The role of macrophages in vascular adaptation to pregnancy in mice

Holly Michelle Groome

The Robinson Research Institute

School of Medicine

Discipline of Obstetrics & Gynaecology

University of Adelaide, Adelaide,

Australia

A thesis submitted to the University of Adelaide in fulfilment of the requirements for the admission to the degree Doctor of Philosophy

FEBRUARY 2021

ABSTRACT

Macrophages are abundant in female reproductive tissues and play crucial roles in the establishment of murine pregnancy through actions in the ovary, and potentially in the uterus. Within the ovary, macrophages support the vascular integrity of the corpus luteum allowing progesterone (P4) production. These ovarian macrophages have been shown to be associated with endothelial cells in the corpora lutea and express the angiogenic marker Tie2. This supports an angiogenic role for ovarian macrophages at the outset of pregnancy.

On the other hand, the role of uterine macrophages during murine pregnancy is not fully understood. It has been postulated that uterine macrophages contribute to immune tolerance and tissue remodelling for embryo implantation, trophoblast invasion, and decidualisation. In addition, some studies have suggested that macrophages are involved in uterine vascular remodelling through interactions with endothelial cells, trophoblast cells, and other immune cell subsets including uterine natural killer (uNK) cells and regulatory T (Treg) cells. Therefore, studies within this thesis sought to investigate the role of uterine macrophages in promoting vascular adaptations to pregnancy.

Previous studies with macrophage-deficient mice or mice transiently depleted of macrophages during pregnancy have shown pregnancy failure (Pollard et al., 1991, Care et al., 2013). Whilst these studies demonstrate macrophages as being indispensable for pregnancy success, the specific physiological role of uterine macrophages has not been confirmed. Studies within this thesis utilised the CD11b-DTR transgenic mouse model to deplete CD11b-expressing cells via administration of diphtheria toxin (DT). Administration of 25 ng/g DT to CD11b-DTR mice elicited >90% depletion of macrophages from the uterus and other tissues 24 h post-DT administration. Importantly, administration of DT to wild type mice had no effect on pregnancy or macrophage numbers.

Data from chapter three demonstrated that macrophage depletion resulted in pregnancy failure from day 7.5 pc, 48 h post-DT administration. Macrophage depletion impaired decidualisation and reduced trophoblast invasion on day 7.5 pc. In addition, vascular remodelling within the uterus was reduced post-macrophage depletion. Pregnancy failure on day 7.5 pc was in part attributable to defects in corpus luteum structure and reduced serum P4. However, hormone supplementation in macrophage-depleted mice failed to fully restore viable pregnancy. This implies a role for macrophages other than in ovarian P4 production and presumably within the uterus during the peri-implantation phase of murine pregnancy.

Whilst near-complete macrophage depletion resulted in pregnancy failure, an attenuated dose of DT was investigated to explore the effect of less extensive macrophage loss. Moderate macrophage depletion during the peri-implantation phase allowed a greater proportion of pregnancies to survive. However, there was a reduced number of viable fetuses and reduced fetal growth measured at day 17.5 pc. Associated

with fetal growth restriction was an impairment in the placental labyrinth zone which had reduced densities of fetal capillaries. In addition, uterine vascular remodelling was impaired during mid-gestation after moderate macrophage depletion, similar to what was observed at the higher DT dose.

To further investigate the involvement of macrophages in uterine vascular remodelling, macrophage or P4 replacement procedures were conducted in DT-treated CD11b-DTR mice. Macrophage replacement improved viable pregnancy rates and restored serum P4, decidualisation, trophoblast invasion, and to an extent, uterine vascular remodelling. Whilst P4 supplementation restored decidualisation, P4 administration failed to improve uterine vascular remodelling and trophoblast invasion after macrophage depletion. In addition, macrophage depletion caused reduced abundance of uNK cells, while P4 or macrophage administration restored uNK cell abundance.

In order to interrogate macrophage-derived products as mediators of uterine vascular remodelling during early to mid-gestation, RNA profiling was performed in the decidua and myometrium on day 7.5 pc. Macrophage depletion resulted in substantial gene expression changes. A majority of these dysregulated genes could be restored by either P4 or macrophage administration. Importantly, macrophage administration restored a larger proportion of the genes dysregulated by macrophage depletion than did P4 supplementation. Notably, *C1q* genes were downregulated after macrophage depletion, independent of P4 administration, but macrophage replacement restored *C1q* expression. *C1q* has been shown to be an important factor for placental development and fetal growth with some evidence to suggest that decidual vascular remodelling is impaired in *C1q*-deficient dams.

To investigate C1Q function in murine pregnancy, C1Q-deficient dams were utilised in allogeneic pregnancy. At late gestation, fetuses were growth restricted and placentas were hypertrophic in C1Q-deficient dams. Importantly, C1Q deficiency caused impaired decidual vascular remodelling and reduced uNK cell abundance. Wild type macrophage administration to C1Q-deficient dams restored decidual vascular remodelling and uNK cells, highlighting that macrophage-derived C1Q can facilitate uterine vascular remodelling during early to mid-gestation.

The data presented in this thesis shows that macrophages play an indispensable role during the peri-implantation phase of murine pregnancy through effects in the uterus, in addition to their known roles within the ovary. Furthermore, macrophage-derived C1Q appears to be a regulator of uterine vascular adaptation during early to mid-gestation and facilitates pregnancy success. This indicates that macrophages and C1Q are essential factors in promoting adequate placentation and fetal growth, and should be further investigated in the context of human pregnancy and gestational disorders.

DECLARATION

I certify that this work contains no material which has been accepted for the award of any other degree or diploma in my name, in any university or other tertiary institution and, to the best of my knowledge and belief, contains no material previously published or written by another person, except where due reference has been made in the text. In addition, I certify that no part of this work will, in the future, be used in a submission in my name, for any other degree or diploma in any university or other tertiary institution without the prior approval of the University of Adelaide and where applicable, any partner institution responsible for the joint-award of this degree.

I give permission for the digital version of my thesis to be made available on the web, via the University's digital research repository, the Library Search and also through web search engines, unless permission has been granted by the University to restrict access for a period of time.

I acknowledge the support I have received for my research through the provision of an Australian Government Research Training Program Scholarship.

Holly Michelle Groome

FEBRUARY 2021

ACKNOWLEDGMENTS

They say what does not kill you only makes you stronger. Well. After this, consider me invincible. From the Imposter Syndrome, to the late nights and weekends, to the constant feeling of working too hard yet feeling unaccomplished, my journey through this PhD is complete. I would not have got to this point without a superior support team behind me.

My principal supervisor, Sarah Robertson, I am truly indebted to you for your encouragement, your guidance, and your ability to always inspire me to achieve the best. Thank you for your thoroughness, patience and giving me the opportunity to undertake research with you. To my co-supervisory team, Loretta Chin, Alison Care, and Claire Roberts, thank you for always providing a strong support base where there was a “no question is too dumb” and “no mistake is on purpose” policy. I am truly grateful for your technical expertise, mental support, and desire to help me achieve my best.

To the entire Robertson lab group, thank you for putting up with me. Thank you for enjoying countless lunches with me and always picking my spirits up when my experiments did not work. From escorting me to hospital, to telling me the centrifuge was on rpm and not RCF, thank you!

To my nearest and dearest friends who I would otherwise never have met until we crossed paths in the Robertson Lab. Kavita, Dexter, Bridget, and Ricky, you made my life infinitely more enjoyable during my PhD. Thank you for always having a meme or dog picture to show me on my darkest days (including the day I dropped all my macrophages) and for giving me the space to be mad or upset when I needed it. Above all, thank you for always having my best interests at heart and supporting me during the difficult times. I am truly blessed by your friendship, hysterical laughing episodes, and being surrounded by kindred spirits. You all mean so much to me. Thank you, Jean, for always discussing the meaning of life during the early mornings and caring enough about my project to source difficult answers for me.

To my family, even though the details of my project were blurry to you, you were all still able to tell me you were proud of me. Thank you, mum for always being available to answer the phone and listen to me cry or have an existential crisis. To nana and papa, thank you for always having Monday Night Dinner and shortbread prepared for me. To Damon, thank you and sorry. Thank you for picking me up when I could not pick myself up and thank you for your patience. My PhD changed me in so many ways but now I hope to get back on with our lives together now it is finished.

I would like to finish my acknowledgements by saying that no one achieves anything alone and that this list of acknowledgments only scratches the surface for the people who have supported me. Unconventionally, I would like to acknowledge my own efforts. Whilst my negative thought processes have often meant I have been overly critical of myself, I have been able to show myself that I am truly capable of achieving anything. Above all, a PhD teaches you more about yourself than anything else.

PUBLICATIONS ARISING FROM THESIS

Groome HM, Care AS, Chin PY, Roberts CT & Robertson SA. *Macrophage-regulated C1Q drives uterine vascular adaptations essential for pregnancy in mice.* In preparation.

Groome HM, Care AS, Chin PY, Roberts CT & Robertson SA. *Moderate macrophage depletion causes fetal growth restriction through altered uterine vascular adaptations in mice*. In preparation.

Groome HM, Care AS, Chin PY, Roberts CT & Robertson SA. *Macrophages as critical mediators of implantation and placentation for pregnancy success (a review).* In preparation.

ABSTRACTS ARISING FROM THESIS

2019

Groome HM, Care AS, Chin PY, Roberts CT & Robertson SA. *Macrophages mediate vascular remodelling required to establish pregnancy in mice.* Oral Presentation at Australian and New Zealand Society for Immunology. Annual Scientific Meeting, Adelaide, Australia. December 2019.

Groome HM, Care AS, Chin PY, Roberts CT & Robertson SA. *Macrophages mediate uterine vascular adaptations to pregnancy in mice.* Oral Presentation at Adelaide Immunology Retreat as part of Australian Society for Immunology. Annual retreat, Hahndorf, Adelaide, Australia. August 2019.

Groome HM, Care AS, Chin PY, Roberts CT & Robertson SA. *Macrophages mediate uterine vascular remodelling required to establish pregnancy in mice.* Oral Presentation at Society for Reproductive Biology. Annual Scientific Meeting, Sydney, Australia. August 2019.

Groome HM, Care AS, Chin PY, Roberts CT & Robertson SA. *Macrophage regulation of decidual vascular remodelling is crucial for pregnancy success in mice.* Poster Presentation at Society for Reproductive Investigation. Annual Scientific Meeting, Paris, France. March 2019.

2018

Groome HM, Chin PY, Care AS, Roberts CT & Robertson SA. Macrophage depletion in the post-implantation phase elicits implantation failure through effects on the ovary and uterus in mice. Poster Presentation at Society for Reproductive Biology. Annual Scientific Meeting, Adelaide, Australia. August 2018.

Groome HM, Care AS, Chin PY, Roberts CT & Robertson SA. Macrophage depletion during the post-implantation phase elicits poor vascular adaptations to pregnancy in mid-gestation in mice. Oral Presentation at Australian Reproduction Update. Annual Scientific Meeting, Melbourne, Australia, November 2018.

2017

Groome HM, Chin PY & Robertson SA. *Macrophages promote adequate development of placental vasculature for healthy pregnancies in mice.* Oral presentation at Australian Society for Medical Research South Australian Division. Annual Scientific Meeting, Adelaide, Australia. June 2017.

Groome HM, Chin PY, Green ES, Wilson RL, Roberts CT & Robertson SA. *Macrophages regulate vascular adaptations associated with placental labyrinth development in mice.* Oral presentation at Adelaide Immunology Retreat as part of Australian Society for Immunology. Annual Retreat, Barossa Valley, Adelaide, Australia. August 2017.

Groome HM, Chin PY, Green ES, Wilson RL, Roberts CT & Robertson SA. *Macrophage regulation of vascular remodelling is required for placental development in mice.* Poster presentation at Society for Reproductive Biology. Annual Scientific Meeting, Perth, Australia. August 2017.

Groome HM, Chin PY, Wilson RL, Roberts CT & Robertson SA. *Macrophage depletion during decidualisation in mice affects placental labyrinth development.* Oral presentation at Robinson Research Institute Symposium. Annual symposium, Adelaide, Australia. November 2017.

Groome HM, Chin PY, Green ES, Wilson RL, Roberts CT & Robertson SA. *Macrophage depletion affects placental labyrinth vascularisation independent of fetal alloantigens.* Special Interest Group oral presentation and poster presentation at Australian Society for Immunology. Annual Scientific Meeting, Brisbane, Australia. November 2017.

TABLE OF CONTENTS

LIST OF FIGURES

LIST OF TABLES

ABBREVIATIONS

°C	degrees Celsius
αSMA	alpha smooth muscle actin
ABC	Avidin-Biotin Complex
Actb	actin beta
ANGPT	angiopoietin
ANOVA	analysis of variance
APC	allophycocyanin
Arg-1	arginase-1
BCIP/NBT	5-bromo-4-chloro-3-indolyl phosphate/nitro blue tetrazolium
BMDM	bone marrow derived macrophages
BMP	bone morphogenetic protein
bp	base pairs
Breg	regulatory B
BSA	bovine serum albumin
BV	brilliant violet
C	complement component
CCL	chemokine (C-C motif) ligand
CCR	CC chemokine receptors
CD	cluster of differentiation
cDNA	complementary DNA
CL	corpus luteum
cm	centimetre
cRPMI	complete RPMI medium
CSF	colony-stimulating factor
Ct	cycle threshold
CTLA4	cytotoxic T-lymphocyte-associated protein 4
CX3C	C-X3-C motif chemokine
CXC	chemokine (C-X-C) motif
Cy	cyanine
DAB	3,3'-diaminobenzidine
DAPI	4,6-diamidino-2-phenylindole dihydrochloride
DBA	dolichos biflorus agglutinin
DC	dendritic cell
Dec	decidua

DMEM	Dulbecco's Modified Eagle's Medium
DNA	deoxyribonucleic acid
dNTPs	deoxyribonucleotide triphosphate
DPX	distrene-80 plasticizer xylene
DT	diphtheria toxin
DTR	diphtheria toxin receptor
e	embryo
E1	estrone
E2	estradiol/estrogen
E3	estriol
ECM	extracellular matrix
EDTA	ethylenediaminetetraacetic acid
EGF	epidermal growth factor
EGFP	enhanced green fluorescent protein
ELISA	enzyme-linked immunosorbent assay
eNOS	endothelial nitric oxide synthase
ER	estrogen receptor
ET-1	endothelin 1
EVT	extravillous trophoblast cell
FACS	fluorescence-activated cell sorting
FBS	fetal bovine serum
FC	fold change
FGF	fibroblast growth factor
FGR	fetal growth restriction
FITC	fluorescein isothiocyanate
Flt1	fms-like tyrosine kinase 1
FMO	fluorescence minus one
FOXP3	forkhead box P3
FSC	forward scatter
FSH	follicle stimulating hormone
g	gram
G	gauge
Gapdh	glyceraldehyde 3-phosphate dehydrogenase
GC	glycogen cell
GDF	growth differentiation factor

GFP	green fluorescent protein
GPCR	G-protein coupled receptor
h	hour
H	hormone supplemented
H&E	haematoxylin & eosin
HBC	Hofbauer cell
hCG	human chorionic gonadotrophin
HIF	hypoxia inducible factor
HLA	human leukocyte antigen
HRP	horseradish peroxidase
i.p.	intraperitoneal
i.v.	intravenous
Icam1	intracellular adhesion molecule 1
IDO	indoleamine 2,3-dioxygenase
IFN	interferon
IGF	insulin growth factor
IHC	immunohistochemistry
IL	interleukin
iNOS	inducible nitric oxide synthase
IPA	Ingenuity Pathway Analysis
ITGAM	integrin alpha M
KDR	kinase insert domain protein receptor
JZ	junctional zone
LH	luteinising hormone
LIF	leukaemia inhibitory factor
LIFR	leukaemia inhibitory factor receptor
LN	lymph node
LPS	lipopolysaccharide
LysM	lysin motif
LZ	labyrinth zone
µg	microgram
µl	microliter
µm	micrometre
µM	micromolar
MØ	macrophage

M1-like	classical activation of macrophages
M2-like	alternative activation of macrophages
M	molar
MD	macrophage-depleted
mg	milligram
MHC	major histocompatibility complex
min	minute
mL	millilitre
MLAp	mesometrial lymphoid aggregate of pregnancy
mm	millimetre
mM	millimolar
MMP	matrix metalloproteinase
ng	nanogram
NK	natural killer
NRP	neuropilin
NO	nitric oxide
O/N	overnight
OCT	optimal cutting temperature
op/op	osteopetrotic mouse
P4	progesterone
PBS	phosphate buffered saline
pc	post coitum
PCR	polymerase chain reaction
PDGF	platelet derived growth factor
PE	phycoerythrin
PE	preeclampsia
PEC	peritoneal exudate cell
Pf4	platelet factor 4
PGR	progesterone receptor
PGRMC1	progesterone receptor membrane component 1
PIGF	progesterone-induced blocking factor
PlGF	placental growth factor
PR	progesterone receptor
PRL	prolactin
PRLR	prolactin receptor

qPCR	quantitative PCR
RBC	red blood cell
RCF	relative centrifugal force
RGB	red, green, and blue
RIN	RNA integrity number
Rn$^{-/-}$	relaxin knock-out
RNA	ribonucleic acid
RO	reverse osmosis
rpm	revolutions per minute
RXFP1	relaxin family peptide receptor 1
s	second
s.c.	subcutaneous
SDS	Dodecyl sodium sulphate
SEM	standard error of the mean
SSC	side scatter
TAMs	tumour associated macrophages
TEMs	Tie2 expressing macrophages
Tg	transgene
TGC	trophoblast giant cell
TGF	transforming growth factor
Th	T helper
TIM-3	T cell immunoglobulin and mucin domain protein 3
TIMP	tissue inhibitors of matrix metalloproteinases
TLR	toll-like receptor
TNF	tumour necrosis factor
Treg	regulatory T cell
uNK	uterine natural killer
UV	ultraviolet
V	volts
V	violet
VEGF	vascular endothelial growth factor
Veh	vehicle pellet
w/v	weight by volume
WT	wild type
x g	gravitational force per unit mass due to gravity

Mouse strains:

C1qa$^{+/+}$	C1Q replete
C1qa$^{-/-}$	C1Q deplete
C1qa$^{-/-}$ + MØ	C1Q deplete administered C1Q replete BMDM
MD^{5}	CD11b-DTR administered 5 ng/g
MD^{10}	CD11b-DTR administered 10 ng/g DT
MD^{25}	CD11b-DTR administered 25 ng/g DT
MD^{25} + H	CD11b-DTR administered 25 ng/g DT, P4 and E2
MD^{25} + MØ	CD11b-DTR administered 25 ng/g DT and WT BMDM
MD^{25} + P4	CD11b-DTR administered 25 ng/g DT and P4
MD^{25} + Veh	CD11b-DTR administered 25 ng/g DT and vehicle pellets
WT	FVB/NJ females administered 25 ng/g DT

CHAPTER 1
LITERATURE REVIEW

Excerpts of this chapter have contributed to the following publication: Groome HM, Care AS, Chin PY, Roberts CT & Robertson SA. *Macrophages as critical mediators of implantation and placentation for pregnancy success (a review)*. In preparation.

1.1 INTRODUCTION

Macrophages are innate immune cells which induce pro-inflammatory immune responses to pathogens yet also regulate tissue remodelling and homeostasis. Macrophages can exert a range of functions, including secretion of both pro-inflammatory and immunoregulatory cytokines, chemokines, and growth factors. Most macrophages differentiate from bone marrow-derived monocytes upon entering tissues where they play roles in antigen uptake and presentation (Geissmann et al., 2010). Here, macrophages phagocytose antigens and cellular debris from apoptotic cells, and present antigens to T and B cells. Macrophages thus act as a bridge between the innate and adaptive immune systems to initiate immune responses directed at pathogens, or dampen immune responses to promote tissue remodelling during growth, development, and wound healing.

Macrophages are thought to be essential for reproductive success where they have substantial potential to act in the uterus and ovary to facilitate adaptations to pregnancy (Tang et al., 2015, Zhang et al., 2017). Notably, the various roles of macrophages in the female reproductive tract are currently under comprehensive investigation for their roles in tissue and vascular remodelling (Riabov et al., 2014, Moldovan et al., 2000, Lash et al., 2016). In mice, the numbers of macrophages in the uterus and ovary fluctuate over the course of the estrous cycle. In the uterus, their numbers increase in the pre-implantation phase of pregnancy where the proportion of macrophages accounts for around 20-30% of all decidual leukocytes (Lessin et al., 1988). As decidualisation occurs, macrophages are excluded and congregate in the myometrium (Mackler et al., 2000, Mackler et al., 1999, van den Heuvel et al., 2005). Macrophages have been implicated as being crucial for several aspects of pregnancy, including implantation, placental development, and parturition (Ning et al., 2016). However, the precise physiological significance of uterine macrophages has been difficult to assess, largely because the genetic models to deplete macrophages are challenging to apply in this context.

Using a diphtheria toxin (DT)-driven genetic mouse model to deplete $CD11b^{+}$ cells, macrophages have been shown to be essential for ovarian corpus luteum development and maintenance (Care et al., 2013, Turner et al., 2011). In preparation for pregnancy and during pregnancy, vascular remodelling is crucial in the ovaries. Development and maintenance of the corpus luteum in mice is essential for maintaining pregnancy and progesterone (P4) production throughout gestation. Failure to adequately remodel and develop the corpora lutea is linked with insufficient P4 and consequently implantation failure (Care et al., 2013, Erlebacher et al., 2004). However, it remains to be investigated whether and how macrophages may function locally within the uterus to support implantation and maintenance of pregnancy.

Greater understanding of how macrophages and other immune cells induce uterine vascular remodelling in early pregnancy is imperative, as the global burden of reproductive disorders, including infertility, subfertility, miscarriage, preeclampsia (PE), fetal growth restriction (FGR), and preterm birth, represents

a significant challenge to overcome. The origins of these conditions have each been linked to early perturbations in pregnancy establishment (Bounds et al., 2015, Kaufmann et al., 2003, Williams et al., 2009). In particular, immune cells are implicated in the development of pregnancy complications due to aberrant phenotypes and/or reduced numbers (Faas et al., 2014, Wang et al., 2011). Moreover, the events which occur during early pregnancy influence the embryo and fetus to program offspring health. Poor origins can compromise later offspring health with diseases arising after birth, including asthma, allergy, metabolic and cardiovascular disorders as well as mental and cognitive dysfunction (Lucas et al., 1999, Andraweera et al., 2020).

Mice provide a useful model for studying pregnancy and the immune response, as placentation is similar to that in women. Both species undergo hemochorial placentation, which involves direct contact of maternal blood with the developing fetal chorion. This method of placental development is more challenging for maintaining immune tolerance to the semi-allogeneic fetus due to the developing fetal cells being in direct contact with maternal immune cells within the blood. In addition, the immune systems of both humans and mice are similar in terms of cellular and molecular composition, regulation, and development. Studies involving mice are also beneficial for ethical reasons, and their short gestation makes mice very useful to assess interventions in pregnancy at defined time points. Mouse gestation is typically 19-21 days, whereas human gestation is approximately 40 weeks. The developmental stages of neonates are strikingly different between these species, where key organ differentiation occurs after delivery in mice but before delivery in humans. Pregnancy perturbations need to be understood in mice before the gaps in knowledge of the pathophysiology of human clinical conditions can be fully addressed.

This review will focus on the known and potential roles of macrophages in the female reproductive tract, and their potential to contribute to successful pregnancy.

1.2 IMMUNOLOGY OF PREGNANCY

Pregnancy depends on versatility in the innate and adaptive immune systems whereby the mother is able to tolerate and supply nutrients to a semi-allogeneic embryo, allowing implantation followed by fetal and placental growth, while still supporting defence against microbial infection and placental overgrowth (Robertson et al., 2015). The embryo is considered semi-allogeneic due to the expression of both maternal and paternal major histocompatibility complex (MHC) antigens. These paternal MHC antigens are recognised as “foreign” by maternal immune cells. Thus, immune tolerance mechanisms must prevent destructive fetal rejection and inflammatory responses, and this is mediated by a range of immunoregulatory cells and agents.

Current understanding suggests that maternal and fetal components cooperate to create an environment suitable for placental development and fetal growth (Robertson et al., 2015). Maternal immune cells in the

vicinity of the semi-allogeneic placenta and fetus are dominated by immunoregulatory M2-like macrophages, uterine natural killer (uNK) cells, tolerogenic dendritic cells (DCs), and Treg cells (Wan et al., 2008). The paradigm of Th1/Th2 cells used in the 1990's to describe the immune response in pregnancy is now recognised as overly simplistic and has been expanded to accommodate the Th1/Th2/Th17/Treg phenomenon (Saito et al., 2010). Innate immune cells prime immunoregulatory adaptive immune cells and together these cells generate a state of active tolerance to the fetus.

The process of generating maternal immune tolerance, required for successful embryo implantation, depends on ovarian steroid hormones and events at coitus. Male seminal fluid, which contains soluble paternal MHC antigens and inflammatory regulators such as transforming growth factor-beta (TGF-β) is deposited into the female reproductive tract at coitus (Robertson et al., 2009a). Signalling molecules in the ejaculate interact with estrogen (E2)-primed epithelial cells in the female reproductive tract (Robertson et al., 1996a). This induces expression of chemokines and other inflammatory signals that in turn cause recruitment of antigen presenting cells (Robertson et al., 1996b). These antigen presenting cells traffic to the uterine-draining lymph nodes which interact with naïve T cells to induce proliferation and differentiation of Treg cells which then circulate via the peripheral blood back to the uterus. This Treg cell generation allows establishment of an optimal uterine microenvironment for the developing fetus (Robertson et al., 2015, Robertson et al., 2009b, Sharkey et al., 2012b). Macrophage and DCs also help prepare the female reproductive tract for pregnancy through clearance of cellular debris and pathogens.

1.2.1 INNATE IMMUNE CELLS

The innate immune system is the first line of defence against foreign bodies and pathogens. From the seminal fluid delivered at coitus, to the developing embryo and the fetus, the mother's immune system must tolerate these foreign cells. The mechanisms of maternal immune tolerance are mediated in the first instance by innate immune cells. Together these cells interact to promote immune tolerance by favouring the priming of adaptive immune cells into tolerogenic subsets. NK cells, DCs and macrophages infiltrate the decidua in early pregnancy and surround the foreign trophoblast cells (Shimada et al., 2006).

NK cells are typically granulated cytotoxic lymphocytes that contribute to clearance of senescent cells, tumour cells and pathogens. However, in the pregnant uterus their phenotype is unique in that it induces tissue and vascular remodelling associated with trophoblast invasion, uterine vascular remodelling, and placental development (Gaynor and Colucci, 2017). In the decidua, approximately 70% of infiltrating uterine leukocytes are NK cells. uNK cells have a biphasic fluctuation in phenotype. During the pre-ovulatory phase, uNK cells are agranular where they become increasing granulated in the post-ovulatory secretory phase. If conception occurs, uNK cells increase in density around trophoblast cells during early pregnancy where their numbers begin to diminish as pregnancy progresses, and finally are virtually

absent at term. Thus, uNK cells appear to be involved in trophoblast invasion and early vascular changes associated with the development of the placenta (Madeja et al., 2011, Hanna et al., 2006).

uNK cells represent the largest proportion of decidual leukocytes. Surprisingly, NK cell knockout mice show minimal impacts on pregnancy outcomes where viable pups are still born (Croy et al., 2003). However, their deficiency is associated with poor decidual and spiral artery remodelling (Croy et al., 2003). Conversely, macrophage-deficient mice are infertile, namely the osteopetrotic (op/op) mouse strain, where there is a defect in colony stimulating factor-1 receptor (CSF1R). This infertility has been directly attributed to female reproductive tract dysfunction rather than defects in paternal signalling (Pollard et al., 1991).

DCs represent approximately 2% of immune cells at the fetal-maternal interface. DCs play an essential role in antigen uptake and presentation to stimulate tolerogenic T cells in the uterine-draining lymph nodes (Wan et al., 2008). DCs can promote Th1 or Th2-skewing of activated T cells through production of interleukin (IL)-12 and IL-10 polarising cytokines, respectively (Steinman and Hemmi, 2006). In addition, the interaction between DCs and Treg cells is crucial to promote pregnancy success and occurs in a dynamic and complex manner depending on signalling factors (Collins et al., 2009). Whilst DC numbers are low in the decidua, their depletion severely impacts embryo implantation and also impairs NK cell maturation, highlighting a crucial role in pregnancy (Krey et al., 2008, Tagliani and Erlebacher, 2011).

Initially, the fetal immune system was regarded as playing minimal roles in promoting tolerance. However, recent studies in humans have shown that fetal antigen presenting cells, mostly fetal DCs, have a higher capacity to induce regulatory T cells than maternal DCs from around 10 weeks of gestation (McGovern et al., 2017). Whilst DCs have not been strictly implicated in vascular remodelling required for pregnancy, their ability to control the uterine microenvironment by priming other immune cells implicates them as key regulatory cells during pregnancy.

The role of neutrophils during pregnancy has not been extensively examined, however key studies indicate that they largely play an immunoregulatory role in the conception environment with limited roles in the uterus thereafter. Neutrophils can be recruited to the uterus via chemokine (C-X-C motif) ligand 8 (CXCL8). Trophoblast cells have been shown to constitutively express CXCL8 which, in addition to recruiting neutrophils, can promote constant turnover and recruitment of other immune cells (Mor et al., 2017). In women, neutrophils exposed to P4 and E2 promote maternal tolerance through inducing Treg cells (Nadkarni et al., 2016). These induced Treg cells are able to produce IL-10, IL-17, and vascular endothelial growth factor (VEGF) *in vitro* to promote vessel growth. In contrast, activated neutrophils have been implicated in the pathogenesis of PE (Gupta et al., 2007). Depletion of maternal neutrophils in mice has been shown to reduce Treg cells, cause growth restriction in fetuses, decrease uteroplacental

circulation, and cause poor spiral artery development (Nadkarni et al., 2016). This implicates neutrophils as mediators of pregnancy immune adaptations.

1.2.2 ADAPTIVE IMMUNE CELLS

The adaptive immune system plays key roles in maintaining immune tolerance during pregnancy. Critical cells involved for maintaining tolerance include B cells, Th2 cells, and Treg cells. Other adaptive immune cells are typically suppressed during pregnancy including Th1, Th17, and CD8 T cells.

B cells account for 5-10% of circulating lymphocytes and are divided into subsets including B1 cells or B2 cells (Fettke et al., 2014). B1 cells are derived from haemopoietic stem cells in the fetal liver where they have self-renewal properties (Stall et al., 1988). B2 cells on the other hand are splenic B cells that originate from the bone marrow where they are short-lived and proliferate upon antigenic stimulation (Gatto and Bachmann, 2005). Furthermore, a new subset of B2 cells was discovered, IL-10 producing B cells (B10 in mice) or regulatory B cells (Breg in humans). These regulatory cells act to control excessive T cell-mediated inflammatory responses (Yanaba et al., 2008). B cells were initially regarded as having no role in pregnancy and were reported to be absent from the decidua during pregnancy. However, other studies have implicated regulatory B cells in immune tolerance during pregnancy through the release of asymmetric antibodies which bind antigens at high affinity without initiating a host immune response (Gentile et al., 1992, Guzman-Genuino et al., 2020).

Altogether T cells comprise 3-10% of immune cells in the decidua (Wicherek et al., 2009). This is divided among Th1, Th2, Th17 and Treg cell subsets (Saito et al., 2010). Th1 cells are typical inflammatory T cells involved in cellular immunity, whereas Th2 cells mediate humoral immunity. T cell immunoglobulin and mucin domain protein 3 (TIM-3) is expressed on interferon-γ (IFN-γ) producing Th1 cells and binds to galectin 9 to induce apoptosis of exhausted T effector cells (Zhu et al., 2005). TIM-3 is also expressed on M2-like macrophages where it regulates maternal immune tolerance (Anderson et al., 2007, Chabtini et al., 2013). In this case, TIM-3 enhances the phagocytic capabilities of macrophages. Macrophages are able to interact with trophoblast cells through TIM-3 and galectin 9 during pregnancy which can educate the decidual microenvironment to promote immune tolerance (Hu et al., 2016).

Th17 cells are typically regarded as pathogenic cells, however new evidence suggests that these cells can be recruited to the decidua to exert anti-apoptotic effects on trophoblast cells through IL-17 secretion (Wu et al., 2014). In addition, IL-17 in the decidua acts as an inflammatory signal to recruit immune cells during trophoblast invasion. However, excessive IL-17 has been correlated with pregnancy pathologies such as PE and FGR, mainly through inhibition of DC maturation and Treg cell responses (Gaffen, 2009, Darmochwal-Kolarz et al., 2012, Darmochwal-Kolarz et al., 2017). Notably, the ratio of Th17:Treg cells has been continually investigated as a way of understanding the pro-inflammatory state in pregnancy. It

has been proposed that toward the end of pregnancy and during parturition, there is a shift in this balance where Th17 cells accumulate in the uterus and initiate an inflammatory cascade that facilitates parturition.

Whilst Treg cell numbers in the uterus are relatively small, their function is essential for maintaining maternal immune tolerance and pregnancy success. Treg cell depletion in allogeneic matings causes implantation failure, however Treg cell depletion in syngeneic matings has little effect on embryo implantation, suggesting an immunological role for Treg cells (Darasse-Jèze et al., 2006). Furthermore, recent studies into Treg cells have identified that Treg depletion can cause increased fetal death and uterine artery vascular dysfunction in murine pregnancy (Care et al., 2018). It remains to be fully investigated how Treg cells regulate other immune cell subsets during pregnancy.

1.3 MACROPHAGES

Macrophages are mononuclear phagocytes from the myeloid haemopoietic cell lineage. Early in fetal development a primitive haemopoietic system exists from day seven post-coitum (pc) in mice and from week three in humans (Tavian and Peault, 2005, Palis et al., 1999). Here, non-bone marrow-derived macrophages arise from the fetal liver or the fetal yolk sac from as early as day 8.5 pc in mice or week four in humans (Gomez Perdiguero et al., 2015). These primitive macrophage subsets can seed developing tissues during fetal organogenesis, and the resulting fetal macrophages are maintained under homeostatic conditions through self-renewal to become tissue-resident macrophages in adult life (Yona et al., 2013). In late fetal development and beyond, bone marrow-derived macrophages and other naïve macrophage subsets differentiate from monocytes upon entering tissues during homeostatic surveillance or provoked by inflammation. Some macrophages can differentiate in the bone marrow or periphery and enter tissues as mature macrophages (Geissmann et al., 2010). Macrophages play key roles in antigen presentation and phagocytosis; tissue growth and remodelling; extracellular matrix (ECM) production and degradation; induction of apoptosis; and secretion of growth factors, cytokines, and chemokines for modulating immune responses (Mosser and Edwards, 2008, Robertson et al., 2015, Tang et al., 2015).

1.3.1 MACROPHAGE PHENOTYPES

Once recruited into peripheral sites, macrophages are broadly defined as classically activated “M1-like” and alternatively activated “M2-like” (Gordon, 2003, Mosser and Edwards, 2008, Murray and Wynn, 2011). M1-like macrophages are typically polarised by IFN-γ, tumour necrosis factor (TNF), and CSF2 yielding a pro-inflammatory response. Conversely, M2-like macrophages are polarised by IL-4, IL-10, and IL-13 to result in an anti-inflammatory, pro-angiogenic, and tissue-remodelling capability (Ning et al., 2016, Pinhal-Enfiled et al., 2012). Importantly, M2 polarisation can be mediated by P4, which plays a role to inhibit nitric oxide (NO) and TNF production (Miller et al., 1996).

These broad classifications do not cover the full extent of macrophage function or the immensely plastic nature of these cells (Gordon, 2003, Xue et al., 2014). Within a single tissue, macrophages make up a heterogeneous population that is highly sensitive to local cytokines and other environmental signals (Amit et al., 2016). Furthermore, recently recruited macrophages respond and differentiate according to the activation status of the tissue microenvironment. These phenotypically diverse macrophage populations can act to initiate immune responses as well as modulate them. For example, vascular-associated macrophages in cancer seem to display phenotypes which can induce tissue and vascular remodelling as well as modulating the adaptive immune response (Mor et al., 2017, Qian and Pollard, 2010). Notably, macrophages in reproductive tissues are postulated to exert similar effects.

Importantly, macrophages phenotype is fluid and reversible such that alterations in environmental stimuli can shift individual macrophages' phenotypes. Macrophage phenotype is not a constant state of the cell and thereby the cells undergo phenotypic switching. In this way, the semantics of labelling macrophages as M1 and M2 is overly simplistic and should be defined by their activation markers and the conditions in which they were cultured or exposed to (Murray et al., 2014).

1.3.1.1 TUMOUR-ASSOCIATED MACROPHAGES (TAMs)

Macrophages in cancer are predominately pro-angiogenic and are referred to as tumour-associated macrophages (TAMs) (Kim et al., 2013). Macrophages recruited to tumour sites can be programmed by CSF1, VEGFA, and chemokine (C-C motif) ligand 2 (CCL2) derived from tumour cells to become TAMs (Qian and Pollard, 2010). Here, TAMs can mediate immune quiescence, ECM remodelling, tumour cell invasion, angiogenesis, and metastasis. Importantly, an increased influx of TAMs around tumours has been associated with a poor prognosis and enhanced tumour metastasis in mice (Leek and Harris, 2002, Lin et al., 2002).

TAMs can be a source of matrix metalloproteinase-9 (MMP-9) which acts to degrade the ECM to free bioactive VEGFA and promote vascularisation in tumour sites (Riabov et al., 2014). Importantly, inhibiting MMP-9 production by macrophages cause reduced production of VEGF and diminished tumour vascularisation in mice (Giraudo et al., 2004). Furthermore, in mice with macrophages deficient in Arginase-1 (Arg-1), a typical M2-like marker, tumour size was reduced by approximately half compared to wild type controls (Colegio et al., 2014). These studies implicate macrophages in vascularisation of tumour masses via specific proteins. However, it remains to be investigated whether macrophages in the female reproductive tract induce tissue and vascular remodelling via similar mechanisms.

1.3.1.2 TIE2 EXPRESSING MACROPHAGES (TEMs)

Another important subset of macrophages involved in vascularisation are the TIE2-expressing macrophage (TEM) population (De Palma et al., 2005, Forget et al., 2014). In mice, TEMs express F4/80,

the classical macrophage marker, and CD31, a classical endothelial cell marker (Pucci et al., 2009). TEMs are pro-angiogenic by responding to angiopoietins (ANGPT), in particular ANGPT2 derived from endothelial cells (Coffelt et al., 2010). Importantly, TEMs have been implicated in the neovascularisation of tumours, growth of endometriotic lesions, and ischemic limb revascularisation (Patel et al., 2013, Capobianco et al., 2011, De Palma et al., 2005). Depletion of TEMs, using a murine model, has been shown to cause disorganised $CD31^+$ endothelial cells and improper vessel formation (Capobianco et al., 2011). Furthermore, TEMs can express IL-10 and CCL17 which acts to block the proliferation of pro-inflammatory T cells and promote expansion of the Treg cell population (Coffelt et al., 2011).

Early in embryogenesis a subset of TEMs exist within the embryo which arises before monocyte-derived macrophages (Fantin et al., 2010, Gomez Perdiguero et al., 2015). These TEMs express Neuropilin 1 (NRP1), a receptor for semaphorins and VEGF isoforms, to mediate an interaction with endothelial tip cells to promote vascular fusion (Fantin et al., 2010). Inadequate vascularisation during embryogenesis may be linked with pregnancy complications, including the inadequate development of fetal capillaries within the placenta.

Moreover, early pregnancy is reliant upon substantial ovarian vascular remodelling. Macrophage depletion in early pregnant and non-pregnant mice results in poor vascularisation, decreased numbers of endothelial cells, and decreased numbers of TIE2 macrophages within the corpora lutea (Care et al., 2013, Turner et al., 2011). It remains to be investigated whether TEMs exist within the uterus to facilitate uterine vascular remodelling during pregnancy.

1.3.1.3 MACROPHAGES AND REGULATION OF VASCULAR DEVELOPMENT

Macrophages are postulated to be involved in vascular remodelling events due to their ability to respond to hypoxic stress and induce vascular changes to restore normoxia (Egners et al., 2016). Importantly, TAMs can respond to hypoxia in tumour masses through production of VEGFA. This recruits additional macrophages and circulating endothelial cells to generate additional blood supply and increased access to nutrients. Similar events occur in pregnancy, where the conceptus initially develops in a hypoxic environment and vascular changes are required to support nutrient delivery for growth and development.

During hypoxia, hypoxia inducible factor-1 α (HIF-1α) is upregulated which can induce expression of VEGFA, TGF-β, fibroblast growth factor (FGF), platelet-derived growth factor (PDGF), and sVEGFR1 (Shweiki et al., 1992, Kourembanas et al., 1990). Hypoxia can also induce M2-like macrophage differentiation and Treg cell recruitment (Corzo et al., 2010, Facciabene et al., 2011). VEGFA and HIF-1α positively regulate each other, forming a positive feedback loop. VEGFA binds to VEGFR1 (VEGF-receptor 1, Flt-1) in two isoforms either membrane-bound VEGFR1 (found on macrophages and endothelial cells) or soluble VEGFR1 (sFlt-1). When VEGFA binds to the membrane-bound receptor,

there is weak signal transduction. Conversely, when VEGFA binds to soluble receptor, there is no cellular transduction (Olsson et al., 2006). Also produced during hypoxia is placental growth factor (PlGF). PlGF can act to recruit macrophages and promote M2-like differentiation (De Falco, 2012). PlGF can bind VEGFR1 with higher affinity than VEGFA. Thus, PlGF acts to induce release of VEGFA from VEGFR1 (Autiero et al., 2003). This free VEGFA can bind to another membrane bound receptor found only on endothelial cells, VEGFR2 (Flk-1). When VEGFA binds to VEGFR2, there is stronger cellular transduction which enhances VEGFA production. This induces signalling along the endothelial cells lining blood vessels which in turn promotes vascular permeability, angiogenesis, and endothelial cell survival and proliferation.

The process of vascular remodelling is crucial in pregnancy where insufficient remodelling of uterine spiral arteries is associated with PE, FGR, and miscarriage (Khong et al., 1986, Ball et al., 2006, Pijnenborg et al., 1991). The balance between membrane-bound and soluble VEGFR1 is tightly regulated where increased levels of sVEGFR1 have been associated with poor vascular adaptations to pregnancy, development of PE, and systemic endothelial dysfunction. Thus, sVEGFR1 levels have been used as an indicator of PE in high-risk pregnancies. However, this method of monitoring PE is outdated and does not recognise the early perturbations to vascular remodelling which can precede development of PE.

1.4 MACROPHAGES IN PREGNANCY

In pregnancy, specific immune adaptations are critical to prevent fetal rejection and optimise fetal growth. In particular, immune cells are implicated in mediating vascular adaptations required for placental development and pregnancy success. Macrophages are the second largest leukocyte subset within the uterine decidua during pregnancy comprising approximately 20% of the immune cells in mice (Vince et al., 1990). Furthermore, macrophages are the predominant leukocyte population in the murine myometrium. Macrophage populations also exist within the ovaries, cervix, and endometrium. Uterine macrophages are postulated to play roles in tissue and vascular remodelling, growth factor and cytokine secretion, and phagocytic removal of apoptotic trophoblast cells to facilitate placental development (Svensson-Arvelund and Ernerudh, 2015). Whilst uterine macrophages are not strictly M2 macrophages, they possess certain features and functions which align them more closely to the immunoregulatory M2-like phenotype than the immunogenic M1-like phenotype.

Notably, macrophages in pregnancy possess high levels of plasticity, enabling them to switch between M1-like and M2-like phenotypes in response to micro-environmental cues to establish appropriate support for fetal development. This phenotypic switching is facilitated by local release of cytokines, growth factors, and tissue-remodelling agents. Recently, three unique macrophage subsets were identified in women in the early pregnancy uterine microenvironment (Jiang et al., 2018). These subsets were $CCR2^{-}CD11c^{lo}$ (~80%), $CCR2^{-}CD11c^{hi}$ (~5%), and $CCR2^{+}CD11c^{hi}$ (~15%). The largest population were found throughout

the decidua. The other two populations embodied both pro- and anti-inflammatory characteristics and were found to associate with CCL2 producing extravillous trophoblast cells (EVTs), which may indicate a vascular remodelling role.

Increasing evidence suggests that both M1-like and M2-like macrophage phenotypes are crucial for fetal growth and development (Zhang et al., 2017). During early pregnancy, increased numbers of M1-like macrophages are hypothesised to be required to initiate events such as trophoblast invasion. Trophoblast invasion requires inflammatory signals to recruit the appropriate cellular mediators and induce apoptosis of some cells (Jaiswal et al., 2012). In contrast, growth and development of the fetus and placenta is hypothesised to be reliant on M2-like macrophages which are likely to be involved in uterine tissue and vascular remodelling. Furthermore, pregnancy maintenance during the second and third trimesters is thought to be controlled by M2-like macrophages which oppose fetal rejection and allow fetal growth (Ning et al., 2016). Parturition requires increased numbers of M1-like macrophages to initiate an inflammatory cascade, inducing labour and bringing an end to the pregnancy (Hamilton et al., 2012).

1.5 MACROPHAGES AND OVARIAN FUNCTION

Macrophages have been shown to be involved in many processes within the ovary during pregnancy and ovarian cycling. Through the timely release of specific cytokines, macrophages contribute to follicle growth and development, ovulation, corpus luteum development and maintenance, luteolysis, and follicle atresia (Care et al., 2013, Wu et al., 2004). Notably, macrophage depletion prior to embryo implantation, using the CD11b-DT receptor (DTR) mouse model, inhibited development and vascularisation of the corpus luteum resulting in reduced serum P4 (Care et al., 2013). Furthermore, depletion of macrophages during different stages of the estrous cycle significantly impacts the ovarian vasculature causing ovarian haemorrhage and loss of endothelial cells within the corpus luteum (Turner et al., 2011). These studies highlight an essential role for macrophages in the ovary and indicate that macrophages are important for maintaining ovarian vascular integrity.

Ovarian structure changes dynamically over the course of the murine estrous and human menstrual cycles. These structural changes are largely dependent on cyclic hormone regulation whereby follicles develop, followed by ovulation, luteogenesis, and luteolysis. These processes are dependent on endocrine hormones as well as interactions with immune cells (Norman and Brannstrom, 1994). The cyclic nature of ovarian processes is reflected in the fluctuating numbers of macrophages across the cycle, suggesting hormone control of macrophage numbers. In murine estrous cycles, macrophage numbers are highest in the proestrus and metestrus stages, immediately prior to and immediately after ovulation (Brännström et al., 1993).

In the process of folliculogenesis, small follicles are induced to grow through granulosa and theca cell proliferation in response to follicle stimulating hormone (FSH) and E2. In mice, only a fraction of developing follicles will release an egg for ovulation where many non-dominant follicles undergo follicle atresia or degradation caused by granulosa cell apoptosis. Macrophages are thought to contribute to inducing apoptosis of granulosa cells through TNF signalling (Kaipia et al., 1996). Macrophages also appear to remove apoptotic granulosa cells to maintain the ovary in a homeostasis and avoid aberrant inflammation (Norman and Brannstrom, 1994, Takaya et al., 1997). Ovarian macrophage function has been investigated in CSF1-deficient *op/op* mice, which exhibit ovarian lesions that impact the estrous cycle and ovulation (Cohen et al., 2002).

Females are born with all the ovarian primordial follicles they will ever have. During embryonic development and adulthood, many of these follicles are lost. This process is essential for maintaining oocyte quality and removing any poorly developed follicles or oocytes to maximise reproductive fitness. In atretic follicles undergoing apoptosis, oocytes become misshapen and granulosa cells shrink. Following this, leukocytes initiate and facilitate further apoptosis and tissue resolution. The process of atresia can occur during any follicular development stage and is characterised by low luteinising hormone (LH) and FSH levels within the follicle, which limits growth and development. Premature loss of primordial follicles during the pre-pubertal phase of life can change ovarian dynamics greatly and can lead to premature ovarian insufficiency, which can bring about early menopause and associated reproductive impairments.

Ovulation involves follicle rupture to allow oocytes to be situated at the ovary surface for transfer to the oviduct. Associated with this process is an array of inflammatory mediators such as prostaglandins, histamine, and multiple cytokines. Macrophages assist in ovulation and are presumed to ensure tissue matrix remodelling to erode the follicle surface and allow oocyte release, since depletion of macrophages has been shown to inhibit ovulation (Van der Hoek et al., 2000). Prior to ovulation, macrophages influx the thecal layers of follicles (Brannstrom et al., 1994). Post-ovulation, the ruptured follicle is remodelled into the corpus luteum in a process referred to as luteogenesis. After its development, P4 is released by luteal cells. Luteal insufficiency resulting in reduced P4 has been shown to decrease pregnancy success in mice and is implicated in reduced fertility in women (Erlebacher et al., 2004). Without luteotrophic signals to the corpus luteum, the structure is lost (luteolysis).

1.5.1 CORPUS LUTEUM DEVELOPMENT

During each estrous or menstrual cycle, the corpus luteum develops from granulosa cells in women whereas the corpus luteum of rodents is comprised of granulosa cells and theca interna layers (Anand-Ivell and Ivell, 2014). If ovulation does not progress to conception, luteolysis occurs and a new ovulatory cycle commences following menstruation in women. However, if conception occurs then the corpus luteum is retained and P4 and E2 production is progressively elevated. In mice, the corpus luteum is

retained over the course of pregnancy, and in late gestation fetal cues signal for corpus luteum degradation and reduced P4, signal for parturition (Meidan, 2016). In rodents, macrophages and T cells have been implicated in the life cycle of the corpus luteum. Healthy corpora lutea have limited macrophage and T cell infiltration. However, early corpus luteum regression is associated with a strong M1-like macrophage influx and by late regression T cells become the predominant immune cell. This suggests that macrophages contribute to initiate T cell influx and further luteal apoptosis (Komatsu et al., 2003)

1.5.2 ROLE OF HORMONES IN PREGNANCY MAINTENANCE

In women, LH and FSH are secreted from the pituitary gland where they induce cyclic release of ovarian steroid hormones, P4 and E2. Interactions between ovarian steroid hormones and gonadotrophins act as the main regulators of the ovarian cycle. P4 and E2 levels surge post-ovulation to create a "window of implantation". If ovulation is followed by conception, the ovarian hormone levels remain high until the 10th week of human gestation when placental trophoblast cells take over hormone synthesis (Tan et al., 1999, Milligan and Finn, 1997, Su and Fazleabas, 2015). LH and FSH regulate various aspects of pregnancy. LH is primarily involved in controlling the length of the female menstrual cycle, including ovulation, stimulating P4 and E2 synthesis, and preparing the uterus for embryo implantation (Kumar and Sait, 2011). A pre-ovulatory surge of LH promotes ovulation and stimulates the development and function of the corpus luteum. Notably, LH can stimulate VEGF production in luteinised granulosa cells which allows angiogenesis in the ovarian follicles and the corpus luteum (Fraser and Wulff, 2003). On the other hand, FSH is responsible for follicle growth and E2 synthesis, as well as corpus luteum development and maintenance (Rama Raju et al., 2013).

1.5.2.1 PROLACTIN (PRL)

Prolactin (PRL) is another hormone produced by the corpus luteum and stimulates LH receptor expression in granulosa cells during luteinisation and corpus luteum formation. PRL can repress the conversion of active P4 into an inactive metabolite, thereby assisting in maintaining pregnancy. PRL receptor (PRLR) knockout female mice are infertile due to implantation failure associated with delayed luteinisation and delayed corpus luteum formation (Ormandy et al., 1997). Interestingly, P4 administration to these knockout mice is able to rescue embryo implantation with a small proportion of the embryos surviving to adulthood (Binart et al., 2000). High embryo mortality indicates an essential role for PRL signalling through its receptor during pregnancy maintenance, where it appears to be heavily involved in luteal function. In mice, trophoblast giant cells (TGCs) are the primary producers of hormones including PRL to support placental morphogenesis. In women, syncytiotrophoblasts produce high levels of PRL and human chorionic gonadotrophin (hCG) (Fujimoto et al., 1986). In addition, PRL signalling induces survival of the corpus luteum during lactation due to suckling pups (Takiguchi et al., 2004).

1.5.2.2 ESTROGEN (E2)

Estrogens have been implicated in uterine angiogenesis and vasodilation and a link between PE and estrogen dysregulation has been established (Berkane et al., 2017, Jobe et al., 2011, Rosenfeld and Rivera, 1978, Clewell et al., 1977). The three most common estrogens during pregnancy include estrone (E1), estradiol (E2), and estriol (E3) – all of which are produced by the placenta, ovary, and adrenal glands in women and in mice (Zhang et al., 2017). The respective receptors can be expressed on immune cell subsets where cognate interaction with estrogen ligands can influence the immunoregulatory phenotype of various immune cell types (Robinson and Klein, 2012). E2 has been shown to have roles in angiogenesis through inducing VEGF production and can cause an increase in trophoblast cell proliferation and differentiation (Caulin-Glaser et al., 1997, Cullinan-Bove and Koos, 1993). In mice, E2 levels are low in early pregnancy, however by mid-gestation E2 levels rise to promote placental development (Milligan and Finn, 1997). Without this increase in E2, placental development fails and pregnancy is lost.

1.5.2.3 PROGESTERONE (P4)

In women, during the first trimester, P4 is primarily produced by the corpus luteum. From around the 11th week of gestation, P4 is then predominantly produced by the trophoblast cells of the placenta. In contrast, P4 is primarily produced by the corpora lutea for the entirety of mouse gestation.

P4 plays key roles in uterine decidualisation and receptivity to embryo implantation. In addition, P4 exerts effects on immune cells and is involved in maintaining an anti-inflammatory state during pregnancy (Gellersen and Brosens, 2014, Druckmann and Druckmann, 2005). In particular, the P4 receptor (PGR) is expressed on macrophages. Cognate binding of P4 and PGR can inhibit NO production in macrophages to promote an immunoregulatory phenotype (Miller et al., 1996). Uterine macrophages can respond directly to E2 and P4 as they express the estrogen receptor (ER) and the PGR (Huang et al., 2008). Notably, under the influence of P4 during early pregnancy, macrophages up-regulate MHC-II allowing an increase in antigen presentation and phagocytosis (Miller et al., 1996). Decidual leukocytes can upregulate expression of PGR and P4-induced blocking factor (PIBF) and these signals appear important in preventing fetal loss by inhibiting the cytotoxicity of NK cells and Th1 cells (Roussev et al., 1993, Szekeres-Bartho et al., 1999).

P4 signalling occurs via nuclear receptors which have two distinct isoforms. P4 signalling induces expression of genes which promote decidualisation, implantation, and parturition (Mulac-Jericevic and Conneely, 2004, Cha et al., 2012, Wetendorf and Demayo, 2014). A mouse model of PGR and P4 signalling ablation, resulted in failure to establish pregnancy (Lydon et al., 1995). Interestingly, rodent granulosa and luteal cells do not express PGR but can bind P4 through P4-binding protein (P4 receptor membrane component 1, PGRMC1) which mediates P4 signalling within the ovary (Peluso et al., 2006).

Studies involving gene knockout mice have shown that when corpus luteum function is disrupted, pregnancy success is decreased. For example, null mutation in TGF-β causes a decrease in plasma P4 and renders females infertile. This infertility was attributed to altered function of the corpus luteum rather than ovulation failure (Ingman et al., 2006). Furthermore, macrophage depletion in the CD11b-DTR model has shown ovarian haemorrhage and disrupted vasculature within the corpus luteum (Turner et al., 2011). Ultimately, loss of P4 signalling leads to luteolysis where small capillaries within the corpus luteum undergo apoptosis via TNF – a known product of macrophages. Larger endothelial vessels are lost in corpus luteum regression where the once mature corpus luteum becomes a connective tissue scar called the corpus albicans.

1.5.2.4 RELAXIN

The hormone relaxin is produced by the corpus luteum and can modulate ovulation, the menstrual cycle and pregnancy success (Marshall et al., 2017, Anand-Ivell and Ivell, 2014). Relaxin primarily acts through a G-protein coupled receptor (GPCR) called, relaxin family peptide receptor 1 (RXFP1), expressed in the uterus (Bathgate et al., 2006). In rodents, relaxin increases towards term. In contrast, relaxin is increased in the first trimester of human pregnancy and remains at a constant intermediate level for the rest of gestation (Bell et al., 1987). Relaxin has been postulated to play roles in uterine remodelling to allow trophoblast invasion. Relaxin knock-out mice ($Rn^{-/-}$) are growth restricted *in utero* and $Rn^{-/-}$ females fail to develop sufficient mammary glands which inhibits lactation (Parry et al., 2009, Gooi et al., 2013, Samuel et al., 2005). Previous studies have implicated relaxin in angiogenesis as relaxin can induce VEGF expression in local endothelial cells (Segal et al., 2012, Unemori et al., 1999). However, relaxin was found not to induce pre-implantation uterine angiogenesis, yet appeared to induce expression of steroid receptors and circulating P4 (Marshall et al., 2016). Interestingly, women with reduced relaxin in early pregnancy appear to have an increased risk of developing PE, as well as recurrent miscarriage (Jeyabalan et al., 2009, Anumba et al., 2009). Therefore, relaxin may be a mediator of pregnancy vascular adaptations.

1.6 MACROPHAGES AT THE FETAL-MATERNAL INTERFACE

During embryo implantation, immune cells infiltrate the decidua to maintain tolerance towards the semi-allogenic fetus. Decidual macrophages are thought to assist in maintaining tolerance through antigen presentation to modulate the responses of other immune cells. There appears to be a link between dysregulated macrophage activation and recurrent spontaneous miscarriage in women (Wang et al., 2011). It has been hypothesised that Treg cells can control the activation status of macrophages at the fetal-maternal interface and this contributes to support the tolerogenic environment. Macrophages are abundant in the cycling uterus and are further recruited into the uterus during early pregnancy by a range of factors including ovarian hormones, seminal fluid signalling molecules, hypoxia, chemokines, and

growth factors (Robertson et al., 2009a, Tremellen et al., 1998). Notably, activation of VEGFR1 on macrophages induces a chemotactic response to recruit additional macrophages to sites of active angiogenesis such as the pre-implantation uterus (Murakami et al., 2008).

Macrophages are abundant in the decidua *in vivo* in humans and mice (Stewart and Mitchell, 1991, Brandon, 1994, Hunt and Robertson, 1996, Givan et al., 1997, Eidukaite and Tamosiunas, 2004). Previous studies have utilised immunohistochemistry and flow cytometry to detect macrophage populations in different compartments of the uterus through the estrous and menstrual cycles of mice and women, respectively, and have also looked at the kinetics of macrophages during early pregnancy.

Macrophage recruitment to the uterus is heightened after coitus and early embryo implantation. This may be a response to placental-derived chemokines, as macrophages been shown *in vitro* to traffic towards trophoblast cells (Fest et al., 2007). In this study, macrophage co-culture with trophoblast cells caused an increase in the expression of macrophage-derived chemokines including CXCL1, CXCL8, CCL2, and CCL5. Trophoblast cells appear to actively recruit macrophages which raises the question of whether macrophages may facilitate trophoblast invasion through release of MMPs to remodel decidual tissue, and/or potentially contribute to clearance of apoptotic uterine and trophoblast cells (Salamonsen, 1998, Hannan et al., 2011).

1.6.1 MACROPHAGE CYTOKINES, CHEMOKINES, AND GROWTH FACTORS

The spectrum of macrophage phenotypes present at the fetal-maternal interface appear to interact to promote the growth and development of the placenta. Within the decidua, M2-like macrophages can secrete high levels of IL-10 which suppresses immunogenic responses (Lash et al., 2016). IL-10 can induce expression of TGF-β and minimise cytotoxic T cell activation (Svensson et al., 2011). Interestingly, macrophages from pregnant women with a high risk of developing PE were found to secrete higher levels of pro-inflammatory cytokines IL-1β and TNF, than those macrophages from women with a low PE risk (Svensson-Arvelund and Ernerudh, 2015). A pro-inflammatory uterine environment can impede invading trophoblast cells and impact placental development.

Trophoblast-derived CCL3 is one chemokine implicated in recruiting macrophages and uNK cells into implantation sites (Lima et al., 2014, Ning et al., 2016). Macrophages have also been shown to be responsive to CCL14 released by endothelial cells after activation by EVTs in an *in vitro* study (Choudhury et al., 2017). Trophoblast-derived IL-6 and CXCL8 act to activate endothelial cells which in turn secrete CCL14 and CXCL6 to recruit macrophages and uNK cells towards spiral arteries. CCL14-responsive macrophages also express CCR1 and CCR5 which bind CXCL6. However, these macrophages were not reliant on CXCL6 for migration, whereas CXCL6 could recruit uNK cells (Choudhury et al., 2017). This

suggests that different subpopulations of macrophages and uNK cells play coordinated roles in spiral artery remodelling.

1.6.1.1 VASCULAR ENDOTHELIAL GROWTH FACTORS (VEGFs)

In pregnancy, VEGF mediates uterine vasculature permeability and angiogenesis (Rabbani and Rogers, 2001). Macrophages are known to promote angiogenesis *in vivo* through release of pro-angiogenic factors including VEGFA and ANGPT (Kofler et al., 2011). VEGF-mediated angiogenesis can also be mediated by NO derived from endothelial NO synthase (eNOS). NO can induce endothelial cell differentiation and migration and can also act to promote vascular permeability and vasodilation (Papapetropoulos et al., 1997, Murohara et al., 1998).

1.6.1.1.1 VEGFA

VEGFA binds to both VEGFR1 and VEGFR2 as well as the soluble form of VEGFR1 (sFlt-1). The membrane bound receptor positively regulates angiogenesis through cellular tyrosine kinase transduction. Conversely, the soluble receptor limits angiogenesis by sequestering free VEGFA, VEGFB, and PlGF (Shibuya, 2011, Shibuya, 2006). *VEGFR1*$^{-/-}$ embryos die during gestation due to overgrowth of the vasculature, suggesting that both forms of the receptor modulate angiogenesis (Fong et al., 1995). Interestingly, the ligand binding domain is crucial for controlling angiogenesis as mice with deletion of the tyrosine kinase part of VEGFR1 show no pregnancy abnormalities (Shibuya, 2011). Another study demonstrated that VEGFR1 is expressed on decidual endothelial cells and that blockade of VEGFR1 was insufficient to cause pregnancy failure, yet did reduce the recruitment of macrophages to the uterus during the onset of pregnancy (Douglas et al., 2014).

VEGFA binds VEGFR2, also called Flk-1, with lower affinity than VEGFR1. However, VEGFA-VEGFR2 binding induces stronger cellular signal transduction than does binding to VEGFR1, leading to increased proliferation of endothelial cells (Douglas et al., 2009). It has been shown that blockade of VEGFR2 *in vivo* during pregnancy resulted in embryonic lethality by day 10.5 pc in murine pregnancy (Douglas et al., 2009). In contrast, blocking VEGFR1 or VEGFR3 did not lead to abnormal pregnancy outcomes.

1.6.1.1.2 VEGFB, VEGFC, AND VEGFD

VEGFB is also a modulator of angiogenesis, however it only binds to VEGFR1 and its role in pregnancy is not well-characterised. Conversely, VEGFC and VEGFD regulate lymphangiogenesis and endothelial cell migration, predominantly by binding VEGFR3 and to a lesser degree VEGFR2 (Alitalo and Carmeliet, 2002, Joukov et al., 1996). uNK cells are known to produce VEGF-C, PlGF, and ANGPT1 to support angiogenesis and vascular remodelling during pregnancy (Lash et al., 2006). Increased eNOS and inducible NOS (iNOS) expression was observed after ovine uterine artery endothelial cells were treated

with VEGFD (Mehta et al., 2014). This suggests VEGFD may play roles in uterine artery vasodilation. However, there has been little research into the function of VEGFD in pregnancy.

1.6.1.1.3 PLACENTAL GROWTH FACTOR (PlGF)

Similar to VEGFB, PlGF only binds to VEGFR1 to induce angiogenesis and facilitate endothelial cell growth, proliferation, migration, and survival (Carmeliet et al., 2001, Nejabati et al., 2017). PlGF plays key roles in the maintenance of pregnancy where insufficiency of PlGF has been linked with PE in women (Andraweera et al., 2012). Excessive PlGF can induce inflammation and cause tissue damage and pregnancy loss in some cases (Kang et al., 2014). On the other hand, PlGF can induce angiogenic factor release from macrophages (Selvaraj et al., 2003).

PlGF primarily functions through occupying VEGFR1 and directing VEGFA toward the more potent angiogenic stimulator, VEGFR2 (Park et al., 1994). When PlGF binds VEGFR1 and VEGFA binds VEGFR2, cross-talk occurs between the cognate receptor-ligand pairs to induce angiogenesis (Autiero et al., 2003). uNK cells, decidual cells, and EVTs produce PlGF during early pregnancy to facilitate embryo implantation (Tayade et al., 2007). PlGF can also be induced via P4 and E2 (Chen et al., 2015). Interestingly, PlGF induced vessels display more stability and maturity than vessels induced with VEGFA alone (Carmeliet et al., 2001).

1.6.1.2 HYPOXIA INDUCIBLE FACTORS (HIFs)

HIFs are transcription factors induced in response to hypoxia. HIF-1 is comprised of a heterodimer of an oxygen-regulated HIF-1α subunit and a constitutively expressed HIF-1β subunit. HIF-2α also binds HIF-1β to form the HIF-2 transcription factor. During normoxia, HIF-1α is rapidly degraded. However, during hypoxia the stability of HIF-1α increases. HIF-1-dependent transcription initiates many genes which promote proliferation, angiogenesis, survival, and tumour-associated genes including invasion and metastasis (Semenza, 2003). Key genes activated by HIF-1 include PlGF, VEGF, ANGPT2, and MMP2. These genes are involved in pregnancy establishment, particularly through regulating uterine and placental angiogenesis and tissue remodelling (Semenza, 2009).

1.6.1.3 COLONY STIMULATING FACTORS (CSFs)

CSF1 and CSF2 are present, along with their receptors, at the fetal-maternal interface (Arceci et al., 1989, Giacomini et al., 1995). CSFs act as growth factors for macrophages and can aid in their differentiation recruitment, and regulation of functional phenotype.

1.6.1.3.1 CSF1 (M-CSF)

CSF1 acts as a macrophage growth factor and exerts a critical role in inducing haemopoietic stem cells to become macrophages *in vivo* and *in vitro* (Pierce et al., 1990, Rathinam et al., 2011). In pregnancy, CSF1 derived from trophoblast cells, in concert with IL-10, can induce the M2-like phenotype in maternal

macrophages (Svensson et al., 2011, Svensson-Arvelund et al., 2015). The CSF1-deficient *op/op* mouse, which has a naturally occurring mutation in the *Csf1* gene, reveals infertility after homozygous matings and reduced fertility in heterozygous matings. This infertility was not due to paternal defects but rather due to defects in the uterus of *op/op* females. Within these mice, there are reduced numbers of uterine macrophages which may contribute to pregnancy failure (Pollard et al., 1991).

1.6.1.3.2 CSF2 (GM-CSF)

CSF2 in the female reproductive tract is positively regulated by E2 and negatively regulated by P4 (Robertson et al., 1996b). In the mouse reproductive tract, seminal fluid contact increases the expression of CSF2. This signalling initiates recruitment of macrophages to the implantation site and induces features of M1 polarisation that are likely to be important for presentation of paternal alloantigens to initiate T cell-mediate tolerance in the peri-conception environment (Tremellen et al., 1998, Svensson et al., 2011). CSF2-deficient mice are prone to adverse fetal development and impaired placental vascularisation (Robertson et al., 1999). CSF2-induced M1 polarisation is likely short-lived and overridden by progressively elevating CSF1 expression in response to rising P4 in the peri-implantation phase (De et al., 1993, Carson et al., 2000). A similar transition occurs from the peri-ovulatory to luteal phase in women (Shinetugs et al., 1999). In women, exaggerated or extended CSF2 expression is correlated with increased M1 macrophage influx and PE (Wu et al., 2012).

1.6.1.4 LEUKAEMIA INHIBITORY FACTOR (LIF)

Leukaemia inhibitory factor (LIF) is a member of the IL-6 family and is essential for embryo implantation in mice (Cheng et al., 2001). LIF can be synthesised by macrophages and endometrial cells. In LIF-null mice, there are implantation defects and altered uterine macrophage populations which cause embryo loss (Stewart et al., 1992b). These mice also exhibit altered glycoprotein expression in the uterus which may explain poor embryo implantation (Fouladi-Nashta et al., 2005). Moreover, LIF-receptor (LIFR) knockout mice exhibit perinatal lethality within 24 h of birth (Ware et al., 1995). Importantly, mice treated with LIFRα antagonist during pregnancy showed abnormalities in placental morphology and decreased pregnancy viability (Winship et al., 2015a). These studies suggest that LIF plays multifaceted roles during pregnancy and may be released by maternal macrophages to facilitate fetal growth and development.

1.6.1.5 MATRIX METALLOPROTEINASES (MMPs)

MMPs are zinc-dependent enzymes which degrade components of the ECM to allow tissue and vascular remodelling. Varieties of MMPs include collagenases, gelatinases, stromelysins, and matrilysins (Raffetto and Khalil, 2008). Macrophages can secrete an array of MMPs to release ECM-bound proteins required for angiogenesis and tissue remodelling. MMPs are initially released from cells as inactive proenzymes but are cleaved extracellularly to become activated (Kessenbrock et al., 2010). A broad range of MMPs and their inhibitory counterparts, tissue inhibitors of MMPs (TIMPs), are expressed at the fetal-maternal

interface (Anacker et al., 2011). Regulation of MMPs and TIMPs is key to controlling the degradative abilities of MMPs and ensuring tissue remodelling is controlled (Nissi et al., 2013). MMP2 and MMP9 both play roles in remodelling endometrial tissue during pregnancy and are postulated to facilitate trophoblast invasion (Lalu et al., 2007, Zhang et al., 2010).

1.6.1.5.1 MMP2

MMP2, also called gelatinase A, along with MMP9 help mobilise VEGF in the ECM and allow it to travel to its cognate receptors. Uterine MMP2 levels are high during early pregnancy where they regulate trophoblast invasion (Kizaki et al., 2008). uNK cells express high levels of MMP2 and TIMP-2 in the placental bed, suggesting a regulatory role in trophoblast invasion (Naruse et al., 2009).

1.6.1.5.2 MMP9

MMP9, also called gelatinase B, plays a significant role in the migration of neutrophils across the basement membrane of blood vessels (Delclaux et al., 1996). MMP9 is crucial for angiogenesis in concert with MMP2. Importantly, MMP9 has been implicated in the recruitment of endothelial stem cells which promote angiogenesis (Heissig et al., 2002). During pregnancy, trophoblast cells can secrete high levels of MMP9 during embryo implantation (Alexander et al., 1996). MMP9 has been implicated as a potential biomarker for PE with evidence suggesting that cytotrophoblasts in PE secrete lower levels of MMP9 (Graham and McCrae, 1996, Rahimi et al., 2013). Pregnant MMP9-deficient mice were susceptible to small and morphologically impaired placentas which was accompanied by poor trophoblast invasion on day 7.5 pc. (Plaks et al., 2013). This study proposed that lack of MMP9 was inhibiting the degradation of ECM components which inhibited the released of VEGF thereby reducing angiogenesis.

1.6.1.6 COMPLEMENT SYSTEM IN PREGNANCY

Activation of the complement system has been linked to adverse pregnancy outcomes in animal models (Munn et al., 1998, Xu et al., 2000, Mellor et al., 2001). The complement system acts to recruit and activate immune cells to phagocytose pathogens. Complement activation leads to a cascading effect involving various proteins, including complement component 3 (C3) and C5, to form a membrane attack complex. This complex embeds itself into cell membranes to rid pathogens. C3a and C5a are referred to as anaphylatoxins as they induce pathogen clearance through increasing vascular permeability and promoting release of pro-inflammatory mediators. These proteins exert their effects through C3aR and C5aR, respectively. Excessive plasma C3a and C5 concentrations are associated with PE in women (Derzsy et al., 2010). Increased C3 and C3aR1 during pregnancy can increase sFlt-1 expression resulting in placental damage (Wang et al., 2012).

Whilst complement activation has been associated with poor pregnancy outcomes, C1q upregulation has been implicated in normal pregnancy progression. C1q secreted by decidual cells can localise in spiral

arteries and trophoblast invasion sites (Bulla et al., 2008). Furthermore, C1q expression during pregnancy is not linked with complement activation suggesting a novel role for C1q. Interestingly, deficiency of C1q in males mated to wild type females resulted in the development of preeclamptic-like symptoms in pregnant mice with increases in sFlt-1 and fetal death (Singh et al., 2011). Furthermore, C1q deficiency in females mated to wild type males was associated with impaired placental development (Agostinis et al., 2010).

1.6.2 MACROPHAGES AND EMBRYO IMPLANTATION

After conception, the pre-implantation embryo traverses the fallopian tube in preparation for implantation. Prior to trophoblast invasion, the blastocyst-stage embryo attaches to the maternal uterus via glycoproteins (Enders, 1995). The blastocyst responds to cytokines and growth factors secreted from maternal oviduct and uterine epithelial cells that influence its development, and embed epigenetic programming as reviewed by (Marcho et al., 2015). In humans, the embryo secretes high levels of hCG which can bind to decidual macrophages and induce the tolerogenic phenotype in DCs (Saito et al., 2010). hCG acts as a luteotrophic molecule which promotes corpus luteum development and maintenance during pregnancy to support P4 production (Makrigiannakis et al., 2017). In addition, hCG can suppress T cell cytotoxic activity, potentially via P4, and promotes Treg cell recruitment to the implantation site (Sharma, 2014).

After copulation in mice, macrophages are recruited to the endometrium via seminal fluid signalling where they play roles in promoting uterine receptivity for embryo attachment (Robertson et al., 1996a). Macrophages secrete an array of cytokines including IL-1β, IL-12, and LIF to induce epithelial cells lining the murine endometrium and decidua to upregulate expression of attachment ligands to mediate embryo implantation (Jasper et al., 2011). During the implantation period, an array of cytokines are released which favour M1-like macrophage polarisation (Jaiswal et al., 2012). Here, M1-like macrophages respond to the "injury" signals released through embryo attachment and can facilitate further recruitment of immune cells to induce tissue remodelling (Mor et al., 2011). As implantation progresses, there is a shift away from M1 and towards M2-like phenotypic features (Brown et al., 2014). It has been observed that macrophage depletion prior to implantation in mice results in pregnancy failure through P4 insufficiency and corpora lutea demise (Care et al., 2013).

1.6.3 MACROPHAGES AND DECIDUALISATION

In mice, decidualisation occurs in response to embryo implantation and only occurs at the implantation site from approximately day 3.5 pc (Matsumoto and Sato, 2006). At this stage, the embryo lies in a crypt opposed to the epithelial layer of the uterus. This epithelial layer then undergoes apoptosis to allow trophoblast invasion into the decidua from day 4.5 pc (Enders and Schlafke, 1984). During this time, P4 levels surge which initiates intense changes to the local uterine cellular and molecular environment to

accommodate invading trophoblast cells and initiate vascular changes. Decidualisation involves endometrial stromal cells transforming into larger, rounder decidual cells, which are glycogen and lipid rich, to create the decidua which lines the uterus during pregnancy and interfaces the fetal placenta.

Macrophages may be involved particularly in the extensive breakdown of ECM components to allow decidualisation (Dekel et al., 2014). This transformation, which allows the invading trophoblast cells of the ectoplacental cone, that will ultimately form the placenta, to enter maternal tissues, is mediated by MMPs and IL-10 (Staun-Ram et al., 2004). Over time, decidual cells become the placental bed. In the decidual bed, decidual leukocytes facilitate immune tolerance and tissue and vascular remodelling during early placental morphogenesis from day 4.5 pc through 9.5 pc in mice (Zhang et al., 2016).

In women, decidualisation occurs in each cycle during the luteal phase, independently of the presence of an embryo (Dunn et al., 2003). Following decidualisation, macrophages have been shown at higher concentrations around the spiral arteries at the site of implantation within the decidua which suggests a crucial role in uterine remodelling and vascularisation in women (Ning et al., 2016).

1.6.4 MACROPHAGES AND TROPHOBLAST INVASION

Following blastocyst attachment in women, cytotrophoblast cells invade the decidua and differentiate into two subsets, the syncytiotrophoblast and the EVTs (Enders, 1995). EVTs migrate into the maternal decidua and influence spiral artery remodelling from the decidua. This remodelling increases uteroplacental blood flow and increases nutrient delivery to the developing conceptus. In time, this structural change is accompanied by altered uterine artery function and more compliant blood vessels, allowing increased blood supply and greater infiltration of leukocytes, including macrophages, as placental morphogenesis proceeds. Macrophages can facilitate trophoblast cell invasion in healthy pregnancy. However, in complicated pregnancies macrophage numbers may be insufficient to promote adequate invasion or aberrant macrophage phenotypes may prevent trophoblast cell invasion (Abrahams et al., 2004).

Mice have less trophoblast invasion into the decidual stroma and spiral arteries than do women and rely more heavily on maternal remodelling of tissues and spiral arteries for placental development (Adamson et al., 2002). Blood vessels are most concentrated around the invading trophoblast cells with a dense network of vessels extending through the decidua and myometrium supporting maternal blood flow to the developing placenta for nutrient delivery (Shawber et al., 2015). In mice, trophoblast cells gain access to the decidual stroma which can induce local immune cell populations, including macrophages, DCs and T cells, to differentiate into phenotypes that support the embryo and allow tolerance (Mor et al., 2011). This is achieved through trophoblast-secreted chemokines and immunoregulatory cytokines, CXCL8 and CCL2, which modulate immune cell phenotypes (Fest et al., 2007).

Trophoblast invasion causes a progressive and continuous induction of apoptosis in the decidua which is facilitated by macrophages to assist in development of the placental bed (Abrahams et al., 2004). Macrophages can induce apoptosis of trophoblast cells to regulate the extent of invasion. This is mediated by TNF and TGF-β (Ning et al., 2016). Furthermore, apoptotic trophoblast cells must be cleared to prevent unwanted inflammation. These cells contain allogeneic paternal MHC antigens which can cause inflammation and immune activation in the maternal tissue if not cleared (Ning et al., 2016). Apoptotic body clearance is a key function of macrophages. During the process of apoptosis surface markers are rearranged on the apoptotic body membrane which allow recognition by the macrophages for phagocytic clean-up (Lash et al., 2016). M2-like macrophages also release pro-apoptotic factors to facilitate apoptotic body clean-up, including fibronectin and Mer receptor tyrosine kinase. This process is tightly regulated to ensure trophoblast-induced remodelling of spiral arteries is limited and not excessive and so that the placenta can detach upon conclusion of pregnancy.

1.6.4.1 INFLAMMATORY MEDIATORS

Trophoblast invasion induces a local inflammatory response which is associated with recruitment of immune cells (Co et al., 2013). IL-17 is a key mediator of recruiting immune cells during trophoblast invasion and is strictly controlled in order to dampen excessive inflammatory responses. Another key pro-inflammatory cytokine is IL-23, produced mainly by macrophages and DCs, that in concert with TGF-β stimulates the differentiation of $CD4^+$ T cells into Th17 cells (Oppmann et al., 2000). IL-23 is able to induce MMP9 expression as well as inducing angiogenesis (Saito et al., 2010). In women, unregulated IL-23 expression has been shown to have adverse effects in pregnancy – including recurrent pregnancy loss, PE, and FGR in women (Cai et al., 2016, Darmochwal-Kolarz et al., 2017).

TGF-β plays critical roles in the decidua during embryo implantation through suppressing secretion of pro-inflammatory cytokines from T and B cells. TGF-β can also prevent phenotypic switching of uNK cells to cytotoxic NK cells. TGF-β acts to reduce proliferation of pro-inflammatory cells and inhibits MHC-II expression on macrophages and DCs (Li et al., 2006). This cytokine, which is abundant in seminal fluid, may be linked with facilitating uterine angiogenesis as introduction of seminal fluid induces angiogenesis-associated gene pathways *in vitro* (Sharkey et al., 2012a). In women, reduced TGF-β expression has been linked with PE and FGR (Darmochwal-Kolarz et al., 2017).

1.7 MACROPHAGES AND VASCULAR ADAPTATIONS TO PREGNANCY

1.7.1 VASCULAR REMODELLING

Vascular remodelling involves three-dimensional remodelling of the vasculature whereby vessels undergo structural changes in response to increases in blood pressure or blood flow; or undergo reactivity changes including increased vasodilation or vasoconstriction. These adaptations rely on four main cellular processes: growth, apoptosis, migration, and ECM metabolism (Kelly et al., 2000, Gibbons and Dzau,

1994). These processes are dependent on regulatory factors such as blood pressure, shear stress, and hormonal and endocrine factors. These factors can work independently or synergistically to promote remodelling. The vascular endothelium can sense and respond to these signalling molecules to commence the cellular proliferation, invasion and/or apoptosis events required for remodelling. Immune cells, particularly macrophages, associated with vessels can also sense and alter the environmental stimuli to induce vascular remodelling. Macrophages could reasonably act directly on the vasculature to induce changes, or might act indirectly through actions on other immune cells, such as NK cells.

Structural changes to the lumen of vessels is referred to as circumferential remodelling (Mulvany et al., 1996). Increases in blood flow or blood pressure can induce changes in lumen dimensions. Furthermore, vessel wall mass during remodelling can increase (hypertrophy), decrease (hypotrophy), or stay constant (eutrophy). This often occurs in conjunction with the narrowing or widening of vessels. Active remodelling of the vessel wall can alter lumen dimensions with no substantial change to wall thickness which, when sustained, can be associated with aneurysm formation (Gibbons and Dzau, 1994). Conversely, in cases where the wall thickness is increased, typically through deposition of smooth muscle, this can be associated with hypertension and increases in vascular reactivity (Mulvany, 1991).

Another determinant of vascular remodelling is changes in cellular reactivity. Primarily, this includes the secretory and contractile properties of smooth muscle cells supporting vessels. During homeostasis, a balance is maintained between vasoactive factors; pro- and anti-inflammatory mediators; and growth promoters and growth restrictors. Alterations to vasodilatory and vasoconstrictive factors, particularly NO and endothelin-1 (ET-1), respectively, can induce vascular remodelling.

NO can be secreted from endothelial cells, through eNOS-mediate synthesis, or from other cells – particularly macrophages – through iNOS-mediated synthesis. NO causes vasodilation through inducing relaxation of vascular smooth muscle cells. In pregnancy, NO contributes to the vascular integrity of the decidua and increases vasodilation (Moncada et al., 1991). Pregnant eNOS$^{-/-}$ mice had altered uterine vascular features specifically decreased lumen diameters of uterine, spiral, and radial arteries (Rennie et al., 2015), as well as decreased uteroplacental blood flow (Kulandavelu et al., 2012). Furthermore, pups born from these mice were growth restricted, yet there was no evidence of altered placental morphology. These studies show that eNOS$^{-/-}$ mice mimic human FGR through fetal hypoxia and changes in uteroplacental blood flow but no gross placental morphology changes (Kulandavelu et al., 2013).

ET-1 is a vasoconstrictive agent released by endothelial cells that acts to induce contraction of vascular smooth muscle cells. ET-1 acts as a balancing factor to NO where ET-1 can induce production of ROS and pro-inflammatory cytokines TNF, IL-1, and IL-6. Imbalances in ET-1 and NO are associated with hemodynamic disorders. There is evidence to suggest that macrophages can secrete ET-1 under

inflammatory conditions, in addition to having the capacity to produce NO (Wahl et al., 2005, McKenna et al., 2015). In women, ET-1 may provide a useful biomarker to determine the extent of endothelial dysfunction in pregnancy complications such as PE.

During adulthood, vessels rarely undergo remodelling except during disease, injury, or reproductive cycles. Vascular adaptations which occur in the uterus of women during the menstrual cycle and pregnancy are notable exceptions to disease or injury. Uterine arteries undergo vascular remodelling to prepare for and accommodate the oxygen and nutrient demands of fetal growth and development. The vascular remodelling observed in pregnancy has similarities to the vascularisation events in cancer (Mor et al., 2017). Both cancer and pregnancy require substantial nutrient delivery to either the tumour mass or the embryonic mass for growth. Improper vascular remodelling has been linked with pregnancy complications such as PE (Osol and Mandala, 2009b, Brennan et al., 2014).

1.7.2 VASCULAR REMODELING IN PREGNANCY

During pregnancy, the maternal vasculature must adapt to support fetal and placental development for up to 40 weeks in women and up to three weeks in mice. Vascular adaptations to pregnancy are significant, where uteroplacental blood flow increases dramatically compared to the non-pregnant state. In rodents, uteroplacental blood flow can increase 10 to 100-fold above the non-pregnant state (Bruce, 1976, Caton and Kalra, 1986, Dowell and Kauer, 1997).

In women, approximately 90% of uterine blood flow is directed to the placenta by term (Dowell and Kauer, 1997). In women, the main uterine artery doubles in size, with a 100% diameter increase occurring by 20 weeks gestation (Assali et al., 1960, Thaler et al., 1990, Palmer et al., 1992).

It is crucial to understand how maternal arteries adapt to the hemodynamic demands of pregnancy as under-perfused placentas and insufficient uteroplacental circulation have been linked with pregnancy pathologies including FGR and PE (Bewley et al., 1991, Bernstein et al., 1998). As healthy pregnancy is often met with a decrease or no change to blood pressure, uterine arteries are remodelled to achieve a decrease in uterine vascular resistance and an increase in the compliance and diameter of the arteries. This is achieved through synergistic mechanisms including enlargement of the entire uterine vascular tree and vasodilation (Osol and Mandala, 2009b, Brennan et al., 2014).

During early pregnancy, VEGF levels positively correlate with macrophage numbers in the maternal decidua (Wheeler et al., 2018b). At excessive concentrations, VEGF can promote an M1-like macrophage phenotype (Wheeler et al., 2018b). In this event, insufficient VEGF signalling at the fetal-maternal interface can induce elevated sFlt expression, suggesting a possible cause of vascular disorders of pregnancy (Andraweera et al., 2012). Furthermore, VEGF can recruit macrophages into the hypoxic

environment of the fetal-maternal interface where vascular changes are required to support nutrient delivery for growth and development of the conceptus (Wheeler et al., 2018b).

During early pregnancy in women, the uterus is relatively hypoxic until week 10 of gestation. After this time, oxygen tension increases, triggering trophoblast cell proliferation and invasion into maternal uterine spiral arteries to promote remodelling (Adamson et al., 2002). A failure to relieve this state of hypoxia compromises the trophoblast's ability to sufficiently invade maternal spiral arteries, decreasing their remodelling ability and leading to under-perfusion of the placenta and increased risk of vascular dysfunction and ensuing PE (Morton et al., 2017, Brennan et al., 2014).

In pregnancy, the entire uterine vascular tree expands to allow greater blood volume into the developing implantation sites to deliver nutrients, and remove wastes, to support fetal growth and development. Figure 1.2 shows the uterine vascular tree during murine mid-gestation and the relative abundance of immune cells in the different compartments of the uterus, particularly uNK cells and macrophages. The main uterine artery branches off from the aorta and runs parallel to the developing implantation sites. The remodelling of this artery occurs to a different extent at either the ovarian end or the cervical end of the artery (Osol and Mandala, 2009a). Uterine radial arteries branch off the main uterine artery and feed into the developing implantation sites. These radial arteries also undergo extensive vascular remodelling (James et al., 2018, Adamson et al., 2002).

These radial arteries branch into the uterus, more specifically into the mesometrial triangle. The vessels are present in the non-pregnant state and as pregnancy progresses, these vessels increase in diameter to facilitate increased blood volume directed towards the developing fetus. These mesometrial triangle vessels branch into the developing decidua and the vessels, now called decidual spiral arteries, become discernible from approximately day 8.5 pc in mice (Adamson et al., 2002). Importantly, the decidual spiral arteries remodel to a greater extent than do the mesometrial triangle arteries as these spiral arteries feed directly into the placenta and are a rate-limiting factor for fetal growth in both mice and women (Ball et al., 2006, Burton et al., 2009, Zenclussen et al., 2015).

1.7.3 MACROPHAGES AND SPIRAL ARTERY REMODELLING

In women, embryonic trophoblast cells invade the maternal spiral arteries for remodelling. This process increases uteroplacental blood flow to allow greater nutrient delivery to the developing conceptus. NO contributes to the vascular integrity of the decidua during pregnancy where it acts to relax smooth muscle cells to increase vasodilation and thereby assist remodelling (Moncada et al., 1991). This structural change in the uterus is accompanied by altered vascular function and more compliant blood vessels, allowing increased blood supply into the embryo implantation site and greater infiltration of leukocytes, including macrophages, as placental morphogenesis proceeds.

Spiral artery remodelling consists of two processes; first, loss of the musculo-elastic structure (thought to be immune cell-dependent); and second, endothelial cell layer breaks (thought to be trophoblast- and immune cell-dependent) (Harris, 2010). Murine spiral artery remodelling begins between days 8.5 and 10.5 pc (Ashkar et al., 2000). A recent study found evidence to suggest that there is cross-talk between trophoblast cells, spiral arteries, and decidual immune cells to mediate immune cell recruitment and spiral artery remodelling (Choudhury et al., 2017). Failure to adequately remodel spiral arteries has been associated with FGR, late miscarriage, and PE in women (Lyall et al., 2013, Ball et al., 2006). In women, uNK cells have been identified as critical mediators of spiral artery remodelling, whereby the uNK cells release ANGPT-1, ANGPT-2, VEGFC, IFNγ and MMPs to induce cell-cell contacts and cell-ECM interactions, leading to arteries that are better able to be penetrated by invading EVTs (Robson et al., 2012).

Macrophages and NK cells are thought to underpin spiral artery remodelling as they are intimately associated with the endothelial cells of decidual spiral arteries. These immune cells can facilitate spiral artery remodelling resulting in increased compliance, diameter, and permeability of the arteries (Lash et al., 2016). Previous findings have indicated a role for uNK cells in remodelling uterine vasculature through interactions with trophoblast and endothelial cells (Madeja et al., 2011). Results from Madeja et al. showed fewer numbers of uNK cells were recruited to the decidua when there was an absence of MHC disparity between the mother and fetus. This resulted in reduced vessel diameter in the decidual spiral arteries on day 8.5 pc which was correlated with decreased placental efficiency. Importantly, uNK cells can pave the way for trophoblasts to invade the maternal spiral arteries to facilitate intravascular remodelling. It is still unclear how macrophages facilitate spiral artery remodelling and whether there is a link between macrophages and uNK cells during this process.

1.8 PLACENTAL MORPHOGENESIS

Both humans and rodents share a common hemochorial placentation strategy, wherein pressure from maternal blood vessels in the intervillous space is kept low to not crush fetal capillaries required for nutrient delivery and waste removal within the placenta (Benirschke, 1983). This is achieved by significant resistance in upstream maternal arteries (Moll et al., 1975). In the murine placenta, three trophoblast layers separate the fetal and maternal circulations, whereas in women only one trophoblast cell layer separates the two circulatory systems (Soncin et al., 2015).

At the outset of murine pregnancy, the outermost trophoblast cells proliferate to form the trophoectoderm which encases the inner cell mass. The embryo develops from the inner cell mass and the trophoectoderm cells develop into the chorioallantoic placenta. The first major event preceding chorioallantoic placental formation is chorioallantoic fusion, where the extra-embryonic ectoderm expands to form the chorionic ectoderm which fuses with the allantoic mesoderm around day 8.5 pc (Rossant and Cross, 2001).

Following this, folds appear which mark where feto-placental blood vessels will develop to generate a placental blood vessel network. This vessel network is comprised of both fetal capillaries and maternal vessels which appear by day 10.0 pc in the labyrinth zone (LZ). The LZ directly faces the fetus and is where exchange of nutrients for metabolic waste products occurs. The trophoblast cells in concert with the fetal capillaries undergo villous branching to allow LZ development. This zone is highly vascularised and perturbations to the development of this zone can impair fetal growth (see Table 1.1).

In conjunction to the chorioallantoic placenta, the murine yolk sac placenta develops early in gestation and remains present until parturition (Burton et al., 2016). The yolk sac placenta is highly vascularised and encapsulates the developing conceptus from around day 6.0 pc where nutrients are absorbed through the visceral layer of the yolk sac placenta. Later in pregnancy, the overlying parietal layer (comprised of trophoblast cells) breaks down and so the visceral layer directly interacts with the uterine epithelium. Perturbations to the yolk sac in early gestation are thought to have profound effects on organogenesis, particularly affecting heart development and giving rise to defects that can manifest as cardiovascular conditions in later life (Burton et al., 2016). There has been minimal research into the yolk sac placenta and its interaction with immune cells. As immune cells can promote adequate vascular remodelling events in the decidua and the chorioallantoic placenta, it is rational to hypothesise that immune cells may play similar roles within the yolk sac placenta.

Once the murine placenta becomes a complete structure, maternal blood flows through the remodelled spiral arteries in the decidua and converges into one main maternal artery before feeding into the placenta (Adamson et al., 2002). Within this main artery, maternal blood passes through the junctional zone (JZ), which interfaces the decidua, and then through the LZ where it reaches the base of the placenta, the chorionic plate. As maternal blood flows through the LZ it contacts fetal capillaries, facilitating exchange between the maternal and fetal circulatory systems. After the maternal blood carrying nutrients and oxygen has reached the chorionic plate, this blood then flows through the LZ and JZ, then back to the maternal circulation. The blood travelling out of the placenta is now relatively hypoxic and contains fetal wastes which are processed by the maternal liver and kidneys for excretion. Maternal blood spaces in the LZ are lined by trophoblast cells and facilitate passive nutrient delivery to fetal circulation. The overlying JZ is comprised of both spongiotrophoblast and glycogen cells (GCs) (Coan et al., 2006, Coan et al., 2004b, Coan et al., 2005). The JZ plays a barrier role at the maternal-fetal interface as well as producing hormones, angiogenic factors, and tissue remodelling agents (Watson and Cross, 2005). This zone is also a rich source of trophoblast stem cells and hosts GCs which migrate into the decidua from around day 14.5 pc. After migrating to the decidua, GCs release their glycogen stores around spiral arteries for uptake and delivery to the LZ and then the fetus (Adamson et al., 2002). This process is maximal in the

last days of mouse gestation and provides a final energy source for a burst of fetal growth in the 48-72 h prior to delivery.

The architecture of the human placenta differs, such that the human placenta is described as being villous and the mouse placenta as labyrinthine. Human placentation involves the development of chorionic villi which encase the fetal vasculature. Maternal spiral artery endothelial cells are predominantly replaced by EVTs as placental morphogenesis proceeds. Similar to the mouse, the human placenta has a chorionic plate where the umbilical cord attaches. Placental villi extend from the chorionic plate to form a lobule which centres over a remodelled maternal spiral artery. Some villi are free-floating in the intervillous space whereas others are anchoring villi. Fetal capillaries are densely packed within the finest villi branches where they interact with the syncytiotrophoblast which is bathed in maternal blood during the second and third trimesters. Maternal blood enters the intervillous space from maternal spiral arteries, whereby exchange between it and fetal capillaries occurs overs a thin syncytiotrophoblast layer as little as 1-2 µm (Burton et al., 2016).

1.8.1 FETAL MACROPHAGES AND PLACENTAL VASCULARISATION

Within the placenta, a unique subset of macrophages exists, Hofbauer cells (HBCs). These macrophages are fetal-derived and are present from day 9.5 pc in the chorionic plate blood vessels in rodents, or at around 4 weeks post-conception in humans (Takahashi et al., 1989). During early gestation, HBCs may arise from mesenchymal stem cells or from monocyte progenitor cells from the yolk-sac (Kim et al., 2009, Seval et al., 2007). HBCs predominate the early placenta and are responsible for stromal fluid regulation, tissue remodelling, controlling the development of chorionic villi, and phagocytosing antigen-antibody complexes to maintain immune tolerance (Takahashi et al., 1991). These fetal macrophages are thought to be derived from fetal haemopoietic stem cells in later gestation (Kim et al., 2008). Whilst HBCs are distinct in origin, they contribute similar roles to decidual macrophages including placental angiogenesis and immune tolerance. They appear to be important for regulating immune tolerance as they are fetal-derived and express paternal antigens. HBCs can appear phenotypically similar to maternal M2-like macrophages (Böckle et al., 2008, Reyes et al., 2017).

HBC constitutively express CD209 and other markers such as CD163, IL-10, and TGF-β (Johnson and Chakraborty, 2012). At day 8.5 pc, the placenta becomes visible in murine models where the chorionic plate is highly vascularised and is populated with HBC on the subsequent day (Moffett and Loke, 2006). Furthermore, increasing evidence suggests that HBC may be involved in assisting placental vascularisation as these cells express high levels of VEGF (Demir et al., 2004). HBCs also express “Sprouty” proteins; regulators of branching morphogenesis and growth factor signalling, further suggesting a likely role in placental vascularisation during the branching stage of villous maturation in

women (Anteby et al., 2005, Seval et al., 2007). In addition, it is likely that HBC play key roles in trophoblast apoptotic body clean-up to limit placental inflammation (Tang et al., 2013). Irregular HBC numbers and phenotypes have been correlated to a range of pregnancy pathologies, with the underlying cause a result of poor placentation (Ilekis et al., 2016). The mechanisms of how HBCs promote vascular remodelling remain under-investigated. Furthermore, it needs to be clarified how maternal macrophages and fetal macrophages interact within the placenta to promote adequate fetal growth.

1.9 MACROPHAGES AND PREGNANCY PATHOLOGIES

Most instances of PE, FGR and related pregnancy pathologies become evident in later gestation, however mounting evidence suggests that these pathologies originate in, or are linked to, abnormalities in early placental development. It is therefore important to understand the early events of pregnancy establishment including decidualisation, trophoblast invasion, and maternal uterine artery vascular remodelling. These processes are crucial for establishing an appropriate environment for placentation that will optimise fetal growth. Importantly, macrophages are implicated as key regulators of these process due to their multi-functional roles in vascular remodelling, abundance, and functional plasticity. Furthermore, macrophages have been associated with pregnancy pathologies, wherein when their numbers are reduced, or their function is altered.

Vascular dysfunction and poor vascular adaptations to pregnancy are associated with pregnancy complications including PE and FGR which affect up to 2-8% of human pregnancies (Khong et al., 1986, Ball et al., 2006, Pijnenborg et al., 1991). These disorders can be associated with early pregnancy perturbations that result in shallow trophoblast invasion. Shallow trophoblast invasion into spiral arteries can reduce the amount of remodelling these arteries undergo and thus can decrease blood flow to the placenta (McMaster et al., 2004). The pathophysiology of PE and FGR is similar in that both disorders exhibit characteristic poor placentation and maternal endothelial dysfunction (Ness and Sibai, 2006, Kaufmann et al., 2003).

PE can be diagnosed when a pregnant woman has hypertension after the 20th week of gestation in conjunction with at least one other symptom including proteinuria, organ dysfunction, or uteroplacental dysfunction (Andraweera et al., 2020). A proposed mechanism behind preeclamptic symptoms is the over expression of sVEGFR1 (sFlt), an anti-angiogenic factor. This overexpression is induced by excessive HIF-1α. When sFlt is heightened, this indicates that the vasculature is under duress, and sFlt is thus considered a stress signal from the placenta. In PE, the dysfunctional placental can release other inflammatory mediators into maternal circulation which impacts systemic maternal vascular function resulting in endothelial dysfunction (Goulopoulou and Davidge, 2015). Maternal endothelial dysfunction can appear both during and post-gestation and may precede elevated risk for later cardiovascular disease in these women (Weissgerber et al., 2016, Andraweera et al., 2020). Currently, the only cure for PE is

delivery of the placenta. Without delivery of the placenta, PE can progress to eclampsia with greater symptoms including stroke.

During PE, a shift toward pro-inflammatory Th1 cells is observed with increased levels of pro-inflammatory cytokines (Saito and Sakai, 2003). Dysregulated inflammatory pathways, caused by increased pro-inflammatory cytokines, were found to be associated with PE and have been correlated with an increase in M1-like macrophages in women (Huda et al., 2017). Furthermore, in cases of FGR and PE, macrophages that secrete TNF have been associated with spiral arteries where they can induce excessive trophoblast apoptosis and prevent spiral artery remodelling required for placentation (Reister et al., 2001). Similarly, macrophage distribution within the decidua and spiral arteries in women with PE differs from women with healthy pregnancies (Reister et al., 1999).

Interestingly, in some cases of PE, normal spiral artery remodelling has occurred. For this reason it has been suggested that the specific sites of altered remodelling within the uteroplacental tree are under researched (Lyall et al., 2013). Another study reported that uterine radial arteries analysed from preeclamptic women were smaller in vessel lumen area with an increased wall thickness that indicates inward eutrophic remodelling, which may explain the increases in uterine vascular resistance associated with this condition (Ong et al., 2005). Ideally, use of three-dimensional uteroplacental vascular trees would predict changes across gestation (Rennie et al., 2016).

FGR occurs in around 5% of human pregnancies with growth restricted infants having a higher risk of mortality and morbidity. FGR also has longer term effects with delays in development and links to metabolic disorders in later life (Godfrey and Barker, 2000). Both maternal and fetal factors can predetermine the risk of FGR, however placental insufficiency appears to be a major cause (Hendrix and Berghella, 2008). Whilst the specific underlying causes of FGR remain unknown, it is becoming increasingly clear that faults in the immune response to pregnancy that affect vascular adaptation and placental development, may be a factor.

One potential mechanism of FGR is complement activation and dysregulated expression of angiogenic factors leading to poor placental development which results in FGR (Girardi et al., 2006). Blockade of complement activation in mice prevented increased sFlt-1 levels and rescued pregnancies which were complicated with fetal resorption and growth restriction (CBA/J X DBA/2, a model where fetal loss shares features similar to human miscarriage) (Girardi et al., 2006). Furthermore, *in vitro* stimulation with the complement cascade upon monocytes directly cause sFlt-1 release suggesting a link between sFlt-1 levels and complement activation potentially involving macrophages (Girardi et al., 2006). Therefore, perturbations to immune system activation and regulation may be factors in mediating optimal fetal growth.

Preterm birth is classed as delivery <37 weeks of gestation where it accounts for around 12% of births worldwide and is associated with significant perinatal mortality and morbidity (Liu et al., 2015). Around 70% of preterm birth is spontaneous due to premature rupture of fetal membranes (Goldenberg et al., 2008). M1-like macrophages are known to contribute to an inflammatory-like cascade to induce labour in women as part of normal pregnancy. However, premature polarisation towards M1-like macrophages has been implicated in spontaneous preterm birth (Hamilton et al., 2012, Mackler et al., 1999, Xu et al., 2016). Therefore, the functions of macrophages during late pregnancy also contribute to pregnancy's success.

1.10 ANIMAL MODELS INVESTIGATING MACROPHAGE FUNCTION

Animal models have been useful to study macrophage function (Murray and Wynn, 2011). Macrophages can be studied using a lineage-marked strain where green fluorescent protein (GFP) is expressed by the *Csf1r* promoter (MacGreen mice). This model allows GFP expression in the majority of the macrophage population (Ovchinnikov et al., 2010). Furthermore, the C-X3-C motif chemokine receptor 1 (CX3CR1) GFP mouse strain (CX3CR1-GFP) can allow *in vivo* tracking of macrophages. Here CX3CR1 is expressed on bone marrow derived macrophages (Jung et al., 2000).

The lox-Cre system for lineage-specific gene deletion has been revolutionary to studying cellular biology, particularly macrophages. Notably, the *LysM*-Cre mouse strain has been utilised to specifically delete genes from cells expressing *LysM*, mostly macrophages (Clausen et al., 1999). This system can be used to transiently deplete macrophage populations using DTR or using tamoxifen-inducible promoters. Other macrophage specific Cre strains include *Tie2*-Cre mice and *Csf1r*-Cre mice (Kisanuki et al., 2001). This gene-targeting approach in macrophages has been applied to an array of genes including VEGFA and HIF-1α (Liyanage et al., 2016, Colegio et al., 2014).

Furthermore, *op/op* mice possess a natural mutation in *Csf1* which results in a reduced number of macrophages in many peripheral tissues including the uterus (Mikkelsen and Thuneberg, 1999, Pollard et al., 1991). Previous studies have found that *op/op* mice have poor recruitment of uterine macrophages and poor mammary gland development (Wood et al., 1997, Pollard and Hennighausen, 1994).

In the CD11b-DTR mouse strain, simian DTR and GFP is expressed under the control of the CD11b promoter (Duffield et al., 2005). Treatment of these mice with diphtheria toxin (DT) renders the $CD11b^+$ cells transiently depleted. The simian DTR binds to DT with high affinity, whereas the murine DTR binds with little or no affinity. Thus, administration of DT to wild type mice results in no adverse effects.

Macrophages can also be depleted by administration of clodronate liposomes (van Rooijen and van Nieuwmegen, 1984). Macrophages phagocytose these liposomes and accumulation of clodronate causes apoptosis. This method depletes phagocytic cells (~75% of macrophages) after 24 h but $CD11c^+$ cell populations are unaffected. This model is ineffective for studying uterine macrophages as liposomes

delivered intravenously or the uterine or peritoneal cavity do not cross into the uterus, therefore uterine macrophages are not depleted.

1.11 SIGNIFICANCE, HYPOTHESES, AND AIMS

Macrophages have been proposed to play roles in a range of reproductive processes relevant to early pregnancy including trophoblast invasion, immune tolerance, decidualisation, and placental development (Zhang et al., 2016, Mori et al., 2016). However, their specific functions and physiological importance in these processes is not fully defined. Furthermore, the mechanisms of uterine vascular remodelling during pregnancy and the contributions of immune cell types other than uNK cells are yet to be confirmed.

Vascular remodelling in early pregnancy is required for fetal and placental growth. This indicates that a rate-limiting factor in pregnancy success is maternal vascular adaptation. During pregnancy, macrophages represent a large proportion of immune cells in the uterus and they appear to localise near to the uterine vasculature. Macrophages have been shown to regulate and induce angiogenesis in specific settings such as cancer. However, the role of macrophages in promoting similarly extensive vascular remodelling during pregnancy has been under-researched. This highlights the need to address the functions of macrophages in promoting vascular remodelling during pregnancy.

In women, perturbed macrophage numbers and phenotypes have been associated with pregnancy complications such as implantation failure, PE, chronic placental inflammation, and recurrent miscarriage (Faas et al., 2014, Khong and Brosens, 2011, Guenther et al., 2012, Kim et al., 2015, Pijnenborg et al., 1991). In cohorts of women, macrophages are present in diverse proportions and numbers, but women with reduced numbers of macrophages or higher proportions of M1-like macrophages may be more prone to pregnancy complications (Brown et al., 2014, Faas et al., 2014). The literature on macrophages and pregnancy disorders contain differing interpretations – for example, one study has found higher numbers of macrophages in women with PE. This was associated with increased macrophage-induced apoptosis of EVTs, thereby limiting their invasion into spiral arteries (Reister et al., 2001). Conversely, another study showed decreased macrophage numbers in the event of PE (Williams et al., 2009). These conflicting notions highlight the need for understanding how macrophages support uterine vascular remodelling and development of placental vasculature during pregnancy. In addition, the interaction of macrophages with other immune cells, specifically Treg cells and uNK cells, and the significance of these interactions for regulating vascular remodelling during pregnancy, is yet to be investigated (Figure 1.1).

HYPOTHESES

- Macrophages play essential roles during the peri-implantation phase of pregnancy
- Macrophages regulate uterine vascular remodelling required for placental development

AIMS

- To define the effect of acute macrophage depletion during the peri-implantation phase on pregnancy success
- To investigate how macrophages promote immune tolerance during early placental development
- To examine the tissue remodelling properties of macrophages and the contribution of macrophage regulators in remodelling of uterine arteries to underpin placental development and fetal growth

Table 1.1: Vascular and placental disorders in murine models during pregnancy.

Perturbation	Phenotype	Reference
Csf2$^{-/-}$	Altered labyrinthine development – reduced maternal blood spaces and trophoblast surface area	(Robertson et al., 1999)
CD40-L overexpression	Decreased decidualisation, decreased trophoblast invasion, reduced spiral artery remodelling, and narrow labyrinthine capillaries	(Matsubara et al., 2016)
C5ar$^{-/-}$ with Malaria infection	Increased placental vascular development	(Conroy et al., 2013)
C1q$^{-/-}$	Decreased spiral artery remodelling, increased sFlt production, FGR, and poor labyrinth vascularisation	(Singh et al., 2011, Agostinis et al., 2010)
Plgf$^{-/-}$	Embryonic lethal after day 9.5, defective branching morphogenesis, and reduced trophoblast invasion	(Perez-Garcia et al., 2018)
LIFRα antagonist	Decreased trophoblast invasion, decreased spiral artery remodelling, decreased pregnancy viability, and decreased labyrinthine zone area	(Winship et al., 2015a)
Rn$^{-/-}$	FGR, reduced uteroplacental perfusion, and uterine artery dysfunction	(Parry et al., 2009, Marshall et al., 2018)
eNOS$^{-/-}$	Decreased uterine artery diameter, decreased uteroplacental blood flow, and FGR	(Rennie et al., 2015), (Kulandavelu et al., 2012)

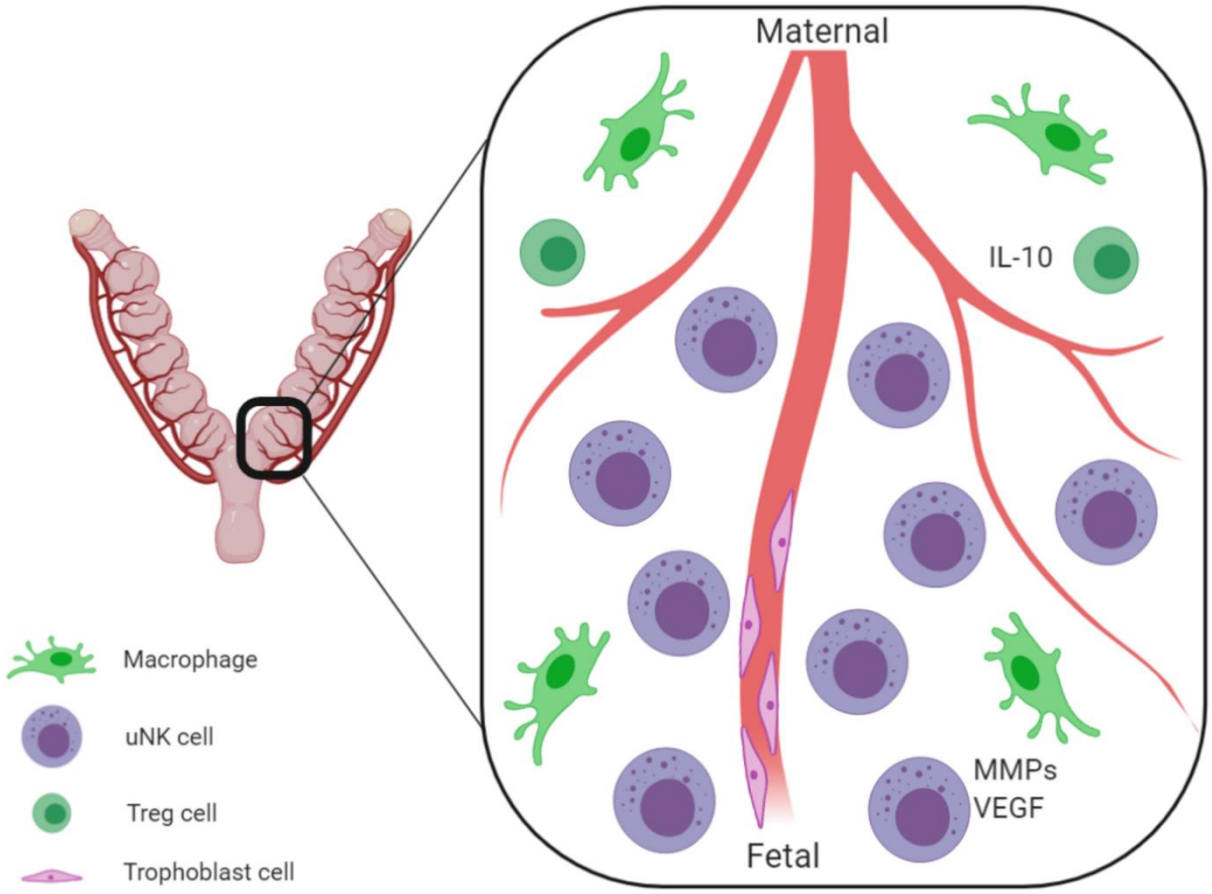

Figure 1.1: Schematic illustrating current understanding of the role of immune cells in uterine vascular adaptations to pregnancy.

Murine pregnancy requires the remodelling of the vasculature within the implantation sites to facilitate placental and fetal growth. This process occurs from the peri-implantation phase up until mid to late gestation. Importantly, uterine arteries must branch into the developing implantation sites and be remodelled to allow nutrient delivery to the embryo. These arteries are remodelled by extravillous trophoblast cells (EVTs), internal to the vessel, and immune cells, external to the vessel. Main drivers of this remodelling include uNK cells, and decidual macrophages are also implicated. Treg cells may also contribute through maintaining macrophages and uNK cells in appropriate phenotype states to facilitate remodelling. The cellular interactions controlling this process are mediated by soluble factors including matrix metalloproteinases (MMPs), vascular endothelial growth factor (VEGF) and interleukin 10 (IL-10).

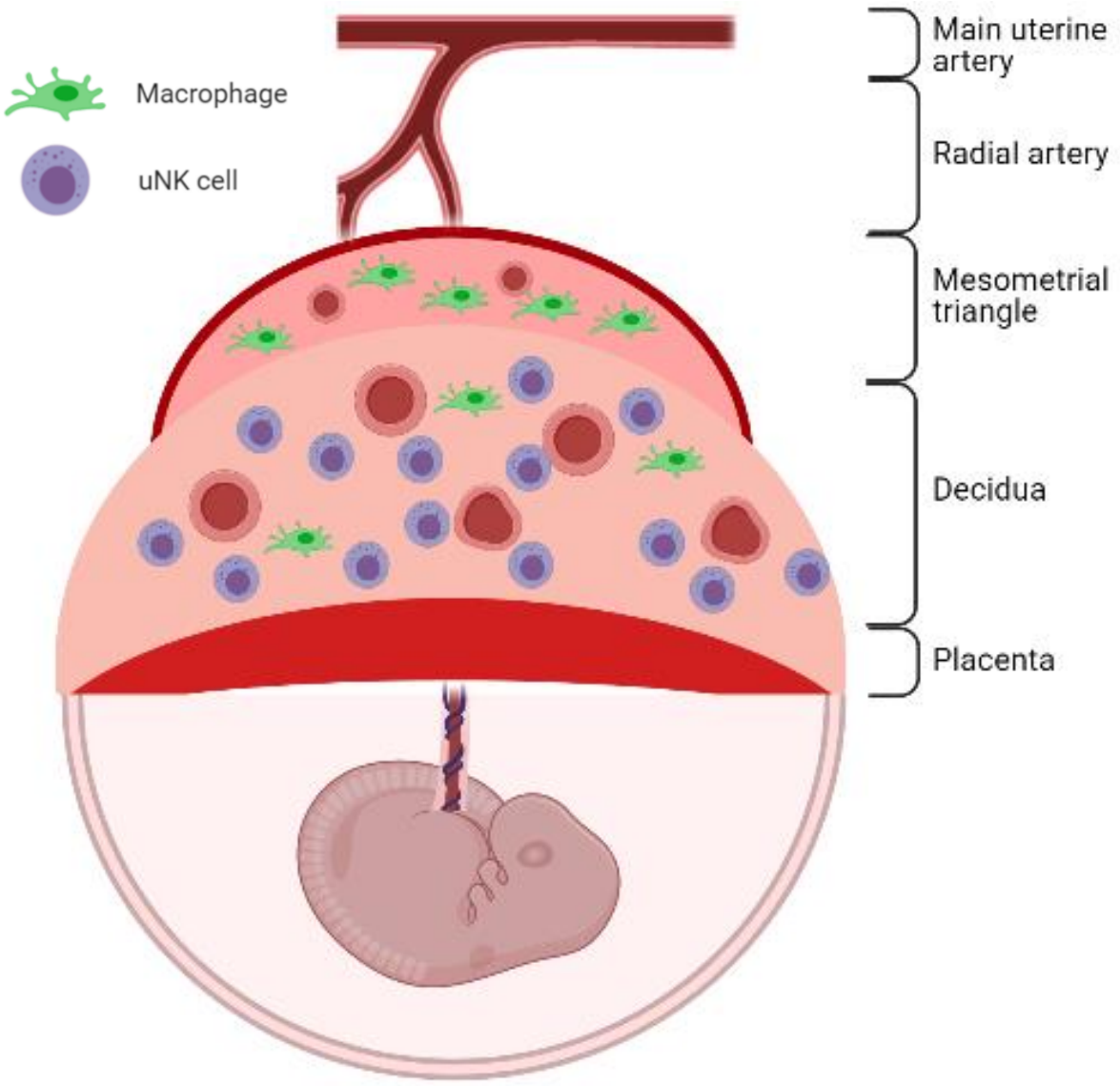

Figure 1.2: Schematic illustrating the immune cell distribution in various compartments of a mid-gestation mouse implantation site.

The uterine vascular tree undergoes remodelling during pregnancy to increase the volume of blood delivered to the developing fetus for growth and development. Main uterine arteries and radial arteries increase in size to allow an increase in blood velocity without turbulent blood flow. The radial arteries branch into the mesometrial triangle of the implantation site. This compartment of the implantation site has a high density of macrophages. These arteries will then further branch into the decidua to form decidual spiral arteries which remodel to a greater extent. The remodelling of these arteries is facilitated by uNK cells, macrophages, and trophoblast cells. These arteries facilitate adequate development of the placenta to support fetal growth.

CHAPTER 2

MATERIALS AND METHODS

2.1 MICE

All mice were housed and bred under specific pathogen-free conditions at the University of Adelaide Medical School Animal House on a 12 h light/12 h dark cycle and were given 10% fat food (Teklad Diets, Envigo, Madison, WI, USA) and water *ad libitum*. Mice were cared for and used in experiments as detailed in the NHMRC Australian Code of Practice for the Care and Use of Animals for Scientific Purposes with ethics approval from the Animal Ethics Committee, University of Adelaide (ethics identifiers: m-2017-029; m-2019-026; m-2019-041; m-2020-008). Genetically Modified Organisms Dealing Authorisation was obtained from the Institutional Biosafety Committee, University of Adelaide (identifiers: 12375 and 15600). Virgin female mice were aged between 8-12 weeks of age upon use in any experiment. Proven-fertile stud males were used for mating from 10 weeks of age until no more than 12 months of age.

FVB-Tg(ITGAM-DTR/EGFP)34Lan, herein referred to as CD11b-DTR, mice express the simian diphtheria toxin receptor (DTR) fused to a green fluorescent protein (GFP) under the control of the CD11b promoter (Duffield et al., 2005). CD11b-DTR mice are on the FVB/NJ background strain. Administration of diphtheria toxin (DT) to CD11b-DTR mice causes ablation of CD11b-expressing cells while administration of DT to wild type (FVB/NJ) control mice has no effect. The murine DTR binds DT with low affinity whereas the simian DTR, expressed in the CD11b-DTR mice, binds DT with high affinity. Wild type DT-treated FVB/NJ are referred to as wild type (WT) controls throughout. Pregnancy outcomes between WT mice with or without DT and CD11b-DTR mice without DT are presented in Appendices 9.30 and 9.31.

C1qa$^{-/-}$, C1Q-deficient, mice are on the C57Bl/6J background and were used to assess *C1qa* deficiency on maternal vascular remodelling during pregnancy. These mice were provided by Associate Professor Wendy Ingman (Robinson Research Institute, University of Adelaide). C57Bl/6J females were used as control mice for these experiments, referred to as *C1qa*$^{+/+}$, C1Q-replete, in figures and text.

2.1.1 GENOTYPING

2.1.1.1 DNA EXTRACTION

Ear notches were acquired from CD11b-DTR and WT mice to confirm the genotype. To extract DNA from these tissues, a salting out method of DNA extraction was utilised whereby tissues were placed in digestion buffer (350 µM Proteinase K (Sigma-Aldrich, St. Louis, USA), 20 mM EDTA (Sigma-Aldrich), 50 mM Tris (Sigma-Aldrich), 120 mM NaCl (Chem-Supply, SA, Australia), and 1% [w/v] SDS (Sigma-Aldrich), pH 8.0) on a shaking incubator at 37^{o}C overnight or were placed on a 55^{o}C heat block for 4 h with regular vortexing. After incubation, 4 M ammonium acetate (pH 7.5; Chem-Supply) was added to the samples (1:1) and the samples were vortexed prior to shaking for 15 min. Samples were then left at room temperature for 10 min prior to centrifugation at 16 100 x g for 10 min. The clear supernatant (1 part) was taken off and added to 100% ethanol (2 parts, Chem-Supply) prior to being vortexed and centrifuged for 8 min at 16 100 x g. Again, the supernatant was carefully removed and discarded before 70% ethanol

was added to wash the pellet. The supernatant was again removed and discarded. The samples were left on a heat block (37^{o}C) to dry. Once the pellet was dry, the DNA was resuspended in MilliQ water and kept at 4^{o}C for up to 2 weeks before transfer to -20^{o}C for long term storage.

2.1.1.2 PCR PRIMERS, CONDITIONS, AND GEL ELECTROPHORESIS

Extracted DNA samples were used to test the presence of an internal positive control (present in both WT mice and CD11b-DTR mice) as well as the transgenic GFP (present only in CD11b-DTR mice). A standard PCR was run to confirm the presence of the GFP gene as detailed by the Jackson Laboratory (Maine, USA). All PCRs were run on the GeneAmp® PCR System 9700 (Applied Biosystems, subsidiary of Thermo Fisher Scientific, Wilmington, DE, USA).

A master mix was prepared for the PCR reactions containing forward and reverse primers for both the positive internal control (forward: 5'-CTAGGCCACAGAATTGAAAGATCT-3' and reverse: 5'-GTAGGTGGAAATTCTAGCATCATCC-3') and GFP (forward: 5'-AAGTTCATCTGCACCACCG-3' and reverse: 5'-TCCTTGAAGAAGATGGTGCG-3') at a final concentration of 0.5 µM (GeneWorks Pty Ltd, Thebarton, SA, Australia). The Kapa 2G HS PCR kit was utilised for the master mix where in $MgCl_2$ (2.6 mM), polymerase reaction buffer (1.3 X) and *Taq* polymerase (0.03 U/µl) were added (Kapa Biosystems, subsidiary of Sigma-Aldrich). dNTPs (Sigma-Aldrich) were added to a final concentration of 0.26 mM, and then glycerol (Sigma-Aldrich) was added at 6.5%, before the master mix was made up with MilliQ water. For each PCR reaction, 10 µl of master mix was added to 2 µl of template DNA. The PCR was carried out with an initial denaturation step at 94^{o}C for 2 min, 10 amplification cycles of 94^{o}C (20 s), 65^{o}C (15 s; with a 0.5^{o}C decrease in temperature per cycle) and 68^{o}C (10 s), followed by a further 28 amplification cycles at 94^{o}C (15 s), 60^{o}C (15 s) and 72^{o}C (10 s), concluding with an elongation step at 72^{o}C for 2 min. Products were stored at 4^{o}C for up to two weeks until gel electrophoresis.

The positive control PCR product was 324 base pairs (bp) and the transgene was 173 bp. The PCR products were separated on a 1.5% (w/v) agarose gel (Promega, WI, USA) made up in 1 x TBE buffer (45 mM Tris base (Sigma-Aldrich), 45 mM Boric acid (Chem-Supply), 1 mM EDTA (Sigma-Aldrich, pH 8.2) with 1 X GelRed™ nucleic acid gel stain (Biotium, CA, America). Prior to loading, samples were mixed with 1 X DNA Gel Loading Buffer (Sigma-Aldrich) and then were applied to the set agarose gel with a pUC19/HpaII molecular weight marker (GeneWorks Pty Ltd) to determine product sizes. The gel was run in 1 X TBE buffer at 90 V for 40 min to separate the products. To localise bands, the gel was placed under a UV light using the GelDoc™ EZ Imager (BioRad Laboratories Inc., Hercules, CA, USA) and images were taken for analysis (Figure 2.1 shows an example of gel image with both WT and CD11b-DTR samples).

This protocol did not allow for distinction between homozygote or heterozygote individuals. To infer zygosity of these mice, ear notch samples were sent to Transnetyx® (Cordova, TN, USA) whereby real-time PCR was performed using a GFP probe. From the relative copy number of GFP, individuals were classified as either homozygotes or heterozygotes based on copy number.

2.2 GENERAL PROCEDURES

Surgical instruments were autoclaved before use and sterilised using 70% ethanol. For terminal anaesthesia, mice received an intraperitoneal (i.p.) injection of 15 µl/g body weight of 2% Avertin (tribromoethanol; Sigma-Aldrich). For surgery with recovery, mice were anaesthetised with 2.5% isoflurane (ISOTHESIA®, Henry Schein®, New York, USA) and received carprofen (Rimadyl; Pfizer, New York, USA) at 0.05 mg/1 g of body weight subcutaneous (s.c.) as analgesia pre-surgery. Surgical wounds were closed with 9 mm stainless steel wound clips (BD Autoclip Wound Closing System, Thermo Fisher Scientific) and remained on the mice until euthanasia. Following anaesthesia, mice were placed on a 37^{o}C heat-pad for recovery.

2.2.1 MACROPHAGE DEPLETION

Transgenic CD11b-DTR mice received DT from *Corynebacterium diphtheria* (Sigma-Aldrich) to elicit CD11b^{+} cell depletion. Various doses of DT were utilised including 5 ng/g (MD^{5}), 10 ng/g (MD^{10}) or 25 ng/g (MD^{25}) bodyweight to achieve varying degrees of macrophage depletion (MD). DT was diluted with sterile phosphate buffered saline (PBS, Thermo Fisher Scientific) to achieve the desired concentration. The dose was given as an i.p. injection between 0800 h – 1000 h on day 5.5 post coitum (pc). DT was made up fresh each day from 1 mg/mL aliquots and the remainder was discarded.

2.2.2 ESTROUS CYCLE TRACKING

Estrous cycles in mice were tracked daily using a cytological vaginal smearing technique for timed mating experiments. Vaginal smears were conducted between 0800 h – 1100 h daily. A small volume of 1 x PBS was flushed into the vagina using a pipette tip and the recovered fluid was expelled onto a microscope slide, with a coverslip, to be viewed as a wet, unstained sample. Stages in the estrous cycle were distinguished as described in previous work (Byers et al., 2012). Briefly, pro-estrus was defined by the presence of rounded epithelial cells and the occasional leukocyte if in early pro-estrus. Estrus was identified by the presence of many cornified epithelial cells. Once these cornified cells began to clump in large numbers, the stage in the cycle was defined as Metestrus-1. Metestrus-2 was specified by large quantities of leukocytes and diestrus was identified when minimal leukocytes and other cells were present. Females in pro-estrus were added to cages of stud males for mating.

2.2.3 MATINGS

Females were housed with fertile stud BALB/c males for allogeneic matings and WT or CD11b-DTR males for syngeneic matings. Females were housed overnight at a maximum of 2:1 ratio with studs and examined the following morning before 1000 h for the presence of a vaginal copulatory plug, a sign of positive mating, which was assumed to occur between 2300 h and 0100 h on the previous night. The presence of a plug signified day 0.5 pc of pregnancy. Before 1200 h was regarded as 0.5 pc of the respective day in pregnancy, and after 1200 h was regarded as 1.0 pc of the respective day in pregnancy.

2.2.4 IDENTIFICATION OF IMPLANTATION SITES

Implantation sites were visible to the naked eye from day 6.5 pc. Resorption sites were defined as haemorrhagic or necrotic masses in the uterus in later pregnancy, whereas at days 7.5 and 9.5 pc resorption was apparent as discolouration at the implantation site. Embryos which failed to develop early in pregnancy appeared as red bands on the uterus on days 9.5 pc, 12.5 pc, and 17.5 pc and were classified as uterine scars. Resorbing fetuses were defined as haemorrhagic, small necrotic areas of the uterus on days 12.5 pc and 17.5 pc. Non-viable fetuses on days 12.5 pc and 17.5 pc were very small and appeared hypoxic (white heads and limbs).

2.2.5 ASSESSMENT OF PREGNANCY OUTCOMES

Pregnant mice were humanely killed by cervical dislocation before 1200 h unless terminal anaesthesia was required for blood collection. In this case, mice were first administered Avertin as in section 2.2. The uterus from each female was excised, and the number of viable, non-viable, and resorbing implantation sites were counted along with uterine scars. A pregnant mother was defined as having viable fetuses on days 12.5 pc and 17.5 pc and as having viable implantation sites on days 6.5 pc, 7.5 pc, and 9.5 pc. On day 17.5 pc, each fetus and placenta were weighed after dissection from the uterus, amniotic sac, and umbilical cord. Two to four placentas from each dam, with a placenta from each horn where possible, were cut along the mid-sagittal plane and collected into individual tissue cassettes and immersed in 10% neutral buffered formalin in PBS. This enabled placental processing to be performed at the mid-sagittal point and for each placenta to be matched to the individual fetus.

2.2.6 ASSESSMENT OF POST-NATAL OUTCOMES

To assess post-natal outcomes, females were monitored every 12 h from day 18.0 pc for signs of labour or pups in the cage bedding. After delivery, pup weights and survival on post-natal days one, eight and twenty-one and the dam's viable litter size were recorded. Dams failing to give birth prior to day 21.0 pc were euthanised and assessed for signs of pregnancy.

2.2.7 COLLECTION OF MATERNAL ARTERIES

Maternal uterine and radial arteries were collected from mice. To maintain artery structure and integrity, mice were humanely killed, and dental floss was utilised to tie-off the maternal uterine artery at both ovarian ends, distal to the ovaries, and the cervical end. The uterus was then carefully dissected ensuring the arteries were still blood-filled to maintain structure. Both uterine horns were fixed in formalin as in section 2.2.5 and then dissected before processing for further histochemical analysis (see section 2.5.5).

2.2.8 DISSECTION OF ARTERIES

Post-fixation (see section 2.5.1.2), maternal uterine and radial arteries were dissected into approximately 1 cm pieces for processing and embedding. To achieve this, the post-fixation uterus was pinned to elongate the vessels. Using spring loaded scissors and fine forceps, the maternal uterine artery was dissected in two places, firstly at the ovarian end, distal to the floss, and secondly at the cervical end. Radial arteries were then dissected. Each artery segment was placed into individual tissue cassettes for further processing. To keep measures consistent, arteries were dissected from uterine horns with roughly the same number of implantation sites across all groups (approximately five – seven sites).

2.2.9 SERUM COLLECTION

Approximately 1 mL of blood was collected by cardiac puncture from terminally anaesthetised mice using a 20G needle (Becton Dickinson, New Jersey, USA). Blood was left at room temperature for at least 30 min before being centrifuged at 1 500 x g for 10 min to recover serum. Serum samples were stored at -80^{o}C for later analysis.

2.2.10 OVARIECTOMIES

Female mice underwent ovariectomy under sterile conditions on day 5.5 pc before progesterone (P4) pellet insertion and DT treatment. Mice were anaesthetised using 2.5% isoflurane and pure oxygen inhalation while in a ventral recumbent position. Mice were swabbed with 70% ethanol at the dorsal mid-lumbar region before a single surgical incision of 0.5 to 1 cm was made on the dorsal midline. This incision was at the caudal edge of the ribcage and once made blunt forceps were utilised to separate the skin from the underlying muscle wall. Upon separating the skin from the underlying muscle wall, the muscle wall was pinched on one side in the approximate location of the fat pad where the ovary is located. A 0.5 to 1 cm retroperitoneal incision was made on the erector spinae muscle below the last rib. The muscle layer was held open with sterile forceps, whilst another pair of forceps was used to gently withdraw the fat pad and the ovary. A cauterising device (Bovie Medical, Clearwater, FL, USA) was utilised to excise the ovary to prevent excess haemorrhage. The caudal portion of the uterus was replaced into the abdominal cavity, then the entire process was repeated on the contralateral side of the mouse to excise both ovaries. The open skin wound was then closed with a surgical wound clip.

2.2.11 PROGESTERONE (P4) PELLETS

P4 (Sigma-Aldrich) pellets were made in laboratory SILASTIC tubing (Dow Corning Corp, Midland, MI, USA – approximately 1.4 cm in length). One end was filled with multi-purpose sealant (Dow Corning Corp) and allowed to dry overnight. The following day the pellets were filled with a P4-sesame oil (Sigma-Aldrich) suspension (~400 mg/mL) before the other end was filled with sealant and left to dry overnight. Pellets were placed in sterile 1 x PBS and then placed on a 37^{o}C heat plate for at least 24 h before surgery. Mice were anaesthetised and an incision was made as in section 2.2.10. Two P4 pellets per mouse were inserted s.c. and the surgical wound was closed with a surgical wound clip. Pellets were inserted on day 5.5 pc before DT treatment.

For experiments performed in chapters five and six, mice that were P4 supplemented were administered 0.2 mg/ml P4 on days 5.5 pc and 6.5 pc via s.c. injection. This protocol was performed to reduce the exogenous stress of surgery and to further replicate previous P4 supplementation protocols established in the laboratory.

2.2.12 ESTROGEN (E2) PELLETS

Estrogen (E2) pellets were made from SILASTIC tubing as in section 2.2.11. The tubing was filled with a 25 µg/mL 17β-estradiol (Sigma-Aldrich) solution dissolved in sesame oil. These pellets were suspended in sterile 1 x PBS from at least 24 h prior to use and placed on a 37^{o}C heat plate. Mice received E2 pellets on day 9.5 pc. Mice underwent surgical procedure for pellet insertion as in section 2.2.10 except the existing wound from the P4 pellet was reopened for pellet insertion by removing the surgical wound clip. One E2 pellet per mouse was inserted s.c. and the wound was closed with a surgical wound clip.

2.3 BONE MARROW-DERIVED MACROPHAGE CULTURE

2.3.1 L929 CONDITIONED MEDIA

The mouse fibroblast cells line L929 (ATCC® number: CCL-1™) was recovered from cryo-storage, resuspended in Dulbecco's Modified Eagle Media (DMEM) supplemented with high glucose, GlutaMAX© (Gibco, Life Technologies, Carlsbad, CA, USA), and 10% fetal bovine serum (FBS, Gibco) and plated on T75 flasks (Corning®, VIC, Australia). Media was replaced every two to three days. Confluent L929 cells were detached from T75 flasks by adding ice-cold Accutase™ (Gibco) to the flask for 15 min at 37^{o}C. Accutase™ with the suspended cells was poured into a 50 mL Falcon tube and the T75 flask was rinsed with 1 x PBS. Collected cells were spun at 300 x g for 5 min and then passaged at 1:10. L929 cells were cultured in DMEM media (described above) at 37^{o}C (5% CO_2) for 7-10 days until media was exhausted (yellow appearance). The exhausted media containing macrophage colony stimulating factor (CSF-1) was separated from cells via centrifugation (300 x g, 5 min), filtered (0.22 µm), aliquoted and stored at -20^{o}C until required.

2.3.2 MACROPHAGE CULTURE AND DIFFERENTIATION

WT or C1Q-replete females were euthanised and hind legs were removed above the hip joint using sterile techniques. Hind legs were placed into sterile PBS on ice. Using sterile instruments and gauze, the fur and muscle was removed from the legs and the foot was removed before the femur and tibia were separated from one another. Each bone had both ends removed to expose the bone marrow and ice-cold PBS was flushed through the bone from both ends using a sterile 5 mL syringe and 26G needle. The cells were filtered (70 µm) into a 50 mL Falcon tube on ice. The harvested cells were centrifuged at 300 x g for 10 min at 4°C. Supernatant was removed and red blood cells lysis was performed as described in section 2.4.5. After centrifugation, cells were resuspended in 1 mL complete RPMI (cRPMI, 10% FBS, 100 U/mL penicillin and 100 mg/mL streptomycin, 1% GlutaMAX©, 1% non-essential amino acids and 20% L929 conditioned media) for cell counting (described in section 2.4.6). Sterile, non-tissue culture-coated 10 cm or 14 cm petri dishes were seeded with 5 x 10^6 or 1 x 10^7 bone marrow cells supplemented with 10 mL or 20 mL cRPMI, respectively.

On the next day, 5 mL or 15 mL of cRPMI was added to the dishes, respectively. By day four, most cells were adherent and so 5 mL or 15 mL of media was removed with 5 mL or 15 mL fresh media added. Due to the presence of non-adherent cells, the removed media was centrifuged at 300 x g for 5 min and plated onto fresh 10 cm petri dishes where media was replaced every second day. On day six, cells had differentiated into macrophages which was confirmed via flow cytometry staining using antibodies to detect macrophage surface markers F4/80 and CD11b (see section 2.4.7 and Appendix 9.34). Macrophages were detached from the petri dishes after repeated washing with ice-cold PBS. Adherent cells were treated with 10 mL Accutase™ for 10-20 min at 37°C. Petri dishes were then further rinsed in PBS and in some cases Accutase™ treatment was repeated. Removed media, Accutase™ suspension, and cells were centrifuged at 300 x g for 10 min at 4°C. Macrophages were then washed twice with serum-free RPMI and cell counts were performed as above. Approximately 5-10 x 10^6 cells were injected per mouse per time point, resuspended in 250 µl RPMI for intravenous (i.v.) injection. Control mice received 250 µl RPMI for i.v. injection. Over 80% of BMDM were positive for F4/80 and CD11b (Appendix 9.32).

2.4 FLOW CYTOMETRIC ANALYSIS OF MACROPHAGE POPULATIONS

Briefly, peritoneal exudate cells (PECs), uteri, and spleens were collected from pregnant mice on day 6.5 pc following cervical dislocation before 1200 h to assess macrophages after DT administration. This analysis was performed to confirm macrophage depletion. In a separate cohort, spleen, uteri, and paraaortic lymph nodes (LNs) were collected on day 7.5 pc to assess other immune cells in addition to macrophages.

2.4.1 PEC COLLECTION

A peritoneal lavage was performed with 5 mL of ice-cold PBS to obtain PECs. The collected cells were washed with complete RPMI media (cRPMI; RPMI + 10% FBS, Thermo Fisher Scientific), centrifuged (300 x g, 5 min, room temperature) and then kept on ice until further processing (see section 2.4.5).

2.4.2 UTERUS COLLECTION

Uteri were trimmed of excess fat and placed in PBS on ice. Each horn was slit lengthways and chopped into small pieces. Uterine pieces were added to an enzymatic digestion mix (cRPMI, 10 mg/mL collagenase from *Clostridum histolyticum* and 25 µg/mL DNase I, Thermo Fisher Scientific) and incubated for 1 h at 37^{o}C, with shaking at 125 rpm. Following incubation, 0.1 M EDTA (Sigma-Aldrich) was added to the samples, which were then returned to the shaking incubator for another 5 min. Following this incubation, samples were placed on ice and the contents were gently ground between the frosted ends of two microscope slides. The cells were then passed through a 70 µm filter where EDTA-FBS (10% 0.1 M EDTA, pH 7.22, 90% FBS) was underlaid and the samples were centrifuged (1000 x g, 7 min, room temperature). Supernatants were removed and the cell pellets were kept on ice until further processing (see section 2.4.5).

2.4.3 SPLEEN COLLECTION

Spleens were harvested into PBS and made into single cell suspensions by pushing the spleen through a 70 µm filter with the plunger end of a 5 mL syringe into a small petri dish containing cRPMI. Single cells were washed with extra cRPMI and centrifuged (300 x g, 5 min, room temperature). The resulting cell pellets were kept on ice until further processing (see section 2.4.5).

2.4.4 PARAAORTIC LYMPH NODE COLLECTION

Lymph nodes (LNs) were collected into PBS and were made into single cell suspensions by crushing the LNs between the frosted ends of two glass slides and passing through a 70 µm filter. Single cells were washed with cRPMI and centrifuged (300 x g, 5 min, room temperature). The resulting cell pellets were kept on ice until further processing (see section 2.4.5).

2.4.5 ERYTHROCYTE LYSIS

Pelleted cells were resuspended in 5 mL pre-warmed red blood cell (RBC) lysis buffer (0.155 M NH_4Cl, 10 mM $KHCO_3$, 99.2 µM EDTA, Sigma-Aldrich, made up in MilliQ water) and incubated for 5 min at 37^{o}C. Suspensions were then centrifuged as described above and resuspended for cell counting.

2.4.6 QUANTIFICATION OF CELL NUMBERS

Uterine and LN suspensions were resuspended to 2 mL and a 1:5 dilution was performed with 0.4% Trypan Blue (Sigma-Aldrich). PEC suspensions were resuspended to 2 mL and diluted to 1:2 with Trypan

Blue. Spleen suspensions were resuspended to 10 mL and a 1:10 dilution was performed. Total cell counts were then performed using a haemocytometer.

Total cell count = average count x dilution factor x 10^4 x volume of cell suspension

Once cell counts were performed, the volumes were adjusted to allow 1 x 10^6 cells/well.

2.4.7 LABELLING SUSPENSIONS

The resuspended cells were plated at 1 x 10^6 cells/well into 96-well U-bottom plates in replicates in 100 µl (where possible). To allow for discrimination between live and dead cells, 50 µl/well of V620 viability dye (BD Biosciences, San Jose, USA) diluted 1/1000 in PBS was added to each well, excluding control wells and incubated at room temperature for 15 min in the dark. Cells were then washed with PBS and centrifuged (400 x g, 2 min, room temperature). Fc receptors were blocked by resuspending all wells in 50 µl of FACS buffer containing 0.5 µg anti-Fc-γIIR antibody (FcBlock, BD Pharmingen, BD Biosciences) for 15 min at room temperature in the dark. Surface markers were labelled by adding 10 µl of an antibody master mix as described in Table 2.1 and 2.2. Single colour control and fluorescence-minus-one (FMO) control wells were included in each experiment. Plates were then incubated at 4°C for 25 min in the dark. For intracellular staining of FOXP3, cells were fixed and permeabilised according to the manufacturer's instructions (eBioscience). Briefly, cells were incubated for 1 h using a 1:4 dilution of concentrate into diluent from the FOXP3 kit. Cells were washed and the FOXP3 antibody was applied for 25 min in the dark at 4°C.

Cells were washed twice with PBS/0.04% sodium azide (Sigma-Aldrich) and centrifuged. Data were acquired using FACS Canto II (BD Biosciences) and FACS Diva Software (BD Biosciences). Data were analysed using FlowJo Software (version 10.1, Tree Star Inc.). Cells were initially gated on their forward scatter (FSC) and side scatter (SSC) properties, indicating size and complexity, respectively. Further gates were applied on FSC/SSC plots to exclude cell debris and doublets followed by live/dead cell discrimination before populations of interest were analysed.

2.5 HISTOLOGY

2.5.1 TISSUE COLLECTION, EMBEDDING, AND SECTIONING

2.5.1.1 FRESH-FROZEN TISSUE

Uteri were collected from pregnant females and trimmed of fat and connective tissue. Two consecutive implantation sites from one uterine horn were embedded in Tissue-Tek OCT compound (Sakura Finetek, Torrance, USA) and frozen in liquid nitrogen-cooled isopentane (Sigma-Aldrich) or dry ice and stored at -80°C. Prior to sectioning, samples were transferred to a -20°C freezer for at least 1 h to allow tissue to equilibrate to the cryostat temperature. Fresh-frozen tissue was sectioned on a Leica CM 1850 cryostat (Leica Microsystems, NSW, Australia) into 6 µm sections and fixed onto Colourfrost microscope slides

(Trajan, VIC, Australia). Slides were stored with desiccant at -80°C or at -20°C if staining was to occur within one month of sectioning.

2.5.1.2 PARAFFIN EMBEDDED TISSUE

Tissues were fixed in 10% neutral buffered formalin (Australian Biostain, VIC, Australia) for approximately 24 h followed by two 1 x PBS washes, each for 24 h, and stored in 70% ethanol until processing. Tissues were processed using a Leica TP1020 Tissue Processor (Leica Microsystems) using the following protocol; 30 min 75% ethanol, 30 min 80% ethanol, 30 min 85% ethanol, 30 min 90% ethanol, 30 min 95% ethanol, 30 min absolute ethanol, 2 x 30 min 100% xylene (Ajax Finechem, NSW, Australia); and 2 x 30 min paraffin wax (Ajax Finechem) for larger tissues, e.g. placentas. For smaller tissues, e.g. ovaries, the processing procedure was as follows 20 min 75% ethanol, 20 min 80% ethanol, 20 min 85% ethanol, 20 min 90% ethanol, 20 min 95% ethanol, 20 min absolute ethanol, 2 x 15 min 100% xylene, and 2 x 30 min paraffin wax. Tissue was then moulded into wax blocks with additional paraffin and stored at -20°C before sectioning on a Leica Rotary Microtome (Leica Microsystems, Wetzlar, Germany). Tissue sections (6 µm) were cut and floated onto Colourfrost slides (Trajan) using a 37°C water bath for histology and immunohistochemistry (IHC). Slides were placed inside a damp folded piece of filter paper and were pressed with a rubber roller to ensure sections were adhered to the slides. The slides were then dried in a slide drier at 50°C for 15 min before being stored at room temperature prior to staining.

2.5.2 HISTOCHEMISTRY PROTOCOL

2.5.2.1 FRESH-FROZEN TISSUE

2.5.2.1.1 HAEMATOXYLIN AND EOSIN (H&E) STAIN

Every 10th implantation site section was stained with H&E to assess the relative location of embryos within uterine sections. These H&E stained sections were utilised for vessel analysis (see section 2.5.5). Briefly, fresh-frozen tissue sections were removed from -80°C or -20°C storage and sections were then fixed in ice-cold 96% ethanol for 10 min at 4°C. Slides were washed in 1 x PBS (3 x 5 min) before being placed in Harris's haematoxylin (Sigma-Aldrich) for 2 min. Sections were washed under running tap water until the water ran clear before being placed in 1% hydrochloric acid (HCl, Chem-Supply) in MilliQ water for 5 s before another tap water rinse and immersion in 0.5% ammonia (Sigma-Aldrich) in MilliQ water for 5 s followed by a tap water rinse. Sections were placed in eosin (Sigma-Aldrich) for 30 s in the dark and then rinsed in tap water and dehydrated in ethanol (1 min in both 90% and 100% followed by 2 min in another 100%). Tissue sections were then cleared in Safsolv (Labchem, VIC, Australia) washes (3 x 5 min) prior to mounting with DPX mounting medium (BDH Industries, Poole, England) to attach coverslips (Trajan). Slides were dried for at least 24 h before removal of excess DPX in preparation for imaging.

2.5.2.1.2 ALKALINE PHOSPHATASE STAIN

Fresh-frozen sections were prepared for staining as above in section 2.5.2.1.1. After the first round of PBS washing, slides were immersed in a SigmaFast™ BCIP/NBT (5-bromo-4-chloro-3-indolyl phosphate/nitro blue tetrazolium; Sigma Aldrich) tablet made up in MilliQ water for 10 min. Sections were washed in PBS (3 x 5 min) and counterstained in eosin at 1:2 with 70% ethanol for 30 s. Tissues were dehydrated and coverslips applied as in section 2.5.2.1.1. The BCIP/NBT substrate is converted to an insoluble purple product by alkaline phosphatase activity.

2.5.2.2 PARAFFIN EMBEDDED TISSUE

2.5.2.2.1 MASSON'S TRICHROME STAIN

Tissue sections were dewaxed in Safsolv (Labchem), twice for 5 min each and were rehydrated through decreasing ethanol dilutions for 2 min each (2 x 100%, 1 x 90%, 1 x 70% and 1 x 50%) followed by 2 min in MilliQ water. Sections were incubated in Weigert's haematoxylin (Sigma-Aldrich) in the dark for 15 min before being washed in running tap water for 10 min. Sections were differentiated in 0.5 % HCl in 70% ethanol for 20 s and rinsed in MilliQ water for 10 s. To identify muscle, sections were stained in acid Ponceau 2R (Sigma-Aldrich) for 1 min before two washes in MilliQ water (10 s each). To differentiate between muscle and cell cytoplasm, tissue sections were differentiated in 1% phosphomolybdic acid (Sigma-Aldrich) for 30 s before rinsing in MilliQ water and staining with 1% methyl blue (Sigma-Aldrich) briefly to detect collagen. Two washes of 30 s each in 1% acetic acid (Ajax Finechem) were performed before dehydration in increasing ethanol concentrations and clearing in Safsolv as in section 2.5.2.1.1. Coverslips were mounted with DPX and slides were dried for at least 24 h.

2.5.2.2.2 HAEMATOXYLIN AND EOSIN (H&E) STAIN

Tissue sections were dewaxed and rehydrated in ethanol as described in section 2.5.2.2.1. Sections were then stained with H&E as in section 2.5.2.1.1. Sections were dehydrated in ethanol and Safsolv before being mounted with coverslips using DPX as in section 2.5.2.1.1.

2.5.3 IMMUNOHISTOCHEMISTRY (IHC) PROTOCOL

2.5.3.1 FRESH-FROZEN TISSUE

2.5.3.1.1 F4/80 STAINING

Sections were fixed in 96% ethanol as in section 2.5.2.1.1. Sections were washed in PBS (3 x 5 min) prior to blocking in 15% rabbit serum in 1% PBS-bovine serum albumin (BSA) for 30 min at room temperature. Sections were again washed in PBS (3 x 2 min) and primary antibody, rat anti-mouse F4/80 (Agilent), was applied at 1:400 diluted in 1.5% rabbit serum (Sigma-Aldrich) diluted in 1% PBS-BSA and incubated overnight (no more than 16h) at 4^{o}C in a humidified chamber. The following morning, sections were washed in PBS (3 x 5 min) and secondary antibody, rabbit anti-rat IgG (Agilent), was made up in 1.5%

rabbit serum diluted in 1% PBS-BSA at 1:500 and applied for 40 min at room temperature. Sections were washed in PBS (3 x 5 min) and Avidin-Biotin Complex (ABC) kit (Vector Laboratories, CA, USA) was applied for 30 min at room temperature. Following this, sections were washed in PBS (3 x 5 min) before 3,3'-diaminobenzidine (DAB; Dako North America, Carpinteria, CA, USA) chromogen was applied for 20 min at room temperature to generate an insoluble brown product at sites of peroxidase activity. Sections were washed in MilliQ water (2 x 5 min) each prior to counterstaining with haematoxylin (5 – 10 s). Sections were washed in running tap water until the water ran clear and then differentiated in 1% HCl and 0.5% ammonium water as in section 2.5.2.1.1. Sections were dehydrated and cleared as above prior to being mounted with DPX and coverslips. Negative and isotype-matched controls for each immunohistochemical stain are presented in Appendix 9.1.

2.5.3.1.2 DOLICHOS BIFLORUS AGGLUTININ (DBA) LECTIN STAINING

Sections were fixed in 96% ethanol as in section 2.5.2.1.1. Sections were then washed in PBS (3 x 5 min) prior to blocking in Carbo-Free™ Blocking Solution (Vector Laboratories) for 30 min at room temperature. Sections were washed in PBS (3 x 2 min) and primary antibody, biotinylated-dolichos biflorus agglutinin (DBA) lectin (Vector Laboratories), was applied at 1:500 diluted in PBS and incubated for 30 min at room temperature. Following this, sections were washed in PBS (3 x 5 min) and ABC kit (Vector Laboratories) was applied for 30 min at room temperature. Sections were washed in PBS (3 x 5 min) and DAB chromogen (Dako) was applied for 1 min at room temperature. Sections were washed in MilliQ water prior to counterstaining with haematoxylin (5 – 10 s). Sections were washed in running tap water until the water ran clear and then differentiated in 1% HCl and 0.5% ammonium water as in section 2.5.2.1.1. Sections were dehydrated and cleared as above prior to being mounted with DPX and coverslips.

2.5.3.2 PARAFFIN EMBEDDED TISSUE

2.5.3.2.1 PLACENTA DOUBLE LABELLING

Placenta sections were dewaxed and rehydrated as in section 2.5.2.2.1. Sections were then washed in PBS (3 x 5 min) and circled using a pap pen (Agilent, Santa Clara, CA, USA). Pronase (Thermo Fisher Scientific) in PBS (1:30) was used for antigen retrieval, in which sections were incubated for 15 min at 37^{o}C. Sections were rinsed in MilliQ water and washed in PBS (3 x 5 min), then treated with hydrogen peroxide as per the manufacturer's instructions using the Mouse-on-Mouse kit (Abcam, Melbourne, VIC, Australia) for 30 min to neutralise endogenous peroxidase activity. Sections were washed in PBS (3 x 5 min) and then Rodent Block from the Mouse-on-Mouse kit was applied for 30 min to block endogenous mouse IgG and Fc receptors. After slides were washed in PBS (3 x 5 min) the primary antibody, Vim3B4 anti-vimentin (Agilent), was diluted in 10% rabbit serum (Sigma-Aldrich) in 1% PBS-BSA (Sigma-Aldrich) to a 1:10 dilution. Primary antibody was incubated overnight in a humidified chamber at room temperature. Negative controls comprised diluent alone or irrelevant isotype-matched primary antibodies.

The following morning, slides were washed and Mouse-on-Mouse horseradish peroxide (HRP) Polymer (Abcam), used to amplify signal of primary antibody binding signal through HRP catalysis, was applied and incubated for 15 min in the dark. Sections were washed in PBS (3 x 5 min) and DAB with 2% ammonium nickel (II) sulphate (Sigma-Aldrich) was applied and incubated for three min before slides were washed in PBS (3 x 5 min). Rodent Block was applied for 30 min and sections were washed prior to application of the second primary antibody, anti-AE1/AE3 (pan) cytokeratin (Agilent), which was diluted in 10% rabbit serum in PBS with 1% BSA and left for 2.5 h at room temperature in a humidified chamber. Diluent was applied to the negative controls. Sections were washed in PBS (3 x 5 min) and Mouse-on-Mouse HRP polymer was added for 15 min before washing in PBS (3 x 5 min) and DAB applied for 10 min. Finally, sections were rinsed in MilliQ water before being counterstained with haematoxylin for 30 s and dehydrated as in section 2.5.2.1.1. Slides were mounted with DPX.

2.5.3.2.2 F4/80 STAINING

Sections were dewaxed and rehydrated as in 2.5.2.2.1. Sections were washed in PBS (3 x 5 min) prior to blocking in 3% H_2O_2 in PBS for 30 min at room temperature. Sections were washed in PBS (3 x 5 min) and then were then stained to detect F4/80 as in section 2.5.3.1.1.

2.5.3.2.3 DBA LECTIN STAINING

Sections were dewaxed and rehydrated as in section 2.5.2.2.1. Sections were then washed in PBS (3 x 5 min) prior to blocking in 3% H_2O_2 in PBS for 30 min at room temperature. Sections were again washed in PBS and then were stained for DBA lectin as in section 2.5.3.1.2.

2.5.3.2.4 ALPHA SMOOTH MUSCLE ACTIN (αSMA) STAINING

Sections were dewaxed and rehydrated as in section 2.5.2.2.1. Sections were then washed in PBS (3 x 5 min) prior to blocking in 3% H_2O_2 in PBS for 30 min at room temperature. Sections were washed in PBS (3 x 5 min) and were then blocked in 10% goat serum in 1% BSA in PBS for 1 h at room temperature. Sections were again washed in PBS (3 x 2 min) and primary antibody, rabbit anti-mouse αSMA (Merck, Millipore), was applied at 1:600 diluted in 2% goat serum (Sigma-Aldrich) diluted in 1% PBS-BSA and incubated for 30 min at room temperature in a humidified chamber. Sections were washed in PBS (3 x 5 min) and secondary antibody, goat anti-rabbit IgG (Agilent), was made up in 2% goat serum diluted in 1% PBS-BSA at 1:500 and applied for 30 min at room temperature. Following this, sections were washed in PBS (3 x 5 min) and ABC kit (Vector Laboratories) was applied for 30 min at room temperature. Sections were washed in PBS (3 x 5 min) and DAB chromogen (Dako) was applied for 10 min at room temperature. Sections were washed in MilliQ water prior to counterstaining with haematoxylin (5 – 10 s). Sections were washed in running tap water until the water ran clear and then differentiated in 1% HCl and 0.5% ammonium water as in section 2.5.2.1.1. Sections were dehydrated and cleared as above prior to being mounted with DPX and coverslips.

2.5.4 IMMUNOFLUORESCENCE PROTOCOL

2.5.4.1 FRESH-FROZEN TISSUE

Fresh-frozen tissue sections were fixed as described in 2.5.2.1.1. Slides were washed in 1 x PBS (3 x 5 min) and blocked with 15% rabbit serum in 1% BSA in PBS for 30 min. Primary antibodies included anti-mouse C1Q (1:100 dilution, Abcam), Alexa Fluor® 488 or 647 conjugated anti-mouse CD31 (1:100 dilution, Biolegend, San Diego, USA) and Alexa Fluor® 594 conjugated anti-mouse F4/80 (1:50 dilution, Biolegend). Unconjugated antibodies were diluted in 1.5% rabbit serum in 1% BSA in PBS and were incubated at 4^{o}C overnight in a humidified chamber. The following morning slides were washed in PBS (3 x 5 min) prior to secondary antibody treatment (rabbit anti-rat IgG Alexa Fluor® 488) for 1 h at room temperature. Following this, sections were washed in PBS (3 x 5 min) and directly conjugated antibodies were diluted in PBS with 1% BSA and 10% mouse serum (Sigma-Aldrich) and were incubated for 2 h in the dark at room temperature. Sections were washed in MilliQ water in the dark before the nucleic acid stain, DAPI (4',6-diamidino-2-phenylindole, 10 mM, Sigma-Aldrich), was applied for 20 min. Slides were washed in MilliQ water and cover slips were mounted using fluorescent mounting medium (Agilent). Slides were then stored at 4^{o}C in the dark until image capture within two weeks of staining.

2.5.5 IMAGE CAPTURE, CELL AND PLACENTAL MORPHOLOGY QUANTIFICATION

Slides were imaged using a Nanozoomer-XR Digital Slide Scanner (Hamamatsu Photonics, Hamamatsu, Japan) at a zoom equivalent to a 40X objective lens. Placental junctional zone (JZ) and labyrinth zone (LZ) areas were calculated via the manual tracing of these regions on the digital image generated by the Nanozoomer using NDP.view2 Viewing software (Hamamatsu Photonics). Glycogen cells (GCs) within the JZ of these placentae were detected and quantified based on their distinct appearance (Appendix 9.6). H&E-stained sections were observed for differences in general morphology of ovarian sections, particularly corpus luteum structure and integrity. All corpora lutea were assessed including those with disorganised/abnormal appearance. The proportion of haemorrhagic corpora lutea were calculated by dividing the number of disorganised/abnormal corpora lutea by the total number of corpora lutea in an H&E-stained ovarian cross-section and multiplying by 100.

Double-labelled IHC placentas were assessed for fetal and maternal capillary densities in the LZ using a 36 L-mertz grid (FIJI, Wayne Rasband, US National Institutes of Health) to count line intercepts of trophoblast cells and crosses were used to count fetal capillaries, maternal blood spaces or trophoblast cells. Ten grids per placental section were analysed. The total number of points was also recorded. To calculate the volume density of fetal capillaries, maternal blood spaces and trophoblast cells each component was divided by the total number of points per placenta. The corresponding volume of each component was then calculated by multiplying the volume density of each component with the placental weight for each placenta analysed. The surface volume of the placenta was calculated using the number

of line intercepts and the diameter of the semi-circles in the grid. The surface area of trophoblast cells in the LZ was calculated using the weight of the LZ (proportion labyrinth multiplied by the placental weight) multiplied by the surface volume. The barrier thickness of the trophoblast cells and the maternal blood spaces was calculated by dividing the volume density of the trophoblast cells or the maternal blood spaces with the surface volume. These methods have been well established in the literature (Roberts et al., 2001, Robertson et al., 1999, Zhang et al., 2015).

Immunofluorescence sections were imaged using an inverted optical microscope (Olympus, IX73, VIC, Australia) using the appropriate filters or using the FV3000 confocal microscope (Olympus) using the appropriate lasers. Two non-serial sections, at least 20 µm apart, per uterus were imaged across the groups with four to six mothers utilised. The mesometrial triangle was the focus point for analysis with four different images around the mesometrial triangle being captured at 40X per section. A total of eight images were analysed per mother per group. Captured images were merged for all the filters applied, i.e. DAPI, C1Q, F4/80 and CD31 images were combined to one image. This merged image was transferred to ImageJ where the merged imaged was red, green, and blue (RGB) split into four images representing DAPI, C1Q, F4/80 and CD31 but inverted to black and white. Using these split images, a colour threshold analysis was performed to identify positive cells. This threshold value was used to determine the density of stained cells. Using the DAPI density, the relative density of C1Q, F4/80 and CD31 positive cells per total DAPI positive cell density was determined. These relative densities across the eight images were averaged to give one relative density for each parameter per mother per treatment group.

For analysis of implantation site decidual vessels a morphometric approach was taken (Kieckbusch et al., 2014). Five vessels within the mesometrial triangle, or decidua, of these implantation sites were assessed at the section defined as the closest to the central plane in reference to embryo location. Vessel analysis was performed on the NDP.view2 software utilising the freehand region tracing and ruler functions. Parameters measured using the software included vessel lumen area and lumen circumference, total vessel area (including the lumen and wall) and total vessel circumference and absolute total vessel area (including the lumen, wall and associated pericytes). Using these measurements, calculation of vessel diameter and the vessel wall thickness was performed (Appendix 9.14). Conceptus area was measured by tracing the area of the trophoblast cells and embryo in the section closest to the central plane.

2.6 RNA ANALYSIS

2.6.1 SAMPLE COLLECTION

To assess gene changes due to macrophage depletion, uteri on day 7.5 pc were removed and trimmed of excess fat. An individual implantation site was dissected and using fine forceps the overlying myometrium was carefully separated from the inner decidua. These tissues were collected into separate

sterile Eppendorf tubes and snap-frozen in liquid nitrogen. Four implantation sites were dissected from each female (n=4/group) and stored at -80^{o}C until RNA extraction.

2.6.2 RNA EXTRACTION, QUANTIFICATION AND QUALITY

Samples were removed from -80^{o}C and transferred directly to ice and then to a homogenising tube with 600 µl of RLT extraction buffer from the Qiagen RNeasy® extraction kit (Qiagen, Hilden, Germany). The homogenising regime for both decidua and myometrium was 3500 rpm for 10 s at 4^{o}C using the PowerLyzer 24 Homogenizer (Mo Bio Laboratories, subsidiary of Qiagen). This was followed by centrifugation at maximum speed for 3 min at 4^{o}C. The RNA extraction protocol was performed with the Qiagen RNeasy® kit using the manufacturer's instructions. Briefly, after centrifugation the supernatant was removed and mixed with 70% ethanol (1:1). Up to 700 µl of this solution and any precipitate was transferred to a RNeasy® mini-spin column. The sample was centrifuged at 8 000 x g for 30 s. The flow through was discarded and RW1 buffer was added prior to centrifugation as before. Flow-through was discarded and the sample was washed with RPE buffer and centrifuged as before. Flow through was again discarded and sample was washed with RPE buffer for 2 min at 8 000 x g. The RNA column was placed into a new collection tube and the sample was centrifuged at maximum speed to dry the membrane. The collection tube was discarded, and the column was placed in a sterile 1.5 mL collection tube where 50 µl RNase free water was applied directly to the membrane and centrifuged at 8 000 x g for 1 min to pellet the RNA. The extracted RNA was kept on ice from this point.

The extracted RNA concentration and absorbance ratio was measured using the Nano-drop Spectrophotometer ND-1000 (Thermo Fisher Scientific). From here, 5 µg of extracted RNA was utilised for DNase treatment using the TURBO DNA-free (Life Technologies, CA, USA) treatment according to the manufacturer's instructions. Briefly, 5 µg of RNA was added to TURBO DNase master mix with 5 µl 1X TURBO DNase buffer and 2 µl TURBO DNase per sample. Sample volume was made to 50 µl using RNase free water and samples were incubated at 37^{o}C for 30 min. Then, 5 µl DNase Inactivation Reagent was added to each sample and mixed periodically throughout the 5 min incubation at room temperature. Samples were then centrifuged at 10 000 x g for 90 s and the clear supernatant was transferred to a new Eppendorf tube. At this stage, RNA concentration and absorbance were measured, then samples were aliquoted for quality checks, testing genomic DNA contamination and for reverse transcription.

RNA quality was assessed on the RNA Agilent Bioanalyser (Agilent) as per the manufacturer's instructions to test RNA integrity number (RIN). Typically, RIN values between 6.5 and 10 are considered acceptable RNA quality. Due to the resorbing nature of some implantation sites on day 7.5 pc, these samples had lower RIN values (minimum reading of 4). A pre-amplification step using the cDNA was performed to enhance complementary DNA (cDNA) quality (see section 2.6.3).

Genomic DNA contamination was assessed for each sample using genomic DNA primers (forward 3'-GGCACTGACTGAGGTCAAAC-5' and reverse 3'-GTCACAATCACAGAGACTTTGA-5'). Real-time quantitative PCR (qPCR) was run using SybR® green technology (Thermo Fisher Scientific) and a QuantStudio™ 3 system (Thermo Fisher Scientific). Briefly, 1 µl of each DNase treated RNA was added to individual wells of a 96-well plate. A SybR® master mix was made with genomic DNA primers and the volume was made up to 20 µl per well using MilliQ water. The plate was sealed and centrifuged at 1 000 rpm for 1 min prior to loading into the QuantStudio™ 3 (Thermo Fisher Scientific) using the following program: 50°C for 2 min, 95°C for 10 min and 40 cycles of 95°C for 15 s and 60°C for 1 min. Samples were confirmed as having no contaminating genomic DNA as there was no product amplification.

2.6.3 REVERSE TRANSCRIPTION AND PRE-AMPLIFICATION PROCEDURES

DNase treated RNA was utilised for reverse transcription where the template RNA (at a final concentration of 50 µg/mL) was added to SuperScript IV VILO master mix (Thermo Fisher Scientific) and the volume was brought to 20 µl using MilliQ water. Each sample was mixed gently and incubated in a thermal cycler at 25°C for 10 min, 50°C for 10 min and 85°C for 5 min. Samples were removed after incubation and were kept at -20°C for up to one week or at -80°C for long term storage.

Briefly, the pre-amplification step was performed on the reverse transcribed cDNA where each sample had to be pre-amplified using two primer pools, pool A and pool B. For each sample, each pool was amplified in separate Eppendorf tubes (two tubes per sample, one for pool A and one for pool B). For each sample and each primer pool, 10 µl of TaqMan® PreAmp Master Mix (Thermo Fisher Scientific) was added to 5 µl of cDNA and 5 µl of either pool A or pool B. The individual sample tubes were mixed and the samples were incubated in a thermal cycler using the following program; 95°C for 10 min, 12 cycles of 95°C for 15 s and 60°C for 4 min and finally 99°C for 10 min. Samples were removed and pool A and pool B products were stored individually at -20°C for later use. Importantly, the pre-amplification step was only required for cDNA samples being used for OpenArray®.

2.6.4 QUANTITATIVE PCR (qPCR)

Reverse transcribed cDNA without pre-amplification was used to perform qPCR. Primer sequences for the genes of interest are listed below in Table 2.6. Each primer set was designed, optimised, and tested for efficiency in-house. Briefly, the qPCR plate was set-up so that each reaction contained cDNA, 1 X Power SYBR® Green PCR Master Mix (Thermo Fisher Scientific), forward and reverse primer (at the desired concentration) and made up in RNase free water to 20 µl. No template control samples, where RNase free water was substituted for cDNA, were utilised for each experiment. qPCR was performed using a QuantStudio™ 3 (Thermo Fisher Scientific) under the following conditions: 50°C for 2 min, 95°C for 2 min and 40 cycles of 95°C for 1 s and 60°C for 30 s. Melt curve analysis was included to ensure no non-specific amplification. Data for these genes analysed is presented in Appendices 9.22 and 9.23.

2.6.4.1 qPCR USING OpenArray® PLATES

Once samples had been pre-amplified, pool A and pool B samples were thawed and mixed together where the final tube had one-part pool A and one-part pool B for each sample. This mixture was diluted 1:20 with MilliQ water. The diluted sample was mixed 1:1 with TaqMan® OpenArray® Master Mix (Thermo Fisher Scientific) and enough solution was prepared for 12 subarrays per each sample as per the manufacturer's instructions. Therefore, on one OpenArray® plate up to four samples were run. The OpenArray® plates utilised were "Mouse Inflammation Panel" (Thermo Fisher Scientific). The PCR reaction was aliquoted into a 384-well sample plate where one well of the 384-well plate was used to load one subarray, thus 12 wells were filled per sample so as to run 12 subarrays per sample and four samples per OpenArray® Plate. Once PCR reactions were aliquoted into the 384-well plate, the plate was covered with adhesive sealing tape and centrifuged at 1 000 rpm for 1 min and returned to ice. The samples from the 384-well plate were transferred to OpenArray® plates using the OpenArray® AccuFill™ System (Thermo Fisher Scientific). Once the machine had loaded the OpenArray® plate, the plate was removed and carefully sealed with a transparent plastic lid and mineral oil was inserted into the space between the OpenArray® plate and the lid and sealed with a plug as per the manufacturer's instructions. From here, the OpenArray® plate was loaded into the QuantStudio™ 12K Flex Real-Time PCR system (Thermo Fisher Scientific) and the "Mouse Inflammation Panel" template was utilised to run the OpenArray® PCR.

2.6.5 qPCR analysis

Amplification plots for each sample were obtained and then cycle threshold (Ct) limits were determined using the Relative Quantification Software (Thermo Fisher Scientific). All samples were run in duplicate for each primer set. Both actin beta (*Actb*) and glyceraldehyde 3-phosphate dehydrogenase (*Gapdh*) were utilised as house-keeping genes, where levels of each gene of interest were expressed relative to either house-keeping gene using the following formula:

$$\text{mRNA expression level} = 2^{-\Delta\Delta Ct}$$

2.6.5.1 qPCR ANALYSIS FOR OpenArray® PLATES

To analyse the differential expression of genes, data was uploaded to the Thermo Fisher Cloud where the Relative Quantification software was utilised. From here, data were separated into biogroups for analysis. Four biogroups were used for analysis; WT; MD^{25}; MD^{25} + P4 and MD^{25} + MØ. The WT group served as the control and gene expression was normalised to this group. The Relative Quantification software enabled the assessment of the quality of the OpenArray® PCR run for each OpenArray® plate to confirm data reliability. The data were assessed using 16 specific endogenous controls. Another 632 genes were assessed per sample. Using the Relative Quantification software, the maximum Ct value was defined as 32 while the remaining settings remained as default as described by the manufacturer (Thermo Fisher Scientific). Each sample was then assessed for outliers using the Data Review function. Outliers

were discarded based on Amplification Status where genes that were not amplified or were inconclusive were omitted from analysis through assessment of the Amplification and Multicomponent plots. Inconclusive genes typically had Ct values >32 or <15. After this, data were analysed for the four biogroups and for each tissue (myometrium or decidua). Data were exported where the fold change boundary was set at $\log_2(2)$ with a corrected p-value boundary at $-\log_{10}(0.05)$. From here, significant differential gene expression was assessed for each biogroup compared to the control biogroup for each tissue.

Furthermore, a second analysis was performed where each of the four groups were analysed for differential gene expression between the decidua and the myometrium. This approach allowed analysis of gene expression differences between the two regions in the uterus. This data is presented in the Appendices Tables 9.20 and 9.21 and Appendix 9.24.

2.7 ASSAYS

An ELISA kit (ALPCO, Salem NH, USA) was used to measure the concentration of P4 in serum recovered. Assays were carried out according to the manufacturer's instructions. For each experiment, DT-treated WT and DT-treated CD11b-DTR mice were measured in a single assay. The lower level of detection was 0.4 ng/mL and upper limit was 100 ng/mL with 0.04 ng/mL sensitivity.

2.8 STATISTICAL ANALYSIS

Data are presented as mean ± SEM (standard error of the mean) unless otherwise specified. Data were analysed using GraphPad Prism Software version 8 for Windows (GraphPad Software, La Jolla CA, USA) unless a mixed-model analysis was utilised, in which case SPSS® software (version 24.0, IBM, Armonk, New York, USA) was utilised. RNA analysis was performed separately as described above in section 2.6.5. To assess for normality within the data, a D'Agostino & Pearson normality test was utilised. For normally distributed data, a parametric test was used, while data that were not normally distributed required a non-parametric test. For comparison between two groups, either unpaired t-tests or Mann-Whitney u-tests were utilised. Data where three or more groups were utilised were analysed using one-way ANOVA with Sidak's multiple comparison test for normally distributed data or the Kruskal-Wallis test for when data was not normally distributed. Pregnancy rate was analysed using a χ^2-squared test and fetal and placental weights were corrected for viable litter size using mixed model analysis on SPSS® to give estimated marginal means for fetal weight, placental weight and fetal:placental weight ratio. Differences between groups were considered significant when $p<0.05$. This is indicated in Figures with *, where *$p<0.05$, **$p<0.01$, ***$p<0.001$, and ****$p<0.0001$. Additional annotations used for specific comparisons are detailed in the corresponding Figure captions.

Table 2.1: Monoclonal antibodies used in flow cytometry on day 6.5 pc

Antigen	Conjugate	Dilution	Clone	Alternative names	Expression	Source
F4/80	V421	1/100	BM8	EMR1, Ly-71	Macrophages, eosinophils	Biolegend
CD11b	APC-Cy7	1/400	M1/70	Mac-1, Ly-40, CR3, CR3A, Integrin αM	Monocytes, granulocytes, NK cells	BD biosciences
B220 (CD19)	FITC	1/400	RA3-6B2	CD45R, Ly-5, Lyt-4, T200, Protein tyrosine phosphatase receptor type C	B lymphocytes	BD biosciences
CD3	PE-Cy7	1/200	17A2	CD3 Molecular Complex	Thymocytes, mature T lymphocytes	BD biosciences

Table 2.2: Monoclonal antibodies used in flow cytometry on day 7.5 pc

Antigen	Conjugate	Dilution	Clone	Alternative names	Expression	Source
F4/80	V421	1/100	BM8	EMR1, Ly-71	Macrophages, eosinophils	Biolegend
CD11b	APC-Cy7	1/400	M1/70	Mac-1, Ly-40, CR3, CR3A, Integrin αM	Monocytes, granulocytes, NK cells, DC	BD biosciences
CD3	PE-Cy7	1/200	17A2	CD3e, T3e	Thymocytes, T lymphocytes, NKT cells	BD biosciences
CD4	BV510	1/400	RM4-5	L3T4, Ly-4	Thymocytes, T lymphocytes, DCs, NKT cells	BD biosciences
CD25	FTIC	1/200	PC61	IL-2R, Ly-43	Thymocytes, T lymphocytes, B lymphocytes, DCs, monocytes	BD biosciences
FOXP3	APC	1/100	FJK-16s	JM2, Scurfin	Thymocytes, T lymphocytes, Treg cells	BD biosciences
CD122	PE	1/200	TM-Bta1	IL15-Rβ, IL-2Rβ	NK cells, mature T lymphocytes, B lymphocytes, monocytes	BD biosciences

Table 2.3: Primary antibodies used for immunofluorescence and immunohistochemistry

Antigen	Reactivity	Dilution	Concentration	Clone	Isotype	Duration	Source
F4/80	Mouse	1/400	1 µg/ml	BM8	Rat IgG2a	Overnight	eBioscience
C1Q	Mouse, Human	1/200	0.5 µg/ml	7H8	Rat IgG1	Overnight	Abcam
αSMA	Mouse, Human	1/600	0.5 µg/ml	ACTA2	Rabbit IgG	30 min	Merck Millipore
Pan-cytokeratin	Mouse, Human	1/250	0.7 µg/ml	AE1/AE3	Mouse IgG1	2.5 h	Agilent
Vimentin	Mouse, Human	1/10	8.2 µg/ml	Vim3B4	Mouse IgG1	Overnight	Agilent

Table 2.4: Secondary antibodies used for immunofluorescence and immunohistochemistry

Antigen isotype	Reactivity	Dilution	Concentration	Duration	Source
Rabbit IgG	Rat IgG	1/500	4 µg/ml	40 min	Abcam
Goat IgG	Rabbit IgG	1/500	3 µg/ml	1 h	Vector Labs
Rabbit IgG-Alexa Fluor 488	Rat IgG	1/400	5 µg/ml	1 h	Abcam

Table 2.5 Directly conjugated antibodies used for immunofluorescence and immunohistochemistry

Directly conjugated antigen	Reactivity	Dilution	Concentration	Clone	Isotype	Duration	Source
F4/80-Alexa Fluor 594	Mouse	1/50	10 µg/ml	BM8	Rat IgG2a	Overnight **or** 2 h	Biolegend
CD31-Alexa Fluor 488	Mouse	1/100	5 µg/ml	390	Rat IgG2a	Overnight **or** 2 h	Biolegend
CD31-Alexa Fluor 647	Mouse	1/100	5 µg/ml	390	Rat IgG2a	Overnight **or** 2 h	Biolegend
Biotinylated-DBA	N/A	1/600	8 µg/ml	N/A	N/A	30 min	Vector Laboratories

Table 2.6: Primer sequences, concentrations, and accession numbers used for qPCR

Gene (protein)	Primer sequence (5' – 3')	Product length (bp)	Concentration	GenBank accession number
Actb (Actin, beta)	Fwd: GTGTGACGTTGACATCCGTAAAG Rev: CTCAGGAGGAGCAATGATCTTGAT	151	0.25 µM	NM_12481
Cxcr4 (CXCR4)	Fwd: TCGTGCACAAGTGGATCTCC Rev: GGGCAGAGCTTTTGAACTTGG	105	0.25 µM	NM_009911
Gapdh (GAPDH)	Fwd: AGAGGCCCTACTCCAACTCG Rev: TCCCTAGGCCCCTCCTGTTA	91	0.25 µM	NM_008084
Icam1 (ICAM-1)	Fwd: CAGACTCTGAAATGCCAGGCC Rev: TGACAGACTTCACCACCCCG	103	0.25 µM	NM_010493

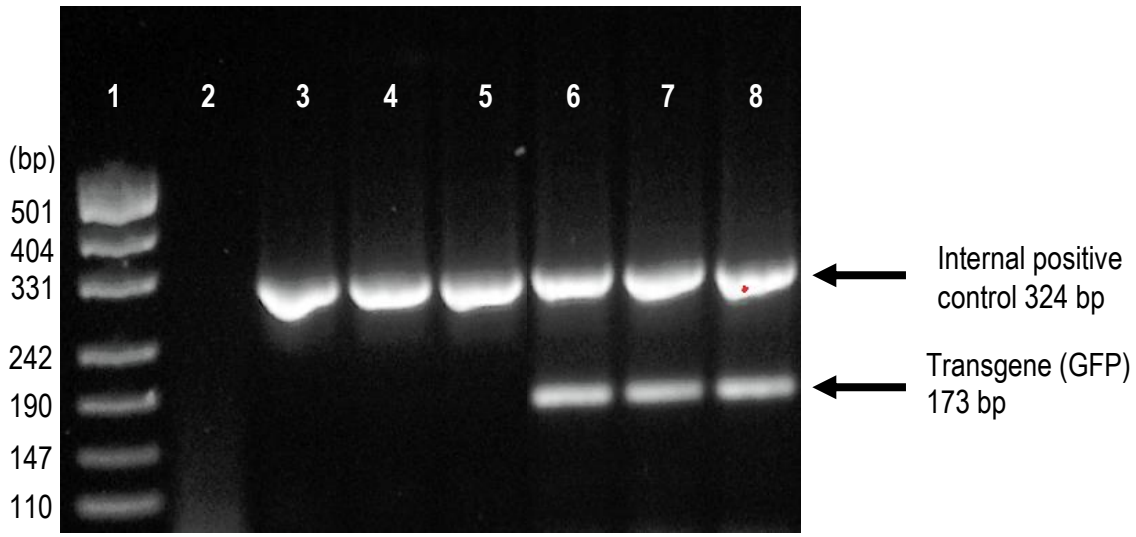

Figure 2.1: Standard PCR assessment of FVB-Tg(ITGAM-DTR/EGFP)34Lan mice for GFP.
To maintain the colony as confirmed FVB-Tg(ITGAM-DTR/EGFP)34Lan mice, PCR was run for wild type and CD11b-DTR mice. Lane 1 indicates the pUC19/HpaII ladder; lane 2 is the negative control; lanes 3-5 are wild type mice and lanes 6-8 are transgenic mice.

CHAPTER 3

EFFECT OF MACROPHAGE DEPLETION IN THE PERI-IMPLANTATION PHASE ON PREGNANCY SUCCESS

3.1 INTRODUCTION

Pregnancy success requires maternal immune tolerance and appropriate hormonal and vascular adaptations to support embryo implantation and placental development (Robertson et al., 2009b, Osol and Mandala, 2009b, Adamson et al., 2002). Macrophages are thought to be involved in immune tolerance through antigen presentation and clearing apoptotic trophoblast cells (Tang et al., 2015). Without regulated clearance, trophoblast cells may be seen as foreign to the maternal immune system, which can lead to initiation of an inflammatory immune response (Abrahams et al., 2004). Excessive inflammatory responses during pregnancy are linked with pregnancy complications such as preeclampsia (PE) in women (Bounds et al., 2015, Weel et al., 2017). Thus, it is postulated that macrophages may regulate immune tolerance to control inflammatory reactions and to further assist in other reproductive processes unique to pregnancy.

Within the body, macrophages are involved in diverse physiological events, including responding to pathogens and facilitating angiogenesis. To achieve specificity in their function, macrophages must be highly responsive to environmental stimuli and have a wide range of activation states. One model for understanding macrophage function separates macrophage populations into pro-inflammatory (M1-like) and anti-inflammatory (M2-like) phenotypes (Zhang et al., 2017). However, this model is overly simplistic as a spectrum of macrophage phenotypes exist, wherein dynamic fluctuations in polarisation status can occur in response to micro-environmental stimuli. In pregnancy, macrophages are likely to have many functions, and understanding their roles over the course of gestation may enlighten potential mechanisms underlying pregnancy disorders including PE (Zhang et al., 2016).

In the pre-implantation phase, macrophages contribute to ovarian remodelling and development of the corpus luteum (Care et al., 2013). Ovarian macrophage numbers fluctuate during the murine estrous cycle in response to steroid hormones (Brannstrom et al., 1994). After ovulation, ovarian macrophages facilitate development of the corpus luteum from the remnants of the ovulated oocyte and its follicle. The corpus luteum is a major source of progesterone (P4) and is the dominant source of P4 during murine pregnancy (Milligan and Finn, 1997). Previous work has demonstrated that depletion of macrophages immediately after conception caused pregnancy failure, which was attributable to defects in corpus luteum structure and decreased serum P4 in mice (Care et al., 2013). In addition, macrophage depletion appears to act to disrupt formation of the microvasculature by impairing angiogenesis in the forming corpus luteum (Turner et al., 2011). Importantly, it was the Tie2-expressing macrophage (TEM) population that were found to be essential for this process (Care et al., 2013). TEMs are key regulators of endothelial cell function and angiogenesis (Kim et al., 2013).

The major hormones of pregnancy, P4 and estrogen (E2), facilitate embryo implantation and placental development (Milligan and Finn, 1997). During both the menstrual cycle in women and the estrous cycle

in mice, P4 and E2 levels fluctuate in order to prepare the female reproductive tract for a potential pregnancy (Byers et al., 2012). Herein, P4 primarily acts to generate a modified lining of the endometrium, a process called decidualisation, to allow embryo implantation. Decidualisation occurs in every menstrual cycle in women but only after fertilisation in mice. E2 works in concert with P4 to facilitate an appropriate uterine environment for embryo implantation. In women, P4 and E2 levels steadily rise until the end of gestation where parturition is initiated by decreasing bioavailability of P4. Here, the P4 receptor changes forms which causes a functional P4 withdrawal (Merlino et al., 2007). In mice, P4 levels are heightened throughout pregnancy then decline toward the end of gestation to stimulate parturition. In contrast, E2 levels remain relatively low throughout murine pregnancy, yet levels dramatically increase toward the end of pregnancy preceding parturition. Within the uterus, macrophage numbers fluctuate in association with these cycling hormone levels, which potential indicates a hormonal control mechanism of macrophage function (Robertson et al., 1996b, Care et al., 2014).

Whilst previous studies have elucidated key roles for macrophages in the ovary through promoting corpus luteum vascularisation to allow P4 synthesis, the role of macrophages in vascular changes within the uterus during early pregnancy remains largely unknown. Reduced macrophage numbers and altered phenotypes have been correlated with PE and fetal growth restriction (FGR) in women (Faas et al., 2014, Brown et al., 2014). However, the pathophysiological mechanisms underpinning these observations are not understood. To this extent, rodent models are excellent tools for understanding and investigating the immunobiology of pregnancy. The short gestation of mice (19 – 21 days) allows for timely manipulations of immune cells to achieve different biological outcomes. In conjunction, events in murine pregnancy, including placentation, are similar to humans, where both species undergo hemochorial placentation (Burton et al., 2016). Thus, murine models are useful to define the role of macrophages in critical events contributing to implantation and placental development, especially vascular adaptations. Therefore, experiments were designed to address the involvement of macrophages in maternal immune tolerance, embryo implantation, placental development, and uterine vascular changes during pregnancy.

To assess the roles of macrophages in murine pregnancy, the CD11b-DTR transgenic mouse model was utilised, which allows for the systemic and transient depletion of macrophages following administration of diphtheria toxin (DT) (refer to section 2.2.1 for detailed protocol). Wild type (WT) mice are resistant to the effects of DT and were used as controls. Herein we depleted macrophages from day 5.5 pc so as to coincide with embryo implantation, decidualisation, and extensive tissue and vascular remodelling prior to placentation. In this chapter, we confirm that macrophage depletion elicited ovarian defects, including disruption and haemorrhage of the corpus luteum. We further demonstrate that ovarian hormone replacement was insufficient to prevent pregnancy failure, suggesting a role for macrophages beyond corpus luteum development with macrophages potentially acting locally within the uterus. Pregnancy failure was also independent of fetal-maternal major histocompatibility complex (MHC) disparity, which

demonstrates that macrophages are involved in roles beyond tolerance induction and indicates potential roles in vascularisation and tissue remodelling in developing implantation sites.

3.2 EFFICIENCY OF MACROPHAGE DEPLETION IN THE CD11b-DTR MODEL

Previous studies have investigated the effects of macrophage depletion either in virgin female mice or early pregnant CD11b-DTR mice prior to implantation. These studies showed extensive macrophage depletion (>90%) in reproductive tissues, as well as depletion in other tissues (Turner et al., 2011, Care et al., 2013). The numbers of most other immune cells, including T and B cells, remain unchanged. There appeared to be decreases in neutrophil and dendritic cell (DC) numbers, but this was not significant in the uterus (Care et al., 2013, Care et al., 2014). Other studies have shown that macrophages become depleted from the kidneys but not from the liver or the lungs in this model (Cailhier et al., 2005).

To establish and confirm the CD11b-DTR model performed as previously reported, flow cytometry (FACS) was firstly utilised to assess macrophage numbers in early pregnancy. Briefly, WT and CD11b-DTR females were mated to BALB/c stud males. Following this, all mice received DT (25 ng/g of body weight) on day 5.5 pc. On day 6.5 pc, single cell suspensions of peritoneal exudate cells (PECs), spleen, and uterus were analysed by FACS, using CD11b and F4/80 to identify granulocytes as $F4/80^{-}CD11b^{+}$ cells and macrophages as $F4/80^{+}CD11b^{+}$ cells. Here data are presented as proportion of live cells for each tissue.

Representative dot plots indicate that DT-treated CD11b-DTR females had decreased proportions of macrophages in the peritoneal cavity and uterus (Figure 3.1 A). The number of macrophages was decreased by 97% in the peritoneal cavity compared to WT controls (mean ± SEM, 11.4 ± 2.3 x 10^4 cells vs 0.3 ± 0.2 x 10^4 cells, WT vs MD^{25}, p=0.011, Table 3.1 and Figure 3.1 B). There was no change to macrophage numbers in the spleen which was expected due to the low expression of CD11b on splenocytes (Table 3.1 and Figure 3.1 C). There was a reduction in uterine macrophages in DT-treated CD11b-DTR mice (17.0 ± 3.9 x 10^3 cells vs 0.2 ± 0.1 x 10^3 cells, p=0.036, Table 3.1 and Figure 3.1 D).

The numbers and proportions of granulocytes ($F4/80^{-}CD11b^{+}$) were also assessed (Table 3.2). There were no changes to the numbers of granulocytes in the peritoneal cavity or the spleen. However, there was a reduction in number of granulocytes in the uterus compared to WT controls (21.2 ± 2.9 x 10^3 cells vs 1.7 ± 0.7 x 10^3 cells, p=0.002, Table 3.2).

To confirm macrophage depletion, implantation sites were stained to detect F4/80 expression (Figure 3.2 A-D). Immunohistochemistry staining showed that the relative F4/80 density in the uterus was decreased by 82% in CD11b-DTR DT-treated mice on day 6.5 pc compared to WT controls (9.6 ± 1.9% vs 1.7 ± 0.3%, p=0.003, Figure 3.2 E). Furthermore, the relative F4/80 density was decreased by 72% in DT-treated CD11b-DTR mice on day 7.5 pc (9.2 ± 1.3% vs 2.5 ± 0.5%, p<0.001, Figure 3.2 F). Due to extensive macrophage depletion in the uterus, CD11b-DTR mice given 25 ng/g DT are henceforth referred to as “macrophage-depleted mice” or “MD^{25}” in figures.

Table 3.1: Proportions and number of macrophages on day 6.5 pc

	%F4/80$^+$CD11b$^+$ (% of Live)		#F4/80$^+$CD11b$^+$	
	WT	MD^{25}	WT	MD^{25}
PECs	10.0 ± 1.2	0.5 ± 0.3*	11.4 ± 2.3 x 10^4 cells	0.3 ± 0.2* x 10^4 cells
Spleen	1.5 ± 0.1	1.5 ± 0.2	2.1 ± 1.5 x 10^6 cells	1.2 ± 0.5 x 10^6 cells
Uterus	1.8 ± 0.3	0.1 ± 0.0*	17.0 ± 3.9 x 10^3 cells	0.2 ± 0.1* x 10^3 cells

Table 3.2: Proportions and number of granulocytes on day 6.5 pc

	%F4/80$^-$CD11b$^+$ (% of Live)		#F4/80$^-$CD11b$^+$	
	WT	MD^{25}	WT	MD^{25}
PECs	9.6 ± 1.2	33.7 ± 11.8*	20.6 ± 6.1 x 10^4 cells	26.5 ± 11.7 x 10^4 cells
Spleen	3.1 ± 0.4	3.2 ± 0.6	3.4 ± 0.4 x 10^6 cells	2.2 ± 0.4 x 10^6 cells
Uterus	3.5 ± 0.5	0.4 ± 0.1*	21.2 ± 2.9 x 10^3 cells	1.7 ± 0.7* x 10^3 cells

Data are presented as mean ± SEM with statistical analysis using an unpaired t-test. * indicates statistical significance ($p<0.05$) for WT vs MD^{25}.

Figure 3.1: DT administration to CD11b-DTR mice elicits macrophage depletion on day 6.5 pc. WT and CD11b-DTR females were mated to BALB/c stud males and all mice were administered 25 ng/g DT on day 5.5 pc. Single cell suspensions of PECs, spleen and uterus were stained to detect CD11b and F4/80 expression by FACS on day 6.5 pc (A). Macrophage numbers were quantified in PECs (B), spleen (C), and uterus (D). FACS plots are representative of 5-12 mice per group. Data are presented as mean ± SEM with statistical analysis using an unpaired t-test. * indicates statistical significance ($p<0.05$) compared to WT controls; *$p<0.05$. MD^{25}; CD11b-DTR females treated with 25 ng/g DT. PECs; peritoneal exudate cells. WT; wild type.

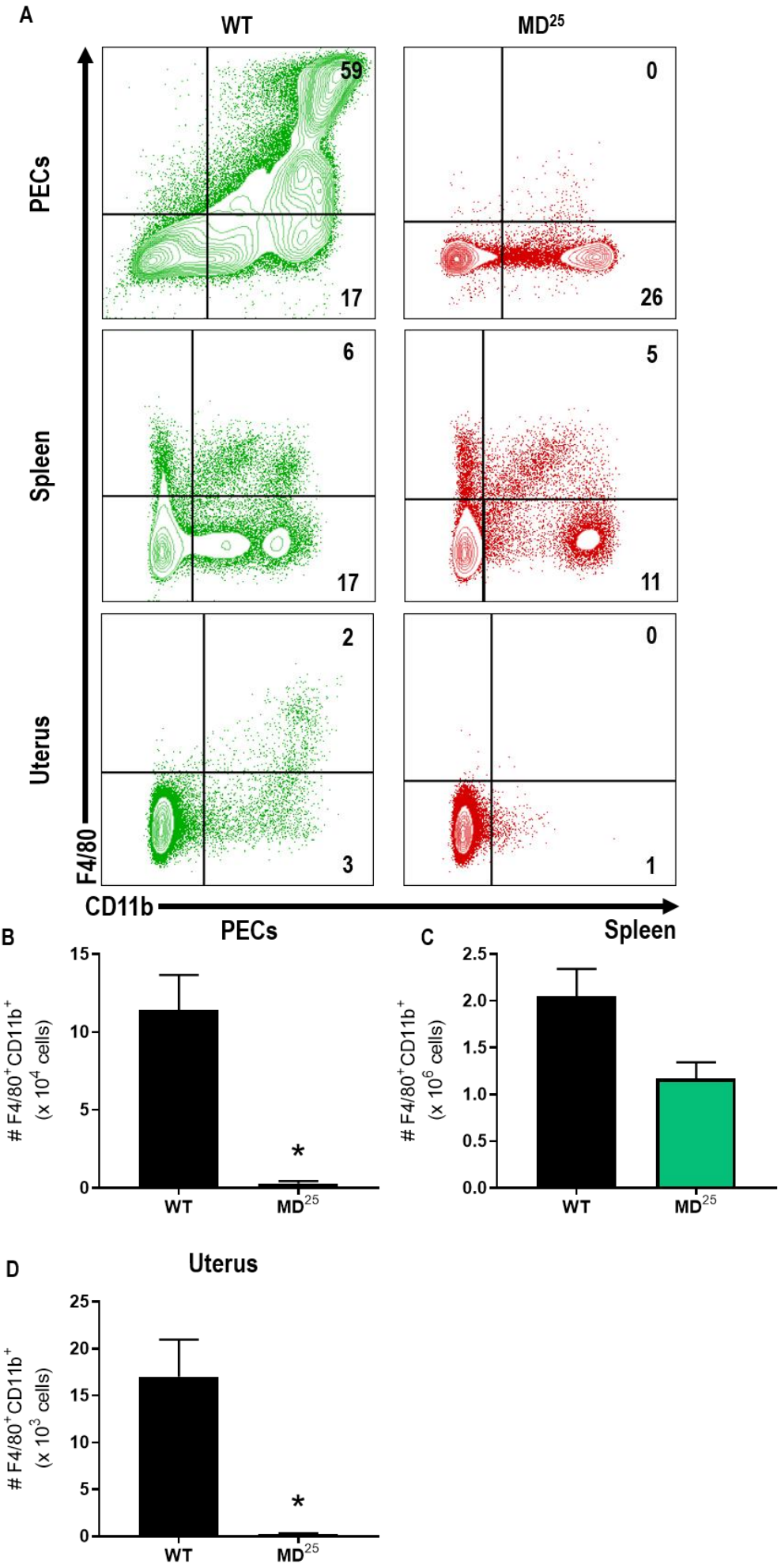
A
WT
MD25
PECs
Spleen
Uterus
F4/80
CD11b
59
17
0
26
6
17
5
11
2
3
0
1
B
PECs
F4/80+CD11b+ (x 10^4 cells)
15
10
5
0
*
WT
MD25
C
Spleen
F4/80+CD11b+ (x 10^6 cells)
2.5
2.0
1.5
1.0
0.5
0.0
WT
MD25
D
Uterus
F4/80+CD11b+ (x 10^3 cells)
25
20
15
10
5
0
*
WT
MD25

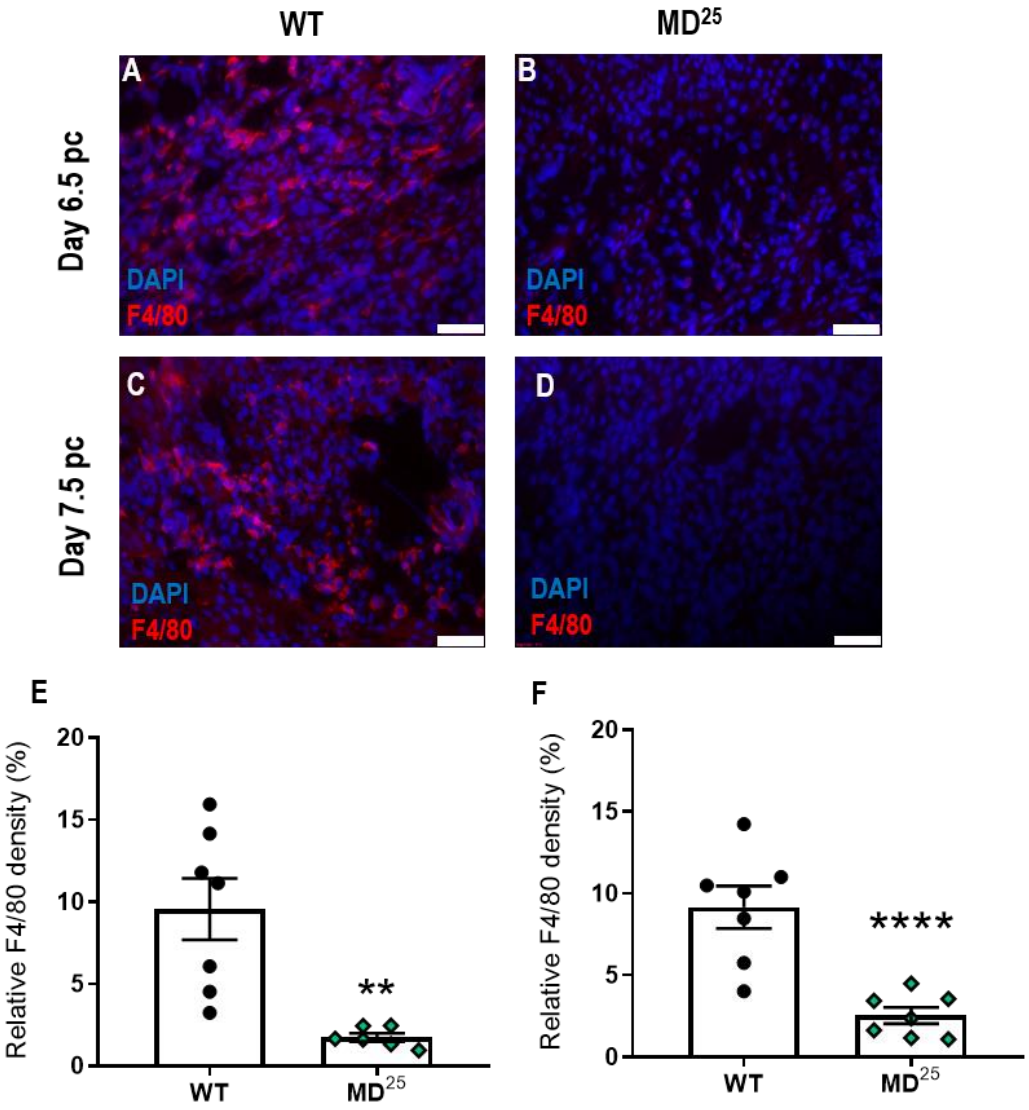

Figure 3.2: DT administration to CD11b-DTR mice elicits macrophage depletion in the uterus on days 6.5 pc and 7.5 pc.

WT and CD11b-DTR females were mated to BALB/c stud males and all mice were administered 25 ng/g DT on day 5.5 pc. Implantation sites were stained with DAPI and anti-F4/80 to assess macrophages in WT (A and C) and DT-treated CD11b-DTR mice (B and D). The relative density of F4/80 was quantified on day 6.5 pc (E) and day 7.5 pc (F). Immunofluorescence images are representative of 6-7 mice per group (scale bar is 50 μm in A-D). Negative and isotype-matched controls are presented in Appendix 9.1. Data are presented as mean ± SEM with statistical analysis using an unpaired t-test, n=6-7 mice/group. * indicates statistical significance ($p<0.05$) compared to WT controls; **$p<0.01$ and ****$p<0.0001$. MD^{25}; CD11b-DTR females treated with 25 ng/g DT. WT; wild type.

3.3 EFFECT OF MACROPHAGE DEPLETION ON EARLY PREGNANCY SUCCESS

After confirming macrophage depletion in CD11b-DTR mice given 25 ng/g DT, implantation site viability was assessed on days 6.5 pc and 7.5 pc. Visual examination of day 6.5 pc implantation sites showed similar viability in both WT and macrophage-depleted mice (Figure 3.3 A, B, E and F). However, on day 7.5 pc implantation sites from macrophage-depleted mice were undergoing resorption (Figure 3.3 C and D). Thus, although there was no change to the number of implantation sites, compared to WT controls, there was a reduction in the number of viable implantation sites in macrophage-depleted mice on day 7.5 pc (mean ± SEM, 9.6 ± 0.6 sites vs 3.5 ± 1.2 sites, WT vs MD[25], p=0.001, Figure 3.3 G and H). On both days 6.5 pc and 7.5 pc, ovaries from macrophage-depleted mice appeared dark red and haemorrhagic compared to WT controls (Figure 3.3 A-D).

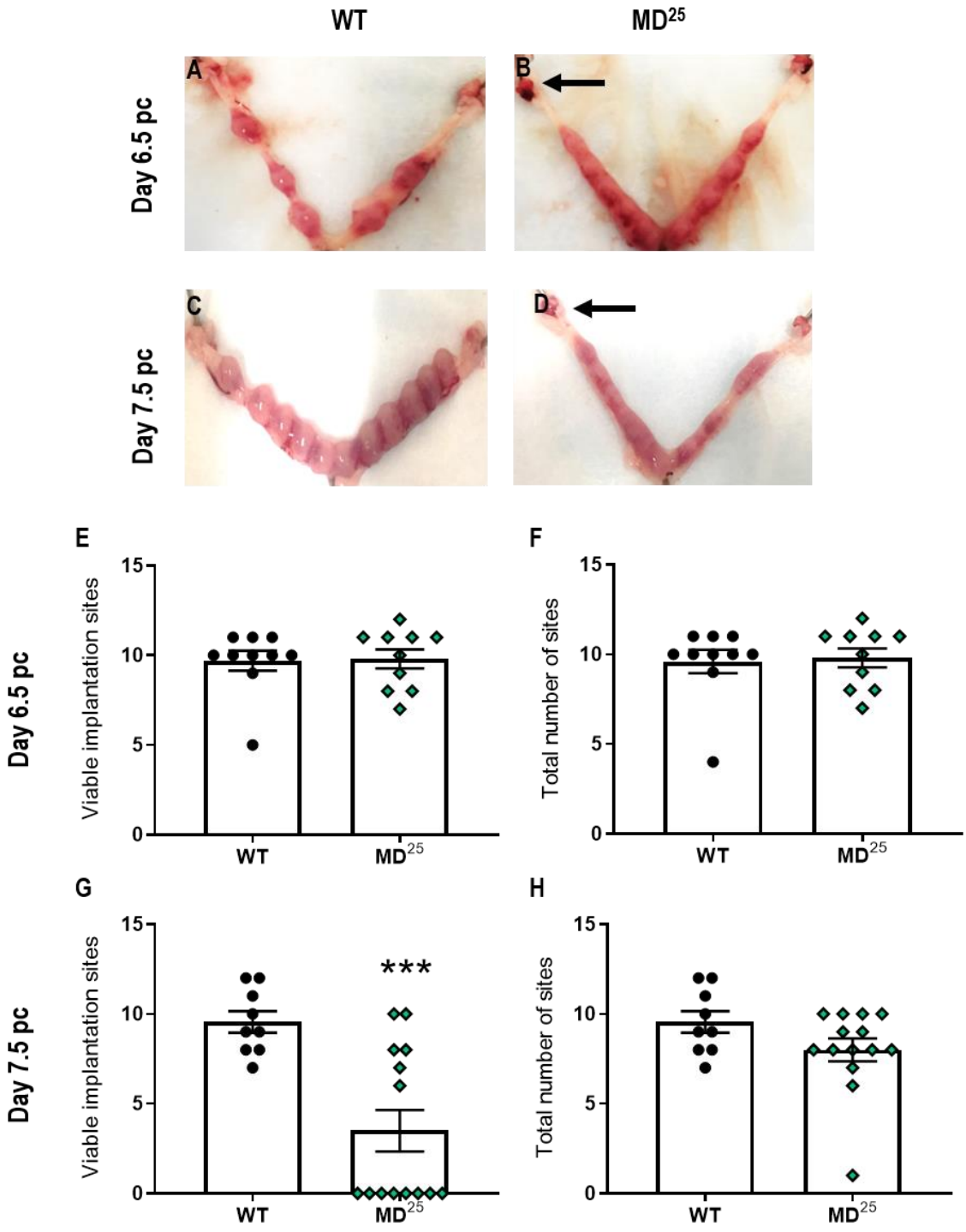

Figure 3.3: Macrophage depletion causes reduced implantation site viability on day 7.5 pc. WT and CD11b-DTR females were mated to BALB/c stud males and all mice were administered 25 ng/g DT on day 5.5 pc. The number of viable implantation sites and the total number of implantation sites were assessed on days 6.5 pc (A, B, E, and F) and 7.5 pc (C, D, G, and H). Data are presented as mean ± SEM with statistical analysis using an unpaired t-test, n=9-14 mice/group. * indicates statistical significance ($p<0.05$) compared to WT controls; ***$p<0.001$. Arrow; haemorrhagic ovary. MD; macrophage-depleted. WT; wild type.

3.3.1 OVARIAN STRUCTURE

To investigate the impact of macrophage depletion on ovarian structure and function, ovaries were stained with haematoxylin and eosin (H&E) and serum P4 concentrations were assessed by ELISA on days 6.5 pc and 7.5 pc. Macrophage-depleted mice showed a profound influx of red blood cells into many corpora lutea compared to corpora lutea from WT controls (Figure 3.4 A-D). This pathology is henceforth referred to as "haemorrhagic corpora lutea". The proportion of haemorrhagic corpora lutea per female was calculated, with macrophage-depleted females having more haemorrhagic corpora lutea than WT controls on day 6.5 pc (mean ± SEM, 0% vs 74 ± 6%, WT vs MD[25], $p<0.001$, Figure 3.4 E). Correspondingly, there was a 24% reduction in serum P4 concentrations in macrophage-depleted mice compared to WT controls on day 6.5 pc (46.7 ± 4.3 ng/mL vs 35.6 ± 3.7 ng/mL, $p=0.024$, Figure 3.4 F).

Similarly, the percentage of haemorrhagic corpora lutea per female was increased in macrophage-depleted females on day 7.5 pc (0% vs 72 ± 4%, $p<0.001$, Figure 3.4 G). Furthermore, there was a 71% reduction in serum P4 concentrations in macrophage-depleted mice on day 7.5 pc (49.9 ± 4.4 ng/mL vs 14.3 ± 2.9 ng/mL, $p<0.001$, Figure 3.4 H). This equated to 60% lower P4 concentrations at day 7.5 pc compared to day 6.5 pc in macrophage-depleted mice.

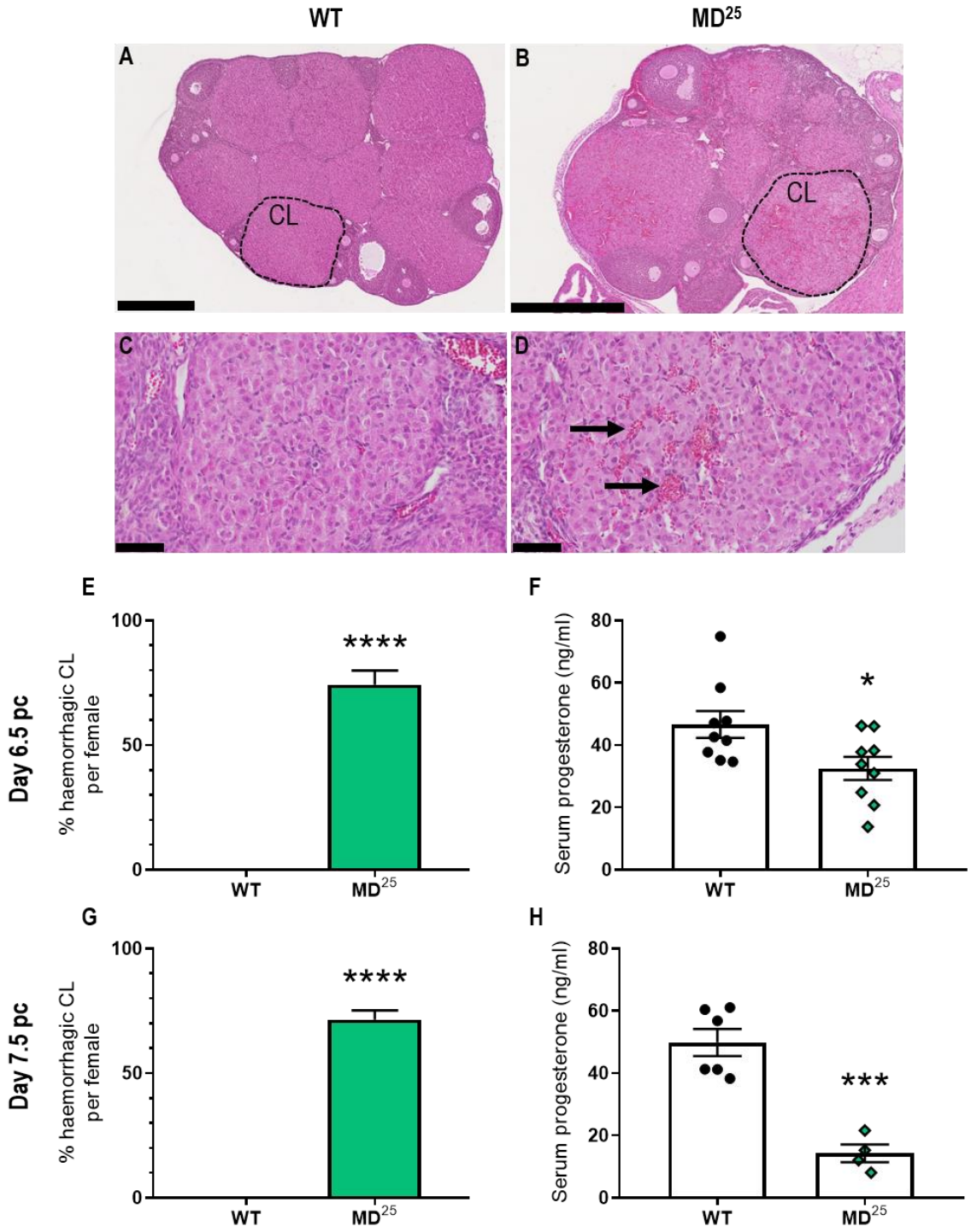

Figure 3.4: Macrophage depletion elicits corpus luteum haemorrhage and decreased serum P4 on days 6.5 pc and 7.5 pc.

WT and CD11b-DTR females were mated to BALB/c stud males and all mice were administered 25 ng/g DT on day 5.5 pc. Ovarian morphology was assessed after H&E staining (A and B; scale bar is 500 µm). Closer inspection of the corpora lutea identified an influx of red blood cells in macrophage-depleted mice compared to WT mice (C and D; scale bar is 50 µm and arrows indicate red blood cells). The proportion of haemorrhagic corpora lutea per female was quantified on days 6.5 pc (E) and 7.5 pc (G). Serum P4 concentration was assessed by ELISA on days 6.5 pc (F) and 7.5 pc (H). Data are presented as mean ± SEM with statistical analysis using unpaired t-test, n=4-6 mice/group. * indicates statistical significance ($p<0.05$) compared to WT controls; *$p<0.05$, ***$p<0.001$, and ****$p<0.0001$. CL; corpora lutea. MD; macrophage-depleted. WT; wild type.

3.3.2 IMPLANTATION SITE STRUCTURE

To determine whether macrophage depletion impaired embryo implantation, implantation sites from days 6.5 pc and 7.5 pc were assessed for alterations to conceptus area and decidualisation. Images in Figure 3.5 (A-D) represent implantation sites stained with alkaline phosphatase. Alkaline phosphatase staining is used as a marker of decidualisation due to high expression of this enzyme in the developing decidua. The decidualisation reaction was quantified through calculating the area of alkaline phosphatase positive tissue as a percentage of the total uterine cross-sectional area (shown in Appendix 9.3). There was no difference in the area of positivity between WT and macrophage-depleted females on day 6.5 pc (Figure 3.5 E). In addition, the area of the embryo and its associated invading trophoblast cells, called the "conceptus area", was also comparable between the two groups on day 6.5 pc (Figure 3.5 F, shown in Appendix 9.3).

In contrast, the extent of decidualisation was decreased by 32% in macrophage-depleted females on day 7.5 pc compared to WT controls (mean ± SEM, 73.6 ± 1.7% vs 50.2 ± 11.4%, WT vs MD[25], p=0.025, Figure 3.5 G). Furthermore, the conceptus area was decreased by 47% in macrophage-depleted mice compared to WT mice on day 7.5 pc (0.47 ± 0.04 mm^2 vs 0.25 ± 0.07 mm^2, p<0.001, Figure 3.5 H).

These data indicate that macrophage depletion impacts ovarian structure which was associated with decreased circulating P4 levels. In addition, decidualisation and the area of the conceptus was reduced on day 7.5 pc after macrophage depletion. Thus, macrophages appear to be involved in maintaining corpora lutea vascular integrity and may be linked with decidualisation and trophoblast invasion in the uterus.

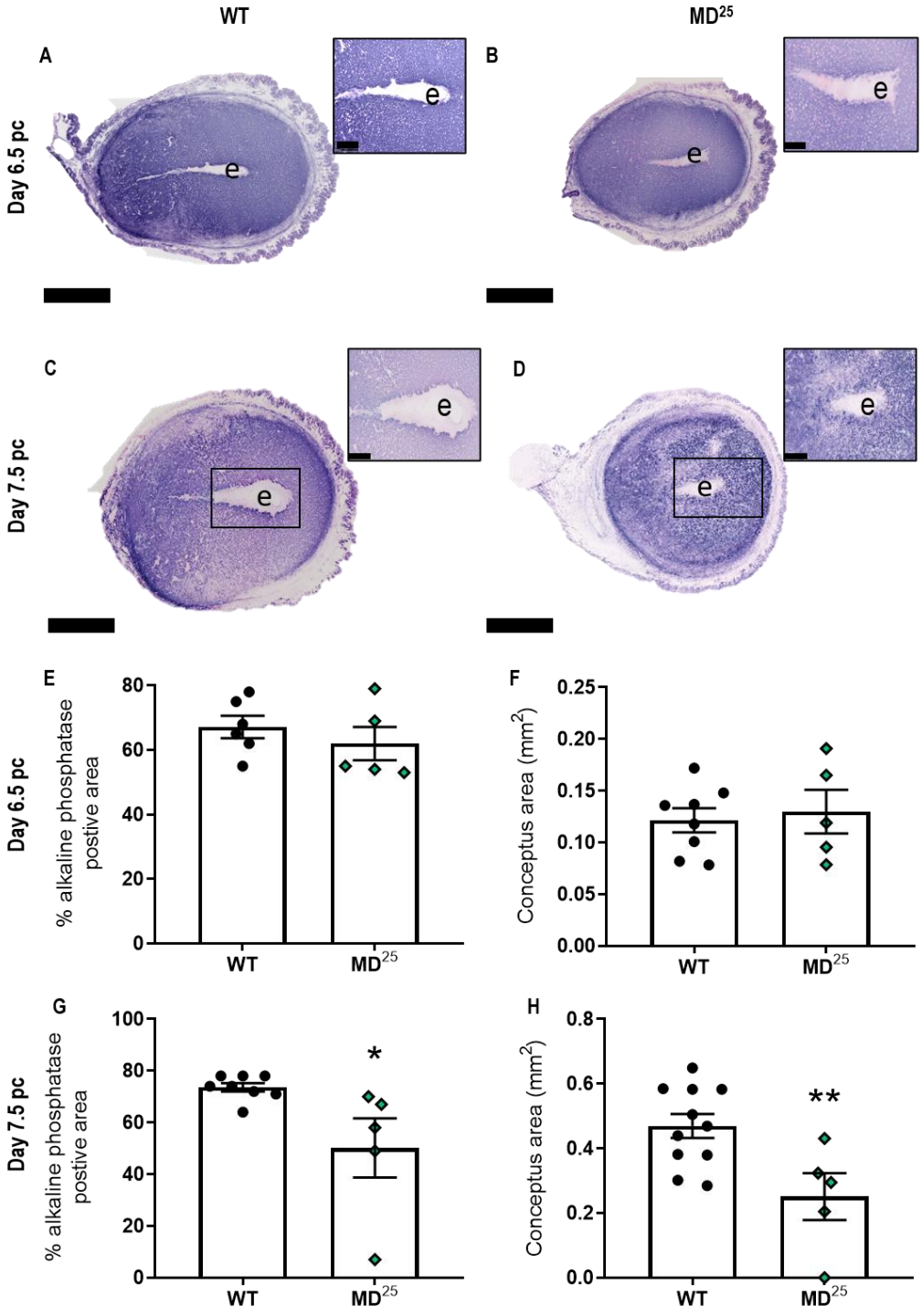

Figure 3.5: Macrophage depletion decreases decidualisation area and conceptus area on day 7.5 pc.

WT and CD11b-DTR females were mated to BALB/c stud males and all mice were administered 25 ng/g DT on day 5.5 pc. Implantation site structure was assessed on days 6.5 pc and 7.5 pc. Alkaline phosphatase-stained implantation sites show the maternal decidua in purple in WT and macrophage-depleted females (A-D; scale bar is 1 mm; inset pictures show conceptus area; scale bar is 250 µm). The extent of decidualisation (see Appendix 9.3) was quantified using alkaline phosphatase staining on day 6.5 pc (E) and day 7.5 pc (G). The conceptus area (see Appendix 9.3) was measured on days 6.5 pc (F) and 7.5 pc (H). Data are presented as mean ± SEM with statistical analysis using unpaired t-test, n=5-8 mice/group. * indicates statistical significance ($p<0.05$) compared to WT controls; *$p<0.05$ and **$p<0.01$. e; embryo. MD; macrophage-depleted. WT; wild type.

3.4 EFFECT OF MACROPHAGE DEPLETION ON PREGNANCY SUCCESS INDEPENDENT OF OVARIAN EFFECTS

Once we identified that macrophage depletion caused corpus luteum haemorrhage and decreased serum P4, the next experiments sought to determine the significance of uterine macrophages, as opposed to ovarian macrophages, in establishing pregnancy. These experiments aimed to clarify the extent to which decreased serum P4 was the cause of reduced pregnancy viability. In previous studies, it has not been possible to distinguish the effects of ovarian macrophages from uterine macrophages, as the mouse models used for macrophage depletion either only deplete ovarian macrophages (using clodronate citrate which is unable to cross into the uterus (Van der Hoek et al., 2000)), or deplete both macrophage populations (CD11b-DTR model, (Care et al., 2013)). The lack of an appropriate model to solely deplete uterine macrophages has proven to be a limitation in understanding the physiological significance of macrophages in female reproductive tissues. The following series of experiments sought to elucidate the specific role of macrophages in the uterus as opposed to the ovary, by determining whether macrophages are required to support pregnancy viability when hormones were administered to compensate for the absence of corpora lutea.

To do this, we investigated various hormone replacement protocols, to find a treatment regimen that was able to replace the impact of failed development of corpora lutea. These were tested in ovariectomised and intact WT and macrophage-depleted mice. Initial attempts show that supplementation of P4 in WT ovariectomised pregnant mice was insufficient to prevent pregnancy failure (see Appendices 9.4 and 9.5). The next approach used a combination of E2 and P4 in the hormone replacement protocol, as reported previously to support gestation in ovariectomised mice (Milligan and Finn, 1997). WT and CD11b-DTR mice were mated to BALB/c studs and ovariectomy was performed on day 5.5 pc. Mice concurrently received P4 pellets and DT on day 5.5 pc, then were administered an E2 pellet on day 9.5 pc. Pregnancy outcomes were assessed at day 17.5 pc.

3.4.1 PREGNANCY OUTCOMES

Supplementation of P4 and E2 in WT ovariectomised females allowed viable pregnancy at day 17.5 pc (Figure 3.6 A). However, macrophage-depleted, ovariectomised females failed to maintain pregnancy despite hormone supplementation, resulting in the presence of resorbing implantation sites on day 17.5 pc (Figure 3.6 B). Overall, there was a reduction in the rate of viable pregnancy in macrophage-depleted mice (90% vs 18%, WT + OVX + H vs MD^{25} + OVX + H, $p<0.001$, Figure 3.6 C). This was associated with a reduction in the average number of viable fetuses in macrophage-depleted mice compared to WT controls (mean ± SEM, 6.1 ± 1.2 fetuses vs 1.4 ± 0.9 fetuses, $p=0.005$, Figure 3.6 D). Correspondingly, macrophage-depleted mice had a greater number of resorbing implantation sites compared to WT controls (3.1 ± 0.8 sites vs 6.6 ± 1.0 sites, $p=0.012$, Figure 3.6 E). To better visualise the range of outcomes, individual females were placed into one of five categories based on the type and extent of

pregnancy loss. These categories were defined as 100% uterine scars (early pregnancy loss), 100% resorptions, >50% resorptions, <50% resorptions, and no resorptions, no scars (Figure 3.6 F). Macrophage-depleted females were more likely to have 100% resorptions compared to WT controls (0% vs 80.9%, Figure 3.6 F).

This experiment shows that despite replacement of the hormones that are deficient due to corpora lutea demise, pregnancy in macrophage-depleted mice is still compromised. This experiment is consistent with a clear requirement for uterine macrophages in implantation and pregnancy progression

Figure 3.6: P4 and E2 supplementation to ovariectomised mice sustains pregnancy but not in macrophage-depleted mice.

WT and CD11b-DTR females were mated to BALB/c stud males and all mice were administered 25 ng/g DT on day 5.5 pc. On day 5.5 pc, ovariectomy was performed and two P4 pellets were subcutaneously inserted into the mid-dorsal region. On day 9.5 pc, an E2 pellet was also inserted subcutaneously. Pregnancy outcomes were then assessed on day 17.5 pc in WT (A) and macrophage-depleted females (B). Viable pregnancy rate was assessed (C) as were the number of viable fetuses (D), the number of resorptions (E), and the total number of sites per litter (F). The pregnancies from each group were categorised by viability (G). Data are presented as mean ± SEM (D-F). Statistical analysis was performed using unpaired t-test, except in C where a χ^2 test was used, n=10-11 mice/group. * indicates statistical significance ($p<0.05$) compared to WT controls; *$p<0.05$, **$p<0.01$, and ****$p<0.0001$. DT; diphtheria toxin. DTR; diphtheria toxin receptor. E2; estrogen. H; hormone-supplemented. MD; macrophage-depleted. OVX; ovariectomised. P4; progesterone. pc; post-coitum. WT; wild type.

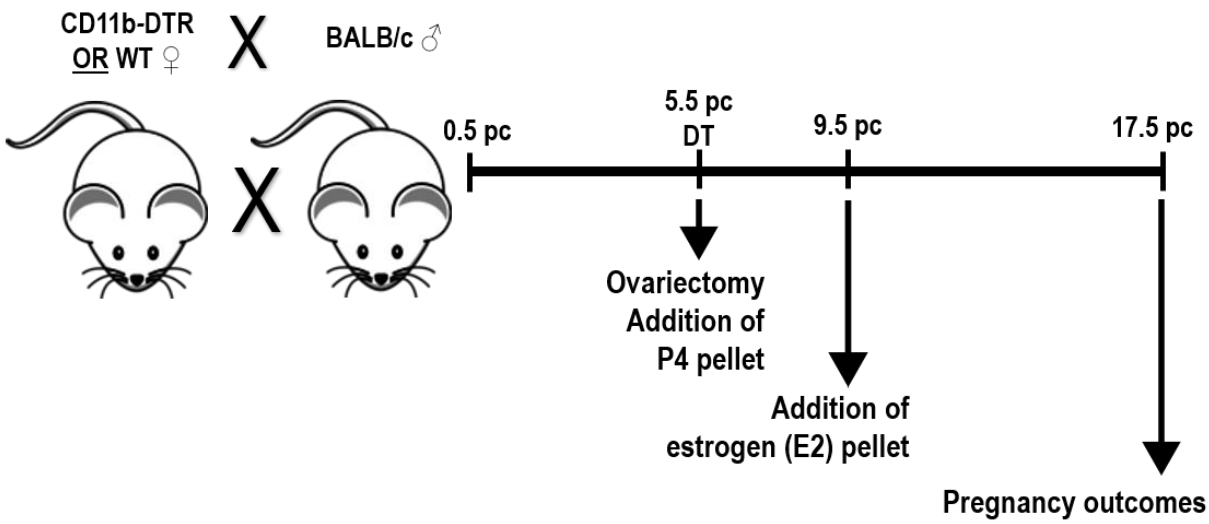
CD11b-DTR
OR WT ♀
X
BALB/c ♂
X
0.5 pc
5.5 pc
DT
9.5 pc
17.5 pc
Ovariectomy
Addition of
P4 pellet
Addition of
estrogen (E2) pellet
Pregnancy outcomes

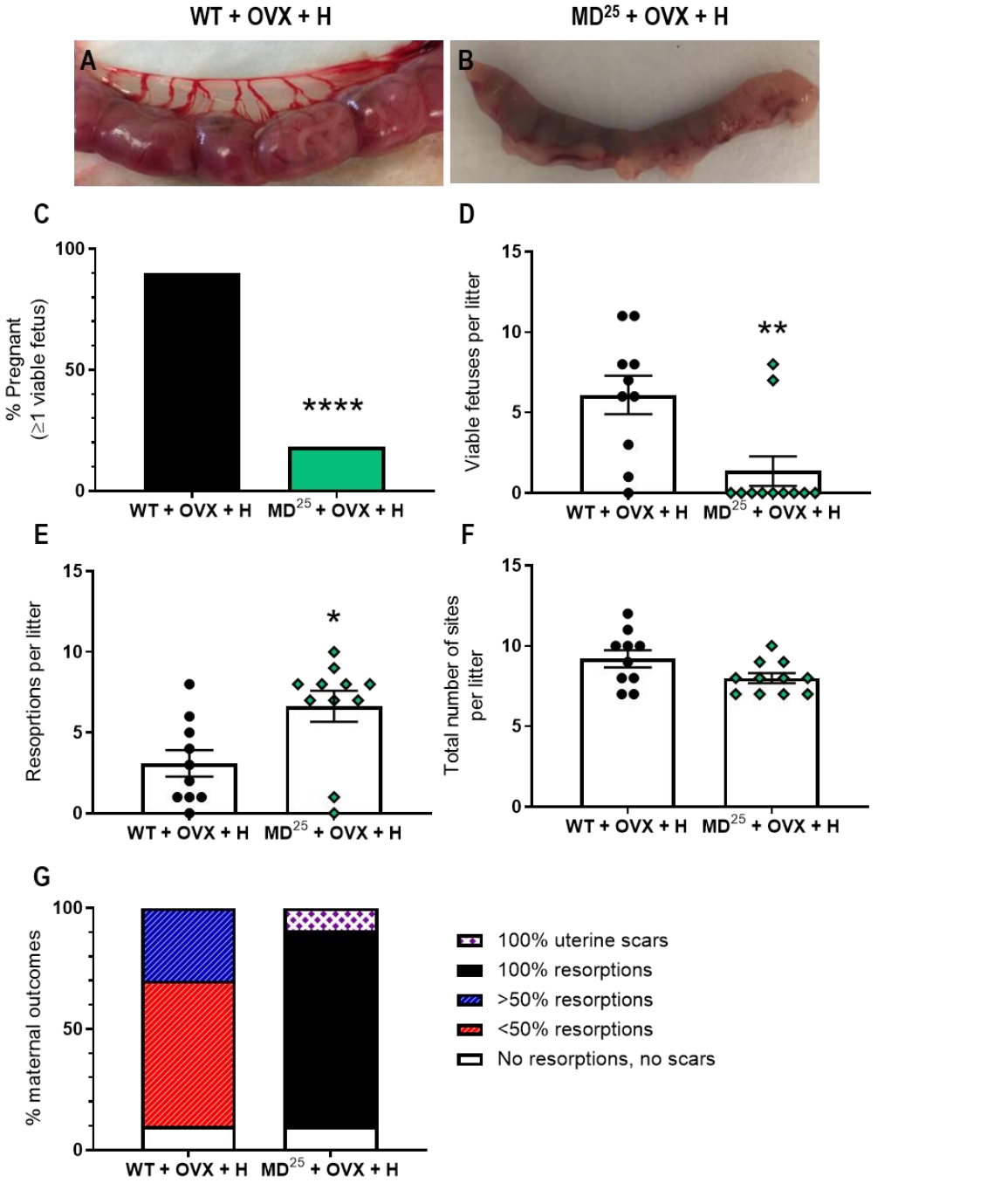
WT + OVX + H
MD25 + OVX + H
A
B
C
% Pregnant
(≥1 viable fetus)
100
50
0
****
WT + OVX + H
MD25 + OVX + H
D
Viable fetuses per litter
15
10
5
0
**
WT + OVX + H
MD25 + OVX + H
E
Resoprtions per litter
15
10
5
0
*
WT + OVX + H
MD25 + OVX + H
F
Total number of sites
per litter
15
10
5
0
WT + OVX + H
MD25 + OVX + H
G
% maternal outcomes
100
50
0
WT + OVX + H
MD25 + OVX + H
100% uterine scars
100% resorptions
>50% resorptions
<50% resorptions
No resorptions, no scars

3.5 EFFECT OF MACROPHAGE DEPLETION ON PREGNANCY SUCCESS INDEPENDENT OF MHC ANTIGENS

Due to the extensive pregnancy loss in ovariectomised, macrophage-depleted mice despite hormone replacement, we next sought to investigate whether macrophage depletion acted to impair pregnancy immune tolerance. Thus, a syngeneic versus allogeneic mating strategy was investigated. Allogeneic matings expose the mother to a higher level of paternally-inherited, disparate MHC antigens compared to syngeneic matings (Erlebacher, 2010). Therefore, an allogeneic mating has a higher demand on immune regulatory mechanisms that provide immune tolerance toward the semi-allogeneic embryo (Darasse-Jèze et al., 2006). This is not the case in syngeneic matings, where there is no maternal-fetal MHC disparity, and so a reduced need for tolerogenic immune responses. Central to the generation of tolerance is the T cell compartment and more specifically, the Treg cell compartment (Robertson et al., 2009a). Studies have shown that there is less proliferation of Treg cells in syngeneic pregnancies compared to allogeneic pregnancies (Robertson et al., 2009a). Importantly, macrophages may assist in generating tolerogenic responses through their roles in antigen presentation (Ning et al., 2016). However, it remains to be investigated how macrophages and Treg cells interact during pregnancy.

Briefly, WT and CD11b-DTR females were mated allogeneically to BALB/c stud males or were mated to males of the same genetic background for syngeneic matings. Females underwent insertion of P4 or vehicle control pellets on day 5.5 pc, and concurrently were administered 25 ng/g DT. At day 9.5 pc, mice either received an E2 pellet or a vehicle control pellet. Females were assessed for pregnancy outcomes on day 17.5 pc. Data here is first presented in regard to allogeneic matings and then syngeneic matings.

3.5.1 PREGNANCY OUTCOMES

Irrespective of mating strategy or hormone supplementation, viable pregnancy rate on day 17.5 pc was reduced after macrophage depletion. After allogeneic mating, macrophage-depleted mice given vehicle pellets showed a 92% reduction in viable pregnancy rate compared to WT controls (100% vs 8%, WT + H vs MD^{25} + Veh, $p<0.001$, Figure 3.7 A). In addition, the number of viable fetuses was decreased in macrophage-depleted mice given vehicle pellets (mean ± SEM, 8.9 ± 0.4 fetuses vs 0.6 ± 0.4 fetuses, $p<0.001$, Figure 3.7 B). There was no change to the number of resorbing implantation sites or the total number of sites, however the number of uterine scars was increased (0 scars vs 6.3 ± 0.6 scars, $p<0.001$, Figure 3.7 C-E). Macrophage-depleted mice given vehicle pellets had an increased proportion of females with uterine scars on day 17.5 pc (Figure 3.7 F).

In allogeneic matings, macrophage-depleted mice given hormones had no viable pregnancies on day 17.5 pc (100% vs 0%, WT + H vs MD^{25} + H, $p<0.001$, Figure 3.7 A and B). These mice had an increased number of resorptions (0.4 ± 0.1 resorptions vs 3.5 ± 1.2 resorptions, $p<0.001$, Figure 3.7 C) and uterine scars compared to WT controls (0 scars vs 4.7 ± 1.2 scars, $p<0.001$, Figure 3.7 D). There was no change

to the total number of implantation sites, however macrophage-depleted mice given hormones were more prone to 100% resorptions and uterine scars on day 17.5 pc compared to WT controls (Figure 3.7 E and F).

For macrophage-depleted mice given vehicle pellets after syngeneic mating, the rate of viable pregnancy was reduced compared to WT controls (95% vs 29%, WT + H vs MD^{25} + Veh, $p<0.001$, Figure 3.8 A). In addition, the number of viable fetuses was decreased (mean ± SEM, 7.2 ± 0.6 fetuses vs 2.5 ± 1.0 fetuses, $p<0.001$, Figure 3.8 B). Unexpectedly, there were fewer resorptions in macrophage-depleted mice given vehicle pellets (2.1 ± 0.3 resorptions vs 0.4 ± 0.2 resorptions, $p=0.023$, Figure 3.8 C) but the number of uterine scars was increased (0 scars vs 4.9 ± 0.9 scars, $p<0.001$, Figure 3.8 D). There was no change to the total number of implantation sites and macrophage-depleted females given vehicle pellets were more prone to uterine scars on day 17.5 pc (Figure 3.8 E and F).

After syngeneic mating, there were no viable pregnancies in macrophage-depleted mice supplemented with hormones (95% vs 0%, WT + H vs MD^{25} + H, $p<0.001$, Figure 3.8 A). However, there was an increase in the number of resorptions compared to WT controls (2.1 ± 0.3 resorptions vs 5.7 ± 1.6 resorptions, $p<0.001$, Figure 3.8 C). Furthermore, the number of uterine scars was increased compared to WT controls (0 scars vs 3.0 ± 1.9 scars, $p=0.049$, Figure 3.8 D). There was no change to the total number of implantation sites and macrophage-depleted mice given hormones were more prone to 100% resorptions on day 17.5 pc (Figure 3.8 E and F).

Overall, macrophage-depleted females given the vehicle pellets were more susceptible to uterine scars compared to macrophage-depleted females supplemented with hormones, where a greater proportion of resorptions was seen (Figure 3.7 F and Figure 3.8 F). There was no difference to viable pregnancy rate between macrophage-depleted mice given vehicle pellets and macrophage-depleted mice given hormones.

Notably, the number of resorptions was increased in WT mice in syngeneic matings compared to WT mice in allogeneic matings (2.1 ± 0.3 resorptions vs 0.4 ± 0.1 resorptions, WT + H syngeneic vs WT + H allogeneic, Figure 3.7 C and Figure 3.8 C).

These data indicate that pregnancy outcome is not improved in syngeneic compared to allogeneic mating, and do not support a role for macrophages in antigen presentation or other aspects of antigen-dependent immune tolerance. However, it is noteworthy that in both syngeneic and allogeneic pregnancies, there was evidence of a shift towards more resorptions and fewer scars in late gestation after hormone supplementation in macrophage-depleted mice. This is consistent with later pregnancy loss, likely around mid-gestation, as opposed to peri-implantation when macrophage-depleted mice are administered exogenous hormones. Moreover, it appears macrophages function locally within the uterus to promote pregnancy success, outside of their well-defined role in the ovary.

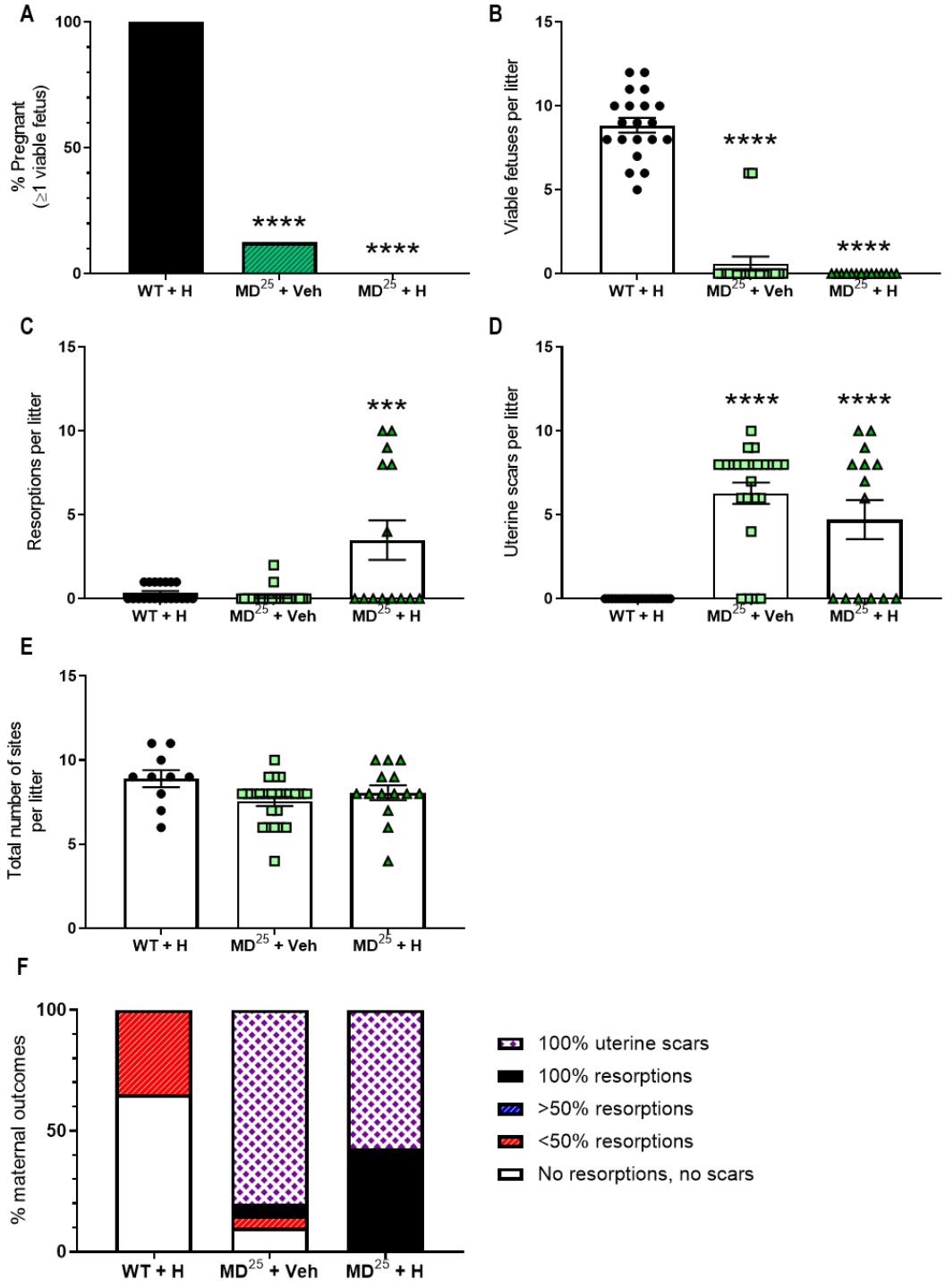

Figure 3.7: Macrophage depletion causes pregnancy failure on day 17.5 pc in allogeneic matings independent of hormone supplementation.

WT and CD11b-DTR females were mated to BALB/c stud males and all mice were administered 25 ng/g DT on day 5.5 pc. On day 5.5 pc, two P4 (or vehicle) pellets were subcutaneously inserted into the mid-dorsal region. On day 9.5 pc, an E2 (or vehicle) pellet was also inserted subcutaneously. Viable pregnancy rate was assessed on day 17.5 pc along with the number of viable fetuses, implantation site resorptions, uterine scars, and total number of implantation sites (A-E). The pregnancies from each group were categorised by viability (F). Data are presented as mean ± SEM (B-E). Statistical analysis was performed using one-way ANOVA with Sidak's multiple comparisons test, except in A where a χ^2 test was used, n=10-24 mice/group. * indicates statistical significance ($p<0.05$) compared to WT controls; ***$p<0.001$ and ****$p<0.0001$. H; hormone-supplemented. MD^{25}; macrophage-depleted. Veh; vehicle control pellet. WT; wild type.

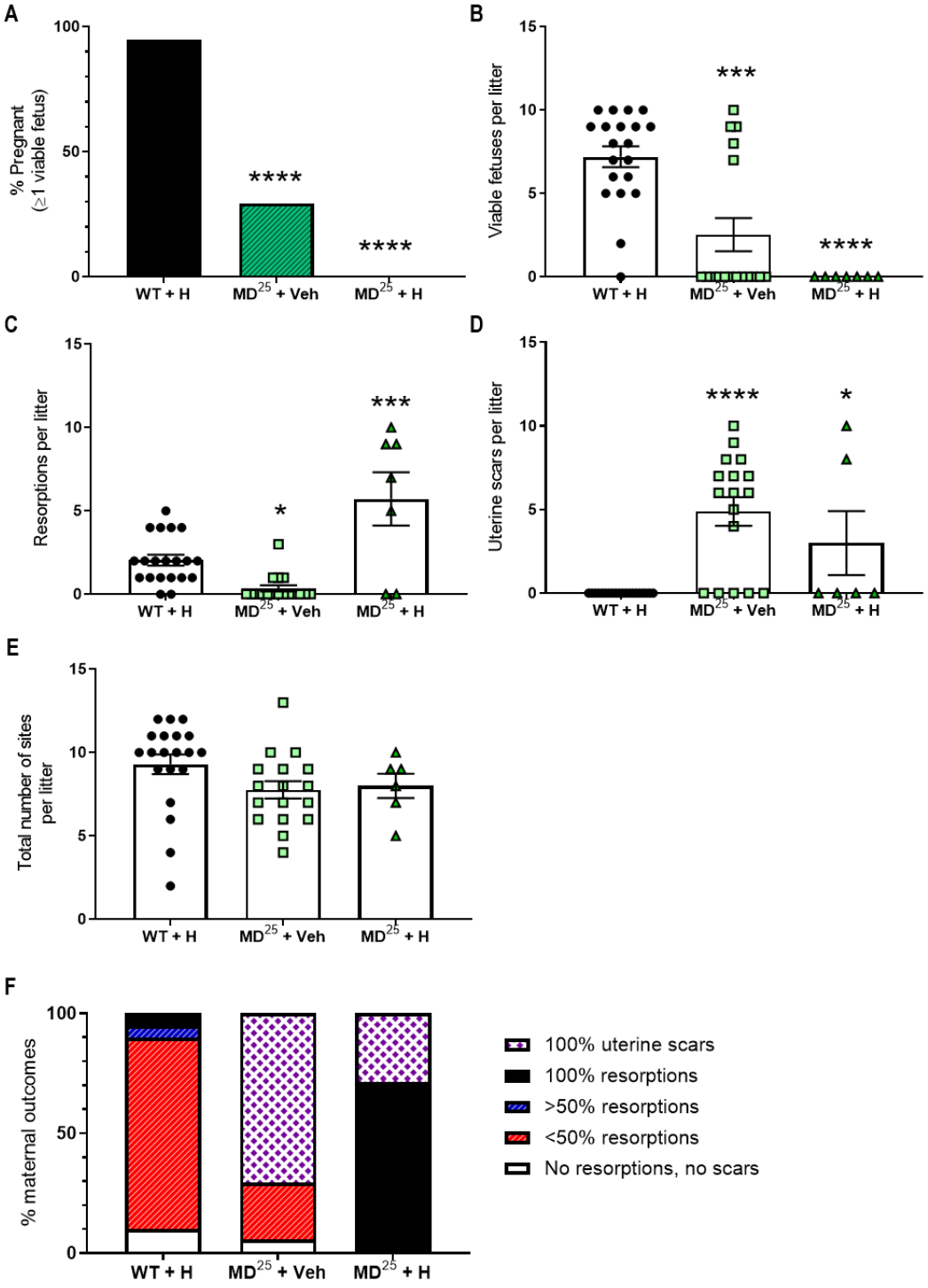

Figure 3.8: Macrophage depletion causes pregnancy failure on day 17.5 pc in syngeneic matings independent of hormone supplementation.

WT and CD11b-DTR females were mated to BALB/c stud males and all mice were administered 25 ng/g DT on day 5.5 pc. On day 5.5 pc, two P4 (or vehicle) pellets were subcutaneously inserted into the mid-dorsal region. On day 9.5 pc, an E2 (or vehicle) pellet was also inserted subcutaneously Viable pregnancy rate was assessed on day 17.5 pc along with the number of viable fetuses, implantation site resorptions, uterine scars and total number of implantation sites (A-E). The pregnancies from each group were categorised by viability (F). Data are presented as mean ± SEM (B-E). Statistical analysis was performed using one-way ANOVA with Sidak's multiple comparisons test, except in A where a χ^2 test was used, n=6-20 mice/group. * indicates statistical significance ($p<0.05$) compared to WT controls; ***$p<0.001$ and ****$p<0.0001$. H; hormone-supplemented. MD^{25}; macrophage-depleted. Veh; vehicle control pellet. WT; wild type.

3.6 EFFECT OF MACROPHAGE DEPLETION AND P4 SUPPLEMENTATION ON PREGNANCY VIABILITY DURING MID-GESTATION

After confirming that pregnancy viability decreased independently of fetal-maternal MHC disparity and hormone replacement, the next series of experiments sought to determine the stage of gestation at which fetal viability declined after hormone replacement. Briefly, WT and CD11b-DTR females were mated to BALB/c stud males. Mice underwent insertion of P4 or vehicle control pellets subcutaneously on day 5.5 pc and concurrently were administered 25 ng/g DT. Pregnancy outcomes were assessed at day 9.5 pc (before the time at which E2 would be administered).

3.6.1 PREGNANCY OUTCOMES

The images in Figure 3.9 (A) show the appearance of implantation sites on day 9.5 pc. Implantation sites from the macrophage-depleted mice given vehicle pellets presented as uterine scars, indicating early loss (Figure 3.9 A). Pregnancy viability rate was decreased by 89% in macrophage-depleted mice given vehicle pellets compared to WT controls (100% vs 11%, WT + P4 vs MD^{25} + Veh, $p<0.001$, Figure 3.9 B). The number of viable implantation sites was also decreased (mean ± SEM, 8.7 ± 1.2 sites vs 0.9 ± 0.9 sites, $p=0.007$, Figure 3.9 C). Whilst the number of resorptions was unchanged (Figure 3.9 D), the number of uterine scars was increased compared to WT controls (0 scars vs 6.1 ± 0.9 scars, $p<0.001$, Figure 3.9 E). The total numbers of implantation sites in these pregnancies were similar (Figure 3.9 F).

Implantation sites from macrophage-depleted mice given P4 appeared viable but were smaller and paler compared to those in WT controls (Figure 3.9 A). Pregnancy viability rate was decreased by 33% when P4 was supplemented to macrophage-depleted mice compared to WT controls (100% vs 67%, WT + P4 vs MD^{25} + P4, $p<0.001$, Figure 3.9 B). The number of viable implantation sites was not different (Figure 3.9 C) but there was a trend toward an increase in the number of resorptions (mean ± SEM, 0 resorptions vs 2.1 ± 1.4 resorptions, $p=0.09$, Figure 3.9 D). The number of uterine scars and the total number of implantation sites were not different (Figure 3.9 E and F).

When comparing macrophage-depleted mice, P4 supplementation increased pregnancy viability by 56% compared to vehicle control administration (11% vs 67%, MD^{25} + Veh vs MD^{25} + P4, $p=0.002$, Figure 3.9 B). Looking at pregnancy viability categories, macrophage depletion without P4 supplementation mainly resulted in uterine scars, whereas P4 supplementation reduced the susceptibility to uterine scars yet increased fetal resorptions, thereby failing to completely restore pregnancy viability (Figure 3.9 G).

Figure 3.9: P4 supplementation to macrophage-depleted mice improves pregnancy viability on day 9.5 pc.

WT and CD11b-DTR females were mated to BALB/c stud males and all mice were administered 25 ng/g DT on day 5.5 pc. On day 5.5 pc, two P4 (or vehicle) pellets were inserted to the s.c. region of the mid-dorsal area. Implantation sites were assessed on day 9.5 pc (A). Pregnancy outcomes, the numbers of viable implantation sites, implantation site resorptions, uterine scars, and total number of sites were assessed (B-F). The pregnancies from each group were categorised based on viability (G). Data are presented as mean ± SEM (C-F). Statistical analysis was performed using one-way ANOVA with Sidak's multiple comparisons test, except in B where a χ^2 test was used, n=6-9 mice/group. * indicates statistical significance ($p<0.05$) compared to WT controls; **$p<0.01$, ***$p<0.001$, and ****$p<0.0001$. ## in B indicates $p<0.01$ for MD^{25} + Veh vs MD^{25} + P4. MD; macrophage-depleted. P4; progesterone. Veh; vehicle control pellet. WT; wild type.

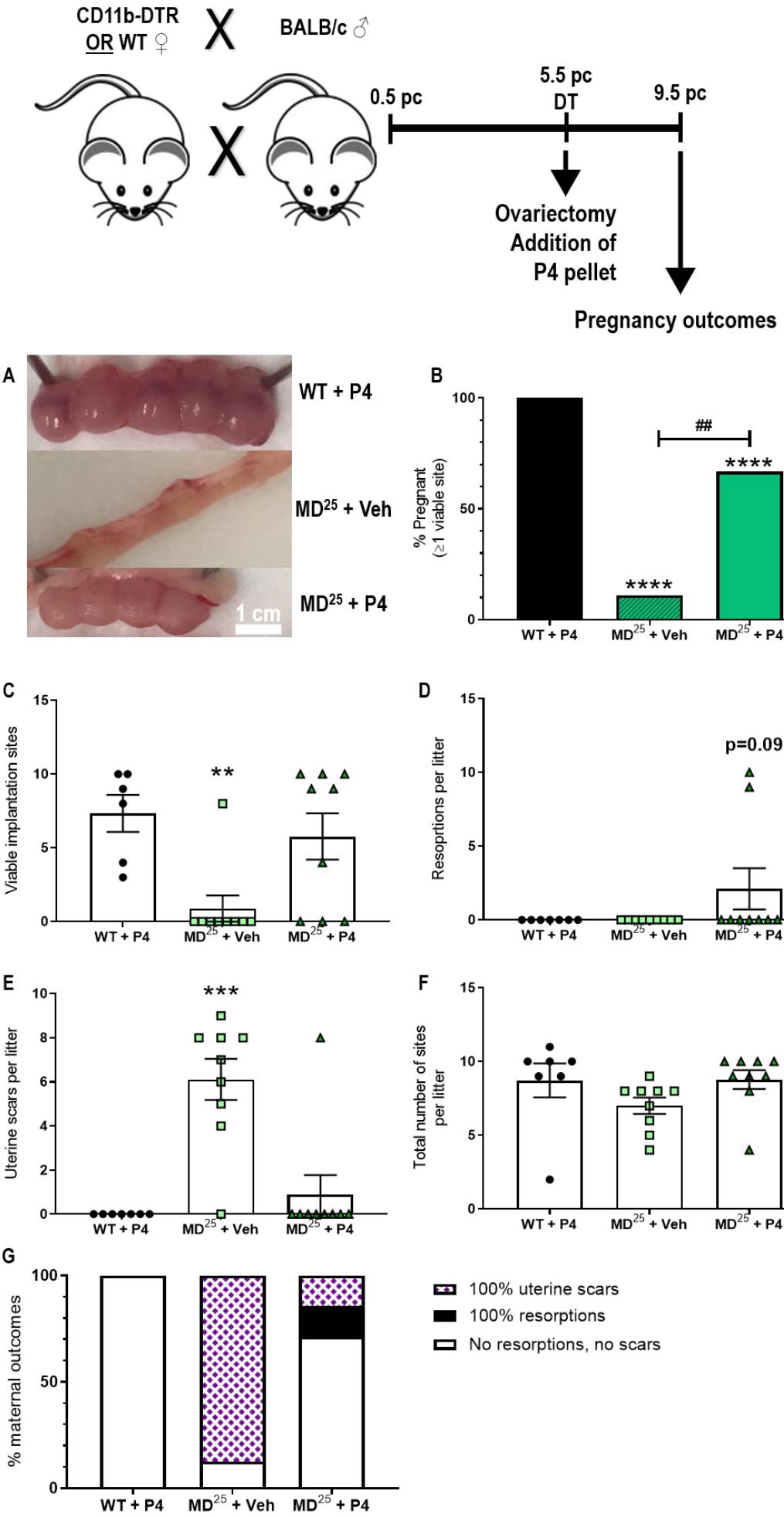
CD11b-DTR
OR WT ♀
X
BALB/c ♂
X
0.5 pc
5.5 pc
DT
9.5 pc
Ovariectomy
Addition of
P4 pellet
Pregnancy outcomes
A
WT + P4
MD25 + Veh
MD25 + P4
1 cm
B
% Pregnant
(≥1 viable site)
100
50
0
##
****
****
WT + P4
MD25 + Veh
MD25 + P4
C
Viable implantation sites
15
10
5
0
**
WT + P4
MD25 + Veh
MD25 + P4
D
Resoprtions per litter
15
10
5
0
p=0.09
WT + P4
MD25 + Veh
MD25 + P4
E
Uterine scars per litter
10
8
6
4
2
0
***
WT + P4
MD25 + Veh
MD25 + P4
F
Total number of sites
per litter
15
10
5
0
WT + P4
MD25 + Veh
MD25 + P4
G
% maternal outcomes
100
50
0
WT + P4
MD25 + Veh
MD25 + P4
100% uterine scars
100% resorptions
No resorptions, no scars

3.6.2 IMPLANTATION SITE STRUCTURE

To further investigate the structure of the day 9.5 pc implantation sites, sections were stained with alkaline phosphatase to assess decidualisation (Figure 3.10 A-F). WT implantation sites had a developing embryo and a large decidual region subjacent to the mesometrial triangle (Figure 3.10 A and D). In macrophage-depleted mice with a vehicle pellet, this distinct structure was lost, the decidual region was small, and there was evidence of cell death where the trophoblast cells of the conceptus should have been invading (Figure 3.10 B and E). In macrophage-depleted mice with P4, the decidual area comprised most of the implantation site, and the embryo appeared very small (Figure 3.10 C and F). The macrophage-depleted mice given the vehicle pellet only yielded one viable pregnancy, and so data are not presented for this group. There was no change to the extent of decidualisation in macrophage-depleted mice given P4 compared to WT controls (Figure 3.10 G).

Again, this data is consistent with the interpretation that administration of P4 acts to protect the conceptus from loss during the early, peri-implantation phase. Whilst this result is improved compared to vehicle control supplementation, it further indicates that macrophages act locally within the uterus to promote pregnancy success.

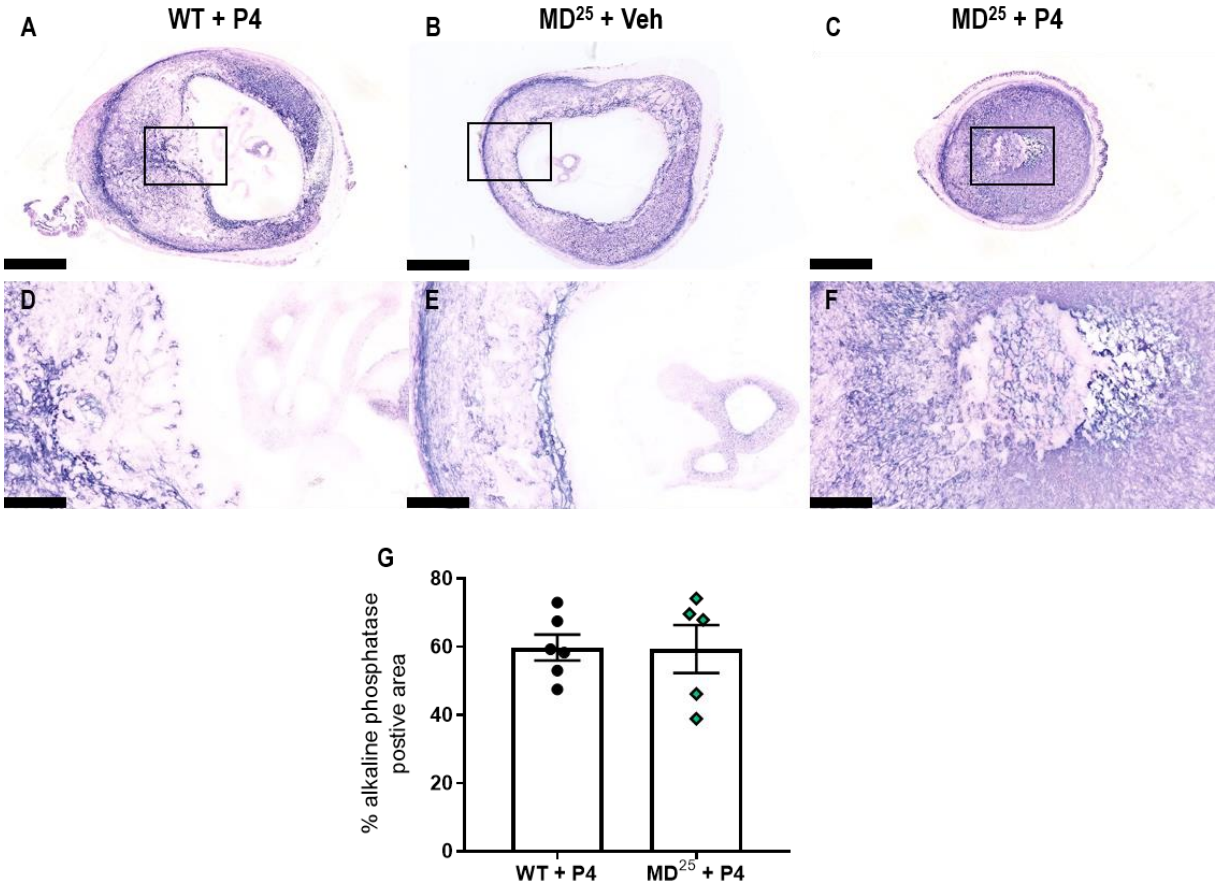

Figure 3.10: Macrophage depletion elicits changes to implantation site structure on day 9.5 pc independent of P4 supplementation.

WT and CD11b-DTR females were mated to BALB/c stud males and all mice were administered 25 ng/g DT on day 5.5 pc. On day 5.5 pc, two P4 (or vehicle) pellets were inserted to the s.c. region of the mid-dorsal area. Alkaline phosphatase-stained implantation sites show the maternal decidua in purple (A-C; scale bar is 1 mm). The conceptus area is shown for each group (D-F; scale bar is 250 µm). The proportion of alkaline phosphatase staining indicated the extent of decidualisation (G). Data are presented as mean ± SEM with statistical analysis using unpaired t-test, n=5-6 mice/group. MD; macrophage-depleted. P4; progesterone. Veh; vehicle control pellet. WT; wild type.

3.7 EFFECT OF MACROPHAGE DEPLETION AND HORMONE SUPPLEMENTATION ON PREGNANCY VIABILITY AT DAY 12.5 PC

As overt pregnancy viability was relatively improved in macrophage-depleted mice given P4 on day 9.5 pc, day 12.5 pc pregnancy outcomes were then assessed. Briefly, WT and CD11b-DTR females were mated to BALB/c stud males. Mice underwent insertion of P4 or vehicle control pellets subcutaneously on day 5.5 pc and concurrently were administered 25 ng/g DT. On day 9.5 pc, females were supplemented with an E2 or vehicle pellet.

3.7.1 PREGNANCY OUTCOMES

WT mice had distinct developing fetuses with growing placentas (Figure 3.11 A). In contrast, macrophage-depleted pregnancies tended to fail independent of hormone supplementation, either early, presenting as uterine scars (Figure 3.11 B), or late, presenting as resorptions (Figure 3.11 C).

The pregnancy viability rate was decreased in macrophage-depleted mice given vehicle pellets compared to WT controls (100% vs 22%, WT + H vs MD^{25} + Veh, $p<0.001$, Figure 3.11 D). The number of viable implantation sites decreased in macrophage-depleted mice given vehicle pellets (mean ± SEM, 9.6 ± 0.5 sites vs 0.9 ± 0.6 sites, $p<0.001$, Figure 3.11 E) whereas the number of uterine scars was increased compared to WT controls (0 scars vs 6.2 ± 1.3 scars, $p<0.001$, Figure 3.11 G). There was no change to the number of resorptions or total number of implantation sites (Figure 3.11 F and H).

Furthermore, macrophage-depleted mice given hormones had no viable pregnancies, thus the number of resorptions was increased compared to WT controls (0.4 ± 0.2 resorptions vs 7.4 ± 1.2 resorptions, WT + H vs MD^{25} + H, $p<0.001$, Figure 3.11 D-F). There was no difference in the number of uterine scars nor in the total number of implantation sites (Figure 3.11 G and H). Overall, pregnancy viability was impaired in macrophage-depleted mice, where mice without hormones were more susceptible to uterine scars, and mice with hormones were more commonly associated with resorptions (Figure 3.11 I).

This experiment confirms that uterine macrophages play critical roles in promoting pregnancy success, outside of the roles of ovarian macrophages. Furthermore, this suggests that macrophage-depletion and hormone supplementation rescues pregnancy viability beyond the early loss occurring in macrophage-depleted mice with vehicle control pellets, yet fails to fully account for the complex role of macrophages locally within the uterus.

Figure 3.11: Pregnancy fails in macrophage-depleted mice on day 12.5 pc independent of hormone supplementation.

WT and CD11b-DTR females were mated to BALB/c stud males and all mice were administered 25 ng/g DT on day 5.5 pc. On day 5.5 pc of pregnancy, two P4 (or vehicle) pellets were inserted to the s.c. region of the mid-dorsal area. On day 9.5 pc, an E2 (or vehicle) pellet was also inserted subcutaneously. Implantation sites from WT, macrophage-depleted + vehicle control and macrophage-depleted + hormone supplemented mice (A-C). Pregnancy outcomes were assessed on day 12.5 pc (D). The numbers of viable implantation sites, implantation site resorptions, uterine scars, and total number of sites were assessed (E-H). Individual mice were categorised into pregnancy viability rankings (I). Data are presented as mean ± SEM (E-H). Statistical analysis was performed using one-way ANOVA with Sidak's multiple comparisons test, except in D where a χ^2 test was used, n=5-11 mice/group. * indicates statistical significance ($p<0.05$) compared to WT controls; ***$p<0.001$ and ****$p<0.0001$. H; hormone-supplemented. MD; macrophage-depleted. Veh; vehicle control pellet. WT; wild type.

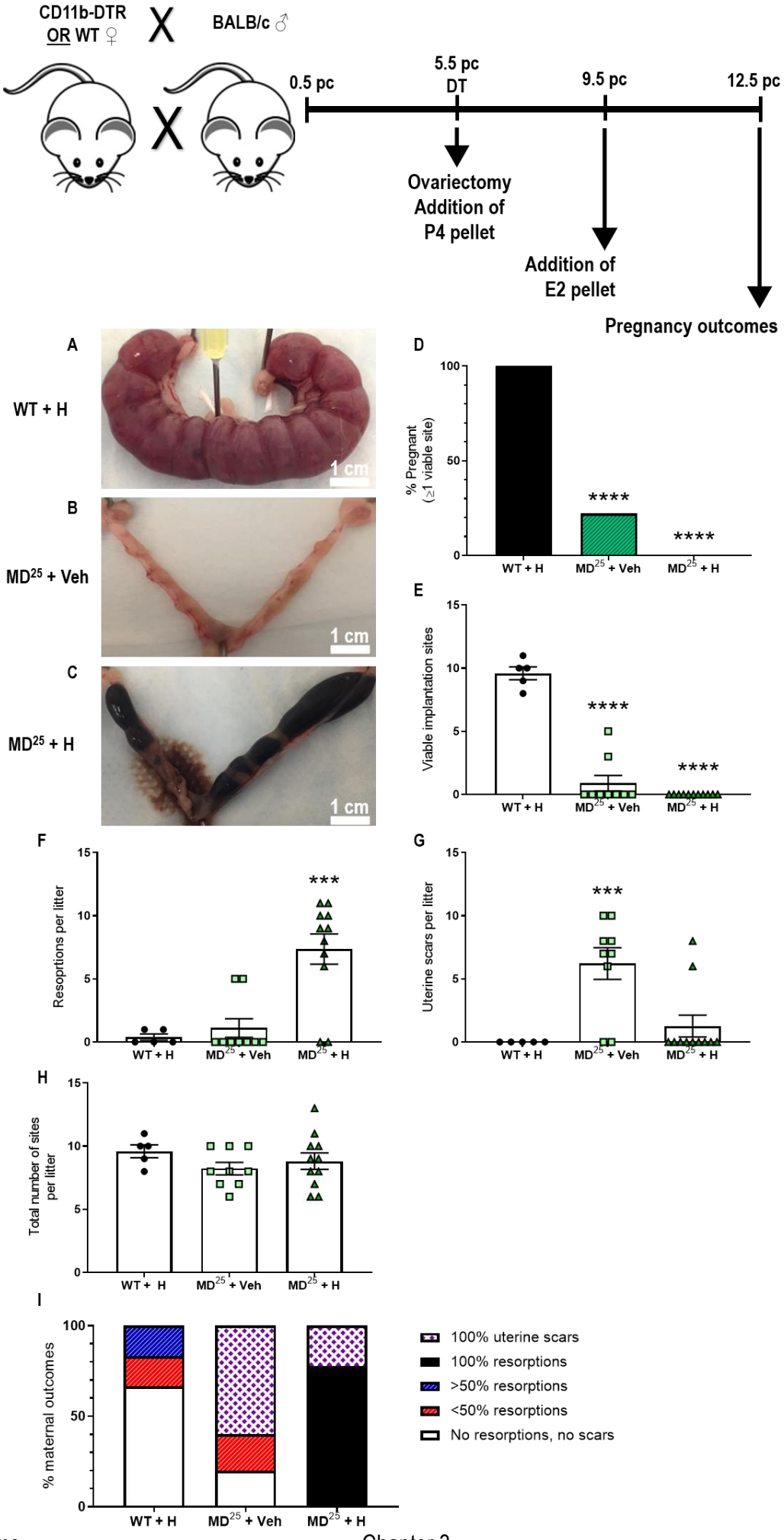
CD11b-DTR
OR WT ♀
X
BALB/c ♂
X
0.5 pc
5.5 pc
DT
9.5 pc
12.5 pc
Ovariectomy
Addition of
P4 pellet
Addition of
E2 pellet
Pregnancy outcomes
A
WT + H
1 cm
B
MD25 + Veh
1 cm
C
MD25 + H
1 cm
D
% Pregnant
(≥1 viable site)
100
50
0
****
****
WT + H
MD25 + Veh
MD25 + H
E
Viable implantation sites
15
10
5
0
****
****
WT + H
MD25 + Veh
MD25 + H
F
Resoprtions per litter
15
10
5
0
***
WT + H
MD25 + Veh
MD25 + H
G
Uterine scars per litter
15
10
5
0
***
WT + H
MD25 + Veh
MD25 + H
H
Total number of sites
per litter
15
10
5
0
WT + H
MD25 + Veh
MD25 + H
I
% maternal outcomes
100
50
0
WT + H
MD25 + Veh
MD25 + H
100% uterine scars
100% resorptions
>50% resorptions
<50% resorptions
No resorptions, no scars

3.8 EFFECT OF MACROPHAGE DEPLETION ON UTERINE VASCULAR REMODELLING

As pregnancy viability decreased from day 7.5 pc without P4 supplementation, and from 9.5 pc with P4 supplementation, it was evident that macrophage depletion caused impairment in other aspects of pregnancy progression aside from maintaining ovarian structure for hormone production. Therefore, vascular remodelling within the uterus was assessed during early to mid-pregnancy. Briefly, WT and CD11b-DTR females were mated to BALB/c stud males. Following this, mice received 25 ng/g DT on day 5.5 pc. For day 9.5 pc outcomes (but not day 7.5 pc outcomes), mice were concurrently given P4 or vehicle control pellets on day 5.5 pc.

3.8.1 UTERINE VASCULAR REMODELLING ON DAY 7.5 PC

To further investigate the defects in implantation site structure and decreased pregnancy viability, the extent of uterine artery remodelling within the mesometrial triangle was investigated on day 7.5 pc (Figure 3.12 A-D). On day 7.5 pc, vessel lumen area was decreased by 56% in macrophage-depleted females compared to WT controls (mean ± SEM, 308.7 ± 50.0 μm^2 vs 134.3 ± 24.6 μm^2, WT vs MD^{25}, p=0.023, Figure 3.12 E). Likewise, vessel diameter was decreased by 39% (23.5 ± 2.5 µm vs 14.4 ± 1.5 µm, p=0.021, Figure 3.12 F). The cross-sectional area trended toward being decreased (1335 ± 194 μm^2 vs 783 ± 143 μm^2, p=0.052, Figure 3.12 G), whereas the total area was decreased compared to WT controls (1706 ± 233 μm^2 vs 922 ± 157 μm^2, p=0.031, Figure 3.12 H). The total area to lumen area ratio was not different (Figure 3.12 I).

Figure 3.12: Macrophage depletion decreases lumen diameter in uterine mesometrial triangle vessels on day 7.5 pc.

WT and CD11b-DTR females were mated to BALB/c stud males and all mice were administered 25 ng/g DT on day 5.5 pc. H&E-stained sections in WT and macrophage-depleted females were used to assess uterine arteries on day 7.5 pc (A-B; scale bar is 1 mm and rectangle shows mesometrial triangle region). The mesometrial triangle region is shown in (C and D; scale bar is 100 μm and black arrows show arteries). Vessel parameters were calculated including vessel lumen area (E), vessel diameter (F), vessel cross-sectional area (G), total vessel area (H), and the ratio of total vessel size to lumen ratio (I). Data are presented as mean ± SEM with statistical analysis using unpaired t-test, n=6-10 mice/group. * indicates statistical significance ($p<0.05$) compared to WT controls; *$p<0.05$. MD; macrophage-depleted. WT; wild type.

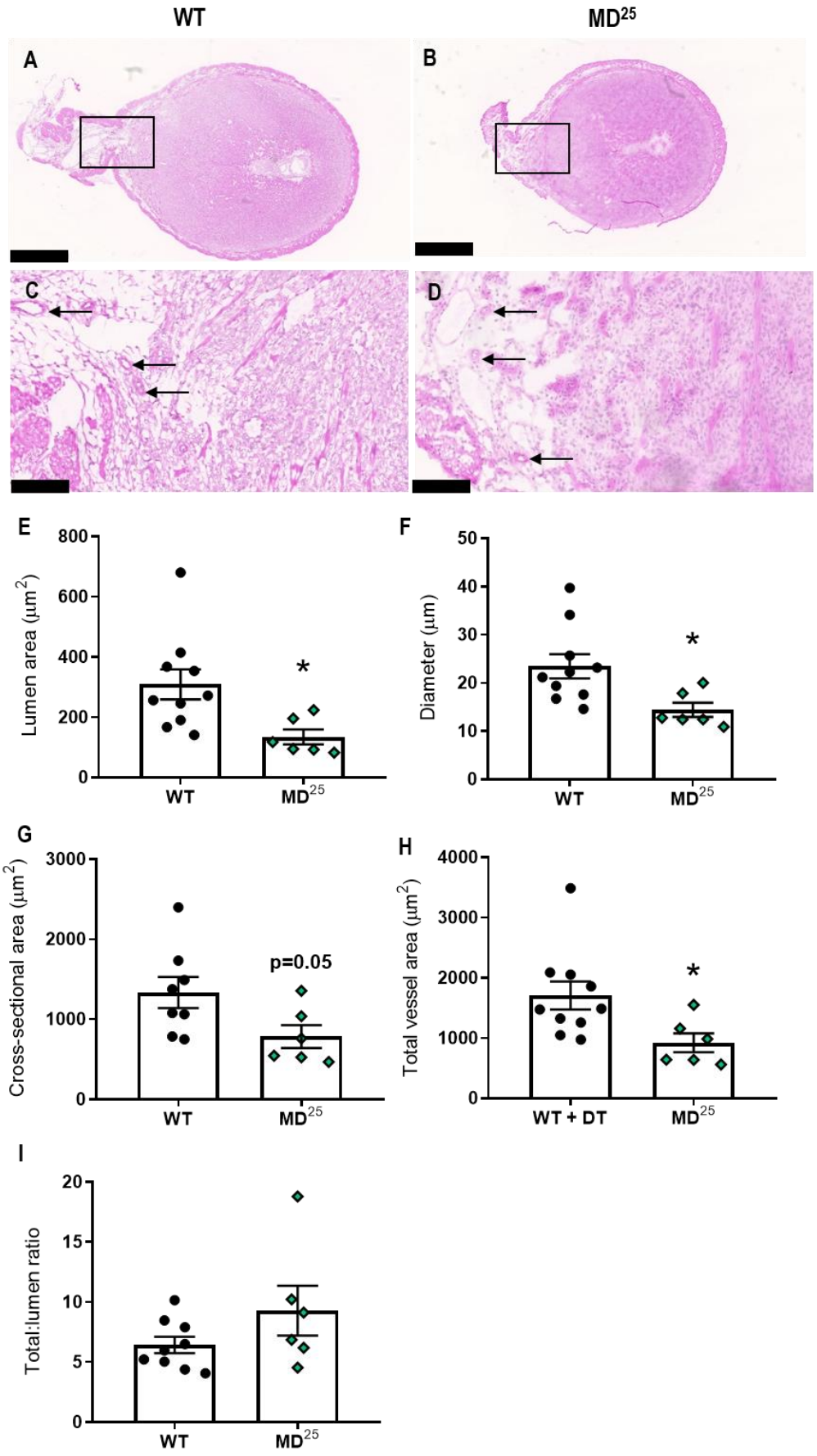
WT
MD25
A
B
C
D
E
Lumen area (μm2)
800
600
400
200
0
*
WT
MD25
F
Diameter (μm)
50
40
30
20
10
0
*
WT
MD25
G
Cross-sectional area (μm2)
3000
2000
1000
0
p=0.05
WT
MD25
H
Total vessel area (μm2)
4000
3000
2000
1000
0
*
WT + DT
MD25
I
Total:lumen ratio
20
15
10
5
0
WT
MD25

3.8.2 UTERINE VASCULAR REMODELLING ON DAY 9.5 PC

Vessel parameters in the mesometrial triangle region of day 9.5 pc implantation sites were also assessed (Figure 3.13 A-F). Importantly, macrophage-depleted mice given the vehicle pellet only yielded one viable pregnancy, and so data are not presented for this group. Nonetheless, vessel lumen area was decreased by 70% in macrophage-depleted mice given P4 compared to WT controls (mean ± SEM, 628.9 ± 81.4 μm^2 vs 186.3 ± 70.6 μm^2, WT vs MD^{25} + P4, p=0.003, Figure 3.13 G). Furthermore, lumen diameter was decreased by 52% (30.5 ± 2.2 µm vs 14.5 ± 2.4 µm, p<0.001, Figure 3.13 H). The vessel cross-sectional area was decreased by 56% (1262 ± 154 μm^2 vs 557 ± 113 μm^2, p=0.006, Figure 3.13 I) and the total area of the vessel was also decreased by 61% compared to WT controls (1891 ± 205 μm^2 vs 733 ± 149 μm^2, p=0.001, Figure 3.13 J). The total vessel area to lumen area ratio was increased by 50% (3.27 ± 0.24 vs 6.64 ± 1.12, p=0.011, Figure 3.13 K).

These experiments indicate that macrophages may be involved in vascular remodelling required for pregnancy success during the peri-implantation phase. Importantly, a deficiency of macrophages is associated with impaired vascular remodelling events within the murine uterus, independent of P4 supplementation.

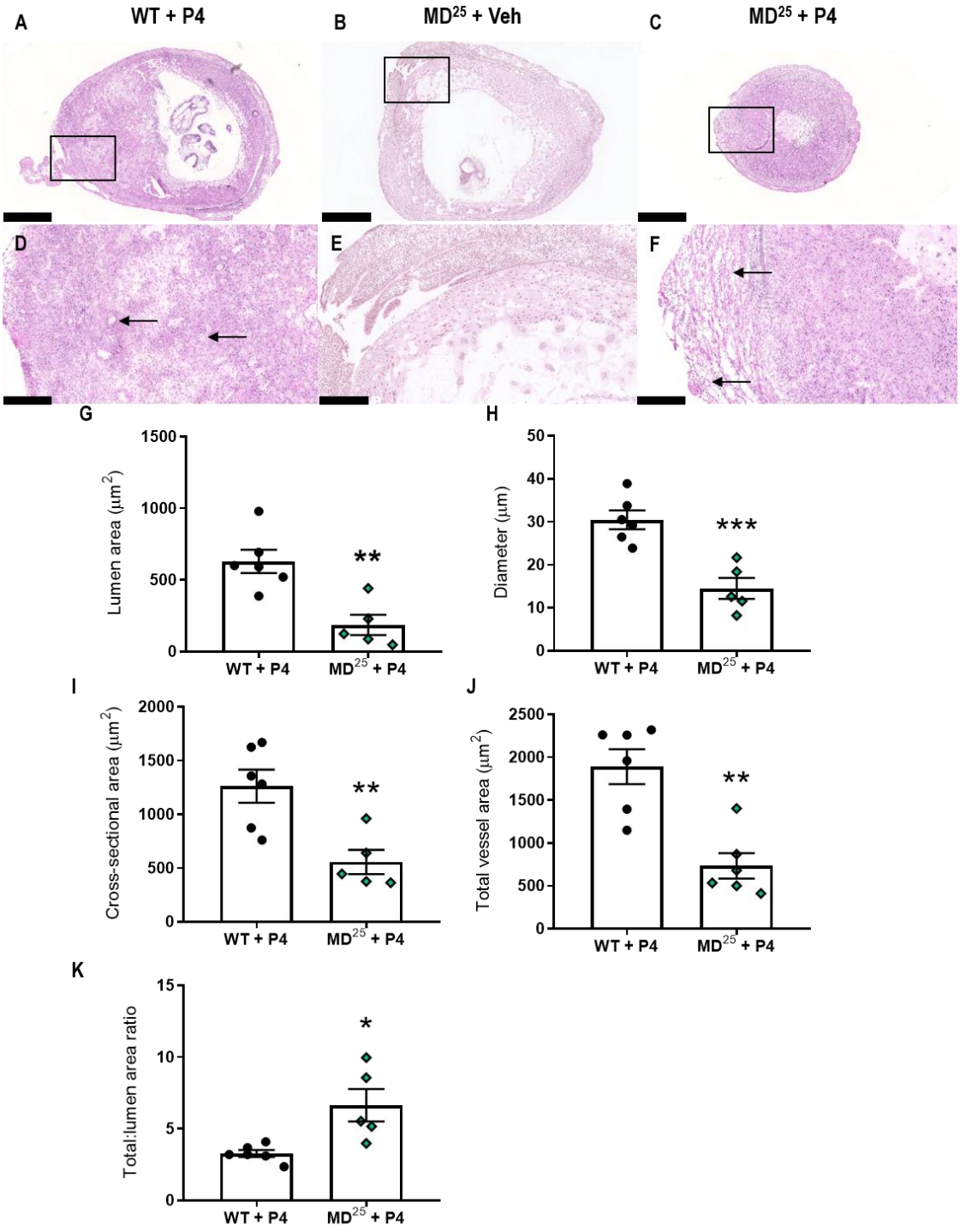

Figure 3.13: Macrophage-depleted mice given P4 have impaired uterine vascular remodelling on day 9.5 pc.

WT and CD11b-DTR females were mated to BALB/c stud males and all mice were administered 25 ng/g DT on day 5.5 pc. On day 5.5 pc, two P4 (or vehicle) pellets were inserted to the s.c. region of the mid-dorsal area. H&E stained sections were used to assess arteries (A-C, scale bar equal 1 mm and rectangle shows mesometrial region). Vessels parameters were assessed within the mesometrial triangle (D-F, scale bar equals 250 µm and black arrows indicate arteries). These parameters included vessel lumen area (G), vessel diameter (H), vessel cross-sectional area (I), total vessel area (J), and the ratio of total vessel size to lumen ratio (K). Data are presented as mean ± SEM with statistical analysis using unpaired t-test, n=5-6 mice/group. * indicates statistical significance ($p<0.05$) compared to WT controls; *$p<0.05$, **$p<0.01$, and ***$p<0.001$. MD; macrophage-depleted. P4; progesterone. WT; wild type.

3.9 DISCUSSION

The data presented in this chapter demonstrate an essential role for macrophages during the peri-implantation phase of murine pregnancy. Using the CD11b-DTR murine model, we systemically depleted macrophages from day 5.5 pc using 25 ng/g DT. Whilst there was some depletion of $CD11b^+$ granulocytes in the uterus in addition to macrophage depletion, many studies in CD11b-DTR mice have reported this, and these previous studies have emphasised these impacts to be minimal, and these impacts have generally not accounted for the observed impact on physiology. Particularly, the numbers of neutrophils and dendritic cells remain largely unaffected in these previous studies (Care et al., 2014, Care et al., 2013). Our data indicate that the depletion of macrophages caused corpus luteum defects and reduced serum P4. Furthermore, hormone supplementation was insufficient to retain viable pregnancy in macrophage-depleted mice. In addition, pregnancy viability was decreased to the same extent in allogeneic and syngeneic matings. Importantly, there was an impairment to uterine vascular remodelling from day 7.5 pc in macrophage-depleted mice.

3.9.1 MACROPHAGE DEPLETION RESULTS IN CORPUS LUTEUM DEFECTS

Depletion of macrophages elicited ovarian haemorrhage. This result was expected as ovarian lesions in the CD11b-DTR model have been well characterised following macrophage depletion (Care et al., 2013, Turner et al., 2011). It is interesting to note that our data add to the previously reported findings by showing that macrophages remain essential for corpus luteum structure even after embryo implantation commences. This result was unexpected as we might have predicted that corpus luteum development would be completed by this time. However, it was surprising to discover that macrophages still remain essential for corpus luteum structure and vascular integrity beyond day 5.5 pc.

A major hormone produced by the ovarian luteal cells is P4. Our data show that macrophage depletion resulted in reduced serum P4 concentrations which was associated with reduced decidualisation within the implantation sites. Importantly, P4 induces decidualisation which generates a modified lining of the endometrium to allow embryo implantation (Milligan and Finn, 1997). Here, decidual cells facilitate tissue and vascular remodelling and support ongoing development of the fetus and its placenta. In the current study, a decrease in the conceptus area was also observed after macrophage depletion, which indicates compromised embryo development that may be caused by impaired decidualisation. Thus, the structural demise in the ovaries post-macrophage depletion was associated with sustained structural defects in the developing implantation sites. This indicates that ovarian macrophages are required to maintain corpus luteum structure which may act to sustain pregnancy viability through P4 production. The direct cause and effect of these pathways remains to be investigated.

3.9.2 HORMONE SUPPLEMENTATION FAILS TO RESCUE PREGNANCY IN MACROPHAGE-DEPLETED MICE

Given that serum P4 concentration decreased, it was important to assess the extent to which macrophage depletion in the ovaries could be reversed through restoring serum P4 concentrations. We predicted that if macrophages have essential roles in the uterus as well as the ovary, P4 would only partly rescue the effect of macrophage depletion. To do this, we developed a hormone supplementation regime and found that P4 alone was insufficient to maintain pregnancy in ovariectomised females (Appendix 9.4). Therefore, we supplemented ovariectomised mice with E2 in conjunction with P4 (Milligan and Finn, 1997). The hormone supplementation protocol was also applied to mice with intact ovaries to ensure no adverse impact of exogenous hormones (Appendix 9.5). This resulted in viable pregnancies in ovariectomised WT females but importantly, did not rescue outcomes in ovariectomised, macrophage-depleted mice.

Most macrophage-depleted mice given hormones exhibited resorptions at day 17.5 pc, an indication that decidualisation and implantation had occurred, but embryo viability was not sustained to late gestation. In contrast, macrophage-depleted females without exogenous hormones presented with uterine scars, indicating early loss. This suggests that whilst hormone supplementation was insufficient to completely rescue pregnancy, it did allow pregnancy to progress further than would have been possible without exogenous hormones. This implies that corpus luteum demise was not the sole cause of pregnancy failure in macrophage-depleted mice. These results therefore suggest that uterine macrophages may also be required to support pregnancy success.

On day 9.5 pc, P4 supplementation in macrophage-depleted mice could rescue decidualisation but embryo development had ceased. This led to pregnancy failure by day 12.5 pc, independent of hormone supplementation. Without P4, pregnancy failed in macrophage-depleted mice from as early as day 7.5 pc with uterine scars apparent from mid-gestation. Interestingly, there appears to be some macrophage-depleted mice with viable pregnancies on day 7.5 pc. This may suggest that some mice are slightly more resistant to the effects of macrophage depletion and manage to retain a viable pregnancy at day 7.5 pc. However, these viable implantation sites still have impaired vascular remodelling and decreased decidualisation. It is likely that decidualisation fails in mice with low P4 concentrations and embryonic development ceases either due to this failed decidualisation and/or other mechanisms involving poor adaptation to pregnancy. Another aspect to consider is that macrophage depletion may impair trophoblast invasion into the decidua, independent to the effects of failed decidualisation or reduced P4. Herein, macrophage depletion may create an unfavourable environment for trophoblast invasion and/or an unreceptive decidua. Again, the precise cause and effect still needs comprehensive interrogation. Having confirmed that hormone supplementation was insufficient to account for pregnancy failure, we next sought to assess whether pregnancy failure could be attributable to loss of immune tolerance to the semi-

allogeneic fetus. Notably, impaired decidualisation has been reported to be associated with FGR and is directly related to impaired immune tolerance in women (Dunk et al., 2019).

3.9.3 PREGNANCY FAILS INDEPENDENT OF FETAL-MATERNAL MHC DISPARITY

As the immune response in pregnancy is complex, we sought to assess how macrophages were contributing to immune tolerance, which is essential for allogeneic but not syngeneic pregnancy. Macrophages are involved in immune tolerance and are also essential to clear apoptotic trophoblast cells, which if not cleared, can release foreign antigens into the maternal circulation resulting in recognition by the immune system to cause effector immunity and promote fetal rejection (Abrahams et al., 2004). Our hypothesis remained that if the depletion of macrophages acted to cause a failure in immune tolerance, then when MHC antigens were not disparate there would be a lesser degree of pregnancy loss. However, our results indicated that pregnancy failure occurred to a similar degree in syngeneic matings and allogeneic matings when macrophages were depleted, independent of hormone supplementation. Thus, while macrophages may contribute to promoting immune tolerance in the first few days after coitus, they appear unnecessary to maintain immune tolerance after day 5.5 pc. Instead they seem more likely to influence pregnancy outcome through roles in uterine tissue and/or vascular remodelling (Ning et al., 2016).

Interestingly, WT syngeneic pregnancies were more prone to resorptions compared to WT allogeneic pregnancies. This suggested that without MHC disparity, pregnancy viability was compromised. One potential mechanism is via a failure to generate enough Treg cells and/or NK cells to promote tissue and vascular remodelling (Aluvihare et al., 2004).

3.9.4 VASCULAR REMODELLING DEFECTS CORRELATE WITH PREGNANCY FAILURE

In order to interrogate the possible causes of pregnancy failure, implantation site vascular parameters were assessed. During pregnancy, uterine arteries undergo extensive remodelling and directly interact with the developing placenta (Osol and Mandala, 2009b, Adamson et al., 2002). Importantly, vascular remodelling is crucial for pregnancy success, as main uterine arteries can expand to become 10 to 100-fold larger than uterine arteries in non-pregnant mice (Mandala and Osol, 2012). Our data show that macrophage depletion led to smaller uterine arteries with smaller diameters in the mesometrial triangle region. In women, failed vascular adaptation to pregnancy has been linked with pregnancy complications including PE, FGR, and recurrent miscarriage (Lyall et al., 2013, Lecarpentier and Tsatsaris, 2016, Saito and Nakashima, 2014). This highlights the importance of understanding vascular remodelling events occurring in early pregnancy, as the mechanisms behind pregnancy failure likely originate during this period.

The uterine arteries in the mesometrial triangle from macrophage-depleted mice were smaller in total, cross-sectional and lumen areas. Furthermore, these vessels also had an increase in total to lumen area

ratio, a proxy measure of vessel remodelling status. These vascular changes were not observed on day 6.5 pc (Appendix 9.7). In pregnancy, outward hypertrophic remodelling is observed which allows arteries to become large diameter and low resistance vessels to accommodate sufficient nutrient delivery to the fetus without damaging the developing placenta (Mandala and Osol, 2012). Our data imply inward hypotrophic remodelling in macrophage-depleted mice which indicates vessels are not adapting to the demands of pregnancy and blood flow is likely decreased (Osol and Mandala, 2009b). A follow-up study investigating blood velocity and pulsitility using Doppler ultrasound would further confirm impaired vascular function in macrophage-depleted mice. Furthermore, further immunohistochemical staining of the blood vessels in these implantation sites may help to identify any differences in blood vessel density.

Whilst implantation sites from macrophage-depleted mice given P4 appeared to progress further than implantation sites from macrophage-depleted mice without exogenous hormones, it was clear that pregnancy success was not improved by hormone administration as embryos still appeared non-viable in both groups. Furthermore, vascular remodelling was also impaired in P4-supplemented macrophage-depleted mice on day 9.5 pc. This, in addition to the changes in vascular structure, points to a requirement for macrophages in mediating uterine vascular remodelling.

Overall, the results in this chapter demonstrate that macrophage depletion impairs pregnancy success. The data imply that not only ovarian macrophages, but also uterine macrophages contribute to establishing pregnancy. The requirement of uterine macrophages to facilitate pregnancy success occurs independent of corpora lutea integrity, P4 supplementation, and MHC disparity. This raises the question of the specific mechanisms by which uterine macrophages act within the uterus to facilitate pregnancy success, yet our data clearly point to mechanisms involving vascular remodelling. Also, whilst macrophage depletion using 25 ng/g DT was extensive and caused >90% pregnancy failure, a question of interest remained whether smaller reductions in macrophage numbers may also alter pregnancy outcomes, and perhaps provide a more physiologically relevant model. This is addressed in chapter four.

CHAPTER 4

EFFECT OF LOW-DOSE DT TREATMENT IN THE PERI-IMPLANTATION PHASE ON FETAL AND PLACENTAL GROWTH AND DEVELOPMENT

4.1 INTRODUCTION

During early pregnancy, substantial maternal vascular remodelling is required to support appropriate placentation and allow it to deliver nutrients and remove waste material in order to accommodate the demands of the developing fetus. The placenta is a unique organ where it develops during pregnancy and is only needed for approximately 40 weeks in humans or two weeks in mice. A key feature of the placenta is that the maternal and fetal circulatory systems must interdigitate in a complete capillary network to facilitate maternal-fetal exchange activity. To accommodate optimal placental development, uterine vessels must be remodelled to reduce resistance and expand in capacity. Under-perfused placentas and failure to remodel uterine arteries are linked with preeclampsia (PE) and fetal growth restriction (FGR) in women (Lyall et al., 2013).

Placental development in humans and mice is similar where both species undergo hemochorial placental development (Georgiades et al., 2002). Specifically, the human placenta is defined as villous and haemomonochorial; whereas the murine placenta is defined as labyrinthine and haemotrichorial (Burton et al., 2016). Importantly, by the end of the first trimester in women, fetal extravillous trophoblast cells (EVTs) have invaded and remodelled maternal spiral arteries allowing a constant flow of maternal blood to the placenta at low velocity and pressure so as to not crush fetal capillaries (Burton et al., 2009). This process is similar in mice; however, murine trophoblast giant cells (TGCs) do not invade uterine arteries to the same extent. The mouse can therefore be used as an information model of uterine vascular adaptation for placental development.

The murine placenta is divided into two distinct zones, the junctional zone (JZ) and the labyrinth zone (LZ). The JZ, or endocrine zone, is responsible for synthesis of hormones and the development of glycogen cells (GCs). GCs act as an energy reserve for the fetus just prior to delivery. Within the mouse, maternal spiral arteries traverse the JZ to deliver blood to the LZ, or exchange zone. Herein, maternal and fetal circulatory systems facilitate exchange of nutrients for waste to promote fetal growth. Failure to adequately vascularise the LZ results in poor nutrient delivery and pregnancy complications (Pardi et al., 2002).

Previous studies have highlighted the relationship between poor uterine vascular remodelling and pregnancy complications in women (Boeldt and Bird, 2017). Animal models have been utilised to recapitulate these conditions. For example, uterine artery ligation during late pregnancy can cause poor blood flow, which can lead to the development of pregnancy complications (Wigglesworth, 1974, Janot et al., 2014). Understanding the mechanisms of early vascular remodelling is therefore crucial for developing preventative treatments and diagnostics for pregnancy complications.

Immune cells have been implicated in vascularisation and angiogenesis in various diseases, but their contributions to uterine vascular remodelling in pregnancy are incompletely understood. Uterine natural

killer (uNK) cells are well-recognised drivers of decidual spiral artery remodelling (Moffett-King, 2002). Larger numbers of uNK cells are situated in the maternal decidua from the beginning of implantation and have an intimate relationship with trophoblast cells and the endothelial cells of the maternal spiral arteries (Robson et al., 2012, Kieckbusch et al., 2014). Whilst the presence of uNK cells facilitates spiral artery remodelling, their absence in murine models does not result in complete pregnancy failure, highlighting a more complex mechanism (Guimond et al., 1997b). Furthermore, the role of macrophages in promoting uterine vascular remodelling remains unclear. Reduced numbers of macrophages or aberrant macrophage phenotypes has been linked with pregnancy complications in women (Faas et al., 2014). In addition, macrophages have been implicated in processes of vascularisation and angiogenesis within tumours and appear to be essential for tumour survival and growth (Condeelis and Pollard, 2006). Macrophage depletion in murine models of cancer results in inhibition of tumour growth and decreased vascularisation (De Palma and Lewis, 2013).

Interestingly, tumour and embryonic tissues have similar properties (Mor et al., 2017). The cells of both tissues will seek to adhere to extracellular matrix (ECM) surfaces and then begin to invade this surface as a means of anchorage or implantation. This invasive behaviour can initiate a cascade of events including recruitment of other immune cell lineages. From here, immune cells can be programmed by the invading mass to facilitate vascularisation. The microenvironment formed by the invading mass and recruited immune cells is dynamic and responds to intercellular signalling cues. By considering the concepts of cancer and pregnancy in conjunction, knowledge from both fields can guide research.

The experiments in this chapter sought to investigate the role of macrophages in facilitating maternal vascular adaptation to pregnancy through promoting uterine vascular remodelling and placental development. These experiments utilise low-dose DT treatment in the CD11b-DTR mouse model to partially deplete macrophages. This partial depletion strategy was used to mimic a more physiologically relevant reduction in macrophage numbers, rather than near-complete depletion shown in chapter three, to understand whether a moderate manipulation of macrophage numbers can result in the development of placental dysfunction and FGR.

4.2 DT DOSE RESPONSE ON PREGNANCY VIABILITY

In order to investigate the effect of reduced macrophage numbers during pregnancy, we utilised the CD11b-DTR model to titrate the dose of DT and investigate how manipulation of macrophage numbers may achieve different biological outcomes. Briefly, WT and CD11b-DTR females were mated to BALB/c stud males and on day 5.5 pc of pregnancy DT was administered to CD11b-DTR mice at either 5 ng/g (MD^5), 10 ng/g (MD^{10}) or 25 ng/g (MD^{25}). A control group of WT mice received 25 ng/g DT throughout. A selection of the relevant data on control and MD^{25} groups from chapter three is included for comparison purposes.

In early pregnancy, day 7.5 pc, females given 5 ng/g DT (MD^5) remained pregnant in all cases whereas MD^{10} females had viable pregnancies in 73% of cases (100% vs 73%, WT vs MD^{10}, $p<0.001$, Figure 4.1 A). In contrast, only 43% of females given 25 ng/g DT (MD^{25}) had viable pregnancies (100% vs 43%, WT vs MD^{25}, $p<0.001$, Figure 4.1 A). The number of viable implantation sites was reduced in the MD^{25} group compared to WT controls (mean ± SEM, 9.3 ± 0.6 sites vs 3.4 ± 1.4 sites, $p<0.001$, Figure 4.1 B).

In mid-gestation, on day 9.5 pc, all CD11b-DTR females given 5 ng/g DT remained pregnant, however there was a 50% reduction in viable pregnancy rate in MD^{10} mice compared to WT controls (100% vs 50%, WT vs MD^{10}, $p<0.001$, Figure 4.1 C). This compared to an 89% reduction in viable pregnancy rate in MD^{25} mice compared to WT controls (100% vs 11%, WT vs MD^{25}, $p<0.001$, Figure 4.1 C). There was a trend towards reduced numbers of viable implantation sites in MD^{10} mice compared to WT controls (mean ± SEM, 7.9 ± 0.7 sites vs 4.5 ± 1.3 sites, WT vs MD^{10}, $p=0.078$, Figure 4.1 D). In addition, the number of viable implantation sites was reduced in MD^{25} mice compared to WT controls (mean ± SEM, 7.9 ± 0.7 sites vs 0.9 ± 0.9 sites, WT vs MD^{25}, $p<0.001$, Figure 4.1 D).

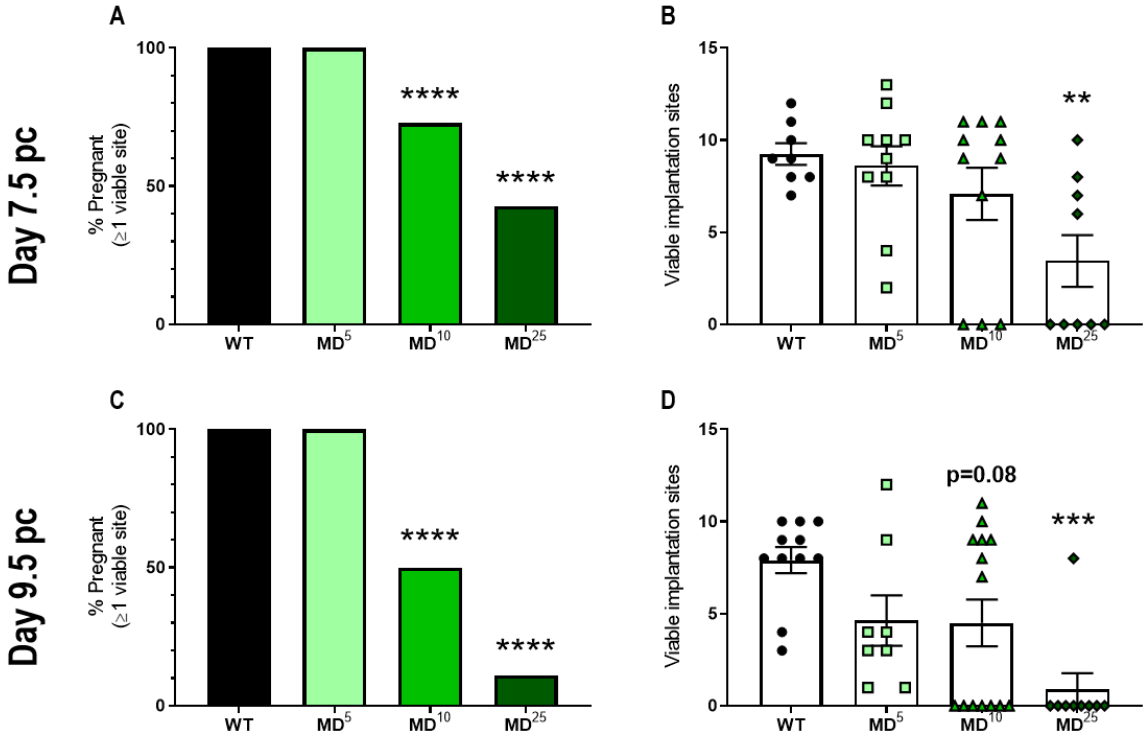

Figure 4.1: Increasing DT dose reduces pregnancy viability at early and mid-gestation.
WT and CD11b-DTR females were mated to BALB/c stud males and on day 5.5 pc of pregnancy, DT was administered at either 5 ng/g (MD^5), 10 ng/g (MD^{10}) or 25 ng/g (MD^{25}). WT mice also received 25 ng/g DT on day 5.5 pc. Pregnancy viability rate was assessed on days 7.5 pc (A) and 9.5 pc (C). The number of viable implantation sites on days 7.5 pc (B) and 9.5 pc (D) were also assessed. Data are presented as mean ± SEM. Statistical analysis was performed using one-way ANOVA with Sidak's multiple comparisons test, except in A and C where a χ^2 test was used, n=8-14 mice/group. * indicates statistical significance ($p<0.05$) compared to WT controls; **$p<0.01$, ***$p<0.001$, and ****$p<0.0001$. MD; macrophage-depleted. WT; wild type.

4.2 EFFECT OF LOW-DOSE DT TREATMENT IN CD11b-DTR MICE

Previous results described in chapter three of this thesis have shown that near-complete macrophage depletion using 25 ng/g DT during the peri-implantation phase of pregnancy elicited pregnancy failure independent of effects on P4 synthesis in the ovary and effects of fetal-maternal MHC disparity. These results implicate macrophages as having a critical role in the uterus during this period. Given that a dose-dependent response to titrated doses of DT was observed on day 7.5 and day 9.5 pc, we next sought to understand how moderate depletion of macrophages during the peri-implantation phase may impact late gestation outcomes by using lower doses of DT administered to CD11b-DTR females. We postulated that pregnancy might progress further yet lead to FGR or other adverse outcomes.

Importantly, administration of either 5 ng/g or 10 ng/g DT to CD11b-DTR mice had no impact on the concentration of P4 on day 7.5 pc, however administration of 25 ng/g DT to CD11b-DTR mice reduced serum P4 compared to WT controls (Table 4.1). For this reason, we continued to investigate the effects of low-dose DT treatment on pregnancy outcomes in CD11b-DTR females without P4 replacement.

Table 4.1: Serum P4 concentration is not changed on day 7.5 pc with low-dose DT administration.

	WT	MD^5	MD^{10}	MD^{25}
Serum P4 (ng/ml)	52.4 ± 4.1	36.8 ± 14.2	39.0 ± 11.3	14.3 ± 2.2*

Data are presented as mean ± SEM with statistical analysis using a one-way ANOVA with Sidak's multiple comparison test. * indicates statistical significance ($p<0.05$) for WT vs MD^{25}, n=5-11 dams/group.

4.2.1 PREGNANCY OUTCOMES

All CD11b-DTR females given 5 ng/g DT (MD^5) remained pregnant on day 17.5 pc (Figure 4.2 A). However, there was a reduction in the average number of viable fetuses compared to WT controls (mean ± SEM, 8.9 ± 0.4 fetuses vs 5.2 ± 1.1 fetuses, WT vs MD^5, p=0.009, Figure 4.2 B). Furthermore, there was an increase in the number of resorptions on day 17.5 pc (0.4 ± 0.1 resorptions vs 2.3 ± 0.8 resorptions, p=0.015, Figure 4.2 C). Females in the MD^5 group were more susceptible to resorptions with nearly 80% of females carrying at least one resorption (Figure 4.2 F). In addition, over 30% of CD11b-DTR females given 5 ng/g DT had greater than 50% resorptions (Figure 4.2 F).

In CD11b-DTR females given 10 ng/g DT (MD^{10}), 43% fewer mice remained pregnant at day 17.5 pc compared to WT controls (100% vs 57%, WT vs MD^{10}, $p<0.001$, Figure 4.2 A). There was also a reduction in the number of viable fetuses (mean ± SEM, 8.9 ± 0.4 fetuses vs 4.3 ± 0.9 fetuses, $p<0.001$, Figure 4.2 B). There was a trend toward an increase in the number of resorptions (0.4 ± 0.1 resorptions vs 1.6 ± 0.5 resorptions, p=0.09, Figure 4.2 C). Over 40% of MD^{10} females had early pregnancy loss, evidenced as

uterine scars, the incidence of which was increased (0 scars vs 3.3 ± 0.6 scars, $p<0.001$, Figure 4.2 D and F). Overall, there was no change to the total number of implantation sites (Figure 4.2 E).

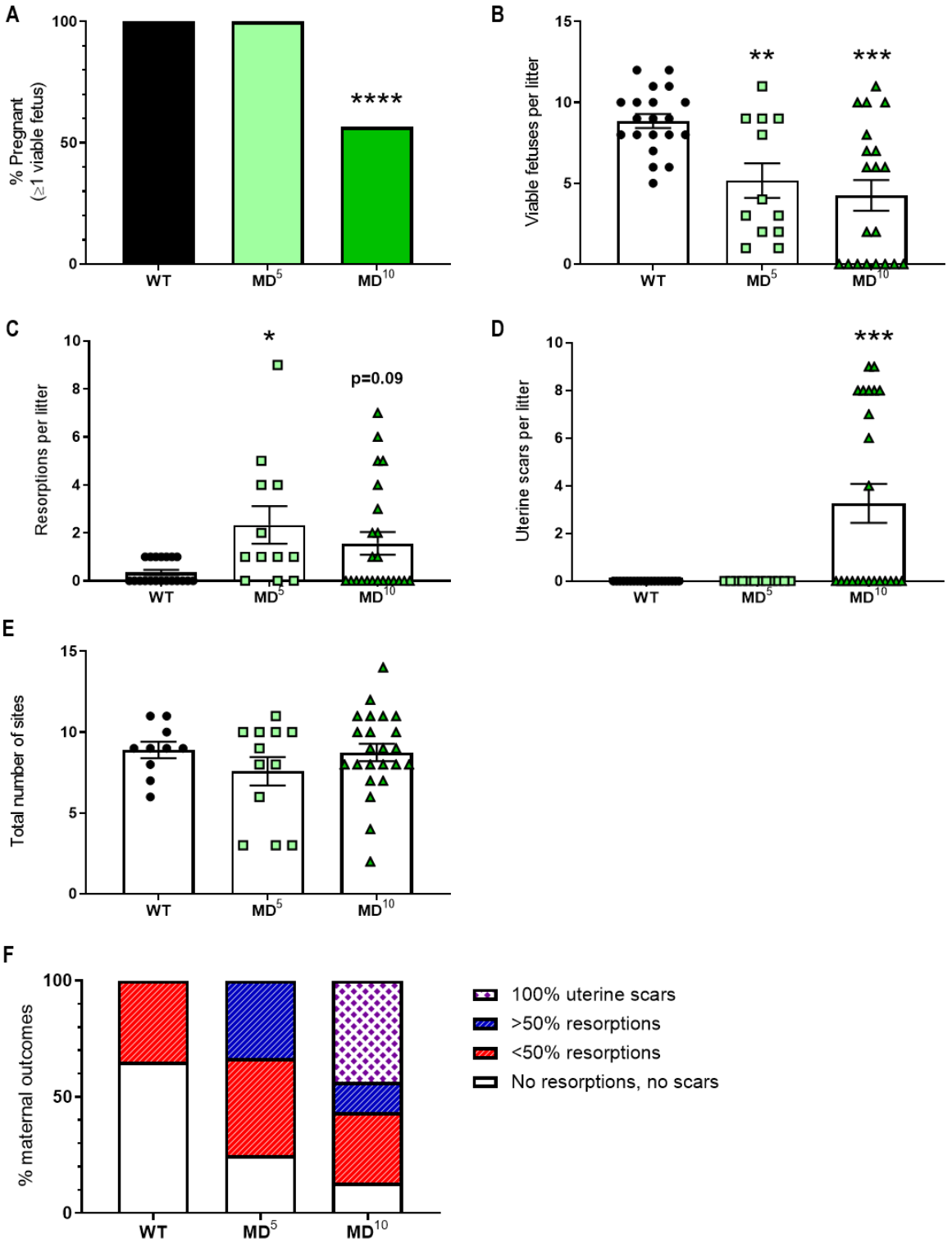

Figure 4.2: Low-dose DT administration causes a reduction in viable pups on day 17.5 pc.
WT and CD11b-DTR females were mated to BALB/c stud males. On day 5.5 pc, DT was administered at either 5 ng/g or 10 ng/g to CD11b-DTR mice and WT mice received DT at 25 ng/g. Pregnancy outcomes were then assessed on day 17.5 pc (A). The number of viable pups (B), implantation site resorptions (C), uterine scars (D), and total number of implantation sites were assessed (E). The pregnancies from each group were categorised into viability rankings (F). Data are presented as mean ± SEM (B-E). Statistical analysis was performed using one-way ANOVA with Sidak's multiple comparisons test, except in A where a χ^2 test was used, n=10-21 mice/group. * indicates statistical significance ($p<0.05$) compared to WT controls; *$p<0.05$, **$p<0.01$, ***$p<0.001$, and ****$p<0.0001$. MD; macrophage-depleted. WT; wild type.

4.2.2 FETAL OUTCOMES

On day 17.5 pc, fetuses from CD11b-DTR mice treated with 5 ng/g DT were 11% smaller than WT controls (estimated marginal means ± SEM, 1034 ± 11 mg vs 916 ± 18 mg, WT vs MD^5, $p<0.001$, Figure 4.3 A). Similarly, fetuses from CD11b-DTR mice given 10 ng/g DT were 4% smaller compared to WT controls (1034 ± 11 mg vs 990 ± 15 mg, WT vs MD^{10}, $p=0.047$, Figure 4.3 A). Unexpectedly, fetuses from CD11b-DTR mice given 5 ng/g DT were 7% smaller than fetuses from CD11b-DTR mice given 10 ng/g DT (916 ± 18mg vs 990 ± 15 mg, MD^5 vs MD^{10}, $p=0.006$, Figure 4.3 A).

Placental weights were not affected in CD11b-DTR mice treated with either 5 ng/g DT or 10 ng/g DT (Figure 4.3 B). As fetal weight was reduced and placental weight remained unchanged, there was a reduction in the fetal to placental weight ratio in both CD11b-DTR treatment groups compared to WT controls (11.5 ± 0.1 vs 10.5 ± 0.2 vs 10.9 ± 0.2, WT vs MD^5 vs MD^{10}, $p=0.002$ for WT vs MD^5 & $p=0.047$ for WT vs MD^{10}, Figure 4.3 C).

These data show that titration of DT dose in CD11b-DTR mice elicits varying impacts on pregnancy viability and fetal growth during late gestation.

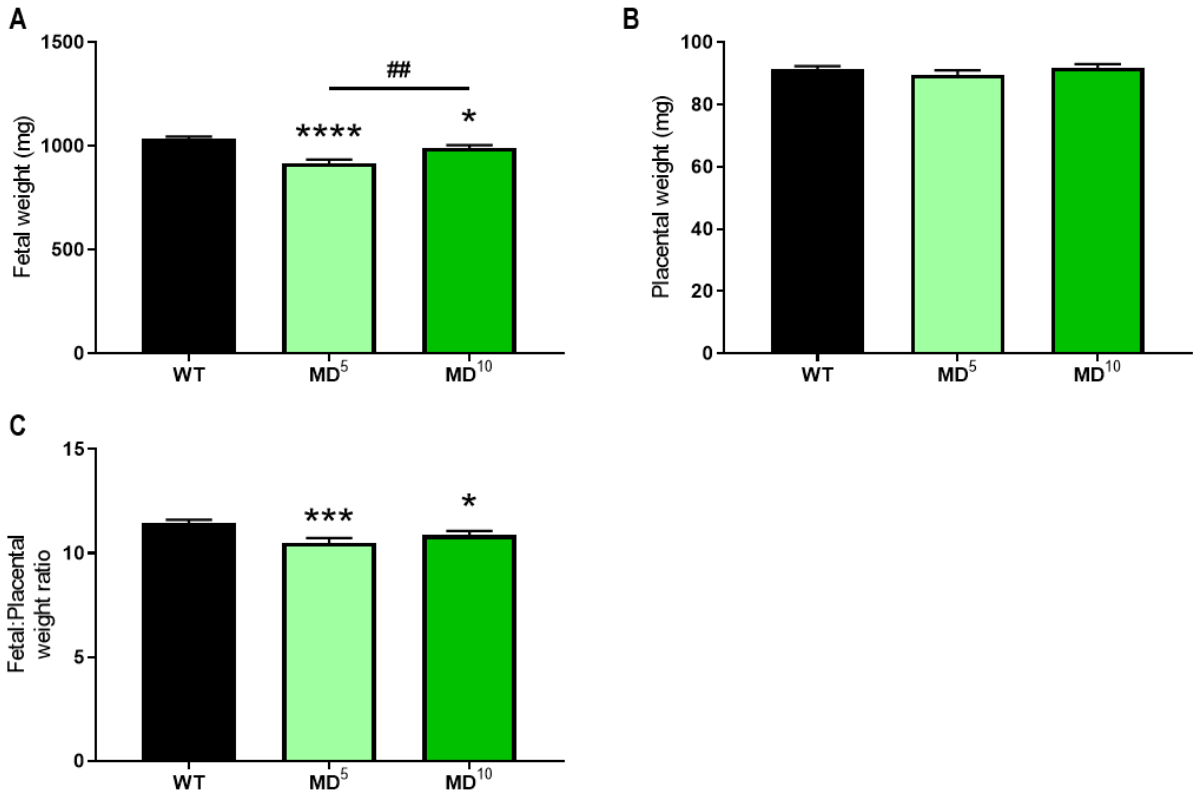

Figure 4.3: Low-dose DT administration causes fetal growth restriction at day 17.5 pc.
WT and CD11b-DTR females were mated to BALB/c stud males. On day 5.5 pc, DT was administered at either 5 ng/g or 10 ng/g to CD11b-DTR mice and WT mice received DT at 25 ng/g. Fetal weight (A), placental weight (B), and fetal to placental weight ratio (C) were all measured on day 17.5 pc. Data are presented as estimated marginal mean ± SEM, where a mixed-model analysis was performed to calculate estimated marginal means using total number of viable sites per litter as the co-variate. Statistical analysis was performed using one-way ANOVA with Sidak's multiple comparisons test, n=10-21 mice/group. * indicates statistical significance ($p<0.05$) compared to WT controls; *$p<0.05$, ***$p<0.001$, and ****$p<0.0001$. # indicates statistical significance ($p<0.05$) compared to MD^5; ## $p<0.01$. MD; macrophage-depleted. WT; wild type.

4.3 EFFICIENCY OF LOW DT DOSE TO DEPLETE MACROPHAGES IN CD11b-DTR MICE

After confirming that titration of DT dose resulted in different biological outcomes, the extent of macrophage reduction after low-dose DT administration was investigated by flow cytometry (FACS) on day 6.5 pc. FACS was performed on peritoneal exudate cells (PECs), spleen, and uterus to assess macrophage numbers post-DT administration on day 5.5 pc. Data here is presented as a proportion of live cells for each of the tissues.

The FACS data indicates that low DT doses reduced macrophage numbers on day 6.5 pc to a smaller extent, compared with the 25 ng/g DT dose which elicited >90% reduction in macrophage numbers. There was no change to the number of macrophages in the peritoneal cavity (Table 4.2 and Figure 4.4 B). However, macrophage numbers were reduced in the spleen with both the 5 ng/g and 10 ng/g DT doses administered to CD11b-DTR dams compared to WT controls (Table 4.2 and Figure 4.4 C). Furthermore, macrophage numbers were reduced by greater than 75% in the uterus using both DT doses (Table 4.2 and Figure 4.4 D).

The numbers of granulocytes were also calculated. There was an increase in the proportion and number of granulocytes within the peritoneal cavity in CD11b-DTR mice given 5 ng/g DT or 10 ng/g DT compared to WT controls (Table 4.3). This result was unsurprising given that macrophages and neutrophils are the major cell lineage in the peritoneal fluid. In contrast, there was a reduction in the number of granulocytes in the spleen in CD11b-DTR females given 10 ng/g DT (Table 4.3). Furthermore, there was no change to the number of granulocytes in the uterus, however there was an increase in the proportion of granulocytes amongst total live cells in CD11b-DTR mice given 5 ng/g DT (Table 4.3).

To confirm partial macrophage depletion in the uterus, implantation sites from CD11b-DTR mice treated with 10 ng/g DT (MD^{10}) were stained to detect F4/80 expression on days 6.5 pc and 7.5 pc (Figure 4.5 A-D). CD11b-DTR mice treated with 10 ng/g DT had an 82% reduction in macrophage density on day 6.5 pc compared to WT controls (mean ± SEM, 9.6 ± 1.9% vs 1.7 ± 0.2%, WT vs MD^{10}, p=0.006, Figure 4.5 E). Similarly, there was a 69% reduction in macrophage density on day 7.5 pc (9.2 ± 1.0% vs 2.9 ± 0.9%, p=0.004, Figure 4.5 F).

This data indicates a reduction in macrophage numbers in the uterus after 5 ng/g or 10 ng/g DT treatment to CD11b-DTR mice. Therefore, CD11b-DTR mice given 5 ng/g or 10 ng/g DT are referred to as moderately macrophage-depleted mice.

Table 4.2: Proportions and number of macrophages on day 6.5 pc.

	%F4/80$^+$CD11b$^+$ (% of Live)			#F4/80$^+$CD11b$^+$		
	WT	MD^5	MD^{10}	WT	MD^5	MD^{10}
PECs	10.3 ± 1.2	6.5 ± 1.1	7.8 ± 1.2	10.5 ± 2.0 x 10^4 cells	14.4 ± 2.8 x 10^4 cells	9.1 ± 2.9 x 10^4 cells
Spleen	1.6 ± 0.1	1.0 ± 0.1*	1.1 ± 0.1*	1.9 ± 0.3 x 10^6 cells	0.6 ± 0.1* x 10^6 cells	0.6 ± 0.1* x 10^6 cells
Uterus	1.9 ± 0.3	3.3 ± 1.0	3.3 ± 1.1	19.5 ± 4.2 x 10^3 cells	3.7 ± 0.7* x 10^3 cells	3.4 ± 1.5 x 10^3 cells

Table 4.3: Proportions and number of granulocytes on day 6.5 pc.

	%F4/80$^-$CD11b$^+$ (% of Live)			#F4/80$^-$CD11b$^+$		
	WT	MD^5	MD^{10}	WT	MD^5	MD^{10}
PECs	12.8 ± 2.0	54.6 ± 5.8*	60.2 ± 3.8*	22.8 ± 6.0 x 10^4 cells	129.3 ± 25.3* x 10^4 cells	104.1 ± 16.5* x 10^4 cells
Spleen	2.9 ± 0.3	2.9 ± 0.3	2.2 ± 0.3	3.1 ± 0.4 x 10^6 cells	1.8 ± 0.3 x 10^6 cells	1.4 ± 1.4* x 10^6 cells
Uterus	3.4 ± 0.4	10.4 ± 2.2*	3.9 ± 1.1	20.7 ± 2.9 x 10^3 cells	18.5 ± 3.7 x 10^3 cells	17.1 ± 4.1 x 10^3 cells

Data are presented as mean ± SEM with statistical analysis using a one-way ANOVA with Sidak's multiple comparison test. * indicates statistical significance ($p<0.05$) compared to WT controls.

Figure 4.4: Low-dose DT elicits moderate macrophage depletion in CD11b-DTR females.
WT and CD11b-DTR females were mated to BALB/c stud males. On day 5.5 pc, DT was administered at either 5 ng/g or 10 ng/g to CD11b-DTR mice and WT mice received DT at 25 ng/g. FACS analysis was performed on day 6.5 pc for the peritoneal exudate cells (PECs), spleen and uterus to assess macrophage depletion using F4/80 and CD11b (A). FACS plots are representative of 8-17 mice/group. The number of macrophages in the PECs (B), spleen (C), and uterus (D) are shown. Data are presented as mean ± SEM with statistical analysis using a one-way ANOVA with Sidak's multiple comparison test. * indicates statistical significance ($p<0.05$) compared to WT controls; *$p<0.05$. MD; macrophage depleted. PECs; peritoneal exudate cells. WT; wild type.

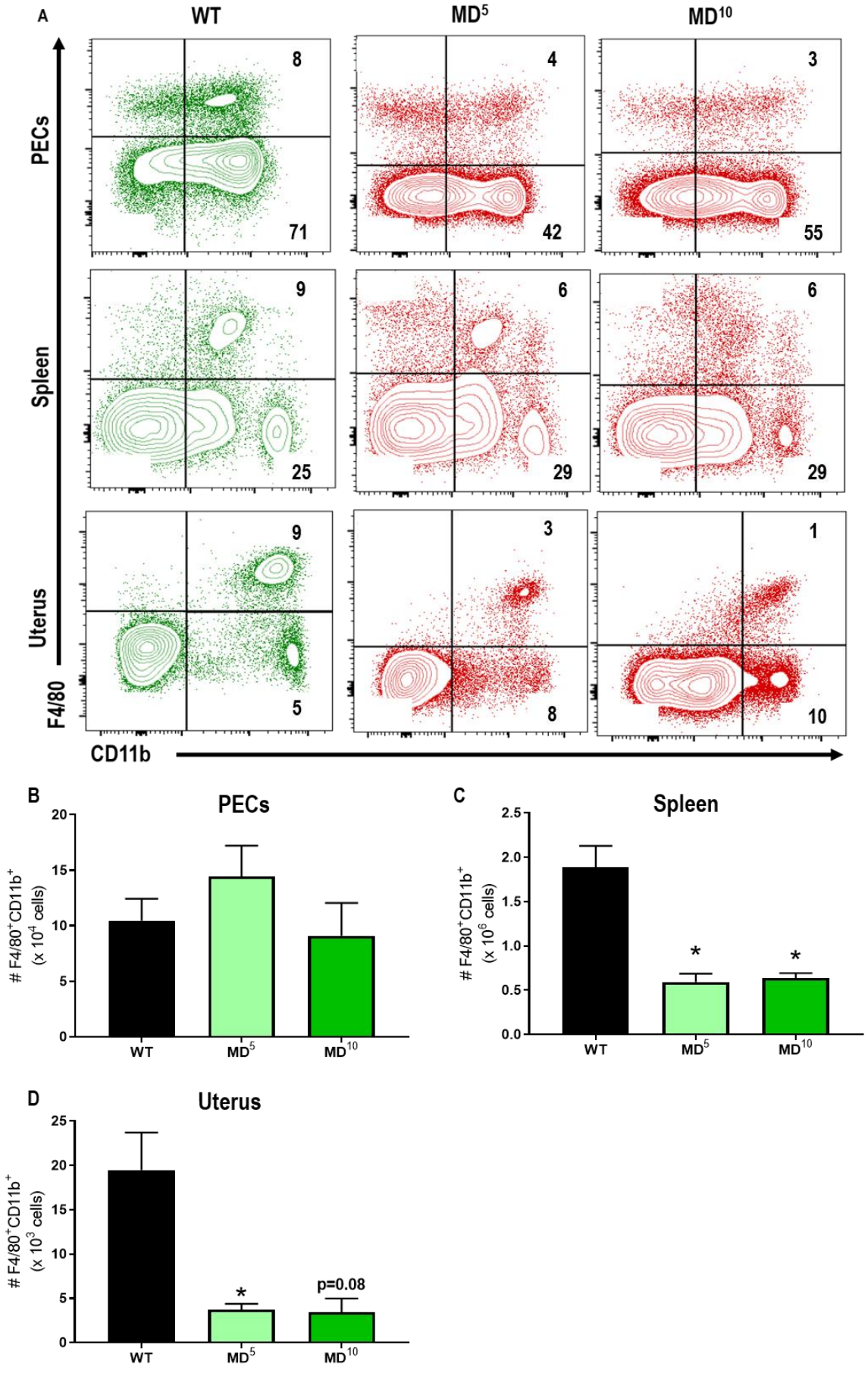
A
WT
MD5
MD10
PECs
Spleen
Uterus
F4/80
CD11b
8
71
4
42
3
55
9
25
6
29
6
29
9
5
3
8
1
10
B
PECs
F4/80+CD11b+ (x 10^4 cells)
WT
MD5
MD10
C
Spleen
F4/80+CD11b+ (x 10^6 cells)
*
*
D
Uterus
F4/80+CD11b+ (x 10^3 cells)
*
p=0.08

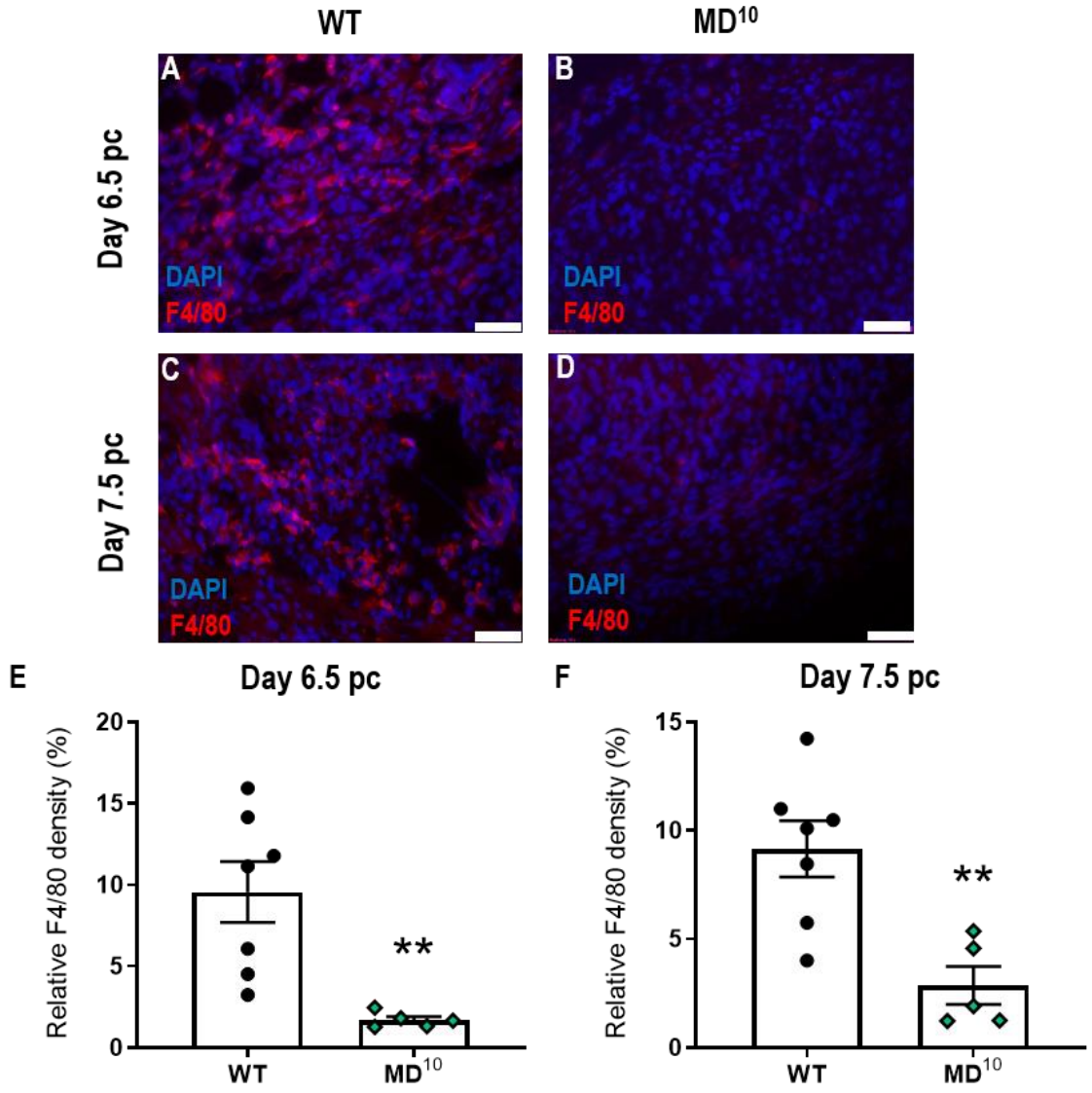

Figure 4.5: Low-dose DT administration to CD11b-DTR mice elicits moderate macrophage depletion in the uterus on days 6.5 pc and 7.5 pc.

WT and CD11b-DTR females were mated to BALB/c stud males. On day 5.5 pc, DT was administered at 10 ng/g to CD11b-DTR mice and WT mice received DT at 25 ng/g. Implantation sites were stained with DAPI and anti-F4/80 to assess macrophages in WT and DT-treated CD11b-DTR females (A-D; scale bar equals 50 µm). The relative density of F4/80 was quantified on days 6.5 pc (E) and 7.5 pc (F). No primary antibody and isotype-matched negative controls are shown in Appendix 9.1. Data are presented as mean ± SEM with statistical analysis using an unpaired t-test, n=5-7 mice/group. * indicates statistical significance ($p<0.05$) compared to WT controls; **$p<0.01$ and ****$p<0.0001$. MD; macrophage-depleted. WT; wild type.

4.4 EFFECT OF LOW-DOSE DT TREATMENT ON PLACENTAL MORPHOLOGY

We next sought to understand a potential mechanism behind the FGR observed on day 17.5 pc. Placental architecture was assessed using Masson's trichrome staining in midsagittal sections of placentas from day 17.5 pc (Figure 4.6 A-C). For this section, data are presented from WT and MD^5 groups first and then WT and MD^{10} groups. Overall, effects were similar between the MD^5 and MD^{10} groups compared to WT controls.

4.4.1 PLACENTAL ARCHITECTURE

The total placental area was increased by 19% in MD^5 mice compared to WT controls (mean ± SEM, 10.6 ± 0.3 mm^2 vs 13.1 ± 0.4 mm^2, WT vs MD^5, $p<0.001$, Figure 4.6 D). There was no difference in JZ area (Figure 4.6 E). Conversely, there was an increase of 26% in the LZ area compared to WT controls (6.4 ± 0.2 mm^2 vs 8.7 ± 0.3 mm^2, $p<0.001$, Figure 4.6 F). Furthermore, there was a reduction in the JZ proportion (39.5 ± 1.2% vs 33.6 ± 1.3%, p=0.003, Figure 4.6 G) and an increase in the LZ proportion compared to WT controls (60.5 ± 1.2% vs 66.4 ± 1.3%, p=0.003, Figure 4.6 H). The LZ to JZ ratio was also increased by 23% compared to WT controls (1.6 ± 0.1 vs 2.1 ± 0.1, p=0.010, Figure 4.6 I). The LZ weight was calculated by multiplying the proportion of LZ with placental weight. The LZ weight was increased by 20% in MD^5 mice compared to WT controls (56.8 ± 1.6 mg vs 71.4 ± 2.7 mg, $p<0.001$, Figure 4.6 J). There was a reduction in the percentage area of GCs in the JZ compared to WT controls (9.1 ± 1.5% vs 4.5 ± 1.0%, p=0.022, Figure 4.6 K).

For MD^{10} mice, there was no difference to total placental area, JZ area or LZ area compared to WT controls (Figure 4.6 D-F). However, there was a reduction in the proportion of JZ (39.5 ± 1.2% vs 33.7 ± 1.4%, WT vs MD^{10}, p=0.009, Figure 4.6 G) and an increase in the proportion of LZ (60.5 ± 1.2% vs 66.3 ± 1.4%, p=0.009, Figure 4.6 H). There was a 20% increase in the LZ to JZ ratio compared to WT controls (1.6 ± 0.1 vs 2.0 ± 0.1, p=0.042, Figure 4.6 I) and there was a 14% increase in the LZ weight (56.8 ± 1.6 mg vs 65.9 ± 2.9 mg, p=0.031, Figure 4.6 J). In addition, there was a trend towards a reduced proportion of GCs in the JZ compared to WT controls (9.1 ± 1.5% vs 4.8 ± 1.4%, p=0.086, Figure 4.6 K).

Figure 4.6: Low-dose DT administration alters placental morphology on day 17.5 pc.
WT and CD11b-DTR females were mated to BALB/c stud males. On day 5.5 pc, DT was administered at either 5 ng/g or 10 ng/g to CD11b-DTR mice and WT mice received DT at 25 ng/g. Masson's trichrome stained placental sections are shown for WT (A) and macrophage-depleted pregnancies (B and C) on day 17.5 pc (scale bar is 500 μm). The total placental area, JZ area, and LZ area were measured (D-F). Proportion of JZ and LZ were calculated (G and H). The LZ to JZ ratio was calculated (I) as was the LZ weight (J). The proportion of GCs in the JZ was calculated (K). Data are presented as mean ± SEM. Statistical analysis was performed using one-way ANOVA with Sidak's multiple comparisons test, n=10-21 mice/group. * indicates statistical significance ($p<0.05$) compared to WT controls; *$p<0.05$, **$p<0.01$, ***$p<0.001$, and ****$p<0.0001$. Dashed line; JZ and LZ border. GCs; glycogen cells. JZ; junctional zone. LZ; labyrinth zone. MD; macrophage-depleted. WT; wild type.

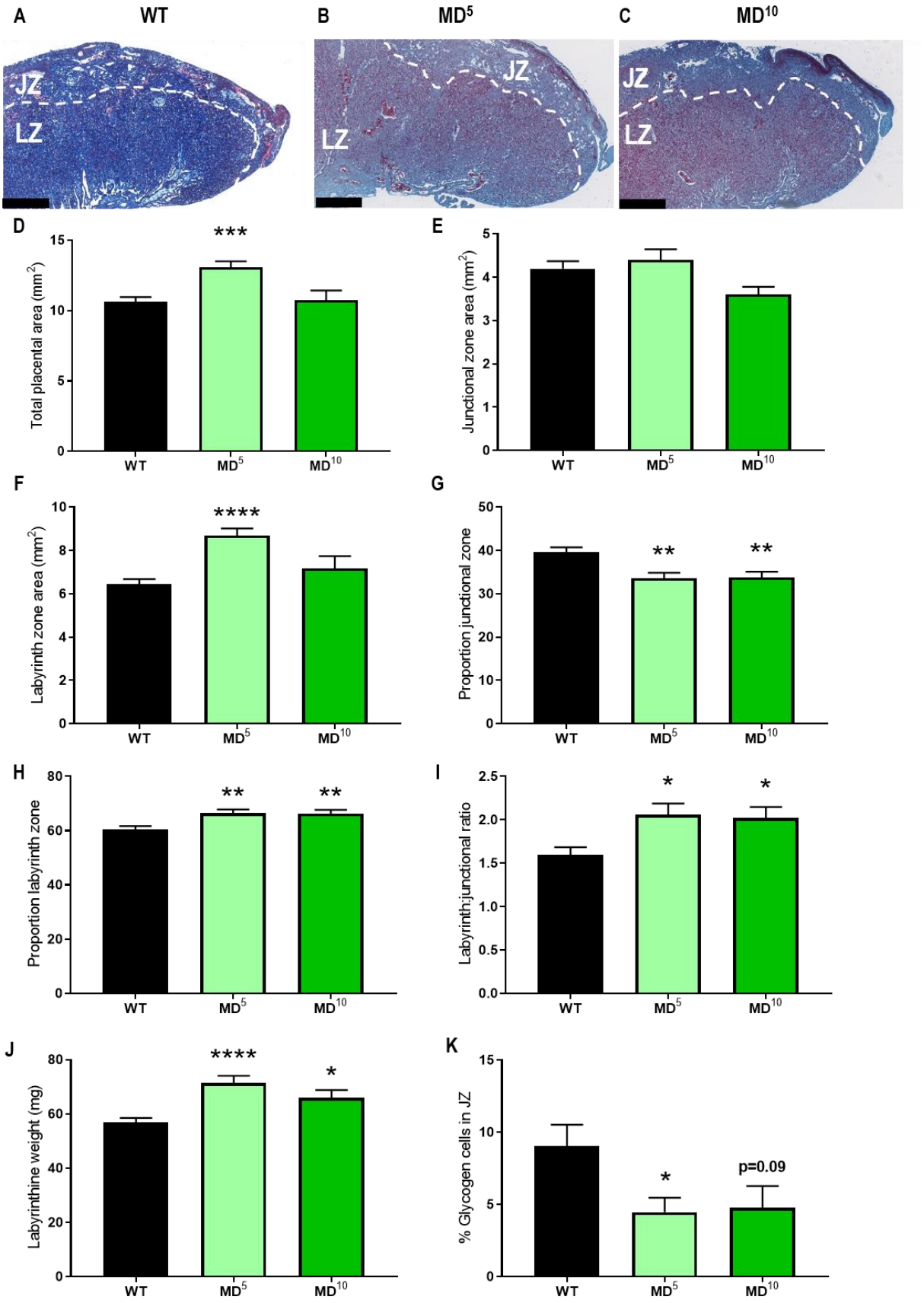
A
WT
B
MD5
C
MD10
JZ
LZ
D
Total placental area (mm2)
E
Junctional zone area (mm2)
F
Labyrinth zone area (mm2)
G
Proportion junctional zone
H
Proportion labyrinth zone
I
Labyrinth:junctional ratio
J
Labyrinthine weight (mg)
K
% Glycogen cells in JZ
p=0.09
WT
MD5
MD10

4.4.2 PLACENTAL VASCULARISATION

Given the observed differences in placental structure, particularly the changes in the LZ, placentas were further assessed for the extent of vascularisation in the LZ. Placentas were immunohistochemically labelled to detect maternal and fetal blood spaces (Figure 4.7 A-C). Again, data here is presented as WT vs MD^5 first and then WT vs MD^{10}.

The density of trophoblast cells in the MD^5 group was increased compared to WT controls (mean ± SEM, 71.3 ± 1.4% vs 82.3 ± 4.2%, WT vs MD^5, p=0.002, Figure 4.7 D). Conversely, there was a decrease in the density of maternal blood spaces (16.2 ± 1.0% vs 12.5 ± 0.7%, p=0.028, Figure 4.7 E) and there was a reduction in the density of fetal capillaries compared to WT controls (12.6 ± 0.5% vs 9.6 ± 0.4%, p=0.001, Figure 4.7 F). There was a 15% increase in trophoblast surface area compared to WT controls (43.4 ± 2.2 cm^2 vs 51.3 ± 2.9 cm^2, p=0.032, Figure 4.7 G). There was no difference to trophoblast barrier thickness, a measure of the distance between fetal and maternal circulation (Figure 4.7 H). Furthermore, there was a 17% reduction in maternal blood barrier thickness compared to WT controls (2.1 ± 0.1 µm vs 1.8 ± 0.1 µm, p=0.004, Figure 4.7 I).

For the MD^{10} group, there was a trend toward an increase density of trophoblast cells compared to WT controls (71.3 ± 1.4% vs 79.9 ± 1.5%, WT vs MD^{10}, p=0.052, Figure 4.7 D). Furthermore, there was a reduction in the density of fetal capillaries compared to WT controls (12.6 ± 0.5% vs 6.6 ± 1.0%, p<0.001, Figure 4.7 F).

These experiments indicate that placental structure, and thus potentially placental function is impacted by the reduction in macrophage numbers during the peri-implantation phase. These placental changes are likely to be causally related to the FGR seen in late gestation.

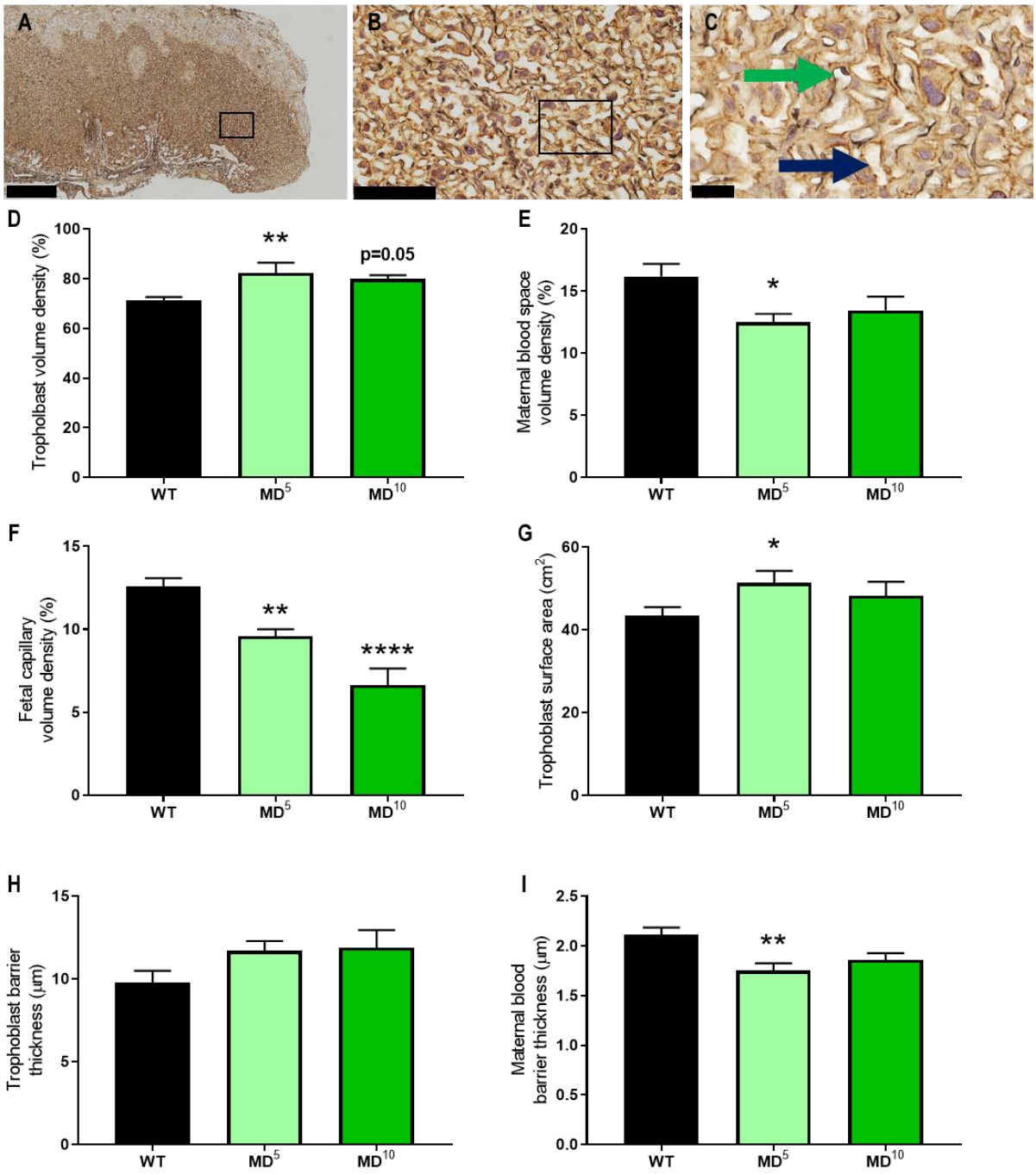

Figure 4.7: Low-dose DT administration alters placental labyrinth vascularisation.
WT and CD11b-DTR females were mated to BALB/c stud males. On day 5.5 pc, DT was administered at either 5 ng/g or 10 ng/g to CD11b-DTR mice and WT mice received DT at 25 ng/g. Placental sections were labelled to detect pan-cytokeratin (trophoblasts, blue arrow in C) and vimentin (fetal capillaries, green arrow in C) in the LZ (A-C; scale bar in A equals 500 µm, scale bar in B equals 100 µm, and scale bar in C equals 25 µm). Trophoblast, maternal blood space, and fetal capillary volume densities were calculated (D-F). The trophoblast surface area was calculated (G). The trophoblast barrier thickness and the maternal blood barrier thickness were calculated (H and I). Data are presented as mean ± SEM. Statistical analysis was performed using one-way ANOVA with Sidak's multiple comparisons test, n=10-21 mice/group. * indicates statistical significance ($p<0.05$) compared to WT controls; *$p<0.05$, **$p<0.01$, and ****$p<0.0001$. MD; macrophage-depleted. WT; wild type.

4.5 EFFECT OF LOW-DOSE DT TREATMENT ON POST-NATAL OUTCOMES

To investigate whether the observed FGR affected pup survival and growth during the post-natal period, CD11b-DTR and WT dams were left to give birth after DT treatment on day 5.5 pc and pups were weighed on days one, eight and twenty-one. In this section, data is presented firstly as WT vs MD^{5} and then as WT vs MD^{10}.

There was a reduction in the number of viable pups compared to WT controls across all time points for CD11b-DTR females given 5 ng/g DT (mean ± SEM, 8.9 ± 0.4 pups vs 5.9 ± 1.0 pups, WT vs MD^{5}, p=0.041 for day one; 8.8 ± 0.4 pups vs 5.4 ± 1.1 pups, p=0.036 for day eight and day twenty-one, Figure 4.8 A). For this group, pup survival was decreased by 11% on day twenty-one compared to WT controls (99% vs 88%, p=0.005, Figure 4.8 B). On day one, there was a 7% reduction in pup weight (1.63 ± 0.03 g vs 1.51 ± 0.03 g, p=0.021, Figure 4.8 C) and there was a 15% reduction in pup weight on day eight (5.05 ± 0.12 g vs 4.28 ± 0.11 g, p<0.001, Figure 4.8 D). On day twenty-one, there was a 7% reduction in pup weight compared to WT controls (9.91 ± 0.19 g vs 9.23 ± 0.19 g, p=0.038, Figure 4.8 E). On day twenty-one, pups were sexed, and the distribution of the sexes revealed no differences (Figure 4.8 F). Day twenty-one pup weights were sorted based on pup sex and there were no differences to the weight of the female pups from CD11b-DTR dams treated with 5 ng/g DT compared to WT controls (Figure 4.8 G). However, there was a 10% reduction in male pup weight on day twenty-one for pups from CD11b-DTR dams treated with 5 ng/g DT compared to WT controls (10.01 ± 0.29 g vs 9.00 ± 0.25 g, p=0.033, Figure 4.8 G).

For the MD^{10} group, there was a reduction in the number of viable pups compared to WT controls across all time points (8.9 ± 0.4 pups vs 4.8 ± 1.0 pups, WT vs MD^{10}, p=0.005 for day one; 8.8 ± 0.4 pups vs 4.7 ± 0.9 pups, p=0.004 for day eight and day twenty-one, Figure 4.8 A). However, pup survival was not different (Figure 4.8 B). On day one, there was a reduction in pup weight of 9% compared to WT controls (1.63 ± 0.03 g vs 1.49 ± 0.03 g, p=0.045, Figure 4.8 C). On day eight, there was a 16% reduction in pup weight (5.05 ± 0.12 g vs 4.25 ± 0.11 g, p<0.001, Figure 4.8 D) and on day twenty-one, there was an 8% reduction in pup weight compared to WT controls (9.91 ± 0.19 g vs 9.13 ± 0.19 g, p=0.012, Figure 4.8 E). On day twenty-one, there was an 8% reduction in male pup weight compared to WT controls (10.01 ± 0.29 g vs 9.24 ± 0.28 g, p=0.097, Figure 4.8 G).

These data highlight that a reduction in macrophage numbers during the peri-implantation phase has lasting impacts on pup growth and survival during the post-natal period.

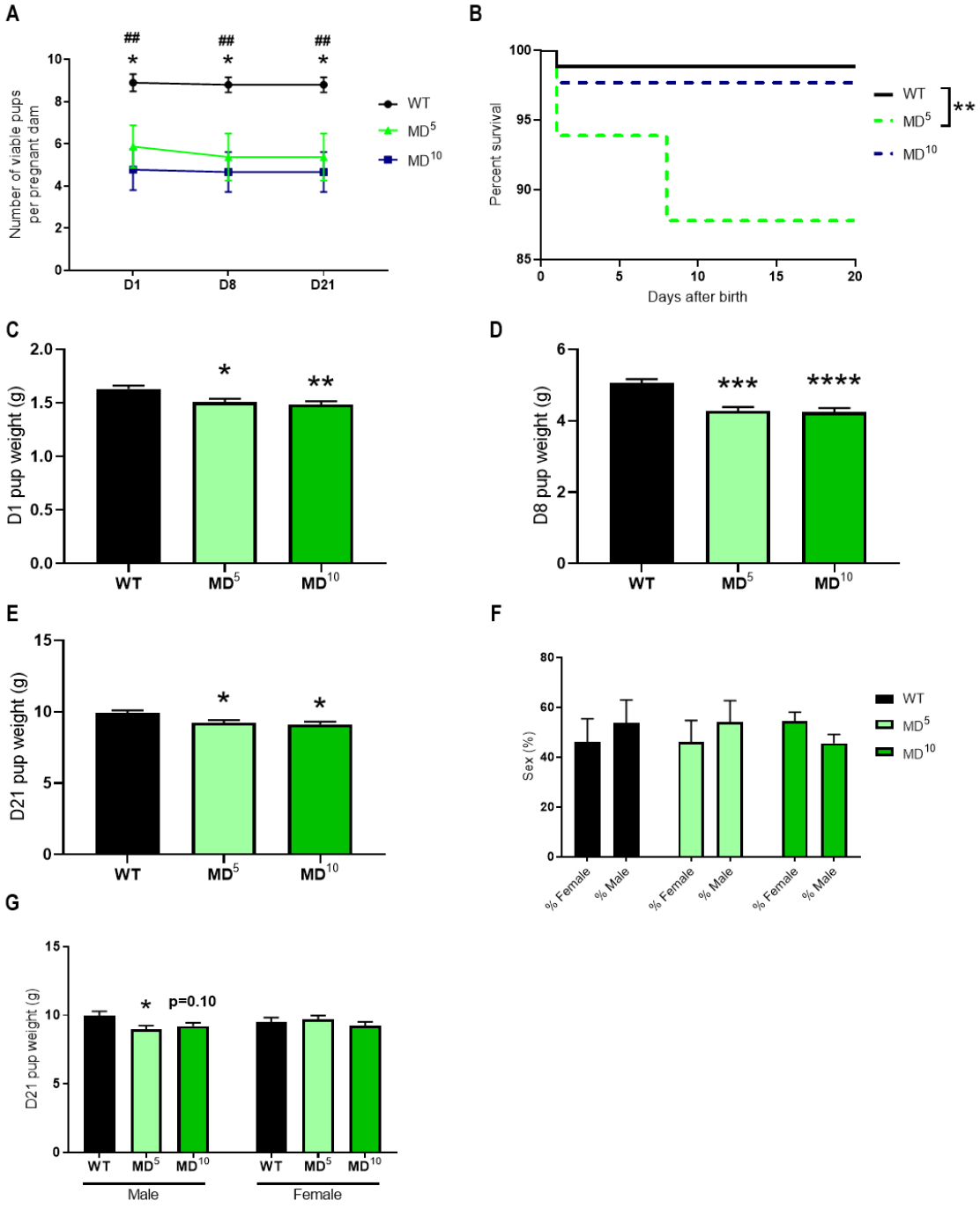

Figure 4.8: Low-dose DT administration alters post-natal growth trajectory.

WT and CD11b-DTR females were mated to BALB/c stud males. On day 5.5 pc, DT was administered at either 5 ng/g or 10 ng/g to CD11b-DTR mice and WT mice received DT at 25 ng/g. The number of viable pups were counted on days one, eight, and twenty-one post-delivery (A). Pup survival was also measured on days one, eight and twenty-one (B). Pup weights were measured on days one (C), eight (D), and twenty-one (E). On day twenty-one, the pups were sexed, and the distribution of sex was calculated (F). Finally, day twenty-one pup weights were separated based on sex (G). Data are presented as mean ± SEM, except in C-E and G where a mixed-model analysis was performed to calculate estimated marginal means using total number of viable pups as the co-variate. Statistical analysis was performed using one-way ANOVA with Sidak's multiple comparisons test, except in B where a survival curve comparison test was used, n=10-17 mice/group. * indicates statistical significance ($p<0.05$) compared to WT controls; *$p<0.05$, **$p<0.01$, ***$p<0.001$, ****$p<0.0001$, and ## in A signifies $p<0.01$ for WT vs MD^{10}. MD; macrophage-depleted. WT; wild type.

4.6 EFFECT OF LOW-DOSE DT TREATMENT ON MID-GESTATION IMPLANTATION SITE STRUCTURE

Due to the reduction in viable pups, FGR, and altered placental morphology, additional experiments were undertaken to understand the mechanisms of FGR in CD11b-DTR mice administered 10 ng/g DT. We used this dose as it was confirmed to cause uterine macrophage depletion and showed pregnancy failure that was apparent from mid-gestation, yet some dams were able to carry fetuses to term. In contrast, the 25 ng/g DT dose resulted in severe macrophage depletion and nearly complete pregnancy loss. Thus, we sought to investigate how the lower DT dose influenced biological outcomes. Mid-gestation, day 9.5 pc, was investigated to determine the impact of moderate macrophage deficiency on implantation site structure and development.

4.6.1 PREGNANCY OUTCOMES

On day 9.5 pc, 10 ng/g DT administered to CD11b-DTR females resulted in 50% pregnancy failure compared to WT controls (100% vs 50%, WT vs MD[10], $p<0.001$, Figure 4.9 A). Furthermore, the number of viable implantation sites was decreased (mean ± SEM, 7.9 ± 0.7 sites vs 4.5 ± 1.3 sites, $p=0.040$, Figure 4.9 B). There was no difference to the number of resorbing implantation sites or total number of implantation sites (Figure 4.9 C and E), however, there was an increase in the number of uterine scars (0 scars vs 3.6 ± 1.2 scars, $p=0.045$, Figure 4.9 D). Approximately half of the low-dose DT-treated dams were unaffected at day 9.5 pc, yet the other half presented with either uterine scars or resorptions (Figure 4.9 F).

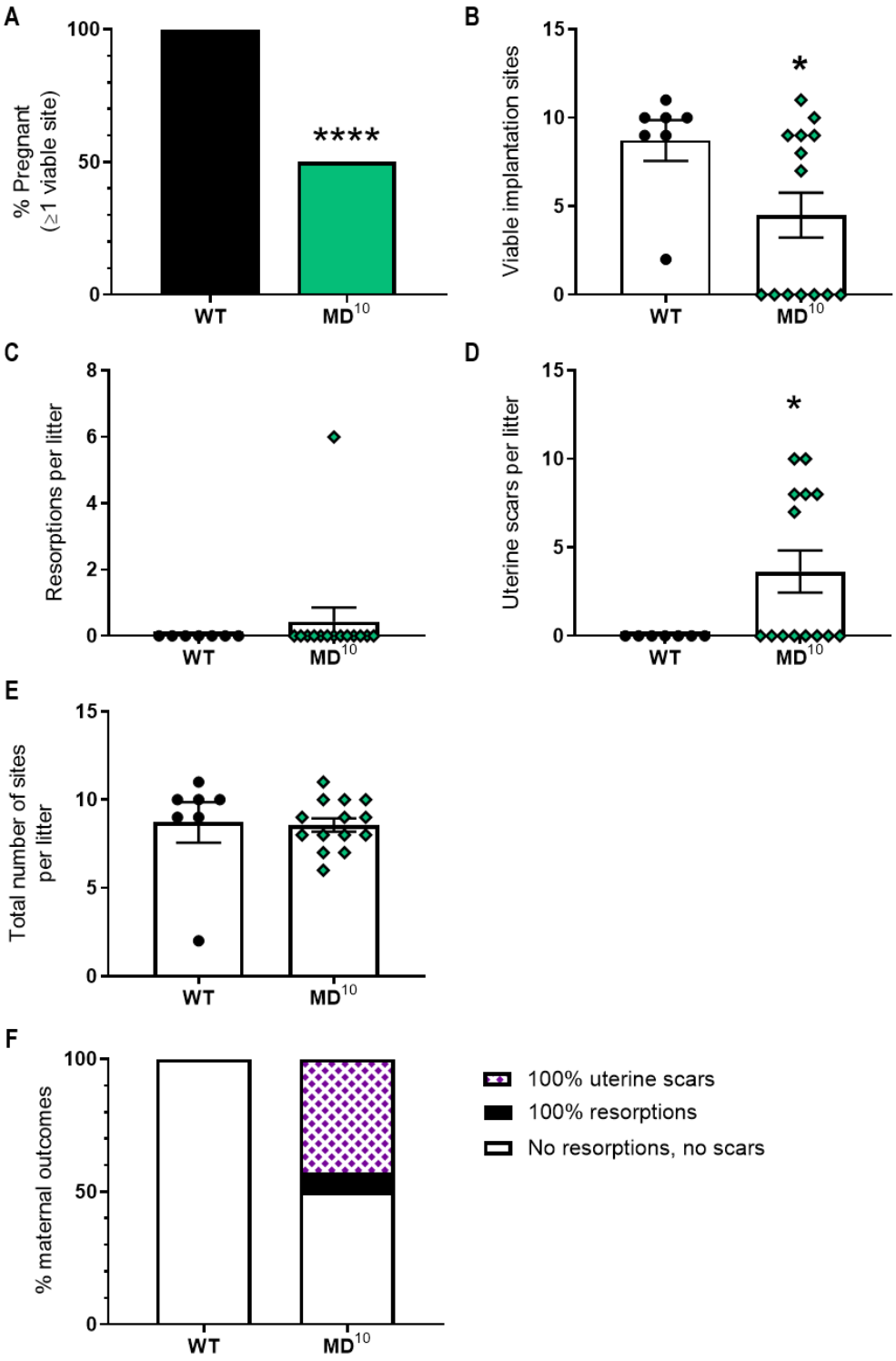

Figure 4.9: Low-dose DT administration reduces pregnancy viability at day 9.5 pc.
WT and CD11b-DTR females were mated to BALB/c stud males. On day 5.5 pc, DT was administered at 10 ng/g to CD11b-DTR mice and WT mice received DT at 25 ng/g. Pregnancy parameters were assessed on day 9.5 pc (A). The numbers of viable implantation sites, resorptions, uterine scars, and total number of implantation sites were assessed (B-E). The pregnancies were categorised into viability rankings (F). Data are presented as mean ± SEM (B-E). Statistical analysis was performed using χ^2 test (A) or unpaired t-test (B-E), n=7-14 mice/group. * indicates statistical significance ($p<0.05$) compared to WT controls; *$p<0.05$ and ****$p<0.0001$. MD; macrophage-depleted. WT; wild type.

4.6.2 IMPLANTATION SITE STRUCTURE

To further investigate the impact of low-dose DT treatment on pregnancy outcomes, day 9.5 pc viable implantation sites were assessed for structural development. Upon inspection, implantation sites from WT dams appeared larger and more developed compared to implantation sites from low-dose DT-treated CD11b-DTR dams (Figure 4.10 A and B). Furthermore, CD11b-DTR dams treated with 10 ng/g DT had implantation sites with smaller mesometrial lymphoid aggregate of pregnancy (MLAp) and decidual areas compared to WT controls (Figure 4.10 C and D). Herein, the MLAp area was decreased by 58% compared to WT controls (mean ± SEM, 2.5 ± 0.2 mm^2 vs 1.1 ± 0.2 mm^2, WT vs MD^{10}, $p<0.001$, Figure 4.10 E) and the decidual area was decreased by 61% (2.6 ± 0.2 mm^2 vs 1.0 ± 0.2 mm^2, $p<0.001$, Figure 4.10 F). In conjunction, placental area was reduced by 38% compared to WT controls (0.9 ± 0.1 mm^2 vs 0.6 ± 0.1 mm^2, $p=0.044$, Figure 4.10 G).

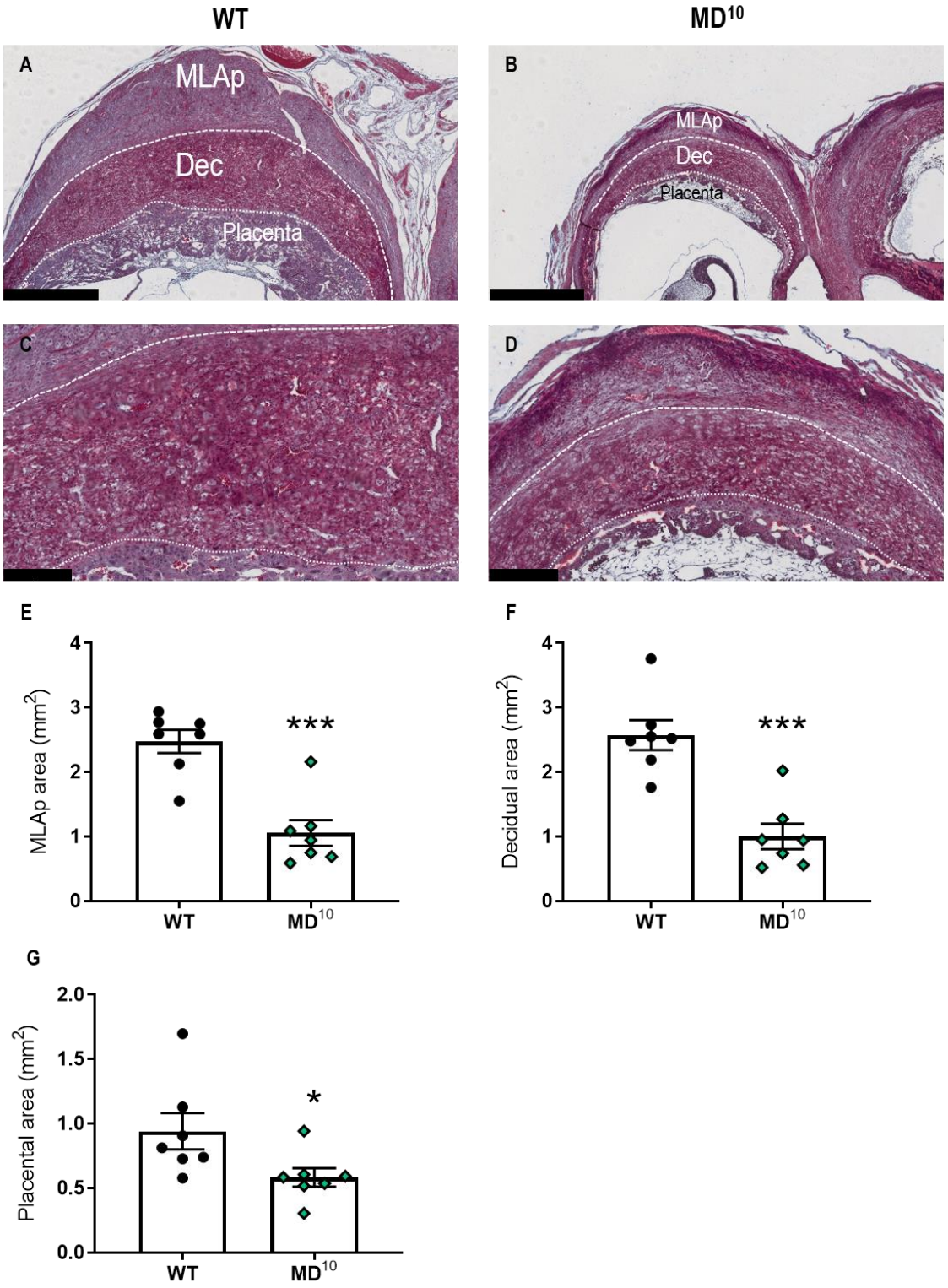

Figure 4.10: Low-dose DT administration impairs implantation site structure on day 9.5 pc. WT and CD11b-DTR females were mated to BALB/c stud males. On day 5.5 pc, DT was administered at 10 ng/g to CD11b-DTR mice and WT mice received DT at 25 ng/g. Masson's trichrome stained implantation site sections on day 9.5 pc (A-D, scale bar is 1 mm in A and B; scale bar is 250 µm in C and D). The areas of the mesometrial lymphoid aggregate of pregnancy (MLAp) (E), the decidua (F), and placenta (G) were measured. Data are presented as mean ± SEM with statistical analysis using unpaired t-tests, n=7 mice/group. * indicates statistical significance ($p<0.05$) compared to WT controls; *$p<0.05$ and ***$p<0.001$. Dec; decidua. MD; macrophage-depleted. MLAp; mesometrial lymphoid aggregate of pregnancy. WT; wild type.

4.6.3 IMMUNE CELLS IN IMPLANTATION SITES

Due to the difference in implantation site structure observed on day 9.5 pc, we sought to investigate whether immune cell populations within these sites were perturbed after macrophage depletion. Immunohistochemical staining showed that the relative DBA density was unchanged between WT and low-dose DT-treated CD11b-DTR dams within the decidua (Figure 4.11 A-E). Furthermore, macrophages were localised in the MLAp and the decidua in both WT and CD11b-DTR dams (Figure 4.12 A-D). At day 9.5 pc, the relative density of decidual F4/80$^+$ cells were decreased in low-dose DT-treated dams by 67% compared to WT controls (6.8 ± 1.1% vs 2.2 ± 1.0%, p=0.009, Figure 4.12 E).

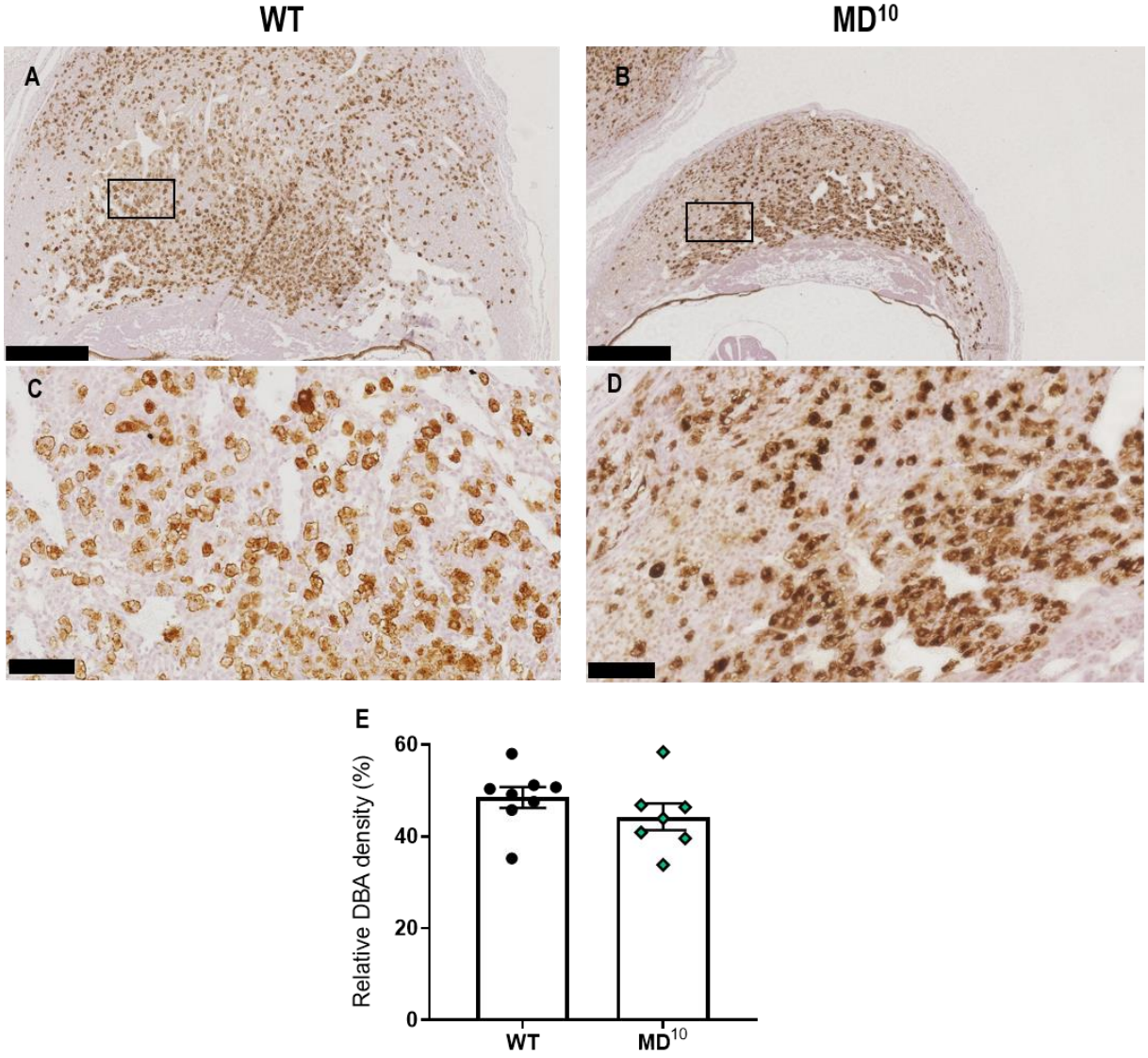

Figure 4.11: Low-dose DT administration has no effect on density of uNK cells on day 9.5 pc. WT and CD11b-DTR females were mated to BALB/c stud males. On day 5.5 pc, DT was administered at 10 ng/g to CD11b-DTR mice and WT mice received DT at 25 ng/g. DBA lectin staining was performed in WT and low-dose DT-treated females on day 9.5 pc (A-D, scale bar is 500 µm in A and B, scale bar is 100 µm in C and D). The relative density of DBA positivity was calculated (E). Data are presented as mean ± SEM with statistical analysis using unpaired t-tests, n=7-8 mice/group. * indicates statistical significance ($p<0.05$) compared to WT controls; **$p<0.01$. MD; macrophage-depleted. WT; wild type.

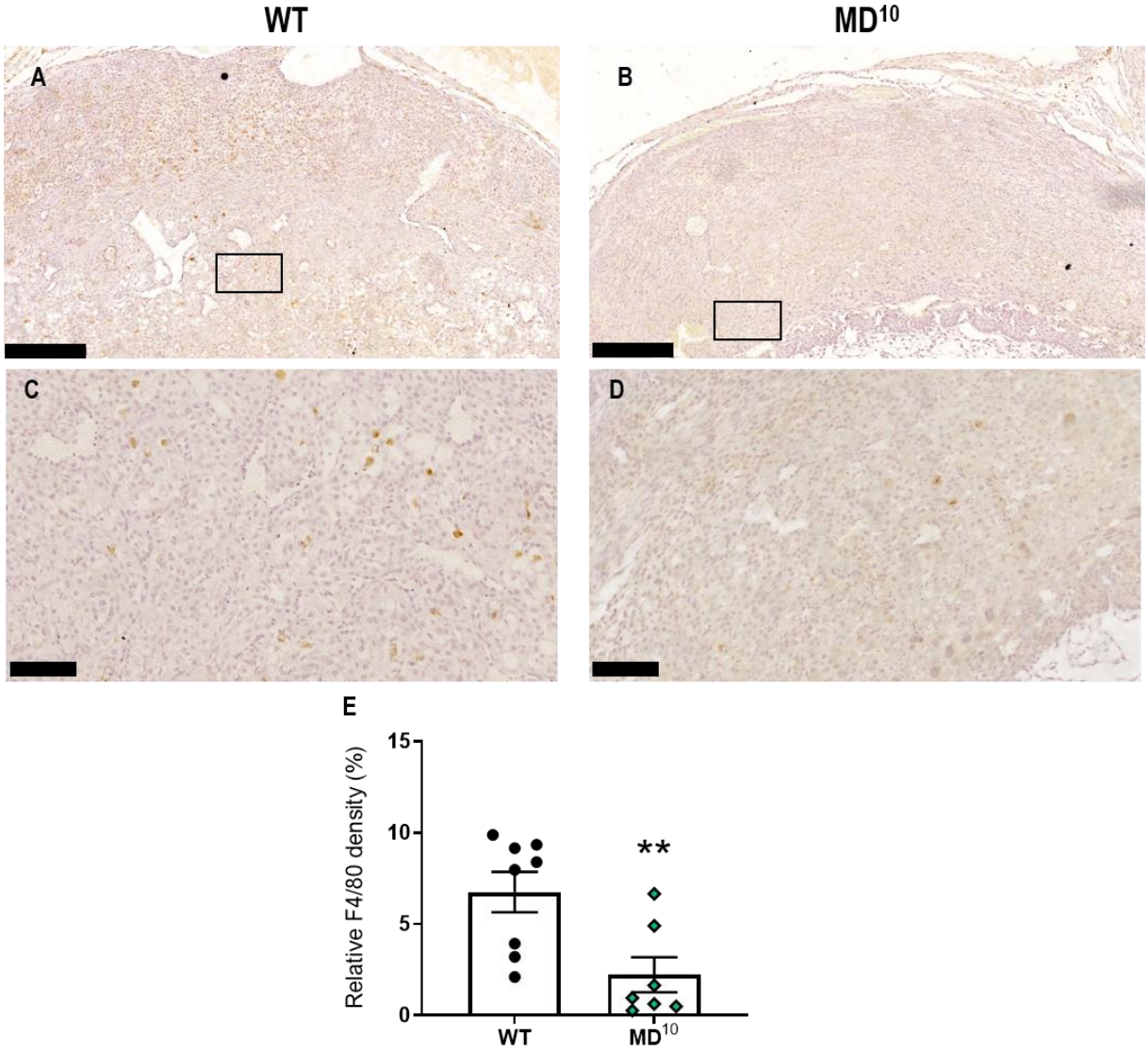

Figure 4.12: Low-dose DT administration reduces density of macrophages on day 9.5 pc.
WT and CD11b-DTR females were mated to BALB/c stud males. On day 5.5 pc, DT was administered at 10 ng/g to CD11b-DTR mice and WT mice received DT at 25 ng/g. F4/80 staining was performed on day 9.5 pc (A-D, scale bar is 250 µm in A and B, scale bar is 100 µm in C and D). The relative density of F4/80 positivity was calculated (E). Data are presented as mean ± SEM with statistical analysis using unpaired t-tests, n=7-8 mice/group. * indicates statistical significance ($p<0.05$) compared to WT controls; **$p<0.01$. MD; macrophage-depleted. WT; wild type.

4.6.4 UTERINE VASCULAR REMODELLING ON DAY 9.5 PC

To further investigate defects in implantation site structure and reduced pregnancy viability after 10 ng/g DT administration to CD11b-DTR females, the extent of uterine artery remodelling within the mesometrial triangle was assessed on day 9.5 pc (Figure 4.13 A-D). On day 9.5 pc, lumen area was decreased by 68% in the MD^{10} group compared to WT controls (mean ± SEM, 629 ± 81 μm^2 vs 200 ± 29 μm^2, WT vs MD^{10}, $p<0.001$, Figure 4.13 E). Furthermore, lumen diameter was decreased by 44% (30 ± 2 µm vs 17 ± 1 µm, $p<0.001$, Figure 4.13 F) and the cross-sectional area was also decreased by 53% compared to WT controls (1262 ± 154 μm^2 vs 597 ± 70 μm^2, $p=0.001$, Figure 4.13 G). In addition, the total vessel area was decreased by 59% (1891 ± 205 μm^2 vs 768 ± 111 μm^2, $p<0.001$, Figure 4.13 H). Conversely, total area to lumen area ratio was increased by 31% compared to WT controls (3.3 ± 0.2 vs 4.7 ± 0.3, $p=0.004$, Figure 4.13 I).

These data show that low-dose DT treatment to CD11b-DTR mice caused reduce numbers of macrophages within implantation sites on day 9.5 pc and resulted in impaired implantation site structural development associated with impaired vascular remodelling of the mesometrial triangle arteries. In addition, there was also impaired vascular remodelling on days 6.5 pc and 7.5 pc in CD11b-DTR mice given low-dose DT (Appendices 9.8 and 9.9).

Figure 4.13: Low-dose DT administration decreases lumen diameter in uterine mesometrial triangle vessels on day 9.5 pc.

WT and CD11b-DTR females were mated to BALB/c stud males. On day 5.5 pc, DT was administered at 10 ng/g to CD11b-DTR mice and WT mice received DT at 25 ng/g. H&E stained sections in WT and CD11b-DTR females were used to assess uterine arteries on day 9.5 pc (A-B; scale bar is 1 mm and rectangle shows mesometrial triangle region). The mesometrial triangle arteries are shown (C and D; scale bar is 50 μm and black arrows show arteries). Vessel parameters were calculated including vessel lumen area (E), vessel diameter (F), vessel cross-sectional area (G), total vessel area (H), and the ratio of total vessel size to lumen ratio (I). Data are presented as mean ± SEM with statistical analysis using unpaired t-test, n=6-8 mice/group. * indicates statistical significance ($p<0.05$) compared to WT controls; **$p<0.01$ and ***$p<0.001$. MD; macrophage-depleted. WT; wild type.

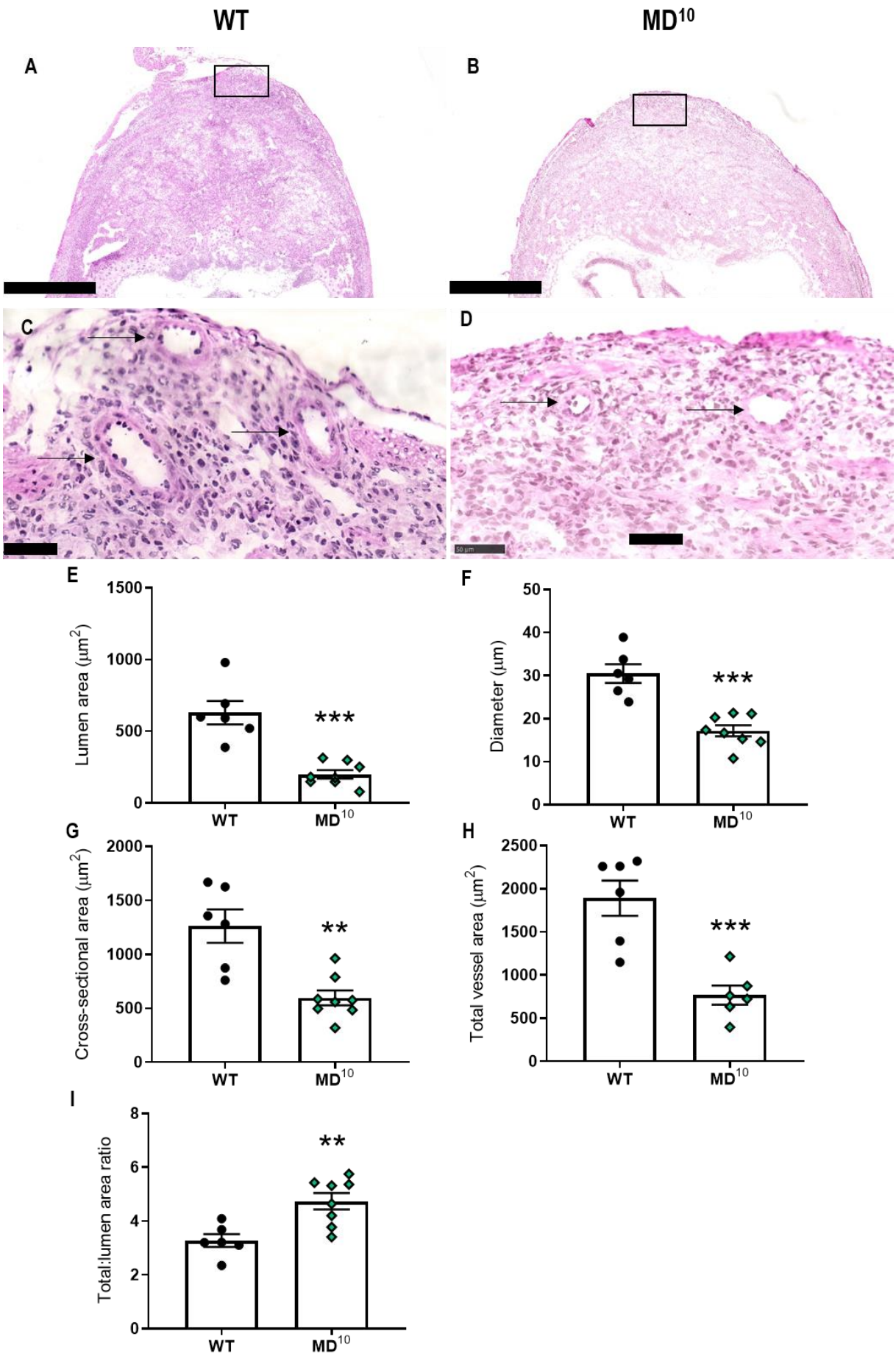
WT
MD10
A
B
C
D
E
Lumen area (μm2)
1500
1000
500
0
***
WT
MD10
F
Diameter (μm)
50
40
30
20
10
0
***
WT
MD10
G
Cross-sectional area (μm2)
2000
1500
1000
500
0
**
WT
MD10
H
Total vessel area (μm2)
2500
2000
1500
1000
500
0
***
WT
MD10
I
Total:lumen area ratio
8
6
4
2
0
**
WT
MD10

4.7 DISCUSSION

The data presented within this chapter provides greater insight on the consequence of macrophage deficiency in the murine uterus during early pregnancy. Herein, relatively small perturbations to macrophage numbers in early pregnancy profoundly affected late pregnancy outcomes and compromised post-natal pup growth and survival. Macrophage depletion was sustained into mid-gestation and was associated with impaired implantation site structure. As previously discussed, the roles of macrophages during pregnancy may include antigen presentation, clearance of apoptotic trophoblast cells, facilitating trophoblast invasion, and tissue and vascular remodelling – all of which have been implicated in placental function and fetal growth (Ning et al., 2016, Lash et al., 2016). In particular, uterine vascular remodelling is crucial for fetal growth where failure to adequately remodel uterine arteries during early pregnancy can lead to pregnancy complications such as FGR and PE in women (Faas et al., 2014, Reynolds et al., 2006).

4.7.1 INCREASED MACROPHAGE DEPLETION CAUSES GREATER PREGNANCY LOSS

Using different doses of DT in the CD11b-DTR murine model elicited a dose-dependent effect on the degree of macrophage depletion and the severity of pregnancy pathology and degree of fetal loss. The highest dose of DT (25 ng/g) elicited greater than 90% macrophage depletion and decreased pregnancy viability from day 7.5 pc. At day 9.5 pc, pregnancy viability was only at 10% using this dose. In addition, the moderate macrophage depletion dose (10 ng/g DT) also impacted viable pregnancy rate on day 7.5 pc, and by day 9.5 pc this fell to 50% where it was maintained until day 17.5 pc. The lowest dose of DT (5 ng/g) resulted in all dams remaining pregnant at each of the time points, however by day 17.5 pc there was a reduction in the number of viable fetuses. There were also minor alterations to pregnancy success on day 12.5 pc in dams treated with either 5 ng/g DT or 10 ng/g DT (Appendix 9.12).

4.7.2 MODERATE MACROPHAGE DEPLETION CAUSES FETAL GROWTH RESTRICTION AND FETAL LOSS

It has become increasingly clear that early perturbations to immune cell numbers can severely impact late pregnancy outcomes (Care et al., 2018, Care et al., 2013). Furthermore, it has been proposed that imbalances in the immune response during early pregnancy can program the pregnancy for complications in later gestation. Results herein show that moderate reductions in macrophage numbers during the peri-implantation phase impact pregnancy viability and fetal growth in late gestation. On day 6.5 pc macrophage numbers were reduced in CD11b-DTR females treated with either 5 ng/g or 10 ng/g DT in the spleen and uterus compared to WT controls. Moreover, immunohistochemistry revealed >65% macrophage depletion from the uterus using 10 ng/g DT on days 6.5 and 7.5 pc in CD11b-DTR mice compared to WT controls, but there was no change to the number of uterine granulocytes.

All CD11b-DTR females administered 5 ng/g DT had viable fetuses on day 17.5 pc. However, these dams were prone to increased numbers of resorptions and FGR. In addition, CD11b-DTR dams given 10 ng/g

also had increased resorptions and FGR, however, only 50% of these dams had viable pups on day 17.5 pc. Thus, a proportion of fetuses were dying *in utero*. Mice are well adapted in dealing with fetal loss *in utero*. Pregnant females appear to deploy mechanisms to eliminate a proportion of fetuses in order to ensure the greatest return on reproductive resources in terms of pup survival after birth. Perturbations to pregnancy can induce the dam to resorb fetal tissues for some, or all, of the fetuses if the pregnancy becomes compromised. This process allows dams to control the amount of energy expended within a single pregnancy. In our case, dams may be adapting to a reduction in macrophages during early pregnancy and act to reduce the number of viable fetuses thereby having a selective response to support embryo development to match available maternal resources. The process of resorption allows the mother to retain the invested nutrients so that future pregnancies are not compromised, and maternal health is maintained.

Interestingly, CD11b-DTR females treated with 5 ng/g DT had fetuses which were more growth restricted than the fetuses from CD11b-DTR dams treated with 10 ng/g DT on day 17.5 pc. This may indicate that CD11b-DTR females treated with 5 ng/g DT may attempt to retain more fetuses after the initial insult of macrophage removal and therefore exhaust more resources keeping more fetuses viable for a longer period of time. In contrast, the initial insult of macrophage removal after 10 ng/g DT may have caused more fetuses to be lost earlier and thus less resources are expended. Therefore, by reducing the number of fetuses earlier, CD11b-DTR dams treated with 10 ng/g DT could invest more nutrients into the smaller number of fetuses, thus promoting increased growth. This may also explain why some of the placental parameters were more greatly affected in the 5 ng/g DT group and not so affected in the 10 ng/g DT group. Furthermore, the fetal to placental weight ratio can be indicative of placental efficiency and was reduced after macrophage reduction, suggesting a poorly functioning placenta (Woods et al., 2018).

4.7.3 PLACENTAL MORPHOLOGY IS PERTURBED AFTER MACROPHAGE DEPLETION

Placental function is key to promoting and sustaining adequate fetal growth. Perturbations to placental architecture causing FGR are often associated with inadequate placental vascularisation (Wilson et al., 2017, Roberts et al., 2003). In addition, differences in the proportions of the JZ and LZ are frequently linked with FGR. An increased JZ area compared to LZ area may indicate insufficient nutrient delivery to the fetus thereby restricting its growth (Woods et al., 2018). Our data indicate that moderate macrophage depletion in early pregnancy resulted in placental structural abnormalities. Most notably, placentas from moderately macrophage-depleted dams had a larger proportion of LZ than JZ, which likely indicates a developmental compensation to achieve greater nutrient delivery. Placentas appear to have a nutrient sensing mechanism in response to fetal development during early pregnancy and adapt to compensate for poor placentation in an attempt to rescue fetal development in later gestation (Wyrwoll et al., 2009). On day 12.5 pc, there were no overt changes to placental structure (Appendix 9.13).

However, it must also be considered that macrophage depletion may have directly resulted in defects in JZ development which could explain the increased LZ proportion. Indicative of defects in the JZ are the reduced proportion of GCs in the JZ on day 17.5 pc. GCs develop during early placental maturation and retain glycogen which later provides an energy source released to the fetus just prior to parturition (Tesser et al., 2010). Immediately prior to parturition, GCs migrate from the JZ into the maternal decidua (Coan et al., 2006). Here these cells release their intracellular glycogen stores which are delivered to the fetus via remodelled spiral arteries as a final energy source from the mother to the fetus *in utero*. A reduced proportion of GCs may also be implicated in the reduced post-natal growth where fetuses prior to delivery were unable to access glycogen stores to promote growth after delivery.

Evaluation of the placental vascular architecture revealed reductions in the fetal capillaries and maternal blood spaces within the LZ after macrophage depletion. Furthermore, there was increased trophoblast cell density in the LZ which suggests an overall reduction in the area occupied by vascular tissue. In addition, the reduced maternal blood space barrier may be indicative of a compensatory mechanism whereby the distance from maternal circulation to fetal circulation is reduced in order to more efficiently shuttle nutrients to the fetus to prevent growth restriction (Coan et al., 2004a). Whilst studies herein did not investigate placental transport mechanisms, it is reasonable to hypothesise that these mechanisms may also be perturbed despite some of the compensatory mechanisms observed in placental architecture (Burton and Fowden, 2012). Future studies could assess these transport mechanisms and whether they can be directly related to FGR in this model.

Another feature of placental architecture is the overall shape of the placenta and whether placentas appear more crescent-shaped or rounded. During early placentation, trophoblast cells invade the maternal decidua and from day 8.5 pc in mice, chorioallantoic fusion occurs (Coan et al., 2004a). If trophoblast cell invasion is not regulated or chorioallantoic fusion occurs irregularly, there can be alterations to overall placental morphology and placental shape (Böing et al., 2018, Burton et al., 2016). Herein, placental shape was not overtly different at autopsy but the extent of trophoblast invasion and chorioallantoic fusion should be further considered in order to determine whether minor changes in placental shape were associated with function of the placenta.

4.7.4 PERI-IMPLANTATION MACROPHAGE DEPLETION AFFECTS POST-NATAL PUP GROWTH

Moderate macrophage depletion revealed FGR at day 17.5 pc and this growth restriction was present in the pups during the post-natal period. Further to this, macrophage-depleted dams gave birth to reduced numbers of viable pups. Future studies should look to assess whether the pups born are non-viable, dying *in utero*, or whether maternal neglect causes these pups to die in the 12 – 24 h post birth. Interestingly, only pups from MD^5 dams were susceptible to a decrease in survival during the post-natal period, indicating that some pups born were not fit for survival. On day eight, pup weights were decreased by

15% whereas pup weight was only 8% reduced on day one. This indicated that whilst pups were growth restricted *in utero*, there was also a defect in their ability to grow during the early post-natal period. This may be due to possible developmental programming on the embryo from the early perturbation of macrophage removal, or may indicate that dams did not provide adequate post-natal nutrition. In particular, it is possible that macrophage depletion may have had lasting impacts on development of the mammary glands to support lactation, which seems feasible given the role of macrophage in mammary gland development (Pollard and Hennighausen, 1994, Dawson et al., 2020, Chua et al., 2010). Thus, the milk provided to the pups during the post-natal period may have been inadequate to promote growth, however this was not further investigated.

Macrophages are implicated in mammary gland development during the estrous cycle of mice where macrophage depletion, using the CD11b-DTR model, prevented the tissue remodelling required for alveolar bud regression (Chua et al., 2010). Therefore, depletion of macrophages during early pregnancy may have impaired initial mammary gland remodelling. Furthermore, a subset of tissue resident macrophages was recently found within the mammary gland which facilitate tissue remodelling (Dawson et al., 2020). These resident macrophages expressed CD11b which would suggest that DT administration to CD11b-DTR mice during early pregnancy could deplete these cells. It is also unknown whether populations of tissue-resident macrophages which become depleted in the CD11b-DTR model can be renewed from bone marrow monocytes considering most of these population arise during embryonic development. A follow-up study could look to cross-foster the pups born from WT dams with dams depleted of macrophages and vice versa to determine the extent to which macrophage depletion impaired mammary gland development and resulting pup growth. In addition, experiments utilising the CD169-DTR murine model could look to investigate the specific depletion of tissue resident macrophages during the peri-implantation phase.

Interestingly, by day twenty-one pup weight appeared to “catch-up” to WT pups where the difference in weight was only 7%. From day eight to day twenty-one pups become more independent and are preparing to be weaned. During this time, pups from macrophage-depleted dams may become progressively less reliant on the milk supplied by their mothers. Whilst there were no differences in the proportions of the sexes across the litters, there was a reduction in male pup weight. This indicates that depletion of macrophages had sex-specific effects on pup growth with males being more susceptible. This further supports the recent notions that fetal sex must be taken into consideration when performing pregnancy outcome experiments as male and female fetuses can be differentially susceptible to various treatment interventions in a context-dependent manner (Cuffe et al., 2014, Zhao et al., 2018, Chin et al., 2019).

4.7.5 MODERATE MACROPHAGE DEPLETION AFFECTS MID-GESTATION IMPLANTATION SITE STRUCTURE AND UTERINE VASCULAR REMODELLING

Due to the observed impacts to fetal growth, the mechanisms underpinning these impairments were investigated in mid-gestation using CD11b-DTR females treated with 10 ng/g DT. Pregnancy outcomes showed that at mid-gestation 40% of dams had uterine scars and only 50% of dams had viable implantation sites, similar to what was observed on day 17.5 pc. Some of the viable implantation sites on day 9.5 pc may have become resorptions in later gestation. During mid-gestation, there are major alterations to the maternal uterine vascular tree as placental development occurs, where complete placental structure is present by day 12.5 pc in mice (Burton et al., 2016, Adamson et al., 2002). At this time, the main uterine arteries, which are connected to the aorta, expand in diameter to provide nutrients for the profound structural changes accompanying mid-gestation placental development (Rennie et al., 2016, Reynolds et al., 2010). Macrophage depletion did not affect the remodelling of these main uterine arteries or the radial arteries which branch from these main arteries (Appendices 9.10 and 9.11).

Nonetheless, implantation site structure was severely impacted on day 9.5 pc. Due to the structural defects, including reduced decidual area, the presence of decidual spiral arteries were difficult to discern and thus there was inconclusive evidence to suggest whether macrophage depletion was impacting decidual artery remodelling. However, arteries within the mesometrial triangle were able to be assessed on day 9.5 pc. Importantly, moderate macrophage depletion impaired the remodelling of these arteries such that they were smaller in lumen area and diameter, potentially indicating poor blood flow into the developing implantation site.

Associated with the aberrant implantation site structure was the reduced density of macrophages on day 9.5 pc. This was accompanied by a smaller area of the MLAp and decidua where these immune cells are primarily located, but the cause and effect relationship between cell number and tissue size are not yet clear (Kieckbusch et al., 2014). In contrast, there was no impact on uNK cell abundance. It is unknown whether moderate macrophage depletion could impair the functions of uNK cells during mid-gestation, and whether effects on the vasculature are mediated via uNK cells. As serum P4 concentration was not impacted by lower DT doses, the change in implantation site structure may be directly related to the deficiency of macrophages and not deficiency of P4. Therefore, the impaired vascular remodelling in the mesometrial triangle appears to be directly related to macrophage insufficiency. The precise casual relationships between these effects in different uterine compartments remains to be investigated.

Next, we aimed to investigate the initial events that arise post macrophage depletion and specifically how vascular remodelling was impaired during early pregnancy. Future experiments utilised the 25 ng/g DT dose administered to CD11b-DTR and WT mice and assessed pregnancy outcomes at day 7.5 pc. The experiments in chapter five and six begin to interrogate specific mechanisms whereby macrophages

promote pregnancy success and facilitate uterine vascular remodelling required for adequate placental development and fetal growth.

CHAPTER 5

EFFECT OF MACROPHAGE DEPLETION AND REPLACEMENT ON IMPLANTATION AND IMMUNE CELL PARAMETERS IN THE PERI-IMPLANTATION PHASE

5.1 INTRODUCTION

Macrophages are thought to play key roles in pregnancy success through a range of functions including tissue and vascular remodelling. Importantly, macrophage depletion in CD11b-DTR mice during early pregnancy results in pregnancy failure (Care et al., 2013). This failure is attributable to a range of factors. These effects appear to be linked to perturbations within the ovary and the uterus. Within the uterus, macrophage depletion appears to include aberrations to implantation, tissue remodelling, and immune regulation. However, there are also effects of macrophage depletion in the ovary which indirectly affect uterine function. Namely, macrophage depletion leads to reduced progesterone (P4) synthesis in the ovaries and the uterine effects can be rescued, at least partly, by P4 supplementation.

The CD11b-DTR mouse model results in systemic macrophage depletion which may damage other tissues outside of the reproductive tract and therefore may result in impacts on pregnancy which could lead to artefactual effects and interpretations. Some examples of such impacts might include systemic inflammation due to macrophage cell death, a toxic impact of DT, or adaptations to injury after macrophage deficiency, including rebound effects on granulocyte numbers. To elucidate the various impacts and effects of macrophage depletion, macrophage replacement is essential. Through administering macrophages and investigating whether effects of macrophage depletion are reversed, we can begin to confirm that results are directly attributable to the actions of macrophage removal and not due to effects on the functions of other cells or other off-target effects. Importantly, through assessing macrophage replacement and P4 replacement, we can further define the essential role of macrophages within the uterus, aside from their crucial roles in the ovary.

Several types of immune cells assist in preparing the maternal reproductive tract for pregnancy through vascular and tissue remodelling, and regulation of the immune response. Collectively, immune cells interact to promote a diverse and responsive immune network which facilitates adaptation to pregnancy. Broadly, the most well studied immune cell during pregnancy is the uterine NK (uNK) cell. uNK cells make up approximately 70% of decidual leukocytes during murine pregnancy and contribute extensively to decidual spiral artery remodelling (Moffett-King, 2002). Whilst uNK cells are abundant and have clear roles in promoting maternal vascular adaptation to pregnancy, mice deficient in NK cells can carry viable pups to term (Guimond et al., 1997a). This suggests that the role of uNK cells may not be essential. In contrast, transient depletion of macrophages leads to pregnancy failure (Care et al., 2013). Furthermore, the interactions between macrophages and uNK cells have not been extensively investigated. As the immune system in pregnancy is now recognised as a network of immune cells, it is reasonable to predict that each of the immune cell subsets interact and can dictate the function of other subsets.

The roles of T cells in pregnancy are being extensively researched due to their spectrum of phenotypes and critical roles in tolerance and effector responses. Importantly, regulatory T cells (Treg) cells are the

main drivers of immune tolerance and are thought to be responsible for controlling phenotypes of other immune cell subsets (Robertson et al., 2009b). Treg cell depletion during murine pregnancy, using the FOXP3-DTR mouse model, causes increased fetal resorptions and increased maternal vascular resistance (Care et al., 2018). Comparatively to uNK cells, Treg cells are relatively sparse in the uterus during pregnancy and are more prevalent in the paraaortic lymph nodes, spleen, and periphery (Robertson et al., 2009a). This implies that Treg cells have broad and systemic roles during pregnancy, whereas uNK cells and macrophages appear to localise to the uterus perhaps suggesting more direct effects in implantation sites. Again, interactions between Treg cells and macrophages are under-researched, and more work is required to investigate their converging roles rather than assessing these subsets independently. A broader approach would be to investigate multiple immune cells simultaneously and determine how changes to individual subsets can affect the entire immune network.

To assess the contributions of macrophages to vascular biology in other tissue settings, various models have been utilised whereby macrophages are depleted, or their phenotype and/or behaviour is altered by specific gene knockouts. These approaches allow researchers to address questions about macrophage biology in specific settings, yet often do not shed light on their interactions with other immune cells.

Previous studies have identified that macrophage depletion in the CD11b-DTR mouse model elicits ovarian haemorrhage and reduced serum P4 during early pregnancy (Care et al., 2013). We have shown that supplementation with P4 was sufficient to restore decidualisation and implantation yet failed to reduce embryo mortality from mid-gestation (chapter three). These findings imply that macrophages have a direct role within the uterus to promote pregnancy success. It was therefore essential to investigate earlier events in pregnancy to identify mechanisms of pregnancy failure and the specific roles of macrophages at this time. Thus, in this chapter, early pregnancy outcomes were evaluated in WT and CD11b-DTR mice. To induce macrophage depletion, CD11b-DTR mice were treated with 25 ng/g DT on day 5.5 pc and were then administered either s.c. P4 or i.v. bone marrow-derived macrophages (BMDM). WT mice were also treated with 25 ng/g DT on day 5.5 pc. Pregnancy outcomes were assessed on day 7.5 pc, including pregnancy viability, corpus luteum structure, serum P4, implantation site structure, decidualisation, and uterine vascular remodelling. Furthermore, the impact of macrophage depletion on the profile of other immune cells was assessed by flow cytometry and immunohistochemistry, wherein macrophage, granulocyte, NK cell, and Treg cell populations were investigated following macrophage depletion.

5.2 EFFECT OF P4 OR BONE MARROW-DERIVED MACROPHAGE (BMDM) ADMINISTRATION ON EARLY PREGNANCY OUTCOMES

To investigate the mechanisms behind pregnancy failure after macrophage depletion, CD11b-DTR and WT females were mated to BALB/c stud males and were administered 25 ng/g DT on day 5.5 pc. P4 administration was conducted such that macrophage-depleted females were supplemented with 0.2 mg/ml P4 on days 5.5 pc and 6.5 pc via s.c. injection (MD^{25} + P4). An additional CD11b-DTR cohort was treated with 25 ng/g DT on day 5.5 pc and were administered WT CSF-1-induced BMDM on days 3.5 pc and 5.5 pc (MD^{25} + MØ). Breeding strategy and treatment regime present in Figure 5.1. This same experimental design is utilised for data presented in chapter six. Some elements of relevant data for the WT and MD^{25} cohorts from chapter three of this thesis are reproduced in this chapter for comparison purposes.

5.2.1 EFFECT OF DT ADMINISTRATION TO CD11b-DTR MICE ON MACROPHAGE AND GRANULOCYTE NUMBERS IN THE UTERUS

Firstly, we sought to investigate whether macrophage and granulocyte populations remained altered 48 h after DT administration in CD11b-DTR mice with and without P4 or BMDM administration. These populations were assessed in the uterus by flow cytometry (FACS) and immunohistochemistry.

5.2.1.1 MACROPHAGES

Implantation sites on day 7.5 pc were assessed for F4/80 density using immunohistochemistry 48 h after macrophage depletion (Figure 5.1 A-D). There was a 72% reduction in F4/80 density in macrophage-depleted females given P4 compared to WT controls (9.2 ± 1.3% vs 2.3 ± 0.4%, $p<0.001$, Figure 5.1 E). In addition, there was a 65% reduction in F4/80 density in the macrophage-depleted mice given BMDM (9.2 ± 1.3% vs 3.0 ± 0.7%, WT vs MD^{25} + MØ, $p<0.001$, Figure 5.1 E), suggesting macrophage numbers were not substantially changed or only partially restored with BMDM treatment. Nevertheless, the experiments reported in this chapter and in chapter six confirm clear effects of macrophage supplementation using the BMDM protocol, implying partial replacement has consequences for pregnancy outcomes.

In addition, CD31 density was assessed to identify the density of endothelial cells on day 7.5 pc (Figure 5.1 A-D). However, there were no alterations to the density of $CD31^+$ cells across treatment groups (Figure 5.1 F). At higher magnification in WT mice there was a close physical association of macrophages with endothelial cells in several tissue sections, which suggests a direct interaction between the two cell types is possible (Figure 5.1 G).

The gating strategy used in the FACS experiment to assess macrophages and granulocytes is detailed in Figure 5.2. Briefly, cells were initially sorted based on size and were discriminated based on various forward and side scatter properties to remove doublet cells and debris allowing a population of single cells

to be assessed. Viable cells were delineated from dead cells and then the various immune cell populations were assessed. Macrophages were defined as $F4/80^{+}CD11b^{+}$ and granulocytes as $F4/80^{-}CD11b^{+}$. Data are shown both as a percentage of viable cells, and as total cell number, determined using cell counts.

On day 7.5 pc, there was no change to the proportion or number of macrophages in macrophage-depleted mice compared to WT controls (Figure 5.3 C and E). However, the proportion of macrophages decreased in macrophage-depleted mice given P4 compared to WT controls (6.0 ± 0.9% vs 2.9 ± 0.3%, WT vs MD^{25} + P4, p=0.005, Figure 5.3 C). Furthermore, the number of macrophages was reduced in this group compared to WT controls (1.4 ± 0.2 x 10^5 cells vs 0.1 ± 0.1 x 10^5 cells, p=0.002, Figure 5.3 E). In macrophage-depleted mice administered BMDM, the macrophage proportion decreased compared to WT controls (6.0 ± 0.9% vs 3.6 ± 0.5%, WT vs MD^{25} + MØ, p=0.026, Figure 5.3 C). However, there was no difference to macrophage numbers compared to WT controls (Figure 5.3 E).

5.2.1.2 GRANULOCYTES

In the uterus, the proportion of $CD11b^{+}F4/80^{-}$ granulocytes was increased in macrophage-depleted mice compared to WT controls on day 7.5 pc (mean ± SEM, 5.3 ± 0.6% vs 37.3 ± 9.6%, WT vs MD^{25}, p=0.014, Figure 5.3 B). The number of granulocytes was also increased in macrophage-depleted mice compared to WT controls (1.2 ± 0.1 x 10^5 cells vs 4.2 ± 1.2 x 10^5 cells, p=0.044, Figure 5.3 D).

P4 supplementation reduced the proportion of granulocytes compared to macrophage-depleted mice and was not different to WT controls (37.3 ± 9.6% vs 9.0 ± 1.6%, MD^{25} vs MD^{25} + P4, p=0.033, Figure 5.3 B). Furthermore, P4 supplementation reduced the number of granulocytes compared to macrophage-depleted mice (4.2 ± 1.2 x 10^5 cells vs 0.3 ± 0.1 x 10^5 cells, p=0.007, Figure 5.3 D).

BMDM supplementation had no effect on granulocytes proportion or number compared to WT controls (Figure 5.3 B and D).

This data suggests that macrophage numbers were not reduced in the MD^{25} group on day 7.5 pc, 48 h after DT administration. This may be reflective of new monocytes and macrophages being recruited to clear tissue debris within these implantation sites. DT-treated CD11b-DTR females supplemented with P4 had reduced macrophages compared to WT controls, suggesting that in viable implantation sites with sufficient P4, macrophage numbers do not return to normal by day 7.5 pc perhaps due to the effects of P4 on suppressing macrophage recruitment. In contrast, macrophage numbers were somewhat restored in DT-treated CD11b-DTR mice given BMDM, highlighting that macrophage administration, unlike P4, does not interfere with restoring macrophages. In addition, DT-treated CD11b-DTR females had increased numbers of granulocytes in the uterus on day 7.5 pc which may reflect the failed decidualisation in these mice or that perhaps P4 also limits the recruitment of granulocytes into the uterus.

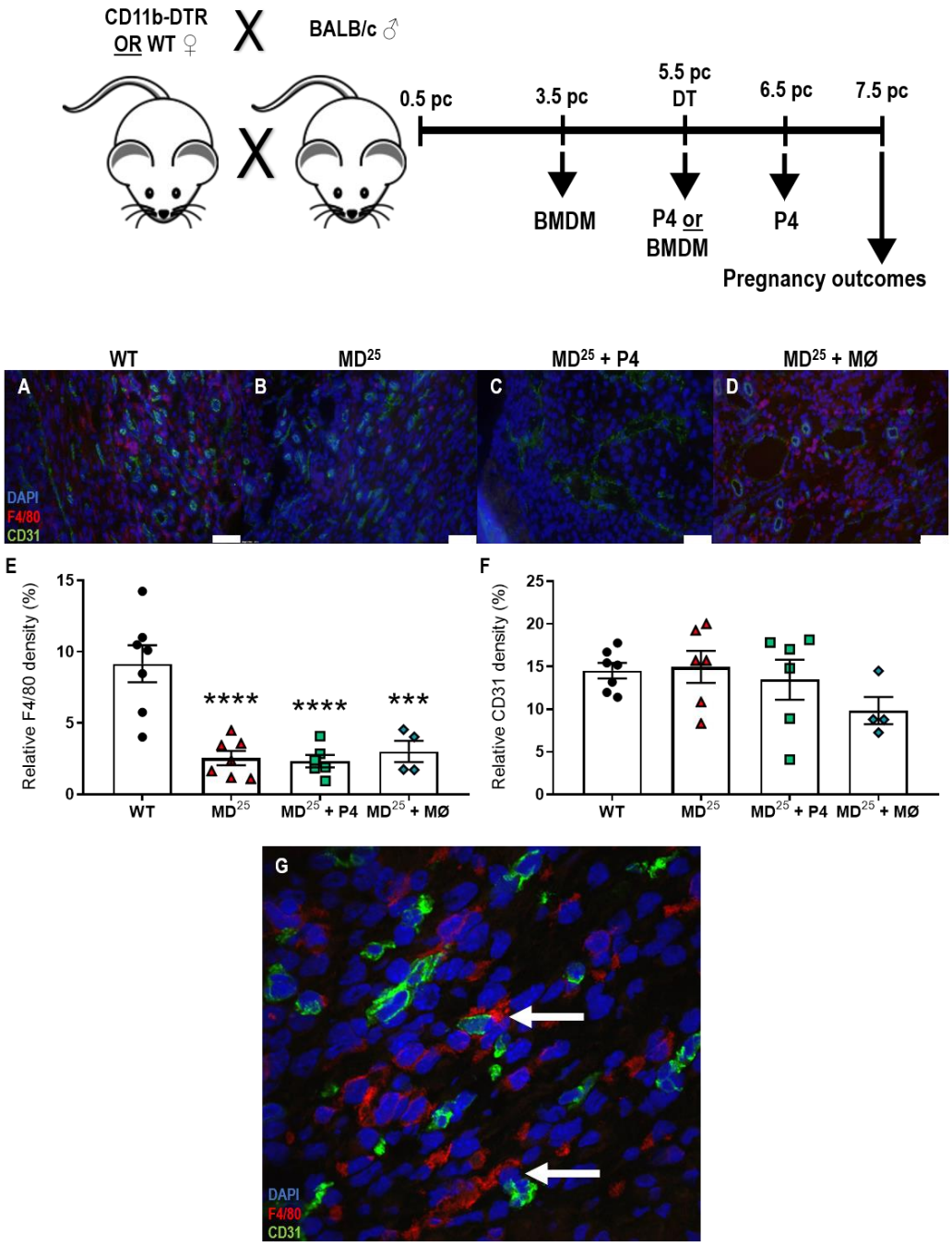

Figure 5.1: DT treatment in CD11b-DTR mice depletes macrophages from the uterine mesometrial triangle on day 7.5 pc.

WT and CD11b-DTR females were mated to BALB/c stud males and 25 ng/g DT was administered on day 5.5 pc. For P4 supplementation, DT-treated CD11b-DTR females were subcutaneously injected with P4 on days 5.5 pc and 6.5 pc. For BMDM administration, DT-treated CD11b-DTR females were intravenously injected with BMDM on days 3.5 pc and 5.5 pc. Macrophage density within the mesometrial triangle was assessed using F4/80 (red). Sections were also stained for CD31 (green) to assess endothelial cells and counterstained with DAPI (blue) on day 7.5 pc (A-D; scale bar is 50 µm). The relative F4/80 density was calculated (E) as was the relative CD31 density (F). A high magnification image (60X magnification) shows the close physical association of $F4/80^+$ and $CD31^+$ cells, indicated by white arrows (G). Data are presented as mean ± SEM with statistical analysis using one-way ANOVA with Sidak's multiple comparisons test, n=4-7 mice/group. * indicates statistical significance ($p<0.05$) compared to WT controls; ***$p<0.001$, ****$p<0.0001$. MD^{25}; macrophage-depleted. MØ; macrophages. P4; progesterone. WT; wild type.

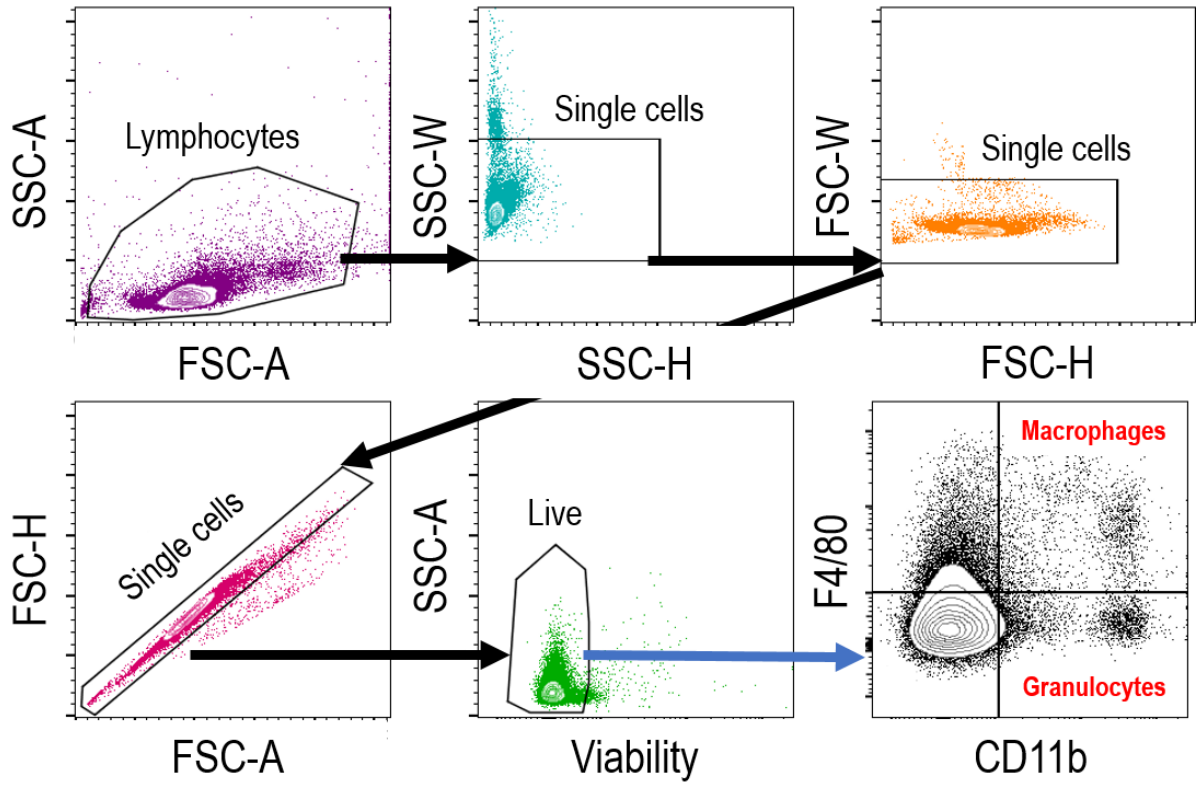

Figure 5.2: Flow cytometry gating strategy to assess macrophages and granulocytes.
WT and CD11b-DTR females were mated to BALB/c stud males and 25 ng/g DT was administered on day 5.5 pc. For P4 supplementation, DT-treated CD11b-DTR females were subcutaneously injected with P4 on days 5.5 pc and 6.5 pc. For BMDM administration, DT-treated CD11b-DTR females were intravenously injected with BMDM on days 3.5 pc and 5.5 pc. Mice were killed on day 7.5 pc and immune cells were analysed by flow cytometry. Initially, cells were gated into lymphocytes, and subsequently cells were discriminated based on single cell status, removing any doublets. Finally, cells were sorted based on viability dye staining into live cells. Using the live cells, macrophages were detected as $F4/80^{+}CD11b^{+}$ and granulocytes as $F4/80^{-}CD11b^{+}$.

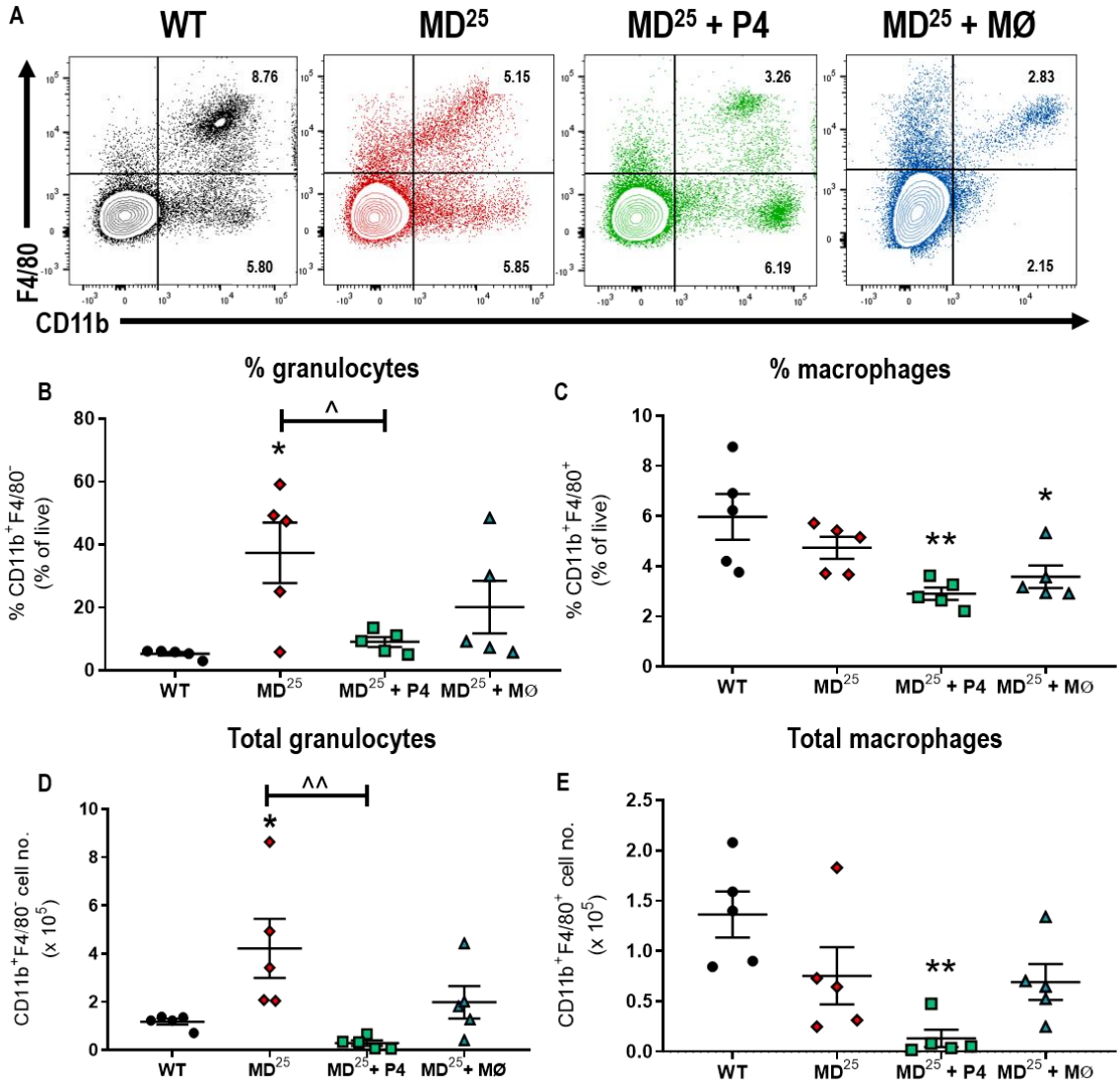

Figure 5.3: Effect of macrophage depletion and macrophage replacement on macrophage and granulocyte populations in the uterus on day 7.5 pc.

WT and CD11b-DTR females were mated to BALB/c stud males and 25 ng/g DT was administered on day 5.5 pc. For P4 supplementation, DT-treated CD11b-DTR females were subcutaneously injected with P4 on days 5.5 pc and 6.5 pc. For BMDM administration, DT-treated CD11b-DTR females were intravenously injected with BMDM on days 3.5 pc and 5.5 pc. Representative FACS plots for CD11b and F4/80 populations in the uterus are shown (A). The proportions of granulocytes (B) and macrophages (C) are presented as a percentage of live cells. From cell counts, granulocyte cell numbers (D) and macrophage cell numbers were calculated (E). Data are presented as mean ± SEM with statistical analysis using one-way ANOVA with Sidak's multiple comparisons test, n=5 mice/group. * indicates statistical significance ($p<0.05$) compared to WT controls; *$p<0.05$, **$p<0.01$. ^ indicates statistical significance ($p<0.05$) compared to MD^{25} mice; ^$p<0.05$ and ^^$p<0.01$. MD^{25}; macrophage-depleted. MØ; macrophages. P4; progesterone. WT; wild type.

5.2.2 PREGNANCY OUTCOMES

Macrophage depletion in CD11b-DTR mice led to pregnancy loss, evidenced by non-viable implantation sites on day 7.5 pc (Figure 5.4 B). Macrophage-depleted females also had haemorrhagic ovaries compared to WT mice (Figure 5.4 A and B). When P4 was supplemented in macrophage-depleted mice, the implantation sites appeared viable, yet the ovaries remained haemorrhagic (Figure 5.4 C). Macrophage-depleted females treated with P4 had an increased rate of viable pregnancy compared to macrophage-depleted mice (43% vs 81%, MD^{25} vs MD^{25} + P4, p=0.022, Figure 5.4 E). P4 supplementation also restored the number of viable implantation sites on day 7.5 pc compared to macrophage-depleted mice (mean ± SEM, 3.5 ± 1.2 sites vs 8.0 ± 1.0 sites, p=0.01, Figure 5.4 F).

The administration of BMDM to macrophage-depleted mice improved both the viability of the implantation sites and the appearance of the ovaries (Figure 5.4 D). Macrophage-depleted females treated with BMDM increased the rate of viable pregnancy compared to macrophage-depleted mice (43% vs 78%, MD^{25} vs MD^{25} + MØ, p=0.040, Figure 5.4 E). BMDM administration indicated some restoration of the numbers of viable implantation sites compared to macrophage-depleted mice (mean ± SEM, 3.5 ± 1.2 sites vs 7.4 ± 1.5 sites, p=0.11, Figure 5.4 F). Importantly, implantation sites from DT-treated CD11b-DTR mice given BMDM appeared larger, and more similar to WT controls, than macrophage-depleted mice given P4 (Figure 5.4 C and D).

There was no difference to the rate of viable pregnancy or the number of viable implantation sites when macrophage-depleted mice were administered either P4 or BMDM (Figure 5.4 E and F).

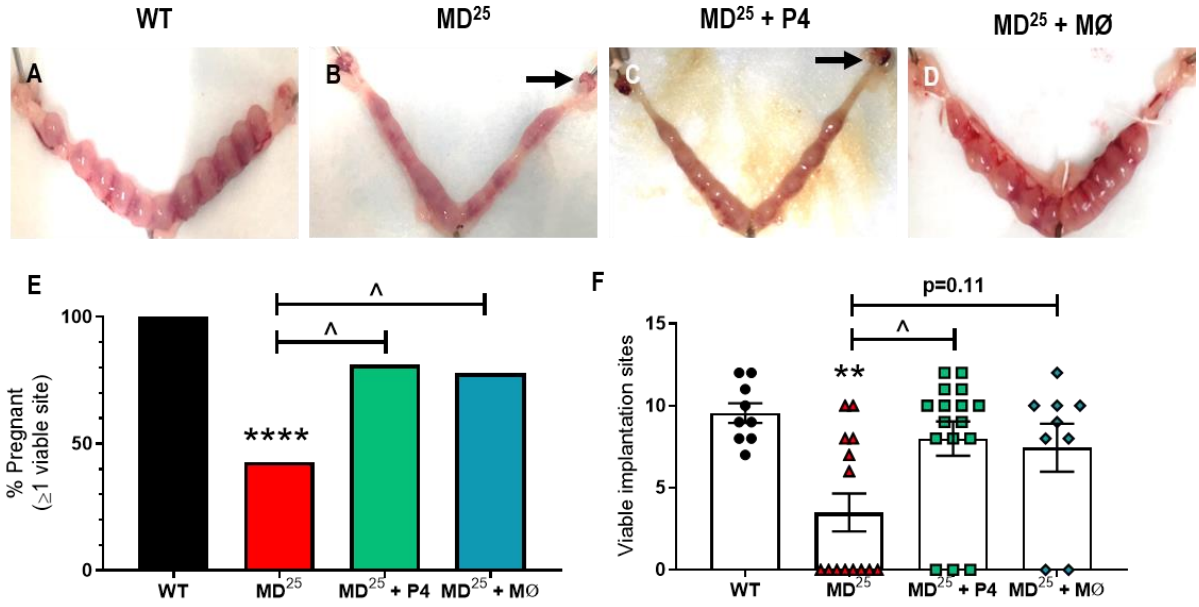

Figure 5.4: P4 or BMDM administration rescues pregnancy viability in macrophage-depleted mice on day 7.5 pc.

WT and CD11b-DTR females were mated to BALB/c stud males and 25 ng/g DT was administered on day 5.5 pc. For P4 supplementation, DT-treated CD11b-DTR females were subcutaneously injected with P4 on days 5.5 pc and 6.5 pc. For BMDM administration, DT-treated CD11b-DTR females were intravenously injected with BMDM on days 3.5 pc and 5.5 pc. Dissected uteri from WT (A), macrophage-depleted (B), macrophage-depleted + P4 (C), and macrophage-depleted + BMDM (D) mice on day 7.5 pc. Pregnancy viability rate (E) and viable implantation site numbers (F) were assessed. Data are presented as mean ± SEM (F). Statistical analysis was performed using a χ^2 test for (E) and a one-way ANOVA with Sidak's multiple comparisons test in (F), n=9-14 mice/group. * indicates statistical significance ($p<0.05$) compared to WT controls; **$p<0.01$ and ****$p<0.0001$. ^ indicates statistical significance ($p<0.05$) compared to MD^{25} mice; ^$p<0.05$. Black arrows; haemorrhagic ovaries. MD^{25}; macrophage-depleted. MØ; macrophages. P4; progesterone. WT; wild type.

5.2.3 OVARIAN STRUCTURE

To determine whether macrophage administration could restore ovarian structure, the structure of the corpora lutea were assessed. The haematoxylin and eosin-stained representative images showed that macrophage depletion led to substantial red blood cell influx into the corpora lutea independent of P4 treatment, referred to as haemorrhagic corpora lutea (Figure 5.5 A-C). The proportion of haemorrhagic corpora lutea remained increased in macrophage-depleted dams given P4 compared to WT controls (mean ± SEM, 0% vs 65 ± 8%, WT vs MD^{25} + P4, $p<0.001$, Figure 5.5 E).

In contrast, administration of BMDM rescued the corpus luteum structure (Figure 5.5 D). BMDM administration reduced the proportion of haemorrhagic corpora lutea compared to macrophage-depleted mice and macrophage-depleted mice given P4 (72 ± 4% vs 65 ± 8% vs 13 ± 8%, MD^{25} vs MD^{25} + P4 vs MD^{25} + BMDM, $p<0.001$, Figure 5.5 E).

In macrophage-depleted mice given P4, there was an increase in serum P4 compared to WT controls (52.4 ± 4.1 ng/ml vs 86.2 ± 9.9 ng/ml, WT vs MD^{25} + P4, $p=0.004$, Figure 5.5 F). Furthermore, P4 supplementation increased serum P4 concentration compared to macrophage-depleted mice (14.3 ± 2.2 ng/ml vs 86.2 ± 9.9 ng/ml, MD^{25} vs MD^{25} + P4, $p<0.001$, Figure 5.5 F).

Macrophage administration restored the concentration of P4 to comparable WT concentrations and increased the concentration of serum P4 compared to macrophage-depleted mice (14.3 ± 2.2 ng/ml vs 55.1 ± 12.5 ng/ml, MD^{25} vs MD^{25} + BMDM, $p=0.044$, Figure 5.5 F). There was no difference in serum P4 concentration between P4 and BMDM groups.

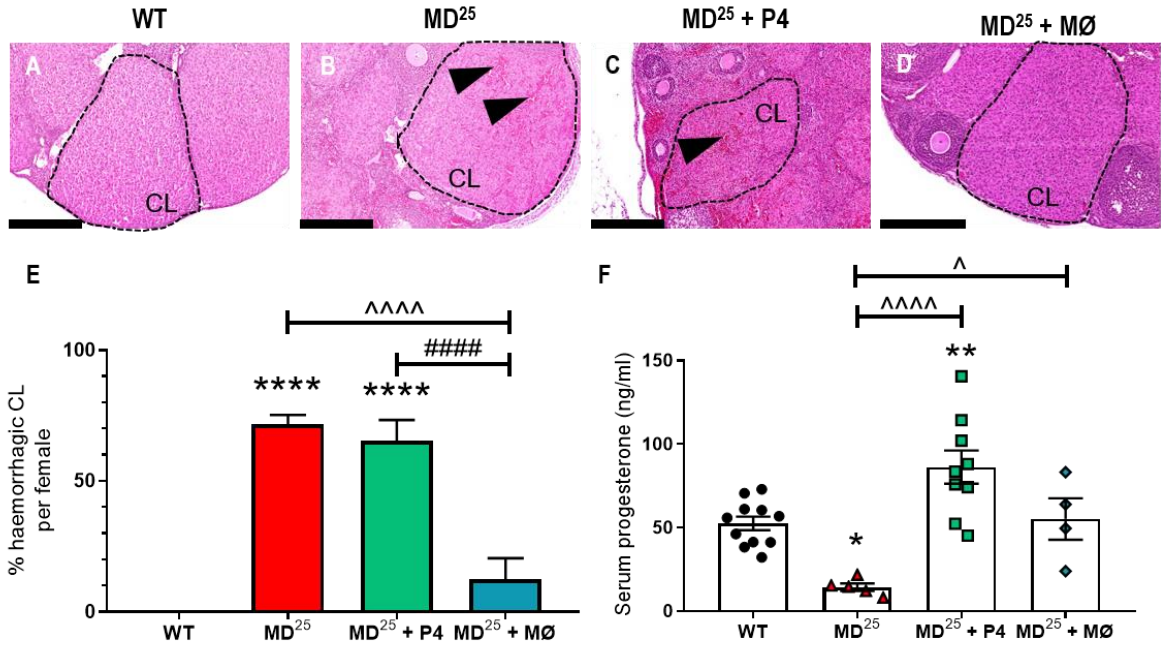

Figure 5.5: BMDM administration rescues ovarian structure and serum P4 concentration in macrophage-depleted mice on day 7.5 pc.

WT and CD11b-DTR females were mated to BALB/c stud males and 25 ng/g DT was administered on day 5.5 pc. For P4 supplementation, DT-treated CD11b-DTR females were subcutaneously injected with P4 on days 5.5 pc and 6.5 pc. For BMDM administration, DT-treated CD11b-DTR females were intravenously injected with BMDM on days 3.5 pc and 5.5 pc. Ovarian morphology was assessed after haematoxylin and eosin staining in WT, macrophage-depleted, macrophage-depleted and P4 supplemented, and macrophage-depleted and BMDM administered mice (A-D; scale bar is 250 µm and influx of red blood cells is shown with black arrows). Proportion of haemorrhagic corpora lutea per female was quantified (E). Serum P4 was measured via ELISA (F). Data are presented as mean ± SEM with statistical analysis using one-way ANOVA with Sidak's multiple comparisons test, n=4-11 mice/group. * indicates statistical significance ($p<0.05$); *$p<0.05$, **$p<0.01$; ****$p<0.0001$. ^ indicates statistical significance ($p<0.05$) compared to MD^{25} mice; ^$p<0.05$ and ^^^^$p<0.0001$. # indicates statistical significance ($p<0.05$) compared to MD^{25} + P4 mice; ####$p<0.0001$. Arrows; red blood cells influx into the corpus luteum. CL; corpus luteum. Dashed lines; corpora lutea. MD^{25}; macrophage-depleted. MØ; macrophages. P4; progesterone. WT; wild type.

5.2.4 IMPLANTATION SITE STRUCTURE

To better understand the effects of P4 or BMDM administration on implantation sites, the extent of decidualisation was assessed using alkaline phosphatase staining (Figure 5.6 A-D). P4 or BMDM administration both increased the area of decidualisation compared to macrophage-depleted mice such that it was not different to WT controls (Figure 5.6 A-D and I).

The mid-sagittal sections were also used to assess conceptus area at a higher magnification (Figure 5.6 E-H). Like macrophage-depleted females without supplements, macrophage-depleted females given P4 had conceptus regions that were smaller and less well-defined compared to WT controls (mean ± SEM, 0.47 ± 0.04 mm^2 vs 0.18 ± 0.07 mm^2, WT vs MD^{25} + P4, p=0.003, Figure 5.6 E-H and J).

In contrast, BMDM administration improved the defective implantation and there was no difference in conceptus area between WT and BMDM administered mice (Figure 5.6 J).

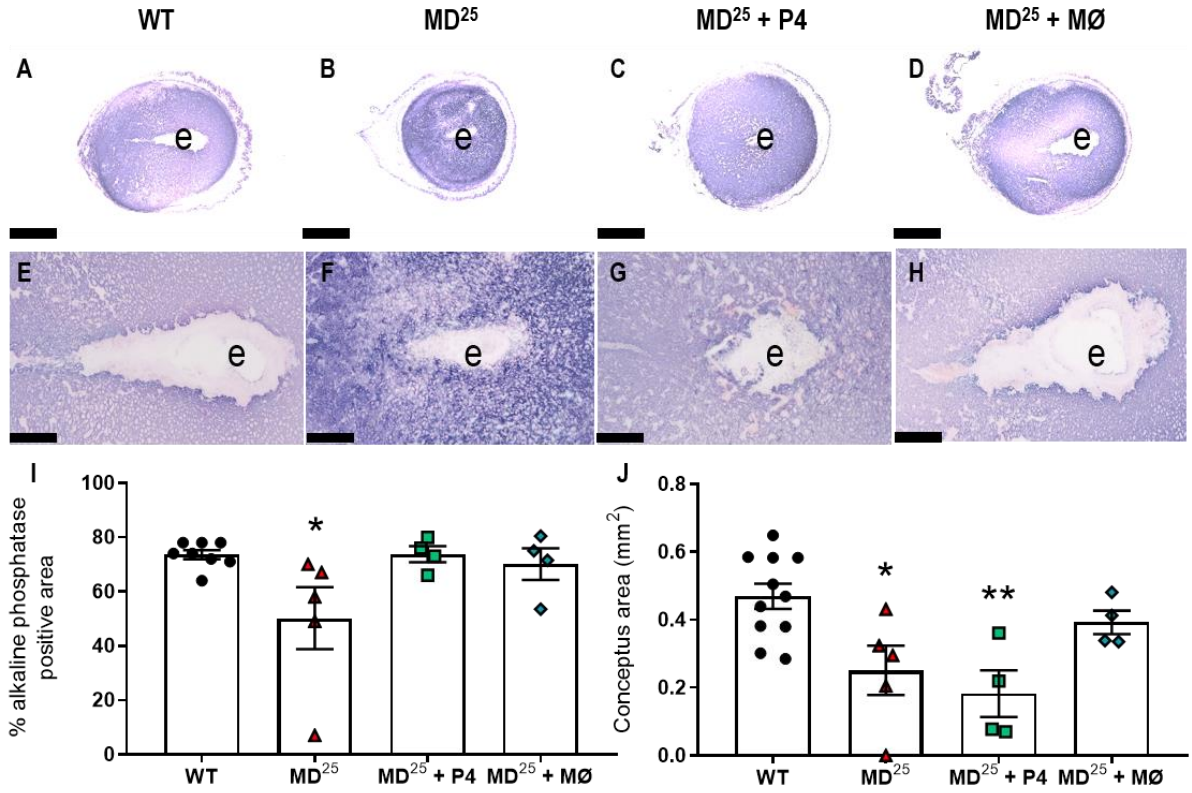

Figure 5.6: BMDM administration improves decidualisation and conceptus area on day 7.5 pc. WT and CD11b-DTR females were mated to BALB/c stud males and 25 ng/g DT was administered on day 5.5 pc. For P4 supplementation, DT-treated CD11b-DTR females were subcutaneously injected with P4 on days 5.5 pc and 6.5 pc. For BMDM administration, DT-treated CD11b-DTR females were intravenously injected with BMDM on days 3.5 pc and 5.5 pc. Alkaline phosphatase stained implantation sites show the maternal decidua in purple in WT, macrophage-depleted, macrophage-depleted and P4 supplemented, and macrophage-depleted and BMDM administered mice (A-D; scale bar is 1 mm). The conceptus area is shown for each of the four groups (E-H; scale bar is 250 µm). The extent of decidualisation was quantified using alkaline phosphatase staining (I). The conceptus area was measured (J). Data are presented as mean ± SEM with statistical analysis using one-way ANOVA with Sidak's multiple comparisons test, n=4-8 mice/group. * indicates statistical significance ($p<0.05$) compared to WT controls; *$p<0.05$, **$p<0.01$. e; embryo. MD^{25}; macrophage-depleted. MØ; macrophages. P4; progesterone. WT; wild type.

5.2.5 UTERINE VASCULAR REMODELLING

To investigate whether P4 or BMDM supplementation improved the defects in vascular remodelling induced by macrophage deficiency, uterine arteries in the mesometrial triangle were assessed on day 7.5 pc (Figure 5.7 A-D). Administration of P4 to macrophage-depleted mice did not alter vessel parameters compared to macrophage-depleted mice. Furthermore, there was a 44% reduction in lumen area in macrophage-depleted mice given P4 compared to WT controls (mean ± SEM, 319.5 ± 42.7 μm^2 vs 138.5 ± 17.1 μm^2, WT vs MD^{25} + P4, p=0.026, Figure 5.7 E). Moreover, vessel diameter was reduced by 17% in macrophage-depleted mice given P4 compared to WT controls (23.3 ± 1.9 µm vs 19.4 ± 4.5 µm, p=0.024, Figure 5.7 F). There was no change to the cross-sectional area, total area, or total to lumen area ratio compared to WT controls (Figure 5.7 G-I).

In contrast, macrophage administration to macrophage-depleted mice largely repaired the vascular defects such that there was no difference compared to WT controls across all vascular parameters measured (Figure 5.7 E-I). Furthermore, the total area to lumen area ratio trended towards between decreased in macrophage-depleted mice administered BMDM compared to macrophage-depleted mice and macrophage-depleted mice given P4 (9.3 ± 2.0 vs 9.5 ± 1.8 vs 4.6 ± 0.6, MD^{25} vs MD^{25} + P4 vs MD^{25} + BMDM, p=0.10 for MD^{25} vs MD^{25} + BMDM & p=0.08 for MD^{25} + P4 vs MD^{25} + BMDM, Figure 5.7 I).

Overall, this data suggests that macrophages function within the uterus to promote embryo implantation and vascular remodelling required for pregnancy success. Furthermore, P4 supplementation appears to be sufficient to restore decidualisation.

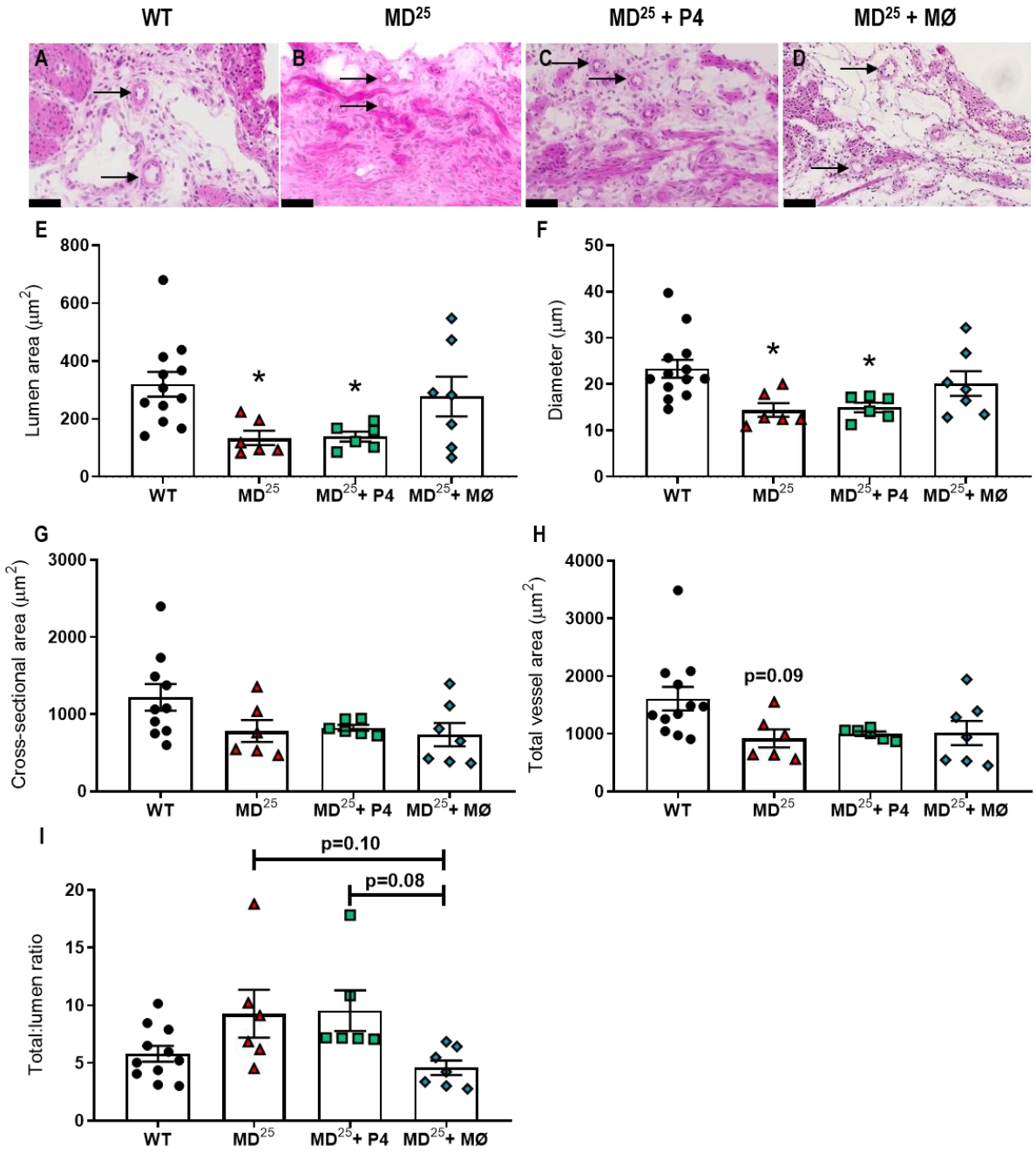

Figure 5.7: BMDM administration rescues implantation site vascularisation in macrophage-depleted mice on day 7.5 pc.

WT and CD11b-DTR females were mated to BALB/c stud males and 25 ng/g DT was administered on day 5.5 pc. For P4 supplementation, DT-treated CD11b-DTR females were subcutaneously injected with P4 on days 5.5 pc and 6.5 pc. For BMDM administration, DT-treated CD11b-DTR females were intravenously injected with BMDM on days 3.5 pc and 5.5 pc. Haematoxylin and eosin-stained sections were used to assess mesometrial triangle vessels (A-D; scale bar is 100 µm, black arrows indicate arteries). Vessel parameters in the mesometrial triangle were calculated including lumen area (E), diameter (F), cross-sectional area (G), total area (H), and the ratio of total vessel area to lumen area (I). Data are presented as mean ± SEM with statistical analysis using one-way ANOVA with Sidak's multiple comparisons test, n=6-12 mice/group. * indicates statistical significance ($p<0.05$) compared to WT controls; *$p<0.05$. MD^{25}; macrophage-depleted. MØ; macrophages. P4; progesterone. WT; wild type.

5.3 EFFECT OF MACROPHAGE DEPLETION ON IMMUNE CELL POPULATIONS

To further investigate the mechanisms whereby macrophages act to promote pregnancy success and vascular adaptations, additional leukocyte populations were assessed by FACS and immunohistochemistry. Here, we sought to investigate whether macrophage depletion caused changes in other leukocyte lineages that might influence receptivity to implantation and/or vascular adaptions to pregnancy. Briefly, the same four treatment groups (WT, MD^{25}, MD^{25} + P4, and MD^{25} + BMDM) were utilised to assess Treg and uNK cells on day 7.5 pc. The time point of 48 h after DT administration was chosen as an appropriate time to evaluate effects of macrophage depletion on other leukocyte lineages.

5.3.1 EFFECT OF MACROPHAGE DEPLETION ON $CD4^+$ T CELL AND REGULATORY T CELL NUMBERS IN THE PARAAORTIC LYMPH NODES

In order to investigate whether macrophage depletion had consequences for T cell generation or maintenance in the uterine draining lymph nodes, the effect of macrophage depletion on $CD4^+$ T cells and Treg cells were assessed on day 7.5 pc, 48 h after macrophage depletion. $CD3^+$ and $CD4^+$ T cells were identified and Treg cells were defined as $CD3^+CD4^+CD25^+FOXP3^+$ cells (Figure 5.8).

5.3.1.1 $CD4^+$ T CELLS

There was no effect of macrophage depletion on $CD4^+$ T cells in the paraaortic lymph nodes. However, there was an increase in the proportion of $CD4^+$ T cells in macrophage-depleted mice given P4 compared to WT controls in the paraaortic lymph nodes (mean ± SEM, 44.8 ± 3.3% vs 54.9 ± 1.5%, WT vs MD^{25} + P4, p=0.021, Figure 5.9 B). In contrast, BMDM supplementation trended toward reducing the proportion of $CD4^+$ T cells compared to macrophage-depleted mice given P4 and was not different to WT controls (54.9% ± 1.5% vs 46.3 ± 1.5%, MD^{25} + P4 vs MD^{25} + MØ, p=0.10, Figure 5.9 B). There was no impact to T cell numbers in the paraaortic lymph nodes.

5.3.1.2 REGULATORY T CELLS

Macrophage depletion did not alter the proportion or number of Treg cells within the paraaortic lymph nodes on day 7.5 pc (Figure 5.10).

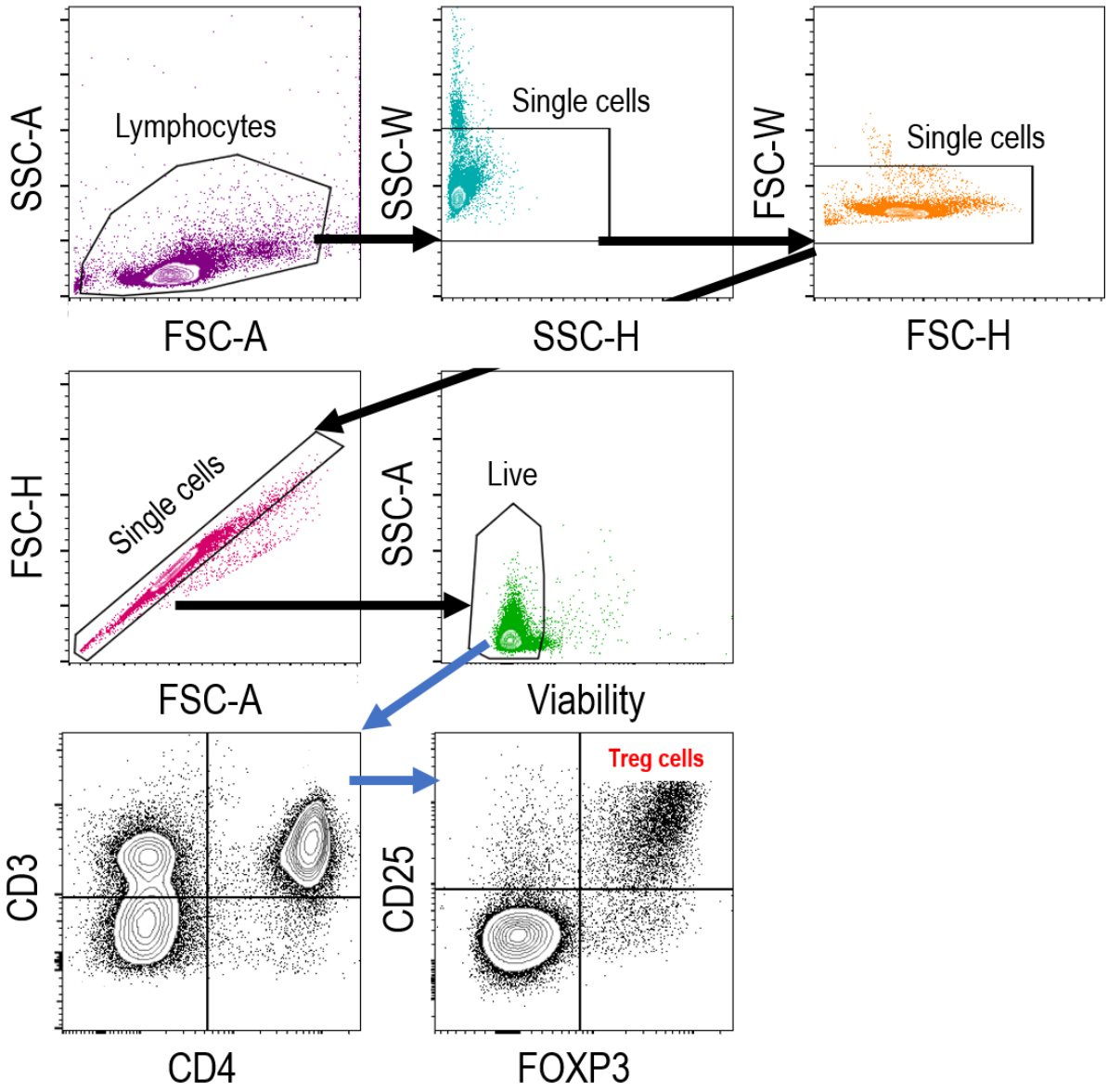

Figure 5.8: Flow cytometry gating strategy to assess CD4+ T cells and regulatory T cells.
WT and CD11b-DTR females were mated to BALB/c stud males and 25 ng/g DT was administered on day 5.5 pc. For P4 supplementation, DT-treated CD11b-DTR females were subcutaneously injected with P4 on days 5.5 pc and 6.5 pc. For BMDM administration, DT-treated CD11b-DTR females were intravenously injected with BMDM on days 3.5 pc and 5.5 pc. Mice were killed on day 7.5 pc and immune cells were analysed by flow cytometry. Initially, cells were gated into lymphocytes, and subsequently cells were discriminated based on single cell status, removing any doublets. Finally, cells were sorted based on viability dye staining into live cells. Using the live cells, $CD3^+CD4^+$ T cells were identified and Treg cells were defined as $CD3^+CD4^+CD25^+FOXP3^+$.

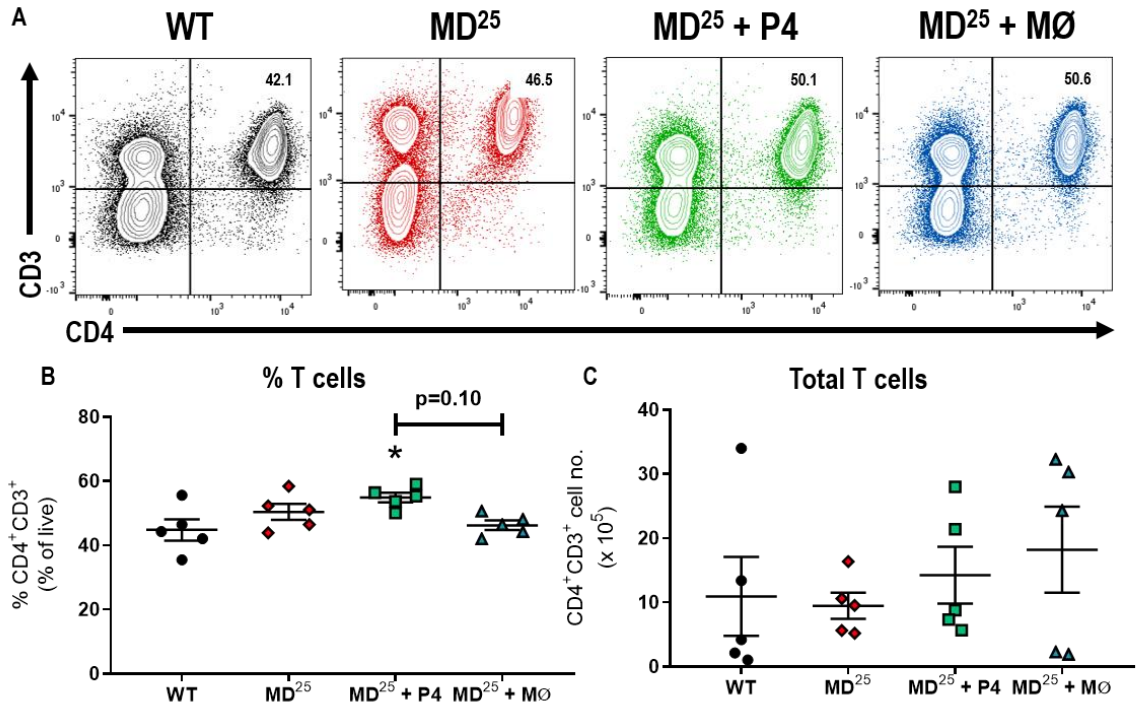

Figure 5.9: Macrophage depletion and macrophage replacement has no effect on T cell populations in the paraaortic lymph nodes on day 7.5 pc.

WT and CD11b-DTR females were mated to BALB/c stud males and 25 ng/g DT was administered on day 5.5 pc. For P4 supplementation, DT-treated CD11b-DTR females were subcutaneously injected with P4 on days 5.5 pc and 6.5 pc. For BMDM administration, DT-treated CD11b-DTR females were intravenously injected with BMDM on days 3.5 pc and 5.5 pc. Representative FACS plots for CD4 and CD3 populations in the paraaortic lymph nodes for the four treatment groups are shown (A). The proportions and numbers of $CD4^+CD3^+$ T cells were assessed (B and C). Data are presented as mean ± SEM with statistical analysis using one-way ANOVA with Sidak's multiple comparisons test, n=5 mice/group. * indicates statistical significance ($p<0.05$) compared to WT controls; *$p<0.05$. MD^{25}; macrophage-depleted. MØ; macrophages. P4; progesterone. WT; wild type.

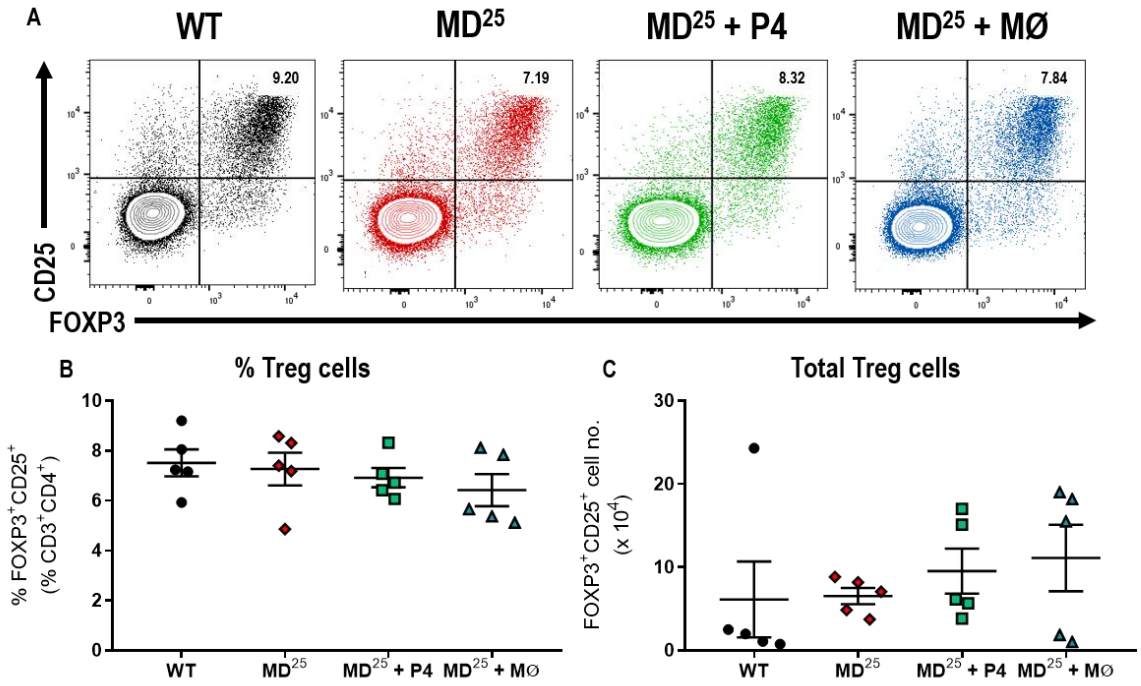

Figure 5.10: Macrophage depletion and macrophage replacement has no effect on Treg cell populations in the paraaortic lymph nodes on day 7.5 pc.

WT and CD11b-DTR females were mated to BALB/c stud males and 25 ng/g DT was administered on day 5.5 pc. For P4 supplementation, DT-treated CD11b-DTR females were subcutaneously injected with P4 on days 5.5 pc and 6.5 pc. For BMDM administration, DT-treated CD11b-DTR females were intravenously injected with BMDM on days 3.5 pc and 5.5 pc. Representative FACS plots for FOXP3 and CD25 populations in the paraaortic lymph nodes for the four treatment groups are shown as a proportion of $CD3^+CD4^+$ cells (A). The proportions of Treg cells were assessed as a percentage of $CD3^+CD4^+$ cells (B). From cell counts, Treg cell numbers were calculated (C). Data are presented as mean ± SEM with statistical analysis using one-way ANOVA with Sidak's multiple comparisons test, n=5 mice/group. MD^{25}; macrophage-depleted. MØ; macrophages. P4; progesterone. WT; wild type.

5.3.2 EFFECT OF MACROPHAGE DEPLETION ON uNK CELL NUMBERS

We next sought to assess how macrophage depletion and subsequent P4 or BMDM administration impacted uNK cell numbers. Representative images of DBA-stained implantation sites are presented in Figure 5.11 (A-D). At increased magnification, uNK cells localised in the primary decidual zone are clearly distinct (Figure 5.11 E-H). When quantified, there was an 87% reduction of DBA^+ cells in macrophage-depleted mice compared to WT controls (mean ± SEM, 46.1 ± 5.9% vs 6.0 ± 2.9%, WT vs MD^{25}, $p<0.003$, Figure 5.11 I).

P4 supplementation increased the density of uNK cells compared to macrophage-depleted mice (6.0 ± 2.9% vs 31.1 ± 5.9%, MD^{25} vs MD^{25} + P4, $p=0.028$, Figure 5.11 I). Furthermore, BMDM supplementation also increased the density of uNK cells compared to macrophage-depleted mice (6.0 ± 2.9% vs 28.8 ± 5.0%, MD^{25} vs MD^{25} + MØ, $p=0.043$, Figure 5.11 I). There was no difference between macrophage-depleted mice given P4 or BMDM and WT controls.

Overall, this data suggests that macrophage depletion does not impact T cell populations 48 h after DT administration yet decreases the density of uNK cells. Administration of either P4 or BMDM is effective in rescuing the reduced uNK cell populations.

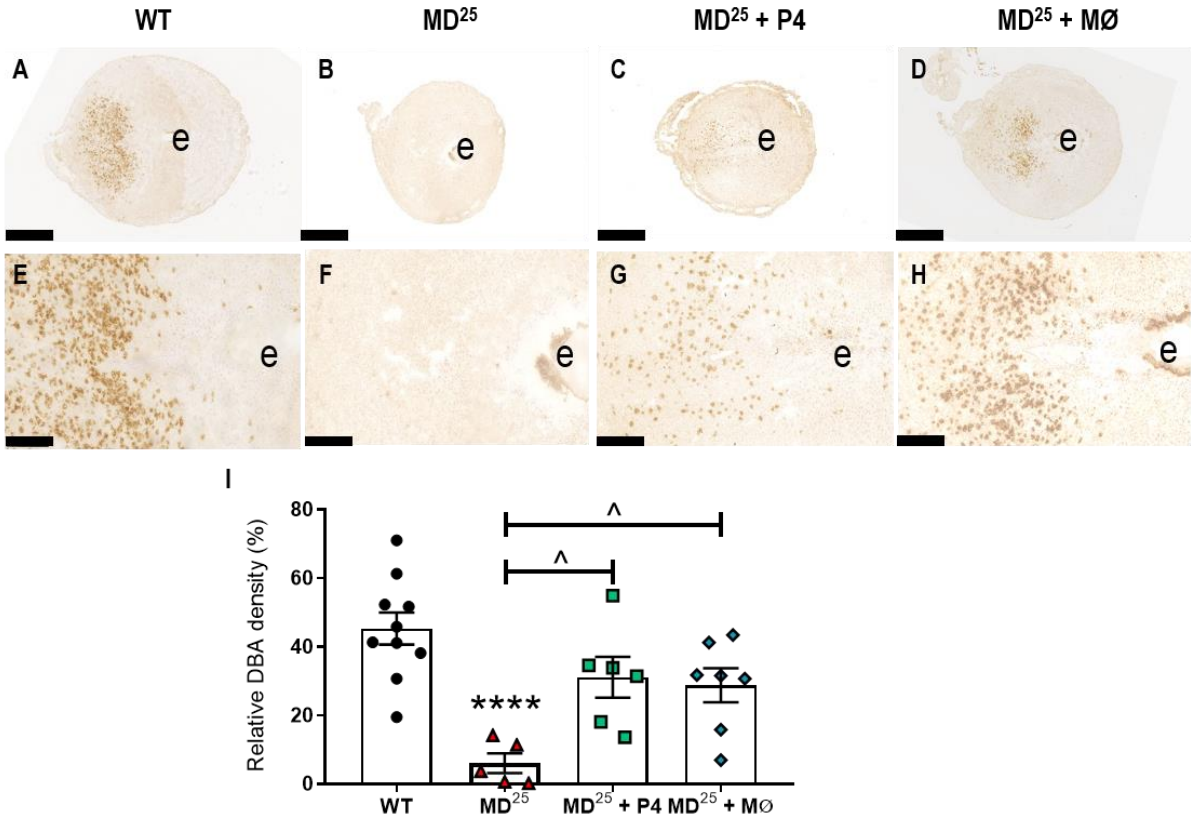

Figure 5.11: Macrophage depletion reduces the abundance of uNK cells on day 7.5 pc.
WT and CD11b-DTR females were mated to BALB/c stud males and 25 ng/g DT was administered on day 5.5 pc. For P4 supplementation, DT-treated CD11b-DTR females were subcutaneously injected with P4 on days 5.5 pc and 6.5 pc. For BMDM administration, DT-treated CD11b-DTR females were intravenously injected with BMDM on days 3.5 pc and 5.5 pc. The localisation of DBA^+ cells in day 7.5 pc implantation sites was assessed in WT, macrophage-depleted, macrophage-depleted and P4 supplemented and macrophage-depleted and BMDM administered (A-D; scale bar is 1 mm). The decidual localisation of DBA^+ cells are shown in the four groups (E – H; scale bar is 250 µm). The relative intensity of DBA staining was then quantified (I). Data are presented as mean ± SEM with statistical analysis using one-way ANOVA with Sidak's multiple comparisons test, n=5-10 mice/group. * indicates statistical significance ($p<0.05$) compared to WT controls; ****$p<0.0001$. ^ indicates statistical significance ($p<0.05$) compared to MD^{25} mice; ^$p<0.05$. e; embryo. MD^{25}; macrophage-depleted. MØ; macrophages. P4; progesterone. WT; wild type.

5.4 DISCUSSION

The data within this chapter demonstrate that macrophages are critical to pregnancy success through direct effects in the uterus and interact with other immune cell subsets in early murine pregnancy. Our data indicate that in the peri-implantation phase of pregnancy, macrophages are involved in tissue and vascular remodelling within the uterus for adequate embryo implantation. We demonstrate that macrophage depletion results in reduced pregnancy viability and suppresses decidualisation, conceptus development, and vascular remodelling, and furthermore reduces the uNK cell population on day 7.5 pc. Through supplementation of P4 in macrophage-depleted mice, we were able to restore decidualisation and the population of uNK cells. However, conceptus area and vascular remodelling were still impaired. Notably, the administration of BMDM rescued ovarian structure, decidualisation, and conceptus area, and improved uterine vascular remodelling and uNK cell numbers. Importantly, BMDM administration improves pregnancy outcomes greater than P4 administration. This further supports the interpretation that macrophages play key roles within the uterus to facilitate tissue and vascular remodelling in addition to their roles within the ovary to sustain luteal production of P4 which indirectly contributes to uterine function.

5.4.1 BMDM ADMINISTRATION RESTORES MACROPHAGE NUMBERS

Within the mesometrial triangle there was a reduction in macrophage density, as assessed by immunohistochemistry, in all the macrophage-depleted groups. To further investigate macrophage numbers 48 h after depletion, FACS was performed on day 7.5 pc. Data here highlighted that in the uterus there was a sustained reduction in the proportion and number of macrophages in DT-treated CD11b-DTR mice given P4. However, there was no change to macrophage numbers in macrophage-depleted mice without P4 or BMDM, which may indicate that P4 acted to suppress macrophage recruitment during the post-depletion rebound phase. It is possible that additional monocytes and macrophages may get recruited to the uterus to assist with the resorption process and wound healing response (Castelucci et al., 2019). Systemically, there was no change in macrophage numbers in other tissues including the spleen and paraaortic lymph nodes at day 7.5 pc, 48 h after macrophage depletion, consistent with the interpretation that macrophages are only transiently affected and then rebound (Appendices 9.15 and 9.16).

The FACS data confirmed some improvement to macrophage numbers in the uterus after BMDM supplementation. However, the number of macrophages given in each transfer may not be sufficient to reach every implantation site or transferred macrophages may preferentially localise to other tissues. It is interesting to consider resident tissue macrophages and whether depletion of macrophages using the CD11b-DTR model depletes tissue-resident populations which may not be fully restored through BMDM administration (Hashimoto et al., 2013). There is little research into defining a population of tissue resident macrophages in the uterus and therefore we cannot confirm the presence or absence of tissue resident macrophages at this time. However, it seems likely that during embryogenesis, when other tissue resident

macrophages are seeding tissues, some embryonic macrophages seed the reproductive tissues to eventually become tissue resident populations (Hoeffel and Ginhoux, 2018).

5.4.2 BMDM ADMINISTRATION IMPROVES PREGNANCY VIABILITY, UTERINE VASCULAR REMODELLING, AND REPAIRS OVARIAN LESIONS

Macrophage depletion elicited pregnancy failure on day 7.5 pc yet administering either P4 or BMDM to macrophage-depleted mice improved overt pregnancy viability. Notably, implantation sites from macrophage-depleted mice given P4 appeared smaller than the WT controls and less vascularised. However, this was rescued with the administration of BMDM, where the implantation sites appeared similar to WT controls in terms of size and structure.

Despite an improvement in the overt viability of implantation sites from macrophage-depleted mice given P4, the area of the conceptus was reduced to a similar extent as macrophage-depleted mice. This may suggest that embryotrophic factors are dysregulated after the depletion of macrophages, independent of P4 treatment. Importantly, administration of BMDM to macrophage-depleted mice restored the conceptus area, indicating that macrophages contribute to the survival and invasion of trophoblast cells during the peri-implantation phase.

Further interrogation into the implantation site structure revealed that macrophage depletion resulted in reduced decidualisation area. Consistently, P4 levels were decreased after macrophage depletion due to corpora lutea haemorrhage. Similarly, ovarian haemorrhage was still apparent in macrophage-depleted mice treated with P4. Importantly, P4 signalling promotes decidualisation (Tan et al., 1999, Lim et al., 1999). Decidualisation area was restored with the administration of either P4 or BMDM as was the concentration of serum P4. Here the P4 treatment substantially increased serum P4 levels above WT levels, demonstrating that the treatment is effective in overcoming P4 loss due to structural demise of the corpora lutea after macrophage depletion.

Importantly, corpus luteum structure was rescued with the supplementation of BMDM and therefore resulted in increased serum P4 concentration compared to macrophage-depleted mice. This confirms that circulating macrophages are essential for maintaining the structure of the corpus luteum during early to mid-pregnancy, beyond the time of implantation as was previously reported (Care et al., 2013). Interestingly, there was a small increase in the percentage of haemorrhagic corpora lutea in the BMDM group which suggests that some of the transfers were not as effective as others. This was likely caused by the number and viability of the injected macrophages varying across experiments.

Vascular remodelling within the mesometrial triangle was impaired after macrophage depletion, independent of P4 supplementation. Crucially, BMDM administration restored these parameters such that they were not different from WT controls. This confirms that the effects seen in macrophage-depleted mice are the consequence of specific physiological actions of macrophages within the uterus, as opposed

to off-target or artefactual effects of the depletion protocol. Furthermore, macrophages are crucial in promoting uterine vascular adaptation to pregnancy and embryo development. In addition, whilst there was no difference in the density of $CD31^+$ cells in the mesometrial triangle, there was a close physical association of macrophages with endothelial cells in WT mice and may implicate macrophages as direct modulators of endothelial cell activity. Furthermore, density does not take into consideration whether these cells are forming functional vessels or the remodelling status of these vessels. Therefore, future studies should look to assess endothelial cell function in response to macrophages.

During pregnancy, uNK cells can function to promote decidual vascular remodelling (Moffett-King, 2002, Kieckbusch et al., 2014, Madeja et al., 2011). Our data highlight that macrophage depletion resulted in a reduced density of uNK cells within the decidua on day 7.5 pc. Interestingly, macrophage depletion also reduced the proportion of NK cells within the spleen and paraaortic lymph nodes (Appendices 9.17 and 9.18). There is some evidence to suggest that uNK cell precursors may arise in the spleen (Chantakru et al., 2002). However, we sought to investigate whether the impaired vascular remodelling observed after macrophage depletion resulted from decreased uNK cell numbers or direct effects of macrophages on vessels within the uterus.

We previously established that macrophage numbers were higher in the myometrium and the mesometrial triangle than in the decidua on day 7.5 pc (Appendix 9.2). Herein, we found that uNK cells were mainly located in the primary decidual zone as previously reported (Madeja et al., 2011). There was an increase in uNK cell density with P4 treatment in macrophage-depleted mice. Interestingly, uNK cell numbers have been linked with P4 levels in previous studies whereby increases to P4 during decidualisation resulted in increased uNK cell numbers (Herington and Bany, 2007b). Therefore, the reduction in serum P4 in macrophage-depleted mice may explain the low uNK cell numbers.

In addition, administration of BMDM increased uNK cell population compared to macrophage-depleted mice. This suggests that, in addition to P4, the presence of macrophages may directly modulate the uNK cell population. As P4 and BMDM supplementation were both able to restore uNK cell population but P4 supplementation did not restore vascular remodelling, these data imply that macrophages directly promote uterine vascular remodelling during the peri-implantation phase of pregnancy. However, it remains to be further investigated whether NK cells have a direct reliance on macrophages to support their population either within the uterus or systemically (Molgora et al., 2019). Although phenotypic markers of uNK cells were not assessed in this thesis, this model provides an interesting avenue of research to determine how macrophages and uNK cells interact. An important research question involves asking whether macrophages can support the uNK cell phenotype to drive vascular remodelling and trophoblast invasion during the peri-implantation phase.

5.4.3 MACROPHAGE DEPLETION DOES NOT AFFECT T CELL POPULATIONS

Overall, there were no major impacts to the numbers of T cells or Treg cells in the paraaortic lymph nodes or spleen (Appendices 9.19 and 9.20). This suggests that the depletion of macrophages did not affect the numbers of Treg cells, unlike its effect on uNK cells. Since specific phenotypic markers were not investigated, we cannot rule out that macrophage depletion may alter the suppressive functions of Treg cells. However, as there were no major impacts to T cell populations, this indicates that macrophages are unlikely to be involved in promoting and maintaining immune tolerance during the peri-implantation phase of murine pregnancy, and that their effects on contributing to uterine vascular remodelling are likely more important.

5.4.4 GRANULOCYTE NUMBERS ARE RESTORED WITH P4 OR BMDM ADMINISTRATION

One of the artefactual consequences of macrophage depletion is the increased proportion of granulocytes within the uterus on day 7.5 pc. This has been confirmed in the literature as a common rebound effect of macrophage depletion (Duffield et al., 2005). This may occur as a result of the injury related to DT treatment, systemic inflammation, or due to macrophage cell death triggering increased bone marrow granulocyte release. Granulocyte number was not changed in macrophage-depleted mice given P4 compared to the increased number of granulocytes in the uterus of macrophage-depleted mice in the uterus. Furthermore, BMDM administration restored the number of granulocytes within the uterus such that it was not different from WT controls. This highlights that granulocyte recruitment is likely to be associated with poor decidualisation since decidualisation was restored in the P4 and BMDM treatment groups but impaired in macrophage-depleted mice. This suggests that this artefact is not a mechanism for the impaired vascular remodelling observed.

In summary, this chapter demonstrates that uterine macrophages are crucial for pregnancy success. The depletion of macrophages ultimately causes pregnancy failure which is likely due to direct actions of uterine macrophages and potentially via macrophage-derived factors influencing the vascular adaptation to pregnancy. Importantly, data within this chapter highlight macrophages as playing key roles in vascular remodelling within the uterus. This was confirmed through macrophage replacement experiments wherein vascular remodelling was rescued, unlike P4 supplementation which was unable to restore the impaired vascular remodelling. In addition, macrophage depletion had minimal effects on other immune cell numbers both systemically and in the uterus. However, an interesting link between macrophages, P4, and uNK cells was revealed. Future research should address whether it is the presence of macrophages that retains uNK cells in the decidua or whether macrophages provide survival signals to the uNK cells via P4-mediated processes. This study is the first of its kind to provide evidence that macrophages potentially contribute to the maintenance of uNK cells. Experiments performed in chapter six look to determine mechanisms whereby macrophages promote pregnancy success through regulating uterine vascular remodelling and the potential interaction between uNK cells and macrophages in the decidua.

CHAPTER 6

EFFECT OF MACROPHAGE DEPLETION AND REPLACEMENT ON UTERINE RNA EXPRESSION IN THE EARLY POST-IMPLANTATION PHASE

6.1 INTRODUCTION

The mechanisms which underpin pregnancy success are complex. Importantly, the maternal vasculature must adapt to the demands of pregnancy in order to provide the optimal environment for fetal and placental growth (Osol and Mandala, 2009b). It is widely accepted that immune cells are crucial for pregnancy success; firstly, by promoting immune tolerance to the semi-allogeneic fetus and secondly, by facilitating tissue and vascular remodelling supporting fetal and placental development (Robertson et al., 2018, Lash et al., 2016). In pregnancy, there is a delicate balance of immune cell subsets to regulate and induce maternal vascular adaptations. Key immune cell populations include macrophages, uterine NK (uNK) cells, and regulatory T (Treg) cells.

In mice, there are two distinct regions of the uterus during early to mid-pregnancy with different resident leukocyte populations. Firstly, the outer region, the myometrium, is a muscular layer populated mainly by macrophages (Erlebacher, 2014). Uterine arteries traverse the myometrium to extend into the developing decidua, supplying nutrients to the trophoblast cells. Secondly, the inner region, the decidua, is formed during decidualisation to allow for an adequate environment for embryo implantation and placental development. High numbers of uNK cells and fewer macrophages populate the decidua (Erlebacher, 2014). Within the decidua, spiral arteries undergo remodelling through interactions with trophoblast cells and uNK cells (Lima et al., 2014). These arteries eventually become low resistance vessels, supplying adequate nutrients via the bloodstream to the newly formed placenta without damaging the delicate fetal capillaries within.

Inflammatory regulators play key roles in decidualisation, embryo implantation, and vascular remodelling during pregnancy. Key proteins involved in decidualisation include prolactin (PRL), bone morphogenetic proteins (BMPs), and insulin-like growth factors (IGFs) (Ormandy et al., 1997, Ni and Li, 2017, Ganeff et al., 2009). Furthermore, other key proteins which promote embryo implantation include the Wnt/β-catenin pathways, epidermal growth factor (EGF) signalling, homeobox transcription factors, and cytokines such as leukemia inhibitory factor (LIF) (Zhang and Yan, 2015, Cai et al., 2003, Winship et al., 2015b). Moreover, the tissue and vascular remodelling events in pregnancy have been linked with the vascular endothelial growth factor (VEGF) family, hypoxia inducible factor (HIF) signalling, and matrix metalloproteinases (MMPs) (Osol and Mandala, 2009b). The actions of these molecules during early pregnancy sets up growth of the fetus by allowing adequate trophoblast invasion to achieve robust placentation. Aberrations to these processes can result in poorly-perfused placentas which can be the underlying cause of pregnancy complications such as preeclampsia (PE) and fetal growth restriction (FGR) (Lyall et al., 2013). Thus, induction of these molecules and their associated pathways must be tightly regulated to promote pregnancy success.

Key markers for decidual macrophages during murine pregnancy include CD163, CD206, and IL-10 (Zhang et al., 2017). These markers are associated with maintaining macrophages in an M2-like state to promote tissue and vascular remodelling (Ning et al., 2016). Key markers for uNK cells include IL-15 and IL-15R among others (Gaynor and Colucci, 2017). Treg cells can express suppressive markers including CTLA4 in addition to the cell type-defining FOXP3 transcription factor (Robertson et al., 2018). Excessive expression of pro-inflammatory molecules can polarise immune cells toward a pro-inflammatory activation status. These molecules include IL-1β, IL-6, and the tumour necrosis factor (TNF) superfamily members (Zhang et al., 2017).

The pre-implantation phase of pregnancy is reliant on pro-inflammatory signalling to recruit immune cells and induce tolerance (Robertson et al., 2018). After embryo implantation and early placentation, pregnancy enters a growth phase. During this phase, inflammatory cytokine expression levels are reduced and growth-promoting factors are heightened (Brown et al., 2014). Irregularities in the concentrations of pro-inflammatory molecules or growth promoting factors or altered dynamics in the progression from pro-inflammatory to anti-inflammatory environments, can impair pregnancy viability.

This chapter investigated how macrophage depletion impacts the expression of inflammation-associated genes during the peri-implantation phase. Wild type (WT) or CD11b-DTR mice were mated with BALB/c stud males and given 25 ng/g diphtheria toxin (DT) on day 5.5 pc. CD11b-DTR mice given DT are referred to as macrophage-depleted (MD^{25}) mice throughout. Additional CD11b-DTR females given DT were either treated with progesterone (P4) or WT CSF1-induced bone marrow-derived macrophages (BMDM). All four treatment groups (WT, MD^{25}, MD^{25} + P4, and MD^{25} + MØ) were assessed on day 7.5 pc where implantation sites were dissected such that the myometrium was removed from the decidua allowing both tissues to be assessed independently. The role of uterine macrophages was investigated through profiling RNA expression in both the decidua and myometrium using OpenArray™ technology. A pre-designed inflammation panel, assessing >600 inflammation-associated genes, was utilised. RNA expression data was compared to the WT group, thus the respective fold changes for all the genes are presented relative to WT, as $\log_2(1)$ fold change (FC). For these experiments, four dams per group were utilised with two implantation sites per dam collected.

6.2 RNA PROFILING OF THE DECIDUA ON DAY 7.5 PC

In the decidua, there were 383 genes that were dysregulated in one or more of the three macrophage-depleted groups compared to WT controls (Figure 6.1 A). Over 70% of these genes were dysregulated in macrophage-depleted mice but attenuated by either or both P4 or BMDM treatment. In particular, we were interested to identify genes that were dysregulated by macrophage deficiency and restored by BMDM administration but not P4. Of the 383 dysregulated genes, 53 were common to both macrophage-depleted mice and macrophage-depleted mice given P4, but were restored through administration of BMDM to macrophage-depleted mice.

From here the genes were sorted into upregulated or downregulated compared to WT (Figure 6.1 B and C). Of the upregulated genes, 49% were found in macrophage-depleted mice (Figure 6.1 B). There were 11 genes were common to macrophage-depleted mice and macrophage-depleted mice given P4, suggesting BMDM administration could rescue the expression of these genes.

Macrophage-depleted mice had 84% of the downregulated genes (Figure 6.1 C). There were 16 commonly downregulated genes between macrophage-depleted mice and macrophage-depleted mice given P4, while BMDM administration restored the expression of these genes to WT levels.

The volcano plots for each of the treatment groups compared to WT are shown in Figure 6.1 (D-F). The volcano plots have a FC cut-off of $\log_2(1)$ and a corrected p-value cut-off of $p<0.05$.

Additional tables showing differential gene expression across each of the groups are presented in Appendices Tables 9.2 – 9.7. Pathway analysis is also presented in Appendices Tables 9.8 – 9.10.

Figure 6.1: Differential decidual RNA expression in macrophage-depleted mice compared to WT controls on day 7.5 pc.

WT and CD11b-DTR females were mated to BALB/c stud males and 25 ng/g DT was administered on day 5.5 pc. For P4 supplementation, DT-treated CD11b-DTR females were subcutaneously injected with P4 on days 5.5 pc and 6.5 pc. For BMDM supplementation, DT-treated CD11b-DTR females were intravenously injected with BMDM on days 3.5 pc and 5.5 pc. Implantation sites were dissected into decidua and myometrium and then RNA profiling was performed using OpenArray™ technology. In the decidua, a total of 383 genes were dysregulated between the WT control and one or more of the treatment groups, as indicated by the Venn diagram (A). The genes that were upregulated (B) and the genes that were downregulated (C) in each treatment are also indicated. The volcano plots for each treatment group are shown compared to WT (D-F). FC; fold change. MØ; macrophages. MD^{25}; macrophage-depleted. P4; progesterone.

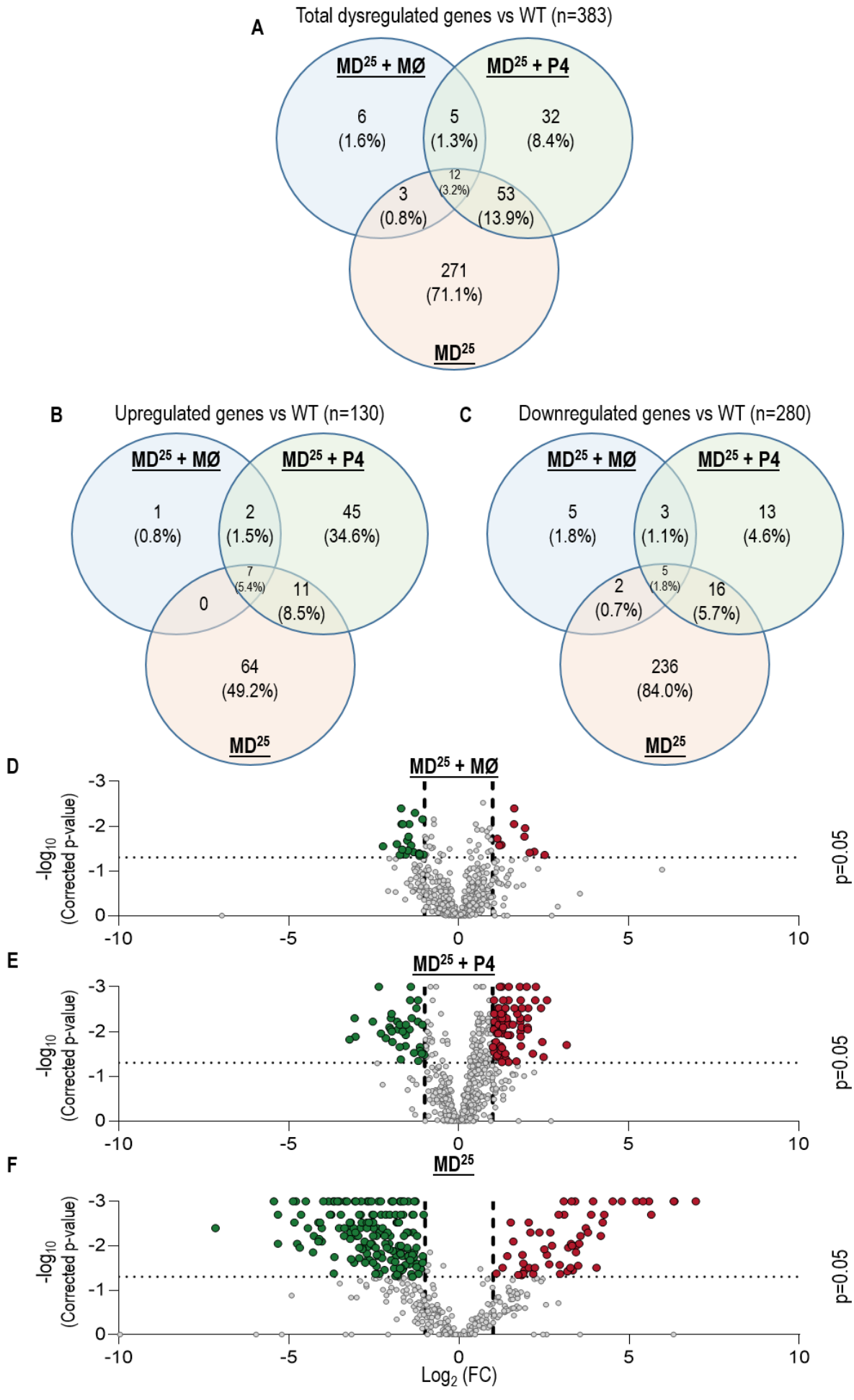
A
Total dysregulated genes vs WT (n=383)
MD25 + MØ
MD25 + P4
MD25
6 (1.6%)
5 (1.3%)
32 (8.4%)
12 (3.2%)
3 (0.8%)
53 (13.9%)
271 (71.1%)
B
Upregulated genes vs WT (n=130)
MD25 + MØ
MD25 + P4
MD25
1 (0.8%)
2 (1.5%)
45 (34.6%)
7 (5.4%)
0
11 (8.5%)
64 (49.2%)
C
Downregulated genes vs WT (n=280)
MD25 + MØ
MD25 + P4
MD25
5 (1.8%)
3 (1.1%)
13 (4.6%)
5 (1.8%)
2 (0.7%)
16 (5.7%)
236 (84.0%)
D
MD25 + MØ
E
MD25 + P4
F
MD25
-log10 (Corrected p-value)
p=0.05
Log2 (FC)

6.2.1 GENES WITH THE LARGEST FOLD CHANGE COMPARED TO WT IN THE DECIDUA

The top ten upregulated and downregulated genes for each treatment group were assessed where the p-value was <0.05 and $1<\log_2 FC<-1$ compared to WT controls (Table 6.1). It is evident that amongst these top ten genes, some appear within only one treatment group, and others appear in more than one, indicating there are different categories of genes that are differentially regulated by macrophages and P4. Genes that meet the stringent FC boundaries but not the p-value boundary are presented in Appendix Table 9.1.

Table 6.1: Top ten upregulated and downregulated genes in the decidua compared to WT on day 7.5 pc ($1<log_2(FC)<-1$ and $p<0.05$)

WT vs MD[25] + MØ			WT vs MD[25] + P4			WT vs MD[25]		
Gene	**log_2FC**	**p-value**	**Gene**	**log_2FC**	**p-value**	**Gene**	**log_2FC**	**p-value**
Gdf15	+ 2.53	0.044	*Gdf15*	+ 3.18	0.020	*Cxcl3*	+ 12.04	<0.001
Prtn3	+ 2.22	0.037	*Prok2*	+ 2.60	0.002	*Cxcl2*	+ 10.92	<0.001
S100a9	+ 2.08	0.039	*S100a9*	+ 2.46	0.017	*Prok2*	+ 9.83	<0.001
Il8rb	+ 1.96	0.011	*Grem1*	+ 2.28	0.001	*Il1b*	+ 8.86	<0.001
Ppbp	+ 1.93	0.017	*Ifnb1*	+ 2.25	0.002	*S100a9*	+ 8.69	<0.001
Il8ra	+ 1.63	0.004	*Prtn3*	+ 2.18	0.031	*Trem1*	+ 8.36	<0.001
Fpr1	+ 1.63	0.009	*Ccl1*	+ 2.05	0.003	*Itgb2l*	+ 8.23	<0.001
Bdkrb2	+ 1.26	0.026	*Tnfsf9*	+ 2.04	0.005	*Il1f9*	+ 8.06	<0.001
Cxcl11	+ 1.19	0.027	*Il8rb*	+ 2.03	0.009	*Fpr1*	+ 7.72	<0.001
Gpr17	+ 1.14	0.019	*Ifnk*	+ 2.03	0.008	*Il8rb*	+ 7.52	<0.001
Il17rb	- 2.22	0.028	*Il13*	- 3.21	0.015	*Cx3cr1*	- 7.38	<0.001
Fgf10	- 1.82	0.025	*Mrc1*	- 3.06	0.005	*Prl7d1*	- 7.16	0.004
Crp	- 1.73	0.044	*Fgf10*	- 2.52	0.006	*Apoa1*	- 6.97	<0.001
Adora3	- 1.69	0.004	*Ccr8*	- 2.51	<0.001	*C1qa*	- 6.97	<0.001
Il31ra	- 1.68	0.009	*Siglec1*	- 2.29	0.011	*C1qb*	- 6.97	<0.001
Tnfrsf19	- 1.66	0.033	*C1qc*	- 2.14	0.014	*C1qc*	- 6.51	<0.001
Ltb4r1	- 1.64	0.009	*C1qa*	- 2.04	0.008	*Mrc1*	- 6.38	<0.001
Cntfr	- 1.56	0.043	*C1qb*	- 1.99	0.009	*Bmp2*	- 6.27	<0.001
Alox5	- 1.51	0.021	*Cntfr*	- 1.99	0.005	*Il17rb*	- 6.27	<0.001
Spp1	- 1.49	0.035	*Cx3cr1*	- 1.97	0.004	*Il31ra*	- 6.27	<0.001

6.2.2 GENES RESTORED BY P4 OR BMDM ADMINISTRATION IN THE DECIDUA

Compared to WT controls, a large proportion of the genes dysregulated by macrophage depletion were restored by P4, as well as by BMDM administration (Figure 6.2 A). The expression of many of these genes was restored with P4 and/or BMDM administration and these categories of genes will be discussed in subsequent sections. Of the 271 genes restored by either treatment, 64 were upregulated and 236 were downregulated. The top ten upregulated and top ten downregulated are presented in Figure 6.2 B and C and Table 6.2. The various clusters of differential gene expression patterns are presented in Appendix 9.21.

Table 6.2: Top genes restored by P4 or BMDM administration in the decidua compared to WT on day 7.5 pc ($1<log_2(FC)<-1$ and $p<0.05$)

	WT vs MD^{25} + MØ		WT vs MD^{25} + P4		WT vs MD^{25}	
Gene	**log_2FC**	**p-value**	**log_2FC**	**p-value**	**log_2FC**	**p-value**
Ccl3	+ 1.07	0.144	- 0.85	0.108	+ 7.34	<0.001
Ccrl2	+ 0.24	0.792	+ 0.00	>0.99	+ 6.33	0.001
Cxcl3	+ 0.61	0.867	- 0.03	>0.99	+ 12.0	<0.001
Il1b	+ 1.46	0.123	+ 0.49	0.252	+ 8.86	<0.001
Il1f9	+ 1.97	0.054	+ 1.38	0.122	+ 8.06	<0.001
Itgb2l	+ 2.33	0.090	+ 1.57	0.187	+ 8.23	<0.001
Nlrp3	+ 0.00	0.768	- 0.79	0.415	+ 6.31	<0.001
Mefv	+ 0.32	>0.99	- 0.30	0.063	+ 7.05	0.001
Saa3	+ 1.36	0.191	+ 1.60	0.093	+ 6.25	<0.001
Trem1	+ 1.27	0.089	+ 0.62	0.033	+ 8.36	<0.001
Adora1	+ 0.08	>0.99	+ 0.38	0.698	- 4.88	<0.001
Aoc3	- 0.63	0.574	- 0.35	0.853	- 4.88	<0.001
Apoa1	- 0.14	>0.99	+ 0.50	0.912	- 6.97	<0.001
Apoa4	- 0.46	0.738	+ 0.06	>0.99	- 6.06	<0.001
Bmp2	- 0.19	>0.99	- 0.03	>0.99	- 6.27	<0.001
Ccl8	- 1.41	0.214	- 0.70	0.627	- 5.32	0.009
Cer1	+ 0.56	0.789	+ 0.32	>0.99	- 4.80	0.001
Prl7d1	- 0.38	>0.99	- 0.12	>0.99	- 7.16	0.004
Tlr3	- 0.06	>0.99	- 0.20	0.931	- 4.84	<0.001
Tnfsf18	+ 0.95	0.388	+ 1.35	0.184	- 6.06	<0.001

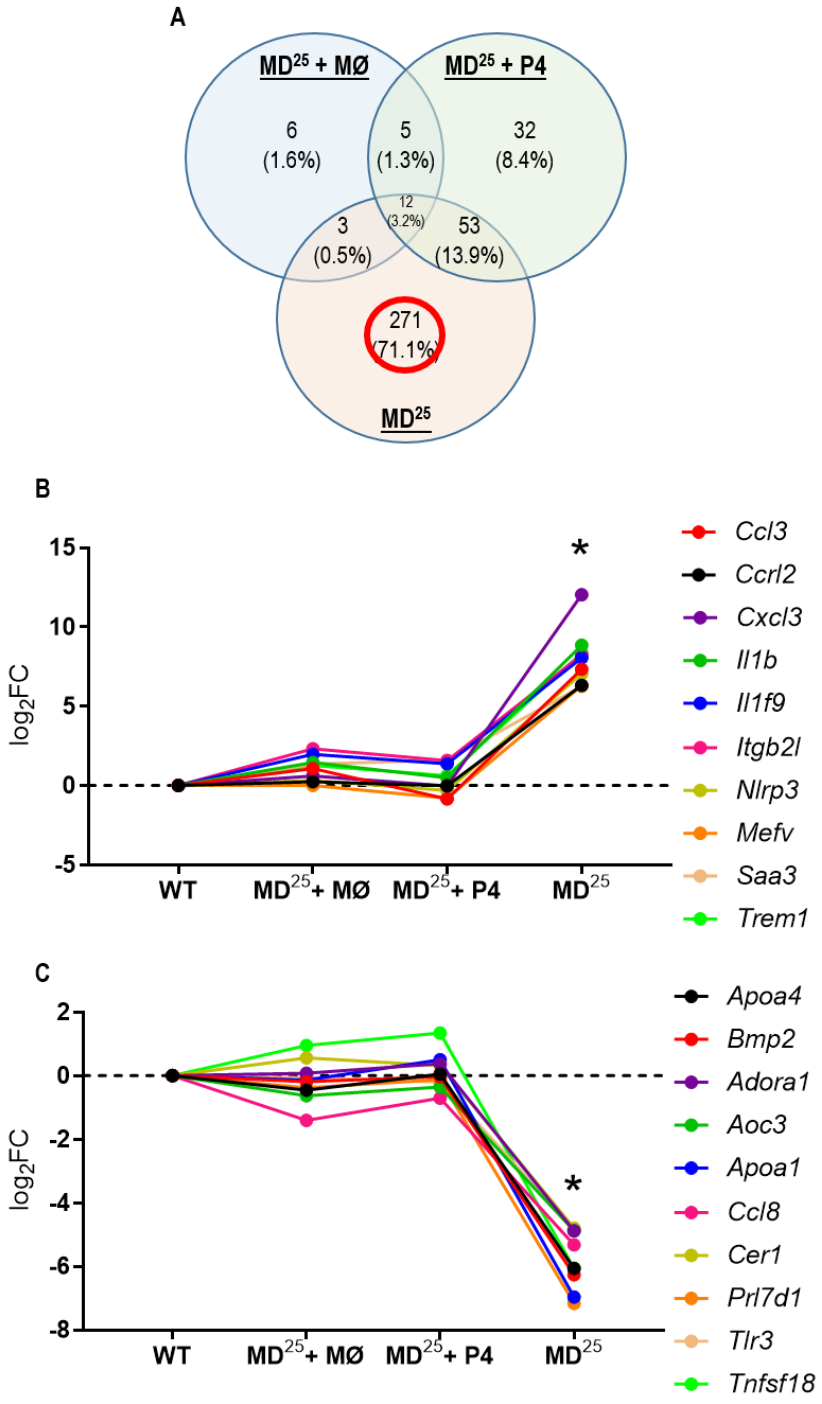

Figure 6.2: Genes restored by P4 or BMDM administration in the decidua compared to WT on day 7.5 pc.

WT and CD11b-DTR females were mated to BALB/c stud males and 25 ng/g DT was administered on day 5.5 pc. For P4 supplementation, DT-treated CD11b-DTR females were subcutaneously injected with P4 on days 5.5 pc and 6.5 pc. For BMDM supplementation, DT-treated CD11b-DTR females were intravenously injected with BMDM on days 3.5 pc and 5.5 pc. Implantation sites were dissected into decidua and myometrium and then RNA profiling was performed using OpenArray™ technology. In the decidua, the dysregulated genes within each treatment group is shown compared to WT and the red circle indicates the dysregulated genes in the MD^{25} group that were restored by either P4 or BMDM treatment (A). The relative fold change of the upregulated genes (B). The relative fold change of the downregulated genes (C). FC; fold change. MØ; macrophages. MD^{25}; macrophage-depleted. P4; progesterone. WT; wild type. * indicates statistical significance ($p<0.05$); compared to WT controls.

6.2.3 GENES RESTORED BY P4 BUT NOT BMDM ADMINISTRATION IN THE DECIDUA

To understand the role of P4 supplementation in macrophage-depleted mice, the genes dysregulated in macrophage-depleted mice and macrophage-depleted mice given BMDM, but restored in macrophage-depleted mice given P4, were assessed. There were three dysregulated genes in this category (Figure 6.3 A). Interleukin 12a (*Il12a*) was reduced in macrophage-depleted mice given BMDM and was increased in macrophage-depleted mice (Figure 6.3 B and Table 6.3). In this way, *Il12a* appears to be restored by both P4 and BMDM administration, however it falls in this category as after BMDM treatment it becomes dysregulated in the opposite direction.

Table 6.3: Genes restored by P4 but not BMDM administration in the decidua compared to WT on day 7.5 pc ($1<\log_2(FC)<-1$ and $p<0.05$)

	WT vs MD^{25} + MØ		WT vs MD^{25} + P4		WT vs MD^{25}	
Gene	**$\log_2$FC**	**p-value**	**$\log_2$FC**	**p-value**	**$\log_2$FC**	**p-value**
Il12a	- 1.15	0.042	- 0.56	0.275	+ 2.58	0.016

	WT vs MD^{25} + MØ		WT vs MD^{25} + P4		WT vs MD^{25}	
Gene	**$\log_2$FC**	**p-value**	**$\log_2$FC**	**p-value**	**$\log_2$FC**	**p-value**
Cd46	- 1.16	0.040	- 0.33	0.516	- 1.64	0.030
Spp1	- 1.49	0.040	- 0.44	0.230	- 1.38	0.020

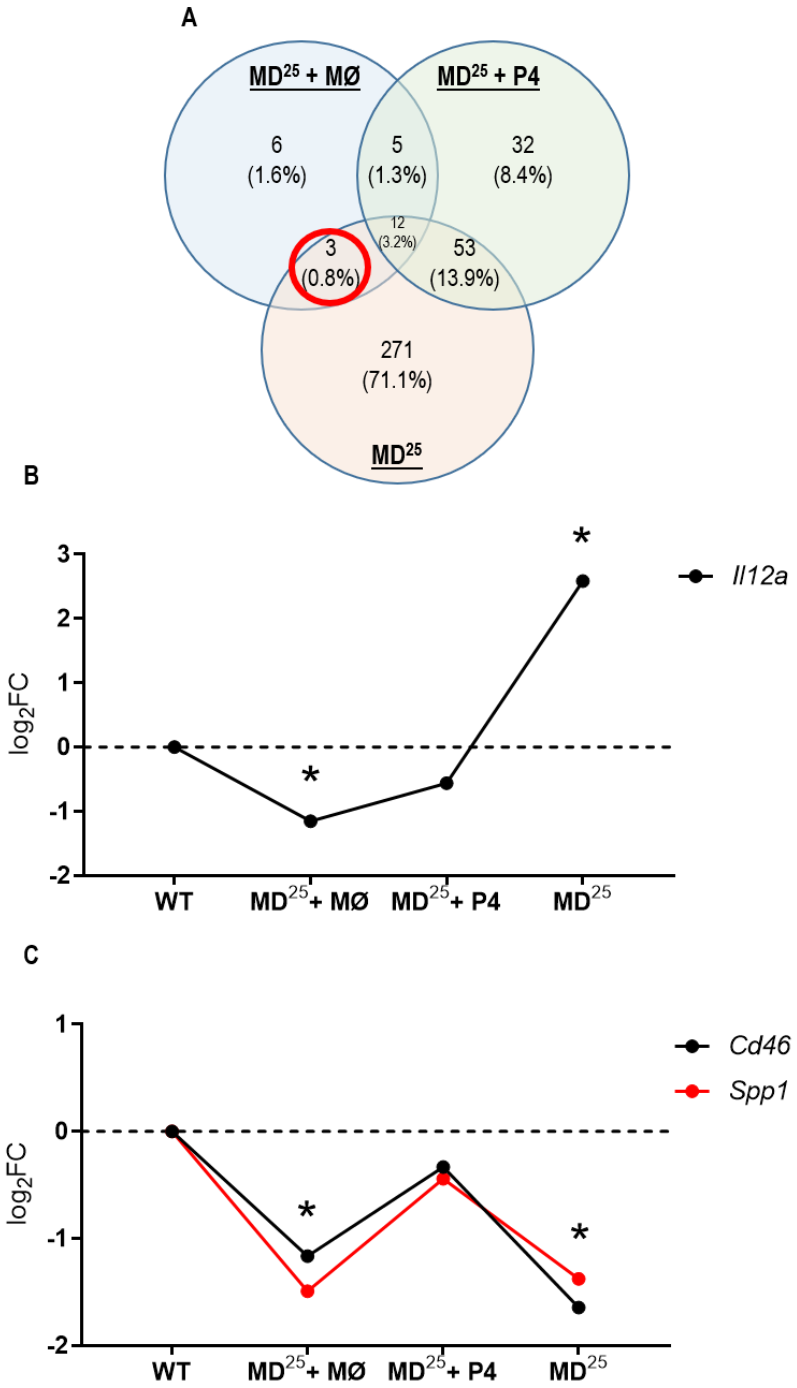

Figure 6.3: Genes restored by P4 but not BMDM administration in the decidua compared to WT on day 7.5 pc.

WT and CD11b-DTR females were mated to BALB/c stud males and 25 ng/g DT was administered on day 5.5 pc. For P4 supplementation, DT-treated CD11b-DTR females were subcutaneously injected with P4 on days 5.5 pc and 6.5 pc. For BMDM supplementation, DT-treated CD11b-DTR females were intravenously injected with BMDM on days 3.5 pc and 5.5 pc. Implantation sites were dissected into decidua and myometrium and then RNA profiling was performed using OpenArray™ technology. In the decidua, the dysregulated genes within each treatment group is shown compared to WT and the red circle indicates the dysregulated genes common to the MD^{25} + MØ and MD^{25} groups but were restored by P4 treatment (A). The relative fold change of the upregulated genes (B). The relative fold change of the downregulated genes (C). FC; fold change. MØ; macrophages. MD^{25}; macrophage-depleted. P4; progesterone. WT; wild type. * indicates statistical significance ($p<0.05$); compared to WT controls.

6.2.4 GENES RESTORED BY BMDM BUT NOT P4 ADMINISTRATION IN THE DECIDUA

To understand the specific mechanism by which macrophages promote pregnancy success, the genes that were dysregulated by macrophage depletion and restored with the administration of BMDM, but not restored when macrophage-depleted mice were given P4, were assessed. This category indicates genes directly related to macrophage function in the uterus. In the decidua, there were 53 dysregulated genes common to macrophage-depleted mice and macrophage-depleted mice given P4 in the decidua on day 7.5 pc (Figure 6.4 A). Table 6.4 shows the top ten upregulated and the top ten downregulated genes in this category (based on highest or lowest fold change for the MD^{25} + P4 group).

Table 6.4: Top genes restored by BMDM but not P4 administration in the decidua compared to WT on day 7.5 pc ($1<log_2(FC)<-1$ and $p<0.05$)

	WT vs MD^{25} + MØ		WT vs MD^{25} + P4		WT vs MD^{25}	
Gene	**log_2FC**	**p-value**	**log_2FC**	**p-value**	**log_2FC**	**p-value**
Clec7a	+ 0.69	0.012	+ 1.43	0.006	+ 3.31	0.001
Csf2	+ 0.64	0.564	+ 1.13	0.011	+ 4.04	0.031
Cxcl2	+ 1.70	0.224	+ 1.47	0.048	+ 10.92	<0.001
Grem1	+ 1.57	0.058	+ 2.28	0.001	+ 4.28	<0.001
Irak2	+ 0.96	0.035	+ 1.41	0.002	+ 2.93	0.002
Lif	+ 0.38	0.812	+ 1.22	0.005	+ 3.08	0.001
Pla2g2e	+ 1.19	0.187	+ 1.31	0.002	+ 3.21	0.011
Pla2g7	+ 0.39	0.176	+ 1.31	0.008	+ 3.29	0.009
Prok2	+ 3.57	0.322	+ 2.72	0.002	+ 9.49	<0.001
Vegfa	+ 1.05	0.065	+ 1.27	0.023	+ 1.28	0.031
C1qa	- 1.00	0.322	- 1.99	0.009	- 6.97	<0.001
C1qb	- 1.20	0.188	- 2.04	0.008	- 6.97	<0.001
C1qc	- 1.10	0.257	- 2.14	0.014	- 6.51	<0.001
Ccr8	- 1.16	0.258	- 2.51	<0.001	- 5.32	0.002
Cd74	- 1.01	0.441	- 4.88	0.021	- 3.52	0.004
Cntfr	- 1.85	0.054	- 1.99	0.005	- 4.72	<0.001
Cx3cr1	- 1.15	0.381	- 1.97	0.004	- 7.38	<0.001
Il13	- 1.88	0.084	- 3.04	0.013	- 4.11	0.007
Mrc1	- 2.04	0.053	- 3.06	0.005	- 6.38	<0.001
Siglec1	- 0.95	0.345	- 2.29	0.011	- 4.44	0.004

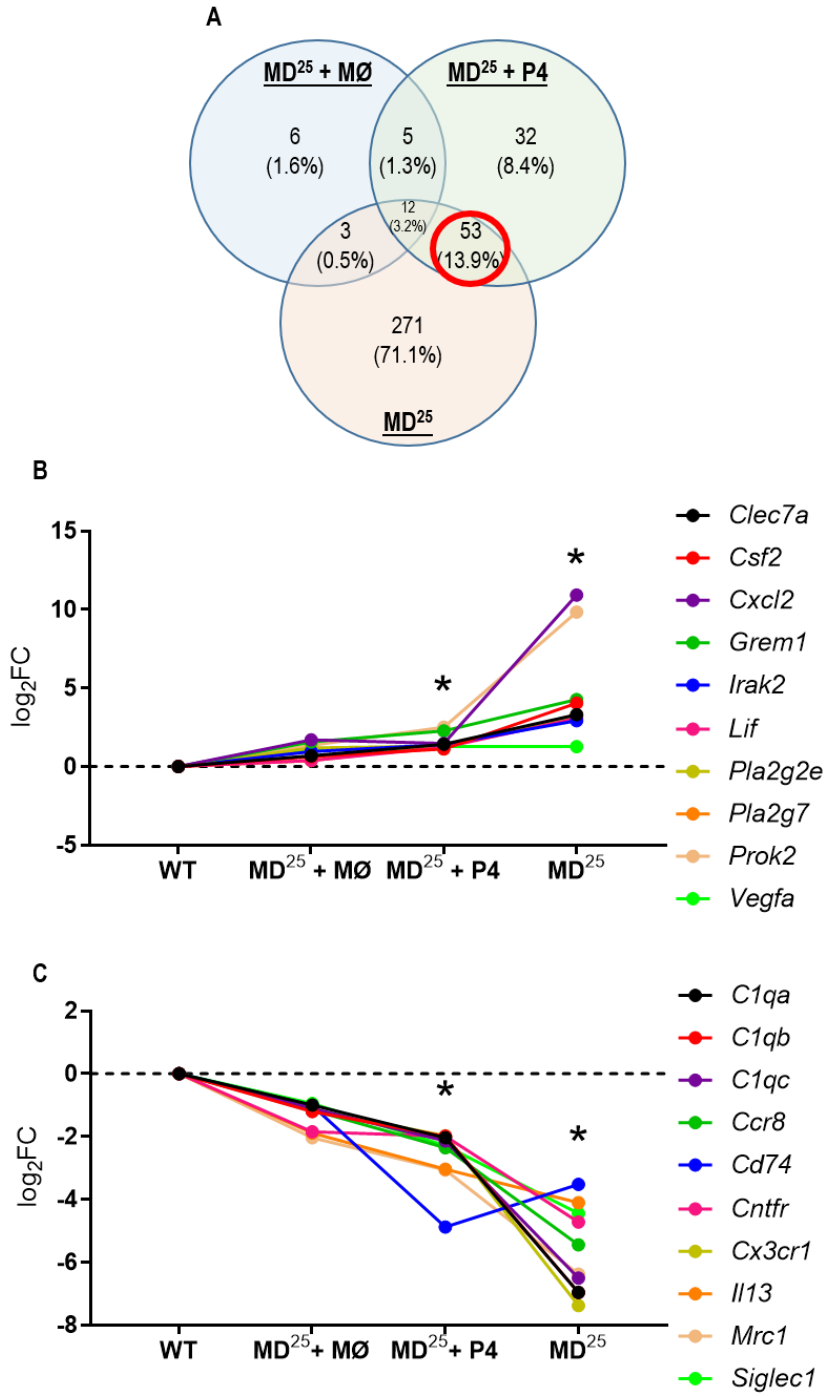

Figure 6.4: Genes restored by BMDM but not P4 administration in the decidua compared to WT on day 7.5 pc.

WT and CD11b-DTR females were mated to BALB/c stud males and 25 ng/g DT was administered on day 5.5 pc. For P4 supplementation, DT-treated CD11b-DTR females were subcutaneously injected with P4 on days 5.5 pc and 6.5 pc. For BMDM supplementation, DT-treated CD11b-DTR females were intravenously injected with BMDM on days 3.5 pc and 5.5 pc. Implantation sites were dissected into decidua and myometrium and then RNA profiling was performed using OpenArray™ technology. In the decidua, the dysregulated genes within each treatment group is shown compared to WT and the red circle indicates the dysregulated genes common to the MD^{25} + P4 and MD^{25} groups but were restored by BMDM treatment (A). The relative fold change of the upregulated genes (B). The relative fold change of the downregulated genes (C). FC; fold change. MØ; macrophages. MD^{25}; macrophage-depleted. P4; progesterone. WT; wild type. * indicates statistical significance ($p<0.05$); compared to WT controls.

6.3 RNA PROFILING OF THE MYOMETRIUM ON DAY 7.5 PC

RNA profiling was also performed in the myometrium on day 7.5 pc, whereby the results from macrophage-depleted and supplemented mice were compared to WT controls. There were 246 genes that were dysregulated in any one or more of the treatment groups compared to WT. Over 80% of these dysregulated genes were in macrophage-depleted mice but were corrected by P4 and/or BMDM (Figure 6.5 A). Again, the genes that were restored by administration of BMDM but not P4 were investigated. There were 23 genes that were dysregulated in both macrophage-depleted mice and macrophage-depleted mice given P4, but restored by BMDM.

There were 90 dysregulated genes that were upregulated and 80% of these were in solely macrophage-depleted mice (Figure 6.5 B). There were six upregulated genes common to both macrophage-depleted mice and macrophage-depleted mice given P4. The remaining 166 genes were downregulated with 80% of these solely in macrophage-depleted mice (Figure 6.5 C). There were 15 downregulated genes common to macrophage-depleted mice and macrophage-depleted mice given P4, indicating that BMDM administration restored the expression of these genes. The representative volcano plots for each of the treatment groups compared to WT are shown in Figure 6.5 (D-F).

Additional tables showing differential gene expression across each of the groups are presented in Appendices Tables 9.12 – 9.16. Pathway analysis is also presented in Appendices Tables 9.17 – 9.19.

Figure 6.5: Differential myometrial RNA expression in macrophage-depleted mice compared to WT on day 7.5 pc.

WT and CD11b-DTR females were mated to BALB/c stud males and 25 ng/g DT was administered on day 5.5 pc. For P4 supplementation, DT-treated CD11b-DTR females were subcutaneously injected with P4 on days 5.5 pc and 6.5 pc. For BMDM supplementation, DT-treated CD11b-DTR females were intravenously injected with BMDM on days 3.5 pc and 5.5 pc. Implantation sites were dissected into decidua and myometrium and then RNA profiling was performed using OpenArray™ technology. In the myometrium, a total of 246 genes were dysregulated between the WT control and one or more of the treatment groups, as indicated by the Venn diagram (A). The genes that were upregulated (B) and the genes that were downregulated (C) in each treatment are also indicated. The volcano plots for each treatment group are shown compared to WT (D-F). FC; fold change. MØ; macrophages. MD^{25}; macrophage-depleted. P4; progesterone.

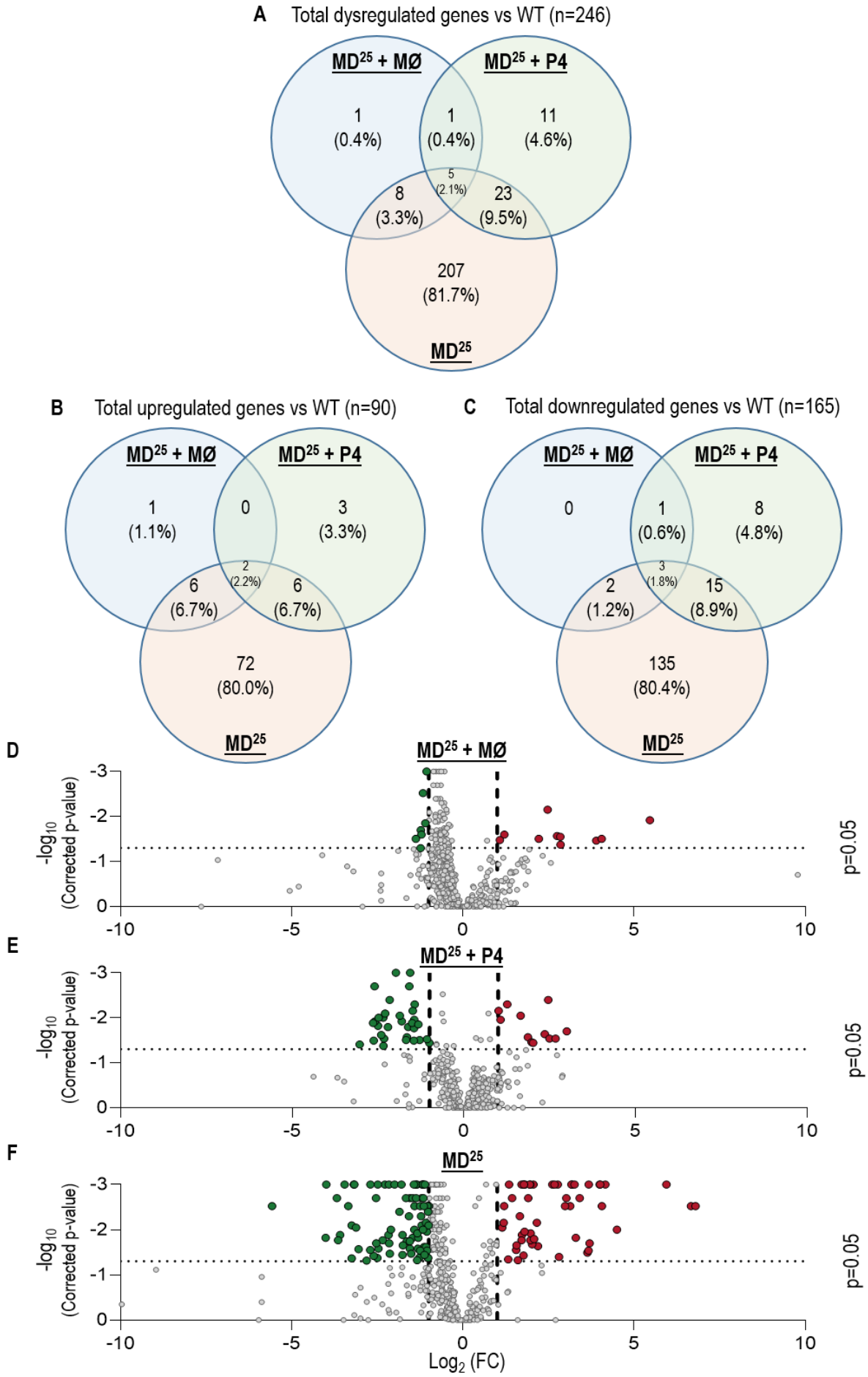
A
Total dysregulated genes vs WT (n=246)
MD25 + MØ
MD25 + P4
MD25
1 (0.4%)
1 (0.4%)
11 (4.6%)
5 (2.1%)
8 (3.3%)
23 (9.5%)
207 (81.7%)
B
Total upregulated genes vs WT (n=90)
MD25 + MØ
MD25 + P4
MD25
1 (1.1%)
0
3 (3.3%)
2 (2.2%)
6 (6.7%)
6 (6.7%)
72 (80.0%)
C
Total downregulated genes vs WT (n=165)
MD25 + MØ
MD25 + P4
MD25
0
1 (0.6%)
8 (4.8%)
3 (1.8%)
2 (1.2%)
15 (8.9%)
135 (80.4%)
D
MD25 + MØ
E
MD25 + P4
F
MD25
-log10 (Corrected p-value)
p=0.05
Log2 (FC)

6.3.1 GENES WITH THE LARGEST FOLD CHANGE COMPARED TO WT IN THE MYOMETRIUM

Next, the relative fold changes of dysregulated genes in each of the three treatment groups were each compared to the WT group. The top ten upregulated and downregulated genes were assessed where 2<FC<0.5 and p-value <0.05 compared to WT (Table 6.5). Again, it is evident that some genes appear within only one treatment group, and others appear in more than one, indicating there are differentially regulated genes. Genes that meet the stringent FC boundaries but not the p-value boundary are presented in Appendix Table 9.11.

Table 6.5: Top ten upregulated and downregulated genes in the myometrium for each group compared to WT on day 7.5 pc ($1<log_2(FC)<-1$ and $p<0.05$)

WT vs MD^{25} + MØ			WT vs MD^{25} + P4			WT vs MD^{25}		
Gene	**log_2FC**	**p-value**	**Gene**	**log_2FC**	**p-value**	**Gene**	**log_2FC**	**p-value**
Saa3	+ 5.46	0.012	*Cxcl2*	+ 3.01	0.020	*S100a9*	+ 8.09	<0.001
S100a8	+ 4.05	0.031	*S100a9*	+ 2.68	0.029	*Saa3*	+ 7.43	<0.001
S100a9	+ 2.85	0.042	*Il24*	+ 2.50	0.029	*Cxcl2*	+ 6.91	<0.001
Prtn3	+ 2.84	0.028	*Gdf15*	+ 2.46	0.004	*Il1b*	+ 6.80	<0.001
Cxcl2	+ 2.75	0.027	*Ifnb1*	+ 2.36	0.023	*S100a8*	+ 6.79	0.003
Chi3l3	+ 2.48	0.007	*Cxcl1*	+ 2.02	0.036	*Il24*	+ 6.64	<0.001
Il8ra	+ 2.22	0.031	*Ccl1*	+ 1.87	0.027	*Trem1*	+ 6.50	<0.001
Ccl2	+ 1.21	0.025	*Vip*	+ 1.66	0.009	*Il8rb*	+ 6.18	<0.001
Ccl4	+ 1.08	0.033	*Hc*	+ 1.27	0.005	*Il8ra*	+ 6.08	<0.001
			Tlr12	+ 1.07	0.011	*Muc4*	+ 6.05	<0.001
Mrc1	- 1.37	0.031	*Ccl8*	- 3.04	0.039	*Pla2g2d*	- 7.38	<0.001
Ccr2	- 1.23	0.020	*Mrc1*	- 2.64	0.013	*Il13ra2*	- 7.16	<0.001
Lilrb3	- 1.21	0.025	*Ccl6*	- 2.63	0.032	*Fcer1a*	- 5.57	0.003
Pxmp2	- 1.21	<0.001	*Cx3cr1*	- 2.60	0.002	*Mrc1*	- 5.06	<0.001
Cd4	- 1.17	0.003	*Fcgr2b*	- 2.59	0.012	*Cx3cr1*	- 4.80	<0.001
Nlrc4	- 1.10	0.014	*C1qc*	- 2.50	0.015	*C1qc*	- 4.51	<0.001
Vegfc	- 1.06	0.001	*Siglec1*	- 2.48	0.010	*Ccr8*	- 4.47	<0.001
			Ccr3	- 2.40	0.024	*Ptn*	- 4.47	<0.001
			Ly86	- 2.35	0.010	*C1qa*	- 4.29	<0.001
			C1qa	- 2.34	0.042	*C1qb*	- 4.16	<0.001

6.3.2 GENES RESTORED BY P4 OR BMDM ADMINISTRATION IN THE MYOMETRIUM

Over 200 genes were dysregulated in macrophage-depleted mice compared to WT controls in the myometrium (Figure 6.6 A). The expression of many of these genes was restored with P4 and/or BMDM administration and these categories of genes will be discussed in subsequent sections. Of these genes, 72 were upregulated and a further 135 genes were downregulated. The top ten upregulated and downregulated genes are presented in Table 6.6 and Figure 6.6 (B and C).

Table 6.6: Genes restored by P4 or BMDM administration in the myometrium compared to WT on day 7.5 pc ($1<log_2(FC)<-1$ and $p<0.05$)

	WT vs MD^{25} + MØ		WT vs MD^{25} + P4		WT vs MD^{25}	
Gene	**log_2FC**	**p-value**	**log_2FC**	**p-value**	**log_2FC**	**p-value**
Cxcl3	+ 0.41	0.997	- 0.13	>0.99	+ 5.89	<0.001
Fpr1	+ 0.46	0.664	- 0.28	0.805	+ 4.65	<0.001
Il1b	+ 1.94	0.054	+ 0.50	0.299	+ 6.80	<0.001
Il1f9	+ 1.91	0.164	+ 0.35	>0.99	+ 5.07	<0.001
Il8rb	+ 1.87	0.095	+ 1.50	0.137	+ 6.18	<0.001
Ltf	+ 2.33	0.074	+ 0.64	0.657	+ 4.92	<0.001
Muc4	+ 1.36	0.438	+ 0.06	>0.99	+ 6.05	<0.001
Pla2g2e	+ 0.94	0.336	+ 0.44	0.281	+ 5.81	<0.001
Prok2	+ 0.06	>0.99	+ 0.57	0.829	+ 5.08	<0.001
Trem1	+ 1.82	0.084	+ 0.38	0.937	+ 6.50	<0.001
A2m	+ 0.34	>0.99	+ 0.81	0.707	- 3.59	0.013
Bmp8a	- 0.15	>0.99	- 0.14	>0.99	- 3.64	0.017
C6	- 1.21	0.238	- 2.31	0.108	- 3.68	0.002
Ccr8	- 0.94	0.634	- 1.74	0.067	- 4.47	<0.001
Fcer1a	- 4.11	0.072	- 3.49	0.261	- 5.57	0.003
Il13	- 0.37	>0.99	- 0.53	>0.99	- 2.82	0.048
Il13ra2	- 2.39	0.183	- 0.31	0.968	- 7.16	<0.001
Il31ra	- 0.17	>0.99	+ 0.21	>0.99	- 3.56	<0.001
Pla2g2d	- 3.38	0.127	- 4.38	0.203	- 7.38	<0.001
Ptn	- 1.16	0.125	- 0.27	0.609	- 4.47	<0.001

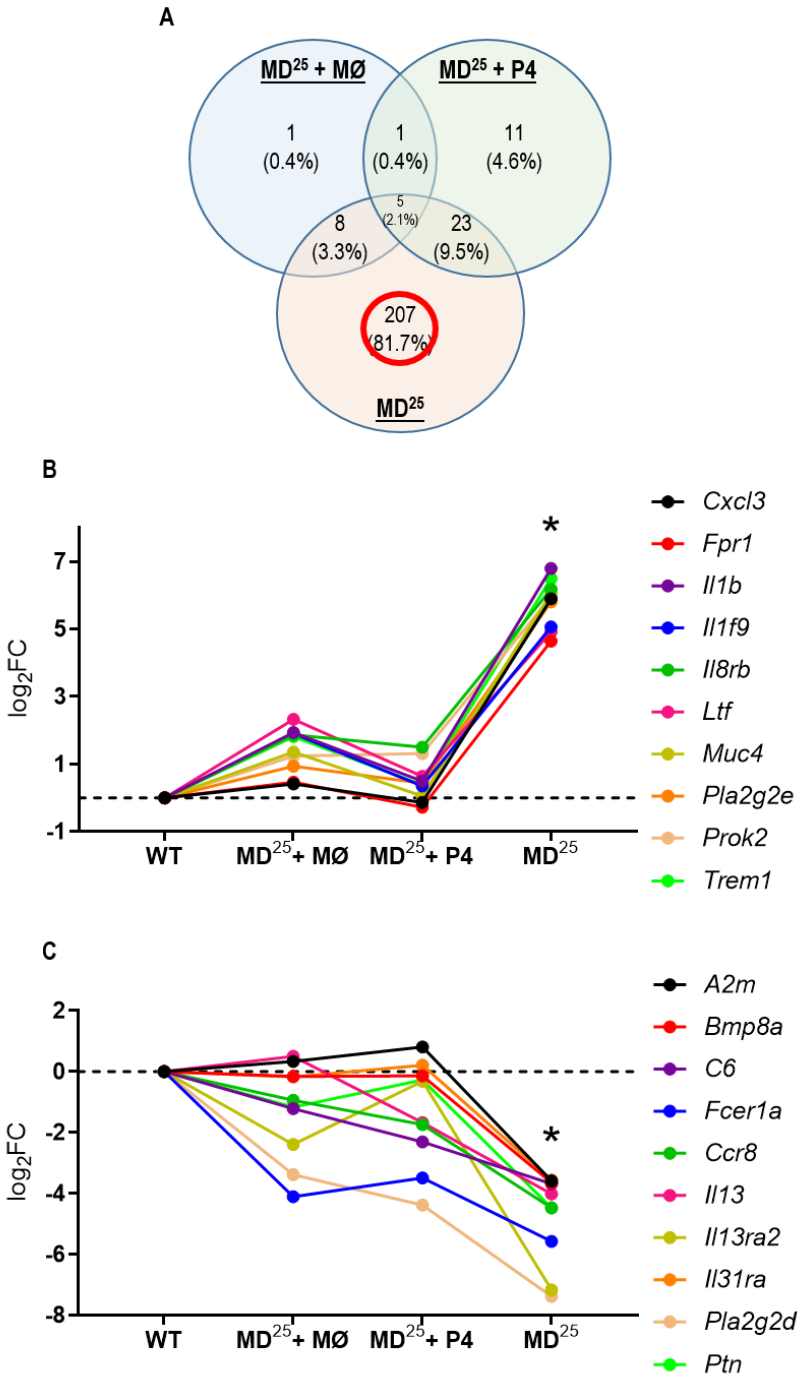

Figure 6.6: Genes restored by P4 or BMDM administration in the myometrium compared to WT on day 7.5 pc.

WT and CD11b-DTR females were mated to BALB/c stud males and 25 ng/g DT was administered on day 5.5 pc. For P4 supplementation, DT-treated CD11b-DTR females were subcutaneously injected with P4 on days 5.5 pc and 6.5 pc. For BMDM supplementation, DT-treated CD11b-DTR females were intravenously injected with BMDM on days 3.5 pc and 5.5 pc. Implantation sites were dissected into decidua and myometrium and then RNA profiling was performed using OpenArray™ technology. In the myometrium, the dysregulated genes within each treatment group is shown compared to WT and the red circle indicates the dysregulated genes in the MD^{25} groups but were restored by either P4 or BMDM treatment (A). The relative fold change of the upregulated genes (B). The relative fold change of the downregulated genes (C). FC; fold change. MØ; macrophages. MD^{25}; macrophage-depleted. P4; progesterone. WT; wild type. * indicates statistical significance ($p<0.05$); compared to WT controls.

6.3.3 GENES RESTORED BY P4 BUT NOT BMDM ADMINISTRATION IN THE MYOMETRIUM

Genes that were restored by P4 supplementation were next assessed. There were eight dysregulated genes that were common to macrophage-depleted mice and macrophage-depleted mice given BMDM, where six were upregulated and two were downregulated (Figure 6.7 and Table 6.7).

Table 6.7: Genes restored by P4 but not BMDM administration in the myometrium compared to WT on day 7.5 pc ($1<log_2(FC)<-1$ and $p<0.05$)

	WT vs MD^{25} + MØ		WT vs MD^{25} + P4		WT vs MD^{25}	
Gene	**log_2FC**	**p-value**	**log_2FC**	**p-value**	**log_2FC**	**p-value**
Ccl2	+ 1.21	0.025	- 0.21	0.956	+ 2.61	<0.001
Chi3l3	+ 2.48	0.007	+ 0.96	0.239	+ 4.16	0.001
Il8ra	+ 2.22	0.031	+ 1.86	0.116	+ 6.08	<0.001
Prtn3	+ 2.84	0.028	+ 0.65	0.542	+ 3.02	0.002
S100a8	+ 4.05	0.031	+ 2.86	0.207	+ 6.79	0.003
Saa3	+ 5.46	0.012	+ 2.72	0.068	+ 7.43	<0.001
Pxmp2	- 1.21	<0.001	- 0.21	0.533	- 1.88	<0.001
Vegfc	- 1.06	0.001	- 0.59	0.012	- 2.09	<0.001

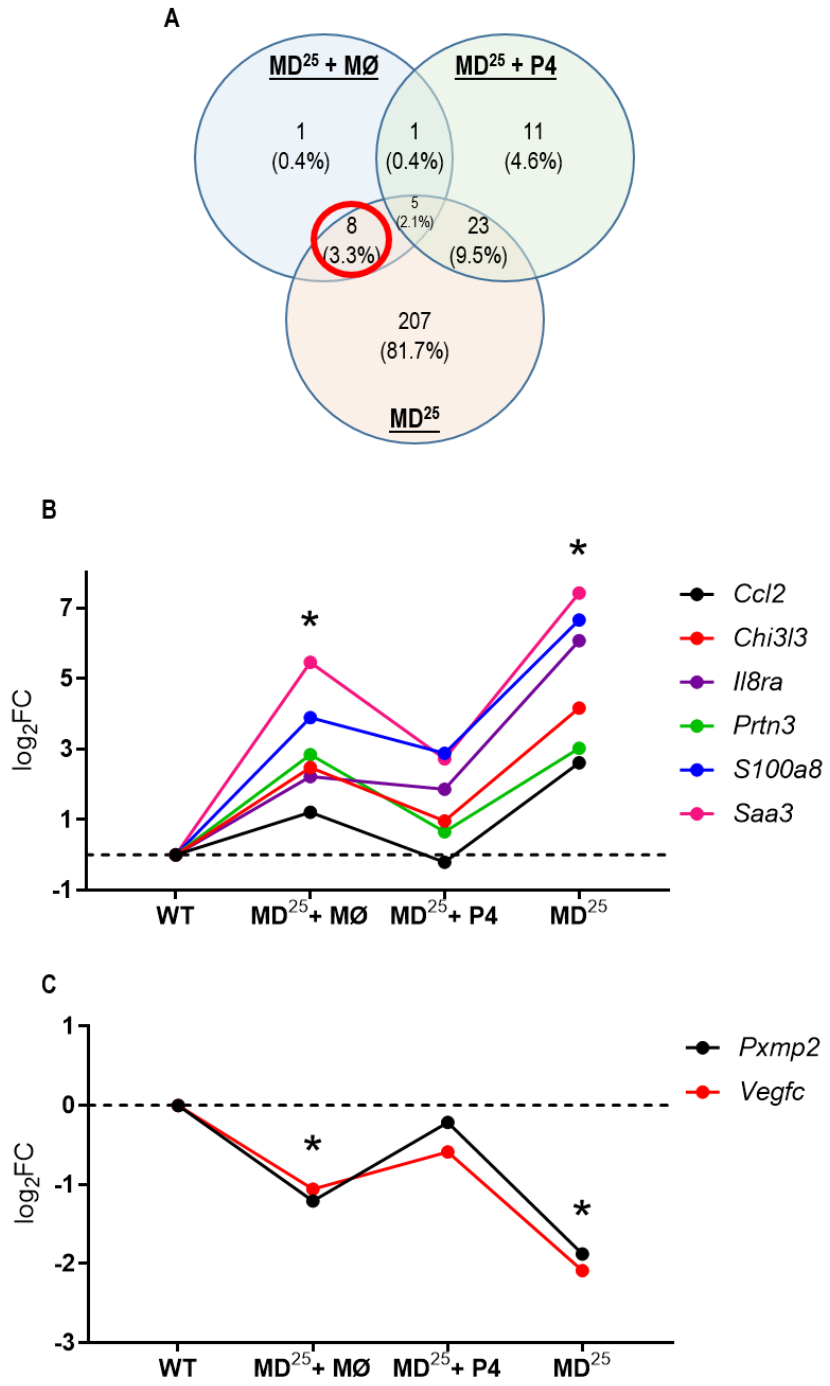

Figure 6.7: Genes restored by P4 but not BMDM administration in the myometrium compared to WT on day 7.5 pc.

WT and CD11b-DTR females were mated to BALB/c stud males and 25 ng/g DT was administered on day 5.5 pc. For P4 supplementation, DT-treated CD11b-DTR females were subcutaneously injected with P4 on days 5.5 pc and 6.5 pc. For BMDM supplementation, DT-treated CD11b-DTR females were intravenously injected with BMDM on days 3.5 pc and 5.5 pc. Implantation sites were dissected into decidua and myometrium and then RNA profiling was performed using OpenArray™ technology. In the myometrium, the dysregulated genes within each treatment group is shown compared to WT and the red circle indicates the dysregulated genes common to the MD^{25} + MØ and MD^{25} groups but were restored by P4 treatment (A). The relative fold change of the upregulated genes (B). The relative fold change of the downregulated genes (C). FC; fold change. MØ; macrophages. MD^{25}; macrophage-depleted. P4; progesterone. WT; wild type. * indicates statistical significance ($p<0.05$); compared to WT controls.

6.3.4 GENES RESTORED BY BMDM BUT NOT P4 ADMINISTRATION IN THE MYOMETRIUM

Dysregulated genes that were restored by BMDM administration but not P4 were also assessed. There were 23 dysregulated genes common to macrophage-depleted mice and macrophage-depleted mice given P4 in the myometrium on day 7.5 pc (Figure 6.8). Table 6.8 shows the upregulated genes and the top ten downregulated genes.

Table 6.8: Top genes restored by BMDM but not P4 administration in the myometrium compared to WT on day 7.5 pc ($1<log_2(FC)<-1$ and $p<0.05$)

	WT vs MD^{25} + MØ		WT vs MD^{25} + P4		WT vs MD^{25}	
Gene	**log_2FC**	**p-value**	**log_2FC**	**p-value**	**log_2FC**	**p-value**
Cxcl1	+ 1.46	0.179	+ 1.98	0.035	+ 4.53	<0.001
Gdf15	+ 1.19	0.277	+ 2.46	0.004	+ 1.97	0.017
Hc	+ 0.31	0.377	+ 1.27	0.005	+ 2.84	<0.001
Ifnb1	+ 1.78	0.128	+ 2.36	0.023	+ 1.77	0.037
Il24	+ 2.57	0.107	+ 2.50	0.029	+ 6.64	<0.001
Ppbp	+ 0.71	0.034	+ 1.02	0.007	+ 2.12	<0.001
C1qa	- 0.67	0.447	- 2.34	0.042	- 4.29	<0.001
C1qb	- 0.89	0.311	- 2.50	0.029	- 4.51	<0.001
C1qc	- 0.78	0.145	- 2.32	0.015	- 4.16	<0.001
Ccl8	- 1.35	0.355	- 3.04	0.039	- 3.25	0.008
Ccr3	- 0.17	>0.99	- 2.40	0.024	- 3.35	0.003
Cx3cr1	- 1.29	0.069	- 2.60	0.002	- 4.80	<0.001
Cybb	- 0.89	0.082	- 2.16	0.004	- 1.99	0.001
Fcgr2b	- 1.01	0.051	- 2.59	0.012	- 1.47	0.015
Ly86	- 1.03	0.124	- 2.35	0.010	- 3.66	<0.001
Siglec1	- 0.68	0.246	- 2.48	0.010	- 3.31	<0.001

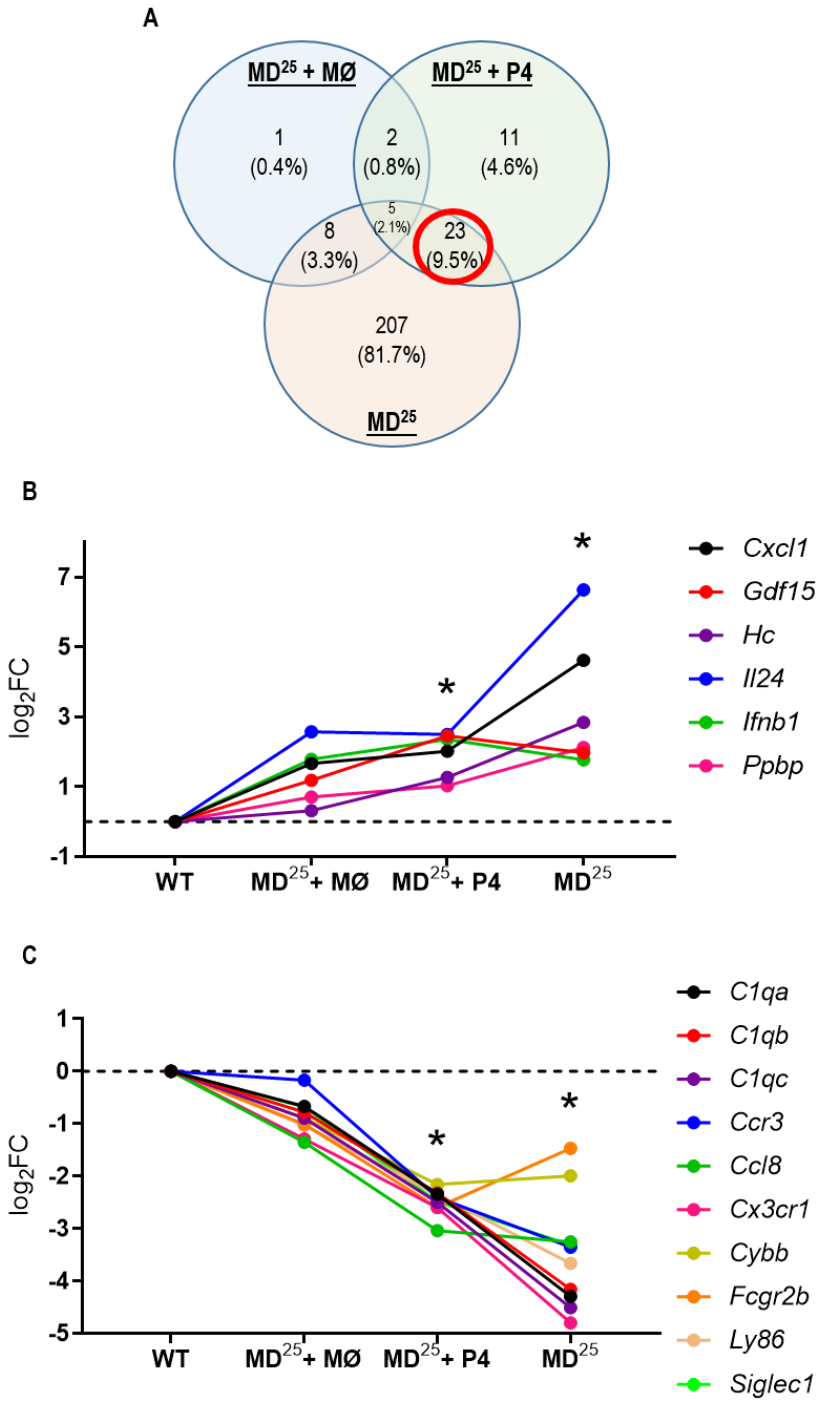

Figure 6.8: Genes restored by BMDM but not P4 administration in the myometrium compared to WT on day 7.5 pc.

WT and CD11b-DTR females were mated to BALB/c stud males and 25 ng/g DT was administered on day 5.5 pc. For P4 supplementation, DT-treated CD11b-DTR females were subcutaneously injected with P4 on days 5.5 pc and 6.5 pc. For BMDM supplementation, DT-treated CD11b-DTR females were intravenously injected with BMDM on days 3.5 pc and 5.5 pc. Implantation sites were dissected into decidua and myometrium and then RNA profiling was performed using OpenArray™ technology. In the myometrium, the dysregulated genes within each treatment group is shown compared to WT and the red circle indicates the dysregulated genes common to the MD^{25} + P4 and MD^{25} groups but were restored by BMDM treatment (A). The relative fold change of the upregulated genes (B). The relative fold change of the downregulated genes (C). FC; fold change. MØ; macrophages. MD^{25}; macrophage-depleted. P4; progesterone. WT; wild type. * indicates statistical significance ($p<0.05$); compared to WT controls.

6.4 DISCUSSION

The gene expression data within this chapter begins to identify a mechanism by which macrophages regulate the decidual and myometrial tissue environment to promote uterine vascular adaptations during the peri-implantation phase. CD11b-DTR mice were used to deplete macrophages on day 5.5 pc and in one cohort, P4 was supplemented and in another cohort, BMDM were administered. All three CD11b-DTR treatment groups were utilised in conjunction with WT controls for RNA profiling of the decidua and the myometrium on day 7.5 pc. The data here show that macrophage depletion strongly impacts RNA expression in both uterine compartments. P4 supplementation to macrophage-depleted mice partially restored the expression of many dysregulated genes, showing in large part the dysregulation after macrophage depletion was due to P4 deficiency. However, BMDM administration to macrophage-depleted mice exceeded P4 supplementation by restoring a greater proportion of the dysregulated genes back to WT control levels. The genes restored after BMDM administration but not P4 treatment identify key macrophage-regulated molecules and mechanisms acting locally in the uterus to promote tissue and vascular remodelling during early pregnancy.

6.4.1 BMDM AND P4 ADMINISTRATION RESTORE SIMILAR GENES POST-MACROPHAGE DEPLETION

The majority of dysregulated genes after macrophage depletion could be restored by either P4 or BMDM administration. Some of the key genes restored include *Ccl3*, *Ccl8*, *Il1b*, *Nlrp3*, and *Prl7d1*. The fact that either treatment restored these genes implies that these genes are likely to be P4-dependent genes that are dysregulated after macrophage depletion because of low P4.

Of these genes, several have already been linked with embryo implantation. There is evidence to suggest *Il1b* plays an important role in establishing implantation in mice and potentially plays a role in maternal immune tolerance (Takacs and Kauma, 1996, Yoshinaga et al., 2014, Paulesu et al., 2008). However, excessive *Il1b* has been shown to cause placental inflammation and *in utero* fetal death (Nadeau-Vallée et al., 2017). The increased expression of *Il1b* in macrophage-depleted mice is likely linked with the resorbing implantation sites on day 7.5 pc. *Nlrp3* is involved in inflammasome activation and may also be upregulated due to resorption. *Nlrp3* expression has been shown to be increased in women with severe PE which was also associated with increased *Il1b* expression in placental villi (Weel et al., 2017). *Ccl3* expression was also increased in macrophage-depleted mice and has been shown to recruit uNK cells and macrophages into the decidua likely due to the deficiency of macrophages (Du et al., 2014, Abrahams et al., 2005).

Conversely, *Ccl8* was downregulated in macrophage-depleted mice. *Ccl8* is known to be produced by macrophages and its expression is increased during early pregnancy (Sakumoto et al., 2017). *Ccl8* has been proposed as being a factor involved in promoting an optimal microenvironment in the uterus required

for embryo implantation (Złotkowska and Andronowska, 2019). There was a reduction in the expression of *Prl7d1*, a member of the prolactin family, in macrophage-depleted mice. Prolactin is involved in decidualisation. A recent study found that deletion of the *Prl7d1* gene in mice caused placental defects and reduced viable litter sizes (Zhang et al., 2019). Therefore, decreased expression of *Ccl8* and *Prl7d1* are likely to be linked with resorption and failed decidualisation. For the P4-regulated pro-inflammatory genes, it is possible that they are causal in fetal loss, or alternatively that their upregulation is a consequence of fetal loss.

6.4.2 P4 SUPPLEMENTATION RESTORES >70% OF DYSREGULATED GENES POST-MACROPHAGE DEPLETION

Notably, P4 supplementation to macrophage-depleted mice was able to restore 70% of the dysregulated genes in the decidua and 84% of the dysregulated genes in the myometrium on day 7.5 pc. Some of the key genes restored include *Spp1* and *Vegfc*. This restoration is likely due to P4-supplemented mice having successful decidualisation on day 7.5 pc whereas macrophage-depleted mice had impaired decidualisation. Therefore, some gene expression changes observed in macrophage-depleted mice may be reflective of the non-viable implantation sites and impaired decidualisation or may be related to wound healing genes to clear the resorbing tissue from the uterus.

Spp1 is expressed mainly by uNK cells in the mouse decidua during embryo implantation with some expression being attributable to macrophages and endometrial cells (Herington and Bany, 2007a). *Spp1* is critical to fetal development including development of cartilage, bones and blood vessels (Singh et al., 2014). The expression of this gene was restored with P4 supplementation. Therefore, when macrophages were depleted, growth factors such as *Spp1* may become lowered which may impair the development and differentiation of trophoblast cells.

Similarly, *Vegfc* expression was restored to an extent with P4 supplementation in the myometrium. The expression of *Vegfc* was reduced in macrophage-depleted mice given P4 but failed to reach the highly stringent FC cut-off boundary. *Vegfc* is primarily involved in lymphangiogenesis with macrophages and uNK cells capable of producing *Vegfc* (Kerjaschki, 2005). Whilst lymphangiogenesis was not specifically investigated, it cannot be ruled out as being disrupted through the depletion of macrophages.

6.4.3 BMDM ADMINISTRATION RESTORES >90% OF DYSREGULATED GENES POST-MACROPHAGE DEPLETION

BMDM supplementation to macrophage-depleted mice was able to restore over 90% of the dysregulated genes in both the decidua and myometrium on day 7.5 pc. Some of the key genes restored include *Lif*, *Cx3cr1*, *Mrc1*, *Siglec1*, *Csf2*, *Cxcl2*, *Vegfa*, and *C1q*. All these genes have previously been linked to various macrophage functions in other tissue settings; thus, it seems likely the BMDM transfer protocol achieved at least partial restoration of macrophage numbers within the uterus. Importantly, BMDM transfer

could restore over 15% more of the dysregulated genes than P4 supplementation, suggesting that BMDM transfer was more effective at restoring the effects of macrophage depletion. This is consistent with the interpretation that macrophages have essential roles in the uterus during early pregnancy, beyond their actions in the ovary.

Lif was upregulated in macrophage-depleted mice given P4 and macrophage-depleted mice in the decidua. *Lif* is involved in decidualisation and embryo implantation where it acts through the *Lif* receptor (*Lifr*) (Jasper et al., 2011). In contrast, *Lifr* was downregulated in macrophage-depleted mice and upregulated in macrophage-depleted mice given P4. This may suggest that the *Lif* pathway is repressed in macrophage-depleted mice potentially due to impaired decidualisation. A recent study highlighted that temporal blocking of LIF during murine pregnancy led to placental defects and impaired vascular morphology (Winship et al., 2015a). Conversely, *Lif* overexpression drove breast cancer cell proliferation and invasion *in vitro* (Shin et al., 2011). It appears that macrophages may regulate the LIF pathway during decidualisation and trophoblast invasion.

BMDM administration was able to restore the expression of some key macrophage markers including *Cx3cr1*, *Mrc1*, and *Siglec1* in both the myometrium and decidua. Furthermore, BMDM administration could restore the expression of chemokines that are involved in the recruitment of macrophages. Namely, *Csf2*, *Cxcl2*, and *Vegfa* were upregulated in the decidua in macrophage-depleted mice and macrophage-depleted mice given P4, but not macrophage depleted mice given BMDM. *Vegfa* most notably induces angiogenesis, however, it has also been shown to stimulate macrophage recruitment under specific circumstances including neovascularisation (Cursiefen et al., 2004). Furthermore, *Vegfa* has been shown to recruit macrophages into the decidua and promote M2 polarisation in human decidual samples (Wheeler et al., 2018a). Thereby, BMDM administration restored the expression of macrophage-recruiting chemokines. Whether this is due to expression by macrophages themselves, or other cells responding to macrophage signals, is unknown.

The expression of the *C1q* gene family (*C1qa*, *C1qb*, and *C1qc*) was increased after BMDM supplementation back to WT control levels. The *C1q* family of genes were decreased after macrophage depletion and the expression of these genes was not restored with P4 administration. Whilst the complement system is often regarded as part of the pro-inflammatory response to pathogens, more recent studies have shown that *C1q* has a unique role in pregnancy (Bulla et al., 2008, Bulla et al., 2012, Agostinis et al., 2010). Studies investigating the *C1q*-knockout mouse have shown that WT females mated with *C1q*-deficient males experience preeclamptic-like symptoms during late gestation and increased fetal death *in utero* (Singh et al., 2011, Agostinis et al., 2010). In addition, maternal *C1q*-deficiency was associated with impaired placental labyrinth development and poor decidual vascular remodelling in mid-gestation (Agostinis et al., 2010). Whilst it has not specifically been investigated during early pregnancy

studies in other tissues suggest *C1q* has regulatory functions that would be suited to a role in maternal vascular adaptation to pregnancy and may be produced by macrophages during this time.

6.4.4 POTENTIAL MARKERS OF MACROPHAGE TISSUE RESIDENCY

Many tissues have distinct populations of resident tissue macrophages that have been defined with specific markers. The uterus is one tissue where tissue resident macrophages have yet to be fully characterised despite their essential roles during pregnancy and normal uterine cycling. Tissue resident populations of macrophages are often established early in embryonic development where monocyte precursor cells seed developing tissues and from here these populations become self-renewing, tissue resident macrophages (Gomez Perdiguero et al., 2015, Yona et al., 2013, Hashimoto et al., 2013). As the uterus is a mucosal surface, it is informative to utilise markers known to be expressed on tissue resident populations in other mucosal tissues such as the intestine and the lungs, to assist in characterising uterine tissue resident macrophages. Some of these tissue resident markers include CX3CR1, CD11b, F4/80, and CD206 (Bain and Schridde, 2018, Hoeffel and Ginhoux, 2018). Furthermore, Kupffer cells in the liver express CD169 as a marker of tissue residency.

Of these markers, *Cx3cr1*, *Mrc1* (CD206), and *Siglec1* (CD169) were all downregulated in macrophage-depleted mice in both the decidua and myometrium. *Cd4* was also downregulated in macrophage-depleted mice. Whilst CD4 protein is classically regarded as a T cell marker, there is evidence that CD4 can be expressed by macrophages during their development and that intestinal tissue-resident macrophages can be defined by CD4 expression (Shaw et al., 2018). Therefore, expression of these markers on macrophages may indicate a tissue resident population in the uterus. Further investigation is required to characterise these macrophage populations and address whether separate populations of uterine macrophages exist; firstly, the recruited macrophages and secondly, the tissue resident macrophages. It is likely that the tissue resident macrophages are critical for tissue and vascular remodelling events.

6.4.5 BEST CANDIDATE GENES

Of the genes restored after BMDM administration but not after P4 supplementation, a shortlist of candidate genes that encode bioactive proteins secreted by macrophages that could potentially influence vascular remodelling was identified. These candidate genes include *C1qa*, *C1qb*, *C1qc*, *Cx3cr1*, and *Siglec1*. *Cx3cr1* and *Siglec1* are both receptors expressed on the surface of macrophages. Of the genes encoding proteins produced by macrophages that could induce vascular remodelling in the uterus, the *C1q* genes were considered the most interesting candidate genes due to their previously noted roles in promoting pregnancy viability, decidual vessel remodelling, and placental development. Our results showed that *C1q* expression is downregulated in both the decidua and myometrium after macrophage-depletion and its expression is restored with BMDM administration, but not P4 supplementation. Thus, experiments in

chapter seven sought to investigate the effect of maternal *C1q* deficiency on murine pregnancy and specifically its impact on placentation and vascular remodelling.

CHAPTER 7

EFFECT OF MATERNAL C1Q DEFICIENCY AND MACROPHAGE SUPPLEMENTATION IN MURINE PREGNANCY

7.1 INTRODUCTION

During pregnancy, maternal immune tolerance facilitates the growth and development of the semi-allogeneic fetus (Robertson et al., 2018). During pregnancy, maternal blood vessels must adapt to the hemodynamic demands of pregnancy to support fetal growth. To achieve this, uterine arteries undergo remodelling to become more compliant, large diameter, and low resistance vessels for the supply of nutrients to the developing fetus (Mandala and Osol, 2012). Failure to adequately remodel uterine arteries during pregnancy is linked with fetal growth restriction (FGR) and preeclampsia (PE) in women (Lyall et al., 2013). PE can be detrimental to maternal health post-pregnancy due to systemic endothelial dysfunction and increased risk of heart disease in later life (Boeldt and Bird, 2017, Andraweera et al., 2020).

Clinical studies have investigated links between inflammatory regulators and PE risk (Geldenhuys et al., 2018). Previously investigated agents associated with the pathophysiology of PE include soluble VEGFR1 (sFlt) and placental growth factor (PlGF). Increases in sFlt and decreases in PlGF have been shown to correlate with PE risk (McKeeman et al., 2004, Chau et al., 2017). Particularly, the sFlt to PlGF ratio is often used as a biomarker of potential PE in women (Zeisler et al., 2016). Other molecules of interest as biomarkers for PE include the complement proteins. A recent study identified an association between reduced serum C1Q and severe early onset PE (Jia et al., 2019). Furthermore, mRNA extracted from placental tissues showed that C1Q gene expression was downregulated in preeclamptic pregnancies compared to healthy controls (Agostinis et al., 2017). Therefore, decreased *C1q* expression may impair the uterine vascular remodelling required for placental development and lead to pregnancy complications including PE and FGR.

The functional C1Q protein requires two subunits from each of the C1QA, C1QB, and C1QC polypeptides, to make up a six-subunit protein. Thus, a deficiency in any of the *C1q* genes renders the C1Q protein non-functional. The multifaceted roles of C1Q are only beginning to be discovered. Aside from its role in promoting the classical complement pathway to clear pathogens, C1Q has been shown to induce macrophages to phagocytose apoptotic cells (Galvan et al., 2012). In addition, C1Q has been shown to prevent the differentiation of monocytes into dendritic cells, thus halting further activation of the adaptive immune response (Son et al., 2012). Furthermore, there appears to be a dynamic interaction between C1Q and HMGB1, whereby cross-linking of LAIR-1 with RAGE and HMGB1 via C1Q promotes macrophages to take on an M2-like phenotype and express high levels of MerTK, CD163, and IL-10 (Son et al., 2016).

Importantly, in murine pregnancy C1Q has been shown to be involved in the vascularisation of the labyrinth zone (LZ) of the placenta where C1Q-deficient dams had aberrant placental development during mid-gestation (Agostinis et al., 2010). Furthermore, paternal deficiency of C1Q has been shown to cause

preeclamptic-like symptoms in wild type dams with increases in serum sFlt and decreases in VEGF suggesting fetal as well as maternal C1Q is important (Singh et al., 2011). This implicates C1Q in both vascular remodelling during early pregnancy and having a role in immune tolerance and function. Importantly, these previous studies do not fully define the dynamic roles of C1Q during pregnancy. Furthermore, these studies have only assessed syngeneic matings and not allogeneic matings, which require a greater contribution of the immune system to maintain immune tolerance to the semi-allogeneic fetus.

This chapter sought to confirm the involvement of C1Q during murine pregnancy and to determine whether macrophage-derived C1Q might be involved in uterine vascular remodelling required for pregnancy success. Briefly, C1Q expression was assessed via immunohistochemistry in WT and CD11b-DTR mice on day 7.5 pc. To induce macrophage depletion, CD11b-DTR mice were treated with 25 ng/g DT on day 5.5 pc. DT-treated CD11b-DTR females were supplemented with s.c. P4 on days 5.5 and 6.5 pc or were supplemented with i.v. bone marrow-derived macrophages (BMDM). WT mice also received DT on day 5.5 pc. The murine *C1qa*$^{-/-}$ strain is deficient in functional C1Q. Therefore, to investigate the role of maternal C1Q in vascular remodelling, *C1qa*$^{+/+}$ and *C1qa*$^{-/-}$ females were mated to BALB/c stud males. Pregnancy outcomes, including uterine vascular parameters and placental development were assessed on days 9.5 pc and 17.5 pc, respectively. Finally, to determine whether macrophages are a major source of C1Q in pregnancy, CSF-1 induced *C1qa*$^{+/+}$ BMDM were supplemented to *C1qa*$^{-/-}$ mice during early pregnancy, and pregnancy outcomes as well as uterine vascular remodelling were assessed on day 9.5 pc.

7.2 C1Q EXPRESSION ON DAY 7.5 PC

In order to confirm C1Q expression during the peri-implantation phase of murine gestation, WT and CD11b-DTR mice were utilised and implantation sites were stained to assess C1Q density on day 7.5 pc (Figure 7.1 A). C1Q expression in the mesometrial triangle was then quantified. There was a trend toward a reduction in C1Q expression in macrophage-depleted mice compared to WT controls on day 7.5 pc (mean ± SEM, 8.2 ± 0.9% vs 4.2 ± 1.5%, WT vs MD[25], p=0.051, Figure 7.1 B). There was no change to C1Q expression in macrophage-depleted mice given P4 or BMDM compared to WT controls (Figure 7.1 B). Confocal imaging revealed the presence of macrophages around $CD31^+$ blood vessels in the mesometrial triangle and high-density expression of C1Q in both the myometrium and decidua in WT mice (Figure 7.1 C). Further to this, macrophages appeared to co-localise with C1Q at these mesometrial blood vessels (Figure 7.1 D). C1Q was also found in the extracellular matrix (ECM) and internal to vessels.

This experiment confirmed C1Q expression within the murine uterus during the peri-implantation phase of pregnancy. Importantly, this experiment revealed that macrophages may be a source of C1Q and that C1Q is located in the proximity of endothelial cells and so appears to be present in the right place and time to initiate remodelling.

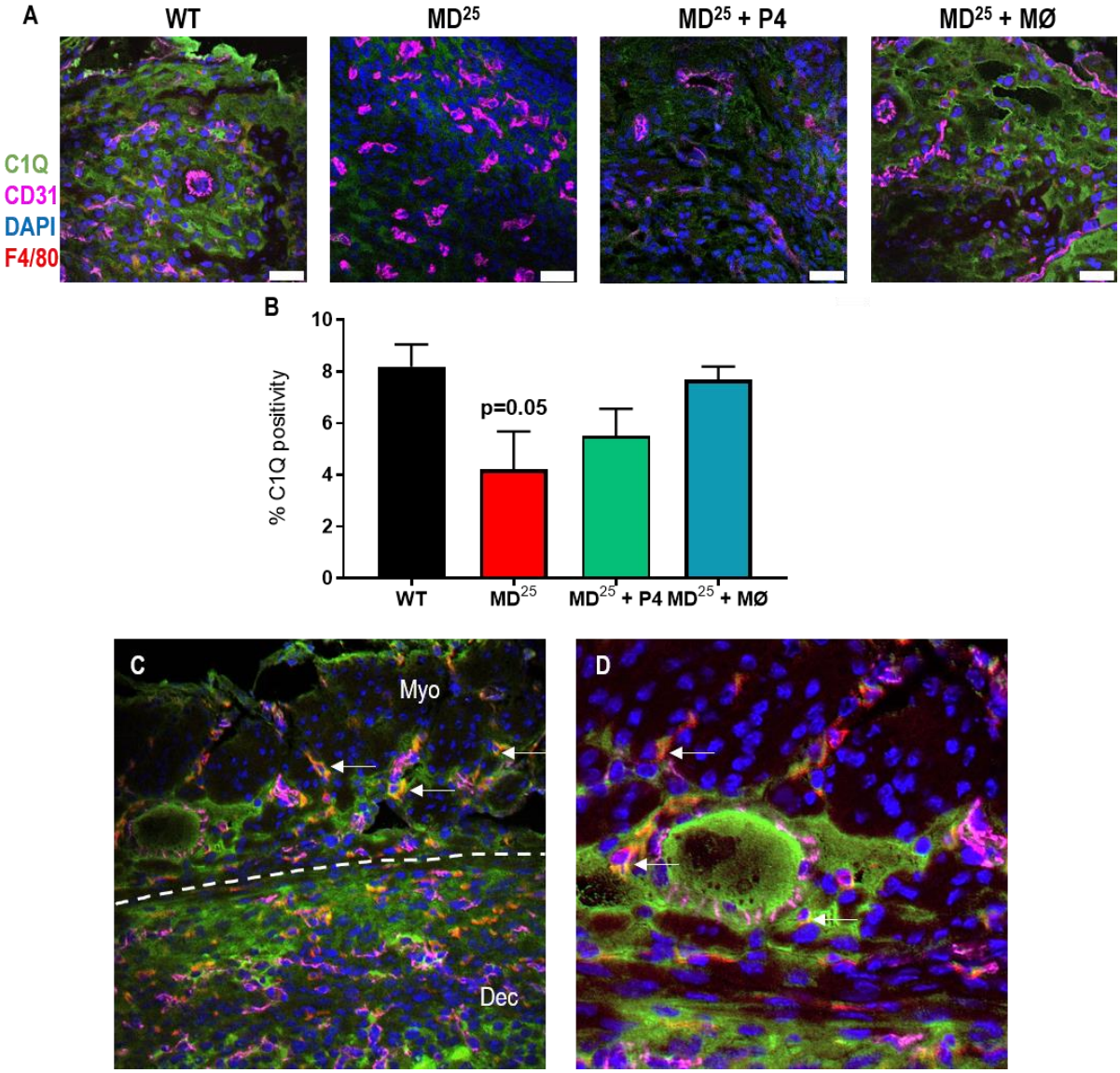

Figure 7.1: Macrophage depletion was associated with a reduction in C1Q expression on day 7.5 pc.

WT and CD11b-DTR females were mated to BALB/c stud males and DT was administered on day 5.5 pc. For P4 supplementation, DT-treated CD11b-DTR females were subcutaneously injected with P4 on days 5.5 pc and 6.5 pc. For BMDM supplementation, DT-treated CD11b-DTR females were intravenously injected with BMDM on days 3.5 pc and 5.5 pc. C1Q (green), CD31 (pink), DAPI (blue), and F4/80 (red) were used to assess C1Q expression in day 7.5 pc implantation sites (A; scale bar is 50 µm). C1Q density was calculated (B). In WT implantation sites, C1Q expression co-localised with the expression of F4/80 in the myometrium and decidua (C, white arrows). A further magnified image (60X magnification) represents the close location of $F4/80^{+}$ cells and C1Q around $CD31^{+}$ vessels, indicated by white arrows (D). Data is presented as mean ± SEM with statistical analysis using one-way ANOVA with Sidak's multiple comparisons test, n= 4-7 mice/group. Dec; decidua. MD^{25}; macrophage-depleted. MØ; macrophages. Myo; myometrium. P4; progesterone. WT; wild type.

7.3 C1Q DEFICIENCY RESULTS IN FETAL GROWTH RESTRICTION AND PLACENTAL HYPERTROPHY

After confirming C1Q expression in the mesometrial triangle and that C1Q expression co-localised with macrophages and endothelial cells, we next hypothesised that macrophages may be a source of C1Q to induce uterine vascular remodelling during early to mid-pregnancy. To further investigate how C1Q was involved in pregnancy, we utilised the *C1qa*$^{-/-}$ mouse strain. To firstly define the impact of C1Q deficiency, knockout (*C1qa*$^{-/-}$) or wild type females (C57BL/6J, referred to as *C1qa*$^{+/+}$) were mated to BALB/c stud males. Late pregnancy outcomes were investigated on day 17.5 pc to determine the impact of maternal C1Q deficiency on fetal and placental growth.

7.3.1 PREGNANCY OUTCOMES

On day 17.5 pc, there was no difference to the rate of viable pregnancy between *C1qa*$^{+/+}$ and *C1qa*$^{-/-}$ dams (Figure 7.2 A). There was also no difference to the number of viable pups per pregnant female (Figure 7.2 B). However, the number of resorptions was increased in *C1qa*$^{-/-}$ dams (mean ± SEM, 0.4 ± 0.2 resorptions vs 1.4 ± 0.4 resorptions, *C1qa*$^{+/+}$ vs *C1qa*$^{-/-}$, p=0.035, Figure 7.2 C). Overall, there were more *C1qa*$^{-/-}$ mice with resorptions than *C1qa*$^{+/+}$ females on day 17.5 pc (Figure 7.2 E).

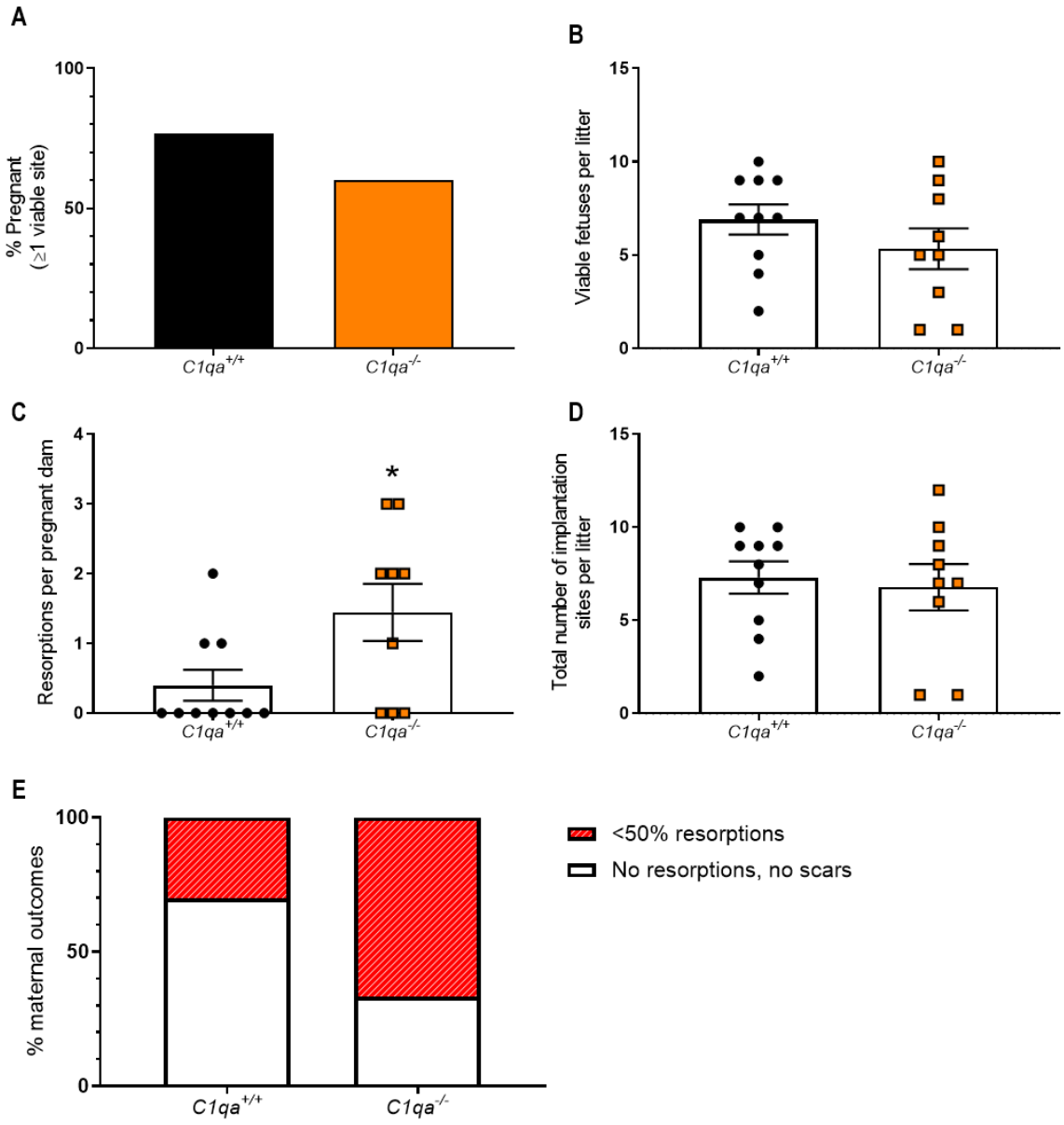

Figure 7.2: C1Q deficiency results in increased number of resorptions on day 17.5 pc.
C1qa$^{+/+}$ and *C1qa*$^{-/-}$ females were mated to BALB/c stud males. Viable pregnancy rate for *C1qa*$^{+/+}$ and *C1qa*$^{-/-}$ dams was assessed on day 17.5 pc (A). The numbers of viable fetuses, implantation site resorptions, and total implantation site numbers were also assessed per litter (B-D). The pregnancies were categorised into viability rankings (E). Data are presented as mean ± SEM (B-D). Statistical analysis was performed using χ^2 test (A) or unpaired t-test (B-D), n=9-10 mice/group. * indicates statistical significance ($p<0.05$); *$p<0.05$.

7.3.2 FETAL OUTCOMES

Fetal outcomes, including fetal and placental weights, were also analysed. Data are presented as estimated marginal means ± SEM with the number of viable pups used as the covariate. Fetuses from *C1qa*$^{-/-}$ dams were 14% smaller than fetuses from *C1qa*$^{+/+}$ dams (1048 ± 16 mg vs 907 ± 19 mg, *C1qa*$^{+/+}$ vs *C1qa*$^{-/-}$, p<0.001, Figure 7.3 A). Conversely, placentas from *C1qa*$^{-/-}$ dams were 11% heavier (107.6 ± 1.7 mg vs 121.0 ± 2.1 mg, p<0.001, Figure 7.3 B). As fetal weight was reduced in *C1qa*$^{-/-}$ dams and placental weight was increased, there was a 22% reduction in fetal to placental weight ratio in *C1qa*$^{-/-}$ dams (9.8 ± 0.2 vs 7.7 ± 0.2, p<0.001, Figure 7.3 C). Interestingly, post-natal pup weights were not different between *C1qa*$^{+/+}$ and *C1qa*$^{-/-}$ mice, yet there were an increased proportion of female pups weaned on day 21 compared to male pups in *C1qa*$^{-/-}$ mice (Appendix 9.28).

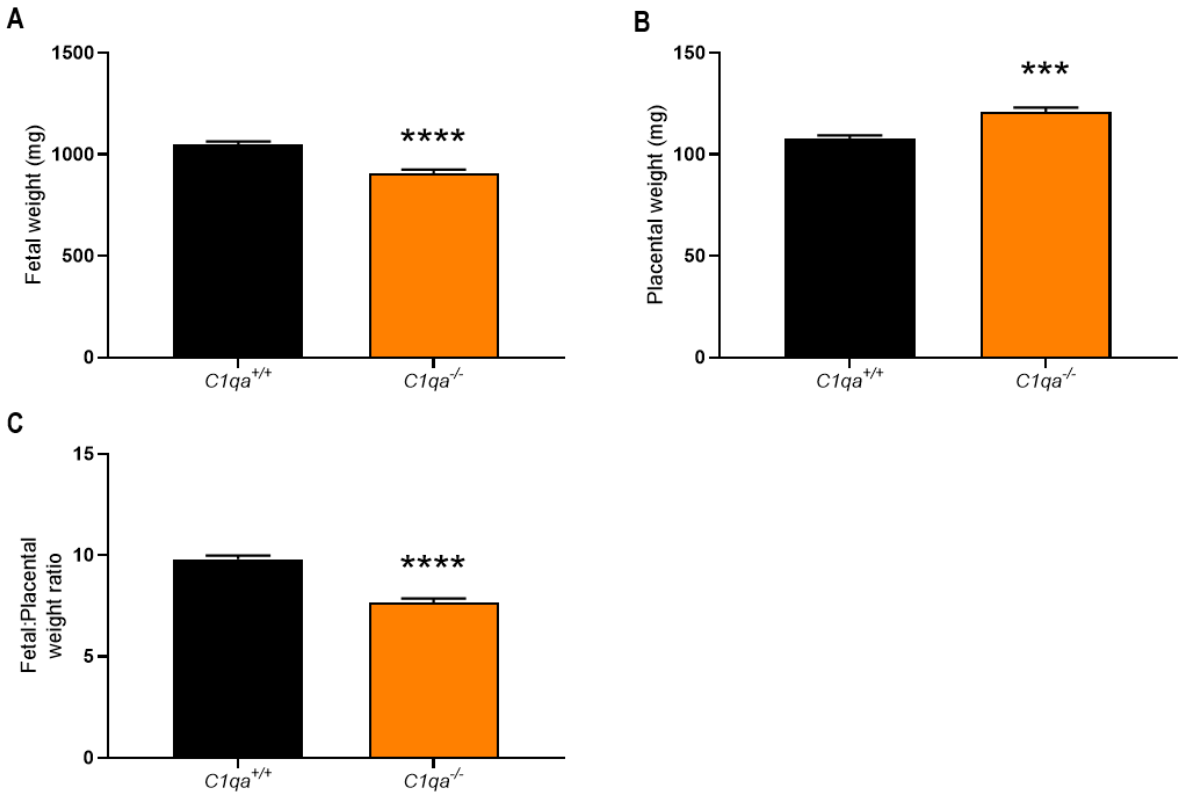

Figure 7.3: C1Q deficiency results in fetal growth restriction on day 17.5 pc.

C1qa$^{+/+}$ and *C1qa*$^{-/-}$ females were mated to BALB/c stud males. Fetal weight (A), placental weight (B), and fetal to placental weight ratio (C) were all measured on day 17.5 pc. Data are presented as estimated marginal mean ± SEM, using total number of viable sites per litter as the covariate. Statistical analysis was performed using unpaired t-test, n=9-10 mice/group. * indicates statistical significance ($p<0.05$); ***$p<0.001$ and ****$p<0.0001$.

7.3.3 PLACENTAL MORPHOLOGY

In order to understand a mechanism of FGR and placental hypertrophy, placental morphology was assessed on day 17.5 pc (Figure 7.4 A and B). There was a 13% increase in the total area of the placentas from *C1qa*$^{-/-}$ mice (mean ± SEM, 11.9 ± 0.3 mm^2 vs 13.6 ± 0.5 mm^2, *C1qa*$^{+/+}$ vs *C1qa*$^{-/-}$, p=0.004, Figure 7.4 C). Furthermore, the junctional zone (JZ) area was increased by 15% in *C1qa*$^{-/-}$ mice (5.3 ± 0.2 mm^2 vs 6.3 ± 0.3 mm^2, p=0.015, Figure 7.4 D). There was also an increase in the LZ area of 11% (6.6 ± 0.2 mm^2 vs 7.4 ± 0.3 mm^2, p=0.012, Figure 7.4 E). Overall, there was no change to the proportions of JZ or LZ and thus there was no difference to the LZ to JZ ratio (Figure 7.4 F, G and H). However, there was a 12% increase in the weight of the LZ in *C1qa*$^{-/-}$ mice (60.0 ± 1.5 mg vs 68.2 ± 2.5 mg, p=0.007, Figure 7.4 I).

Due to the observed differences in placental area, placental vascular architecture was assessed to determine trophoblast, maternal blood space, and fetal capillary volumes within the LZ. Placentas stained with antibodies against pan-cytokeratin and vimentin where used to assess placental vascularisation on day 17.5 pc (Figure 7.5 A-C). The volume of trophoblast cells trended toward being increased in *C1qa*$^{-/-}$ mice (0.040 ± 0.002 cm^3 vs 0.050 ± 0.003 cm^3, p=0.10, Figure 7.5 D). There was no difference to the volume of maternal blood spaces or the volume of fetal capillaries (Figure 7.5 E and F). In contrast, there was an increase in the trophoblast surface area in *C1qa*$^{-/-}$ mice (32.6 ± 1.8 cm^2 vs 41.6 ± 2.5 cm^2, p=0.009, Figure 7.5 G). However, there was no change to the barrier thickness of the trophoblast cells or the barrier thickness of the maternal blood spaces (Figure 7.5 H and I).

These experiments highlight that maternal C1Q is required for fetal growth and placental development. C1Q deficiency led to FGR and altered placental morphology consistent with impaired vascular remodelling during early to mid-pregnancy. In addition, fetal heterozygosity for C1Q may also be a factor to explain some of the results observed.

Figure 7.4: C1Q deficiency causes placental hypertrophy on day 17.5 pc.
C1qa$^{+/+}$ and *C1qa*$^{-/-}$ females were mated to BALB/c stud males. Masson's trichrome stained placental sections are shown for *C1qa*$^{+/+}$ and *C1qa*$^{-/-}$ pregnancies (A and B; scale bar is 500 μm). The total area, JZ area, and LZ area were measured (C-E). The proportion of JZ and LZ were calculated (F and G). The LZ to JZ ratio was calculated (H) as was the LZ weight (I). Data are presented as mean ± SEM. Statistical analysis was performed using unpaired t-test, n=9-10 mice/group. * indicates statistical significance ($p<0.05$). *$p<0.05$ and **$p<0.01$. JZ; junctional zone. LZ; labyrinth zone.

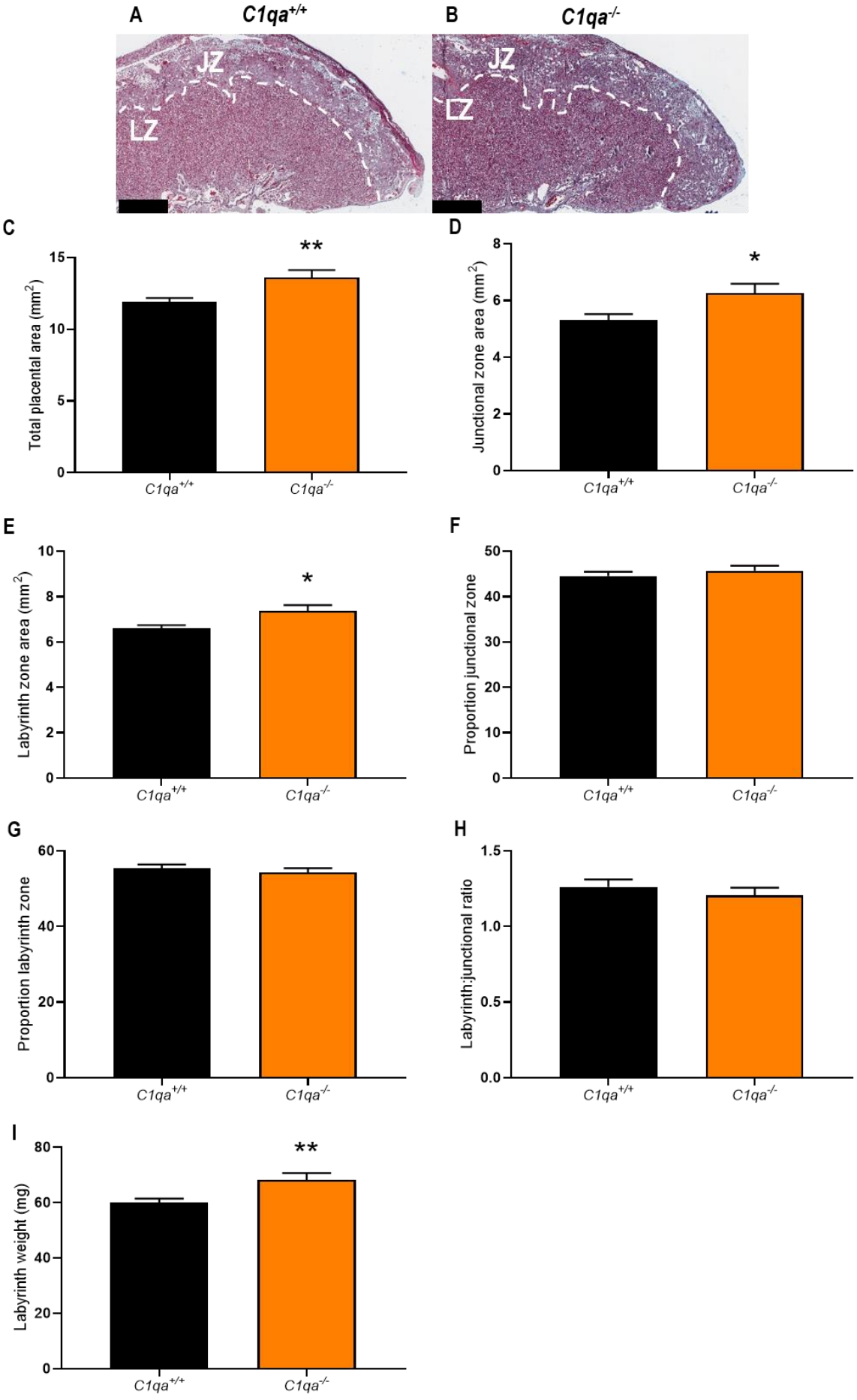
A
C1qa+/+
B
C1qa-/-
JZ
LZ
JZ
LZ
C
Total placental area (mm2)
15
10
5
0
**
C1qa+/+
C1qa-/-
D
Junctional zone area (mm2)
8
6
4
2
0
*
C1qa+/+
C1qa-/-
E
Labyrinth zone area (mm2)
10
8
6
4
2
0
*
C1qa+/+
C1qa-/-
F
Proportion junctional zone
50
40
30
20
10
0
C1qa+/+
C1qa-/-
G
Proportion labyrinth zone
60
40
20
0
C1qa+/+
C1qa-/-
H
Labyrinth:junctional ratio
1.5
1.0
0.5
0.0
C1qa+/+
C1qa-/-
I
Labyrinth weight (mg)
80
60
40
20
0
**
C1qa+/+
C1qa-/-

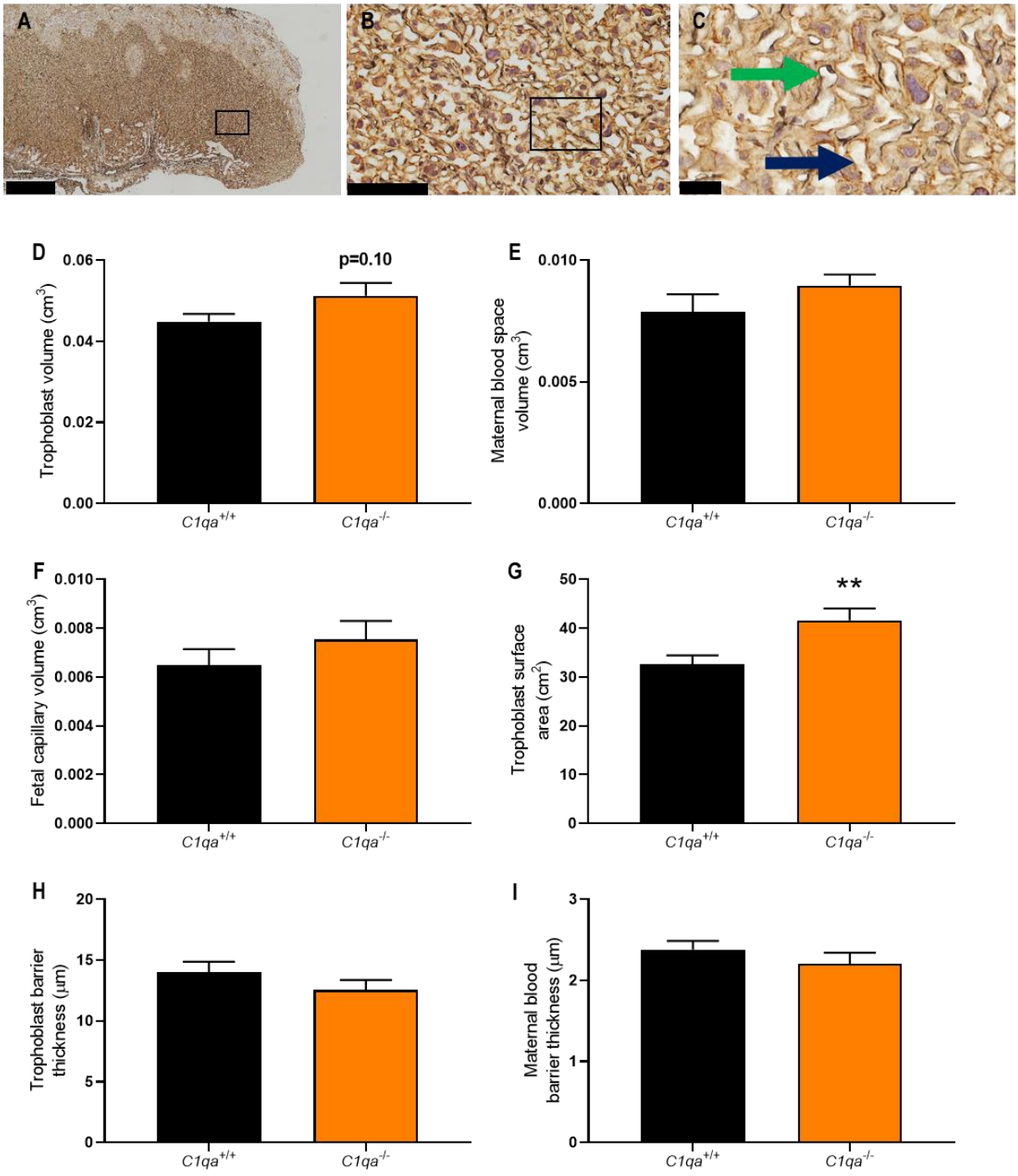

Figure 7.5: C1Q deficiency causes increased trophoblast surface area within placentas.
C1qa$^{+/+}$ and *C1qa*$^{-/-}$ females were mated to BALB/c stud males. Placental sections were labelled to detect pan-cytokeratin (trophoblasts, blue arrow in C) and vimentin (fetal capillaries, green arrow in C) in the LZ (A-C; scale bar in A equals 500 µm, scale bar in B equals 100 µm, and scale bar in C equals 25 µm). Trophoblast, maternal blood space, and fetal capillary volume densities were calculated (D-F). The trophoblast surface area was calculated (G). The trophoblast barrier thickness and the maternal blood barrier thickness were calculated (H and I). Data are presented as mean ± SEM. Statistical analysis was performed using unpaired t-test, n=9-10 mice/group. * indicates statistical significance ($p<0.05$). **$p<0.01$.

7.4 C1Q DEFICIENCY IMPAIRS EARLY PREGNANCY UTERINE VASCULAR REMODELLING

As *C1qa*$^{-/-}$ dams had growth restricted fetuses during late gestation, we next sought to investigate whether this was due to defects in vascular remodelling during mid-gestation. *C1qa*$^{+/+}$ and *C1qa*$^{-/-}$ females were mated to BALB/c stud males and on day 9.5 pc, pregnancy outcomes and decidual vascular remodelling parameters were assessed.

7.4.1 PREGNANCY OUTCOMES

On day 9.5 pc, there was no impact to viable pregnancy rate between *C1qa*$^{+/+}$ and *C1qa*$^{-/-}$ females (Figure 7.6 A). Furthermore, there was no difference to the number of viable implantation sites, resorptions or total number of sites at this time point (Figure 7.6 B-E).

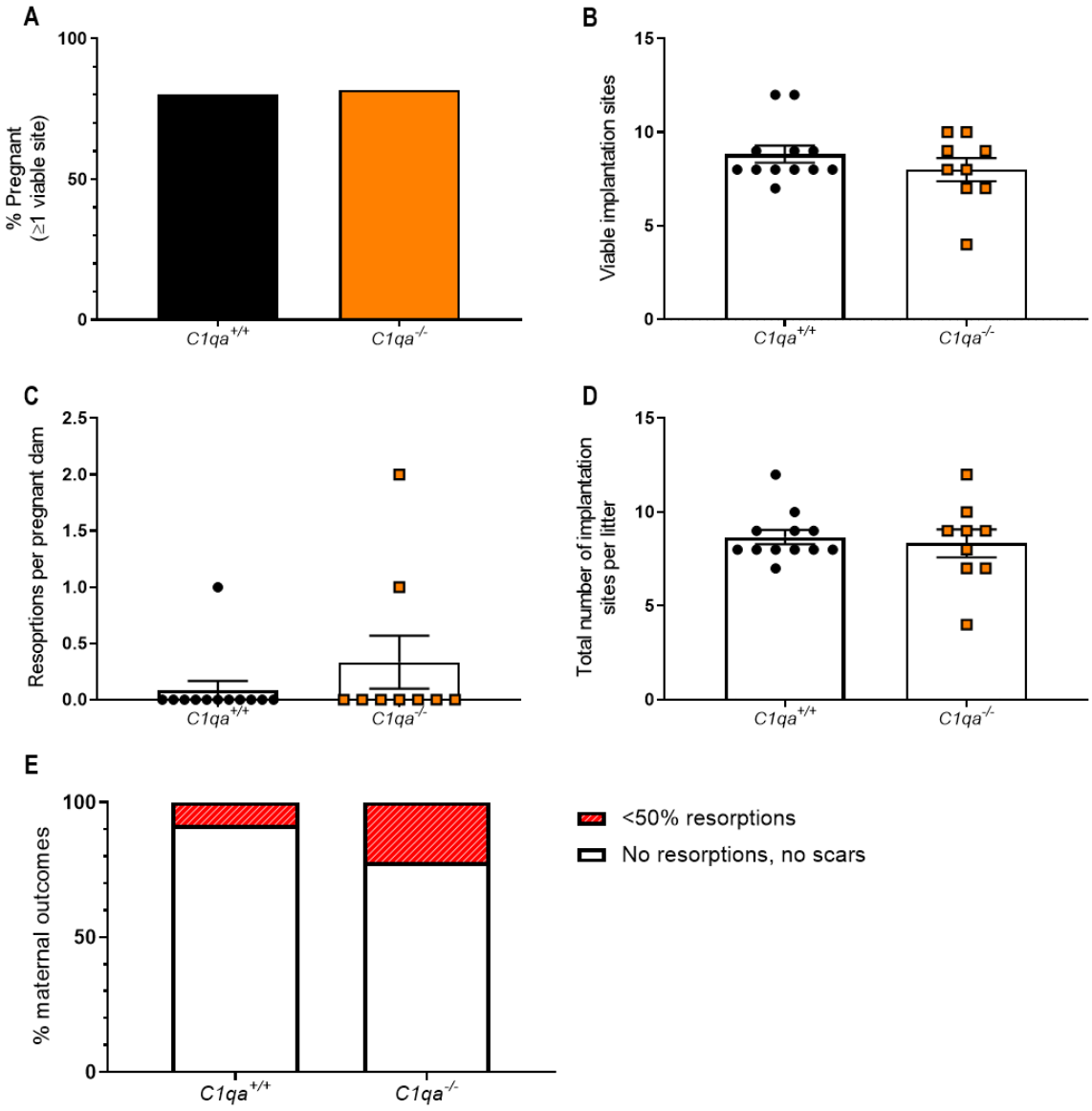

Figure 7.6: C1Q deficiency does not change maternal pregnancy outcomes on day 9.5 pc.
C1qa$^{+/+}$ and *C1qa*$^{-/-}$ females were mated to BALB/c stud males. Viable pregnancy rate for *C1qa*$^{+/+}$ and *C1qa*$^{-/-}$ dams was assessed on day 9.5 pc (A). The numbers of viable pups, implantation site resorptions, and total implantation site numbers were also assessed per litter (B-D). The pregnancies were categorised into viability rankings (E). Data are presented as mean ± SEM (B-D). Statistical analysis was performed using χ^2 test (A) or unpaired t-test (B-D), n=9-12 mice/group.

7.4.2 UTERINE VASCULAR REMODELLING

Decidual vascular remodelling was assessed on day 9.5 pc (Figure 7.7 A-D). The lumen area of decidual vessels was reduced by 41% in *C1qa*$^{-/-}$ dams on day 9.5 pc compared to *C1qa*$^{+/+}$ dams (mean ± SEM, 1802 ± 190 μm^2 vs 1055 ± 95 μm^2, *C1qa*$^{+/+}$ vs *C1qa*$^{-/-}$, p=0.004, Figure 7.7 E). Furthermore, there was a 25% reduction in lumen diameter (50.8 ± 2.8 μm vs 38.1 ± 1.1 μm, p=0.001, Figure 7.7 F). The cross-sectional area of the vessels was also reduced by 20% (1462 ± 122 μm^2 vs 1171 ± 28 μm^2, p=0.045, Figure 7.7 G) and the total vessel area was reduced by 32% (3263 ± 300 μm^2 vs 2225 ± 101 μm^2, p=0.007, Figure 7.7 H). In contrast, there was an increase in the total area to lumen area ratio (1.87 ± 0.04 vs 2.31 ± 0.10, p<0.001, Figure 7.7 I).

As uNK cells are implicated in driving vascular remodelling during early pregnancy, the density of uNK cells was calculated within the decidua on day 9.5 pc (Figure 7.8 A-D). Within the decidua, there was a reduced density of uNK cells in *C1qa*$^{-/-}$ mice on day 9.5 pc (47.3 ± 1.1% vs 41.2 ± 0.9%, p<0.001, Figure 7.8 E). Furthermore, there was a reduction in the density of macrophages in *C1qa*$^{-/-}$ mice on day 9.5 pc (12.2 ± 0.8% vs 9.8 ± 0.5%, p=0.033, Figure 7.9 A-C). To further investigate decidual spiral artery structure, day 9.5 pc implantation sites were assessed for smooth muscle actin retention. During decidual spiral artery remodelling, smooth muscle actin is lost as the arteries increase in compliance and diameter. The density of smooth muscle actin was increased in *C1qa*$^{-/-}$ mice (5.2 ± 0.7% vs 12.8 ± 2.1%, p=0.003, Figure 7.10 A-E).

There was no change to the vascular parameters of the uterine and radial arteries between *C1qa*$^{+/+}$ and *C1qa*$^{-/-}$ mice (Appendices 9.25 – 9.27)

These experiments indicate that C1Q is involved in decidual vascular remodelling during mid-gestation. Furthermore, C1Q deficiency was associated with alterations to uNK cells in the decidua, implying the effect of C1Q deficiency on vessels may be in part mediated via the agency of uNK cells.

Figure 7.7: C1Q deficiency decreases decidual spiral artery remodelling on day 9.5 pc.
C1qa$^{+/+}$ and *C1qa*$^{-/-}$ females were mated to BALB/c stud males. The decidual spiral arteries from day 9.5 pc implantation sites where assessed (A and B; scale bar equals 500 µm and C and D; scale bar equals 50 µm). Artery parameters were calculated including lumen area (E), diameter (F), cross-sectional area (G), total vessel area (H), and the ratio of total vessel size to lumen ratio (I). Data are presented as mean ± SEM with statistical analysis using unpaired t-test, n=8-9 mice/group. * indicates statistical significance ($p<0.05$). *$p<0.05$, **$p<0.01$ and ***$p<0.001$. Black arrow; spiral artery.

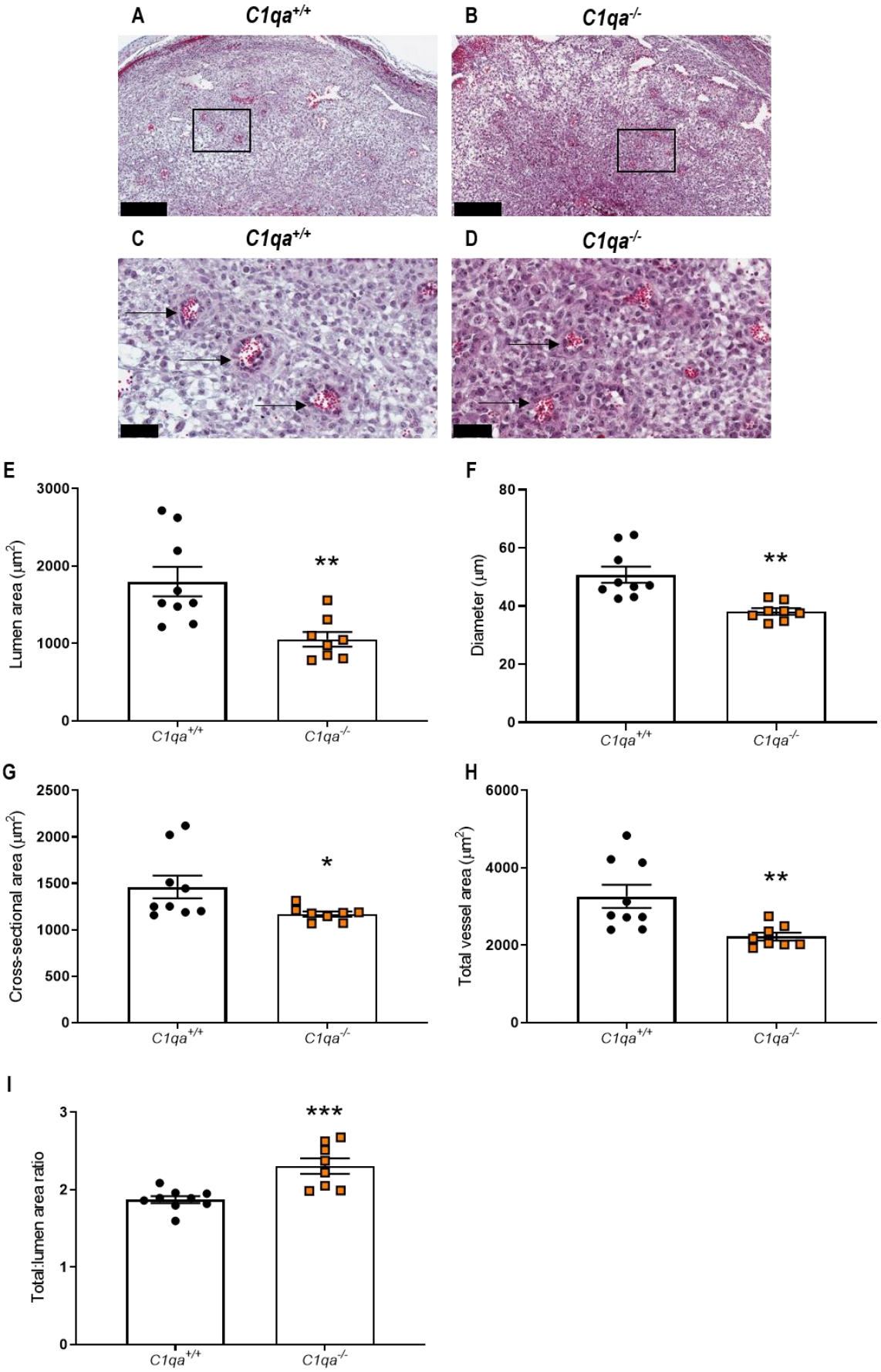
A
C1qa+/+
B
C1qa-/-
C
C1qa+/+
D
C1qa-/-
E
Lumen area (μm2)
3000
2000
1000
0
**
C1qa+/+
C1qa-/-
F
Diameter (μm)
80
60
40
20
0
**
C1qa+/+
C1qa-/-
G
Cross-sectional area (μm2)
2500
2000
1500
1000
500
0
*
C1qa+/+
C1qa-/-
H
Total vessel area (μm2)
6000
4000
2000
0
**
C1qa+/+
C1qa-/-
I
Total:lumen area ratio
3
2
1
0
***
C1qa+/+
C1qa-/-

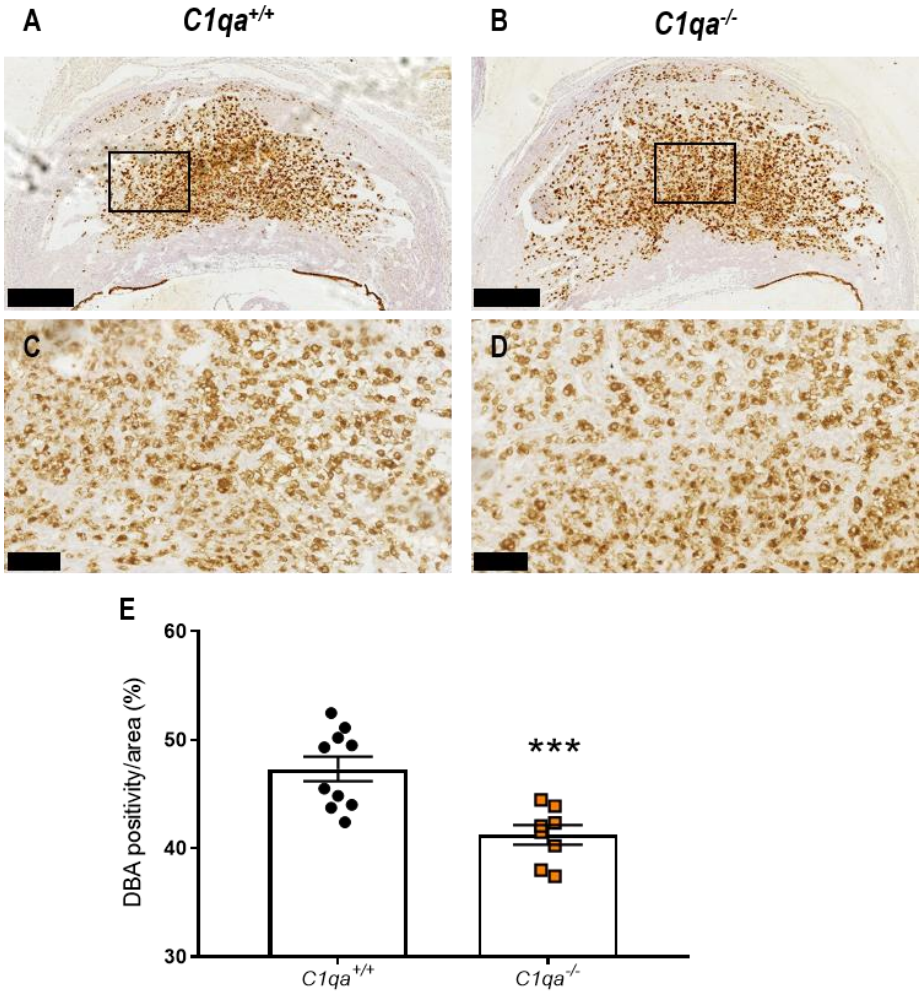

Figure 7.8: C1Q deficiency decreases uNK cells in the decidua on day 9.5 pc.
C1qa$^{+/+}$ and *C1qa*$^{-/-}$ females were mated to BALB/c stud males. DBA stained implantation sites from *C1qa*$^{+/+}$ and *C1qa*$^{-/-}$ females on day 9.5 pc (A-D; scale bar equals 500 µm in A and B and scale bar equals 100 µm in C and D). The density of DBA^{+} cells in the decidua were calculated (E). Data are presented as mean ± SEM with statistical analysis using unpaired t-test, n=8-10 mice/group. * indicates statistical significance ($p<0.05$). ***$p<0.001$.

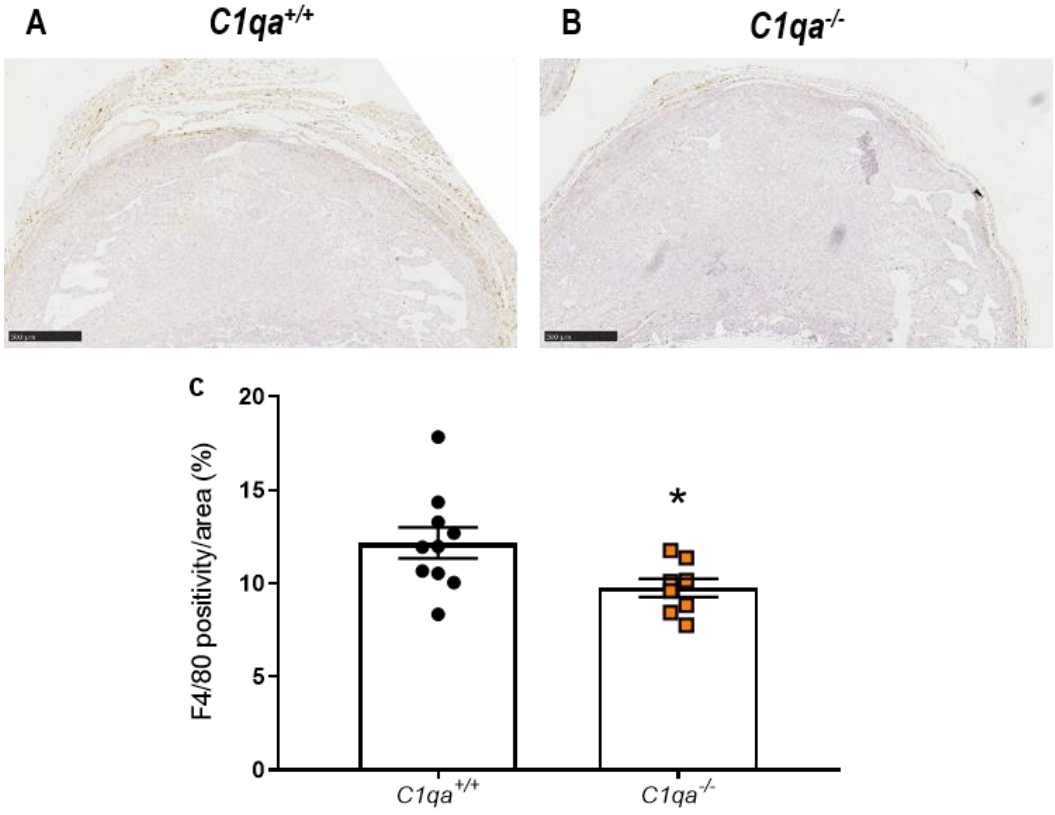

Figure 7.9: C1Q deficiency decreases macrophage density in the decidua on day 9.5 pc.
C1qa$^{+/+}$ and *C1qa*$^{-/-}$ females were mated to BALB/c stud males. F4/80 stained implantation sites from *C1qa*$^{+/+}$ and *C1qa*$^{-/-}$ females on day 9.5 pc (A and B; scale bar is 500 µm). The density of F4/80^{+} cells in the decidua were calculated (C). Data are presented as mean ± SEM with statistical analysis using unpaired t-test. * indicates statistical significance ($p<0.05$); *$p<0.05$.

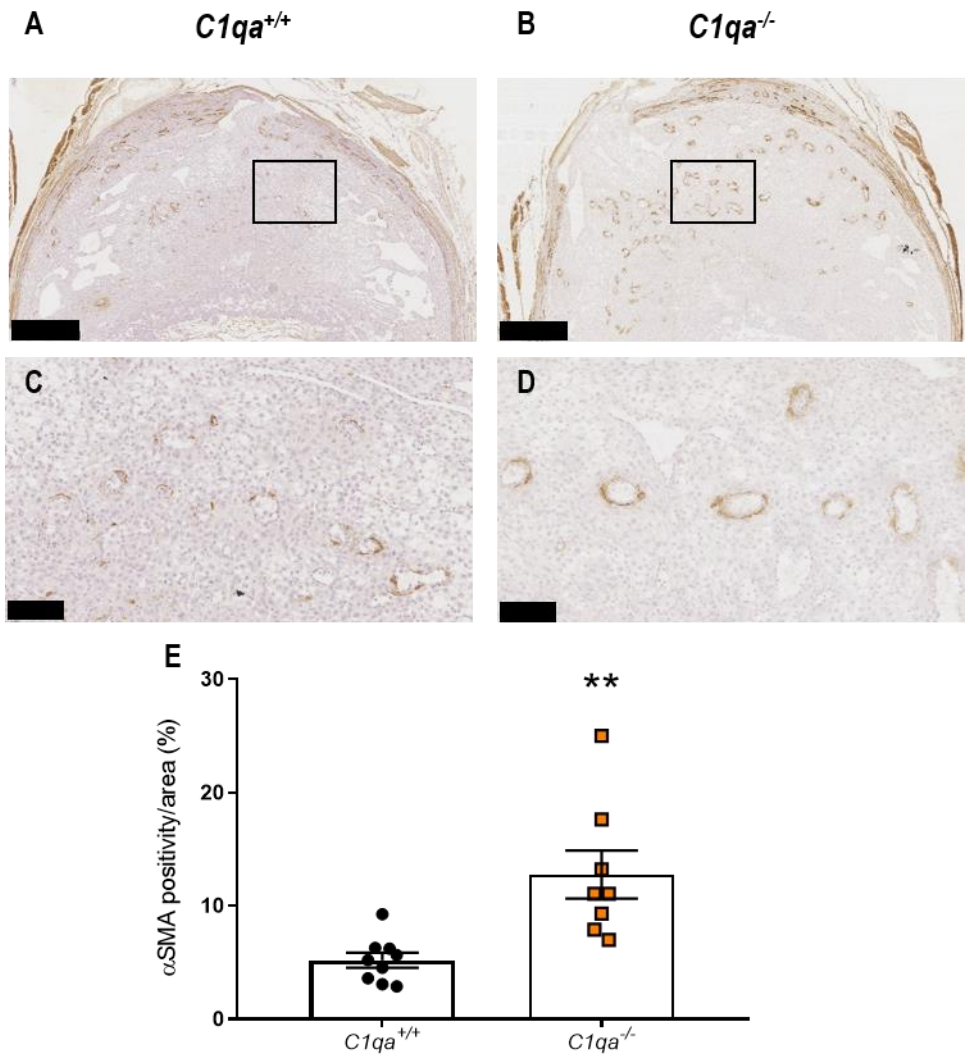

Figure 7.10: C1Q deficiency increases the density of smooth muscle actin density around decidual spiral arteries on day 9.5 pc.

C1qa$^{+/+}$ and *C1qa*$^{-/-}$ females were mated to BALB/c stud males. αSMA stained implantation sites from *C1qa*$^{+/+}$ and *C1qa*$^{-/-}$ females on day 9.5 pc (A-D; scale bar equals 500 µm in A and B and scale bar equals 100 µm in C and D). The density of αSMA^{+} cells in the decidua were calculated (E). Data are presented as mean ± SEM with statistical analysis using unpaired t-test, n=8-10 mice/group. * indicates statistical significance ($p<0.05$). **$p<0.01$. αSMA; alpha smooth muscle actin.

7.5 BONE MARROW-DERIVED MACROPHAGES RESCUE UTERINE VASCULAR REMODELLING IN C1Q-DEFICIENT MICE

To investigate whether macrophage-derived C1Q is physiologically important, we next investigated whether supplementation of CSF-1-induced wild type *C1qa*$^{+/+}$ BMDM during early pregnancy in *C1qa*$^{-/-}$ dams could rescue decidual spiral artery remodelling. Data presented in this section on the *C1qa*$^{+/+}$ and *C1qa*$^{-/-}$ groups is repeated from the above section for comparison. The breeding regime and treatment protocol are presented in Figure 7.11.

7.5.1 PREGNANCY OUTCOMES

BMDM supplementation had no effect on viable pregnancy rate, the number of viable implantation sites, or the total number of implantation sites (Figure 7.11 A, B, and D). There was an increase in the number of resorbing implantations sites in *C1qa*$^{-/-}$ mice given BMDM compared to *C1qa*$^{+/+}$ mice (mean ± SEM, 0.1 ± 0.1 resorptions vs 0.9 ± 0.3 resorptions, *C1qa*$^{+/+}$ vs *C1qa*$^{-/-}$ + MØ, p=0.014, Figure 7.11 C). Furthermore, there was an increase in the proportion of females that carried resorptions on day 9.5 pc in the *C1qa*$^{-/-}$ mice given BMDM compared to C1Q-replete mice (Figure 7.11 E).

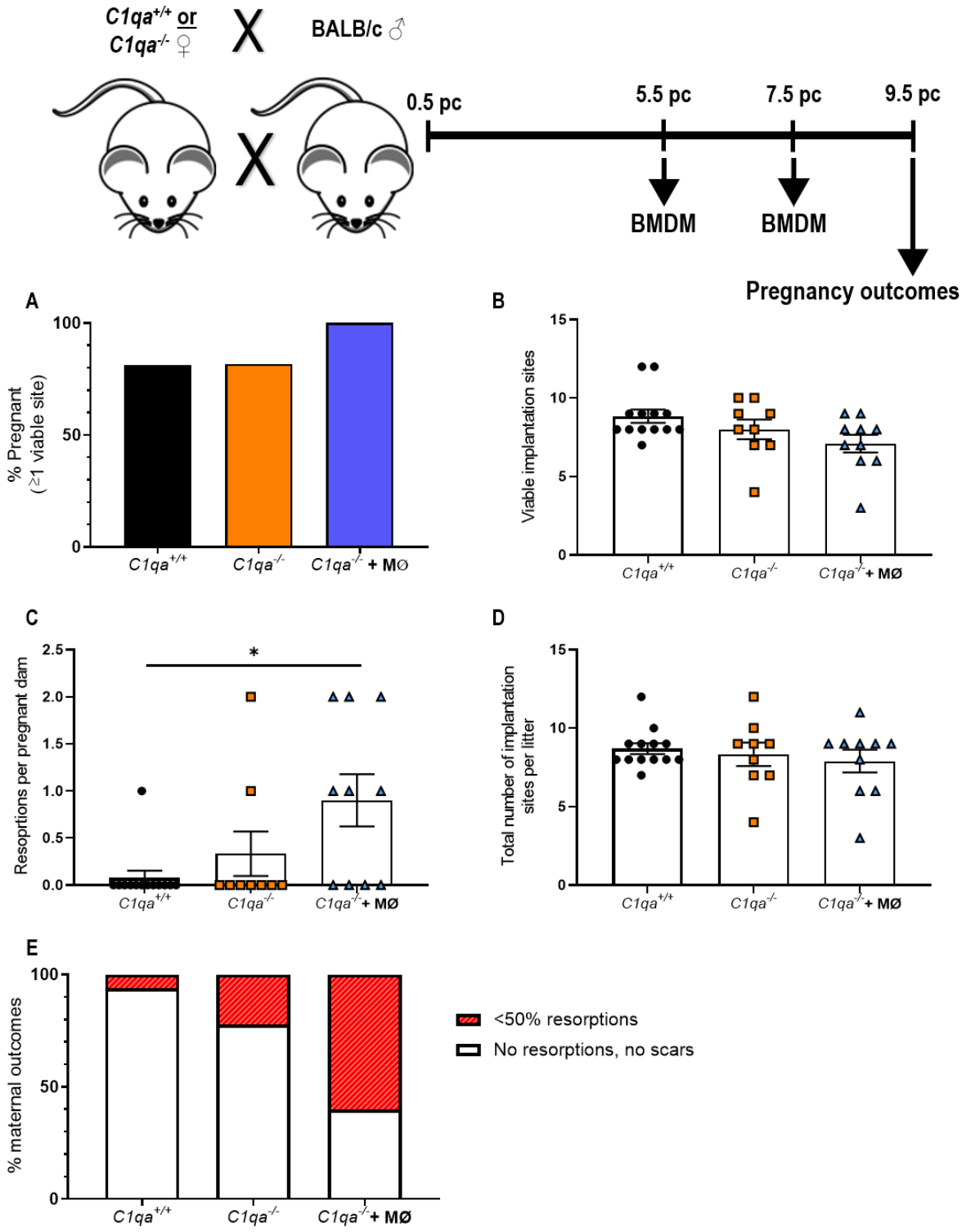

Figure 7.11: BMDM transfer to C1Q-deficient females increases the number of resorptions on day 9.5 pc compared to *C1qa*$^{+/+}$ controls.

C1qa$^{+/+}$ and *C1qa*$^{-/-}$ females were mated to BALB/c stud males. *C1qa*$^{-/-}$ females were supplemented with BMDM on days 5.5 and 7.5 pc. Viable pregnancy rate for *C1qa*$^{+/+}$, *C1qa*$^{-/-}$, and *C1qa*$^{-/-}$ + MØ pregnancies was assessed on day 9.5 pc (A). The numbers of viable pups, implantation site resorptions, and total implantation site numbers were also assessed per litter (B-D). The pregnancies were categorised into viability rankings (E). Data are presented as mean ± SEM (B-D). Statistical analysis was performed using χ^2 test (A) or one-way ANOVA with Sidak's multiple comparisons test (B-D), n=9-13 mice/group. * indicates statistical significance ($p<0.05$), *$p<0.05$. MØ; macrophages.

7.5.2 UTERINE VASCULAR REMODELLING

To investigate whether wild type *C1qa*$^{+/+}$ macrophages are involved in vascular remodelling during pregnancy via C1Q, we next assessed decidual vascular remodelling parameters on day 9.5 pc. Here, we showed that BMDM supplementation to *C1qa*$^{-/-}$ mice was able to rescue the poor decidual vascular remodelling observed in *C1qa*$^{-/-}$ mice on day 9.5 pc (Figure 7.12 A-D). The data is this section is presented as mean ± SEM with unpaired t-test between the *C1qa*$^{-/-}$ and *C1qa*$^{-/-}$ + MØ groups. The *C1qa*$^{+/+}$ group is shown for comparison. Firstly, lumen area was increased by 31% in *C1qa*$^{-/-}$ mice given BMDM compared to *C1qa*$^{-/-}$ dams (mean ± SEM, 1055 ± 95 μm^2 vs 1520 ± 122 μm^2, *C1qa*$^{-/-}$ vs *C1qa*$^{-/-}$ + MØ, p=0.011, Figure 7.12 E). Correspondingly, lumen diameter was also increased by 19% (38.1 ± 1.1 μm vs 47.2 ± 1.9 μm, p=0.001, Figure 7.12 F). There was no difference to cross-sectional area (Figure 7.12 G). There was an increase in total vessel area in *C1qa*$^{-/-}$ mice given BMDM (2225 ± 101 μm^2 vs 2804 ± 194 μm^2, p=0.026, Figure 7.12 H). Finally, the total to lumen area ratio was decreased in *C1qa*$^{-/-}$ mice given BMDM (2.3 ± 0.1 vs 1.9 ± 0.0, p=0.001, Figure 7.12 I).

The density of decidual uNK cells were assessed in the *C1qa*$^{-/-}$ mice given BMDM compared to *C1qa*$^{-/-}$ mice (Figure 7.13 A-D). The density of uNK cells was increased in *C1qa*$^{-/-}$ mice given BMDM compared to *C1qa*$^{-/-}$ dams (41.2 ± 0.9% vs 47.9 ± 1.2%, p<0.001, Figure 7.13 E). There was no change to the density of macrophages after BMDM treatment (Figure 7.14 A-C). In addition, smooth muscle actin density was decreased when BMDM were supplemented to C1Q-deficient dams (12.8 ± 2.1% vs 5.1 ± 0.8%, p=0.007, Figure 7.15 A-E). In addition, BMDM supplementation appeared to increase C1Q expression in the mesometrial triangle (Appendix 9.29).

These data further implicate macrophage-derived C1Q as a driver of vascular remodelling during early pregnancy. Furthermore, macrophage-derived C1Q appears to be involved in regulating uNK cell number within the decidua.

Figure 7.12: Macrophage transfer rescues decidual spiral artery remodelling in C1Q-deficient dams on day 9.5 pc.

C1qa$^{+/+}$ and *C1qa*$^{-/-}$ females were mated to BALB/c stud males. *C1qa*$^{-/-}$ females were supplemented with BMDM on days 5.5 and 7.5 pc. Implantation sites from *C1qa*$^{-/-}$ and *C1qa*$^{-/-}$ + MØ females (A and B; scale bar equals 250 μm). The decidual spiral arteries from day 9.5 pc implantation sites (C and D; scale bar equals 50 μm). Artery parameters were calculated including lumen area (E), diameter (F), cross-sectional area (G), total vessel area (H), and the ratio of total vessel size to lumen ratio (I). Data are presented as mean ± SEM with statistical analysis using unpaired t-test between *C1qa*$^{-/-}$ and *C1qa*$^{-/-}$ + MØ females, n=8-10 mice/group. * indicates statistical significance ($p<0.05$). *$p<0.05$, **$p<0.01$, ***$p<0.001$. MØ; macrophages.

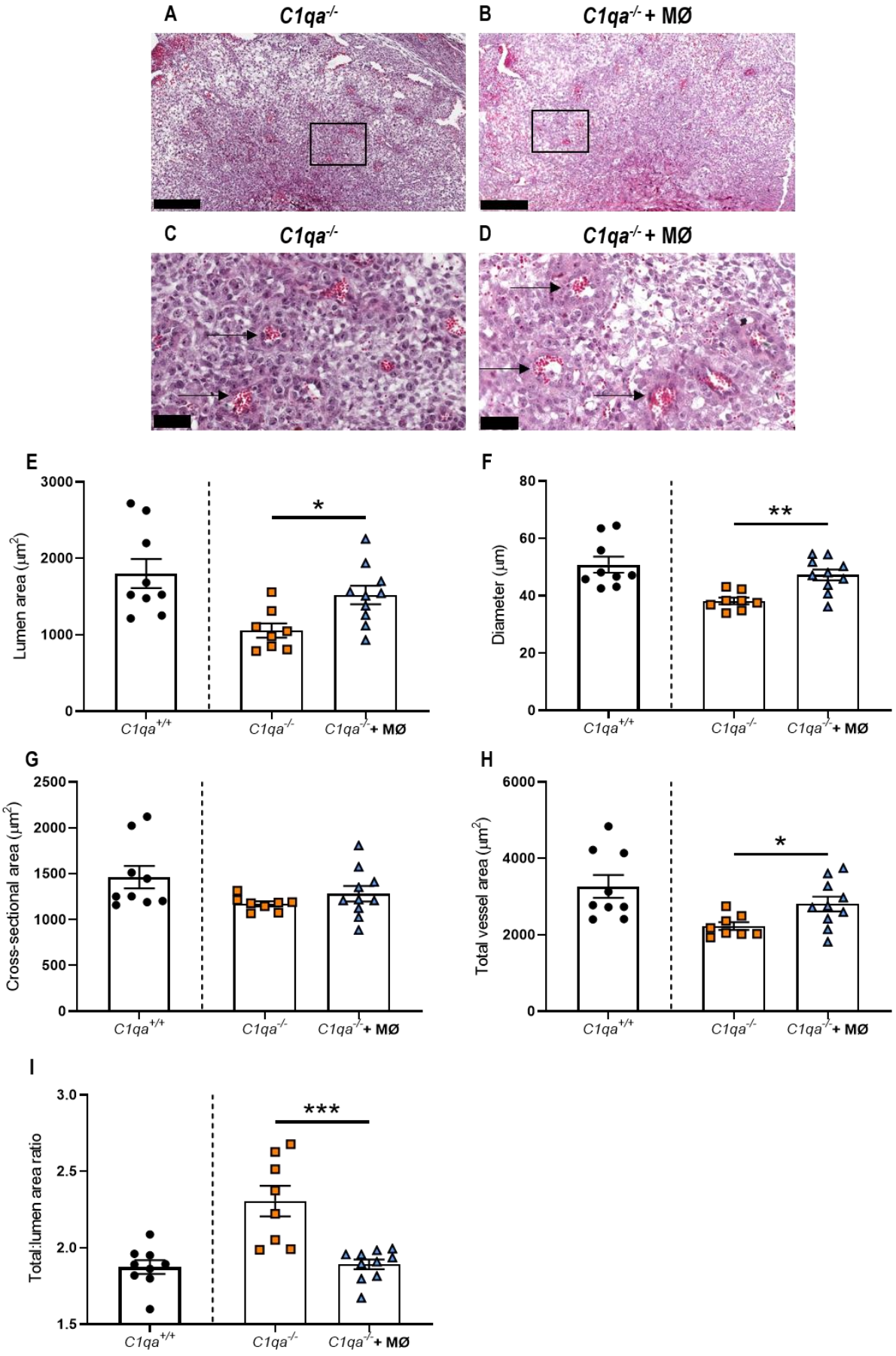
A
C1qa-/-
B
C1qa-/- + MØ
C
C1qa-/-
D
C1qa-/- + MØ
E
Lumen area (µm2)
3000
2000
1000
0
*
C1qa+/+
C1qa-/-
C1qa-/- + MØ
F
Diameter (µm)
80
60
40
20
0
**
C1qa+/+
C1qa-/-
C1qa-/- + MØ
G
Cross-sectional area (µm2)
2500
2000
1500
1000
500
0
C1qa+/+
C1qa-/-
C1qa-/- + MØ
H
Total vessel area (µm2)
6000
4000
2000
0
*
C1qa+/+
C1qa-/-
C1qa-/- + MØ
I
Total:lumen area ratio
3.0
2.5
2.0
1.5
***
C1qa+/+
C1qa-/-
C1qa-/- + MØ

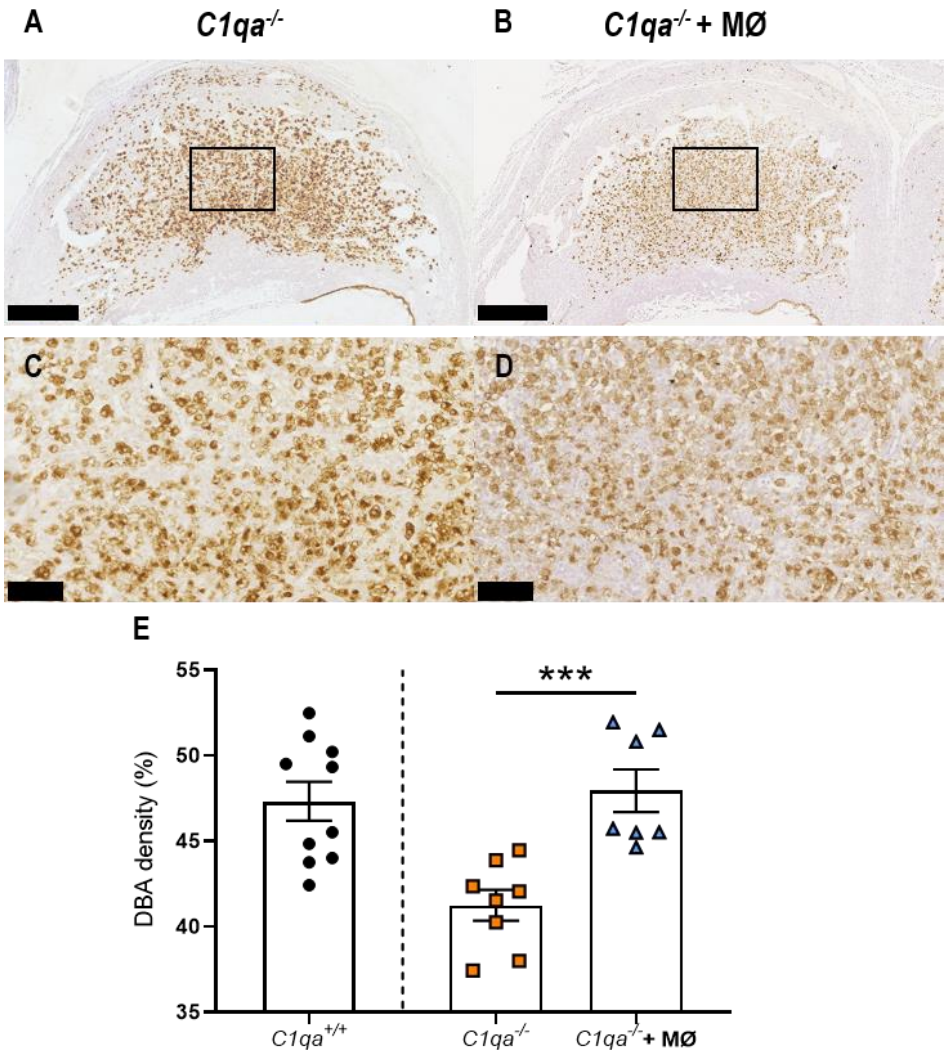

Figure 7.13: BMDM supplementation to C1Q-deficient dams increases uNK cell density in the decidua on day 9.5 pc.

C1qa$^{+/+}$ and *C1qa*$^{-/-}$ females were mated to BALB/c stud males. *C1qa*$^{-/-}$ females were supplemented with BMDM on days 5.5 and 7.5 pc. DBA stained implantation sites from *C1qa*$^{+/+}$ and *C1qa*$^{-/-}$ females (A-D; scale bar equals 500 µm in A and B and scale bar equals 100 µm in C and D). The density of DBA^{+} cells in the decidua were calculated (E). Data are presented as mean ± SEM with statistical analysis using unpaired t-test between *C1qa*$^{-/-}$ and *C1qa*$^{-/-}$ + MØ females, n=7-10 mice/group. * indicates statistical significance ($p<0.05$). ***$p<0.001$. MØ; macrophages.

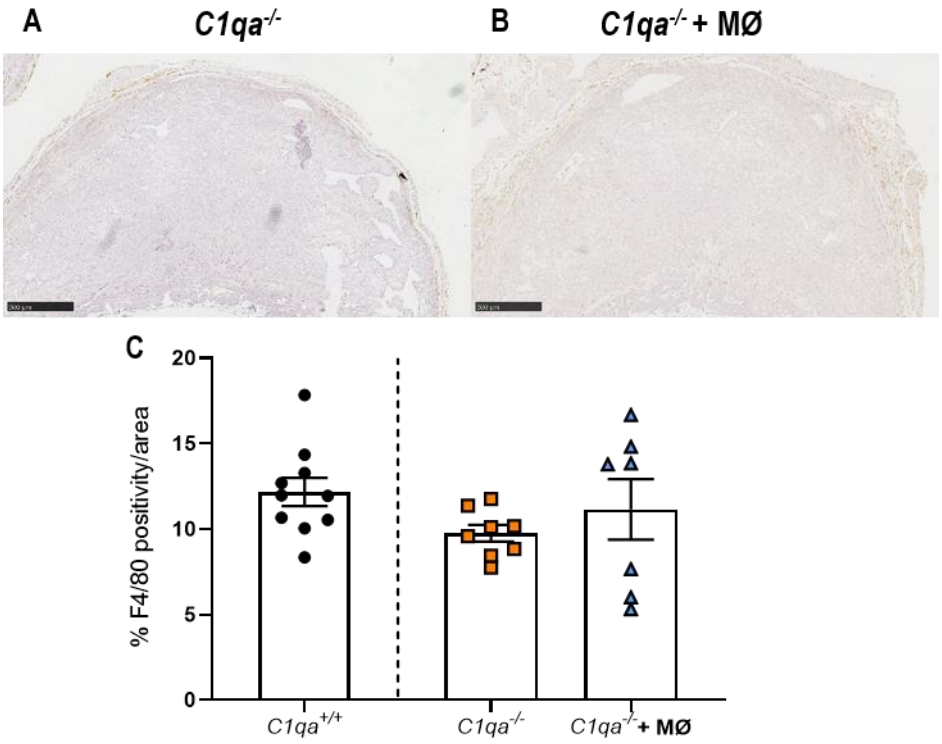

Figure 7.14: BMDM supplementation does not affect macrophage density in the decidua on day 9.5 pc.

C1qa$^{+/+}$ and *C1qa*$^{-/-}$ females were mated to BALB/c stud males. *C1qa*$^{-/-}$ females were administered BMDM on days 5.5 and 7.5 pc. F4/80 stained implantation sites from *C1qa*$^{+/+}$ and *C1qa*$^{-/-}$ females (A and B; scale bar equals 500 µm). The density of F4/80^{+} cells in the decidua were calculated (C). Data are presented as mean ± SEM with statistical analysis using unpaired t-test between *C1qa*$^{-/-}$ and *C1qa*$^{-/-}$ + MØ females. MØ; macrophages.

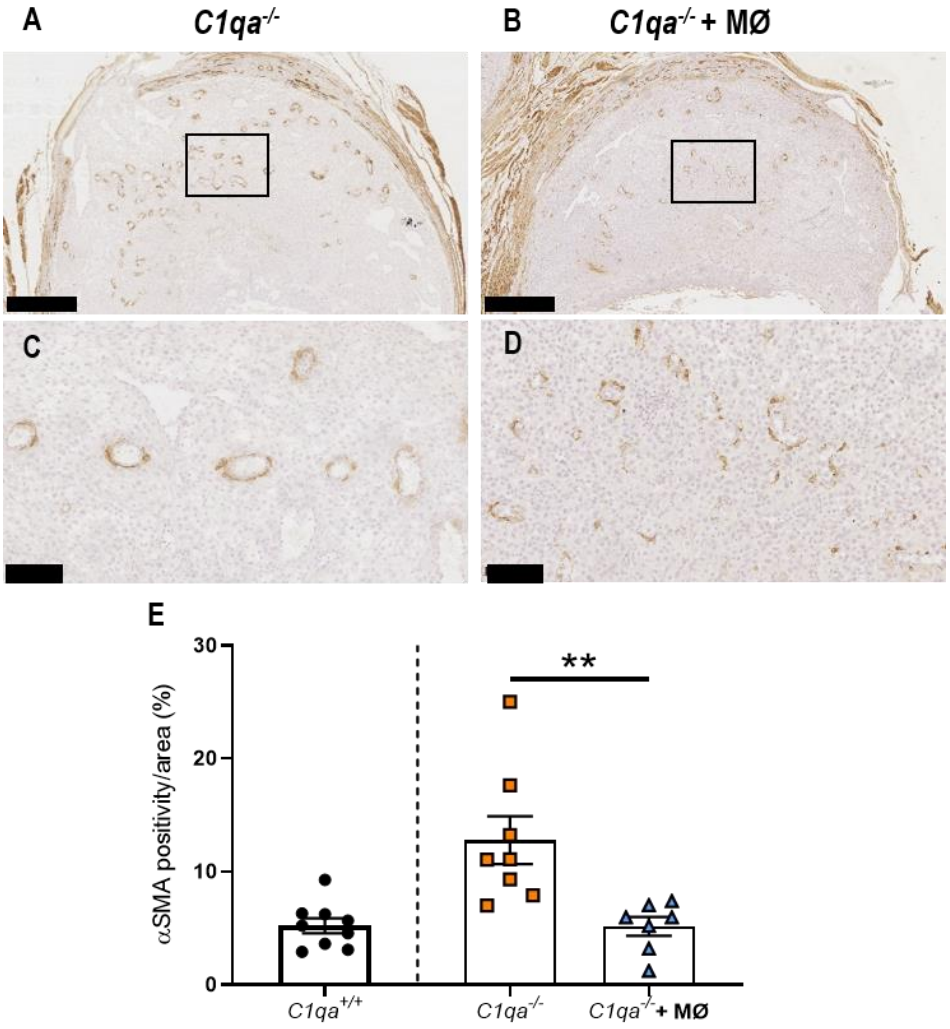

Figure 7.15: BMDM supplementation decreases the density of alpha smooth muscle actin around decidual spiral arteries on day 9.5 pc in C1Q-deficient dams.

C1qa$^{+/+}$ and *C1qa*$^{-/-}$ females were mated to BALB/c stud males. *C1qa*$^{-/-}$ females were supplemented with BMDM on days 5.5 and 7.5 pc. αSMA stained implantation sites from *C1qa*$^{+/+}$ and *C1qa*$^{-/-}$ females (A-D; scale bar equals 500 µm in A and B and scale bar equals 100 µm in C and D). The density of αSMA^{+} cells in the decidua were calculated (E). Data are presented as mean ± SEM with statistical analysis using unpaired t-test between *C1qa*$^{-/-}$ and *C1qa*$^{-/-}$ + MØ females, n=7-10 mice/group. * indicates statistical significance ($p<0.05$). **$p<0.01$. αSMA; alpha smooth muscle actin. MØ; macrophages.

7.6 DISCUSSION

The data in this chapter provide evidence to suggest that C1Q plays an important role in promoting uterine vascular remodelling during pregnancy and that macrophages are a source of C1Q to facilitate these vascular remodelling events. C1Q deficiency primarily led to FGR and placental hypertrophy on day 17.5 pc where an aberration to decidual vascular remodelling on day 9.5 pc highlighted a potential mechanism. Importantly, immunofluorescence staining suggested that macrophages are a source of C1Q during early to mid-pregnancy. Thus, BMDM supplementation was performed to assess whether C1Q derived from macrophages could improve decidual vascular remodelling. Here we present that wild type BMDM supplementation in C1Q-deficient females increases mid-pregnancy decidual vascular remodelling.

7.6.1 FETAL GROWTH IS RESTRICTED IN C1Q-DEFICIENT FEMALES

Previous studies have shown that C1Q deficiency in murine models causes impaired decidual vascular remodelling and poor vascularisation of the placental LZ during mid-pregnancy (Agostinis et al., 2010). However, these studies only investigated syngeneic matings where C1Q-deficient females were mated to C57BL/6J, C1Q-replete males. Interestingly, other studies have shown that the deficiency of C1Q in males mated to C57BL/6J, C1Q-replete females led to symptoms of PE in the dams including hypertension and proteinuria (Singh et al., 2011). Thus, it is unknown whether C1Q deficiency in females mated to an allogeneic stud male would give similar or worse outcomes than in syngeneic matings. We showed for the first time that C1Q-deficient females mated to BALB/c stud males caused FGR, placental hypertrophy, and poor vascular adaptations to pregnancy. This is important as allogeneic pregnancies require a greater level of immune tolerance than syngeneic pregnancies due to disparity in MHC antigens between mother and fetus in an allogeneic pregnancy (Aluvihare et al., 2004, Darasse-Jèze et al., 2006, Robertson et al., 2009b). In addition, pregnant women have MHC disparity with their fetus, thus allogeneic matings in mice more closely replicate pregnancy in women.

In addition to FGR, there was an increase in fetal resorptions on day 17.5 pc in C1Q-deplete dams. However, there was no difference to the number of resorptions on day 9.5 pc between C1Q-replete and C1Q-deplete dams. This suggested that fetal loss was occurring after mid-gestation when substantial growth of the fetus occurs prior to delivery. This may indicate that nutrient delivery toward the end of gestation may be compromised and some of the developing fetuses were not fit for survival. Our data suggest this may be due to an impairment in the initial vascular remodelling events setting up a poor trajectory for fetal and placental development.

7.6.2 C1Q DEFICIENCY CAUSES PLACENTAL ABNORMALITIES

To understand the mechanisms of FGR in C1Q-deficient dams, placentas were assessed for the vascularisation of the LZ. Broadly, placentas from C1Q-deficient dams were larger. There were no alterations to the relative proportions of the JZ or LZ in comparison to C1Q-replete dams. This is similar

to what occurs in various models of maternal nutrient restriction, hypoxia, and restricted uterine blood flow (Fowden et al., 2009). These models suggest that in nutrient-deprived conditions, the placenta can adapt to the demands of the fetus and grow in an attempt to deliver more nutrients to the fetus to support its growth. Furthermore, vascularisation of the LZ was minimally impacted by the deficiency of C1Q but there was an increase in the volume of trophoblast cells. This suggests that these placentas had an overall decrease in the vascular spaces in the LZ and that there was a higher density of trophoblast cells. The increased trophoblast surface area may explain the FGR due to poor nutrient delivery through a decrease in vascularisation (Burton and Jauniaux, 2018). Further investigations should aim to understand placental transport mechanisms and whether these are impaired in C1Q-deficient dams to result in FGR.

7.6.3 VASCULAR REMODELLING IS IMPAIRED IN C1Q-DEFICIENT FEMALES

Due to the observed FGR, mid-pregnancy decidual vascular remodelling was assessed to identify one of the upstream mechanisms causing FGR. C1Q-deficient dams exhibited poor decidual vascular remodelling during mid-gestation including reduced lumen area and diameter of the decidual spiral arteries. This pathophysiology has great implications for the developing placenta as small reductions in artery lumen diameter can have a drastic effect on blood velocity (Rennie et al., 2016, Reynolds et al., 2006). Disruptions to the structure of these arteries can cause turbulent blood flow which can damage the delicate fetal capillaries in the developing placenta (Burton et al., 2009, Harris, 2010). This can cause significant impairment to placental development and fetal growth. Furthermore, failure to adequately remodel these arteries during mid-gestation is linked with pregnancy complications including PE in women (Lyall et al., 2013).

In addition to the reduced decidual spiral artery lumen area, there was an increase in the total area to lumen area ratio of these vessels and increased smooth muscle actin retention around these arteries in C1Q-deficient dams. This indicates that the process of remodelling was not occurring to the same extent as in the C1Q-replete dams. Vascular remodelling in pregnancy is defined as outward hypertrophic remodelling whereas the remodelling observed in C1Q-deficient dams indicated inward hypertrophic remodelling which suggested reduced blood flow (Osol and Mandala, 2009b). Typically, as remodelling occurs smooth muscle actin is lost to increase the compliance of the arteries and reduce the resistance of the vessels (Boeldt and Bird, 2017). This enables the arteries to become relaxed to increase nutrient delivery. In time, maternal endothelial cells are replaced by fetal trophoblast cells (Adamson et al., 2002).

This process has largely been linked with uNK cells and trophoblast cells which induce substantial remodelling required for placental development (Croy et al., 2003, Moffett-King, 2002). C1Q-deficient mice had reduced proportions of uNK cells in the decidua associated with their poor decidual vascular remodelling. In addition, these implantation sites had reduced macrophage densities. Here we observed that a reduced proportion of macrophages without capacity to produce C1Q was linked with a reduced

proportion of uNK cells and poor vascular remodelling events in mid-gestation. This further supports the notion of local interaction between uNK cells and macrophages in the decidua and that their populations may both be required to mutually support the other to facilitate vascular remodelling.

7.6.4 MACROPHAGES ARE A SOURCE OF C1Q TO PROMOTE VASCULAR REMODELLING

In order to confirm that macrophages promote uterine vascular remodelling via C1Q, C1Q-deficient females were supplemented with C1Q-replete macrophages during the peri-implantation phase of murine pregnancy. At mid-gestation, there was no effect on the viability of the BMDM-supplemented pregnancies compared to C1Q-deficient dams. Interestingly, there were increased resorptions in C1Q-deficient mice given BMDM compared to C1Q-replete mice but not compared to C1Q-deficient mice. This result was unexpected but may highlight that the transferred BMDM could facilitate a quality control mechanism to remove sub-optimally developed fetuses.

In C1Q-deficient mice, the initial embryo implantation and decidualisation occurred without C1Q-replete BMDM and thus may not have occurred adequately. Therefore, when C1Q-replete macrophages were transferred, they may have responded to poor implantation or decidualisation and acted to reduce the number of viable implantation sites in order to promote healthy development of the remaining embryos. In murine pregnancy, resorptions occur as a result of maternal constraints on poor embryo or decidualisation quality, in order to conserve resources for optimal outcomes of the remaining fetuses. Despite this, the number of resorptions was not excessive and therefore did not overtly impact pregnancy viability.

Importantly, the structure of the implantation sites and the vascular remodelling after BMDM supplementation was investigated. The supplementation of BMDM to C1Q-deficient dams was able to increase lumen area and lumen diameter of the decidual spiral arteries compared to C1Q-deficient dams. Furthermore, there was no difference to the vascular remodelling on day 9.5 pc comparing C1Q-replete and C1Q-deplete dams given BMDM. The transfer of BMDM to C1Q-deficient dams restored the total area to lumen area ratio and this was further reflected in the smooth muscle actin staining. Smooth muscle actin density was reduced in C1Q-deficient dams given BMDM suggesting that C1Q acts to promote outward hypertrophic remodelling in decidual spiral arteries. Furthermore, whilst there was no specific niche for these transferred macrophages, as there previously has been via the removal of macrophages, it was interesting to note that these transferred macrophages could still act to promote vascular remodelling.

Whilst the density of macrophages was not different in the BMDM group compared to C1Q-deficient dams, there was an increase in the density of uNK cells. This further supports the idea that macrophages are drivers of maintaining the uNK cell population during mid-gestation. The functional consequences of this relationship are not yet clear. The only difference between the macrophages in C1Q-deficient mice

compared to wild type mice is their ability to express C1Q. As previously mentioned, a novel role of C1Q involves promoting an M2-like phenotype in macrophages and this may support both the vascular remodelling events and the uNK cell population in the decidua (Son et al., 2016, Spivia et al., 2014). The specific mechanism of action behind C1Q, and how the functions of macrophages in C1Q-replete and C1Q-deplete pregnancies differ, still need to be clarified.

These data are consistent with previous reports in non-pregnant *C1qa*$^{-/-}$ mice where serum C1Q expression was increased after a single transfer of 10^7 wild type bone marrow-derived cells (Petry et al., 2001). Furthermore, supplementation of wild type bone marrow cells led to an attenuation of autoimmune diseases associated with *C1q* deficiency in mice (Cortes-Hernandez et al., 2004). These findings add confidence that transfer of BMDM to C1Q-deficient mice can increase circulating C1Q. However, the pattern of C1Q expression during murine pregnancy needs to be verified to confirm that the high levels of C1Q during the peri-implantation phase directly correlate to macrophage release of C1Q to promote decidual vascular remodelling. Importantly, decidual endothelial cells can synthesise *C1q* and the deposition of C1Q onto these endothelial cells is a pregnancy dependent process, where it is not observed in the non-pregnant state (Bulla et al., 2008). Endothelial C1Q expression was only upregulated during wound healing responses in the skin and not during homeostasis suggesting a role for C1Q in vessel formation and remodelling (Bossi et al., 2014).

Importantly, C1Q expression appeared to increase moderately from the non-pregnant state to mid-gestation in wild type controls (Appendix 9.31). However, this was only quantified using immunofluorescence. Future studies should investigate C1Q RNA and protein levels throughout early pregnancy. At mid-gestation, BMDM supplementation in C1Q-deficient mice increased C1Q density in the uterus compared to C1Q-deficient mice (Appendix 9.31). Notably, there was some expression of C1Q protein in the C1Q-deficient dams which may suggest that C1Q could be produced by trophoblast cells or other embryonic cells, including embryonic macrophages, to assist in facilitating vascular remodelling in the absence of maternal C1Q expression. This is consistent with data from matings of C1Q-null males and wild type females, where these females experienced PE-like symptoms during late gestation and reduced numbers of viable fetuses (Singh et al., 2011, Agostinis et al., 2010).

C1Q-deficient females mated to BALB/c stud males imply that fetuses will be heterozygous for the C1Q gene and thus some C1Q expression may be attributable to fetal cells. Whether fetal-derived C1Q can also act to induce vascular remodelling during pregnancy has not been investigated. However, this C1Q may be transported into maternal blood via the placental vascular tree and thus aid in vascular remodelling. However, supplementation with BMDM to C1Q-deficient females improved outcomes beyond these potential effects as it restored vascular remodelling above the C1Q-deficient group, indicating macrophage-derived C1Q is important regardless of C1Q derived from the fetus. It would be

interesting to note whether syngeneic matings of male and female C1Q-deficient mice where the fetuses would also be C1Q deficient, exhibit further impaired vascular remodelling, FGR, and placental abnormalities. This experiment would provide greater evidence of the role of fetal C1Q during early pregnancy.

Future experiments should look to discriminate the effects of the individual components which regulate spiral artery remodelling. For example, C1Q-deficient dams have decreased uNK cells, macrophages, and C1Q. Thus, it is critical to determine how these individual components integrate to promote remodelling and what other factors C1Q-sufficient macrophages may produce to further help regulate decidual vascular remodelling.

Overall, results from this chapter implicate macrophages as a source of C1Q required to drive uterine vascular remodelling during mid-gestation to promote fetal growth. Furthermore, this data highlights that while C1Q is important for vascular remodelling, the impacts of C1Q deficiency are not severe enough to cause pregnancy loss, but are severe enough to cause FGR. Our data also suggest that macrophages directly regulate uNK cell populations, potentially via C1Q-mediated pathways. Future experiments should seek to clarify how C1Q-replete macrophages versus C1Q-deficient macrophages act within the decidua to promote vascular remodelling and the specific pathways that differ between the two macrophage subsets. Furthermore, it would be interesting to investigate late gestation outcomes to determine whether BMDM supplementation improves fetal growth in C1Q-deficient mice.

CHAPTER 8
GENERAL DISCUSSION AND CONCLUSIONS

8.1 INTRODUCTION

Macrophages play numerous roles in the immune response where they can act in pro-inflammatory, immune-modulating, and tissue-remodelling roles. Pro-inflammatory or classically activated macrophages are referred to as "M1" macrophages and are typically induced in response to pathogens. Conversely, tissue-remodelling or alternatively activated macrophages are referred to as "M2" macrophages. Macrophage phenotypes are diverse and although their activation status is typically referred to as "M1-like" or "M2-like" there is still an implication of an exclusive commitment to one or the other phenotypes. However, in practise these states exist amongst a vast spectrum of phenotypes between which individual cells appear to flux in a dynamic manner (Gordon, 2003). Macrophages involved in the uterine response to pregnancy are thought to have properties which encompass both pro-inflammatory and tissue remodelling phenotypes (Zhang et al., 2017). Therefore, uterine macrophages seem to have the capacity to be involved in a range of processes including assisting the recruitment and priming of regulatory T (Treg) cells to induce maternal immune tolerance; as well as facilitating uterine tissue and vascular remodelling events to allow fetal and placental growth (Ning et al., 2016). Given their range of possible phenotypes and functions, experiments in this thesis sought to clarify the essential roles of macrophages during the peri-implantation phase of murine pregnancy. In particular, we focussed on their potential to induce uterine tissue- and vascular remodelling.

Pregnancy success requires maternal immune tolerance to alloantigens expressed by the semi-allogeneic fetus, in order to support its growth and development (Robertson et al., 2018). Pregnancy also requires substantial uterine tissue and vascular remodelling to facilitate placentation (Mandala and Osol, 2012). The murine macrophage depletion model, CD11b-DTR, was utilised to assess the role of macrophages during the peri-implantation phase. Experiments within this thesis confirmed previous work showing a requirement for macrophages to maintain the vascular integrity of the corpus luteum in early pregnancy to support progesterone (P4) production (Care et al., 2013, Turner et al., 2011). As well, experiments in this thesis identified that uterine macrophages play essential roles in pregnancy success independent of ovarian macrophages. Notably, these studies provide compelling evidence implicating macrophages in facilitating uterine vascular remodelling required for early placental development, and suggest that macrophage-derived C1Q may be a key regulator of uterine vascular remodelling during early pregnancy.

8.2 MACROPHAGES ARE ESSENTIAL DURING THE PERI-IMPLANTATION PHASE TO SUPPORT DECIDUALISATION AND TROPHOBLAST CELL INVASION

Experiments in chapter three of this thesis investigated the effect on pregnancy outcome of administration of 25 ng/g diphtheria toxin (DT) to CD11b-DTR mice during the peri-implantation phase to induce >90% macrophage depletion. Extensive macrophage depletion during the peri-implantation phase resulted in ovarian haemorrhage and decreased serum P4. This confirms that macrophages are essential for maintaining the corpus luteum vasculature to support P4 production.

To allow investigation into the role of macrophages in the uterus, a hormone replacement protocol was established. This approach was utilised to exclude ovarian insufficiency and reduced serum P4 after macrophage depletion. Moreover, these experiments also aimed to confirm whether the absence of ovarian macrophages was the direct cause of pregnancy failure, independent of uterine macrophage depletion. These experiments revealed that macrophage depletion and hormone supplementation was successful in delaying pregnancy loss but was unable to support pregnancy through mid- to late gestation. This suggests that whilst macrophages play an essential role in maintaining corpus luteum structure, macrophages also facilitate essential processes within the uterus to support robust placental development and ongoing fetal development for pregnancy success.

To further consolidate a role for uterine macrophages during pregnancy, wild type CSF-1-induced bone marrow-derived macrophages (BMDM) were administered to macrophage-depleted mice. These experiments were conducted to confirm that macrophage removal caused the adverse outcomes observed rather than artefactual mechanisms occurring as a consequence of the model. These experiments also helped to identify key pathways related to macrophage function in pregnancy. We showed either P4 or BMDM administration to macrophage-depleted mice could restore pregnancy viability to day 7.5 pc. Importantly, we sought to understand how uterine macrophages were contributing to pregnancy viability through mechanisms in addition to promoting P4 production.

The mechanisms of loss were also investigated. Macrophage depletion led to reduced decidualisation on day 7.5 pc, but this was restored with administration of either P4 or BMDM. Decidualisation is dependent on P4 signalling whereby endometrial cells undergo transformation to become decidual cells in response to embryo implantation in mice. Whilst P4 supplementation did not restore ovarian structure, the increased P4 was associated with improved decidualisation. On the other hand, BMDM administration could restore ovarian structure, serum P4, and decidualisation. This implies that uterine macrophages may be dispensable for decidualisation, but are essential to maintain the corpus luteum structure and promote decidualisation via P4. Unsurprisingly, the expression of a prolactin gene, *Prl7d1*, involved in decidualisation, was decreased after macrophage depletion consistent with impaired decidualisation due to reduced P4. *Prl7d1* expression was restored with either P4 or BMDM administration.

After confirming that P4 or BMDM administration could both adequately support decidualisation, we next sought to understand whether uterine macrophages acted to facilitate pregnancy success independent of their actions within the ovary. Our results showed that macrophage depletion was associated with reduced conceptus area on day 7.5 pc. This was not restored with P4 treatment, yet was restored with BMDM administration. This supports the interpretation that uterine macrophages promote trophoblast invasion during early pregnancy.

This conclusion was also supported by the uterine gene expression data where some markers of trophoblast invasion were dysregulated after macrophage depletion. Some of these dysregulated genes included the bone morphogenetic protein (BMP) family, the fibroblast growth factor (FGF) family, epidermal growth factor (EGF), and the growth differentiation factor (GDF) family. *Fgf10* was downregulated after macrophage depletion and was not restored with P4 or BMDM administration. *Fgf10* has been shown to promote invasion and outgrowth of trophoblast cells and is involved in branching morphogenesis (Natanson-Yaron et al., 2007). Branching morphogenesis is required for early placental development and sufficient development of the chorionic villous tree required for nutrient transfer in the mature placenta (Knöfler and Pollheimer, 2013). Reduced *Fgf10* may be linked with poor trophoblast invasion after macrophage depletion. Importantly, *Fgf10* expression was lower in macrophage-depleted mice and macrophage-depleted mice given P4 compared to macrophage-depleted mice administered BMDM. This suggests that as well as P4, uterine macrophages also directly regulate *Fgf10* expression.

In contrast, *Gdf15* expression was increased after macrophage depletion and its expression was not restored with P4 or BMDM. *Gdf15* has been shown to play roles in promoting trophoblast apoptosis (Li et al., 2014). Serum GDF-15 protein expression has been shown to be increased in women with PE and placental *Gdf15* mRNA was also increased in preeclamptic pregnancies (Sugulle et al., 2009). Thus, the heightened expression of *Gdf15* could be either a cause of or a response to the impaired trophoblast invasion in macrophage-depleted mice. Consistent with this interpretation, BMDM administration acted to restore expression of *Gdf15* better than P4 administration.

Il13 expression was decreased in macrophage-depleted mice and macrophage-depleted mice given P4, but was restored with BMDM administration. *Il13* has been shown to be expressed by EVTs during the first trimester of human pregnancy (Naruse et al., 2010). Thus, decreased *Il13* may be attributable to reduced trophoblast invasion after macrophage depletion. Furthermore, *Il13* can induce macrophages to take on an “M2-like” phenotype (Svensson-Arvelund et al., 2015, Gordon, 2003). Thus, we speculate that trophoblast cells may release *Il13* to drive macrophages towards an M2-like tissue remodelling phenotype to facilitate trophoblast invasion. However, this proposal requires further investigation.

Lif was upregulated in macrophage-depleted mice and macrophage-depleted mice given P4, yet its expression was restored with BMDM administration. So far, *Lif* overexpression studies have not been conducted in murine pregnancy. However, *Lif* may play roles in promoting adequate trophoblast invasion in addition to its known roles in decidualisation (Jasper et al., 2011, Marwood et al., 2009, Stewart et al., 1992a). There is some evidence to suggest that serum LIF levels are reduced in women with recurrent pregnancy loss, which potentially highlights a role for LIF in embryo implantation through tissue and vascular remodelling (Comba et al., 2015).

Furthermore, experiments in chapter three confirmed that the reduced pregnancy viability after macrophage depletion was due to a mechanism other than maintenance of immune tolerance. Syngeneic mating experiments caused the same extent of pregnancy failure as allogeneic mating experiments, independent of hormone supplementation. Thus, these experiments suggested that uterine macrophages are involved in uterine tissue and vascular remodelling, but unlikely to be required for generation of alloantigen tolerance. Thus, we next investigated whether moderate reductions to macrophage numbers caused alterations to fetal and placental growth.

8.3 MODERATE MACROPHAGE REDUCTION IMPACTS LATE PREGNANCY OUTCOMES AND PLACENTAL VASCULATURE

Experiments performed in chapter four of this thesis investigated a moderate reduction in macrophage numbers to recapitulate a more physiologically relevant scenario than the near complete depletion protocol used in chapter three. In the general population, numbers of circulating macrophages fluctuate between individuals due to various environmental and genetic factors. Reduced macrophage numbers have been linked with pregnancy complications (Faas et al., 2014). In addition, while macrophage phenotypes must be tightly regulated to maintain immune tolerance during pregnancy, some degree of inflammation is required at implantation sites to induce tissue and vascular remodelling for placental development (Ning et al., 2016). Lower DT doses (5 ng/g and 10 ng/g) administered to CD11b-DTR mice induced moderate macrophage depletion. Whilst our studies did not specifically investigate macrophage phenotypes, there was evidence to suggest that reduced macrophage numbers impacted uterine vascular remodelling during the peri-implantation phase of pregnancy, which had lasting consequences for fetal and placental growth.

Macrophage function in vascular remodelling has been comprehensively investigated in cancer research. Tumour associated macrophages (TAMs) are drivers of cancer growth and progression by facilitating angiogenesis (Qian and Pollard, 2010). Studies in mice have shown that reduced numbers of macrophages at tumour sites led to decreased tumour growth and vascularisation (Fritz et al., 2014, Zeisberger et al., 2006). As cancer and pregnancy both rely on substantial vascular remodelling events, it is reasonable to compare the process of vascularisation in tumours to that of embryo implantation sites (Mor et al., 2017).

Reduced numbers of macrophages led to fetal growth restriction (FGR) both prior to parturition and during the post-natal period, with pup weights consistently reduced until the time of weaning. Interestingly, male offspring from macrophage-depleted dams were more affected than female offspring. Associated with FGR was reduced vascularisation of the placental labyrinth zone (LZ). Placental structure is highly dynamic whereby fetal demand can initiate placental adaptations to compensate for compromised implantation and placental morphogenesis. In this way, the placenta can remodel itself to increase

vascular blood supply allowing a greater delivery of nutrients to the fetus. Under some circumstances, increased placental vascularisation does not equate to better nutrient delivery, as placental transport mechanisms can be compromised. Placental transport mechanisms after macrophage depletion therefore need to be further investigated, to determine the specific mechanisms of fetal growth impairment when macrophages are limited.

8.4 MACROPHAGE DEPLETION IMPAIRS uNK CELL NUMBERS DURING THE PERI-IMPLANTATION PHASE

Experiments in chapter five investigated the immune profile of uterine tissue on day 7.5 pc, 48 hours post-macrophage depletion. Pregnancy is characterised by synergistic immune interactions to limit inflammation elicited by the semi-allogeneic fetus and promote immunological tolerance (Erlebacher, 2013, Robertson et al., 2015). Immune cells are also involved in tissue and vascular remodelling events to allow fetal and placental growth.

After macrophage depletion, there was a reduction in the abundance of uNK cells on day 7.5 pc. uNK cells are well-characterised to facilitate vascular remodelling in the decidua during mid-pregnancy (Moffett-King, 2002). Furthermore, mounting evidence suggests that uNK cells are reliant on a sufficient degree of MHC disparity between mother and fetus for optimal decidual spiral artery remodelling (Madeja et al., 2011, Kieckbusch et al., 2014). Despite uNK cells facilitating decidual vascular remodelling, pregnant NK cell-deficient mice only have slightly impaired pregnancies, and live pups are born (Guimond et al., 1997b). In contrast, macrophage removal results in pregnancy failure, suggesting an indispensable role for macrophages in promoting pregnancy success that is not fully accounted for by a reduction in uNK cell abundance. Nevertheless, this is a novel potential function for uterine macrophages and future experiments should look to assess the interactions between uterine macrophages and uNK cells in early pregnancy.

Interestingly, both P4 and/or BMDM administration could restore the abundance of uNK cells on day 7.5 pc suggesting the critical mechanisms by which macrophages influence uNK cells is via maintaining corpus luteum integrity and P4 release. This finding is novel in that there is only limited evidence for a hormonal control of uNK cells in mice during the peri-implantation phase. It has been shown *in vitro* that P4 signalling leads to uNK cell recruitment (Herington and Bany, 2007b). Another *in vitro* study showed that NK cell recruitment was enhanced when endometrial stromal cells were cultured in the presence of P4 leading to an upregulation of NK cell chemokines (Carlino et al., 2008). One of the upregulated chemokines was *Cxcl11*. *Cxcl11* has been shown to recruit NK cells in the human endometrium through P4 signalling (Sentman et al., 2004). Interestingly, our data show that *Cxcl11* was upregulated in macrophage-depleted mice and macrophage-depleted mice given BMDM. *Cxcl11* expression may be increased in these treatment groups as a compensation mechanism to recruit additional uNK cells. In

contrast, the heightened P4 concentration in macrophage-depleted mice given P4 may have been sufficient to restore the P4 requirement for uNK cell recruitment. The link between P4, uNK cells, and macrophages during the peri-implantation phase of murine pregnancy needs to be further investigated, in particular to determine whether there are local effects of uterine macrophages on uNK cell parameters.

Il15 is a key survival signal for NK cells (Carson et al., 1994). *Il15* expression was decreased in macrophage-depleted mice. There was a similar level of reduction in macrophage-depleted mice given BMDM, but only a slight reduction in macrophage-depleted mice given P4 replacement. Therefore, *Il15* production appears to be hindered post-macrophage depletion due to their requirement for P4 synthesis, and P4-mediated IL-15 synthesis contribute to the reduced uNK cell abundance. *Il15*-deficient mice have reduced numbers of NK cells and poor CD8 T cell responses (Liu et al., 2000). There is currently minimal evidence to suggest macrophages produce *Il15* to support uNK cell function – however, future studies should clarify whether macrophages regulate uNK cells though regulating IL-15 release. Interestingly, a recent study revealed that macrophages at the murine fetal-maternal interface are also able to respond to IL-15 (Gordon et al., 2020)

P4 administration to macrophage-depleted mice increased the abundance of uNK cells and restored the expression of some key NK cell genes including *Spp1.* However, while *Spp1* was normalised by P4 administration, it was not restored after BMDM administration. This is consistent with the number and/or function of uNK cells being altered after macrophage depletion, in large part due to reduced P4.

In women, uNK cells facilitate and regulate the extent of trophoblast invasion (Faas and de Vos, 2017, Lash et al., 2010). Moreover, uNK cells facilitate trophoblast-mediated spiral artery remodelling (Gaynor and Colucci, 2017). As in mice, uNK cell function during human pregnancy appears to be reliant upon antigenic recognition of specific HLA markers on trophoblast cells (King et al., 2000, Kieckbusch et al., 2014). Furthermore, this interaction allows growth and angiogenic factors to be released from uNK cells to facilitate remodelling (Lash et al., 2011).

Importantly, macrophage and uNK cells can be involved in early decidual spiral artery remodelling prior to trophoblast-mediated spiral artery remodelling (Smith et al., 2009). This highlights an essential role for immune cells in initiating vascular remodelling events. Therefore, we continued to interrogate the precise role of macrophages in facilitating uterine vascular remodelling during early pregnancy.

Whilst there were no differences to the numbers of Treg cells after macrophage depletion, Treg cells may act to regulate macrophage phenotype. Thus, depletion of macrophages would seem unlikely to affect Treg populations if these cells are acting upstream of macrophages. Treg cells are well-known regulators of immune tolerance during pregnancy, however their roles in regulating and promoting uterine vascular adaptations during pregnancy are only just beginning to be explored. Recently, depletion of Treg cells in a murine model revealed increased fetal death and impaired uterine artery function (Care et al., 2018).

This implies that Treg cells act to modulate vascular function during pregnancy, and it is possible that this is partly due to their influence on macrophages. Therefore, the interactions between Treg cells, uNK cells, and macrophages needs to be investigated.

8.5 MACROPHAGE DEPLETION CAUSES REDUCED UTERINE VASCULAR REMODELLING AND REDUCED C1Q EXPRESSION ON DAY 7.5 PC

Experiments from chapters three and five indicate that macrophage depletion caused reduced uterine vascular remodelling on day 7.5 pc in the mesometrial triangle. Macrophage-depleted mice supplemented with P4 also had poor vascular remodelling on both day 7.5 pc and 9.5 pc. Importantly, BMDM administration to macrophage-depleted mice in part restored uterine vascular remodelling on day 7.5 pc. This suggested that macrophages function to drive uterine vascular remodelling during early pregnancy. Therefore, we sought to assess potential molecular mechanisms by which macrophages influence remodelling events during the peri-implantation phase.

Mesometrial triangle vessels were chosen for analysis in chapters three and five as macrophage depletion led to pregnancy failure from as early as day 7.5 pc. On day 7.5 pc, decidual spiral arteries are still developing and are not discernible in the cross-sections of the implantation sites. In contrast, the mesometrial triangle arteries, which feed directly from the uterine and radial arteries, are present consistently, even in non-pregnant mice. For this reason, we were only able to assess vascular remodelling in the mesometrial triangle arteries in macrophage-depleted mice on day 7.5 pc as less than 10% of macrophage-depleted dams remained pregnant at day 9.5 pc when decidual spiral arteries are discernible.

Vascular remodelling during pregnancy enables maternal uterine arteries to be transformed into low resistance and large diameter arteries. This remodelling allows maternal blood to flow at low velocity and high volume to the developing fetus and placenta. Insufficient or reduced vascular remodelling during early pregnancy can cause increased blood velocity and turbulent blood flow. This turbulent flow can damage the trophoblast surface and delicate fetal capillaries within the developing placenta. Furthermore, reduced uterine vascular remodelling is linked with placental insufficiency and pregnancy complications including PE and FGR (Brennan et al., 2014, Boeldt and Bird, 2017, Goulopoulou and Davidge, 2015, Lyall et al., 2013).

After macrophage depletion, RNA expression was assessed on day 7.5 pc in both the decidua and myometrium. In order to identify the functions of macrophages, the genes that were dysregulated in both macrophage-depleted mice and macrophage-depleted mice given P4, but restored with BMDM administration, were investigated. Importantly, BMDM administration rescued more dysregulated genes than did P4 supplementation. The key genes rescued by BMDM administration and not P4 supplementation included the *C1q* family. Macrophages are known producers of C1Q and C1Q has

defined roles in angiogenesis, wound healing, and pregnancy (Agostinis et al., 2010, Bossi et al., 2014, Cortes-Hernandez et al., 2004).

Maternal C1Q deficiency in murine pregnancy has been reported to cause poor development of the placental LZ evident from day 10.5 pc (Bulla et al., 2008, Agostinis et al., 2010). Furthermore, paternal deficiency in C1Q revealed preeclamptic-like symptoms in wild type dams with increased serum sFlt-1, suggesting fetal haplo-insufficiency is sufficient to cause a phenotype (Singh et al., 2011). The role of C1Q in human pregnancy is still unresolved. Some studies indicate that serum C1Q expression is reduced in preeclamptic women compared to healthy controls (Agostinis et al., 2016, Jia et al., 2019, Lokki et al., 2014). However, other studies have shown increased C1Q deposition in placental tissue in women with PE compared to healthy controls – but whether this is a causal factor or constitutes an adaptive response is not clear (Sinha et al., 1984). These conflicting notions may be reconciled by the differences in timing of tissue collection and whether early-onset or late-onset PE was investigated. Results in this thesis suggest that C1Q may be an early determinant of impaired vascular remodelling and could potentially be targeted as a therapeutic for early-onset PE. Furthermore, C1Q has dynamic roles whereby it can act to initiate pro-inflammatory responses or wound healing responses. The context of C1Q expression needs to be investigated and therefore the precise mechanism of C1Q in vascular remodelling is yet to be determined.

8.6 C1Q DEFICIENCY CAUSES FETAL GROWTH RESTRICTION AND POOR VASCULAR ADAPTATION TO PREGNANCY AT MID-GESTATION

Experiments performed in chapter seven of this thesis investigated maternal C1Q deficiency during allogeneic pregnancy. These experiments identified that C1Q deficiency led to FGR on day 17.5 pc and increased placental weight, suggesting decreased efficiency of the placenta. Investigation of placental architecture highlighted hypertrophy in both the JZ and LZ, a common feature of placental compensatory adaptation in models of FGR (Burton et al., 2016, Burton and Jauniaux, 2018, Coan et al., 2004a).

Maternal C1Q deficiency resulted in decidual spiral arteries which were smaller in lumen area and diameter and had an increased total area to lumen area ratio in mid-gestation. This result is consistent with under-remodelled arteries and is linked with pregnancy complications including PE (Osol and Mandala, 2009a). Total area to lumen area ratio can be used as a measure of the remodelling status of arteries. As pregnancy progresses, spiral arteries lose smooth muscle cells and trophoblast cells infiltrate these arteries to increase compliance and diameter. Our data show that absence of maternal C1Q led to retention of smooth muscle cells indicating that remodelling was impaired. Future studies should interrogate trophoblast invasion in C1Q-deficient mice and should look to assess blood flow velocity to determine whether reduced blood flow to these developing implantation sites is related to the FGR observed during late gestation.

Furthermore, maternal C1Q deficiency was associated with reduced abundance of uNK cells. Previous studies have not linked C1Q expression with uNK cells during vascular remodelling events. It remains to be investigated how macrophages, C1Q, and uNK cells interact in the uterine microenvironment to promote spiral artery remodelling. One rational hypothesis is that C1Q exerts its vascular remodelling effects via modulating the numbers and potentially functions of uNK cells.

8.7 MACROPHAGES ARE A SOURCE OF C1Q TO PROMOTE VASCULAR ADAPTATION TO PREGNANCY

Results from chapter seven show that macrophages are a source of C1Q. Importantly, wild-type BMDM supplementation could increase lumen area and diameter of decidual spiral arteries in C1Q-deficient mice and also reduced the density of smooth muscle actin. This highlights that vascular remodelling was occurring to a similar extent to that observed in C1Q-replete mice after BMDM administration to C1Q-deficient mice. Interestingly, BMDM supplementation could also restore the abundance of uNK cells, supporting a potential role for macrophages and C1Q in promoting uNK cell function. It remains to be investigated how wild type macrophages and C1Q-deficient macrophages differ and how C1Q may act to mediate the effects of macrophages or potentially modulate other aspects of macrophage function or phenotype required for vascular remodelling.

Cancer studies have shown that C1Q can induce vascularisation of tumours to promote growth. Furthermore, tumour cells can hijack macrophage-derived C1Q to promote their growth (Roumenina et al., 2019). Studies such as this suggest context-dependent and cell-dependent C1Q expression can act to promote inflammation during times of infection, and can also act to promote tissue and vascular remodelling. Therefore, the specificity of macrophage and C1Q function needs investigation, as well as whether these differences are observed in women with pregnancy complications.

8.8 LIMITATIONS

Experiments within this thesis sought to clarify the role of macrophages in early pregnancy and in uterine vascular remodelling. These experiments utilised murine models which do not completely replicate human pregnancy. Placental development and uterine immune cell localisation differ in important ways between the two species. Thus, further research is required to confirm how macrophages function in the human uterus, to investigate C1Q expression by human uterine macrophages, and to evaluate the direct and indirect consequences of reduced macrophage numbers during human pregnancy.

The CD11b-DTR murine model causes systemic macrophage depletion. Macrophage depletion in this model may have had indirect or artefactual impacts on other tissues rather than just depletion from reproductive tissues. However, experiments within this thesis utilised hormone and macrophage administration protocols to, at least partly, account for off-target and artefactual impacts. Importantly, future studies should investigate murine models which allow transient and specific depletion of uterine

macrophages rather than systemic depletion. For example, lox-Cre mouse models to target uterine macrophages for depletion would be useful.

To further interrogate the specific roles of uterine macrophage subsets during pregnancy, the CD169-DTR model could be used to deplete tissue resident macrophages. This would help to identify whether the contributing actions of macrophages within the uterus arise from circulating bone marrow-derived monocyte populations, or whether these effects reflect actions of embryonic-derived tissue resident macrophages. Tissue resident macrophage populations within the uterus are not yet defined. By comparing results from CD11b-DTR mice with data from CD169-DTR mice, it would be possible to clarify the ontogeny of uterine macrophages that have key functions in pregnancy.

In addition, the C1Q-deficient mouse model utilised is a systemic depletion of C1Q. A better model could delete C1Q from macrophages alone to confirm the specific role of macrophage-derived C1Q. In addition, a uterine-specific C1Q-deficient model would help to elucidate whether uterine C1Q production is essential for vascular remodelling events during pregnancy or whether systemic C1Q expression can induce the remodelling events. Again, the lox-Cre system could be manipulated such that C1Q is either not expressed by macrophages or is not expressed within uterine tissues.

Future studies should aim to investigate the expression of C1Q in decidual biopsies from women. As our studies within this thesis investigated early pregnancy vascular remodelling, it would be beneficial to investigate uterine tissue from early terminations for C1Q expression and macrophage markers. The clinical correlation between C1Q expression and macrophage numbers is yet to be investigated and is yet to be quantified across the course of gestation. It would also be interesting to assess the pattern of expression of C1Q within the decidua and whether C1Q expression levels are correlated to significant vascular remodelling stages of pregnancy. Furthermore, it would be beneficial to assess whether serum C1Q expression is representative of uterine C1Q expression, which could justify studies to investigate whether C1Q can be used as a biomarker for vascular disorders of pregnancy.

8.8 FINAL CONCLUSIONS

In conclusion, this thesis has shown that uterine macrophages are essential for pregnancy success. This finding extends earlier observations that ovarian macrophages are crucial for maintaining the vascular integrity of the corpus luteum during early pregnancy. The role of macrophages within the uterus is predominantly to drive uterine vascular remodelling during the peri-implantation phase via C1Q release. Macrophage depletion during early pregnancy led to near-complete pregnancy failure by day 9.5 pc. Surprisingly, uterine macrophages appear to be dispensable for pregnancy immune tolerance. Conversely, macrophages appear essential to support uNK cells during early pregnancy through actions that appear to involve facilitating corpus luteum P4 production, as well as possible local interactions in the uterus. Importantly, we propose that the uterine vascular adaptations required for pregnancy success are

regulated largely by macrophage-derived C1Q. The precise actions of C1Q, and the extent to which these are mediated via uNK cells or independently, require further investigation. The possibility that Treg cells modulate macrophage production of C1Q is also a key question to resolve.

Importantly, these results raise the prospect that macrophage-derived C1Q is involved in the failed vascular adaptations that lead to hypertensive disorders of human gestation. Future studies are required to define the role of uterine macrophages and their functional relationship with C1Q production and uNK regulation in facilitating uterine vascular remodelling during human pregnancy, and the potential contribution of this nexus in implantation failure, and disorders of placentation such as PE and FGR.

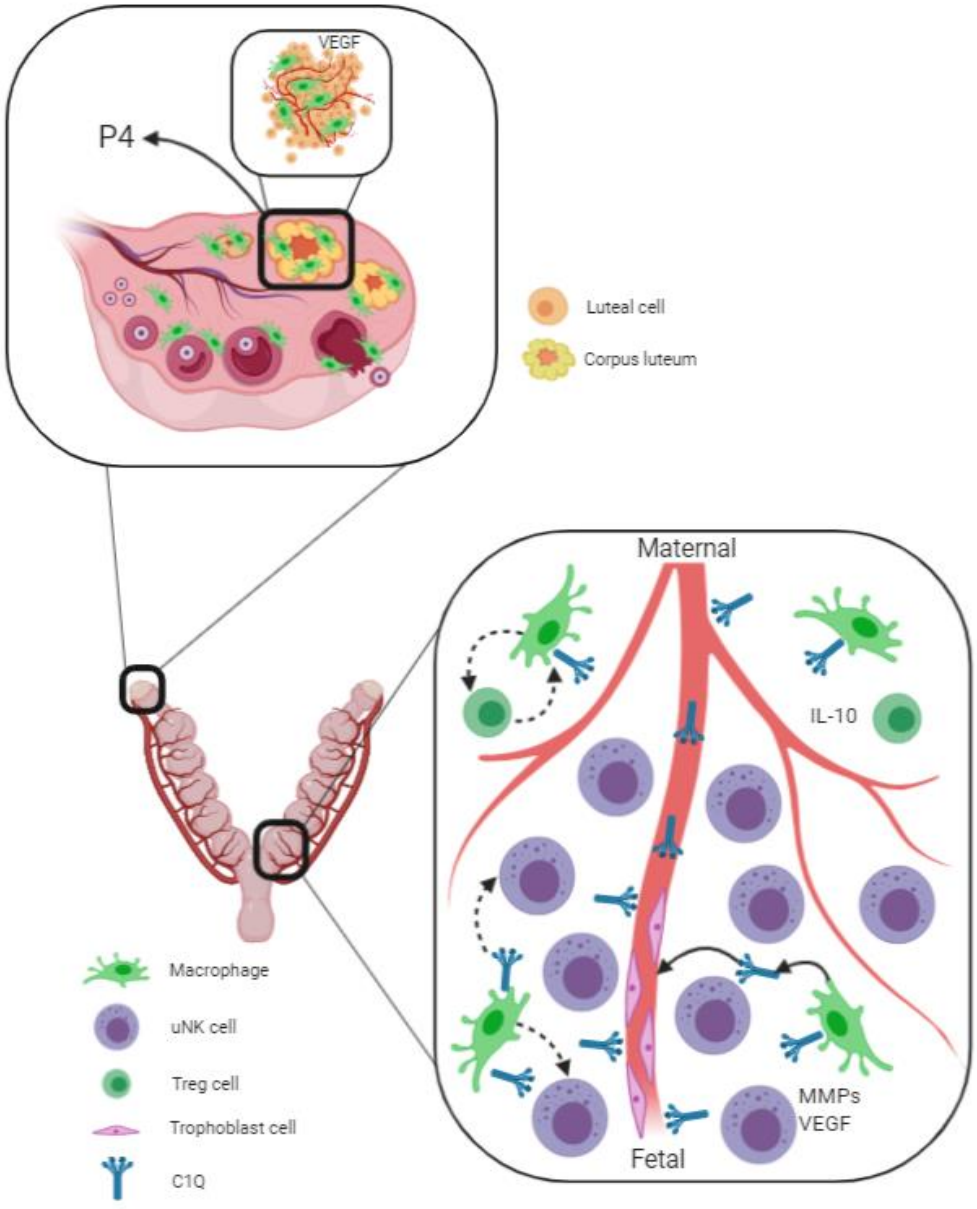

Figure 8.1: Macrophage-derived C1Q facilitates uterine vascular adaptations to pregnancy. This illustration depicts the known and proposed roles of macrophages within the ovary and the uterus. Studies in this thesis have confirmed that macrophages are essential for supporting the vascular integrity of the corpus luteum to facilitate progesterone (P4) production. Previous studies have shown that ovarian macrophages can secrete vascular endothelial growth factor (VEGF) within the corpus luteum and macrophage depletion severely impacts the vasculature within the ovary and reduces serum P4 (Care et al., 2013, Turner et al., 2011). This illustration also depicts immune cells involved in remodelling the uterine vasculature during early pregnancy. This process can be mediated by matrix metalloproteinases (MMPs), VEGF, and interleukin 10 (IL-10). Studies within this thesis demonstrate macrophages as being a source of C1Q to facilitate these remodelling events. C1Q expression was co-localised with macrophages and endothelial cells within the uterus. Furthermore, some C1Q expression was noted within intravascular spaces. C1Q-deficiency was further linked with fetal growth restriction and reduced uNK cell abundance. Future studies should clarify the mechanism of action of macrophage-derived C1Q within the developing implantation sites. Furthermore, whether C1Q directly acts on uNK cells needs clarification as do the interactions between macrophages, uNK cells, and Treg cells. Image adapted from BioRender.

CHAPTER 9

APPENDICES

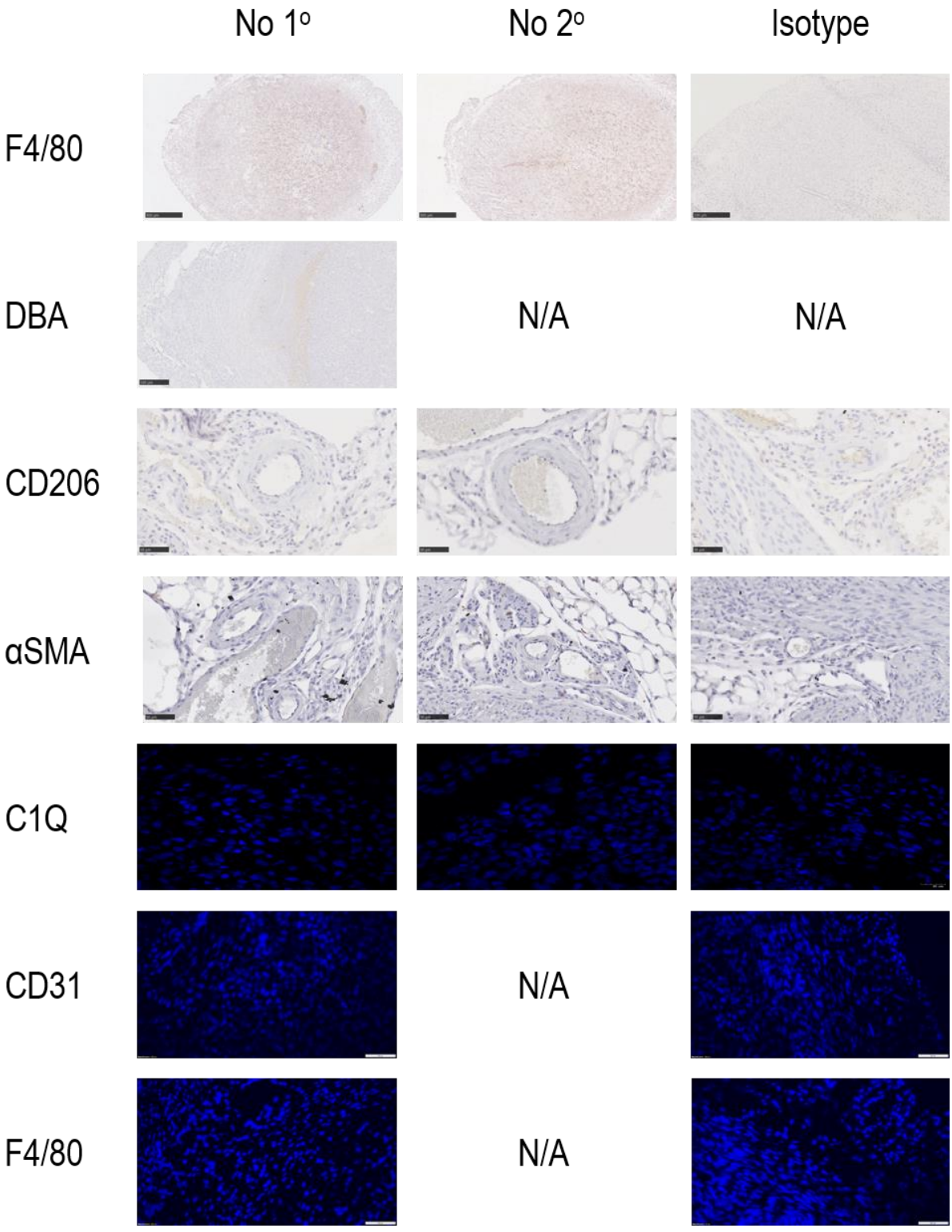

Figure 9.1: No primary antibody and isotype-control sections for immunohistochemistry and immunofluorescence staining

The specificity of the primary (1°) and secondary (2°) antibodies was assessed by substituting these antibodies with serum-only controls or with an isotype-matched control.

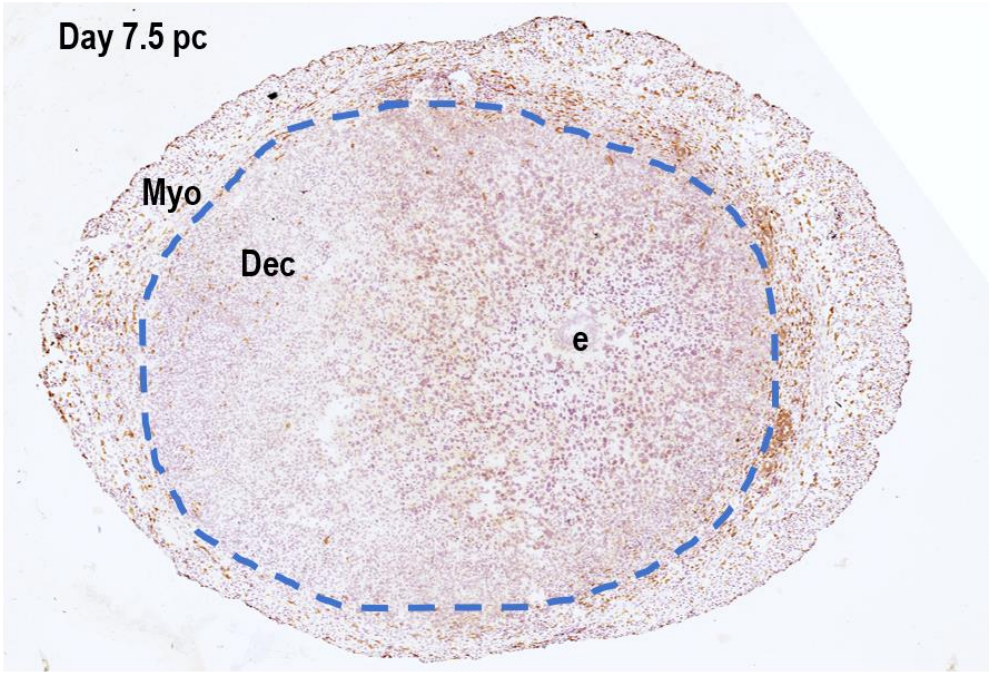

Figure 9.2: Macrophages predominantly localise to the myometrium on day 7.5 pc.
Implantation site on day 7.5 pc stained with anti-rat F4/80. The two regions of the uterus are shown (myometrium, Myo and decidua, Dec). Within the decidua situates the embryo (e).

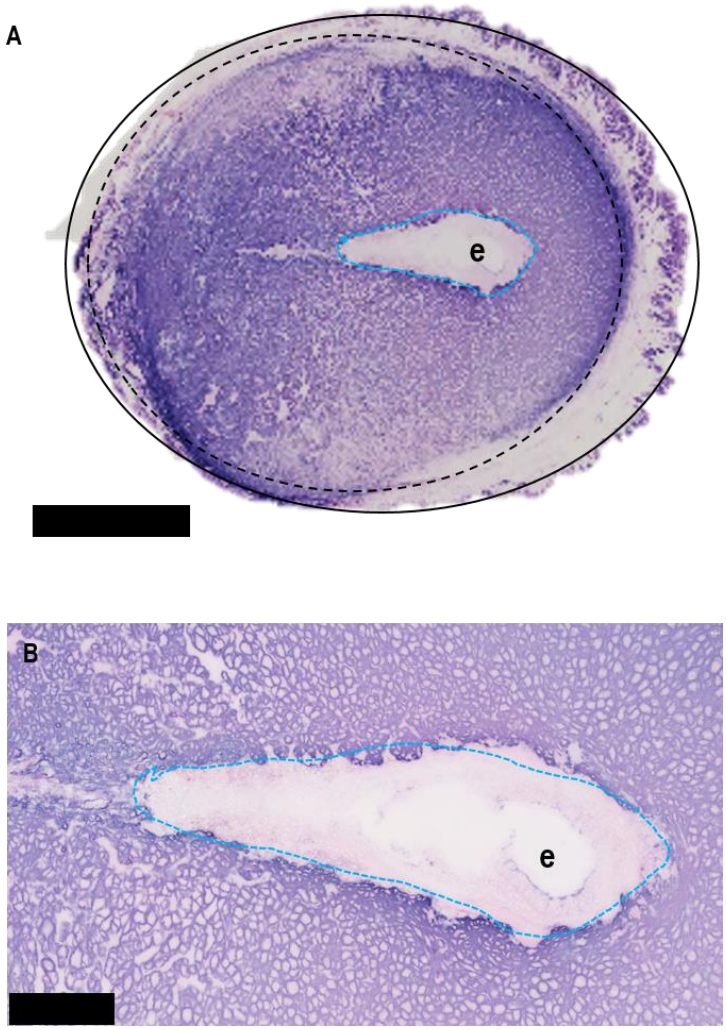

Figure 9.3: Alkaline phosphatase staining allows decidual area to be calculated.
Implantation site on day 7.5 pc stained with alkaline phosphatase. The solid black line in A represents the total implantation site area and the dashed black line in A represents the decidual area (scale bar in A equals 1 mm). The dashed blue line in A and B signifies the conceptus area (scale bar in B equals 250 μm). The decidual area minus the conceptus area was divided by the total area to give the area of decidualisation (%). e; embryo (e).

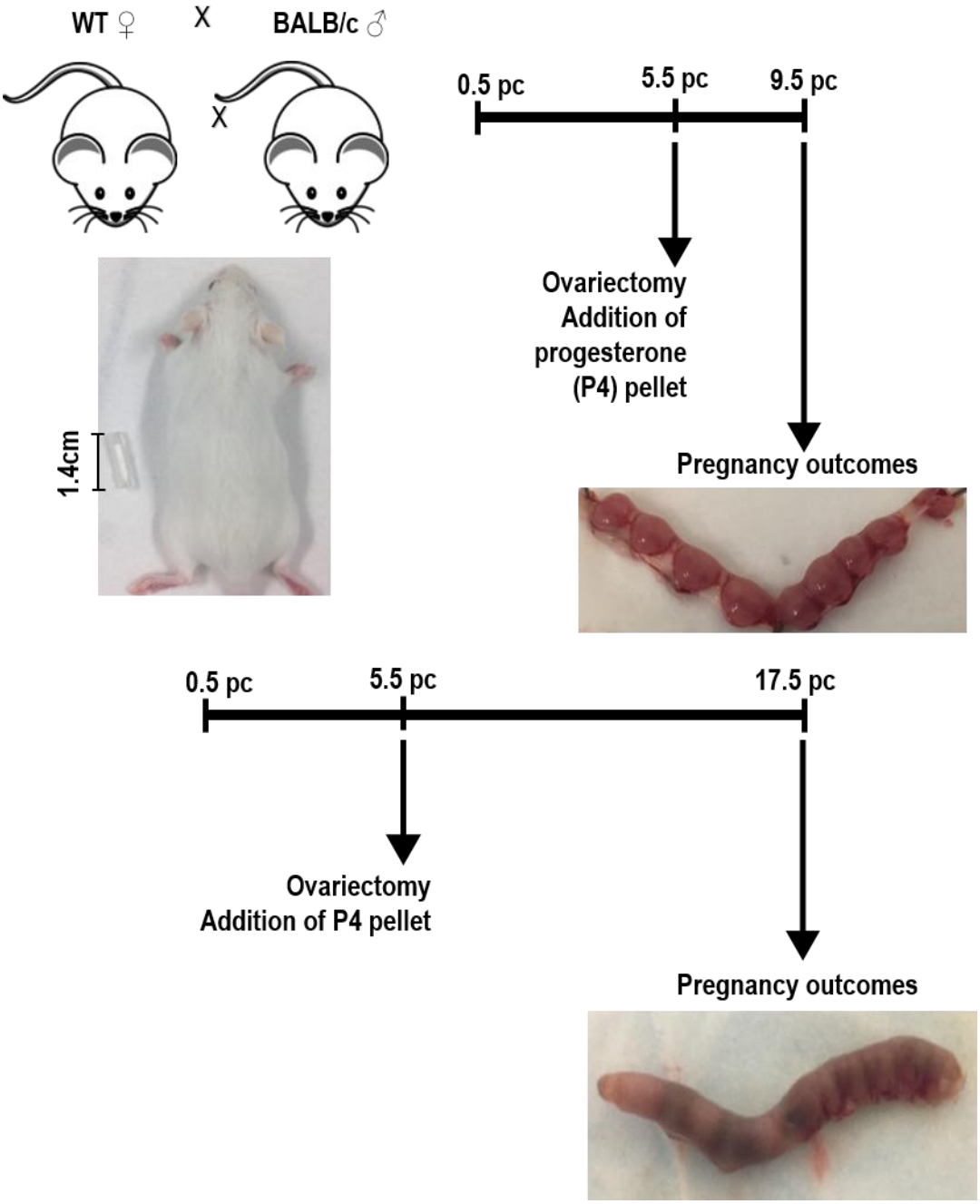

Figure 9.4: Hormone supplementation in ovariectomised FVB mice requires more than P4 for pregnancy viability.

Briefly, WT females were mated to BALB/c stud males. Mice underwent ovariectomy on day 5.5 pc and concurrently received two s.c. P4 pellets. Females were assessed for pregnancy outcomes on days 9.5 pc and 17.5 pc. P4; progesterone. pc; post-coitum. WT; wild type.

Figure 9.5: Macrophage depletion causes pregnancy failure independent of hormone supplementation on day 17.5 pc.

WT and CD11b-DTR females were mated to BALB/c stud males and all mice were administered 25 ng/g DT on day 5.5 pc. On day 5.5 pc of pregnancy, two P4 (or vehicle) pellets was inserted subcutaneously into the mid-dorsal region. On day 9.5 pc, an E2 (or vehicle) pellet was also inserted. Pregnancy outcomes were then assessed on day 17.5 pc in WT (A), macrophage-depleted females with vehicle pellets (B) and macrophage-depleted females given hormone pellets (C). Viable pregnancy rate was assessed on day 17.5 pc (D). The number of viable pups, implantation site resorptions, and uterine scars were also assessed (E-G). The pregnancies from each group were categorised by pregnancy viability (H). Data are presented as mean (D) and mean ± SEM (E-G). Statistical analysis was performed using one-way ANOVA with Sidak's multiple comparisons test (E-G) except in (D) where a χ^2 test was used. * indicates statistical significance ($p<0.05$) compared to WT controls; ***$p<0.001$ and ****$p<0.0001$. Black arrow; resorption. Red arrow; uterine scar. DT; diphtheria toxin. DTR; diphtheria toxin receptor. E2; estrogen. H; hormone-supplemented. MD; macrophage-depleted. P4; progesterone. pc; post-coitum. Veh; vehicle control pellet. WT; wild type.

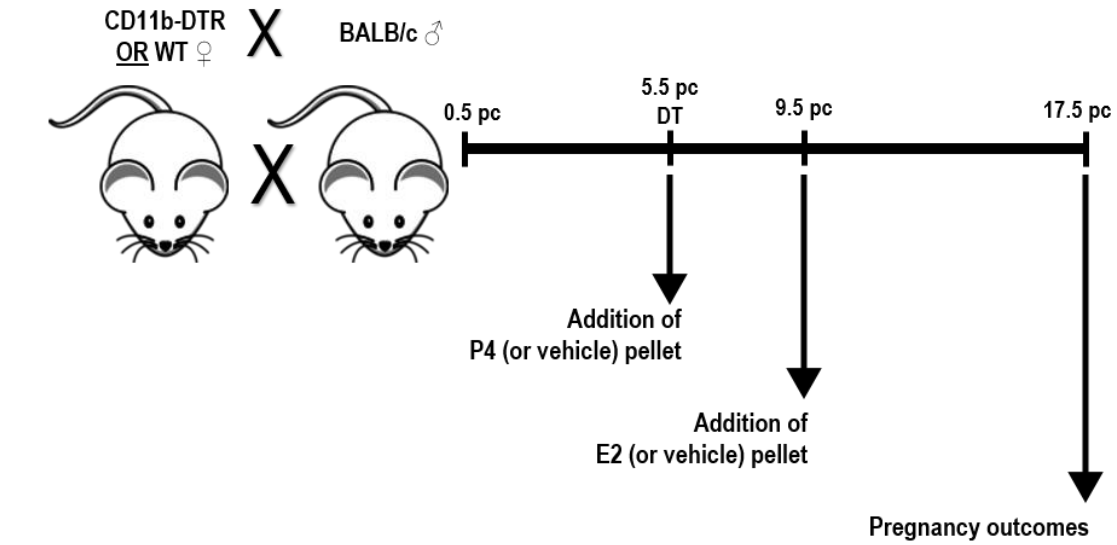
CD11b-DTR
OR WT ♀
X
BALB/c ♂
X
0.5 pc
5.5 pc
DT
9.5 pc
17.5 pc
Addition of
P4 (or vehicle) pellet
Addition of
E2 (or vehicle) pellet
Pregnancy outcomes

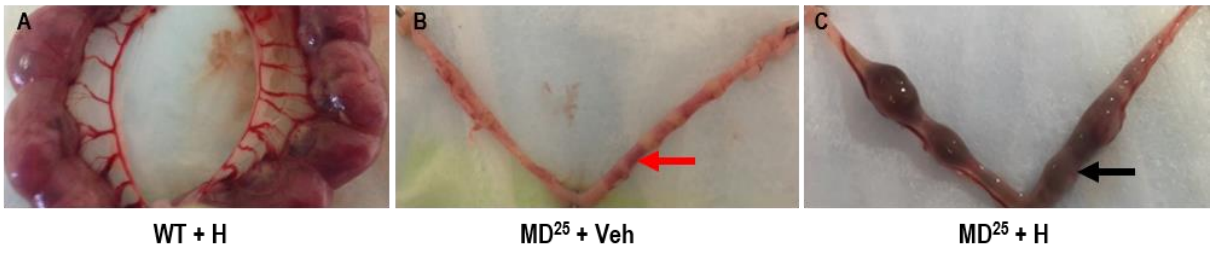
A
B
C
WT + H
MD25 + Veh
MD25 + H

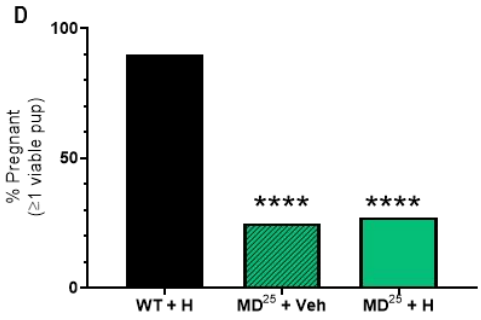
D
% Pregnant
(≥1 viable pup)
100
50
0
****
****
WT + H
MD25 + Veh
MD25 + H

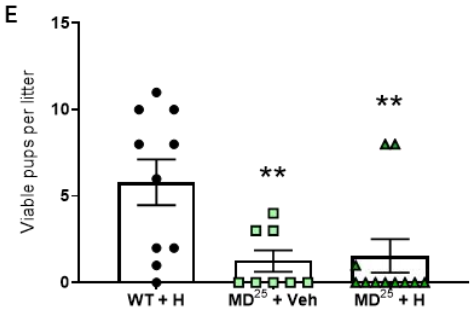
E
Viable pups per litter
15
10
5
0
**
**
WT + H
MD25 + Veh
MD25 + H

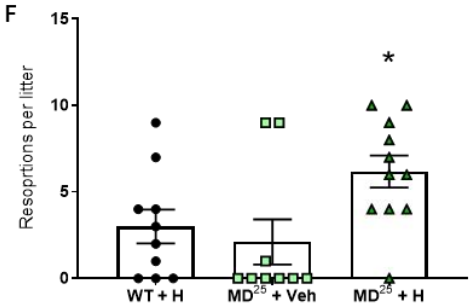
F
Resoprtions per litter
15
10
5
0
*
WT + H
MD25 + Veh
MD25 + H

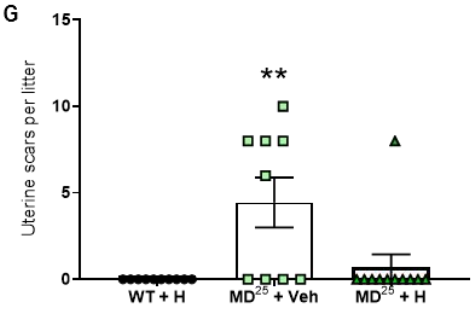
G
Uterine scars per litter
15
10
5
0
**
WT + H
MD25 + Veh
MD25 + H

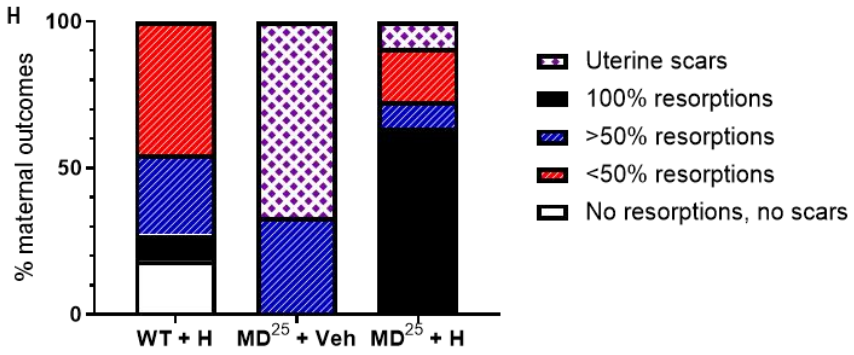
H
% maternal outcomes
100
50
0
WT + H
MD25 + Veh
MD25 + H
Uterine scars
100% resorptions
>50% resorptions
<50% resorptions
No resorptions, no scars

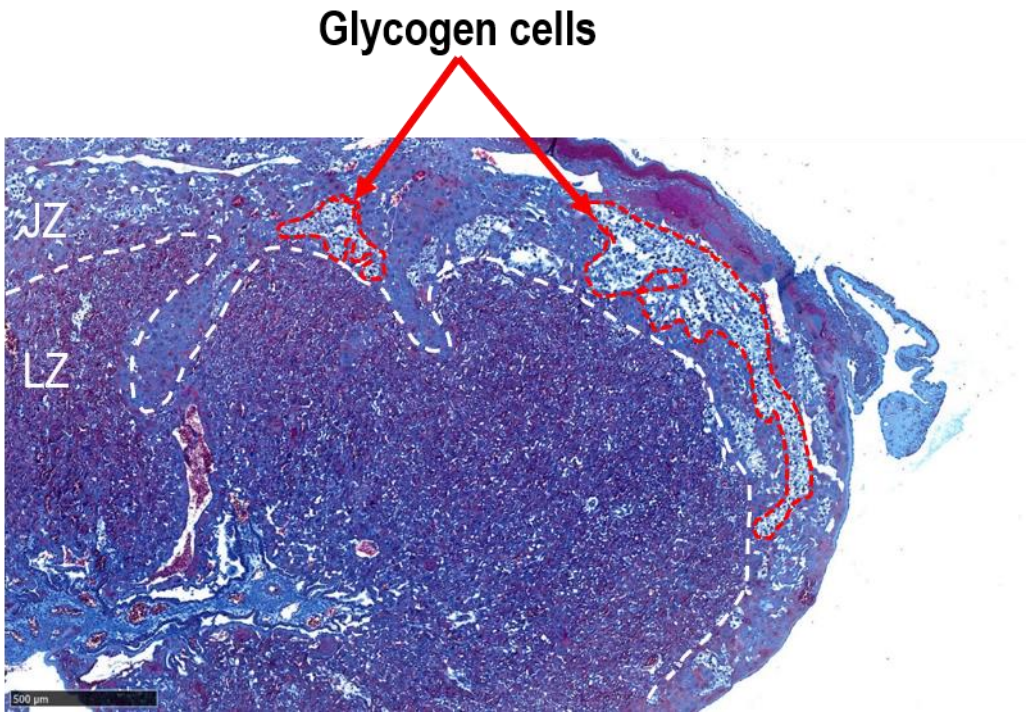

Figure 9.6: Glycogen cells are situated in the junctional zone in day 17.5 pc placentas.
Placentas were stained with Masson's Trichrome to identify the junctional zone (JZ) and labyrinth zone (LZ), separated by white dashed line. Glycogen cells (GCs) were visible in the JZ, shown in the red dashed regions. The area of GCs was divided by the area of JZ to give the proportion of GCs within the JZ.

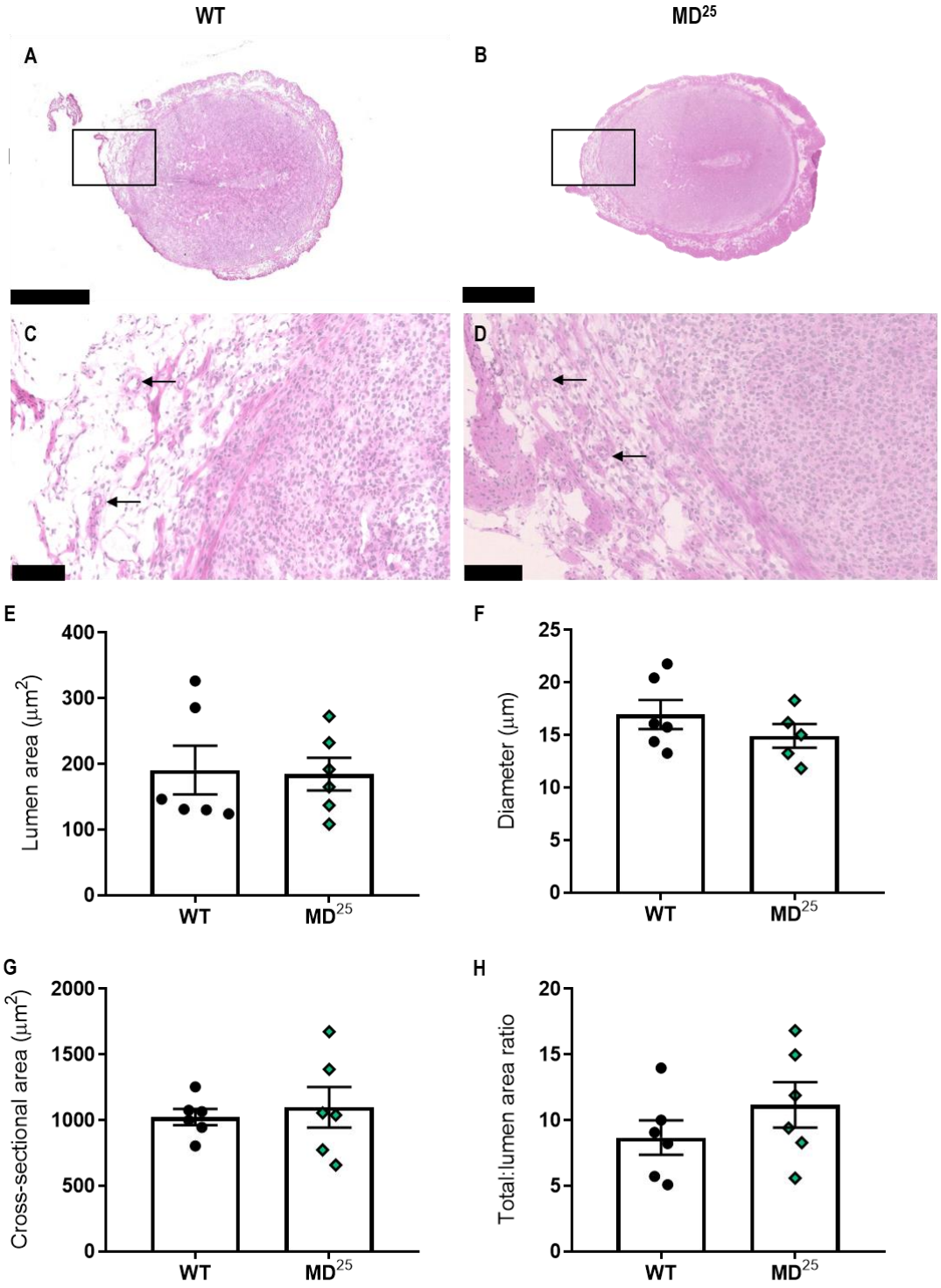

Figure 9.7: Macrophage depletion elicits no changes to uterine vascular remodelling on day 6.5 pc.

WT and CD11b-DTR females were mated to BALB/c stud males and all mice were administered 25 ng/g DT on day 5.5 pc. H&E-stained sections in WT and macrophage-depleted females were used to assess mesometrial triangle arteries on day 6.5 pc (A-B; scale bar is 1 mm). The mesometrial triangle region is shown in (C and D; scale bar is 100 µm). Vessel parameters in the mesometrial triangle were calculated including vessel lumen area (C), vessel diameter (D), vessel cross-sectional area (E), and the ratio of total vessel size to lumen ratio (F). Data are presented as mean ± SEM with statistical analysis using unpaired t-test. Arrow; artery. MD; macrophage-depleted. Triangle; mesometrial triangle region of the implantation site. WT; wild type.

Figure 9.8: Low-dose DT elicits changes to implantation site structure on day 6.5 pc.
WT and CD11b-DTR females were mated to BALB/c stud males. On day 5.5 pc, CD11b-DTR mice were administered 10 ng/g DT. WT mice received DT at 25 ng/g on day 5.5 pc. The number of viable implantation sites were counted on day 6.5 pc (A). The relative density of F4/80$^+$ cells within these implantation sites were calculated (B). The percentage of haemorrhagic corpora lutea in the ovaries were calculated (C). The concentration of P4 in serum was measured via ELISA (D). The extent of decidualisation was quantified using alkaline phosphatase staining (E). The conceptus area was measured (F). Vessel parameters in the mesometrial triangle were also calculated including vessel lumen area (G), vessel diameter (H), vessel cross-sectional area (I), and the ratio of total vessel size to lumen ratio (J). Data are presented as mean ± SEM with statistical analysis using unpaired t-tests. * indicates statistical significance ($p<0.05$); *$p<0.05$, **$p<0.01$, and ****$p<0.0001$. CL; corpora lutea. MD; macrophage-depleted. WT; wild type.

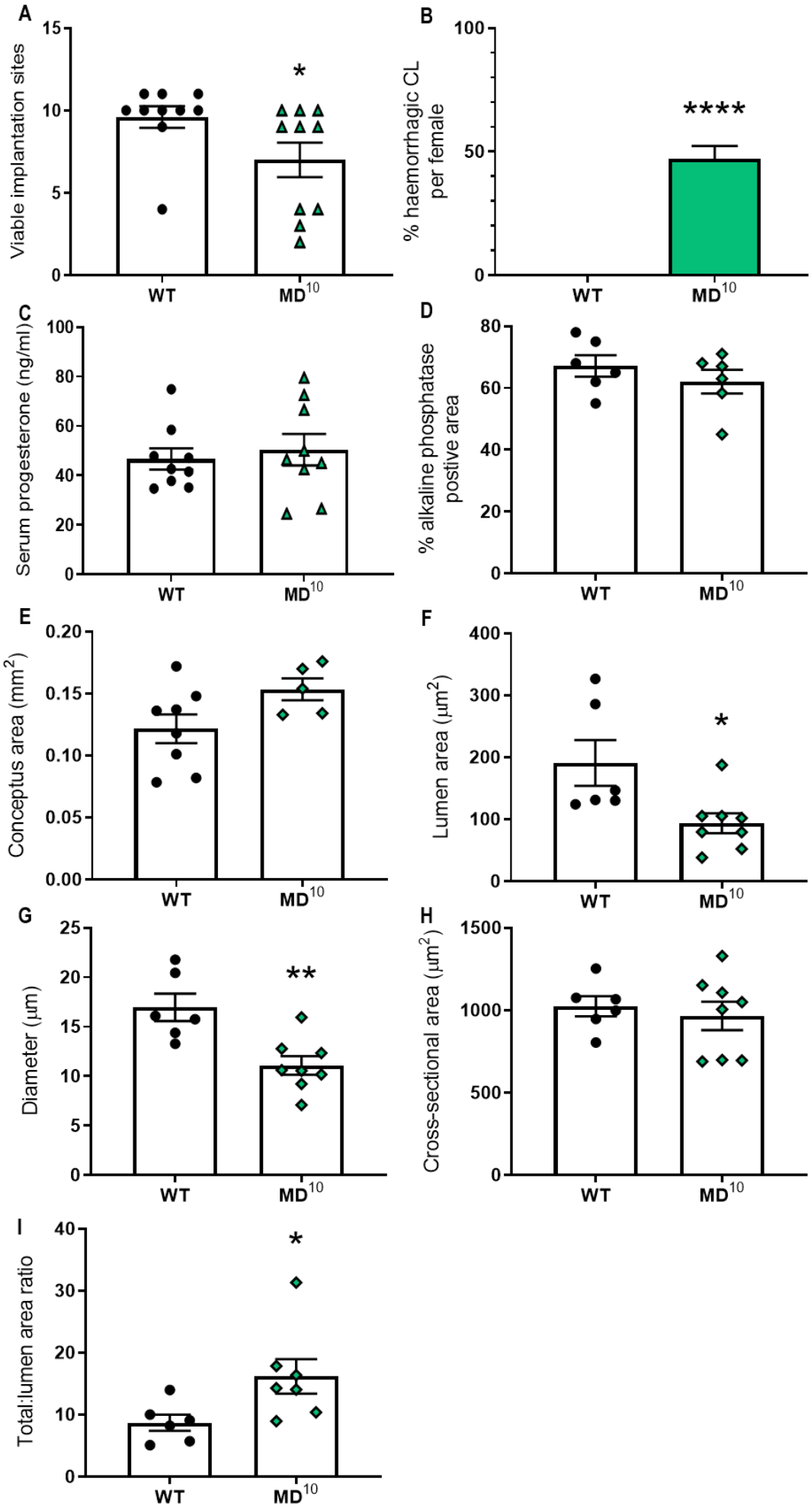
A
Viable implantation sites
15
10
5
0
*
WT
MD10
B
% haemorrhagic CL per female
100
50
0
****
WT
MD10
C
Serum progesterone (ng/ml)
100
80
60
40
20
0
WT
MD10
D
% alkaline phosphatase postive area
80
60
40
20
0
WT
MD10
E
Conceptus area (mm2)
0.20
0.15
0.10
0.05
0.00
WT
MD10
F
Lumen area (µm2)
400
300
200
100
0
*
WT
MD10
G
Diameter (µm)
25
20
15
10
5
0
**
WT
MD10
H
Cross-sectional area (µm2)
1500
1000
500
0
WT
MD10
I
Total:lumen area ratio
40
30
20
10
0
*
WT
MD10

Figure 9.9: Low-dose DT elicits changes to implantation site structure on day 7.5 pc.
WT and CD11b-DTR females were mated to BALB/c stud males. On day 5.5 pc, CD11b-DTR mice were administered 10 ng/g DT. WT mice received 25 ng/g DT on day 5.5 pc. The number of viable implantation sites were counted on day 7.5 pc (A). The relative density of F4/80$^+$ cells within these implantation sites were calculated (B). The percentage of haemorrhagic corpora lutea in the ovaries were calculated (C). The concentration of P4 in serum was measured via ELISA (D). The extent of decidualisation was quantified using alkaline phosphatase staining (E). The conceptus area was measured (F). Vessel parameters in the mesometrial triangle were also calculated including vessel lumen area (G), vessel diameter (H), vessel cross-sectional area (I), and the ratio of total vessel size to lumen ratio (J). Data are presented as mean ± SEM with statistical analysis using unpaired t-tests. * indicates statistical significance ($p<0.05$); *$p<0.05$, **$p<0.01$, and ****$p<0.0001$. CL; corpora lutea. MD; macrophage-depleted. WT; wild type.

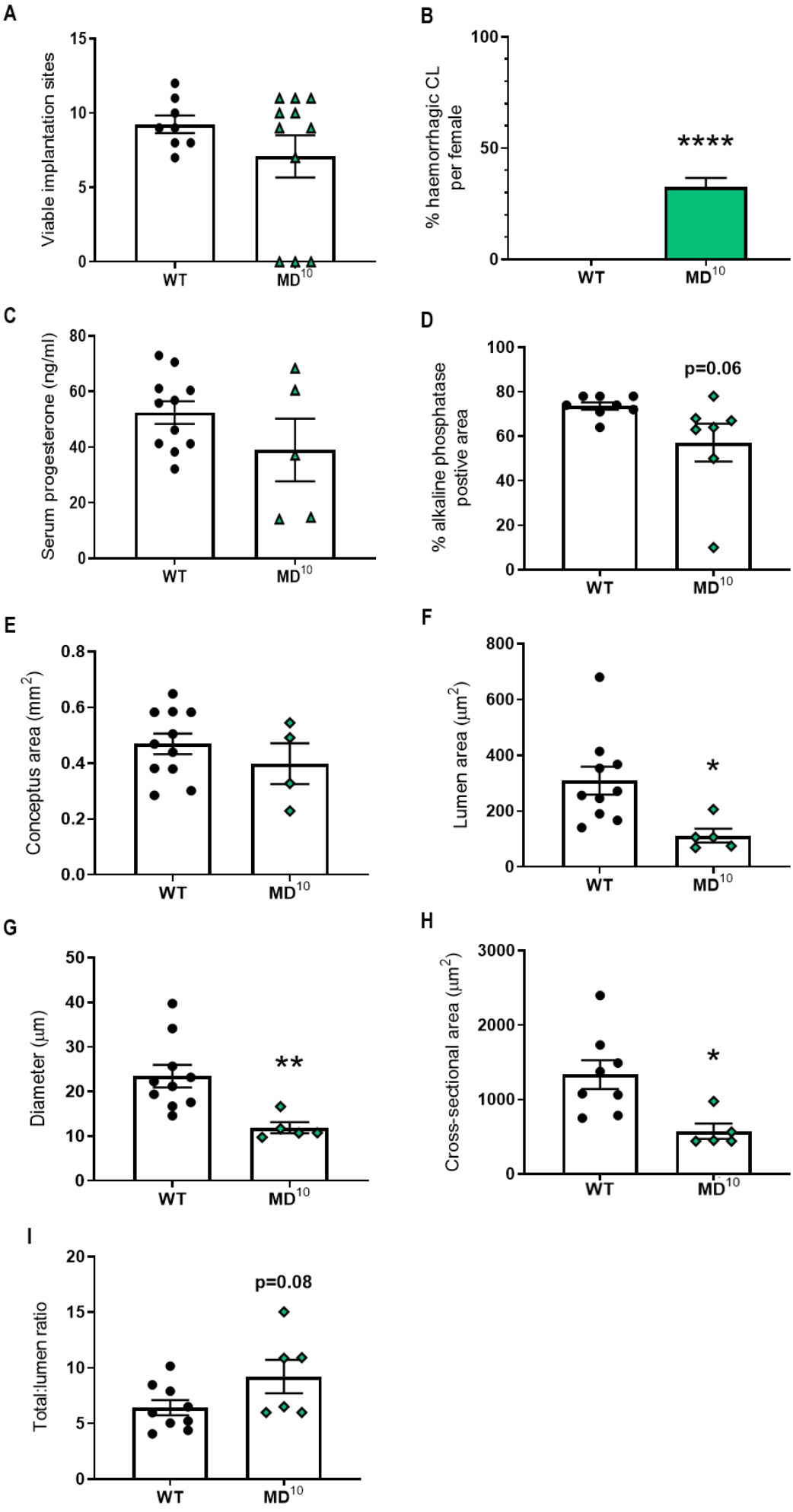
A
Viable implantation sites
15
10
5
0
WT
MD10
B
% haemorrhagic CL per female
100
50
0
****
WT
MD10
C
Serum progesterone (ng/ml)
80
60
40
20
0
WT
MD10
D
% alkaline phosphatase postive area
100
80
60
40
20
0
p=0.06
WT
MD10
E
Conceptus area (mm2)
0.8
0.6
0.4
0.2
0.0
WT
MD10
F
Lumen area (µm2)
800
600
400
200
0
*
WT
MD10
G
Diameter (µm)
50
40
30
20
10
0
**
WT
MD10
H
Cross-sectional area (µm2)
3000
2000
1000
0
*
WT
MD10
I
Total:lumen ratio
20
15
10
5
0
p=0.08
WT
MD10

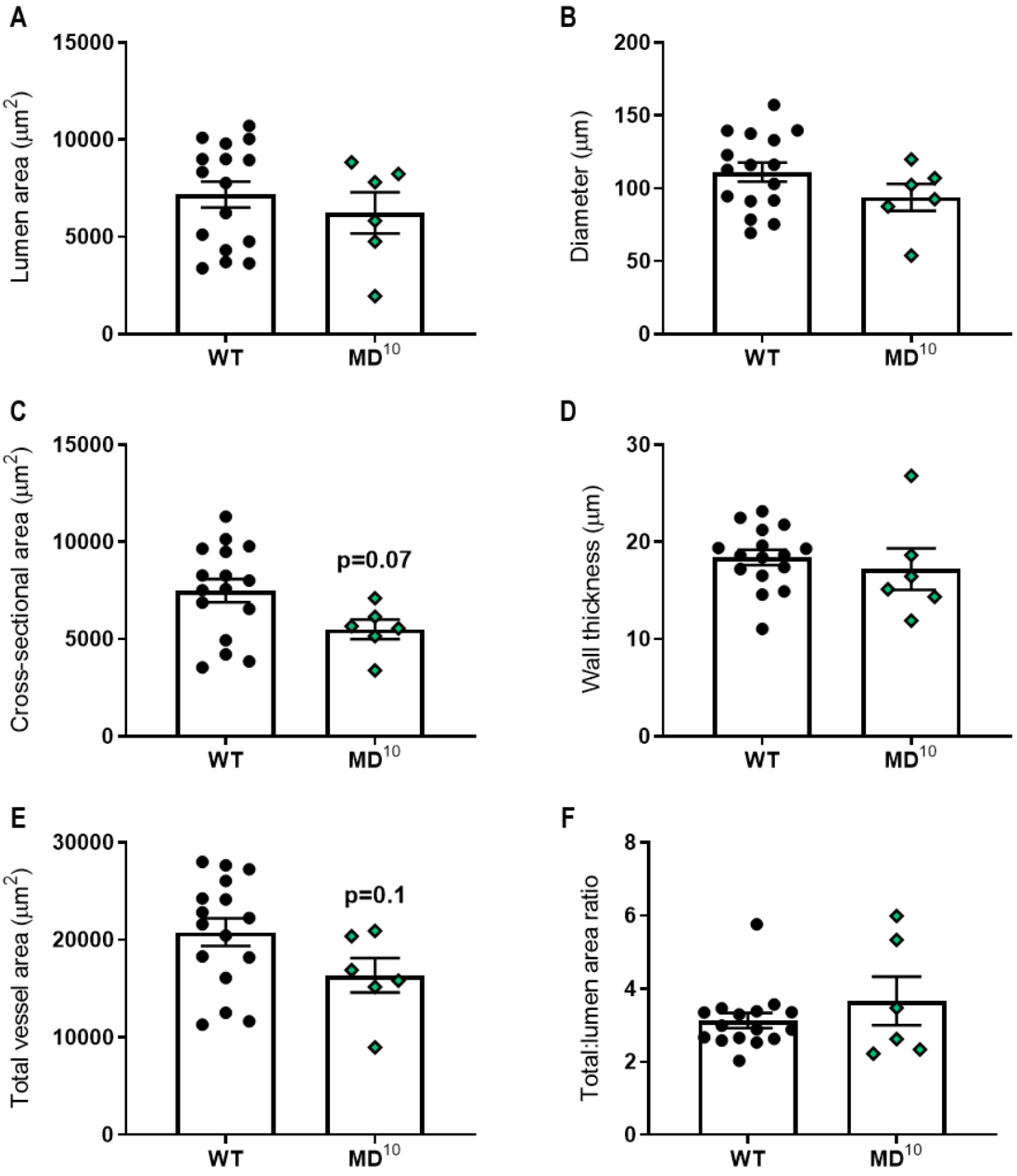

Figure 9.10: Low-dose DT administration mildly reduces main uterine artery size on day 9.5 pc. WT and CD11b-DTR females were mated to BALB/c stud males. On day 5.5 pc, CD11b-DTR mice were administered 10 ng/g DT. WT mice received 25 ng/g DT on day 5.5 pc. Artery parameters on day 9.5 pc were measured including lumen area (A), diameter (B), cross-sectional area (C), wall thickness (D), total area (E), and the ratio of total vessel area to lumen area (F). Data are presented as mean ± SEM with statistical analysis using unpaired t-tests. MD; macrophage-depleted. WT; wild type.

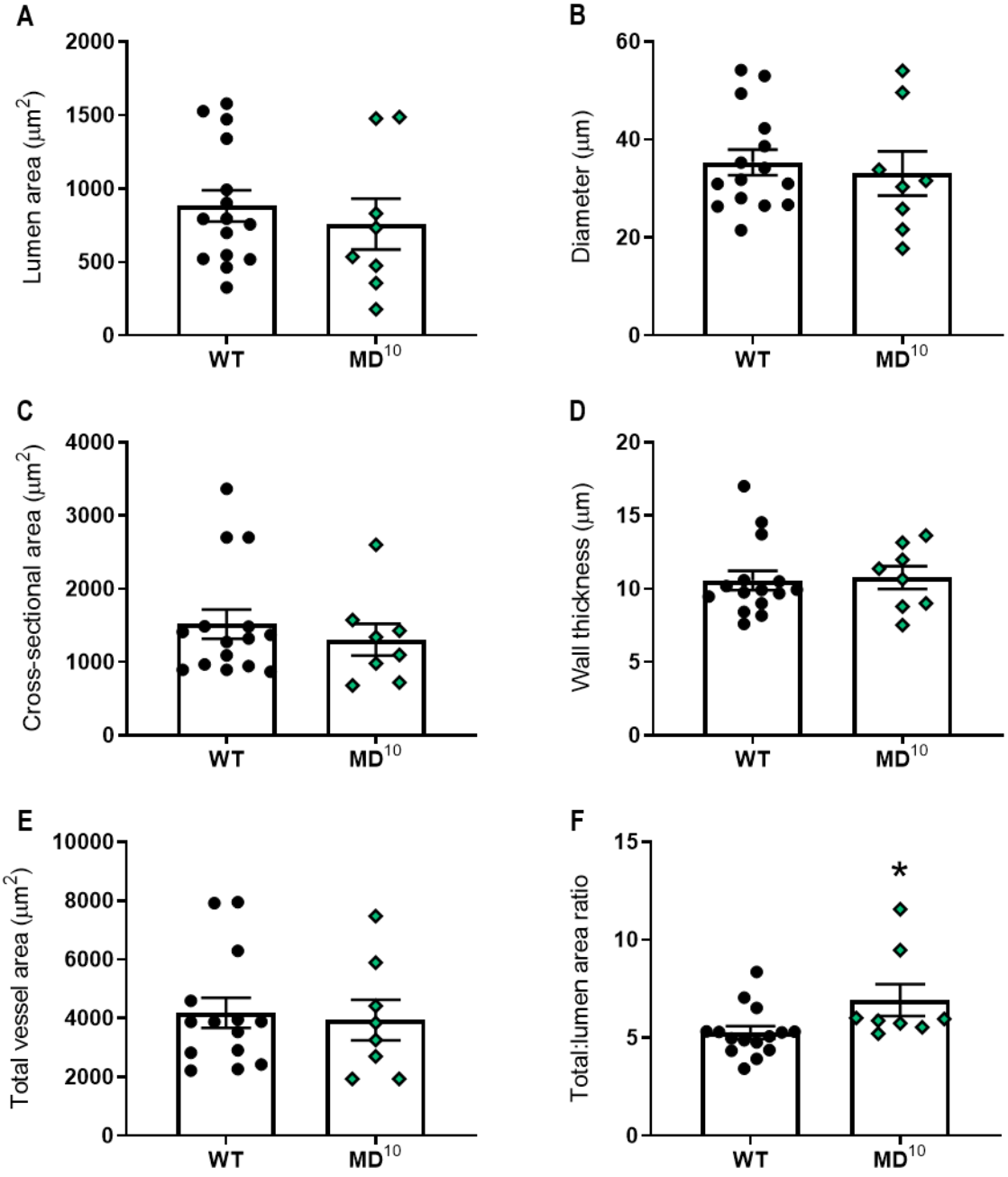

Figure 9.11: Low-dose DT administration increases the total area to lumen area ratio of radial arteries on day 9.5 pc.

WT and CD11b-DTR females were mated to BALB/c stud males. On day 5.5 pc, CD11b-DTR mice were administered 10 ng/g DT. WT mice received 25 ng/g DT on day 5.5 pc. Artery parameters on day 9.5 pc were measured including lumen area (A), diameter (B), cross-sectional area (C), wall thickness (D), total area (E), and the ratio of total vessel area to lumen area (F). Data are presented as mean ± SEM with statistical analysis using unpaired t-tests. * indicates statistical significance ($p<0.05$); *$p<0.05$. MD; macrophage-depleted. WT; wild type.

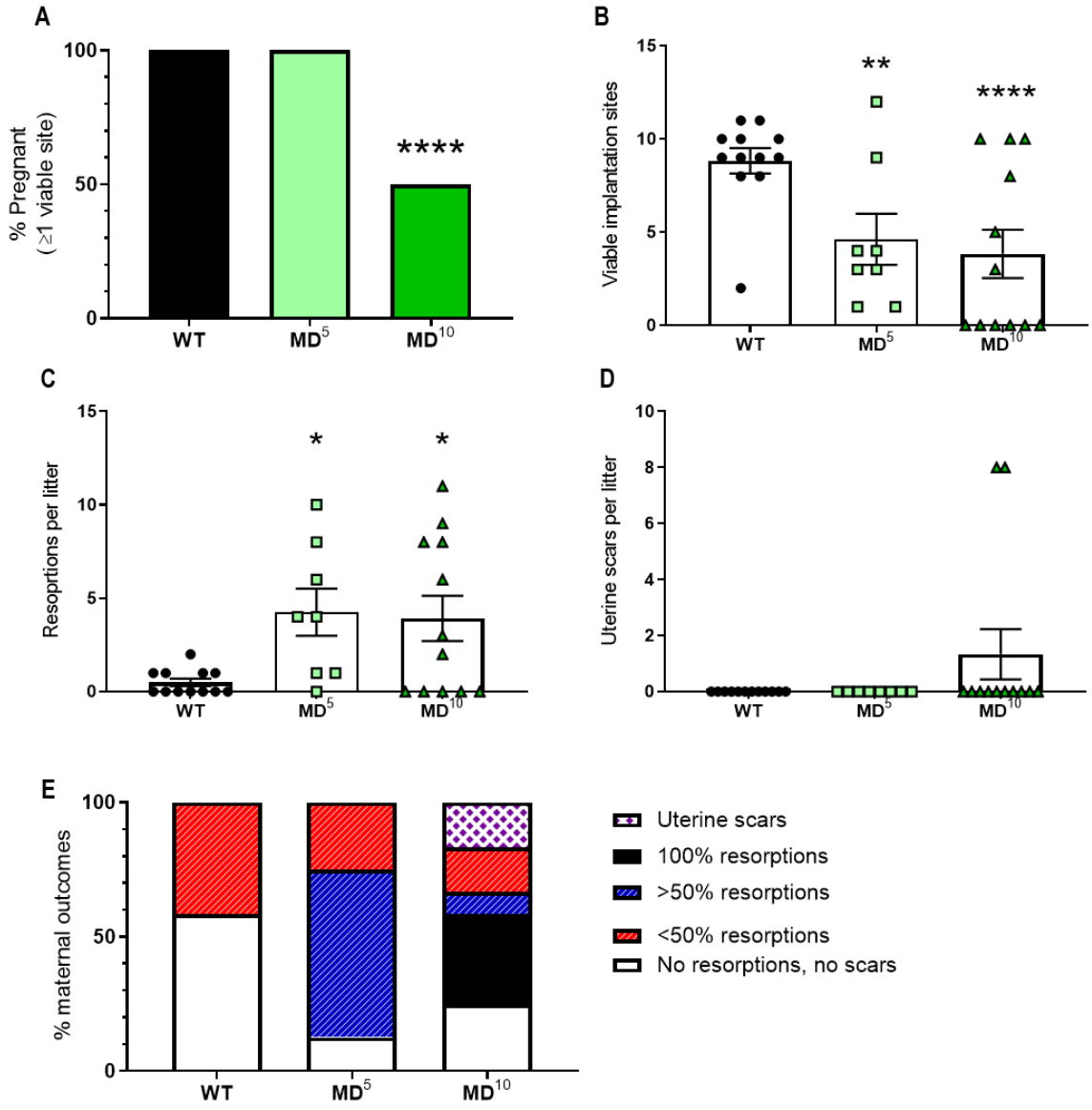

Figure 9.12: Low-dose DT causes a reduction in viable fetuses on day 12.5 pc.

WT and CD11b-DTR females were mated to BALB/c stud males. On day 5.5 pc, CD11b-DTR mice were administered 5 ng/g or 10 ng/g DT. WT mice received 25 ng/g DT on day 5.5 pc. Pregnancy outcomes were assessed on day 12.5 pc (A). The number of viable implantation sites (B), implantation site resorptions (C), and uterine scars were assessed (D). The pregnancies from each group were categorised into viability rankings (E). Data are presented as mean ± SEM, except in A where it is just mean. Statistical analysis was performed using one-way ANOVA with Sidak's multiple comparisons test, except in A where a χ^2 test was used. * indicates statistical significance ($p<0.05$) compared to WT controls; *$p<0.05$, **$p<0.01$, and ****$p<0.0001$. MD; macrophage-depleted. WT; wild type.

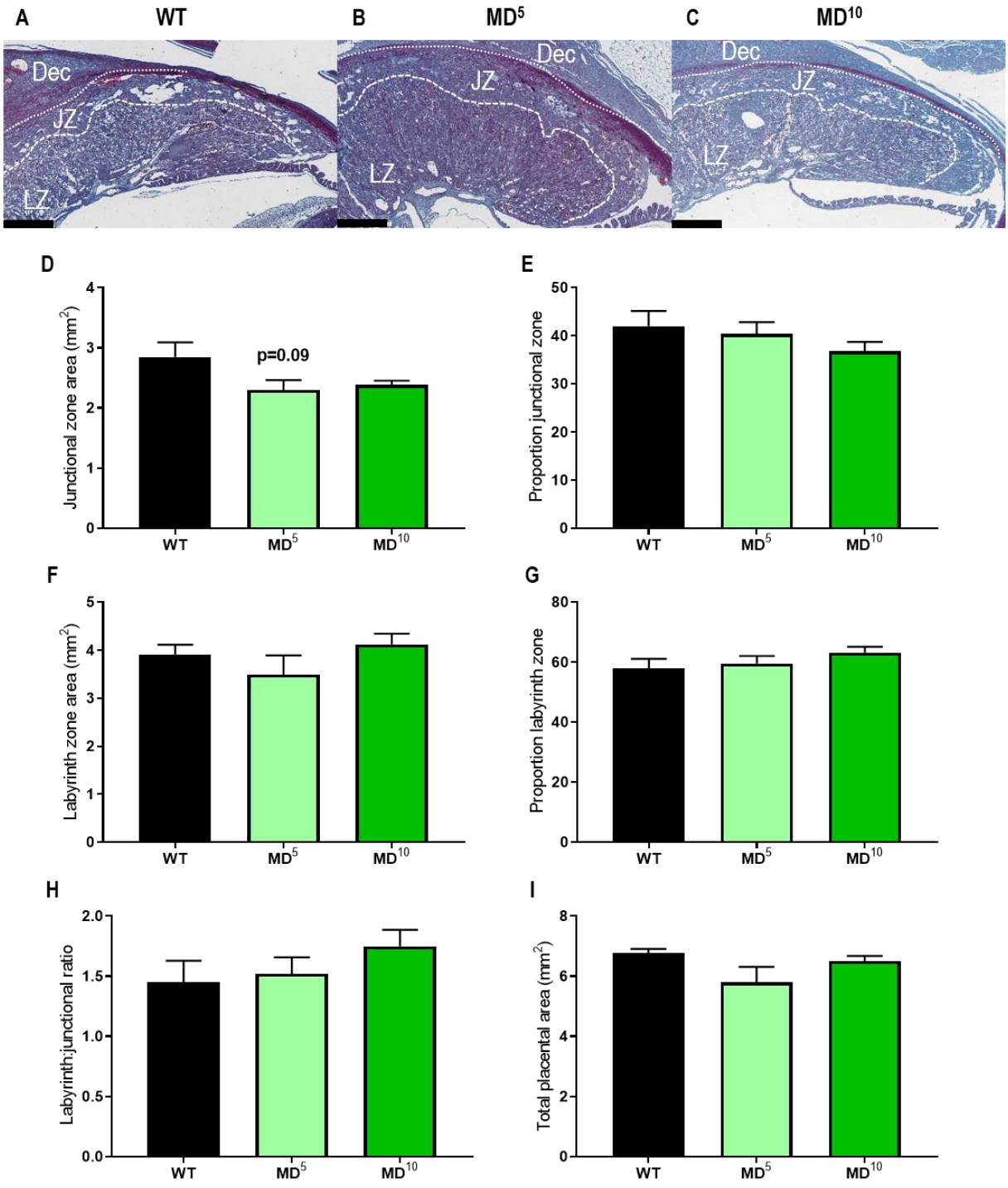

Figure 9.13: Low-dose DT does not alter placental morphology on day 12.5 pc.
WT and CD11b-DTR females were mated to BALB/c stud males. On day 5.5 pc, CD11b-DTR mice were administered 5 ng/g or 10 ng/g DT. WT mice received 25 ng/g DT on day 5.5 pc. Masson's trichrome stained placental sections are shown for WT (A) and macrophage-depleted pregnancies (B and C). JZ and LZ areas were measured (D and F). Proportion of JZ and LZ were calculated (E and G). The LZ to JZ ratio was calculated (H) as was the total placental area (I). Data are presented as mean ± SEM. Statistical analysis was performed using one-way ANOVA with Sidak's multiple comparisons test. Dec; decidua. JZ; junctional zone. LZ; labyrinth zone. MD; macrophage-depleted. WT; wild type.

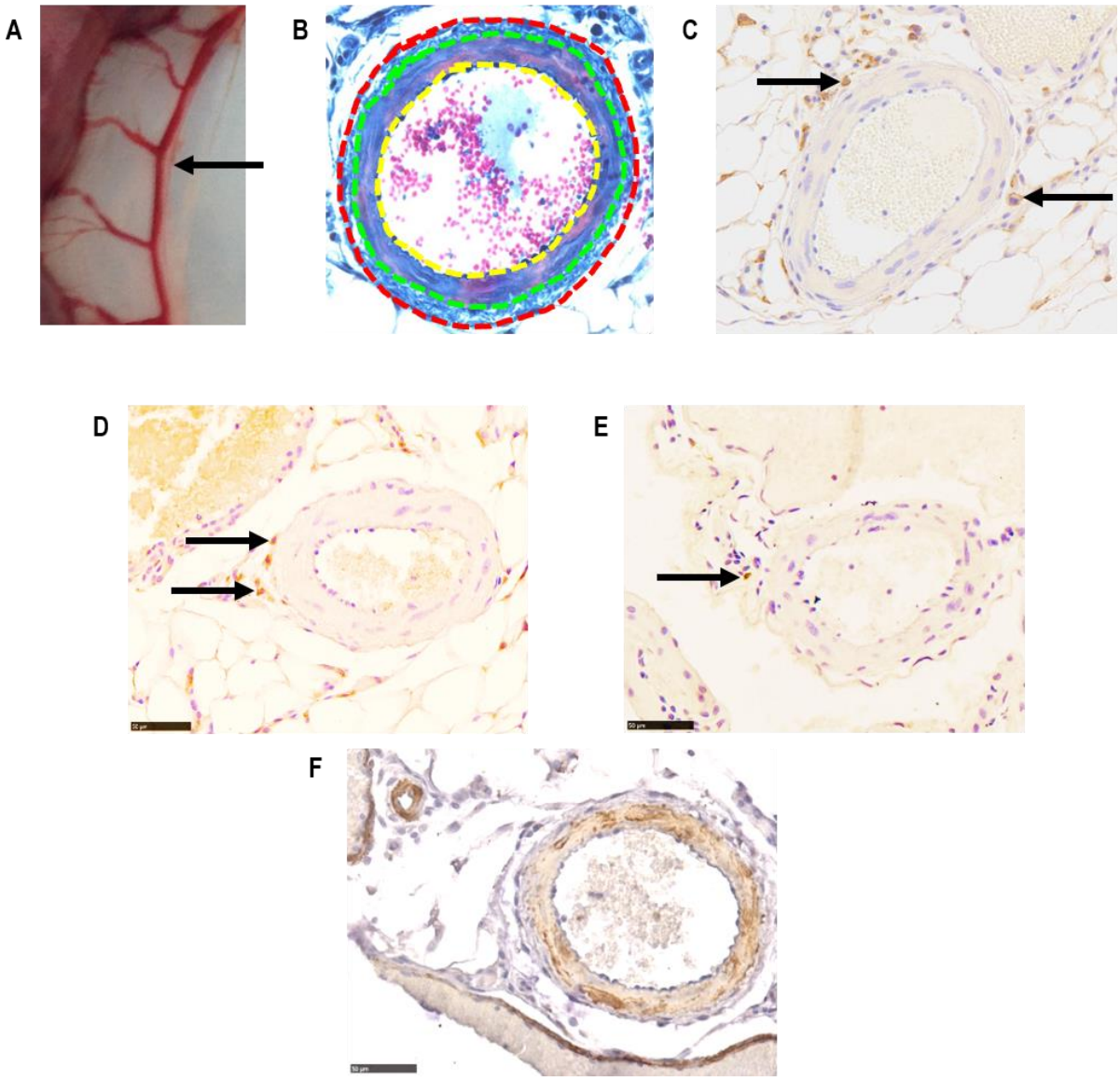

Figure 9.14: Macrophages localise around main uterine arteries.
The main uterine artery (arrow) shown prior to dissection (A). After sectioning and staining with Masson's Trichrome, the distinct portions of the artery are shown (dashed lines) (B). Artery parameters measured include total vessel area (red dashed line), lumen area (yellow dashed line), cross-sectional area and wall thickness (total area – lumen area; green dashed line), and total to lumen area ratio. Lumen diameter was calculated using circumference divided by π. F4/80$^+$ macrophages at the main uterine artery (C). CD206$^+$ cells at the main uterine artery (D). DBA$^+$ cells at the main uterine artery (E). αSMA staining of the main uterine artery (F).

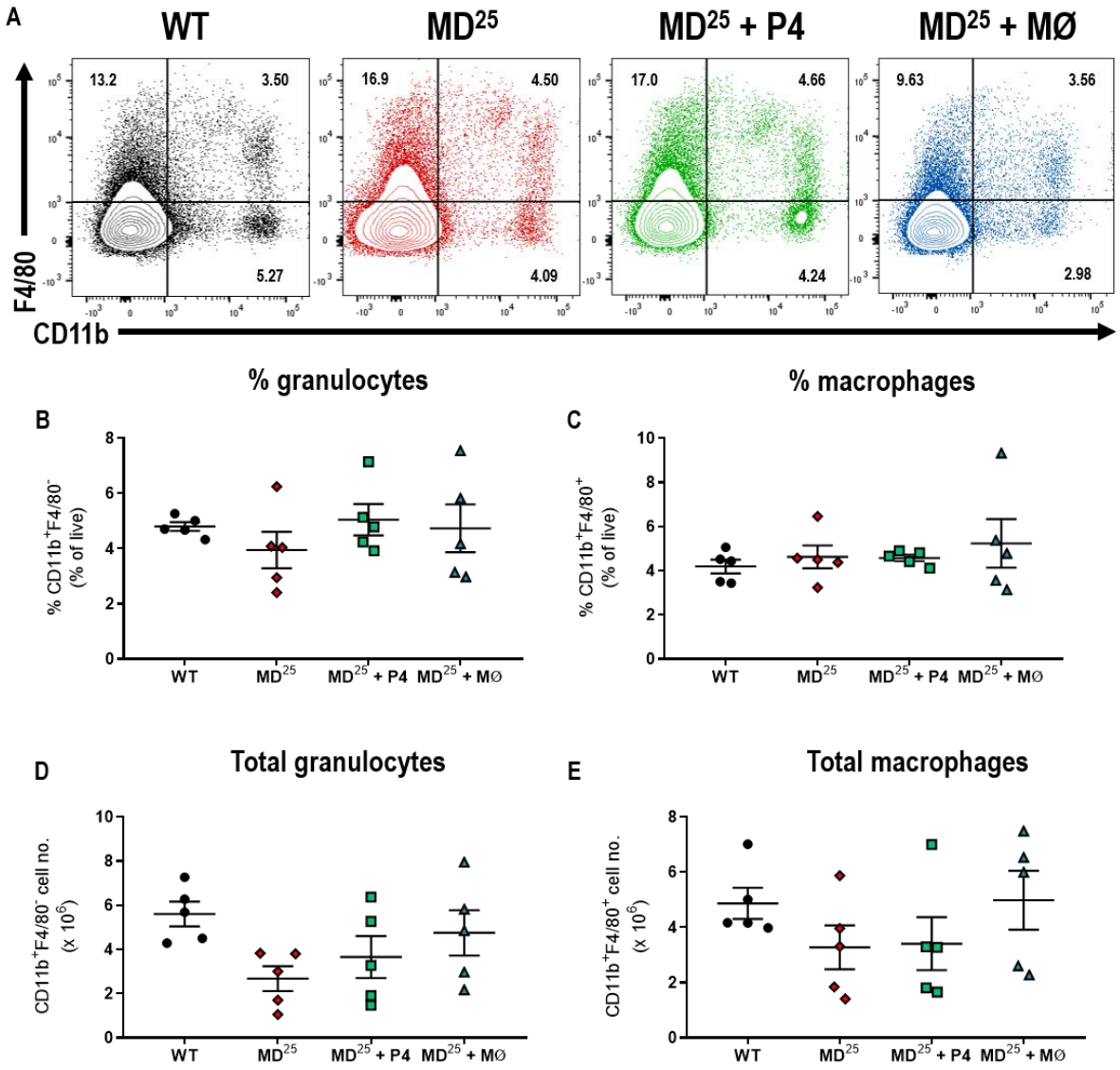

Figure 9.15: Macrophage and granulocyte populations are not changed in the spleen on day 7.5 pc.

WT and CD11b-DTR females were mated to BALB/c stud males and 25 ng/g DT was administered on day 5.5 pc. For P4 supplementation, DT-treated CD11b-DTR females were subcutaneously injected with P4 on days 5.5 pc and 6.5 pc. For BMDM supplementation, DT-treated CD11b-DTR females were intravenously injected with BMDM on days 3.5 pc and 5.5 pc. Representative FACS plots for CD11b and F4/80 populations in the spleen are shown (A). The proportions of granulocytes (B) and macrophages (C) are presented as a percentage of live cells. From cell counts, granulocyte cell numbers (D) and macrophage numbers were calculated (E). Data are presented as mean ± SEM with statistical analysis using one-way ANOVA with Sidak's multiple comparisons test. MD; macrophage-depleted. MØ; macrophages. P4; progesterone. WT; wild type.

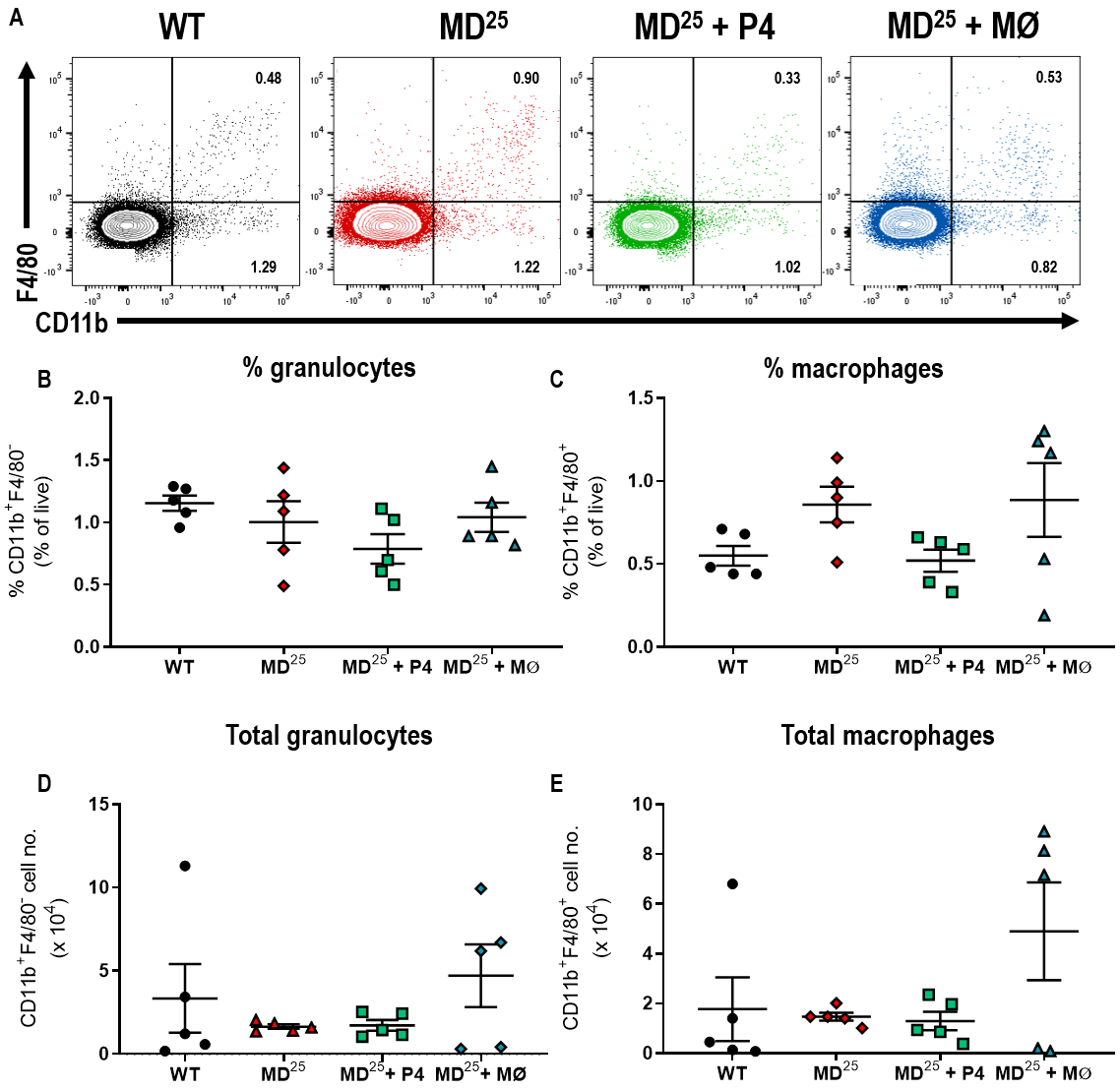

Figure 9.16: Macrophage and granulocyte populations are not changed in the paraaortic lymph nodes on day 7.5 pc.

WT and CD11b-DTR females were mated to BALB/c stud males and 25 ng/g DT was administered on day 5.5 pc. For P4 supplementation, DT-treated CD11b-DTR females were subcutaneously injected with P4 on days 5.5 pc and 6.5 pc. For BMDM supplementation, DT-treated CD11b-DTR females were intravenously injected with BMDM on days 3.5 pc and 5.5 pc. Representative FACS plots for CD11b and F4/80 populations in the paraaortic lymph nodes are shown (A). The proportions of granulocytes (B) and macrophages (C) are presented as a percentage of live cells. From cell counts, granulocyte cell numbers (D) and macrophage cell numbers were calculated (E). Data are presented as mean ± SEM with statistical analysis using one-way ANOVA with Sidak's multiple comparisons test. MD; macrophage-depleted. MØ; macrophages. P4; progesterone. WT; wild type.

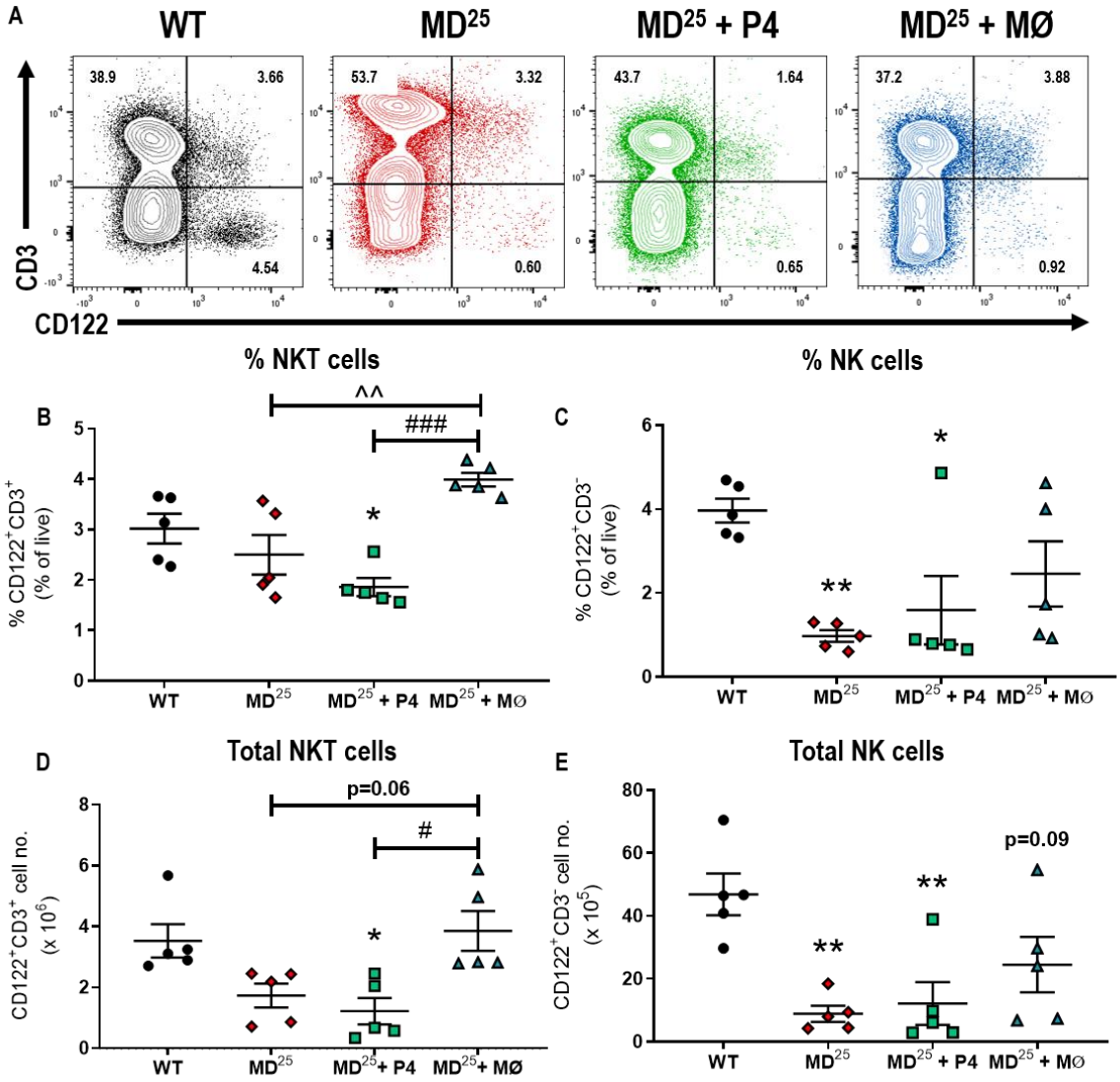

Figure 9.17: Macrophage depletion reduces NK cell numbers in the spleen on day 7.5 pc.
WT and CD11b-DTR females were mated to BALB/c stud males and 25 ng/g DT was administered on day 5.5 pc. For P4 supplementation, DT-treated CD11b-DTR females were subcutaneously injected with P4 on days 5.5 pc and 6.5 pc. For BMDM supplementation, DT-treated CD11b-DTR females were intravenously injected with BMDM on days 3.5 pc and 5.5 pc. Representative FACS plots for CD122 and CD3 populations in the spleen for the four treatment groups are shown (A). The proportions of NKT cells (B) and NK cells (C) are presented as a percentage of live cells. From cell counts, NKT cell numbers (D) and NK cell numbers were calculated (E). Data are presented as mean ± SEM with statistical analysis using one-way ANOVA with Sidak's multiple comparisons test. * indicates statistical significance ($p<0.05$) compared to WT controls; *$p<0.05$ and **$p<0.01$. ^ indicates statistical significance ($p<0.05$) compared to MD^{25} mice; ^^$p<0.01$. # indicates statistical significance ($p<0.05$) compared to MD^{25} + P4 mice; #$p<0.05$ and ###$p<0.001$. MD; macrophage-depleted. MØ; macrophages. P4; progesterone. WT; wild type.

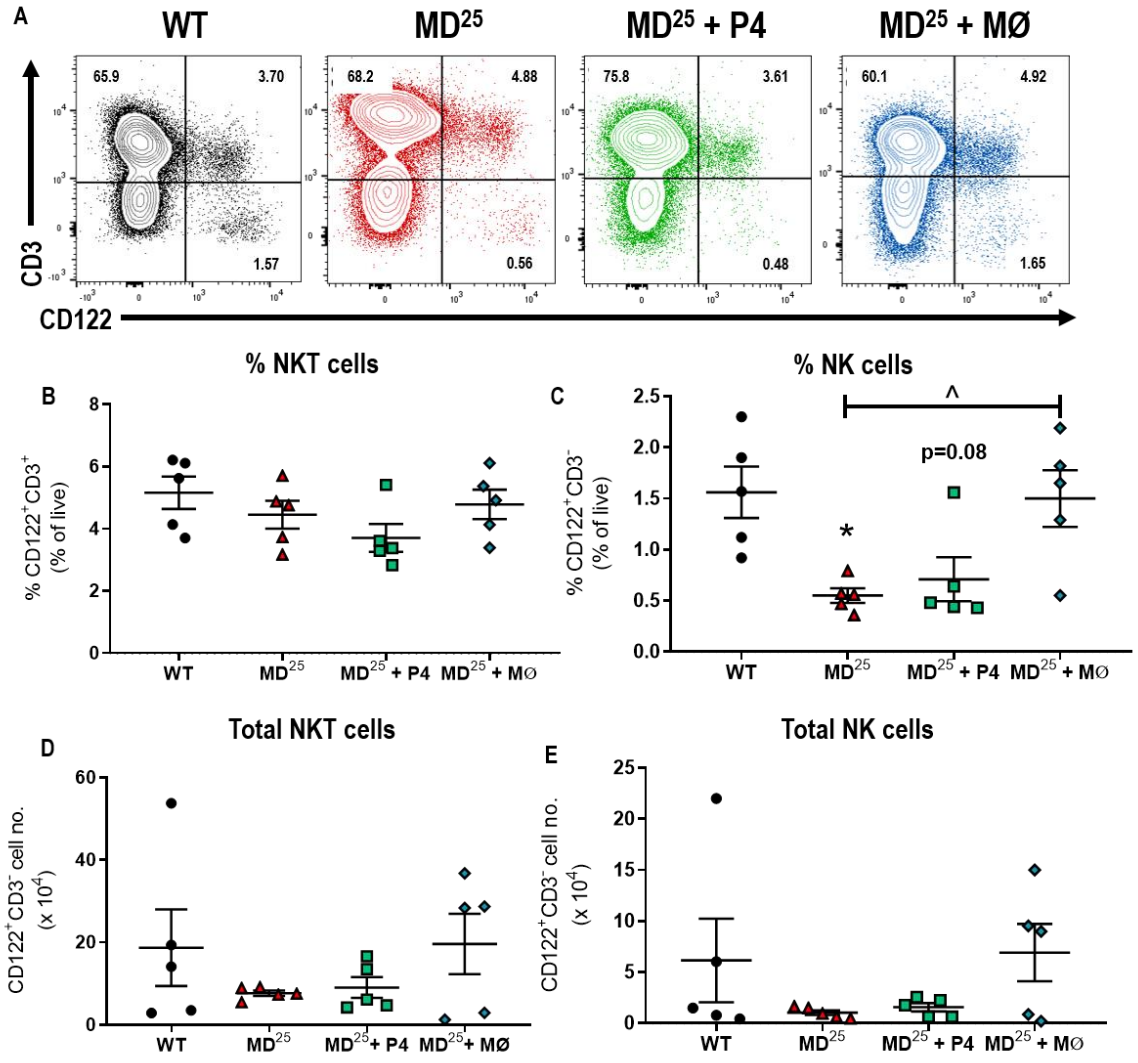

Figure 9.18: BMDM supplementation restores NK cell proportion in the paraaortic lymph nodes on day 7.5 pc.

WT and CD11b-DTR females were mated to BALB/c stud males and 25 ng/g DT was administered on day 5.5 pc. For P4 supplementation, DT-treated CD11b-DTR females were subcutaneously injected with P4 on days 5.5 pc and 6.5 pc. For BMDM supplementation, DT-treated CD11b-DTR females were intravenously injected with BMDM on days 3.5 pc and 5.5 pc. Representative FACS plots for CD122 and CD3 populations in the paraaortic lymph nodes for the four treatment groups are shown (A). The proportions of NKT cells (B) and NK cells (C) are presented as a percentage of live cells. From cell counts, NKT cell numbers (D) and NK cell numbers were calculated (E). Data are presented as mean ± SEM with statistical analysis using one-way ANOVA with Sidak's multiple comparisons test. * indicates statistical significance ($p<0.05$) compared to WT controls; *$p<0.05$. ^ indicates statistical significance ($p<0.05$) compared to MD^{25} mice; ^$p<0.05$. MD; macrophage-depleted. MØ; macrophages. P4; progesterone. WT; wild type.

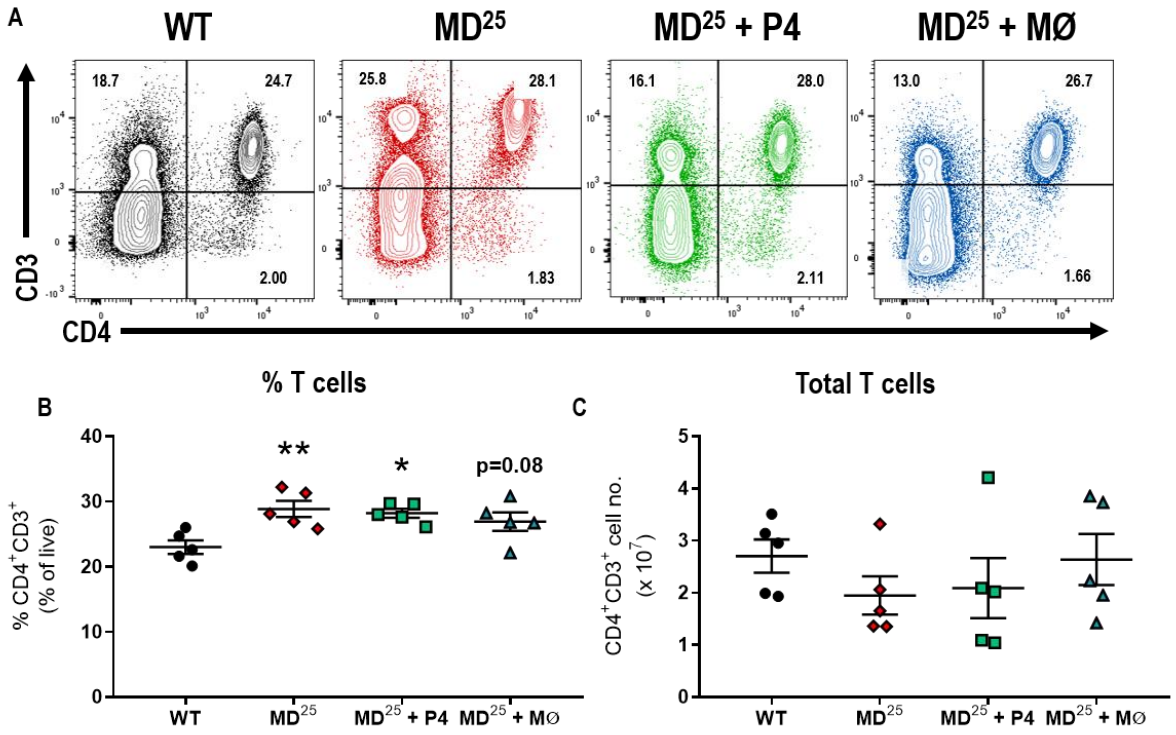

Figure 9.19: Macrophage depletion increases T cell proportions in the spleen on day 7.5 pc. WT and CD11b-DTR females were mated to BALB/c stud males and 25 ng/g DT was administered on day 5.5 pc. For P4 supplementation, DT-treated CD11b-DTR females were subcutaneously injected with P4 on days 5.5 pc and 6.5 pc. For BMDM supplementation, DT-treated CD11b-DTR females were intravenously injected with BMDM on days 3.5 pc and 5.5 pc. Representative FACS plots for CD4 and CD3 populations in the spleen for the four treatment groups are shown (A). The proportion of T cells (B) is presented as a percentage of live cells. From cell counts, T cell numbers were calculated (C). Data are presented as mean ± SEM with statistical analysis using one-way ANOVA with Sidak's multiple comparisons test. * indicates statistical significance ($p<0.05$) compared to WT controls; *$p<0.05$ and **$p<0.01$. MD; macrophage-depleted. MØ; macrophages. P4; progesterone. WT; wild type.

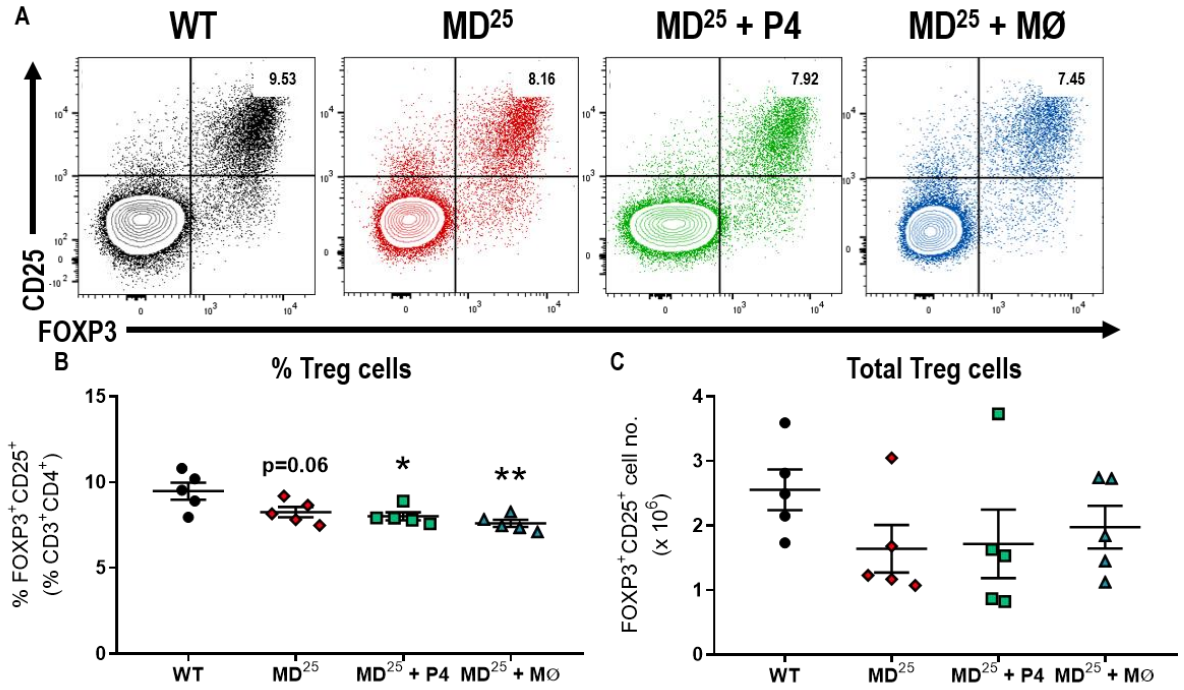

Figure 9.20: Macrophage depletion causes reduced Treg cell proportions in the spleen on day 7.5 pc.

WT and CD11b-DTR females were mated to BALB/c stud males and 25 ng/g DT was administered on day 5.5 pc. For P4 supplementation, DT-treated CD11b-DTR females were subcutaneously injected with P4 on days 5.5 pc and 6.5 pc. For BMDM supplementation, DT-treated CD11b-DTR females were intravenously injected with BMDM on days 3.5 pc and 5.5 pc. Representative FACS plots for FOXP3 and CD25 populations in the spleen for the four treatment groups are shown as a proportion of $CD3^+CD4^+$ cells (A). The proportion of Treg cells (B) is presented as a percentage of $CD3^+CD4^+$ cells. From cell counts, Treg cell numbers were calculated (C). Data are presented as mean ± SEM with statistical analysis using one-way ANOVA with Sidak's multiple comparisons test. * indicates statistical significance ($p<0.05$) compared to WT controls; *$p<0.05$ and **$p<0.01$. MD; macrophage-depleted. MØ; macrophages. P4; progesterone. WT; wild type.

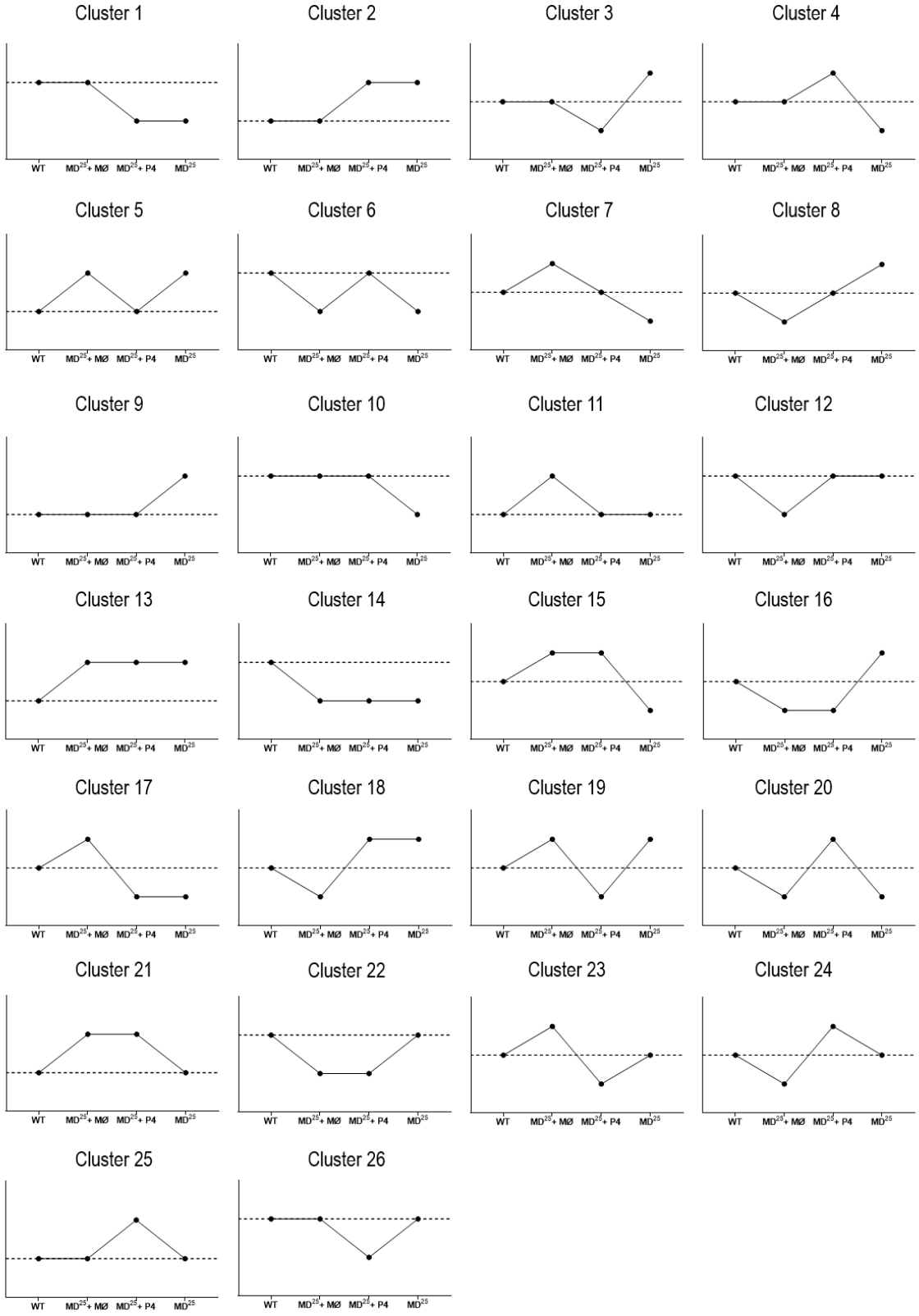

Figure 9.21: RNA expression cluster analysis for day 7.5 pc decidual and myometrial samples. WT and CD11b-DTR females were mated to BALB/c stud males and 25 ng/g DT was administered on day 5.5 pc. For P4 supplementation, DT-treated CD11b-DTR females were subcutaneously injected with P4 on days 5.5 pc and 6.5 pc. For BMDM administration, DT-treated CD11b-DTR females were intravenously injected with BMDM on days 3.5 pc and 5.5 pc. Implantation sites were dissected into decidua and myometrium and then RNA profiling was performed using OpenArray™ technology. The pattern of expression was sorted into clusters 1-26. Clusters 1 and 2 identified key genes regulated by macrophages. MD; macrophage-depleted. MØ; macrophages. P4; progesterone. WT; wild type.

Table 9.1: Top ten upregulated and downregulated genes in the decidua for each group compared to WT on day 7.5 pc ($1<log_2FC<-1$)

WT vs MD^{25} + MØ			WT vs MD^{25} + P4			WT vs MD^{25}		
Gene	**log_2FC**	**p-value**	**Gene**	**log_2FC**	**p-value**	**Gene**	**log_2FC**	**p-value**
Il22	+ 5.99	0.093	*Gdf15*	+ 3.18	0.020	*Cxcl3*	+ 12.04	<0.001
Prok2	+ 3.57	0.322	*Il3*	+ 2.72	>0.99	*Cxcl2*	+ 10.92	<0.001
Il1rapl2	+ 2.92	0.625	*Prok2*	+ 2.60	0.002	*Prok2*	+ 9.83	<0.001
Il3	+ 2.74	>0.99	*S100a9*	+ 2.46	0.017	*Il1b*	+ 8.86	<0.001
Gdf15	+ 2.53	0.044	*Vip*	+ 2.42	0.003	*S100a9*	+ 8.69	<0.001
Itgb2l	+ 2.34	0.090	*Grem1*	+ 2.28	0.001	*Trem1*	+ 8.36	<0.001
Prtn3	+ 2.22	0.037	*Ifnb1*	+ 2.25	0.002	*Itgb2l*	+ 8.23	<0.001
S100a9	+ 2.08	0.039	*S100a8*	+ 2.22	0.078	*Il1f9*	+ 8.06	<0.001
Il1f9	+ 1.97	0.054	*Prtn3*	+ 2.18	0.031	*Fpr1*	+ 7.72	<0.001
Il8rb	+ 1.96	0.011	*Ccl1*	+ 2.05	0.003	*Il8rb*	+ 7.52	<0.001
Il17rb	- 2.22	0.028	*Il13*	- 3.21	0.015	*Cx3cr1*	- 7.38	<0.001
Xcr1	- 2.08	0.282	*Mrc1*	- 3.06	0.005	*Prl7d1*	- 7.16	0.004
Mrc1	- 2.04	0.053	*Fgf10*	- 2.52	0.006	*Apoa1*	- 6.97	<0.001
Il13	- 1.88	0.084	*Ccr8*	- 2.51	<0.001	*C1qa*	- 6.97	<0.001
Orm1	- 1.86	0.295	*Pla2g2d*	- 2.40	0.051	*C1qb*	- 6.97	<0.001
Cntfr	- 1.85	0.054	*Siglec1*	- 2.29	0.011	*C1qc*	- 6.51	<0.001
Fgf10	- 1.82	0.025	*Cd163*	- 2.24	0.154	*Mrc1*	- 6.38	<0.001
Crp	- 1.73	0.044	*C1qc*	- 2.14	0.014	*Bmp2*	- 6.27	<0.001
Adora3	- 1.69	0.004	*C1qa*	- 2.04	0.008	*Il17rb*	- 6.27	<0.001
Il31ra	- 1.68	0.009	*C1qb*	- 1.99	0.009	*Il31ra*	- 6.27	<0.001

Table 9.2: Commonly dysregulated genes across all treatment groups in the decidua compared to WT on day 7.5 pc ($1<log_2FC<-1$ and $p<0.05$)

	WT vs MD^{25} + MØ		WT vs MD^{25} + P4		WT vs MD^{25}	
Gene	**log_2FC**	**p-value**	**log_2FC**	**p-value**	**log_2FC**	**p-value**
Fpr1	+ 1.63	0.009	+ 1.04	0.029	+ 7.72	<0.001
Gdf15	+ 2.53	0.044	+ 3.18	0.020	+ 3.09	0.002
Il8ra	+ 1.63	0.004	+ 1.73	0.004	+ 6.85	<0.001
Il8rb	+ 1.96	0.011	+ 2.03	0.009	+ 7.52	<0.001
Ppbp	+ 1.93	0.017	+ 1.28	0.005	+ 4.48	<0.001
Prtn3	+ 2.23	0.037	+ 2.18	0.031	+ 3.31	0.010
S100a9	+ 2.08	0.039	+ 2.36	0.017	+ 8.69	<0.001
Cntfr	- 1.56	0.043	- 1.73	0.007	- 4.38	<0.001
Fgf10	- 1.82	0.025	- 2.52	0.006	- 5.11	<0.001
Il17rb	- 2.22	0.028	- 1.55	0.007	- 6.27	<0.001
Il31ra	- 1.68	0.009	- 1.79	<0.001	- 6.27	<0.001
Tnfrsf19	- 1.66	0.033	- 1.73	0.022	- 3.88	<0.001

Table 9.3: Commonly downregulated genes between MD^{25} + MØ and MD^{25} + P4 groups in the decidua compared to WT on day 7.5 pc ($1<log_2FC<-1$ and $p<0.05$)

	WT vs MD^{25} + MØ		WT vs MD^{25} + P4		WT vs MD^{25}	
Gene	**log_2FC**	**p-value**	**log_2FC**	**p-value**	**log_2FC**	**p-value**
Bdkrb2	+ 1.26	0.026	+ 1.80	0.001	+ 1.54	0.260
Gpr17	+ 1.14	0.019	+ 1.47	0.002	- 1.30	0.510
Adora3	- 1.69	0.004	- 1.24	0.003	+ 0.03	>0.99
Fcgr2b	- 1.04	0.043	- 1.94	0.017	+ 1.14	0.410
Ltb4r1	- 1.64	0.009	- 1.09	0.031	+ 1.60	0.250

Table 9.4: **Top ten genes upregulated in MD^{25} + P4 group and downregulated in MD^{25} group in the decidua compared to WT on day 7.5 pc (1<log_2FC<-1 and p<0.05)**

	WT vs MD^{25} + MØ		WT vs MD^{25} + P4		WT vs MD^{25}	
Gene	**log_2FC**	**p-value**	**log_2FC**	**p-value**	**log_2FC**	**p-value**
Ccl1	+ 0.83	0.399	+ 2.05	0.003	- 2.00	0.021
Ccrl1	+ 0.86	0.259	+ 1.83	0.021	- 3.08	0.024
Hpse	+ 0.91	0.011	+ 1.83	0.002	- 2.52	0.046
Il6ra	+ 0.67	0.208	+ 1.44	0.012	- 1.46	0.026
Lifr	+ 0.32	0.557	+ 1.47	0.001	- 3.44	<0.001
Klkb1	+ 0.23	0.734	+ 1.38	0.031	- 1.58	0.027
Masp1	+ 0.76	0.230	+ 1.60	0.007	- 3.68	0.042
Slurp1	+ 0.72	0.323	+ 1.83	0.013	- 2.93	0.011
Thpo	+ 0.42	0.492	+ 1.86	0.003	- 3.80	0.002
Vip	+ 0.74	0.081	+ 2.42	0.003	- 1.88	0.023

Table 9.5: **Genes downregulated in MD^{25} + P4 group and upregulated in MD^{25} group in the decidua compared to WT on day 7.5 pc (1<log_2FC<-1 and p<0.05)**

	WT vs MD^{25} + MØ		WT vs MD^{25} + P4		WT vs MD^{25}	
Gene	**log_2FC**	**p-value**	**log_2FC**	**p-value**	**log_2FC**	**p-value**
Ccl6	- 1.01	0.054	- 1.78	0.009	+ 4.52	0.001
Ebi3	+ 0.01	>0.99	- 1.01	0.033	+ 2.65	0.026

Table 9.6: **Dysregulated genes in the decidua for MD^{25} + MØ group compared to WT on day 7.5 pc (1<log_2FC<-1 and p<0.05)**

	WT vs MD^{25} + MØ		WT vs MD^{25} + P4		WT vs MD^{25}	
Gene	**log_2FC**	**p-value**	**log_2FC**	**p-value**	**log_2FC**	**p-value**
Cxcl11	+ 1.19	0.027	+ 0.22	0.685	+ 1.70	0.262
Alox5	- 1.47	0.009	- 0.48	0.179	- 0.92	>0.99
Crp	- 1.73	0.044	- 1.43	0.109	- 2.73	0.083
Hrh1	- 1.15	0.046	- 0.78	0.213	- 0.43	0.538
Il15	- 1.29	0.005	- 0.85	0.016	- 1.38	0.127
Itgb2	- 1.06	0.007	- 0.66	0.095	+ 1.82	0.110

Table 9.7: Top ten upregulated and downregulated genes in the decidua for MD^{25} + P4 group compared to WT on day 7.5 pc ($1<log_2FC<-1$ and $p<0.05$)

	WT vs MD^{25} + MØ		WT vs MD^{25} + P4		WT vs MD^{25}	
Gene	**log_2FC**	**p-value**	**log_2FC**	**p-value**	**log_2FC**	**p-value**
Bmp7	+ 0.71	0.077	+ 1.82	0.006	- 0.24	0.652
Cmtm2a	- 0.08	>0.99	+ 1.40	0.041	- 1.19	0.188
Gh	- 0.19	>0.99	+ 1.85	0.008	+ 0.32	0.962
Ifna2	+ 1.09	0.106	+ 1.82	0.005	+ 0.14	0.834
Ifnb1	+ 1.11	0.161	+ 2.25	0.002	- 0.31	>0.99
Ifnk	+ 1.13	0.059	+ 2.03	0.008	- 1.33	0.077
Olr1	+ 0.79	0.379	+ 1.70	0.046	- 0.88	0.330
Procr	+ 0.37	0.573	+ 2.00	0.001	- 2.14	0.182
Tnfrsf11b	+ 0.42	0.511	+ 1.64	0.003	- 1.27	0.283
Tnfsf9	+ 0.99	0.160	+ 2.04	0.005	- 1.62	0.179
C3ar1	- 1.03	0.187	- 1.81	0.006	- 1.66	0.323
Cd86	- 0.70	0.439	- 1.05	0.030	+ 1.38	0.260
Cybb	- 0.56	0.657	- 1.14	0.027	+ 1.70	0.229
Hgf	- 1.04	0.315	- 1.41	0.001	- 0.96	0.085
Il13	- 0.29	>0.99	- 3.21	0.015	- 3.51	0.071
Lilrb3	- 1.06	0.162	- 1.31	0.030	+ 1.72	0.152
Nlrc4	- 1.19	0.132	- 1.64	0.010	+ 1.00	0.538
Slco1a4	+ 0.13	>0.99	- 1.70	0.042	- 0.38	>0.99
Tlr1	- 1.24	0.140	- 1.19	0.002	- 0.43	0.923

Table 9.8: Canonical pathways identified in the MD[25] + MØ group compared to WT in the decidua on day 7.5 pc (2<Z score<-2 and p<0.05)

Canonical Pathway	Z score	Ratio	p-value
T Cell Exhaustion Pathway	- 2.24	3.2%	8.91×10^{-05}

Table 9.9: Canonical pathways identified in the MD[25] + P4 group compared to WT in the decidua on day 7.5 pc (2<Z score<-2 and p<0.05)

Canonical Pathway	Z score	Ratio	p-value
GP6 Signalling Pathway	- 2.00	3.0%	4.37×10^{-02}
Activation of IRF by Cytosolic Pattern Recognition Receptors	+ 3.16	19.2%	7.94×10^{-11}
Ceramide Signalling	+ 2.65	7.1%	6.17×10^{-05}
Role of RIG1-like Receptors in Antiviral Innate Immunity	+ 2.65	21.2%	3.09×10^{-08}
STAT3 Pathway	+ 2.53	12.9%	2.00×10^{-14}
LPS/IL-1 Mediated Inhibition of RXR Function	+ 2.24	4.4%	2.14×10^{-04}
IL-6 Signalling	+ 2.14	10.5%	6.31×10^{-11}
cAMP-mediated Signalling	+ 2.12	3.7%	1.62×10^{-03}
IL-8 Signalling	+ 2.11	5.6%	5.01×10^{-06}
Endocannabinoid Cancer Inhibition Pathway	+ 2.11	7.1%	4.68×10^{-07}
Production of Nitric Oxide and Reactive Oxygen Species in Macrophages	+ 2.11	6.5%	3.72×10^{-07}

Table 9.10: Canonical pathways identified in the MD[25] group compared to WT in the decidua on day 7.5 pc (2<Z score<-2 and p<0.05)

Canonical Pathway	Z score	Ratio	p-value
FGF Signalling	- 3.16	10.9%	6.31×10^{-06}
Thrombin Signalling	- 3.16	4.8%	4.57×10^{-03}
Cardiac Hypertrophy Signalling	- 3.00	6.8%	6.17×10^{-06}
Neuroinflammation Signalling Pathway	- 2.99	20.6%	3.16×10^{-45}
NF-κB Signalling	- 2.83	17.9%	7.94×10^{-23}
CD40 Signalling	- 2.83	12.5%	1.74×10^{-06}
UVB-Induced MAPK Signalling	- 2.83	11.9%	2.69×10^{-05}
CNTF Signalling	- 2.83	11.4%	3.72×10^{-05}
EGF Signalling	- 2.83	11.4%	3.72×10^{-05}
NF-κB Activation by Viruses	- 2.83	8.4%	3.24×10^{-04}
Cyclins and Cell Cycle Regulation	+ 2.00	7.7%	2.88×10^{-03}

Table 9.11: Top ten upregulated and downregulated genes in the myometrium for each group compared to WT on day 7.5 pc ($1<log_2FC<-1$)

WT vs MD^{25} + MØ			WT vs MD^{25} + P4			WT vs MD^{25}		
Gene	**log_2FC**	**p-value**	**Gene**	**log_2FC**	**p-value**	**Gene**	**log_2FC**	**p-value**
Il1rapl2	+ 9.79	0.196	*Cxcl2*	+ 3.01	0.020	*S100a9*	+ 8.09	<0.001
Saa3	+ 5.46	0.012	*S100a8*	+ 2.88	0.191	*Saa3*	+ 7.43	<0.001
S100a8	+ 4.05	0.031	*Saa3*	+ 2.72	0.068	*Cxcl2*	+ 6.91	<0.001
S100a9	+ 2.85	0.042	*S100a9*	+ 2.68	0.029	*Il1b*	+ 6.80	<0.001
Prtn3	+ 2.84	0.028	*Il24*	+ 2.50	0.029	*S100a8*	+ 6.79	0.003
Cxcl2	+ 2.75	0.027	*Gdf15*	+ 2.46	0.004	*Il24*	+ 6.64	<0.001
Il24	+ 2.57	0.107	*Ifnb1*	+ 2.36	0.023	*Trem1*	+ 6.50	<0.001
Chi3l3	+ 2.48	0.007	*Lep*	+ 2.29	0.759	*Il8rb*	+ 6.18	<0.001
Ltf	+ 2.33	0.074	*Cxcl1*	+ 2.02	0.036	*Il8ra*	+ 6.08	<0.001
Il8ra	+ 2.22	0.031	*Ccl1*	+ 1.87	0.027	*Muc4*	+ 6.05	<0.001
Apoa4	- 7.16	0.092	*Pla2g2d*	- 4.38	0.203	*Il3*	- 9.97	0.448
Cfd	- 5.06	0.443	*Il3*	- 3.68	0.214	*Apoa4*	- 8.97	0.077
Il3	- 4.80	0.358	*Fcer1a*	-3.49	0.261	*Pla2g2d*	- 7.38	<0.001
Fcer1a	- 4.11	0.072	*Cfd*	- 3.21	0.722	*Il13ra2*	- 7.16	<0.001
Pla2g2d	- 3.38	0.127	*Ccl8*	- 3.04	0.039	*Cd163*	- 5.87	0.110
Cd163	- 3.20	0.165	*Mrc1*	- 2.64	0.013	*Cfd*	- 5.87	0.401
Mbl2	- 2.40	0.443	*Ccl6*	- 2.63	0.032	*Fcer1a*	- 5.57	0.003
Apoa1	- 2.39	0.329	*Cx3cr1*	- 2.60	0.002	*Mrc1*	- 5.06	<0.001
Il13ra2	- 2.39	0.183	*Fcgr2b*	- 2.59	0.012	*Cx3cr1*	- 4.80	<0.001
Lep	- 2.39	0.740	*C1qc*	- 2.50	0.015	*C1qc*	- 4.51	<0.001

Table 9.12: Commonly dysregulated genes across all treatment groups in the myometrium compared to WT on day 7.5 pc (1<log_2FC<-1 and p<0.05)

	WT vs MD^{25} + MØ		WT vs MD^{25} + P4		WT vs MD^{25}	
Gene	log_2FC	p-value	log_2FC	p-value	log_2FC	p-value
Cxcl2	+ 2.75	0.027	+ 3.01	0.020	+ 6.91	<0.001
S100a9	+ 2.85	0.042	+ 2.68	0.029	+ 8.09	<0.001
Ccr2	- 1.23	0.020	- 1.59	0.002	- 2.44	<0.001
Cd4	- 1.17	0.003	- 1.51	<0.001	- 2.89	<0.001
Mrc1	- 1.37	0.031	- 2.64	0.013	- 8.38	<0.001

Table 9.13: Commonly dysregulated genes between MD^{25} + MØ and MD^{25} + P4 groups in the myometrium compared to WT on day 7.5 pc (1<log_2FC<-1 and p<0.05)

	WT vs MD^{25} + MØ		WT vs MD^{25} + P4		WT vs MD^{25}	
Gene	log_2FC	p-value	log_2FC	p-value	log_2FC	p-value
Lilrb3	- 1.21	0.025	- 2.21	0.016	- 1.09	0.070
Nlrc4	- 1.10	0.014	- 2.29	0.008	- 0.11	>0.99

Table 9.14: Genes downregulated in MD^{25} + P4 and upregulated in MD^{25} group in the myometrium compared to WT on day 7.5 pc (1<log_2FC<-1 and p<0.05)

	WT vs MD^{25} + MØ		WT vs MD^{25} + P4		WT vs MD^{25}	
Gene	log_2FC	p-value	log_2FC	p-value	log_2FC	p-value
Ccr1	+ 0.09	0.241	- 1.66	0.027	+ 1.27	<0.001
Il10	- 0.15	>0.99	- 1.68	0.031	+ 2.02	<0.001

Table 9.15: Dysregulated genes in the myometrium for MD^{25} + MØ group compared to WT on day 7.5 pc (1<log_2FC<-1 and p<0.05)

	WT vs MD^{25} + MØ		WT vs MD^{25} + P4		WT vs MD^{25}	
Gene	log_2FC	p-value	log_2FC	p-value	log_2FC	p-value
Ccl4	+ 1.08	0.033	- 0.28	0.688	+ 0.62	0.105

Table 9.16: Dysregulated genes in the myometrium for MD^{25} + P4 group compared to WT on day 7.5 pc ($1<log_2FC<-1$ and $p<0.05$)

	WT vs MD^{25} + MØ		WT vs MD^{25} + P4		WT vs MD^{25}	
Gene	**log_2FC**	**p-value**	**log_2FC**	**p-value**	**log_2FC**	**p-value**
Ccl1	+ 1.40	0.167	+ 1.87	0.027	+ 0.08	>0.99
Tlr12	+ 0.01	>0.99	+ 1.07	0.011	+ 0.05	>0.99
Vip	+ 1.04	0.115	+ 1.66	0.009	+ 0.83	0.102
Ccl6	- 0.41	0.884	- 2.63	0.032	- 0.75	0.336
Ebi3	- 0.58	0.332	- 1.86	0.009	- 0.80	0.133
Itgam	+ 0.05	>0.99	- 1.29	0.031	+ 0.98	0.022
Ncf1	+ 0.10	>0.99	- 1.07	0.030	+ 0.49	0.131
Nfam1	- 0.63	0.174	- 1.44	0.011	- 0.63	0.119
Ptafr	- 0.47	0.449	- 1.46	0.032	- 0.15	>0.99
Tlr1	- 0.51	0.124	- 1.43	0.005	- 0.24	0.516
Tlr13	+ 0.00	>0.99	- 1.51	0.013	- 0.65	0.087

Table 9.17: Canonical pathways identified in the MD^{25} + MØ group compared to WT in the myometrium on day 7.5 pc (2<Z score<-2 and p<0.05)

Canonical Pathway	Z score	Ratio	p-value
Neuroinflammation Signalling Pathway	- 4.00	5.6%	5.01×10^{-13}
Colorectal Cancer Metastasis Signalling	- 3.32	5.6%	1.58×10^{-11}
STAT3 Pathway	- 3.16	9.1%	1.58×10^{-11}
HMGB1 Signalling	- 3.16	7.5%	8.71×10^{-10}
NF-κB Signalling	- 3.16	5.6%	1.45×10^{-08}
Tec Kinase Signalling	- 3.00	6.1%	6.61×10^{-09}
Cardiac Hypertrophy Signalling	- 3.00	3.8%	1.91×10^{-06}
Pancreatic Adenocarcinoma Signalling	- 2.83	9.2%	1.26×10^{-11}
Type 1 Diabetes Mellitus Signalling	- 2.83	7.8%	3.09×10^{-08}
IL-6 Signalling	- 2.83	6.0%	2.45×10^{-07}
PPARα/RXRα Activation	+ 2.33	5.1%	1.78×10^{-07}
Antioxidant Action of Vitamin C	+ 2.24	4.9%	1.38×10^{-04}

Table 9.18: Canonical pathways identified in the MD^{25} group compared to WT in the myometrium on day 7.5 pc (2<Z score<-2 and p<0.05)

Canonical Pathway	Z score	Ratio	p-value
Th1 Pathway	- 3.27	21.8%	2.51×10^{-22}
3-phosphoinositide Biosynthesis	- 3.16	5.1%	2.14×10^{-03}
Superpathway of Inositol Phosphate Compounds	- 3.16	4.4%	6.61×10^{-03}
Tec Kinase Signalling	- 3.05	10.3%	4.27×10^{-09}
STAT3 Pathway	- 2.99	24.2%	7.94×10^{-28}
Fc Epsilon RI Signalling	- 2.89	12.2%	3.39×10^{-09}
FLT3 Signalling in Haematopoietic Progenitor Cells	- 2.83	8.8%	1.78×10^{-04}
Thrombin Signalling	- 2.83	3.9%	2.75×10^{-02}
iCOS-iCOSL Signalling in T Helper Cells	- 2.71	11.9%	1.62×10^{-08}
Role of NFAT in Regulation of the Immune Response	- 2.67	7.7%	3.72×10^{-06}
Aryl Hydrocarbon Receptor Signalling	+ 3.00	6.7%	5.75×10^{-04}
Wnt/β-catenin Signalling	+ 2.12	4.8%	8.91×10^{-03}
Role of IL-17F in Allergic Inflammatory Airway Diseases	+ 2.00	15.0%	5.89×10^{-05}

Table 9.19: Canonical pathways identified in the MD^{25} + P4 group compared to WT in the myometrium on day 7.5 pc (2<Z score<-2 and p<0.05)

Canonical Pathway	Z score	Ratio	p-value
Role of Pattern Recognition Receptors in Recognition of Bacteria and Viruses	- 2.65	7.7%	2.00×10^{-12}

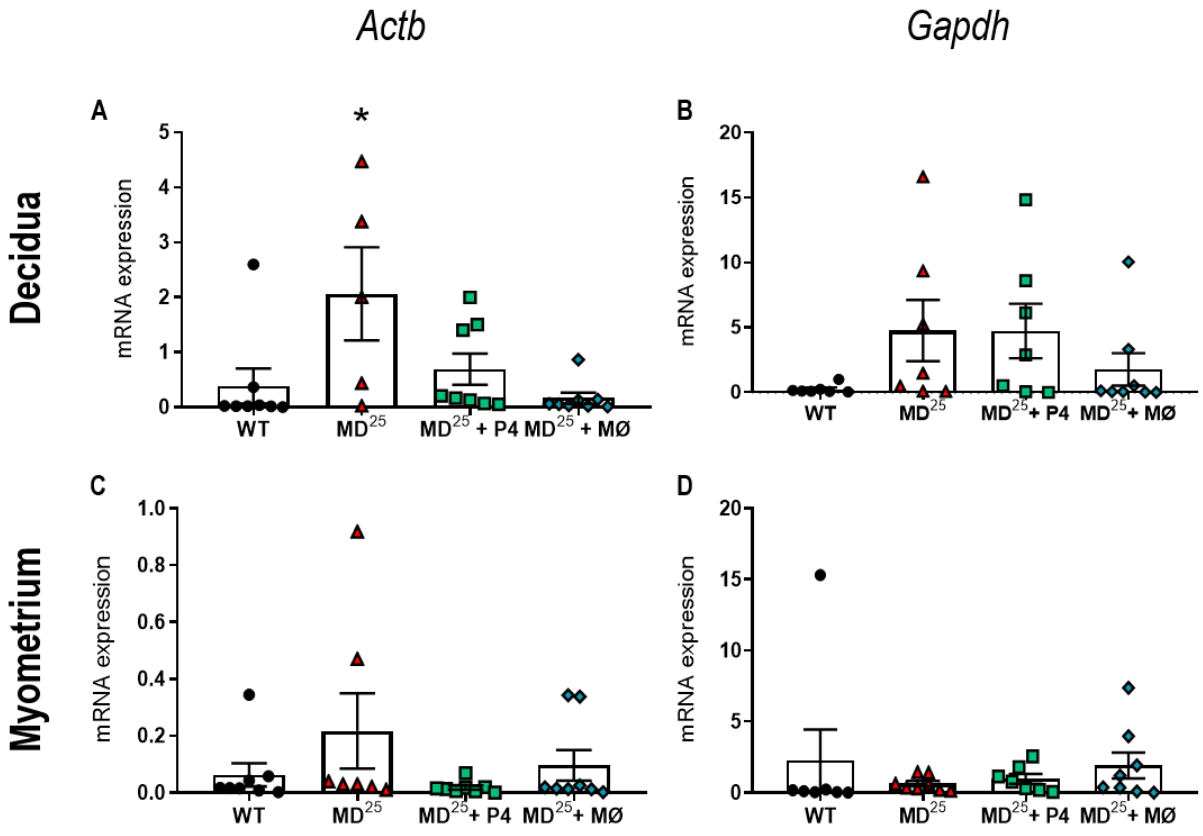

Figure 9.22: *Icam* expression in the decidua and myometrium on day 7.5 pc.
WT and CD11b-DTR females were mated to BALB/c stud males and 25 ng/g DT was administered on day 5.5 pc. For P4 supplementation, DT-treated CD11b-DTR females were subcutaneously injected with P4 on days 5.5 pc and 6.5 pc. For BMDM administration, DT-treated CD11b-DTR females were intravenously injected with BMDM on days 3.5 pc and 5.5 pc. Implantation sites were dissected into decidua and myometrium and *Icam* expression was determined in the decidua (A and B) and myometrium (C and D) using qPCR. Relative expression was calculated using housekeeping genes *Actb* (A and C) or *Gapdh* (B and D). Data are presented as mean ± SEM with statistical analysis using one-way ANOVA with Sidak's multiple comparisons test, n=4 dams/group. * indicates statistical significance ($p<0.05$) compared to WT controls; *$p<0.05$. MD; macrophage-depleted. MØ; macrophages. P4; progesterone. WT; wild type.

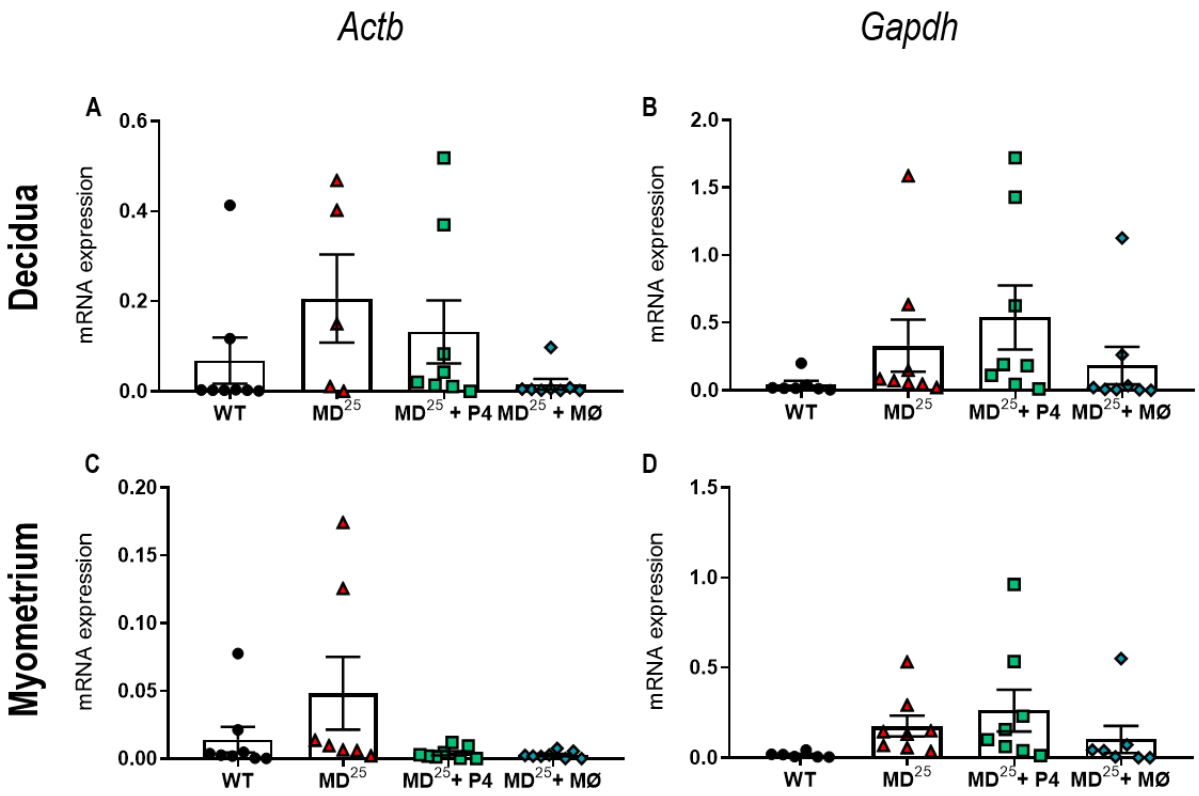

Figure 9.23: *Cxcr4* expression in the decidua and myometrium on day 7.5 pc.
WT and CD11b-DTR females were mated to BALB/c stud males and 25 ng/g DT was administered on day 5.5 pc. For P4 supplementation, DT-treated CD11b-DTR females were subcutaneously injected with P4 on days 5.5 pc and 6.5 pc. For BMDM administration, DT-treated CD11b-DTR females were intravenously injected with BMDM on days 3.5 pc and 5.5 pc. Implantation sites were dissected into decidua and myometrium and *Cxcr4* expression was determined in the decidua (A and B) and myometrium (C and D) using qPCR. Relative expression was calculated using housekeeping genes *Actb* (A and C) or *Gapdh* (B and D). Data are presented as mean ± SEM with statistical analysis using one-way ANOVA with Sidak's t-test. MØ; macrophages. MD; macrophage-depleted. P4; progesterone.

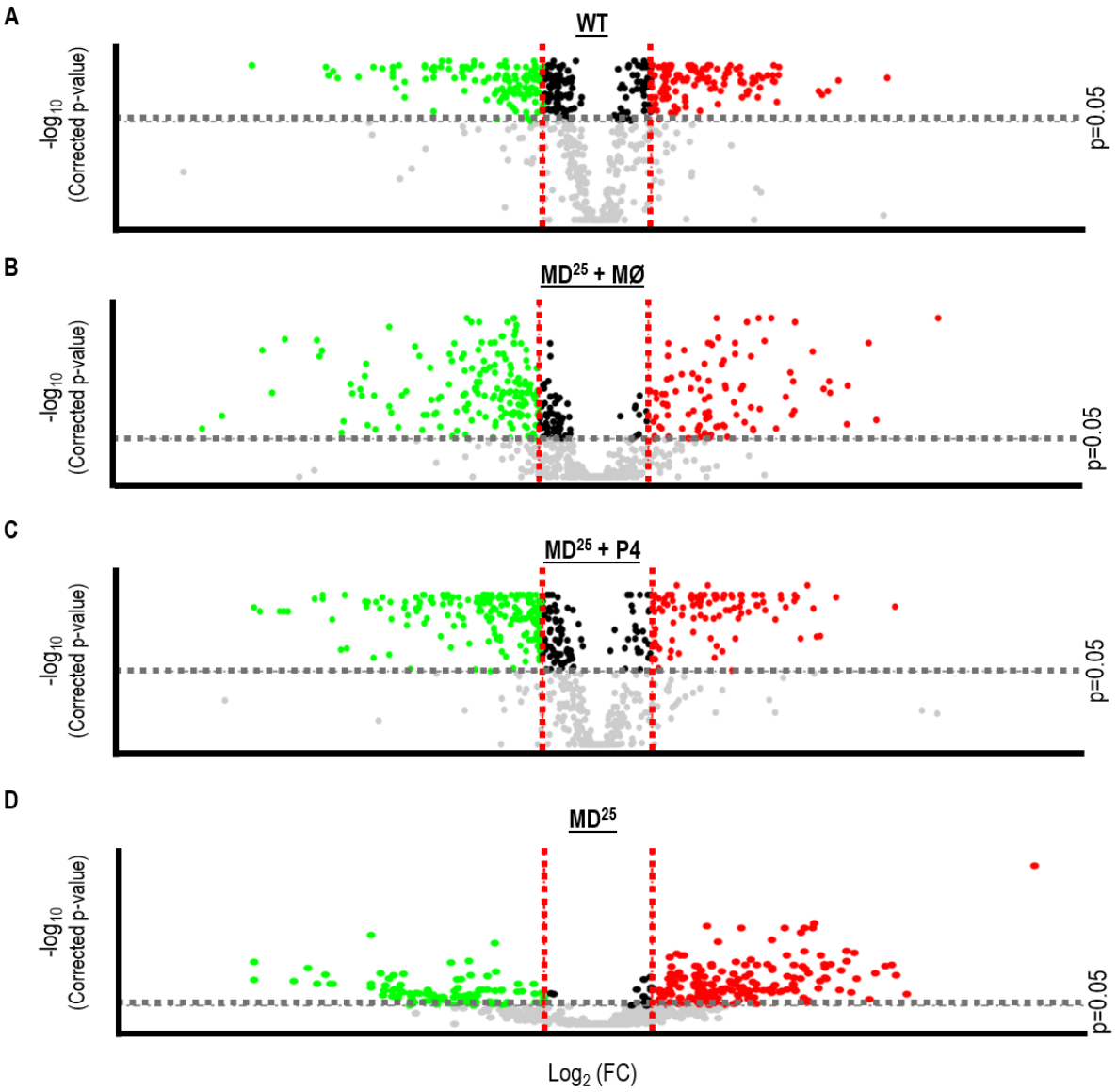

Figure 9.24: RNA expression across the treatment groups for the myometrium compared to decidual gene expression.

WT and CD11b-DTR females were mated to BALB/c stud males and 25 ng/g DT was administered on day 5.5 pc. For P4 supplementation, DT-treated CD11b-DTR females were subcutaneously injected with P4 on days 5.5 pc and 6.5 pc. For BMDM administration, DT-treated CD11b-DTR females were intravenously injected with BMDM on days 3.5 pc and 5.5 pc. Implantation sites were dissected into decidua and myometrium and then RNA profiling was performed using OpenArray™ technology. RNA profiling was compared between the myometrium and the decidua for each of the four treatment groups. MØ; macrophages. MD; macrophage-depleted. P4; progesterone.

Table 9.20: Top ten upregulated and downregulated genes in the myometrium for each group compared to decidual expression on day 7.5 pc (2<FC<0.5)

WT			MD^{25} + MØ			MD^{25} + P4			MD^{25}		
Gene	**log_2FC**	**p-value**	**Gene**	**log_2FC**	**p-value**	**Gene**	**log_2FC**	**p-value**	**Gene**	**log_2FC**	**p-value**
Fcer1a	+ 5.36	0.013	*Sectm1b*	+ 6.30	<0.001	*Lep*	+ 6.21	0.283	*Aoc3*	+ 8.10	<0.001
Il3	+ 5.30	0.873	*Saa3*	+ 5.17	0.011	*Cd163*	+ 5.93	0.250	*Sectm1b*	+ 5.73	0.008
Sectm1b	+ 4.46	0.014	*Crp*	+ 5.03	<0.001	*Sectm1b*	+ 5.43	0.004	*Alox15*	+ 5.53	<0.001
Ccl20	+ 4.27	0.020	*Cxcl15*	+ 4.64	0.001	*Cxcl12*	+ 4.36	0.002	*Gdf5*	+ 5.45	<0.001
Cd163	+ 4.16	0.022	*Xcr1*	+ 4.63	0.016	*Crp*	+ 4.07	0.012	*Serpina1a*	+ 5.33	<0.001
Cxcl5	+ 4.10	0.020	*Ccl20*	+ 4.32	0.001	*Ccl20*	+ 4.00	0.012	*Ltbp4*	+ 5.14	<0.001
Aoc3	+ 3.36	0.010	*Serpina1a*	+ 4.30	0.001	*Serpina3c*	+ 3.96	0.054	*Ccl8*	+ 5.03	0.018
Reg3g	+ 3.36	0.012	*Alox15*	+ 4.20	0.001	*Alox15*	+ 3.94	0.004	*Tnfsf10*	+ 4.80	0.001
Serpina1a	+ 3.32	0.028	*Il33*	+ 4.00	<0.001	*Slco1a4*	+ 3.83	0.001	*C1qa*	+ 4.75	<0.001
Cd70	+ 3.28	0.015	*Aoc3*	+ 3.68	<0.001	*Cxcl5*	+ 3.71	0.013	*Ccl28*	+ 4.70	0.006
Prl7d1	- 7.64	0.233	*Prl7d1*	- 7.16	0.022	*Prl7d1*	- 6.80	0.165	*Ccl3*	- 6.38	<0.001
S100a8	- 6.38	0.009	*Apoa4*	- 6.80	0.008	*Bmp8a*	- 6.27	0.004	*Cxcl13*	- 6.38	0.001
Tnfsf4	- 5.01	0.010	*Bmp8a*	- 5.88	0.001	*Reg3a*	- 6.16	0.004	*Cd274*	- 5.64	0.001
Ereg	- 4.97	0.012	*Apoa1*	- 5.64	0	*S100a8*	- 5.80	0.004	*Ccl4*	- 5.38	<0.001
Bmp8a	- 4.88	0.011	*C8a*	- 5.38	1.000	*Bmp2*	- 5.72	0.004	*Il1rn*	- 5.21	0.001
Il1a	- 4.80	0.013	*Il3*	- 5.11	0.604	*Tnfsf18*	- 5.16	0.003	*Ccr1l1*	- 5.06	<0.001
Bmp2	- 4.41	0.013	*Tnfsf18*	- 5.06	0	*Il1a*	- 5.01	0.003	*Ccrl2*	- 4.97	0.001
Apoa1	- 4.21	0.052	*Cer1*	- 5.01	0	*Kng1*	- 5.01	0.002	*Cxcl2*	- 4.92	0.001
Areg	- 4.13	0.010	*Fabp4*	- 4.97	0	*Tnfsf4*	- 4.84	0.006	*Il13ra2*	- 4.21	<0.001
Ptx3	- 3.97	0.010	*Retn*	- 4.61	0.031	*Apoa1*	- 4.68	0.021	*Nlrp3*	- 4.21	0.003

Table 9.21: Top ten upregulated and downregulated genes in the myometrium for each group compared to decidual expression on day 7.5 pc (2<FC<0.5, p<0.05)

WT			MD^{25} + MØ			MD^{25} + P4			MD^{25}		
Gene	**log_2FC**	**p-value**	**Gene**	**log_2FC**	**p-value**	**Gene**	**log_2FC**	**p-value**	**Gene**	**log_2FC**	**p-value**
Fcer1a	+ 9.79	0.013	*Sectm1b*	+ 6.30	<0.001	*Sectm1b*	+ 5.43	0.004	*Aoc3*	+ 8.10	<0.001
Sectm1b	+ 5.46	0.014	*Saa3*	+ 5.17	0.011	*Cxcl12*	+ 4.36	0.002	*Sectm1b*	+ 5.73	0.008
Ccl20	+ 4.05	0.020	*Crp*	+ 5.03	<0.001	*Crp*	+ 4.07	0.012	*Alox15*	+ 5.53	<0.001
Cd163	+ 2.85	0.022	*Cxcl15*	+ 4.64	0.001	*Ccl20*	+ 4.00	0.012	*Gdf5*	+ 5.45	<0.001
Cxcl5	+ 2.84	0.020	*Xcr1*	+ 4.63	0.016	*Alox15*	+ 3.94	0.004	*Serpina1a*	+ 5.33	<0.001
Aoc3	+ 2.75	0.010	*Ccl20*	+ 4.32	0.001	*Slco1a4*	+ 3.83	0.001	*Ltbp4*	+ 5.14	<0.001
Reg3g	+ 2.57	0.012	*Serpina1a*	+ 4.30	0.001	*Cxcl5*	+ 3.71	0.013	*Ccl8*	+ 5.03	0.018
Serpina1a	+ 2.48	0.028	*Alox15*	+ 4.20	0.001	*Aoc3*	+ 3.60	0.002	*Tnfsf10*	+ 4.80	0.001
Cd70	+ 2.33	0.015	*Il33*	+ 4.00	<0.001	*Xcl1*	+ 3.64	0.002	*C1qa*	+ 4.75	<0.001
Sftpa1	+ 2.22	0.009	*Aoc3*	+ 3.68	<0.001	*Tnfsf13b*	+ 3.60	0.003	*Ccl28*	+ 4.70	0.006
S100a8	- 6.38	0.009	*Prl7d1*	- 7.16	0.022	*Bmp8a*	- 6.27	0.004	*Ccl3*	- 6.38	<0.001
Tnfsf4	- 5.01	0.010	*Apoa4*	- 6.80	0.008	*Reg3a*	- 6.16	0.004	*Cxcl13*	- 6.38	0.001
Ereg	- 4.97	0.012	*Bmp8a*	- 5.88	0.001	*S100a8*	- 5.80	0.004	*Cd274*	- 5.64	0.001
Bmp8a	- 4.88	0.011	*Apoa1*	- 5.64	<0.001	*Bmp2*	- 5.72	0.004	*Ccl4*	- 5.38	<0.001
Il1a	- 4.80	0.013	*Tnfsf18*	- 5.06	<0.001	*Tnfsf18*	- 5.16	0.003	*Il1rn*	- 5.21	0.001
Bmp2	- 4.41	0.013	*Cer1*	- 5.01	<0.001	*Il1a*	- 5.01	0.003	*Ccr1l1*	- 5.06	<0.001
Areg	- 4.13	0.010	*Fabp4*	- 4.97	<0.001	*Kng1*	- 5.01	0.002	*Ccrl2*	- 4.97	0.001
Ptx3	- 3.97	0.010	*Retn*	- 4.61	0.031	*Tnfsf4*	- 4.84	0.006	*Cxcl2*	- 4.92	0.001
Ctla4	- 3.78	0.010	*Bmp2*	- 4.57	0.013	*Apoa1*	- 4.68	0.021	*Il13ra2*	- 4.21	<0.001
Tnfsf18	- 3.78	0.011	*Ptx3*	- 4.44	0.001	*Ereg*	- 4.61	0.002	*Nlrp3*	- 4.21	0.003

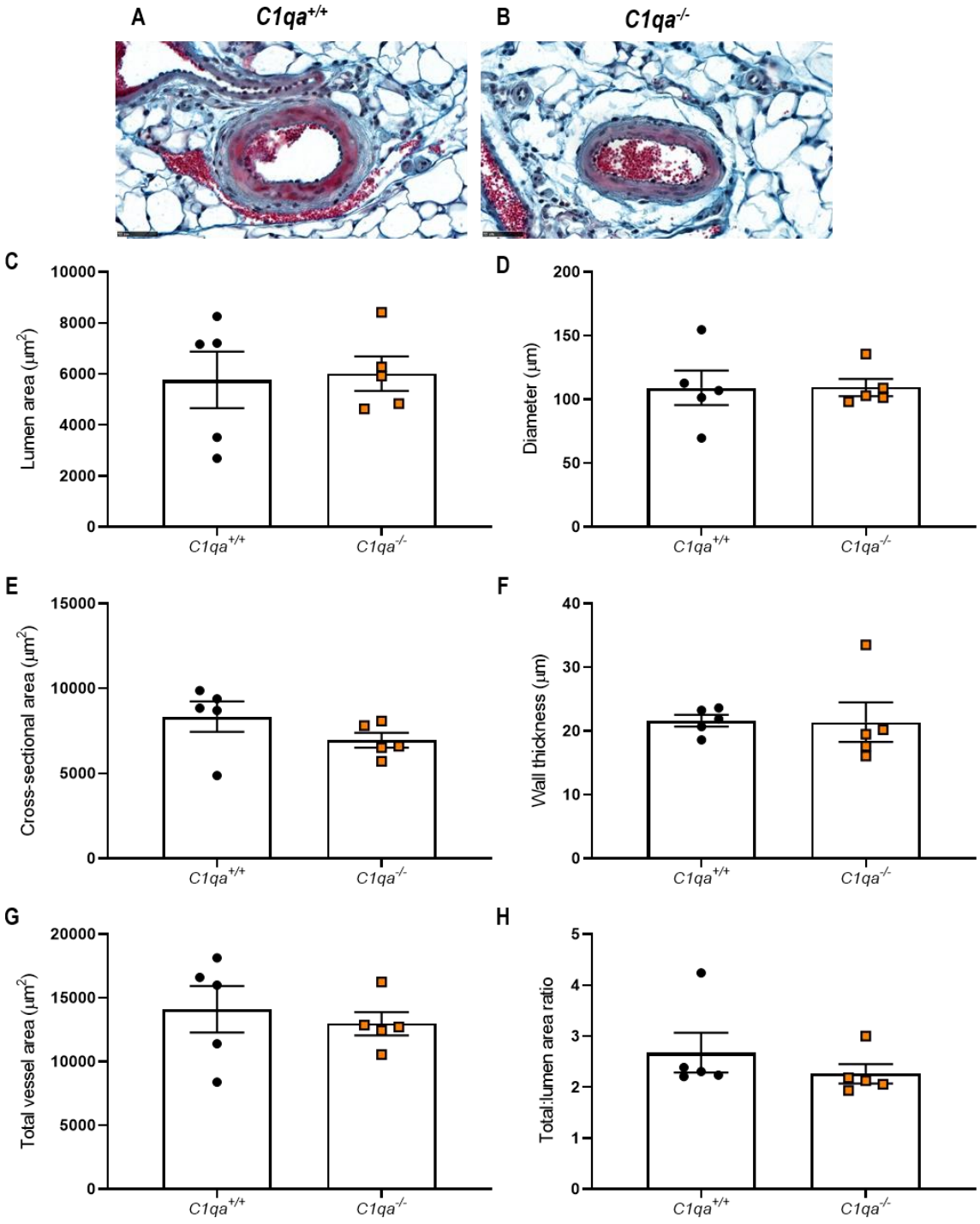

Figure 9.25: C1Q deficiency does not change vascular remodelling at the cervical end of the main uterine artery on day 9.5 pc.

C1qa$^{+/+}$ and *C1qa*$^{-/-}$ females were mated to BALB/c stud males. On day 9.5 pc, the cervical end of the main uterine artery from *C1qa*$^{+/+}$ and *C1qa*$^{-/-}$ females was dissected and sectioned for analysis (A and B). Artery parameters were calculated including lumen area (C), diameter (D), cross-sectional area (E), wall thickness (F), total vessel area (G), and the ratio of total vessel size to lumen ratio (H). Data are presented as mean ± SEM with statistical analysis using unpaired t-tests.

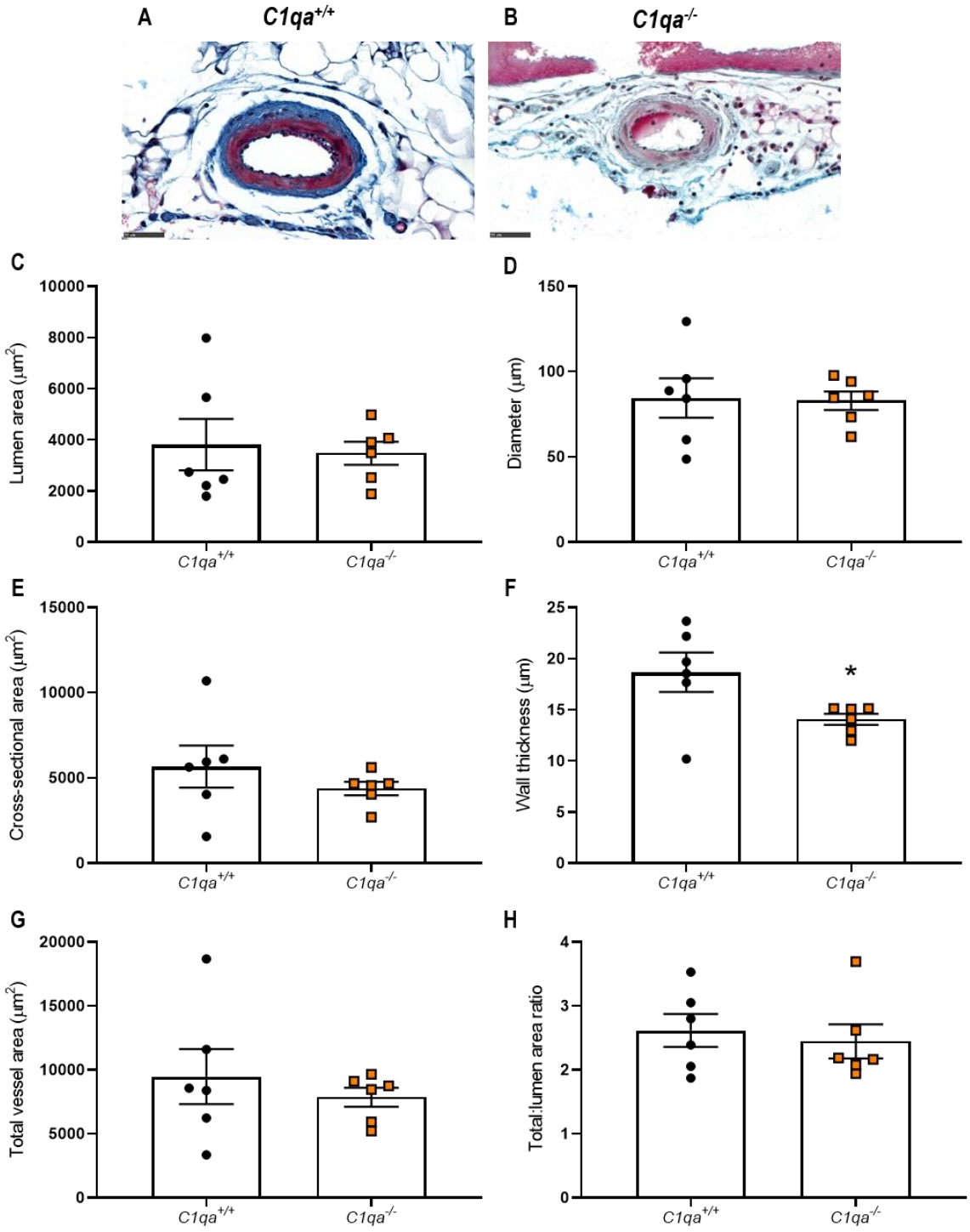

Figure 9.26: C1Q deficiency decrease main uterine artery wall thickness at the ovarian end on day 9.5 pc.

C1qa$^{+/+}$ and *C1qa*$^{-/-}$ females were mated to BALB/c stud males. On day 9.5 pc, the ovarian end of the main uterine artery from *C1qa*$^{+/+}$ and *C1qa*$^{-/-}$ females was dissected and sectioned for analysis (A and B). Artery parameters were calculated including lumen area (C), diameter (D), cross-sectional area (E), wall thickness (F), total vessel area (G), and the ratio of total vessel size to lumen ratio (H). Data are presented as mean ± SEM with statistical analysis using unpaired t-tests. * indicates statistical significance ($p<0.05$); *$p<0.05$.

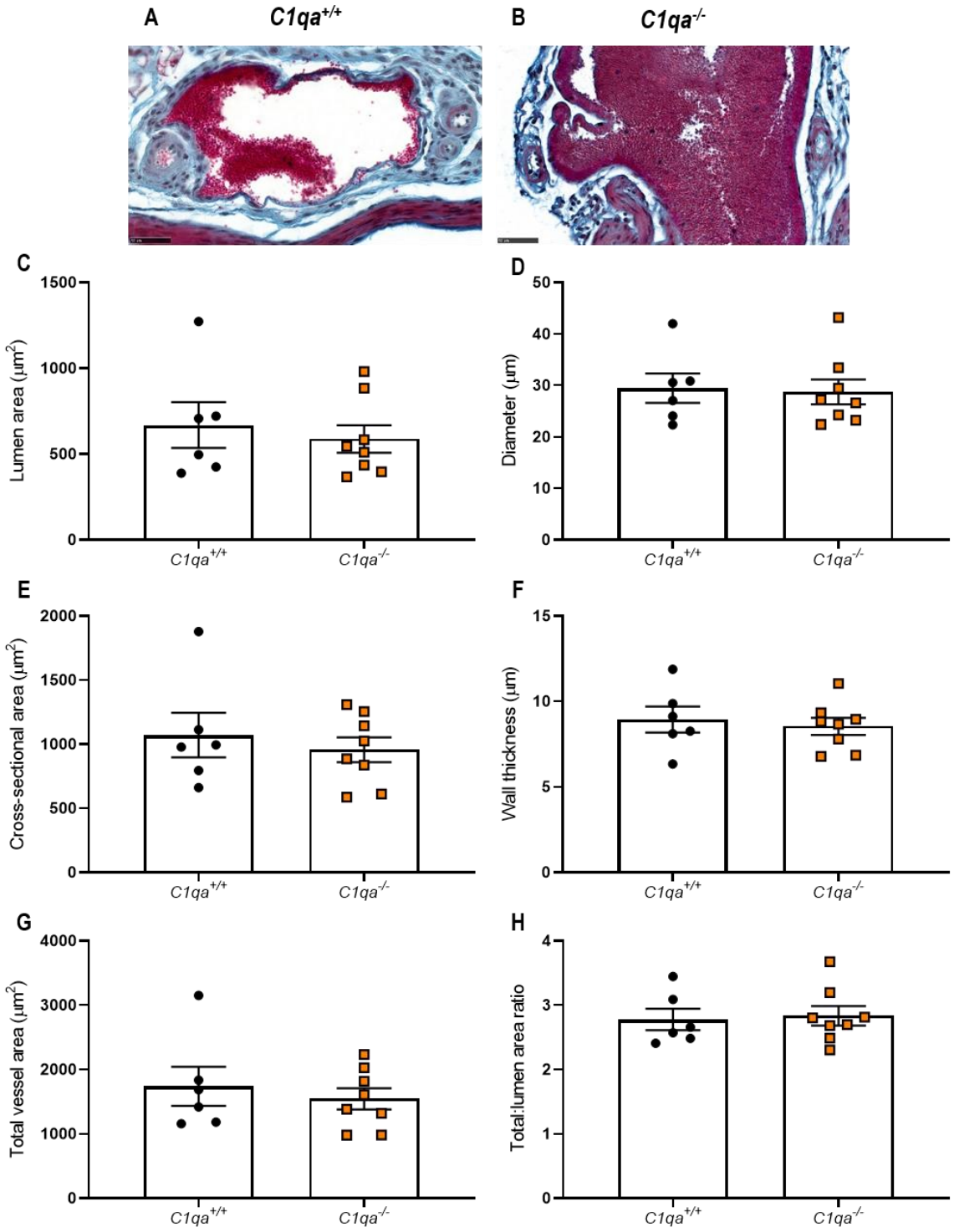

Figure 9.27: C1Q deficiency does not change radial artery remodelling on day 9.5 pc.
C1qa$^{+/+}$ and *C1qa*$^{-/-}$ females were mated to BALB/c stud males. On day 9.5 pc, the uterine radial arteries from *C1qa*$^{+/+}$ and *C1qa*$^{-/-}$ females was dissected and sectioned for analysis (A and B). Artery parameters were calculated including lumen area (C), diameter (D), cross-sectional area (E), wall thickness (F), total vessel area (G), and the ratio of total vessel size to lumen ratio (H). Data are presented as mean ± SEM with statistical analysis using unpaired t-tests.

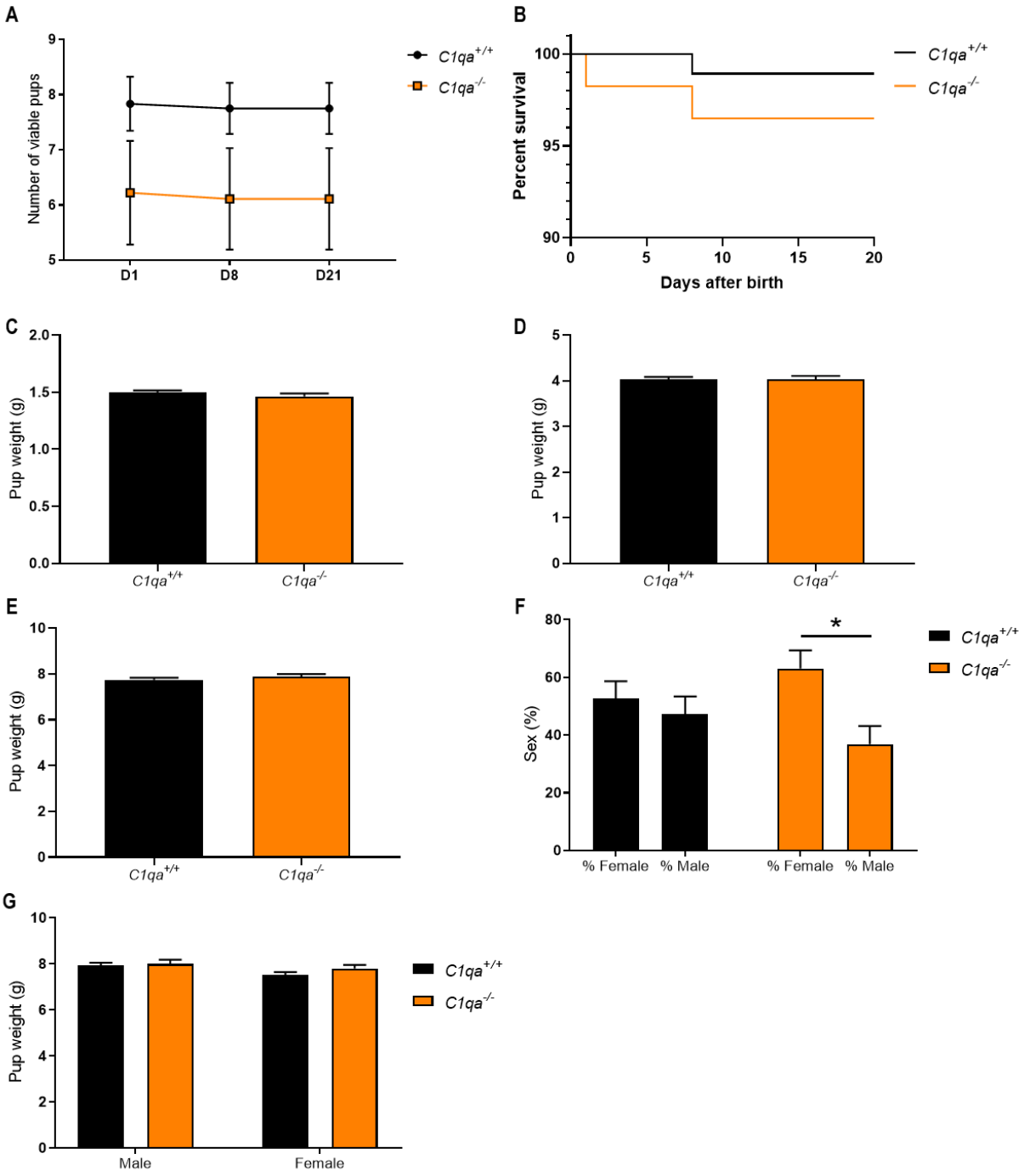

Figure 9.28: Maternal C1Q deficiency results in skewed gender ratios on day 21.

C1qa$^{+/+}$ and *C1qa*$^{-/-}$ females were mated to BALB/c stud males. The number of viable pups were counted on days one, eight, and twenty-one post-delivery (A). Pup survival was also measured on days one, eight, and twenty-one (B). Pup weights were measured on days one (C), eight (D), and twenty-one (E). On day twenty-one, the pups were sexed, and the distribution of sex was calculated (F). Finally, day 21 pup weights were separated based on sex (G). Data are presented as mean ± SEM, except in C-E and G where a mixed-model analysis was performed to calculate estimated marginal means using total number of viable pups as the co-variate. Statistical analysis was performed using unpaired t-test, except in B where a survival curve comparison test was used. * indicates statistical significance ($p<0.05$); *$p<0.05$.

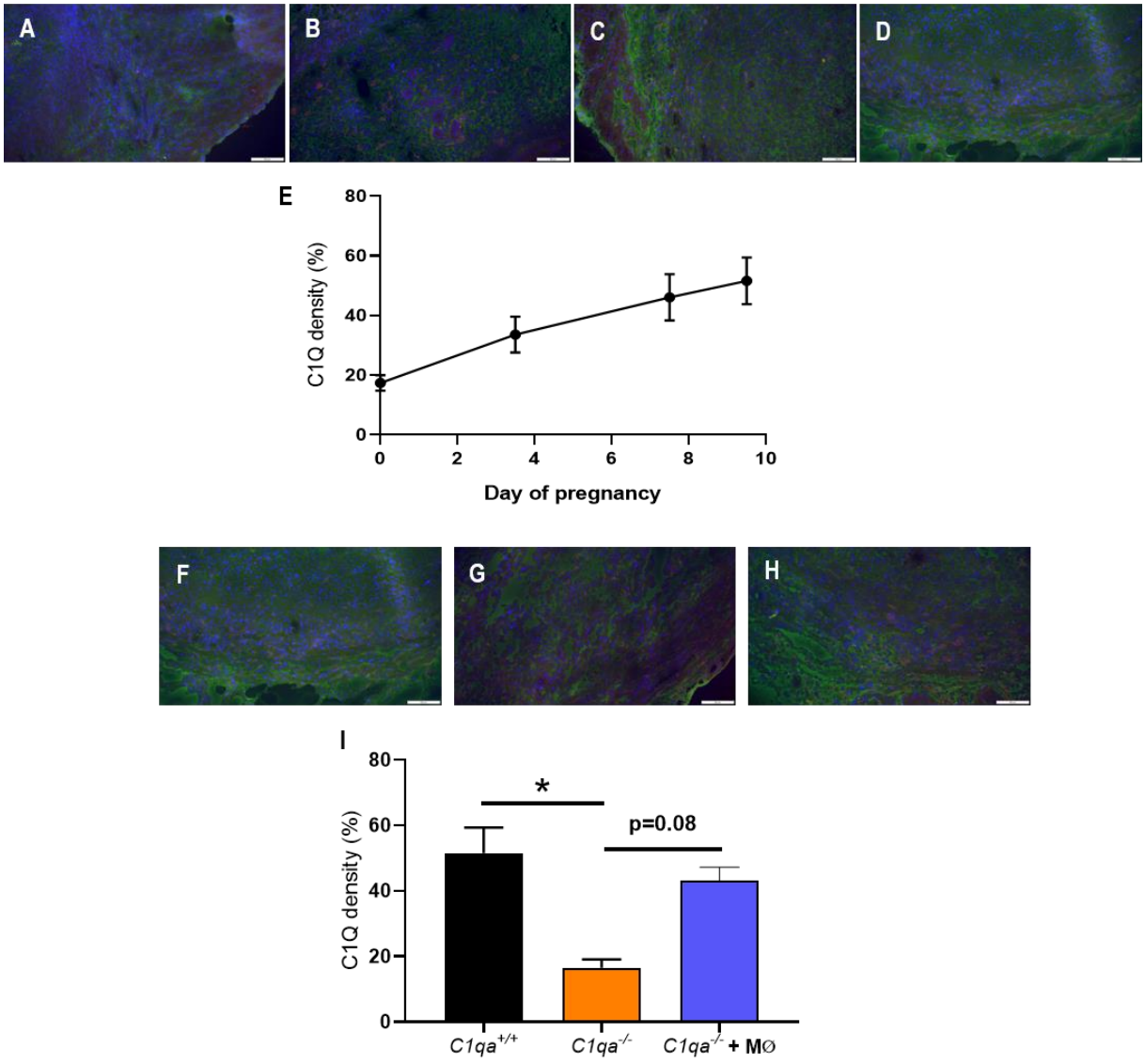

Figure 9.29: C1Q expression increases during pregnancy and with BMDM supplementation. *C1qa*$^{+/+}$ and *C1qa*$^{-/-}$ females were mated to BALB/c stud males. *C1qa*$^{-/-}$ females were administered BMDM on days 5.5 and 7.5 pc. *C1qa*$^{+/+}$ females' implantation sites from days 3.5 pc, 7.5 pc, and 9.5 pc were stained to assess C1Q expression across pregnancy and from virgin mice (A-E; scale bar is 50 µm in A-D). C1Q density was then measured in *C1qa*$^{+/+}$, *C1qa*$^{-/-}$, and *C1qa*$^{-/-}$ + BMDM mice on day 9.5 pc (F-I; scale bar is 50 µm in F-H). Statistical analysis was performed using one-way ANOVA with Sidak's multiple comparisons test. * indicates statistical significance ($p<0.05$) compared to *C1qa*$^{+/+}$ mice; *$p<0.05$.

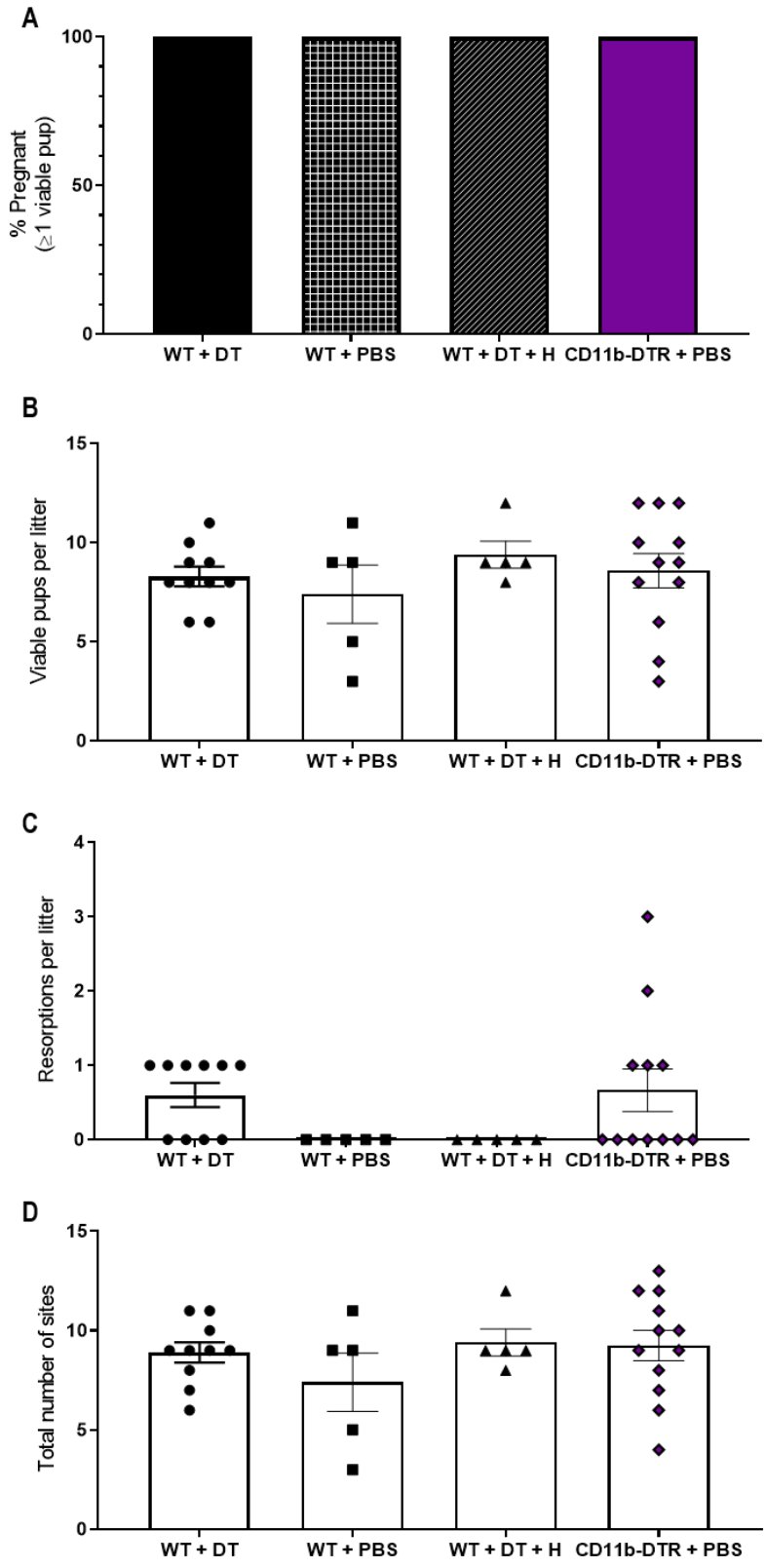

Figure 9.30: DT treatment has no impact on WT pregnancy viability on day 17.5 pc.
WT and CD11b-DTR females were mated to BALB/c stud males and all mice were administered either 25 ng/g DT or PBS on day 5.5 pc. On day 5.5 pc, a cohort of WT mice received P4 pellets prior to DT administration and received an E2 pellet on day 9.5 pc. Viable pregnancy rate was assessed on day 17.5 pc (A). The numbers of viable pups, implantation site resorptions, and total implantation site numbers were also assessed per litter (B-D). Data are presented as mean ± SEM (B-D). Statistical analysis was performed using χ^2 test (A) or one-way ANOVA with Sidak's multiple comparisons test (B-D).

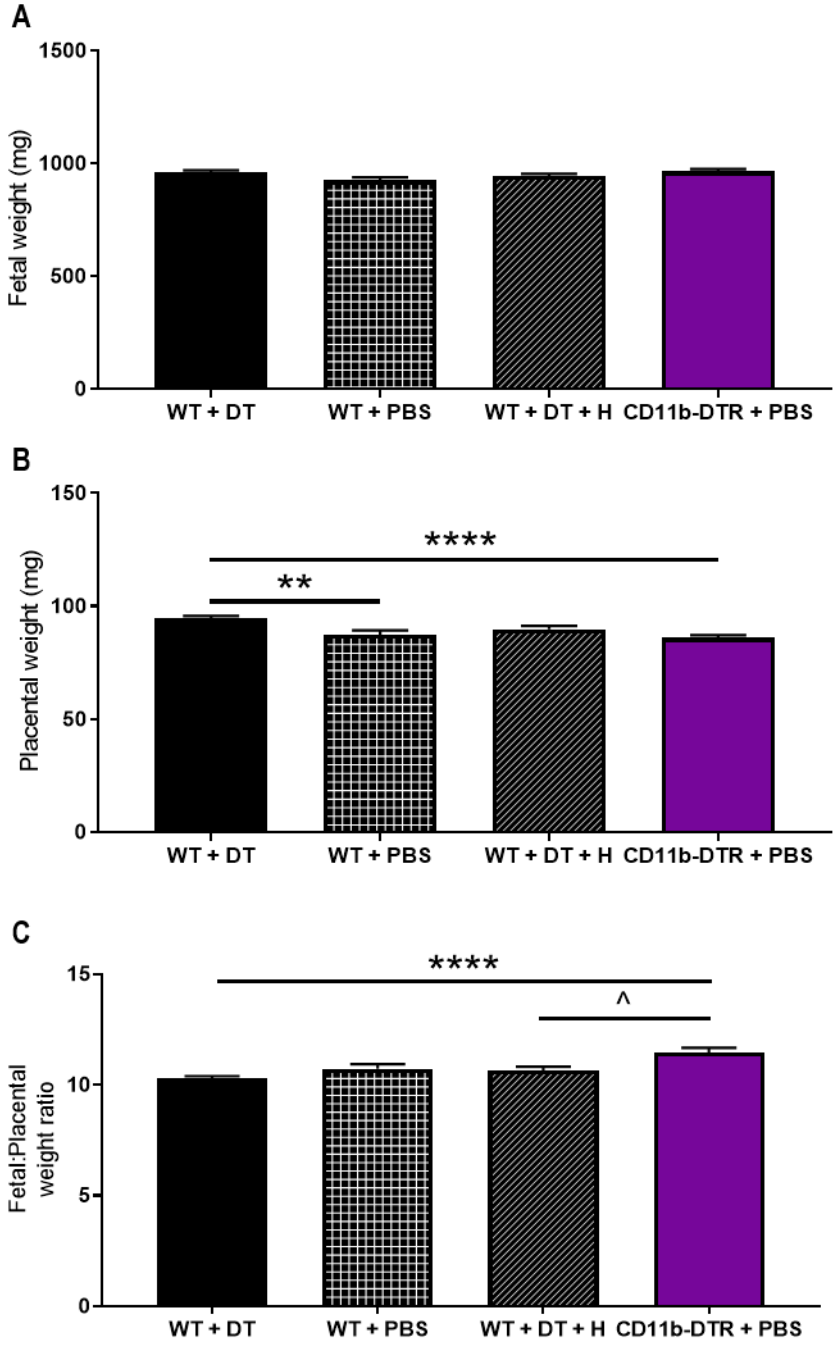

Figure 9.31: DT treatment has no impact on fetal growth in WT mice on day 17.5 pc.
WT and CD11b-DTR females were mated to BALB/c stud males and all mice were administered either 25 ng/g DT or PBS on day 5.5 pc. On day 5.5 pc, a cohort of WT mice received P4 pellets prior to DT administration and received an E2 pellet on day 9.5 pc. Fetal weight (A), placental weight (B), and fetal to placental weight ratio (C) was calculated. Data are presented as estimated marginal means ± SEM where a mixed-model analysis was performed to calculate estimated marginal means using total number of viable pups as the co-variate Statistical analysis was performed using one-way ANOVA with Sidak's multiple comparisons test. * indicates statistical significance ($p<0.05$) compared to WT + DT mice; **$p<0.01$ and ****$p<0.0001$. ^ indicates statistical significance ($p<0.05$) compared to WT + DT + H mice; ^$p<0.05$.

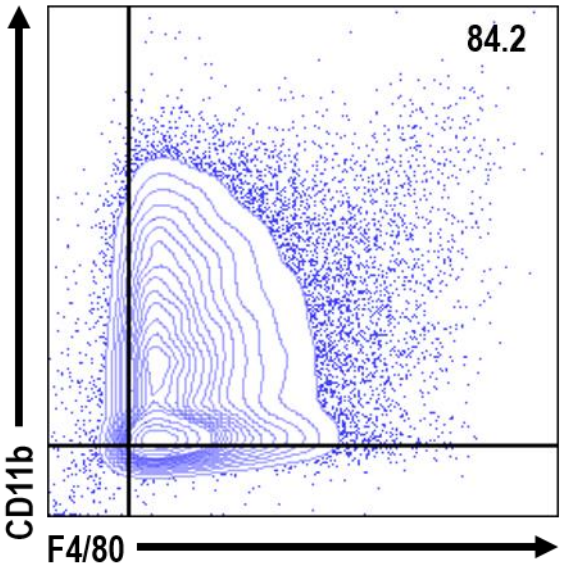

Figure 9.32: Over 80% of BMDM express F4/80 and CD11b prior to transfer.
BMDM were removed from petri dishes and stained to assess F4/80 and CD11b expression to confirm that the cells were macrophages prior to i.v. injection.

CHAPTER 10
BIBLIOGRAPHY

ABRAHAMS, V. M., KIM, Y. M., STRASZEWSKI, S. L., ROMERO, R. & MOR, G. 2004. Macrophages and apoptotic cell clearance during pregnancy. *American Journal of Reproductive Immunology,* 51**,** 275-282.

ABRAHAMS, V. M., VISINTIN, I., ALDO, P. B., GULLER, S., ROMERO, R. & MOR, G. 2005. A role for TLRs in the regulation of immune cell migration by first trimester trophoblast cells. *J Immunol,* 175**,** 8096-104.

ADAMSON, S. L., LU, Y., WHITELEY, K. J., HOLMYARD, D., HEMBERGER, M., PFARRER, C. & CROSS, J. C. 2002. Interactions between Trophoblast Cells and the Maternal and Fetal Circulation in the Mouse Placenta. *Developmental Biology,* 250**,** 358-373.

AGOSTINIS, C., BULLA, R., TRIPODO, C., GISMONDI, A., STABILE, H., BOSSI, F., GUARNOTTA, C., GARLANDA, C., DE SETA, F., SPESSOTTO, P., SANTONI, A., GHEBREHIWET, B., GIRARDI, G. & TEDESCO, F. 2010. An Alternative Role of C1q in Cell Migration and Tissue Remodeling: Contribution to Trophoblast Invasion and Placental Development. *The Journal of Immunology,* 185**,** 4420-4429.

AGOSTINIS, C., STAMPALIJA, T., TANNETTA, D., LOGANES, C., VECCHI BRUMATTI, L., DE SETA, F., CELEGHINI, C., RADILLO, O., SARGENT, I., TEDESCO, F. & BULLA, R. 2016. Complement component C1q as potential diagnostic but not predictive marker of preeclampsia. *American Journal of Reproductive Immunology,* 76**,** 475-481.

AGOSTINIS, C., TEDESCO, F. & BULLA, R. 2017. Alternative functions of the complement protein C1q at embryo implantation site. *Journal of Reproductive Immunology,* 119**,** 74-80.

ALEXANDER, C. M., HANSELL, E. J., BEHRENDTSEN, O., FLANNERY, M. L., KISHNANI, N. S., HAWKES, S. P. & WERB, Z. 1996. Expression and function of matrix metalloproteinases and their inhibitors at the maternal-embryonic boundary during mouse embryo implantation. *Development,* 122**,** 1723-1736.

ALITALO, K. & CARMELIET, P. 2002. Molecular mechanisms of lymphangiogenesis in health and disease. *Cancer cell,* 1**,** 219-227.

ALUVIHARE, V. R., KALLIKOURDIS, M. & BETZ, A. G. 2004. Regulatory T cells mediate maternal tolerance to the fetus. *Nature Immunology,* 5**,** 266-271.

AMIT, I., WINTER, D. R. & JUNG, S. 2016. The role of the local environment and epigenetics in shaping macrophage identity and their effect on tissue homeostasis. *Nat Immunol,* 17**,** 18-25.

ANACKER, J., SEGERER, S. E., HAGEMANN, C., FEIX, S., KAPP, M., BAUSCH, R. & KÄMMERER, U. 2011. Human decidua and invasive trophoblasts are rich sources of nearly all human matrix metalloproteinases. *Molecular human reproduction,* 17**,** 637-652.

ANAND-IVELL, R. & IVELL, R. 2014. Regulation of the reproductive cycle and early pregnancy by relaxin family peptides. *Molecular and Cellular Endocrinology,* 382**,** 472-479.

ANDERSON, A. C., ANDERSON, D. E., BREGOLI, L., HASTINGS, W. D., KASSAM, N., LEI, C., CHANDWASKAR, R., KARMAN, J., SU, E. W., HIRASHIMA, M., BRUCE, J. N., KANE, L. P., KUCHROO, V. K. & HAFLER, D. A. 2007. Promotion of Tissue Inflammation by the Immune Receptor Tim-3 Expressed on Innate Immune Cells. *Science,* 318**,** 1141-1143.

ANDRAWEERA, P., DEKKER, G. & ROBERTS, C. 2012. The vascular endothelial growth factor family in adverse pregnancy outcomes. *Human reproduction update,* 18**,** 436-457.

ANDRAWEERA, P. H., GATFORD, K. L., CARE, A. S., BIANCO-MIOTTO, T., LASSI, Z. S., DEKKER, G. A., ARSTALL, M. & ROBERTS, C. T. 2020. Mechanisms linking exposure to preeclampsia in utero and the risk for cardiovascular disease. *J. Dev. Orig. Health Dis,* 19**,** 1-8.

ANTEBY, E. Y., NATANSON-YARON, S., GREENFIELD, C., GOLDMAN-WOHL, D., HAIMOV-KOCHMAN, R., HOLZER, H. & YAGEL, S. 2005. Human Placental Hofbauer Cells Express Sprouty Proteins: a Possible Modulating Mechanism of Villous Branching. *Placenta,* 26**,** 476-483.

ANUMBA, D. O. C., EL GELANY, S., ELLIOTT, S. L. & LI, T. C. 2009. Serum relaxin levels are reduced in pregnant women with a history of recurrent miscarriage, and correlate with maternal uterine artery Doppler indices in first trimester. *European Journal of Obstetrics & Gynecology and Reproductive Biology,* 147**,** 41-45.

ARCECI, R. J., SHANAHAN, F., STANLEY, E. R. & POLLARD, J. W. 1989. Temporal expression and location of colony-stimulating factor 1 (CSF-1) and its receptor in the female reproductive tract are consistent with CSF-1-regulated placental development. *Proc Natl Acad Sci U S A,* 86**,** 8818-22.

ASHKAR, A. A., DI SANTO, J. P. & CROY, B. A. 2000. Interferon γ Contributes to Initiation of Uterine Vascular Modification, Decidual Integrity, and Uterine Natural Killer Cell Maturation during Normal Murine Pregnancy. *The Journal of Experimental Medicine,* 192**,** 259-270.

ASSALI, N. S., RAURAMO, L. & PELTONEN, T. 1960. Measurement of uterine blood flow and uterine metabolism. VIII. Uterine and fetal blood flow and oxygen consumption in early human pregnancy. *Am J Obstet Gynecol,* 79**,** 86-98.

AUTIERO, M., WALTENBERGER, J., COMMUNI, D., KRANZ, A., MOONS, L., LAMBRECHTS, D., KROLL, J., PLAISANCE, S., DE MOL, M. & BONO, F. 2003. Role of PlGF in the intra-and intermolecular cross talk between the VEGF receptors Flt1 and Flk1. *Nature Medicine,* 9**,** 936-943.

BAIN, C. C. & SCHRIDDE, A. 2018. Origin, Differentiation, and Function of Intestinal Macrophages. *Frontiers in Immunology,* 9.

BALL, E., BULMER, J. N., AYIS, S., LYALL, F. & ROBSON, S. C. 2006. Late sporadic miscarriage is associated with abnormalities in spiral artery transformation and trophoblast invasion. *J Pathol,* 208**,** 535-42.

BATHGATE, R. A., IVELL, R., SANBORN, B. M., SHERWOOD, O. D. & SUMMERS, R. J. 2006. Recommendations for the Nomenclature of Receptors for Relaxin Family Peptides. *Pharmacological Reviews,* 58**,** 7-31.

BELL, R. J., EDDIE, L. W., LESTER, A. R., WOOD, E. C., JOHNSTON, P. D. & NIALL, H. D. 1987. Relaxin in Human Pregnancy Serum Measured With an Homologous Radioimmunoassay. *Obstetrics & Gynecology,* 69**,** 585-589.

BENIRSCHKE, K. 1983. Placentation. *Journal of Experimental Zoology,* 228**,** 385-389.

BERKANE, N., LIERE, P., OUDINET, J.-P., HERTIG, A., LEFÈVRE, G., PLUCHINO, N., SCHUMACHER, M. & CHABBERT-BUFFET, N. 2017. From Pregnancy to Preeclampsia: A Key Role for Estrogens. *Endocrine Reviews,* 38**,** 123-144.

BERNSTEIN, I. M., MEYER, M. C., OSOL, G. & WARD, K. 1998. Intolerance to volume expansion: a theorized mechanism for the development of preeclampsia. *Obstetrics & Gynecology,* 92**,** 306-308.

BEWLEY, S., COOPER, D. & CAMPBELL, S. 1991. Doppler investigation of uteroplacental blood flow resistance in the second trimester: a screening study for pre-eclampsia and intrauterine growth retardation. *Br J Obstet Gynaecol,* 98**,** 871-9.

BINART, N., HELLOCO, C., ORMANDY, C. J., BARRA, J., CLEMENT-LACROIX, P., BARAN, N. & KELLY, P. A. 2000. Rescue of preimplantatory egg development and embryo implantation in prolactin receptor-deficient mice after progesterone administration. *Endocrinology,* 141**,** 2691-7.

BÖCKLE, B. C., SÖLDER, E., KIND, S., ROMANI, N. & SEPP, N. T. 2008. DC-SIGN+ CD163+ Macrophages Expressing Hyaluronan Receptor LYVE-1 Are Located within Chorion Villi of the Placenta. *Placenta,* 29**,** 187-192.

BOELDT, D. S. & BIRD, I. M. 2017. Vascular adaptation in pregnancy and endothelial dysfunction in preeclampsia. 232**,** R27.

BÖING, M., BRAND-SABERI, B. & NAPIREI, M. 2018. Murine transcription factor Math6 is a regulator of placenta development. *Scientific Reports,* 8**,** 14997.

BOSSI, F., TRIPODO, C., RIZZI, L., BULLA, R., AGOSTINIS, C., GUARNOTTA, C., MUNAUT, C., BALDASSARRE, G., PAPA, G., ZORZET, S., GHEBREHIWET, B., LING, G. S., BOTTO, M. & TEDESCO, F. 2014. C1q as a unique player in angiogenesis with therapeutic implication in wound healing. 111**,** 4209-4214.

BOUNDS, K. R., NEWELL-ROGERS, M. K. & MITCHELL, B. M. 2015. Four Pathways Involving Innate Immunity in the Pathogenesis of Preeclampsia. *Frontiers in Cardiovascular Medicine,* 2.

BRANDON, J. M. 1994. Distribution of macrophages in the mouse uterus from one day to three months after parturition, as defined by the immunohistochemical localization of the macrophage-restricted antigens F4/80 and macrosialin. *Anat Rec,* 240**,** 233-42.

BRÄNNSTRÖM, M., MAYRHOFER, G. & ROBERTSON, S. A. 1993. Localization of Leukocyte Subsets in the Rat Ovary during the Periovulatory Period1. *Biology of Reproduction,* 48**,** 277-286.

BRANNSTROM, M., PASCOE, V., NORMAN, R. J. & MCCLURE, N. 1994. Localization of leukocyte subsets in the follicle wall and in the corpus luteum throughout the human menstrual cycle**Supported by a Queen Elizabeth Hospital Fellowships, Woodville, South Australia, and by grant 4982 from the Swedish Medical Research Council, Assar Gabrie Research Foundation, Tore Nilssons Foundation, and Goteborg Medical Society, Goteborg, Sweden. *Fertility and Sterility,* 61**,** 488-495.

BRENNAN, L. J., MORTON, J. S. & DAVIDGE, S. T. 2014. Vascular dysfunction in preeclampsia. *Microcirculation,* 21**,** 4-14.

BROWN, M. B., VON CHAMIER, M., ALLAM, A. B. & REYES, L. 2014. M1/M2 Macrophage Polarity in Normal and Complicated Pregnancy. *Frontiers in Immunology,* 5**,** 606.

BRUCE, N. W. 1976. The distribution of blood flow to the reproductive organs of rats near term. *J Reprod Fertil,* 46**,** 359-62.

BULLA, R., AGOSTINIS, C., BOSSI, F., RIZZI, L., DEBEUS, A., TRIPODO, C., RADILLO, O., DE SETA, F., GHEBREHIWET, B. & TEDESCO, F. 2008. Decidual endothelial cells express surface-bound C1q as a molecular bridge between endovascular trophoblast and decidual endothelium. *Molecular Immunology,* 45**,** 2629-2640.

BULLA, R., BOSSI, F. & TEDESCO, F. 2012. The Complement System at the Embryo Implantation Site: Friend or Foe? *Frontiers in Immunology,* 3.

BURTON, G. J. & FOWDEN, A. L. 2012. Review: The placenta and developmental programming: balancing fetal nutrient demands with maternal resource allocation. *Placenta,* 33 Suppl**,** S23-7.

BURTON, G. J., FOWDEN, A. L. & THORNBURG, K. L. 2016. Placental Origins of Chronic Disease. *Physiol Rev,* 96**,** 1509-65.

BURTON, G. J. & JAUNIAUX, E. 2018. Pathophysiology of placental-derived fetal growth restriction. *American Journal of Obstetrics & Gynecology,* 218**,** S745-S761.

BURTON, G. J., WOODS, A. W., JAUNIAUX, E. & KINGDOM, J. C. 2009. Rheological and physiological consequences of conversion of the maternal spiral arteries for uteroplacental blood flow during human pregnancy. *Placenta,* 30**,** 473-82.

BYERS, S. L., WILES, M. V., DUNN, S. L. & TAFT, R. A. 2012. Mouse estrous cycle identification tool and images. *PloS one,* 7**,** e35538.

CAI, J., LI, M., HUANG, Q., FU, X. & WU, H. 2016. Differences in cytokine expression and STAT3 activation between healthy controls and patients of unexplained recurrent spontaneous abortion (URSA) during early pregnancy. *PloS one,* 11**,** e0163252.

CAI, L., ZHANG, J. & DUAN, E. 2003. Dynamic distribution of epidermal growth factor during mouse embryo peri-implantation. *Cytokine,* 23**,** 170-8.

CAILHIER, J. F., PARTOLINA, M., VUTHOORI, S., WU, S., KO, K., WATSON, S., SAVILL, J., HUGHES, J. & LANG, R. A. 2005. Conditional Macrophage Ablation Demonstrates That Resident Macrophages Initiate Acute Peritoneal Inflammation. *The Journal of Immunology,* 174**,** 2336-2342.

CAPOBIANCO, A., MONNO, A., COTTONE, L., VENNERI, M. A., BIZIATO, D., DI PUPPO, F., FERRARI, S., DE PALMA, M., MANFREDI, A. A. & ROVERE-QUERINI, P. 2011. Proangiogenic Tie2+ Macrophages Infiltrate Human and Murine Endometriotic Lesions and Dictate Their Growth in a Mouse Model of the Disease. *The American Journal of Pathology,* 179**,** 2651-2659.

CARE, A. S., BOURQUE, S. L., MORTON, J. S., HJARTARSON, E. P., ROBERTSON, S. A. & DAVIDGE, S. T. 2018. Reduction in Regulatory T Cells in Early Pregnancy Causes Uterine Artery Dysfunction in Mice. *Hypertension,* 72**,** 177-187.

CARE, A. S., DIENER, K. R., JASPER, M. J., BROWN, H. M., INGMAN, W. V. & ROBERTSON, S. A. 2013. Macrophages regulate corpus luteum development during embryo implantation in mice. *Journal of Clinical Investigation,* 123**,** 3472-87.

CARE, A. S., INGMAN, W. V., MOLDENHAUER, L. M., JASPER, M. J. & ROBERTSON, S. A. 2014. Ovarian Steroid Hormone-Regulated Uterine Remodeling Occurs Independently of Macrophages in Mice. *Biology of Reproduction,* 91.

CARLINO, C., STABILE, H., MORRONE, S., BULLA, R., SORIANI, A., AGOSTINIS, C., BOSSI, F., MOCCI, C., SARAZANI, F., TEDESCO, F., SANTONI, A. & GISMONDI, A. 2008. Recruitment of circulating NK cells through decidual tissues: a possible mechanism controlling NK cell accumulation in the uterus during early pregnancy. *Blood,* 111**,** 3108-15.

CARMELIET, P., MOONS, L., LUTTUN, A., VINCENTI, V., COMPERNOLLE, V., DE MOL, M., WU, Y., BONO, F., DEVY, L. & BECK, H. 2001. Synergism between vascular endothelial growth factor and placental growth factor contributes to angiogenesis and plasma extravasation in pathological conditions. *Nature medicine,* 7**,** 575-583.

CARSON, D. D., BAGCHI, I., DEY, S. K., ENDERS, A. C., FAZLEABAS, A. T., LESSEY, B. A. & YOSHINAGA, K. 2000. Embryo implantation. *Developmental biology,* 223**,** 217-237.

CARSON, W. E., GIRI, J. G., LINDEMANN, M. J., LINETT, M. L., AHDIEH, M., PAXTON, R., ANDERSON, D., EISENMANN, J., GRABSTEIN, K. & CALIGIURI, M. A. 1994. Interleukin (IL) 15 is a novel cytokine that activates human natural killer cells via components of the IL-2 receptor. *The Journal of experimental medicine,* 180**,** 1395-1403.

CASTELUCCI, B. G., CONSONNI, S. R., ROSA, V. S. & JOAZEIRO, P. P. 2019. Recruitment of monocytes and mature macrophages in mouse pubic symphysis relaxation during pregnancy and postpartum recovery. *Biology of reproduction,* 101**,** 466-477.

CATON, D. & KALRA, P. S. 1986. Endogenous hormones and regulation of uterine blood flow during pregnancy. *Am J Physiol,* 250**,** R365-9.

CAULIN-GLASER, T., GARCÍA-CARDEÑA, G., SARREL, P., SESSA, W. C. & BENDER, J. R. 1997. 17β-Estradiol Regulation of Human Endothelial Cell Basal Nitric Oxide Release, Independent of Cytosolic Ca2+ Mobilization. *Circulation Research,* 81**,** 885-892.

CHA, J., SUN, X. & DEY, S. K. 2012. Mechanisms of implantation: strategies for successful pregnancy. *Nat Med,* 18**,** 1754-1767.

CHABTINI, L., MFARREJ, B., MOUNAYAR, M., ZHU, B., BATAL, I., DAKLE, P. J., SMITH, B. D., BOENISCH, O., NAJAFIAN, N., AKIBA, H., YAGITA, H. & GULERIA, I. 2013. TIM-3 Regulates Innate Immune Cells To Induce Fetomaternal Tolerance. *The Journal of Immunology,* 190**,** 88-96.

CHANTAKRU, S., MILLER, C., ROACH, L. E., KUZIEL, W. A., MAEDA, N., WANG, W.-C., EVANS, S. S. & CROY, B. A. 2002. Contributions from self-renewal and trafficking to the uterine NK cell population of early pregnancy. *The Journal of Immunology,* 168**,** 22-28.

CHAU, K., HENNESSY, A. & MAKRIS, A. 2017. Placental growth factor and pre-eclampsia. *Journal of human hypertension,* 31**,** 782-786.

CHEN, X., JIN, X., LIU, L., MAN, C. W., HUANG, J., WANG, C. C., ZHANG, S. & LI, T. C. 2015. Differential expression of vascular endothelial growth factor angiogenic factors in different endometrial compartments in women who have an elevated progesterone level before oocyte retrieval, during in vitro fertilization–embryo transfer treatment. *Fertility and sterility,* 104**,** 1030-1036.

CHENG, J. G., CHEN, J. R., HERNANDEZ, L., ALVORD, W. G. & STEWART, C. L. 2001. Dual control of LIF expression and LIF receptor function regulate Stat3 activation at the onset of uterine receptivity and embryo implantation. *Proc Natl Acad Sci U S A,* 98**,** 8680-5.

CHIN, P. Y., DORIAN, C., SHARKEY, D. J., HUTCHINSON, M. R., RICE, K. C., MOLDENHAUER, L. M. & ROBERTSON, S. A. 2019. Toll-Like Receptor-4 Antagonist (+)-Naloxone Confers Sexually Dimorphic Protection From Inflammation-Induced Fetal Programming in Mice. *Endocrinology,* 160**,** 2646-2662.

CHOUDHURY, R. H., DUNK, C. E., LYE, S. J., APLIN, J. D., HARRIS, L. K. & JONES, R. L. 2017. Extravillous Trophoblast and Endothelial Cell Crosstalk Mediates Leukocyte Infiltration to the Early Remodeling Decidual Spiral Arteriole Wall. *The Journal of Immunology*.

CHUA, A. C. L., HODSON, L. J., MOLDENHAUER, L. M., ROBERTSON, S. A. & INGMAN, W. V. 2010. Dual roles for macrophages in ovarian cycle-associated development and remodelling of the mammary gland epithelium. *Development,* 137**,** 4229-4238.

CLAUSEN, B. E., BURKHARDT, C., REITH, W., RENKAWITZ, R. & FORSTER, I. 1999. Conditional gene targeting in macrophages and granulocytes using LysMcre mice. *Transgenic Res,* 8**,** 265-77.

CLEWELL, W. H., CARSON, B. A. & MESCHIA, G. 1977. Comparison of uterotrophic and vascular effects of estradiol-17β and estriol in the mature organism. *American Journal of Obstetrics and Gynecology,* 129**,** 384-388.

CO, E. C., GORMLEY, M., KAPIDZIC, M., ROSEN, D. B., SCOTT, M. A., STOLP, H. A. R., MCMASTER, M., LANIER, L. L., BÁRCENA, A. & FISHER, S. J. 2013. Maternal Decidual Macrophages Inhibit NK Cell Killing of Invasive Cytotrophoblasts During Human Pregnancy1. *Biology of Reproduction,* 88**,** 155, 1-9-155, 1-9.

COAN, P. M., CONROY, N., BURTON, G. J. & FERGUSON-SMITH, A. C. 2006. Origin and characteristics of glycogen cells in the developing murine placenta. *Dev Dyn,* 235**,** 3280-94.

COAN, P. M., FERGUSON-SMITH, A. C. & BURTON, G. J. 2004a. Developmental dynamics of the definitive mouse placenta assessed by stereology. *Biol Reprod,* 70**,** 1806-13.

COAN, P. M., FERGUSON-SMITH, A. C. & BURTON, G. J. 2004b. Developmental Dynamics of the Definitive Mouse Placenta Assessed by Stereology1. *Biology of Reproduction,* 70**,** 1806-1813.

COAN, P. M., FERGUSON-SMITH, A. C. & BURTON, G. J. 2005. Ultrastructural changes in the interhaemal membrane and junctional zone of the murine chorioallantoic placenta across gestation. *Journal of anatomy,* 207**,** 783-796.

COFFELT, S. B., CHEN, Y. Y., MUTHANA, M., WELFORD, A. F., TAL, A. O., SCHOLZ, A., PLATE, K. H., REISS, Y., MURDOCH, C., DE PALMA, M. & LEWIS, C. E. 2011. Angiopoietin 2 stimulates TIE2-expressing monocytes to suppress T cell activation and to promote regulatory T cell expansion. *J Immunol,* 186**,** 4183-90.

COFFELT, S. B., TAL, A. O., SCHOLZ, A., DE PALMA, M., PATEL, S., URBICH, C., BISWAS, S. K., MURDOCH, C., PLATE, K. H., REISS, Y. & LEWIS, C. E. 2010. Angiopoietin-2 Regulates Gene Expression in TIE2-Expressing Monocytes and Augments Their Inherent Proangiogenic Functions. *Cancer Research,* 70**,** 5270-5280.

COHEN, P. E., ZHU, L., NISHIMURA, K. & POLLARD, J. W. 2002. Colony-Stimulating Factor 1 Regulation of Neuroendocrine Pathways that Control Gonadal Function in Mice. *Endocrinology,* 143**,** 1413-1422.

COLEGIO, O. R., CHU, N.-Q., SZABO, A. L., CHU, T., RHEBERGEN, A. M., JAIRAM, V., CYRUS, N., BROKOWSKI, C. E., EISENBARTH, S. C., PHILLIPS, G. M., CLINE, G. W., PHILLIPS, A. J. &

MEDZHITOV, R. 2014. Functional polarization of tumour-associated macrophages by tumour-derived lactic acid. *Nature,* 513**,** 559-563.

COLLINS, M. K., TAY, C.-S. & ERLEBACHER, A. 2009. Dendritic cell entrapment within the pregnant uterus inhibits immune surveillance of the maternal/fetal interface in mice. *The Journal of clinical investigation,* 119**,** 2062-2073.

COMBA, C., BASTU, E., DURAL, O., YASA, C., KESKIN, G., OZSURMELI, M., BUYRU, F. & SERDAROGLU, H. 2015. Role of inflammatory mediators in patients with recurrent pregnancy loss. *Fertility and Sterility,* 104**,** 1467-1474.e1.

CONDEELIS, J. & POLLARD, J. W. 2006. Macrophages: Obligate Partners for Tumor Cell Migration, Invasion, and Metastasis. *Cell,* 124**,** 263-266.

CONROY, A. L., SILVER, K. L., ZHONG, K., RENNIE, M., WARD, P., SARMA, J. V., MOLYNEUX, M. E., SLED, J., FLETCHER, J. F., ROGERSON, S. & KAIN, K. C. 2013. Complement activation and the resulting placental vascular insufficiency drives fetal growth restriction associated with placental malaria. *Cell Host Microbe,* 13**,** 215-26.

CORTES-HERNANDEZ, J., FOSSATI-JIMACK, L., PETRY, F., LOOS, M., IZUI, S., WALPORT, M. J., COOK, H. T. & BOTTO, M. 2004. Restoration of C1q levels by bone marrow transplantation attenuates autoimmune disease associated with C1q deficiency in mice. *Eur J Immunol,* 34**,** 3713-22.

CORZO, C. A., CONDAMINE, T., LU, L., COTTER, M. J., YOUN, J. I., CHENG, P., CHO, H. I., CELIS, E., QUICENO, D. G., PADHYA, T., MCCAFFREY, T. V., MCCAFFREY, J. C. & GABRILOVICH, D. I. 2010. HIF-1alpha regulates function and differentiation of myeloid-derived suppressor cells in the tumor microenvironment. *J Exp Med,* 207**,** 2439-53.

CROY, B. A., HE, H., ESADEG, S., WEI, Q., MCCARTNEY, D., ZHANG, J., BORZYCHOWSKI, A., ASHKAR, A. A., BLACK, G. P., EVANS, S. S., CHANTAKRU, S., VAN DEN HEUVEL, M., PAFFARO, V. A. & YAMADA, A. T. 2003. Uterine Natural Killer Cells: Insights to their Cellular and Molecular Biology from Mouse Modelling. *Reproduction (Cambridge, England),* 126**,** 149-160.

CUFFE, J. S. M., WALTON, S. L., SINGH, R. R., SPIERS, J. G., BIELEFELDT-OHMANN, H., WILKINSON, L., LITTLE, M. H. & MORITZ, K. M. 2014. Mid- to late term hypoxia in the mouse alters placental morphology, glucocorticoid regulatory pathways and nutrient transporters in a sex-specific manner. *The Journal of Physiology,* 592**,** 3127-3141.

CULLINAN-BOVE, K. & KOOS, R. D. 1993. Vascular endothelial growth factor/vascular permeability factor expression in the rat uterus: rapid stimulation by estrogen correlates with estrogen-induced increases in uterine capillary permeability and growth. *Endocrinology,* 133**,** 829-37.

CURSIEFEN, C., CHEN, L., BORGES, L. P., JACKSON, D., CAO, J., RADZIEJEWSKI, C., D'AMORE, P. A., DANA, M. R., WIEGAND, S. J. & STREILEIN, J. W. 2004. VEGF-A stimulates lymphangiogenesis and hemangiogenesis in inflammatory neovascularization via macrophage recruitment. *J Clin Invest,* 113**,** 1040-50.

DARASSE-JÈZE, G., KLATZMANN, D., CHARLOTTE, F., SALOMON, B. L. & COHEN, J. L. 2006. CD4+CD25+ regulatory/suppressor T cells prevent allogeneic fetus rejection in mice. *Immunology Letters,* 102**,** 106-109.

DARMOCHWAL-KOLARZ, D., KLUDKA-STERNIK, M., TABARKIEWICZ, J., KOLARZ, B., ROLINSKI, J., LESZCZYNSKA-GORZELAK, B. & OLESZCZUK, J. 2012. The predominance of Th17 lymphocytes and decreased number and function of Treg cells in preeclampsia. *Journal of reproductive immunology,* 93**,** 75-81.

DARMOCHWAL-KOLARZ, D., MICHALAK, M., KOLARZ, B., PRZEGALINSKA-KALAMUCKA, M., BOJARSKA-JUNAK, A., SLIWA, D. & OLESZCZUK, J. 2017. The Role of Interleukin-17, Interleukin-23, and Transforming Growth Factor-β in Pregnancy Complicated by Placental Insufficiency. *BioMed Research International,* 2017**,** 5.

DAWSON, C. A., PAL, B., VAILLANT, F., GANDOLFO, L. C., LIU, Z., BLERIOT, C., GINHOUX, F., SMYTH, G. K., LINDEMAN, G. J., MUELLER, S. N., RIOS, A. C. & VISVADER, J. E. 2020. Tissue-resident ductal macrophages survey the mammary epithelium and facilitate tissue remodelling. *Nature Cell Biology*.

DE FALCO, S. 2012. The discovery of placenta growth factor and its biological activity. *Exp Mol Med,* 44**,** 1-9.

DE, M., SANFORD, T. & WOOD, G. W. 1993. Relationship between macrophage colony-stimulating factor production by uterine epithelial cells and accumulation and distribution of macrophages in the uterus of pregnant mice. *J Leukoc Biol,* 53**,** 240-8.

DE PALMA, M., VENNERI, M. A., GALLI, R., SERGI, L. S., POLITI, L. S., SAMPAOLESI, M. & NALDINI, L. 2005. Tie2 identifies a hematopoietic lineage of proangiogenic monocytes required for tumor vessel formation and a mesenchymal population of pericyte progenitors. *Cancer Cell,* 8**,** 211-226.

DE PALMA, M. & LEWIS, CLAIRE E. 2013. Macrophage Regulation of Tumor Responses to Anticancer Therapies. *Cancer Cell,* 23**,** 277-286.

DEKEL, N., GNAINSKY, Y., GRANOT, I., RACICOT, K. & MOR, G. 2014. The Role of Inflammation for a Successful Implantation. *American Journal of Reproductive Immunology,* 72**,** 141-147.

DELCLAUX, C., DELACOURT, C., D'ORTHO, M. P., BOYER, V., LAFUMA, C. & HARF, A. 1996. Role of gelatinase B and elastase in human polymorphonuclear neutrophil migration across basement membrane. *American Journal of Respiratory Cell and Molecular Biology,* 14**,** 288-295.

DEMIR, R., KAYISLI, U. A., SEVAL, Y., CELIK-OZENCI, C., KORGUN, E. T., DEMIR-WEUSTEN, A. Y. & HUPPERTZ, B. 2004. Sequential Expression of VEGF and its Receptors in Human Placental Villi During Very Early Pregnancy: Differences Between Placental Vasculogenesis and Angiogenesis. *Placenta,* 25**,** 560-572.

DERZSY, Z., PROHASZKA, Z., RIGO, J., JR., FUST, G. & MOLVAREC, A. 2010. Activation of the complement system in normal pregnancy and preeclampsia. *Mol Immunol,* 47**,** 1500-6.

DOUGLAS, N. C., TANG, H., GOMEZ, R., PYTOWSKI, B., HICKLIN, D. J., SAUER, C. M., KITAJEWSKI, J., SAUER, M. V. & ZIMMERMANN, R. C. 2009. Vascular Endothelial Growth Factor Receptor 2 (VEGFR-2) Functions to Promote Uterine Decidual Angiogenesis during Early Pregnancy in the Mouse. *Endocrinology,* 150**,** 3845-3854.

DOUGLAS, N. C., ZIMMERMANN, R. C., TAN, Q. K., SULLIVAN-PYKE, C. S., SAUER, M. V., KITAJEWSKI, J. K. & SHAWBER, C. J. 2014. VEGFR-1 blockade disrupts peri-implantation decidual angiogenesis and macrophage recruitment. *Vascular cell,* 6**,** 16.

DOWELL, R. T. & KAUER, C. D. 1997. Maternal hemodynamics and uteroplacental blood flow throughout gestation in conscious rats. *Methods Find Exp Clin Pharmacol,* 19**,** 613-25.

DRUCKMANN, R. & DRUCKMANN, M.-A. 2005. Progesterone and the immunology of pregnancy. *The Journal of Steroid Biochemistry and Molecular Biology,* 97**,** 389-396.

DU, M.-R., WANG, S.-C. & LI, D.-J. 2014. The integrative roles of chemokines at the maternal-fetal interface in early pregnancy. *Cellular & molecular immunology,* 11**,** 438-448.

DUFFIELD, J. S., FORBES, S. J., CONSTANDINOU, C. M., CLAY, S., PARTOLINA, M., VUTHOORI, S., WU, S. J., LANG, R. & IREDALE, J. P. 2005. Selective depletion of macrophages reveals distinct, opposing roles during liver injury and repair. *Journal of Clinical Investigation,* 115**,** 56-65.

DUNK, C., KWAN, M., HAZAN, A., WALKER, S., WRIGHT, J. K., HARRIS, L. K., JONES, R. L., KEATING, S., KINGDOM, J. C. P., WHITTLE, W., MAXWELL, C. & LYE, S. J. 2019. Failure of Decidualization and Maternal Immune Tolerance Underlies Uterovascular Resistance in Intra Uterine Growth Restriction. *Frontiers in Endocrinology,* 10.

DUNN, C. L., KELLY, R. W. & CRITCHLEY, H. O. D. 2003. Decidualization of the human endometrial stromal cell: an enigmatic transformation. *Reproductive BioMedicine Online,* 7**,** 151-161.

EGNERS, A., ERDEM, M. & CRAMER, T. 2016. The Response of Macrophages and Neutrophils to Hypoxia in the Context of Cancer and Other Inflammatory Diseases. *Mediators of Inflammation,* 2016**,** 10.

EIDUKAITE, A. & TAMOSIUNAS, V. 2004. Endometrial and peritoneal macrophages: expression of activation and adhesion molecules. *Am J Reprod Immunol,* 52**,** 113-7.

ENDERS, A. 1995. Transition from lacunar to villous stage of implantation in the macaque, including establishment of the trophoblastic shell. *Cells Tissues Organs,* 152**,** 151-169.

ENDERS, A. C. & SCHLAFKE, S. 1984. Morphology of development in the primate: Blastocyst to villous placental stage. *Journal of Biosciences,* 6**,** 53-61.

ERLEBACHER, A. 2010. Immune surveillance of the maternal/fetal interface: controversies and implications. *Trends in endocrinology and metabolism: TEM,* 21**,** 428-434.

ERLEBACHER, A. 2013. Immunology of the maternal-fetal interface. *Annual Review of Immunology,* 31**,** 387-411.

ERLEBACHER, A. 2014. 19 - Leukocyte Population Dynamics and Functions at the Maternal–Fetal Interface A2 - Croy, B. Anne. *In:* YAMADA, A. T., DEMAYO, F. J. & ADAMSON, S. L. (eds.) *The Guide to Investigation of Mouse Pregnancy.* Boston: Academic Press.

ERLEBACHER, A., ZHANG, D., PARLOW, A. F. & GLIMCHER, L. H. 2004. Ovarian insufficiency and early pregnancy loss induced by activation of the innate immune system. *The Journal of Clinical Investigation,* 114**,** 39-48.

FAAS, M. M. & DE VOS, P. 2017. Uterine NK cells and macrophages in pregnancy. *Placenta,* 56**,** 44-52.

FAAS, M. M., SPAANS, F. & DE VOS, P. 2014. Monocytes and Macrophages in Pregnancy and Pre-Eclampsia. *Frontiers in Immunology,* 5**,** 298.

FACCIABENE, A., PENG, X., HAGEMANN, I. S., BALINT, K., BARCHETTI, A., WANG, L. P., GIMOTTY, P. A., GILKS, C. B., LAL, P., ZHANG, L. & COUKOS, G. 2011. Tumour hypoxia promotes tolerance and angiogenesis via CCL28 and T(reg) cells. *Nature,* 475**,** 226-30.

FANTIN, A., VIEIRA, J. M., GESTRI, G., DENTI, L., SCHWARZ, Q., PRYKHOZHIJ, S., PERI, F., WILSON, S. W. & RUHRBERG, C. 2010. Tissue macrophages act as cellular chaperones for vascular anastomosis downstream of VEGF-mediated endothelial tip cell induction. *Blood,* 116**,** 829-840.

FEST, S., ALDO, P. B., ABRAHAMS, V. M., VISINTIN, I., ALVERO, A., CHEN, R., CHAVEZ, S. L., ROMERO, R. & MOR, G. 2007. Trophoblast-macrophage interactions: a regulatory network for the protection of pregnancy. *American Journal of Reproductive Immunology,* 57**,** 55-66.

FETTKE, F., SCHUMACHER, A., COSTA, S.-D. & ZENCLUSSEN, A. C. 2014. B Cells: The Old New Players in Reproductive Immunology. *Frontiers in Immunology,* 5.

FONG, G.-H., ROSSANT, J., GERTSENSTEIN, M. & BREITMAN, M. L. 1995. Role of the Flt-1 receptor tyrosine kinase in regulating the assembly of vascular endothelium. *Nature,* 376**,** 66-70.

FORGET, M. A., VOORHEES, J. L., COLE, S. L., DAKHLALLAH, D., PATTERSON, I. L., GROSS, A. C., MOLDOVAN, L., MO, X., EVANS, R., MARSH, C. B. & EUBANK, T. D. 2014. Macrophage Colony-Stimulating Factor Augments Tie2-Expressing Monocyte Differentiation, Angiogenic Function, and Recruitment in a Mouse Model of Breast Cancer. *PLoS ONE,* 9**,** e98623.

FOULADI-NASHTA, A. A., JONES, C. J. P., NIJJAR, N., MOHAMET, L., SMITH, A., CHAMBERS, I. & KIMBER, S. J. 2005. Characterization of the uterine phenotype during the peri-implantation period for LIF-null, MF1 strain mice. *Developmental Biology,* 281**,** 1-21.

FOWDEN, A. L., SFERRUZZI-PERRI, A. N., COAN, P. M., CONSTANCIA, M. & BURTON, G. J. 2009. Placental efficiency and adaptation: endocrine regulation. *The Journal of Physiology,* 587**,** 3459-3472.

FRASER, H. M. & WULFF, C. 2003. Angiogenesis in the corpus luteum. *Reproductive Biology and Endocrinology,* 1**,** 88.

FRITZ, J. M., TENNIS, M. A., ORLICKY, D. J., YIN, H., JU, C., REDENTE, E. F., CHOO, K. S., STAAB, T. A., BOUCHARD, R. J., MERRICK, D. T., MALKINSON, A. M. & DWYER-NIELD, L. D. 2014. Depletion of Tumor-Associated Macrophages Slows the Growth of Chemically Induced Mouse Lung Adenocarcinomas. *Frontiers in Immunology,* 5.

FUJIMOTO, S., HAMASAKI, K., UEDA, H. & KAGAWA, H. 1986. Immunoelectron microscope observations on secretion of human placental lactogen (hPL) in the human chorionic villi. *The Anatomical Record,* 216**,** 68-72.

GAFFEN, S. L. 2009. Structure and signalling in the IL-17 receptor family. *Nature Reviews Immunology,* 9**,** 556-567.

GALVAN, M. D., GREENLEE-WACKER, M. C. & BOHLSON, S. S. 2012. C1q and phagocytosis: the perfect complement to a good meal. *Journal of Leukocyte Biology,* 92**,** 489-497.

GANEFF, C., CHATEL, G., MUNAUT, C., FRANKENNE, F., FOIDART, J. M. & WINKLER, R. 2009. The IGF system in in-vitro human decidualization. *Mol Hum Reprod,* 15**,** 27-38.

GATTO, D. & BACHMANN, M. F. 2005. Function of Marginal Zone B Cells in Antiviral B-Cell Responses. 25**,** 331-342.

GAYNOR, L. M. & COLUCCI, F. 2017. Uterine Natural Killer Cells: Functional Distinctions and Influence on Pregnancy in Humans and Mice. *Frontiers in immunology,* 8**,** 467-467.

GEISSMANN, F., MANZ, M. G., JUNG, S., SIEWEKE, M. H., MERAD, M. & LEY, K. 2010. Development of Monocytes, Macrophages, and Dendritic Cells. *Science,* 327**,** 656-661.

GELDENHUYS, J., ROSSOUW, T. M., LOMBAARD, H. A., EHLERS, M. M. & KOCK, M. M. 2018. Disruption in the Regulation of Immune Responses in the Placental Subtype of Preeclampsia. *Frontiers in immunology,* 9**,** 1659-1659.

GELLERSEN, B. & BROSENS, J. J. 2014. Cyclic Decidualization of the Human Endometrium in Reproductive Health and Failure. *Endocrine Reviews,* 35**,** 851-905.

GENTILE, T., BOREL, I. M., ANGELUCCI, J., MIRANDA, S. & MARGNI, R. A. 1992. Preferential synthesis of asymmetric antibodies in rats immunized with paternal particulate antigens. Effect on pregnancy. *Journal of Reproductive Immunology,* 22**,** 173-183.

GEORGIADES, P., FERGUSON-SMITH, A. C. & BURTON, G. J. 2002. Comparative Developmental Anatomy of the Murine and Human Definitive Placentae. *Placenta,* 23**,** 3-19.

GIACOMINI, G., TABIBZADEH, S. S., SATYASWAROOP, P. G., BONSI, L., VITALE, L., BAGNARA, G. P., STRIPPOLI, P. & JASONNI, V. M. 1995. Epithelial cells are the major source of biologically active granulocyte macrophage colony-stimulating factor in human endometrium. *Hum Reprod,* 10**,** 3259-63.

GIBBONS, G. H. & DZAU, V. J. 1994. The Emerging Concept of Vascular Remodeling. *New England Journal of Medicine,* 330**,** 1431-1438.

GIRARDI, G., YARILIN, D., THURMAN, J. M., HOLERS, V. M. & SALMON, J. E. 2006. Complement activation induces dysregulation of angiogenic factors and causes fetal rejection and growth restriction. *The Journal of Experimental Medicine,* 203**,** 2165-2175.

GIRAUDO, E., INOUE, M. & HANAHAN, D. 2004. An amino-bisphosphonate targets MMP-9–expressing macrophages and angiogenesis to impair cervical carcinogenesis. *The Journal of Clinical Investigation,* 114**,** 623-633.

GIVAN, A. L., WHITE, H. D., STERN, J. E., COLBY, E., GOSSELIN, E. J., GUYRE, P. M. & WIRA, C. R. 1997. Flow cytometric analysis of leukocytes in the human female reproductive tract: comparison of fallopian tube, uterus, cervix, and vagina. *Am J Reprod Immunol,* 38**,** 350-9.

GODFREY, K. M. & BARKER, D. J. 2000. Fetal nutrition and adult disease. *Am J Clin Nutr,* 71**,** 1344S-52S.

GOLDENBERG, R. L., CULHANE, J. F., IAMS, J. D. & ROMERO, R. 2008. Epidemiology and causes of preterm birth. *The Lancet,* 371**,** 75-84.

GOMEZ PERDIGUERO, E., KLAPPROTH, K., SCHULZ, C., BUSCH, K., AZZONI, E., CROZET, L., GARNER, H., TROUILLET, C., DE BRUIJN, M. F., GEISSMANN, F. & RODEWALD, H.-R. 2015. Tissue-resident macrophages originate from yolk-sac-derived erythro-myeloid progenitors. *Nature,* 518**,** 547-551.

GOOI, J. H., RICHARDSON, M. L., JELINIC, M., GIRLING, J. E., WLODEK, M. E., TARE, M. & PARRY, L. J. 2013. Enhanced Uterine Artery Stiffness in Aged Pregnant Relaxin Mutant Mice Is Reversed with Exogenous Relaxin Treatment1. *Biology of Reproduction,* 89**,** 18, 1-11-18, 1-11.

GORDON, S. 2003. Alternative activation of macrophages. *Nature Reviews Immunology,* 3**,** 23-35.

GORDON, S. M., NISHIGUCHI, M. A., CHASE, J. M., MANI, S., MAINIGI, M. A. & BEHRENS, E. M. 2020. IFNs Drive Development of Novel IL-15–Responsive Macrophages. *The Journal of Immunology***,** ji2000184.

GOULOPOULOU, S. & DAVIDGE, S. T. 2015. Molecular mechanisms of maternal vascular dysfunction in preeclampsia. *Trends in molecular medicine,* 21**,** 88-97.

GRAHAM, C. H. & MCCRAE, K. R. 1996. Altered expression of gelatinase and surface-associated plasminogen activator activity by trophoblast cells isolated from placentas of preeclamptic patients. *American journal of obstetrics and gynecology,* 175**,** 555-562.

GUENTHER, S., VREKOUSSIS, T., HEUBLEIN, S., BAYER, B., ANZ, D., KNABL, J., NAVROZOGLOU, I., DIAN, D., FRIESE, K., MAKRIGIANNAKIS, A. & JESCHKE, U. 2012. Decidual Macrophages Are Significantly Increased in Spontaneous Miscarriages and Over-Express FasL: A Potential Role for Macrophages in Trophoblast Apoptosis. *International Journal of Molecular Sciences,* 13**,** 9069.

GUIMOND, M.-J., LUROSS, J. A., WANG, B., TERHORST, C., DANIAL, S. & ANNE CROY, B. 1997a. Absence of Natural Killer Cells during Murine Pregnancy is Associated with Reproductive Compromise in TgE26 Mice1. *Biology of Reproduction,* 56**,** 169-179.

GUIMOND, M. J., LUROSS, J. A., WANG, B., TERHORST, C., DANIAL, S. & CROY, B. A. 1997b. Absence of natural killer cells during murine pregnancy is associated with reproductive compromise in TgE26 mice. *Biol Reprod,* 56**,** 169-79.

GUPTA, A. K., HASLER, P., HOLZGREVE, W. & HAHN, S. 2007. Neutrophil NETs: a novel contributor to preeclampsia-associated placental hypoxia? *Semin Immunopathol,* 29**,** 163-7.

GUZMAN-GENUINO, R. M., HAYBALL, J. D. & DIENER, K. R. 2020. Regulatory B Cells: Dark Horse in Pregnancy Immunotherapy? *J Mol Biol*.

HAMILTON, S., OOMOMIAN, Y., STEPHEN, G., SHYNLOVA, O., TOWER, C. L., GARROD, A., LYE, S. J. & JONES, R. L. 2012. Macrophages infiltrate the human and rat decidua during term and preterm labor: evidence that decidual inflammation precedes labor. *Biol Reprod,* 86**,** 39.

HANNA, J., GOLDMAN-WOHL, D., HAMANI, Y., AVRAHAM, I., GREENFIELD, C., NATANSON-YARON, S., PRUS, D., COHEN-DANIEL, L., ARNON, T. I., MANASTER, I., GAZIT, R., YUTKIN, V., BENHARROCH, D., PORGADOR, A., KESHET, E., YAGEL, S. & MANDELBOIM, O. 2006. Decidual NK cells regulate key developmental processes at the human fetal-maternal interface. *Nat Med,* 12**,** 1065-1074.

HANNAN, N. J., EVANS, J. & SALAMONSEN, L. A. 2011. Alternate roles for immune regulators: establishing endometrial receptivity for implantation. *Expert Review of Clinical Immunology,* 7**,** 789-802.

HARRIS, L. K. 2010. Review: Trophoblast-Vascular Cell Interactions in Early Pregnancy: How to Remodel a Vessel. *Placenta,* 31**,** S93-S98.

HASHIMOTO, D., CHOW, A., NOIZAT, C., TEO, P., BEASLEY, MARY B., LEBOEUF, M., BECKER, CHRISTIAN D., SEE, P., PRICE, J., LUCAS, D., GRETER, M., MORTHA, A., BOYER, SCOTT W., FORSBERG, E. C., TANAKA, M., VAN ROOIJEN, N., GARCÍA-SASTRE, A., STANLEY, E. R., GINHOUX, F., FRENETTE, PAUL S. & MERAD, M. 2013. Tissue-Resident

Macrophages Self-Maintain Locally throughout Adult Life with Minimal Contribution from Circulating Monocytes. *Immunity,* 38**,** 792-804.

HEISSIG, B., HATTORI, K., DIAS, S., FRIEDRICH, M., FERRIS, B., HACKETT, N. R., CRYSTAL, R. G., BESMER, P., LYDEN, D., MOORE, M. A. S., WERB, Z. & RAFII, S. 2002. Recruitment of Stem and Progenitor Cells from the Bone Marrow Niche Requires MMP-9 Mediated Release of Kit-Ligand. *Cell,* 109**,** 625-637.

HENDRIX, N. & BERGHELLA, V. 2008. Non-Placental Causes of Intrauterine Growth Restriction. *Seminars in Perinatology,* 32**,** 161-165.

HERINGTON, J. L. & BANY, B. M. 2007a. The conceptus increases secreted phosphoprotein 1 gene expression in the mouse uterus during the progression of decidualization mainly due to its effects on uterine natural killer cells. *Reproduction,* 133**,** 1213-21.

HERINGTON, J. L. & BANY, B. M. 2007b. Effect of the Conceptus on Uterine Natural Killer Cell Numbers and Function in the Mouse Uterus During Decidualization1. *Biology of Reproduction,* 76**,** 579-588.

HOEFFEL, G. & GINHOUX, F. 2018. Fetal monocytes and the origins of tissue-resident macrophages. *Cell Immunol,* 330**,** 5-15.

HU, X.-H., TANG, M.-X., MOR, G. & LIAO, A.-H. 2016. Tim-3: Expression on immune cells and roles at the maternal-fetal interface. *Journal of Reproductive Immunology,* 118**,** 92-99.

HUANG, H., HE, J., YUAN, Y., AOYAGI, E., TAKENAKA, H., ITAGAKI, T., SANNOMIYA, K., TAMAKI, K., HARADA, N., SHONO, M., SHIMIZU, I. & TAKAYAMA, T. 2008. Opposing effects of estradiol and progesterone on the oxidative stress-induced production of chemokine and proinflammatory cytokines in murine peritoneal macrophages. *The Journal of Medical Investigation,* 55**,** 133-141.

HUDA, S., JORDAN, F., BRAY, J., LOVE, G., PAYNE, R., SATTAR, N. & FREEMAN, D. J. 2017. Visceral adipose tissue activated macrophage content and inflammatory adipokine secretion is higher in pre-eclampsia than in healthy pregnancy. *Clinical Science*.

HUNT, J. S. & ROBERTSON, S. A. 1996. Uterine macrophages and environmental programming for pregnancy success. *J Reprod Immunol,* 32**,** 1-25.

ILEKIS, J. V., TSILOU, E., FISHER, S., ABRAHAMS, V. M., SOARES, M. J., CROSS, J. C., ZAMUDIO, S., ILLSLEY, N. P., MYATT, L., COLVIS, C., COSTANTINE, M. M., HAAS, D. M., SADOVSKY, Y., WEINER, C., RYTTING, E. & BIDWELL, G. 2016. Placental origins of adverse pregnancy outcomes: potential molecular targets: an Executive Workshop Summary of the Eunice Kennedy Shriver National Institute of Child Health and Human Development. *American Journal of Obstetrics and Gynecology,* 215**,** S1-S46.

INGMAN, W. V., ROBKER, R. L., WOITTIEZ, K. & ROBERTSON, S. A. 2006. Null Mutation in Transforming Growth Factor β1 Disrupts Ovarian Function and Causes Oocyte Incompetence and Early Embryo Arrest. *Endocrinology,* 147**,** 835-845.

JAISWAL, M. K., MALLERS, T. M., LARSEN, B., KWAK-KIM, J., CHAOUAT, G., GILMAN-SACHS, A. & BEAMAN, K. D. 2012. V-ATPase upregulation during early pregnancy: a possible link to establishment of an inflammatory response during preimplantation period of pregnancy. *Reproduction,* 143**,** 713-25.

JAMES, J. L., SAGHIAN, R., PERWICK, R. & CLARK, A. R. 2018. Trophoblast plugs: impact on utero-placental haemodynamics and spiral artery remodelling. *Human Reproduction,* 33**,** 1430-1441.

JANOT, M., CORTES-DUBLY, M.-L., RODRIGUEZ, S. & HUYNH-DO, U. 2014. Bilateral uterine vessel ligation as a model of intrauterine growth restriction in mice. *Reproductive biology and endocrinology : RB&E,* 12**,** 62-62.

JASPER, M. J., CARE, A. S., SULLIVAN, B., INGMAN, W. V., APLIN, J. D. & ROBERTSON, S. A. 2011. Macrophage-Derived LIF and IL1B Regulate Alpha(1,2)Fucosyltransferase 2 (Fut2) Expression in Mouse Uterine Epithelial Cells During Early Pregnancy1. *Biology of Reproduction,* 84**,** 179-188.

JEYABALAN, A., STEWART, D. R., MCGONIGAL, S. C., POWERS, R. W. & CONRAD, K. P. Low relaxin concentrations in the first trimester are associated with increased risk of developing preeclampsia. Reproductive Sciences, 2009. SAGE PUBLICATIONS INC 2455 TELLER RD, THOUSAND OAKS, CA 91320 USA, 101A-101A.

JIA, K., MA, L., WU, S. & YANG, W. 2019. Serum Levels of Complement Factors C1q, Bb, and H in Normal Pregnancy and Severe Pre-Eclampsia. *Med Sci Monit,* 25**,** 7087-7093.

JIANG, X., DU, M.-R., LI, M. & WANG, H. 2018. Three macrophage subsets are identified in the uterus during early human pregnancy. *Cellular & Molecular Immunology*.

JOBE, S. O., FLING, S. N., RAMADOSS, J. & MAGNESS, R. R. 2011. A novel role for an endothelial adrenergic receptor system in mediating catecholestradiol-induced proliferation of uterine artery endothelial cells. *Hypertension,* 58**,** 874-81.

JOHNSON, E. L. & CHAKRABORTY, R. 2012. Placental Hofbauer cells limit HIV-1 replication and potentially offset mother to child transmission (MTCT) by induction of immunoregulatory cytokines. *Retrovirology,* 9**,** 101.

JOUKOV, V., PAJUSOLA, K., KAIPAINEN, A., CHILOV, D., LAHTINEN, I., KUKK, E., SAKSELA, O., KALKKINEN, N. & ALITALO, K. 1996. A novel vascular endothelial growth factor, VEGF-C, is a ligand for the Flt4 (VEGFR-3) and KDR (VEGFR-2) receptor tyrosine kinases. *EMBO J,* 15**,** 1751.

JUNG, S., ALIBERTI, J., GRAEMMEL, P., SUNSHINE, M. J., KREUTZBERG, G. W., SHER, A. & LITTMAN, D. R. 2000. Analysis of fractalkine receptor CX(3)CR1 function by targeted deletion and green fluorescent protein reporter gene insertion. *Mol Cell Biol,* 20**,** 4106-14.

KAIPIA, A., CHUN, S. Y., EISENHAUER, K. & HSUEH, A. J. 1996. Tumor necrosis factor-alpha and its second messenger, ceramide, stimulate apoptosis in cultured ovarian follicles. *Endocrinology,* 137**,** 4864-4870.

KANG, M.-C., PARK, S. J., KIM, H. J., LEE, J., YU, D. H., BAE, K. B., JI, Y. R., PARK, S. J., JEONG, J. & JANG, W. Y. 2014. Gestational loss and growth restriction by angiogenic defects in placental growth factor transgenic mice. *Arteriosclerosis, thrombosis, and vascular biology,* 34**,** 2276-2282.

KAUFMANN, P., BLACK, S. & HUPPERTZ, B. 2003. Endovascular trophoblast invasion: implications for the pathogenesis of intrauterine growth retardation and preeclampsia. *Biol Reprod,* 69**,** 1-7.

KELLY, B., STONE, S. & POSTON, L. 2000. Cardiovascular adaptation to pregnancy: the role of altered vascular structure. *Fetal and Maternal Medicine Review,* 11**,** 105-116.

KERJASCHKI, D. 2005. The crucial role of macrophages in lymphangiogenesis. *The Journal of clinical investigation,* 115**,** 2316-2319.

KESSENBROCK, K., PLAKS, V. & WERB, Z. 2010. Matrix metalloproteinases: regulators of the tumor microenvironment. *Cell,* 141**,** 52-67.

KHONG, T. Y., DE WOLF, F., ROBERTSON, W. B. & BROSENS, I. 1986. Inadequate maternal vascular response to placentation in pregnancies complicated by pre-eclampsia and by small-for-gestational age infants. *Br J Obstet Gynaecol,* 93**,** 1049-59.

KHONG, Y. & BROSENS, I. 2011. Defective deep placentation. *Best Practice & Research Clinical Obstetrics & Gynaecology,* 25**,** 301-311.

KIECKBUSCH, J., GAYNOR, L. M., MOFFETT, A. & COLUCCI, F. 2014. MHC-dependent inhibition of uterine NK cells impedes fetal growth and decidual vascular remodelling. *Nature communications,* 5**,** 3359.

KIM, C. J., ROMERO, R., CHAEMSAITHONG, P. & KIM, J.-S. 2015. Chronic inflammation of the placenta: definition, classification, pathogenesis, and clinical significance. *American Journal of Obstetrics and Gynecology,* 213**,** S53-S69.

KIM, J. S., ROMERO, R., KIM, M. R., KIM, Y. M., FRIEL, L., ESPINOZA, J. & KIM, C. J. 2008. Involvement of Hofbauer cells and maternal T cells in villitis of unknown aetiology. *Histopathology,* 52**,** 457-464.

KIM, M. J., ROMERO, R., KIM, C. J., TARCA, A. L., CHHAUY, S., LAJEUNESSE, C., LEE, D.-C., DRAGHICI, S., GOTSCH, F., KUSANOVIC, J. P., HASSAN, S. S. & KIM, J.-S. 2009. Villitis of Unknown Etiology Is Associated with a Distinct Pattern of Chemokine Up-Regulation in the Feto-

Maternal and Placental Compartments: Implications for Conjoint Maternal Allograft Rejection and Maternal Anti-Fetal Graft-versus-Host Disease. *The Journal of Immunology,* 182**,** 3919-3927.

KIM, O.-H., KANG, G.-H., NOH, H., CHA, J.-Y., LEE, H.-J., YOON, J.-H., MAMURA, M., NAM, J.-S., LEE, D. H., KIM, Y. A., PARK, Y. J., KIM, H. & OH, B.-C. 2013. Proangiogenic TIE2(+)/CD31(+) Macrophages Are the Predominant Population of Tumor-Associated Macrophages Infiltrating Metastatic Lymph Nodes. *Molecules and Cells,* 36**,** 432-438.

KING, A., HIBY, S., GARDNER, L., JOSEPH, S., BOWEN, J., VERMA, S., BURROWS, T. & LOKE, Y. 2000. Recognition of trophoblast HLA class I molecules by decidual NK cell receptors—a review. *Placenta,* 21**,** S81-S85.

KISANUKI, Y. Y., HAMMER, R. E., MIYAZAKI, J., WILLIAMS, S. C., RICHARDSON, J. A. & YANAGISAWA, M. 2001. Tie2-Cre transgenic mice: a new model for endothelial cell-lineage analysis in vivo. *Dev Biol,* 230**,** 230-42.

KIZAKI, K., USHIZAWA, K., TAKAHASHI, T., YAMADA, O., TODOROKI, J., SATO, T., ITO, A. & HASHIZUME, K. 2008. Gelatinase (MMP-2 and-9) expression profiles during gestation in the bovine endometrium. *Reproductive Biology and Endocrinology,* 6**,** 66.

KNÖFLER, M. & POLLHEIMER, J. 2013. Human placental trophoblast invasion and differentiation: a particular focus on Wnt signaling. *Frontiers in genetics,* 4**,** 190-190.

KOFLER, N. M., SHAWBER, C. J., KANGSAMAKSIN, T., REED, H. O., GALATIOTO, J. & KITAJEWSKI, J. 2011. Notch Signaling in Developmental and Tumor Angiogenesis. *Genes & Cancer,* 2**,** 1106-1116.

KOMATSU, K., MANABE, N., KISO, M., SHIMABE, M. & MIYAMOTO, H. 2003. Changes in localization of immune cells and cytokines in corpora lutea during luteolysis in murine ovaries. *Journal of Experimental Zoology Part A: Comparative Experimental Biology,* 296A**,** 152-159.

KOUREMBANAS, S., HANNAN, R. L. & FALLER, D. V. 1990. Oxygen tension regulates the expression of the platelet-derived growth factor-B chain gene in human endothelial cells. *The Journal of clinical investigation,* 86**,** 670-674.

KREY, G., FRANK, P., SHAIKLY, V., BARRIENTOS, G., CORDO-RUSSO, R., RINGEL, F., MOSCHANSKY, P., CHERNUKHIN, I. V., METODIEV, M., FERNÁNDEZ, N., KLAPP, B. F., ARCK, P. C. & BLOIS, S. M. 2008. In vivo dendritic cell depletion reduces breeding efficiency, affecting implantation and early placental development in mice. *J Mol Med (Berl),* 86**,** 999-1011.

KULANDAVELU, S., WHITELEY, K. J., BAINBRIDGE, S. A., QU, D. & ADAMSON, S. L. 2013. Endothelial NO Synthase Augments Fetoplacental Blood Flow, Placental Vascularization, and Fetal Growth in Mice. *Hypertension,* 61**,** 259-266.

KULANDAVELU, S., WHITELEY, K. J., QU, D., MU, J., BAINBRIDGE, S. A. & ADAMSON, S. L. 2012. Endothelial Nitric Oxide Synthase Deficiency Reduces Uterine Blood Flow, Spiral Artery

Elongation, and Placental Oxygenation in Pregnant MiceNovelty and Significance. *Hypertension,* 60**,** 231-238.

KUMAR, P. & SAIT, S. F. 2011. Luteinizing hormone and its dilemma in ovulation induction. *Journal of Human Reproductive Sciences,* 4**,** 2-7.

LALU, M. M., XU, H. & DAVIDGE, S. T. 2007. Matrix metalloproteinases: control of vascular function and their potential role in preeclampsia. *Front Biosci,* 12**,** 2484-2493.

LASH, G. E., NARUSE, K., ROBSON, A., INNES, B. A., SEARLE, R. F., ROBSON, S. C. & BULMER, J. N. 2011. Interaction between uterine natural killer cells and extravillous trophoblast cells: effect on cytokine and angiogenic growth factor production. *Human Reproduction,* 26**,** 2289-2295.

LASH, G. E., OTUN, H. A., INNES, B. A., PERCIVAL, K., SEARLE, R. F., ROBSON, S. C. & BULMER, J. N. 2010. Regulation of extravillous trophoblast invasion by uterine natural killer cells is dependent on gestational age. *Human Reproduction,* 25**,** 1137-1145.

LASH, G. E., PITMAN, H., MORGAN, H. L., INNES, B. A., AGWU, C. N. & BULMER, J. N. 2016. Decidual macrophages: key regulators of vascular remodeling in human pregnancy. *Journal of Leukocyte Biology*.

LASH, G. E., SCHIESSL, B., KIRKLEY, M., INNES, B. A., COOPER, A., SEARLE, R. F., ROBSON, S. C. & BULMER, J. N. 2006. Expression of angiogenic growth factors by uterine natural killer cells during early pregnancy. *Journal of Leukocyte Biology,* 80**,** 572-580.

LECARPENTIER, E. & TSATSARIS, V. 2016. Angiogenic balance (sFlt-1/PlGF) and preeclampsia. *Annales d'Endocrinologie*.

LEEK, R. D. & HARRIS, A. L. 2002. Tumor-Associated Macrophages in Breast Cancer. *Journal of Mammary Gland Biology and Neoplasia,* 7**,** 177-189.

LESSIN, D. L., HUNT, J. S., KING, C. R. & WOOD, G. W. 1988. Antigen expression by cells near the maternal-fetal interface. *Am J Reprod Immunol Microbiol,* 16**,** 1-7.

LI, M. O., WAN, Y. Y., SANJABI, S., ROBERTSON, A.-K. L. & FLAVELL, R. A. 2006. Transforming growth factor-β regulation of immune responses. *Annu. Rev. Immunol.,* 24**,** 99-146.

LI, S., WANG, Y., CAO, B., WU, Y., JI, L., LI, Y.-X., LIU, M., ZHAO, Y., QIAO, J., WANG, H., WANG, H., HAN, C. & WANG, Y.-L. 2014. Maturation of Growth Differentiation Factor 15 in Human Placental Trophoblast Cells Depends on the Interaction With Matrix Metalloproteinase-26. *The Journal of Clinical Endocrinology & Metabolism,* 99**,** E2277-E2287.

LIM, H., MA, L., MA, W.-G., MAAS, R. L. & DEY, S. K. 1999. Hoxa-10 Regulates Uterine Stromal Cell Responsiveness to Progesterone during Implantation and Decidualization in the Mouse. *Molecular Endocrinology,* 13**,** 1005-1017.

LIMA, P. D. A., ZHANG, J., DUNK, C., LYE, S. J. & ANNE CROY, B. 2014. Leukocyte driven-decidual angiogenesis in early pregnancy. *Cell Mol Immunol,* 11**,** 522-537.

LIN, E. Y., GOUON-EVANS, V., NGUYEN, A. V. & POLLARD, J. W. 2002. The Macrophage Growth Factor CSF-1 in Mammary Gland Development and Tumor Progression. *Journal of Mammary Gland Biology and Neoplasia,* 7**,** 147-162.

LIU, C.-C., PERUSSIA, B. & YOUNG, J. D.-E. 2000. The emerging role of IL-15 in NK-cell development. *Immunology Today,* 21**,** 113-116.

LIU, L., OZA, S., HOGAN, D., PERIN, J., RUDAN, I., LAWN, J. E., COUSENS, S., MATHERS, C. & BLACK, R. E. 2015. Global, regional, and national causes of child mortality in 2000–13, with projections to inform post-2015 priorities: an updated systematic analysis. *The Lancet,* 385**,** 430-440.

LIYANAGE, S. E., FANTIN, A., VILLACAMPA, P., LANGE, C. A., DENTI, L., CRISTANTE, E., SMITH, A. J., ALI, R. R., LUHMANN, U. F., BAINBRIDGE, J. W. & RUHRBERG, C. 2016. Myeloid-Derived Vascular Endothelial Growth Factor and Hypoxia-Inducible Factor Are Dispensable for Ocular Neovascularization—Brief Report. *Arteriosclerosis, Thrombosis, and Vascular Biology,* 36**,** 19-24.

LOKKI, A. I., HEIKKINEN-ELORANTA, J., JARVA, H., SAISTO, T., LOKKI, M.-L., LAIVUORI, H. & MERI, S. 2014. Complement Activation and Regulation in Preeclamptic Placenta. *Frontiers in Immunology,* 5.

LUCAS, A., FEWTRELL, M. & COLE, T. 1999. Fetal origins of adult disease—the hypothesis revisited. *Bmj,* 319**,** 245-249.

LYALL, F., ROBSON, S. C. & BULMER, J. N. 2013. Spiral Artery Remodeling and Trophoblast Invasion in Preeclampsia and Fetal Growth Restriction. *Hypertension,* 62**,** 1046.

LYDON, J. P., DEMAYO, F. J., FUNK, C. R., MANI, S. K., HUGHES, A. R., MONTGOMERY, C. A., SHYAMALA, G., CONNEELY, O. M. & O'MALLEY, B. W. 1995. Mice lacking progesterone receptor exhibit pleiotropic reproductive abnormalities. *Genes & Development,* 9**,** 2266-2278.

MACKLER, A. M., GREEN, L. M., MCMILLAN, P. J. & YELLON, S. M. 2000. Distribution and activation of uterine mononuclear phagocytes in peripartum endometrium and myometrium of the mouse. *Biol Reprod,* 62**,** 1193-200.

MACKLER, A. M., IEZZA, G., AKIN, M. R., MCMILLAN, P. & YELLON, S. M. 1999. Macrophage trafficking in the uterus and cervix precedes parturition in the mouse. *Biol Reprod,* 61**,** 879-83.

MADEJA, Z., YADI, H., APPS, R., BOULENOUAR, S., ROPER, S. J., GARDNER, L., MOFFETT, A., COLUCCI, F. & HEMBERGER, M. 2011. Paternal MHC expression on mouse trophoblast affects uterine vascularization and fetal growth. *Proceedings of the National Academy of Sciences,* 108**,** 4012-4017.

MAKRIGIANNAKIS, A., VREKOUSSIS, T., ZOUMAKIS, E., KALANTARIDOU, S. & JESCHKE, U. 2017. The Role of HCG in Implantation: A Mini-Review of Molecular and Clinical Evidence. *International Journal of Molecular Sciences,* 18**,** 1305.

MANDALA, M. & OSOL, G. 2012. Physiological remodelling of the maternal uterine circulation during pregnancy. *Basic & clinical pharmacology & toxicology,* 110**,** 12-18.

MARCHO, C., CUI, W. & MAGER, J. 2015. Epigenetic dynamics during preimplantation development. *Reproduction (Cambridge, England),* 150**,** R109-R120.

MARSHALL, S. A., NG, L., UNEMORI, E. N., GIRLING, J. E. & PARRY, L. J. 2016. Relaxin deficiency results in increased expression of angiogenesis- and remodelling-related genes in the uterus of early pregnant mice but does not affect endometrial angiogenesis prior to implantation. *Reproductive Biology and Endocrinology,* 14**,** 11.

MARSHALL, S. A., SENADHEERA, S. N., JELINIC, M., O'SULLIVAN, K., PARRY, L. J. & TARE, M. 2018. Relaxin Deficiency Leads to Uterine Artery Dysfunction During Pregnancy in Mice. *Frontiers in Physiology,* 9.

MARSHALL, S. A., SENADHEERA, S. N., PARRY, L. J. & GIRLING, J. E. 2017. The Role of Relaxin in Normal and Abnormal Uterine Function During the Menstrual Cycle and Early Pregnancy. *Reproductive Sciences,* 24**,** 342-354.

MARWOOD, M., VISSER, K., SALAMONSEN, L. A. & DIMITRIADIS, E. 2009. Interleukin-11 and leukemia inhibitory factor regulate the adhesion of endometrial epithelial cells: implications in fertility regulation. *Endocrinology,* 150**,** 2915-23.

MATSUBARA, K., MATSUBARA, Y., MORI, M., UCHIKURA, Y., HAMADA, K., FUJIOKA, T., HASHIMOTO, H. & MATSUMOTO, T. 2016. Immune activation during the implantation phase causes preeclampsia-like symptoms via the CD40-CD40 ligand pathway in pregnant mice. *Hypertens Res,* 39**,** 407-414.

MATSUMOTO, H. & SATO, E. 2006. Uterine angiogenesis during implantation and decidualization in mice. *Reproductive Medicine and Biology,* 5**,** 81-86.

MCGOVERN, N., SHIN, A., LOW, G., LOW, D., DUAN, K., YAO, L. J., MSALLAM, R., LOW, I., SHADAN, N. B., SUMATOH, H. R., SOON, E., LUM, J., MOK, E., HUBERT, S., SEE, P., KUNXIANG, E. H., LEE, Y. H., JANELA, B., CHOOLANI, M., MATTAR, C. N. Z., FAN, Y., LIM, T. K. H., HONG, D. K., TAN, K.-K., TAM, J. K. C., SCHUSTER, C., ELBE-BÜRGER, A., WANG, X.-N., BIGLEY, V., COLLIN, M., HANIFFA, M., SCHLITZER, A., POIDINGER, M., ALBANI, S., LARBI, A., NEWELL, E. W., CHAN, J. K. Y. & GINHOUX, F. 2017. Human fetal dendritic cells promote prenatal T-cell immune suppression through arginase-2. *Nature,* advance online publication.

MCKEEMAN, G. C., ARDILL, J. E. S., CALDWELL, C. M., HUNTER, A. J. & MCCLURE, N. 2004. Soluble vascular endothelial growth factor receptor-1 (sFlt-1) is increased throughout gestation in patients

who have preeclampsia develop. *American Journal of Obstetrics and Gynecology,* 191**,** 1240-1246.

MCKENNA, S., GOSSLING, M., BUGARINI, A., HILL, E., ANDERSON, A. L., RANCOURT, R. C., BALASUBRAMANIYAN, N., EL KASMI, K. C. & WRIGHT, C. J. 2015. Endotoxemia Induces IkappaBbeta/NF-kappaB-Dependent Endothelin-1 Expression in Hepatic Macrophages. *J Immunol,* 195**,** 3866-79.

MCMASTER, M. T., ZHOU, Y. & FISHER, S. J. Abnormal placentation and the syndrome of preeclampsia. Seminars in nephrology, 2004. Elsevier, 540-547.

MEHTA, V., ABI-NADER, K. N., SHANGARIS, P., SHAW, S. S., FILIPPI, E., BENJAMIN, E., BOYD, M., PEEBLES, D. M., MARTIN, J. & ZACHARY, I. 2014. Local over-expression of VEGF-D ΔNΔC in the uterine arteries of pregnant sheep results in long-term changes in uterine artery contractility and angiogenesis. *PloS one,* 9**,** e100021.

MEIDAN, R. 2016. *The Life Cycle of the Corpus Luteum*, Springer.

MELLOR, A. L., SIVAKUMAR, J., CHANDLER, P., SMITH, K., MOLINA, H., MAO, D. & MUNN, D. H. 2001. Prevention of T cell–driven complement activation and inflammation by tryptophan catabolism during pregnancy. *Nature immunology,* 2**,** 64.

MERLINO, A. A., WELSH, T. N., TAN, H., YI, L. J., CANNON, V., MERCER, B. M. & MESIANO, S. 2007. Nuclear progesterone receptors in the human pregnancy myometrium: evidence that parturition involves functional progesterone withdrawal mediated by increased expression of progesterone receptor-A. *J Clin Endocrinol Metab,* 92**,** 1927-33.

MIKKELSEN, H. B. & THUNEBERG, L. 1999. Op/op mice defective in production of functional colony-stimulating factor-1 lack macrophages in muscularis externa of the small intestine. *Cell Tissue Res,* 295**,** 485-93.

MILLER, L., ALLEY, E. W., MURPHY, W. J., RUSSELL, S. W. & HUNT, J. S. 1996. Progesterone inhibits inducible nitric oxide synthase gene expression and nitric oxide production in murine macrophages. *J Leukoc Biol,* 59**,** 442-50.

MILLIGAN, S. R. & FINN, C. A. 1997. Minimal progesterone support required for the maintenance of pregnancy in mice. *Hum Reprod,* 12**,** 602-7.

MOFFETT-KING, A. 2002. Natural killer cells and pregnancy. *Nature Reviews Immunology,* 2**,** 656-663.

MOFFETT, A. & LOKE, C. 2006. Immunology of placentation in eutherian mammals. *Nature Reviews Immunology,* 6**,** 584-594.

MOLDOVAN, N. I., GOLDSCHMIDT-CLERMONT, P. J., PARKER-THORNBURG, J., SHAPIRO, S. D. & KOLATTUKUDY, P. E. 2000. Contribution of monocytes/macrophages to compensatory neovascularization: the drilling of metalloelastase-positive tunnels in ischemic myocardium. *Circ Res,* 87**,** 378-84.

MOLGORA, S., ACQUATI, C., FENAROLI, V. & SAITA, E. 2019. Dyadic coping and marital adjustment during pregnancy: A cross-sectional study of Italian couples expecting their first child. *International Journal of Psychology,* 54**,** 277-285.

MOLL, W., KUNZEL, W. & HERBERGER, J. 1975. Hemodynamic implications of hemochorial placentation. *Eur J Obstet Gynecol Reprod Biol,* 5**,** 67-74.

MONCADA, S., PALMER, R. M. & HIGGS, E. A. 1991. Nitric oxide: physiology, pathophysiology, and pharmacology. *Pharmacol Rev,* 43**,** 109-42.

MOR, G., ALDO, P. & ALVERO, A. B. 2017. The unique immunological and microbial aspects of pregnancy. *Nature Reviews Immunology,* 17**,** 469.

MOR, G., CARDENAS, I., ABRAHAMS, V. & GULLER, S. 2011. Inflammation and pregnancy: the role of the immune system at the implantation site. *Annals of the New York Academy of Sciences,* 1221**,** 80-87.

MORI, M., BOGDAN, A., BALASSA, T., CSABAI, T. & SZEKERES-BARTHO, J. 2016. The decidua—the maternal bed embracing the embryo—maintains the pregnancy. *Seminars in Immunopathology***,** 1-15.

MORTON, J. S., CARE, A. S. & DAVIDGE, S. T. 2017. Mechanisms of Uterine Artery Dysfunction in Pregnancy Complications. *J Cardiovasc Pharmacol,* 69**,** 343-359.

MOSSER, D. M. & EDWARDS, J. P. 2008. Exploring the full spectrum of macrophage activation. *Nature Reviews Immunology,* 8**,** 958-969.

MULAC-JERICEVIC, B. & CONNEELY, O. M. 2004. Reproductive tissue selective actions of progesterone receptors. *Reproduction,* 128**,** 139-146.

MULVANY, M. J. Structure and Function of Resistance Vessels in Hypertension. *In:* BRUSCHI, G. & BORGHETTI, A., eds. Cellular Aspects of Hypertension, 1991// 1991 Berlin, Heidelberg. Springer Berlin Heidelberg, 3-11.

MULVANY, M. J., BAUMBACH, G. L., AALKJAER, C., HEAGERTY, A. M., KORSGAARD, N., SCHIFFRIN, E. L. & HEISTAD, D. D. 1996. Vascular remodeling. *Hypertension,* 28**,** 505-6.

MUNN, D. H., ZHOU, M., ATTWOOD, J. T., BONDAREV, I., CONWAY, S. J., MARSHALL, B., BROWN, C. & MELLOR, A. L. 1998. Prevention of allogeneic fetal rejection by tryptophan catabolism. *Science,* 281**,** 1191-1193.

MURAKAMI, M., ZHENG, Y., HIRASHIMA, M., SUDA, T., MORITA, Y., OOEHARA, J., EMA, H., FONG, G.-H. & SHIBUYA, M. 2008. VEGFR1 Tyrosine Kinase Signaling Promotes Lymphangiogenesis as Well as Angiogenesis Indirectly via Macrophage Recruitment. *Arteriosclerosis, Thrombosis, and Vascular Biology,* 28**,** 658-664.

MUROHARA, T., ASAHARA, T., SILVER, M., BAUTERS, C., MASUDA, H., KALKA, C., KEARNEY, M., CHEN, D., SYMES, J. F., FISHMAN, M. C., HUANG, P. L. & ISNER, J. M. 1998. Nitric oxide

synthase modulates angiogenesis in response to tissue ischemia. *The Journal of Clinical Investigation,* 101**,** 2567-2578.

MURRAY, PETER J., ALLEN, JUDITH E., BISWAS, SUBHRA K., FISHER, EDWARD A., GILROY, DEREK W., GOERDT, S., GORDON, S., HAMILTON, JOHN A., IVASHKIV, LIONEL B., LAWRENCE, T., LOCATI, M., MANTOVANI, A., MARTINEZ, FERNANDO O., MEGE, J.-L., MOSSER, DAVID M., NATOLI, G., SAEIJ, JEROEN P., SCHULTZE, JOACHIM L., SHIREY, KARI A., SICA, A., SUTTLES, J., UDALOVA, I., VAN GINDERACHTER, JO A., VOGEL, STEFANIE N. & WYNN, THOMAS A. 2014. Macrophage Activation and Polarization: Nomenclature and Experimental Guidelines. *Immunity,* 41**,** 14-20.

MURRAY, P. J. & WYNN, T. A. 2011. Obstacles and opportunities for understanding macrophage polarization. *Journal of Leukocyte Biology,* 89**,** 557-563.

NADEAU-VALLÉE, M., CHIN, P.-Y., BELARBI, L., BRIEN, M.-È., PUNDIR, S., BERRYER, M. H., BEAUDRY-RICHARD, A., MADAAN, A., SHARKEY, D. J., LUPIEN-MEILLEUR, A., HOU, X., QUINIOU, C., BEAULAC, A., BOUFAIED, I., BOUDREAULT, A., CARBONARO, A., DOAN, N.-D., JOYAL, J.-S., LUBELL, W. D., OLSON, D. M., ROBERTSON, S. A., GIRARD, S. & CHEMTOB, S. 2017. Antenatal Suppression of IL-1 Protects against Inflammation-Induced Fetal Injury and Improves Neonatal and Developmental Outcomes in Mice. 1601600.

NADKARNI, S., SMITH, J., SFERRUZZI-PERRI, A. N., LEDWOZYW, A., KISHORE, M., HAAS, R., MAURO, C., WILLIAMS, D. J., FARSKY, S. H. P., MARELLI-BERG, F. M. & PERRETTI, M. 2016. Neutrophils induce proangiogenic T cells with a regulatory phenotype in pregnancy. *Proceedings of the National Academy of Sciences,* 113**,** E8415-E8424.

NARUSE, K., INNES, B. A., BULMER, J. N., ROBSON, S. C., SEARLE, R. F. & LASH, G. E. 2010. Secretion of cytokines by villous cytotrophoblast and extravillous trophoblast in the first trimester of human pregnancy. *J Reprod Immunol,* 86**,** 148-50.

NARUSE, K., LASH, G. E., INNES, B. A., OTUN, H. A., SEARLE, R. F., ROBSON, S. C. & BULMER, J. N. 2009. Localization of matrix metalloproteinase (MMP)-2, MMP-9 and tissue inhibitors for MMPs (TIMPs) in uterine natural killer cells in early human pregnancy. *Human Reproduction,* 24**,** 553-561.

NATANSON-YARON, S., ANTEBY, E. Y., GREENFIELD, C., GOLDMAN-WOHL, D., HAMANI, Y., HOCHNER-CELNIKIER, D. & YAGEL, S. 2007. FGF 10 and Sprouty 2 modulate trophoblast invasion and branching morphogenesis. *Mol Hum Reprod,* 13**,** 511-9.

NEJABATI, H. R., LATIFI, Z., GHASEMNEJAD, T., FATTAHI, A. & NOURI, M. 2017. Placental growth factor (PlGF) as an angiogenic/inflammatory switcher: lesson from early pregnancy losses. *Gynecological Endocrinology***,** 1-7.

NESS, R. B. & SIBAI, B. M. 2006. Shared and disparate components of the pathophysiologies of fetal growth restriction and preeclampsia. *Am J Obstet Gynecol,* 195**,** 40-9.

NI, N. & LI, Q. 2017. TGFβ superfamily signaling and uterine decidualization. *Reproductive biology and endocrinology : RB&E,* 15**,** 84-84.

NING, F., LIU, H. & LASH, G. E. 2016. The Role of Decidual Macrophages During Normal and Pathological Pregnancy. *American Journal of Reproductive Immunology*.

NISSI, R., TALVENSAARI-MATTILA, A., KOTILA, V., NIINIMÄKI, M., JÄRVELÄ, I. & TURPEENNIEMI-HUJANEN, T. 2013. Circulating matrix metalloproteinase MMP-9 and MMP-2/TIMP-2 complex are associated with spontaneous early pregnancy failure. *Reproductive Biology and Endocrinology,* 11**,** 2.

NORMAN, R. J. & BRANNSTROM, M. 1994. White cells and the ovary – incidental invaders or essential effectors? *Journal of Endocrinology,* 140**,** 333-336.

OLSSON, A. K., DIMBERG, A., KREUGER, J. & CLAESSON-WELSH, L. 2006. VEGF receptor signalling - in control of vascular function. *Nature Reviews Molecular Cell Biology,* 7**,** 359-371.

ONG, S. S., BAKER, P. N., MAYHEW, T. M. & DUNN, W. R. 2005. Remodeling of myometrial radial arteries in preeclampsia. *Am J Obstet Gynecol,* 192**,** 572-9.

OPPMANN, B., LESLEY, R., BLOM, B., TIMANS, J. C., XU, Y., HUNTE, B., VEGA, F., YU, N., WANG, J. & SINGH, K. 2000. Novel p19 protein engages IL-12p40 to form a cytokine, IL-23, with biological activities similar as well as distinct from IL-12. *Immunity,* 13**,** 715-725.

ORMANDY, C. J., CAMUS, A., BARRA, J., DAMOTTE, D., LUCAS, B., BUTEAU, H., EDERY, M., BROUSSE, N., BABINET, C., BINART, N. & KELLY, P. A. 1997. Null mutation of the prolactin receptor gene produces multiple reproductive defects in the mouse. *Genes Dev,* 11**,** 167-78.

OSOL, G. & MANDALA, M. 2009a. Maternal uterine vascular remodeling during pregnancy. *Physiology (Bethesda, Md.),* 24**,** 58-71.

OSOL, G. & MANDALA, M. 2009b. Maternal uterine vascular remodeling during pregnancy. *Physiology (Bethesda),* 24**,** 58-71.

OVCHINNIKOV, D. A., DEBATS, C. E., SESTER, D. P., SWEET, M. J. & HUME, D. A. 2010. A conserved distal segment of the mouse CSF-1 receptor promoter is required for maximal expression of a reporter gene in macrophages and osteoclasts of transgenic mice. *J Leukoc Biol,* 87**,** 815-22.

PALIS, J., ROBERTSON, S., KENNEDY, M., WALL, C. & KELLER, G. 1999. Development of erythroid and myeloid progenitors in the yolk sac and embryo proper of the mouse. *Development,* 126**,** 5073-84.

PALMER, S. K., ZAMUDIO, S., COFFIN, C., PARKER, S., STAMM, E. & MOORE, L. G. 1992. Quantitative estimation of human uterine artery blood flow and pelvic blood flow redistribution in pregnancy. *Obstet Gynecol,* 80**,** 1000-6.

PAPAPETROPOULOS, A., GARCÍA-CARDEÑA, G., MADRI, J. A. & SESSA, W. C. 1997. Nitric oxide production contributes to the angiogenic properties of vascular endothelial growth factor in human endothelial cells. *The Journal of Clinical Investigation,* 100**,** 3131-3139.

PARDI, G., MARCONI, A. M. & CETIN, I. 2002. Placental-fetal Interrelationship in IUGR Fetuses—A Review. *Placenta,* 23**,** S136-S141.

PARK, J. E., CHEN, H. H., WINER, J., HOUCK, K. A. & FERRARA, N. 1994. Placenta growth factor. Potentiation of vascular endothelial growth factor bioactivity, in vitro and in vivo, and high affinity binding to Flt-1 but not to Flk-1/KDR. *Journal of Biological Chemistry,* 269**,** 25646-25654.

PARRY, L. J., VODSTRCIL, L. A., MADDEN, A., AMIR, S. H., BALDWIN, K., WLODEK, M. E. & NICHOLAS, K. R. 2009. Normal mammary gland growth and lactation capacity in pregnant relaxin-deficient mice. *Reproduction, Fertility and Development,* 21**,** 549-560.

PATEL, A. S., SMITH, A., NUCERA, S., BIZIATO, D., SAHA, P., ATTIA, R. Q., HUMPHRIES, J., MATTOCK, K., GROVER, S. P., LYONS, O. T., GUIDOTTI, L. G., SIOW, R., IVETIC, A., EGGINTON, S., WALTHAM, M., NALDINI, L., DE PALMA, M. & MODARAI, B. 2013. TIE2-expressing monocytes/macrophages regulate revascularization of the ischemic limb. *EMBO Molecular Medicine,* 5**,** 858-869.

PAULESU, L., JANTRA, S., IETTA, F., BRIZZI, R. & BIGLIARDI, E. 2008. Interleukin-1 in reproductive strategies. *Evol Dev,* 10**,** 778-88.

PELUSO, J. J., PAPPALARDO, A., LOSEL, R. & WEHLING, M. 2006. Progesterone membrane receptor component 1 expression in the immature rat ovary and its role in mediating progesterone's antiapoptotic action. *Endocrinology,* 147**,** 3133-40.

PEREZ-GARCIA, V., FINEBERG, E., WILSON, R., MURRAY, A., MAZZEO, C. I., TUDOR, C., SIENERTH, A., WHITE, J. K., TUCK, E., RYDER, E. J., GLEESON, D., SIRAGHER, E., WARDLE-JONES, H., STAUDT, N., WALI, N., COLLINS, J., GEYER, S., BUSCH-NENTWICH, E. M., GALLI, A., SMITH, J. C., ROBERTSON, E., ADAMS, D. J., WENINGER, W. J., MOHUN, T. & HEMBERGER, M. 2018. Placentation defects are highly prevalent in embryonic lethal mouse mutants. *Nature,* 555**,** 463.

PETRY, F., BOTTO, M., HOLTAPPELS, R., WALPORT, M. J. & LOOS, M. 2001. Reconstitution of the Complement Function in C1q-Deficient (C1qa−/−) Mice with Wild-Type Bone Marrow Cells. *The Journal of Immunology,* 167**,** 4033-4037.

PIERCE, J. H., DI MARCO, E., COX, G. W., LOMBARDI, D., RUGGIERO, M., VARESIO, L., WANG, L. M., CHOUDHURY, G. G., SAKAGUCHI, A. Y., DI FIORE, P. P. & ET AL. 1990. Macrophage-colony-stimulating factor (CSF-1) induces proliferation, chemotaxis, and reversible monocytic differentiation in myeloid progenitor cells transfected with the human c-fms/CSF-1 receptor cDNA.

Proceedings of the National Academy of Sciences of the United States of America, 87**,** 5613-5617.

PIJNENBORG, R., ANTHONY, J., DAVEY, D. A., REES, A., TILTMAN, A., VERCRUYSSE, L. & VAN ASSCHE, A. 1991. Placental bed spiral arteries in the hypertensive disorders of pregnancy. *Br J Obstet Gynaecol,* 98**,** 648-55.

PINHAL-ENFILED, G., VASAN, N. S. & LEIBOVICH, J. 2012. The Role of Macrophages in the Placenta. New Jersey, USA: New Jersey Medical School.

PLAKS, V., RINKENBERGER, J., DAI, J., FLANNERY, M., SUND, M., KANASAKI, K., NI, W., KALLURI, R. & WERB, Z. 2013. Matrix metalloproteinase-9 deficiency phenocopies features of preeclampsia and intrauterine growth restriction. *Proceedings of the National Academy of Sciences,* 110**,** 11109-11114.

POLLARD, J. W. & HENNIGHAUSEN, L. 1994. Colony stimulating factor 1 is required for mammary gland development during pregnancy. *Proc Natl Acad Sci U S A,* 91**,** 9312-6.

POLLARD, J. W., HUNT, J. S., WIKTOR-JEDRZEJCZAK, W. & STANLEY, E. R. 1991. A pregnancy defect in the osteopetrotic (opop) mouse demonstrates the requirement for CSF-1 in female fertility. *Developmental Biology,* 148**,** 273-283.

PUCCI, F., VENNERI, M. A., BIZIATO, D., NONIS, A., MOI, D., SICA, A., DI SERIO, C., NALDINI, L. & DE PALMA, M. 2009. A distinguishing gene signature shared by tumor-infiltrating Tie2-expressing monocytes, blood "resident" monocytes, and embryonic macrophages suggests common functions and developmental relationships. *Blood,* 114**,** 901-914.

QIAN, B. Z. & POLLARD, J. W. 2010. Macrophage diversity enhances tumor progression and metastasis. *Cell,* 141**,** 39-51.

RABBANI, M. & ROGERS, P. 2001. Role of vascular endothelial growth factor in endometrial vascular events before implantation in rats. *Reproduction,* 122**,** 85-90.

RAFFETTO, J. D. & KHALIL, R. A. 2008. Matrix metalloproteinases and their inhibitors in vascular remodeling and vascular disease. *Biochemical Pharmacology,* 75**,** 346-359.

RAHIMI, Z., RAHIMI, Z., SHAHSAVANDI, M. O., BIDOKI, K. & REZAEI, M. 2013. MMP-9 (-1562 C: T) polymorphism as a biomarker of susceptibility to severe pre-eclampsia. *Biomarkers,* 7**,** 93-98.

RAMA RAJU, G., CHAVAN, R., DEENADAYAL, M., GUNASHEELA, D., GUTGUTIA, R., HARIPRIYA, G., GOVINDARAJAN, M., PATEL, N. & PATKI, A. 2013. Luteinizing hormone and follicle stimulating hormone synergy: A review of role in controlled ovarian hyper-stimulation. *Journal of Human Reproductive Sciences,* 6**,** 227-234.

RATHINAM, C., POUEYMIROU, W. T., ROJAS, J., MURPHY, A. J., VALENZUELA, D. M., YANCOPOULOS, G. D., RONGVAUX, A., EYNON, E. E., MANZ, M. G. & FLAVELL, R. A. 2011.

Efficient differentiation and function of human macrophages in humanized CSF-1 mice. *Blood, The Journal of the American Society of Hematology,* 118**,** 3119-3128.

REISTER, F., FRANK, H. G., HEYL, W., KOSANKE, G., HUPPERTZ, B., SCHRÖDER, W., KAUFMANN, P. & RATH, W. 1999. The Distribution of Macrophages in Spiral Arteries of the Placental Bed in Pre-eclampsia Differs from that in Healthy Patients. *Placenta,* 20**,** 229-233.

REISTER, F., FRANK, H. G., KINGDOM, J. C., HEYL, W., KAUFMANN, P., RATH, W. & HUPPERTZ, B. 2001. Macrophage-induced apoptosis limits endovascular trophoblast invasion in the uterine wall of preeclamptic women. *Lab Invest,* 81**,** 1143-52.

RENNIE, M. Y., RAHMAN, A., WHITELEY, K. J., SLED, J. G. & ADAMSON, S. L. 2015. Site-Specific Increases in Utero- and Fetoplacental Arterial Vascular Resistance in eNOS-Deficient Mice Due to Impaired Arterial Enlargement1. *Biology of Reproduction,* 92**,** 48, 1-11-48, 1-11.

RENNIE, M. Y., WHITELEY, K. J., ADAMSON, S. L. & SLED, J. G. 2016. Quantification of Gestational Changes in the Uteroplacental Vascular Tree Reveals Vessel Specific Hemodynamic Roles During Pregnancy in Mice. *Biology of Reproduction*.

REYES, L., WOLFE, B. & GOLOS, T. 2017. Hofbauer cells: placental macrophages of fetal origin. *Results and Problems in Cell Differentiation,* 62**,** 45-60.

REYNOLDS, L. P., BOROWICZ, P. P., CATON, J. S., VONNAHME, K. A., LUTHER, J. S., BUCHANAN, D. S., HAFEZ, S. A., GRAZUL-BILSKA, A. T. & REDMER, D. A. 2010. Uteroplacental vascular development and placental function: an update. *Int J Dev Biol,* 54**,** 355-66.

REYNOLDS, L. P., CATON, J. S., REDMER, D. A., GRAZUL-BILSKA, A. T., VONNAHME, K. A., BOROWICZ, P. P., LUTHER, J. S., WALLACE, J. M., WU, G. & SPENCER, T. E. 2006. Evidence for altered placental blood flow and vascularity in compromised pregnancies. *J Physiol,* 572**,** 51-8.

RIABOV, V., GUDIMA, A., WANG, N., MICKLEY, A., OREKHOV, A. & KZHYSHKOWSKA, J. 2014. Role of tumor associated macrophages in tumor angiogenesis and lymphangiogenesis. *Front Physiol,* 5**,** 75.

ROBERTS, C. T., SOHLSTROM, A., KIND, K. L., EARL, R. A., KHONG, T. Y., ROBINSON, J. S., OWENS, P. C. & OWENS, J. A. 2001. Maternal Food Restriction Reduces the Exchange Surface Area and Increases the Barrier Thickness of the Placenta in the Guinea-pig. *Placenta,* 22**,** 177-185.

ROBERTS, C. T., WHITE, C. A., WIEMER, N. G., RAMSAY, A. & ROBERTSON, S. A. 2003. Altered Placental Development in Interleukin-10 Null Mutant Mice. *Placenta,* 24**,** S94-S99.

ROBERTSON, S. A., CARE, A. S. & MOLDENHAUER, L. M. 2018. Regulatory T cells in embryo implantation and the immune response to pregnancy. *The Journal of Clinical Investigation,* 128**,** 4224-4235.

ROBERTSON, S. A., GUERIN, L. R., BROMFIELD, J. J., BRANSON, K. M., AHLSTRÖM, A. C. & CARE, A. S. 2009a. Seminal fluid drives expansion of the CD4+ CD25+ T regulatory cell pool and induces tolerance to paternal alloantigens in mice. *Biology of reproduction,* 80**,** 1036-1045.

ROBERTSON, S. A., GUERIN, L. R., MOLDENHAUER, L. M. & HAYBALL, J. D. 2009b. Activating T regulatory cells for tolerance in early pregnancy — the contribution of seminal fluid. *Journal of Reproductive Immunology,* 83**,** 109-116.

ROBERTSON, S. A., MAU, V. J., TREMELLEN, K. P. & SEAMARK, R. F. 1996a. Role of high molecular weight seminal vesicle proteins in eliciting the uterine inflammatory response to semen in mice. *Journal of Reproduction and Fertility,* 107**,** 265-277.

ROBERTSON, S. A., MAYRHOFER, G. & SEAMARK, R. F. 1996b. Ovarian steroid hormones regulate granulocyte-macrophage colony-stimulating factor synthesis by uterine epithelial cells in the mouse. *Biol Reprod,* 54**,** 183-96.

ROBERTSON, S. A., PETROFF, M. G. & HUNT, S. J. 2015. Immunology of Pregnancy. *Knobil and Neill's Physiology of Reproduction.* Fourth ed.: Elsevier.

ROBERTSON, S. A., ROBERTS, C. T., FARR, K. L., DUNN, A. R. & SEAMARK, R. F. 1999. Fertility Impairment in Granulocyte-Macrophage Colony-Stimulating Factor-Deficient Mice. *Biology of Reproduction,* 60**,** 251-261.

ROBINSON, D. P. & KLEIN, S. L. 2012. Pregnancy and pregnancy-associated hormones alter immune responses and disease pathogenesis. *Hormones and Behavior,* 62**,** 263-271.

ROBSON, A., HARRIS, L. K., INNES, B. A., LASH, G. E., ALJUNAIDY, M. M., APLIN, J. D., BAKER, P. N., ROBSON, S. C. & BULMER, J. N. 2012. Uterine natural killer cells initiate spiral artery remodeling in human pregnancy. *The FASEB Journal,* 26**,** 4876-4885.

ROSENFELD, C. R. & RIVERA, R. 1978. Circulatory responses to systemic infusions of estrone and estradiol-17α in nonpregnant, oophorectomized ewes. *American Journal of Obstetrics and Gynecology,* 132**,** 442-448.

ROSSANT, J. & CROSS, J. C. 2001. Placental development: Lessons from mouse mutants. *Nature Reviews Genetics,* 2**,** 538-548.

ROUMENINA, L. T., DAUGAN, M. V., NOÉ, R., PETITPREZ, F., VANO, Y. A., SANCHEZ-SALAS, R., BECHT, E., MEILLEROUX, J., LE CLEC'H, B. & GIRALDO, N. A. 2019. Tumor cells hijack macrophage-produced complement C1q to promote tumor growth. *Cancer immunology research,* 7**,** 1091-1105.

ROUSSEV, R. G., HIGGINS, N. G. & MCINTYRE, J. A. 1993. Phenotypic characterization of normal human placental mononuclear cells. *Journal of Reproductive Immunology,* 25**,** 15-29.

SAITO, S. & NAKASHIMA, A. 2014. A review of the mechanism for poor placentation in early-onset preeclampsia: the role of autophagy in trophoblast invasion and vascular remodeling. *Journal of Reproductive Immunology,* 101–102**,** 80-88.

SAITO, S., NAKASHIMA, A., SHIMA, T. & ITO, M. 2010. Th1/Th2/Th17 and Regulatory T-Cell Paradigm in Pregnancy. *American Journal of Reproductive Immunology,* 63**,** 601-610.

SAITO, S. & SAKAI, M. 2003. Th1/Th2 balance in preeclampsia. *Journal of Reproductive Immunology,* 59**,** 161-173.

SAKUMOTO, R., HAYASHI, K.-G., FUJII, S., KANAHARA, H., HOSOE, M., FURUSAWA, T. & KIZAKI, K. 2017. Possible Roles of CC- and CXC-Chemokines in Regulating Bovine Endometrial Function during Early Pregnancy. *International journal of molecular sciences,* 18**,** 742.

SALAMONSEN, L. A. 1998. Current Concepts of the Mechanisms of Menstruation: A Normal Process of Tissue Destruction. *Trends in Endocrinology & Metabolism,* 9**,** 305-309.

SAMUEL, C. S., ZHAO, C., BATHGATE, R. A., DU, X. J., SUMMERS, R. J., AMENTO, E. P., WALKER, L. L., MCBURNIE, M., ZHAO, L. & TREGEAR, G. W. 2005. The relaxin gene-knockout mouse: a model of progressive fibrosis. *Ann N Y Acad Sci,* 1041**,** 173-81.

SEGAL, M. S., SAUTINA, L., LI, S., DIAO, Y., AGOULNIK, A. I., KIELCZEWSKI, J., MCGUANE, J. T., GRANT, M. B. & CONRAD, K. P. 2012. Relaxin increases human endothelial progenitor cell NO and migration and vasculogenesis in mice. *Blood,* 119**,** 629-636.

SELVARAJ, S. K., GIRI, R. K., PERELMAN, N., JOHNSON, C., MALIK, P. & KALRA, V. K. 2003. Mechanism of monocyte activation and expression of proinflammatory cytochemokines by placenta growth factor. *Blood,* 102**,** 1515-1524.

SEMENZA, G. L. 2003. Targeting HIF-1 for cancer therapy. *Nat Rev Cancer,* 3**,** 721-732.

SEMENZA, G. L. 2009. Defining the role of hypoxia-inducible factor 1 in cancer biology and therapeutics. *Oncogene,* 29**,** 625-634.

SENTMAN, C. L., MEADOWS, S. K., WIRA, C. R. & ERIKSSON, M. 2004. Recruitment of uterine NK cells: induction of CXC chemokine ligands 10 and 11 in human endometrium by estradiol and progesterone. *J Immunol,* 173**,** 6760-6.

SEVAL, Y., KORGUN, E. T. & DEMIR, R. 2007. Hofbauer Cells in Early Human Placenta: Possible Implications in Vasculogenesis and Angiogenesis. *Placenta,* 28**,** 841-845.

SHARKEY, D. J., MACPHERSON, A. M., TREMELLEN, K. P., MOTTERSHEAD, D. G., GILCHRIST, R. B. & ROBERTSON, S. A. 2012a. TGF-beta mediates proinflammatory seminal fluid signaling in human cervical epithelial cells. *J Immunol,* 189**,** 1024-35.

SHARKEY, D. J., TREMELLEN, K. P., JASPER, M. J., GEMZELL-DANIELSSON, K. & ROBERTSON, S. A. 2012b. Seminal Fluid Induces Leukocyte Recruitment and Cytokine and Chemokine mRNA Expression in the Human Cervix after Coitus. *Journal of Immunology,* 188**,** 2445-2454.

SHARMA, S. 2014. Natural killer cells and regulatory T cells in early pregnancy loss. *The International journal of developmental biology,* 58**,** 219-229.

SHAW, T. N., HOUSTON, S. A., WEMYSS, K., BRIDGEMAN, H. M., BARBERA, T. A., ZANGERLE-MURRAY, T., STRANGWARD, P., RIDLEY, A. J. L., WANG, P., TAMOUTOUNOUR, S., ALLEN, J. E., KONKEL, J. E. & GRAINGER, J. R. 2018. Tissue-resident macrophages in the intestine are long lived and defined by Tim-4 and CD4 expression. *The Journal of Experimental Medicine,* 215**,** 1507-1518.

SHAWBER, C. J., LIN, L., GNARRA, M., SAUER, M. V., PAPAIOANNOU, V. E., KITAJEWSKI, J. K. & DOUGLAS, N. C. 2015. Vascular Notch proteins and Notch signaling in the peri-implantation mouse uterus. *Vascular cell,* 7**,** 9.

SHIBUYA, M. 2006. Vascular endothelial growth factor receptor-1 (VEGFR-1/Flt-1): a dual regulator for angiogenesis. *Angiogenesis,* 9**,** 225-230.

SHIBUYA, M. 2011. Vascular Endothelial Growth Factor (VEGF) and Its Receptor (VEGFR) Signaling in Angiogenesis. *Genes & Cancer,* 2**,** 1097-1105.

SHIMADA, S., NISHIDA, R., TAKEDA, M., IWABUCHI, K., KISHI, R., ONOÉ, K., MINAKAMI, H. & YAMADA, H. 2006. Natural Killer, Natural Killer T, Helper and Cytotoxic T Cells in the Decidua from Sporadic Miscarriage. *American Journal of Reproductive Immunology,* 56**,** 193-200.

SHIN, J. E., PARK, S. H. & JANG, Y. K. 2011. Epigenetic up-regulation of leukemia inhibitory factor (LIF) gene during the progression to breast cancer. *Molecules and cells,* 31**,** 181-189.

SHINETUGS, B., RUNESSON, E., BONELLO, N., BRÄNNSTRÖM, M. & NORMAN, R. 1999. Colony stimulating factor-1 concentrations in blood and follicular fluid during the human menstrual cycle and ovarian stimulation: possible role in the ovulatory process. *Human Reproduction,* 14**,** 1302-1306.

SHWEIKI, D., ITIN, A., SOFFER, D. & KESHET, E. 1992. Vascular endothelial growth factor induced by hypoxia may mediate hypoxia-initiated angiogenesis. *Nature,* 359**,** 843-5.

SINGH, J., AHMED, A. & GIRARDI, G. 2011. Role of complement component C1q in the onset of preeclampsia in mice. *Hypertension,* 58**,** 716-24.

SINGH, M., DALAL, S. & SINGH, K. 2014. Osteopontin: At the cross-roads of myocyte survival and myocardial function. *Life Sci,* 118**,** 1-6.

SINHA, D., WELLS, M. & FAULK, W. P. 1984. Immunological studies of human placentae: complement components in pre-eclamptic chorionic villi. *Clinical and Experimental Immunology,* 56**,** 175.

SMITH, S. D., DUNK, C. E., APLIN, J. D., HARRIS, L. K. & JONES, R. L. 2009. Evidence for immune cell involvement in decidual spiral arteriole remodeling in early human pregnancy. *The American journal of pathology,* 174**,** 1959-1971.

SON, M., PORAT, A., HE, M., SUURMOND, J., SANTIAGO-SCHWARZ, F., ANDERSSON, U., COLEMAN, T. R., VOLPE, B. T., TRACEY, K. J., AL-ABED, Y. & DIAMOND, B. 2016. C1q and HMGB1 reciprocally regulate human macrophage polarization. *Blood,* 128**,** 2218-2228.

SON, M., SANTIAGO-SCHWARZ, F., AL-ABED, Y. & DIAMOND, B. 2012. C1q limits dendritic cell differentiation and activation by engaging LAIR-1. *Proceedings of the National Academy of Sciences,* 109**,** E3160-E3167.

SONCIN, F., NATALE, D. & PARAST, M. M. 2015. Signaling pathways in mouse and human trophoblast differentiation: a comparative review. *Cellular and Molecular Life Sciences,* 72**,** 1291-1302.

SPIVIA, W., MAGNO, P. S., LE, P. & FRASER, D. A. 2014. Complement protein C1q promotes macrophage anti-inflammatory M2-like polarization during the clearance of atherogenic lipoproteins. *Inflamm Res,* 63**,** 885-93.

STALL, A. M., FARIÑAS, M. C., TARLINTON, D. M., LALOR, P. A., HERZENBERG, L. A., STROBER, S. & HERZENBERG, L. A. 1988. Ly-1 B-cell clones similar to human chronic lymphocytic leukemias routinely develop in older normal mice and young autoimmune (New Zealand Black-related) animals. *Proceedings of the National Academy of Sciences,* 85**,** 7312-7316.

STAUN-RAM, E., GOLDMAN, S., GABARIN, D. & SHALEV, E. 2004. Expression and importance of matrix metalloproteinase 2 and 9 (MMP-2 and-9) in human trophoblast invasion. *Reproductive Biology and Endocrinology,* 2**,** 59.

STEINMAN, R. M. & HEMMI, H. 2006. Dendritic cells: translating innate to adaptive immunity. *From innate immunity to immunological memory.* Springer.

STEWART, C. L., KASPAR, P., BRUNET, L. J., BHATT, H., GADI, I., KÖNTGEN, F. & ABBONDANZO, S. J. 1992a. Blastocyst implantation depends on maternal expression of leukaemia inhibitory factor. *Nature,* 359**,** 76-79.

STEWART, C. L., KASPAR, P., BRUNET, L. J., BHATT, H., GADI, I., KÖNTGEN, F. & ABBONDANZO, S. J. 1992b. Blastocyst implantation depends on maternal expression of leukaemia inhibitory factor. *Nature,* 359**,** 76.

STEWART, I. J. & MITCHELL, B. S. 1991. The distribution of uterine macrophages in virgin and early pregnant mice. *Journal of anatomy,* 179**,** 183-196.

SU, R.-W. & FAZLEABAS, A. T. 2015. Implantation and Establishment of Pregnancy in Human and Nonhuman Primates. *Advances in anatomy, embryology, and cell biology,* 216**,** 189-213.

SUGULLE, M., DECHEND, R., HERSE, F., WEEDON-FEKJAER, M. S., JOHNSEN, G. M., BROSNIHAN, K. B., ANTON, L., LUFT, F. C., WOLLERT, K. C., KEMPF, T. & STAFF, A. C. 2009. Circulating and placental growth-differentiation factor 15 in preeclampsia and in pregnancy complicated by diabetes mellitus. *Hypertension (Dallas, Tex. : 1979),* 54**,** 106-112.

SVENSSON-ARVELUND, J. & ERNERUDH, J. 2015. The Role of Macrophages in Promoting and Maintaining Homeostasis at the Fetal–Maternal Interface. *American Journal of Reproductive Immunology,* 74**,** 100-109.

SVENSSON-ARVELUND, J., MEHTA, R. B., LINDAU, R., MIRRASEKHIAN, E., RODRIGUEZ-MARTINEZ, H., BERG, G., LASH, G. E., JENMALM, M. C. & ERNERUDH, J. 2015. The Human Fetal Placenta Promotes Tolerance against the Semiallogeneic Fetus by Inducing Regulatory T Cells and Homeostatic M2 Macrophages. *The Journal of Immunology,* 194**,** 1534-1544.

SVENSSON, J., JENMALM, M. C., MATUSSEK, A., GEFFERS, R., BERG, G. & ERNERUDH, J. 2011. Macrophages at the fetal-maternal interface express markers of alternative activation and are induced by M-CSF and IL-10. *J Immunol,* 187**,** 3671-82.

SZEKERES-BARTHO, J., BARAKONYI, A., POLGAR, B., PAR, G., FAUST, Z., PALKOVICS, T. & SZEREDAY, L. 1999. The Role of γ/δ T Cells in Progesterone-Mediated Immunomodulation During Pregnancy: A Review. *American Journal of Reproductive Immunology,* 42**,** 44-48.

TAGLIANI, E. & ERLEBACHER, A. 2011. Dendritic cell function at the maternal–fetal interface. *Expert review of clinical immunology,* 7**,** 593-602.

TAKACS, P. & KAUMA, S. 1996. The expression of interleukin-1 alpha, interleukin-1 beta, and interleukin-1 receptor type I mRNA during preimplantation mouse development. *J Reprod Immunol,* 32**,** 27-35.

TAKAHASHI, K., NAITO, M., KATABUCHI, H. & HIGASHI, K. 1991. Development, differentiation, and maturation of macrophages in the chorionic villi of mouse placenta with special reference to the origin of Hofbauer cells. *Journal of Leukocyte Biology,* 50**,** 57-68.

TAKAHASHI, K., YAMAMURA, F. & NAITO, M. 1989. Differentiation, maturation, and proliferation of macrophages in the mouse yolk sac: a light-microscopic, enzyme-cytochemical, immunohistochemical, and ultrastructural study. *Journal of Leukocyte Biology,* 45**,** 87-96.

TAKAYA, R., FUKAYA, T., SASANO, H., SUZUKI, T., TAMURA, M. & YAJIMA, A. 1997. Macrophages in normal cycling human ovaries; immunohistochemical localization and characterization. *Human Reproduction,* 12**,** 1508-1512.

TAKIGUCHI, S., SUGINO, N., ESATO, K., KARUBE-HARADA, A., SAKATA, A., NAKAMURA, Y., ISHIKAWA, H. & KATO, H. 2004. Differential regulation of apoptosis in the corpus luteum of pregnancy and newly formed corpus luteum after parturition in rats. *Biol Reprod,* 70**,** 313-8.

TAN, J., PARIA, B. C., DEY, S. K. & DAS, S. K. 1999. Differential Uterine Expression of Estrogen and Progesterone Receptors Correlates with Uterine Preparation for Implantation and Decidualization in the Mouse. *Endocrinology,* 140**,** 5310-5321.

TANG, M. X., HU, X. H., LIU, Z. Z., KWAK-KIM, J. & LIAO, A. H. 2015. What are the roles of macrophages and monocytes in human pregnancy? *Journal of Reproductive Immunology,* 112**,** 73-80.

TANG, Z., BUHIMSCHI, I. A., BUHIMSCHI, C. S., TADESSE, S., NORWITZ, E., NIVEN-FAIRCHILD, T., HUANG, S.-T. J. & GULLER, S. 2013. Decreased levels of folate receptor-β and reduced numbers of fetal macrophages (Hofbauer cells) in placentas from pregnancies with severe pre-eclampsia. *American Journal of Reproductive Immunology,* 70**,** 104-115.

TAVIAN, M. & PEAULT, B. 2005. Embryonic development of the human hematopoietic system. *Int J Dev Biol,* 49**,** 243-50.

TAYADE, C., HILCHIE, D., HE, H., FANG, Y., MOONS, L., CARMELIET, P., FOSTER, R. A. & CROY, B. A. 2007. Genetic deletion of placenta growth factor in mice alters uterine NK cells. *The Journal of Immunology,* 178**,** 4267-4275.

TESSER, R. B., SCHERHOLZ, P. L., DO NASCIMENTO, L. & KATZ, S. G. 2010. Trophoblast glycogen cells differentiate early in the mouse ectoplacental cone: putative role during placentation. *Histochem Cell Biol,* 134**,** 83-92.

THALER, I., MANOR, D., ITSKOVITZ, J., ROTTEM, S., LEVIT, N., TIMOR-TRITSCH, I. & BRANDES, J. M. 1990. Changes in uterine blood flow during human pregnancy. *Am J Obstet Gynecol,* 162**,** 121-5.

TREMELLEN, K. P., SEAMARK, R. F. & ROBERTSON, S. A. 1998. Seminal Transforming Growth Factor β1, Stimulates Granulocyte-Macrophage Colony-Stimulating Factor Production and Inflammatory Cell Recruitment in the Murine Uterus1. *Biology of Reproduction,* 58**,** 1217-1225.

TURNER, E. C., HUGHES, J., WILSON, H., CLAY, M., MYLONAS, K. J., KIPARI, T., DUNCAN, W. C. & FRASER, H. M. 2011. Conditional ablation of macrophages disrupts ovarian vasculature. *Reproduction,* 141**,** 821-831.

UNEMORI, E. N., ERIKSON, M. E., ROCCO, S. E., SUTHERLAND, K. M., PARSELL, D. A., MAK, J. & GROVE, B. H. 1999. Relaxin stimulates expression of vascular endothelial growth factor in normal human endometrial cells in vitro and is associated with menometrorrhagia in women. *Human Reproduction,* 14**,** 800-806.

VAN DEN HEUVEL, M. J., CHANTAKRU, S., XIE, X., EVANS, S. S., TEKPETEY, F., MOTE, P. A., CLARKE, C. L. & CROY, B. A. 2005. Trafficking of Circulating Pro-NK Cells to the Decidualizing Uterus: Regulatory Mechanisms in the Mouse and Human. *Immunological Investigations,* 34**,** 273-293.

VAN DER HOEK, K. H., MADDOCKS, S., WOODHOUSE, C. M., VAN ROOIJEN, N., ROBERTSON, S. A. & NORMAN, R. J. 2000. Intrabursal Injection of Clodronate Liposomes Causes Macrophage Depletion and Inhibits Ovulation in the Mouse Ovary. *Biology of Reproduction,* 62**,** 1059-1066.

VAN ROOIJEN, N. & VAN NIEUWMEGEN, R. 1984. Elimination of phagocytic cells in the spleen after intravenous injection of liposome-encapsulated dichloromethylene diphosphonate. An enzyme-histochemical study. *Cell Tissue Res,* 238**,** 355-8.

VINCE, G. S., STARKEY, P. M., JACKSON, M. C., SARGENT, I. L. & REDMAN, C. W. G. 1990. Flow cytometric characterisation of cell populations in human pregnancy decidua and isolation of decidual macrophages. *Journal of Immunological Methods,* 132**,** 181-189.

WAHL, J. R., GOETSCH, N. J., YOUNG, H. J., VAN MAANEN, R. J., JOHNSON, J. D., PEA, A. S. & BRITTINGHAM, A. 2005. Murine macrophages produce endothelin-1 after microbial stimulation. *Exp Biol Med (Maywood),* 230**,** 652-8.

WAN, H., VERSNEL, M. A., LEIJTEN, L. M. E., VAN HELDEN-MEEUWSEN, C. G., FEKKES, D., LEENEN, P. J. M., KHAN, N. A., BENNER, R. & KIEKENS, R. C. M. 2008. Chorionic gonadotropin induces dendritic cells to express a tolerogenic phenotype. *Journal of Leukocyte Biology,* 83**,** 894-901.

WANG, W.-J., HAO, C.-F. & LIN, Q.-D. 2011. Dysregulation of macrophage activation by decidual regulatory T cells in unexplained recurrent miscarriage patients. *Journal of Reproductive Immunology,* 92**,** 97-102.

WANG, W., IRANI, R. A., ZHANG, Y., RAMIN, S. M., BLACKWELL, S. C., TAO, L., KELLEMS, R. E. & XIA, Y. 2012. Autoantibody-mediated complement C3a receptor activation contributes to the pathogenesis of preeclampsia. *Hypertension (Dallas, Tex. : 1979),* 60**,** 712-721.

WARE, C. B., HOROWITZ, M. C., RENSHAW, B. R., HUNT, J. S., LIGGITT, D., KOBLAR, S. A., GLINIAK, B. C., MCKENNA, H. J., PAPAYANNOPOULOU, T., THOMA, B. & ET AL. 1995. Targeted disruption of the low-affinity leukemia inhibitory factor receptor gene causes placental, skeletal, neural and metabolic defects and results in perinatal death. *Development,* 121**,** 1283-99.

WATSON, E. D. & CROSS, J. C. 2005. Development of Structures and Transport Functions in the Mouse Placenta. *Physiology,* 20**,** 180-193.

WEEL, I., ROMAO-VEIGA, M., MATIAS, M. L., FIORATTI, E. G., PERACOLI, J. C., BORGES, V. T., ARAUJO, J. P., JR. & PERACOLI, M. T. 2017. Increased expression of NLRP3 inflammasome in placentas from pregnant women with severe preeclampsia. *J Reprod Immunol,* 123**,** 40-47.

WEISSGERBER, T. L., MILIC, N. M., MILIN-LAZOVIC, J. S. & GAROVIC, V. D. 2016. Impaired Flow-Mediated Dilation Before, During, and After Preeclampsia: A Systematic Review and Meta-Analysis. *Hypertension,* 67**,** 415-23.

WETENDORF, M. & DEMAYO, F. J. 2014. Progesterone receptor signaling in the initiation of pregnancy and preservation of a healthy uterus. *The International journal of developmental biology,* 58**,** 95-106.

WHEELER, K. C., JENA, M. K., PRADHAN, B. S., NAYAK, N., DAS, S., HSU, C.-D., WHEELER, D. S., CHEN, K. & NAYAK, N. R. 2018a. VEGF may contribute to macrophage recruitment and M2 polarization in the decidua. *PloS one,* 13**,** e0191040-e0191040.

WHEELER, K. C., JENA, M. K., PRADHAN, B. S., NAYAK, N., DAS, S., HSU, C. D., WHEELER, D. S., CHEN, K. & NAYAK, N. R. 2018b. VEGF may contribute to macrophage recruitment and M2 polarization in the decidua. *PLoS One,* 13**,** e0191040.

WICHEREK, L., BASTA, P., PITYNSKI, K., MARIANOWSKI, P., KIJOWSKI, J., WIATR, J. & MAJKA, M. 2009. The Characterization of the Subpopulation of Suppressive B7H4+ Macrophages and the Subpopulation of CD25+ CD4+ and FOXP3+ Regulatory T-cells in Decidua during the Secretory Cycle Phase, Arias Stella Reaction, and Spontaneous Abortion – A Preliminary Report. *American Journal of Reproductive Immunology,* 61**,** 303-312.

WIGGLESWORTH, J. S. 1974. Fetal growth retardation. Animal model: uterine vessel ligation in the pregnant rat. *The American journal of pathology,* 77**,** 347-350.

WILLIAMS, P. J., BULMER, J. N., SEARLE, R. F., INNES, B. A. & ROBSON , S. C. 2009. Altered decidual leucocyte populations in the placental bed in pre-eclampsia and foetal growth restriction: a comparison with late normal pregnancy. *Reproduction,* 138**,** 177-184.

WILSON, R. L., LEEMAQZ, S. Y., GOH, Z., MCANINCH, D., JANKOVIC-KARASOULOS, T., LEGHI, G. E., PHILLIPS, J. A., COLAFELLA, K. M., TRAN, C., O'LEARY, S., BUCKBERRY, S., PEDERSON, S., ROBERTSON, S. A., BIANCO-MIOTTO, T. & ROBERTS, C. T. 2017. Zinc is a critical regulator of placental morphogenesis and maternal hemodynamics during pregnancy in mice. *Scientific Reports,* 7**,** 15137.

WINSHIP, A., CORREIA, J., KRISHNAN, T., MENKHORST, E., CUMAN, C., ZHANG, J.-G., NICOLA, N. A. & DIMITRIADIS, E. 2015a. Blocking Endogenous Leukemia Inhibitory Factor During Placental Development in Mice Leads to Abnormal Placentation and Pregnancy Loss. *Scientific Reports,* 5**,** 13237.

WINSHIP, A., CORREIA, J., ZHANG, J. G., NICOLA, N. A. & DIMITRIADIS, E. 2015b. Leukemia Inhibitory Factor (LIF) Inhibition during Mid-Gestation Impairs Trophoblast Invasion and Spiral Artery Remodelling during Pregnancy in Mice. *Plos One,* 10.

WOOD, G. W., HAUSMANN, E. & CHOUDHURI, R. 1997. Relative role of CSF-1, MCP-1/JE, and RANTES in macrophage recruitment during successful pregnancy. *Mol Reprod Dev,* 46**,** 62-9; discussion 69-70.

WOODS, L., PEREZ-GARCIA, V. & HEMBERGER, M. 2018. Regulation of Placental Development and Its Impact on Fetal Growth—New Insights From Mouse Models. *Frontiers in Endocrinology,* 9.

WU, H.-X., JIN, L.-P., XU, B., LIANG, S.-S. & LI, D.-J. 2014. Decidual stromal cells recruit Th17 cells into decidua to promote proliferation and invasion of human trophoblast cells by secreting IL-17. *Cell Mol Immunol,* 11**,** 253-262.

WU, R., VAN DER HOEK, K. H., RYAN, N. K., NORMAN, R. J. & ROBKER, R. L. 2004. Macrophage contributions to ovarian function. *Human Reproduction Update,* 10**,** 119-133.

WU, Z. M., YANG, H., LI, M., YEH, C. C., SCHATZ, F., LOCKWOOD, C. J., DI, W. & HUANG, S. J. 2012. Pro-inflammatory cytokine-stimulated first trimester decidual cells enhance macrophage-induced apoptosis of extravillous trophoblasts. *Placenta,* 33**,** 188-194.

WYRWOLL, C. S., SECKL, J. R. & HOLMES, M. C. 2009. Altered placental function of 11beta-hydroxysteroid dehydrogenase 2 knockout mice. *Endocrinology,* 150**,** 1287-1293.

XU, C., MAO, D., HOLERS, V. M., PALANCA, B., CHENG, A. M. & MOLINA, H. 2000. A critical role for murine complement regulator crry in fetomaternal tolerance. *Science,* 287**,** 498-501.

XU, Y., ROMERO, R., MILLER, D., KADAM, L., MIAL, T. N., PLAZYO, O., GARCIA-FLORES, V., HASSAN, S. S., XU, Z., TARCA, A. L., DREWLO, S. & GOMEZ-LOPEZ, N. 2016. An M1-like Macrophage Polarization in Decidual Tissue during Spontaneous Preterm Labor That Is Attenuated by Rosiglitazone Treatment. *The Journal of Immunology,* 196**,** 2476-2491.

XUE, J., SCHMIDT, SUSANNE V., SANDER, J., DRAFFEHN, A., KREBS, W., QUESTER, I., DE NARDO, D., GOHEL, TRUPTI D., EMDE, M., SCHMIDLEITHNER, L., GANESAN, H., NINO-CASTRO, A., MALLMANN, MICHAEL R., LABZIN, L., THEIS, H., KRAUT, M., BEYER, M., LATZ, E., FREEMAN, TOM C., ULAS, T. & SCHULTZE, JOACHIM L. 2014. Transcriptome-Based Network Analysis Reveals a Spectrum Model of Human Macrophage Activation. *Immunity,* 40**,** 274-288.

YANABA, K., BOUAZIZ, J.-D., HAAS, K. M., POE, J. C., FUJIMOTO, M. & TEDDER, T. F. 2008. A Regulatory B Cell Subset with a Unique CD1dhiCD5+ Phenotype Controls T Cell-Dependent Inflammatory Responses. *Immunity,* 28**,** 639-650.

YONA, S., KIM, K.-W., WOLF, Y., MILDNER, A., VAROL, D., BREKER, M., STRAUSS-AYALI, D., VIUKOV, S., GUILLIAMS, M., MISHARIN, A., HUME, D. A., PERLMAN, H., MALISSEN, B., ZELZER, E. & JUNG, S. 2013. Fate mapping reveals origins and dynamics of monocytes and tissue macrophages under homeostasis. *Immunity,* 38**,** 79-91.

YOSHINAGA, K., DAVIES, C., WHITE, K., CARON, K., GOLOS, T., FAZLEABAS, A., PARIA, B., MOR, G., PAUL, S., YE, X., DEY, S. K., SPENCER, T. & ROBERTS, R. M. 2014. Interdisciplinary collaborative team for blastocyst implantation research: inception and perspectives. *American journal of reproductive immunology (New York, N.Y. : 1989),* 71**,** 1-11.

ZEISBERGER, S. M., ODERMATT, B., MARTY, C., ZEHNDER-FJÄLLMAN, A. H. M., BALLMER-HOFER, K. & SCHWENDENER, R. A. 2006. Clodronate-liposome-mediated depletion of tumour-associated macrophages: a new and highly effective antiangiogenic therapy approach. *British Journal of Cancer,* 95**,** 272-281.

ZEISLER, H., LLURBA, E., CHANTRAINE, F., VATISH, M., STAFF, A. C., SENNSTRÖM, M., OLOVSSON, M., BRENNECKE, S. P., STEPAN, H. & ALLEGRANZA, D. 2016. Predictive value of the sFlt-1: PlGF ratio in women with suspected preeclampsia. *N Engl J Med,* 374**,** 13-22.

ZENCLUSSEN, M. L., LINZKE, N., SCHUMACHER, A., FEST, S., MEYER, N., CASALIS, P. A. & ZENCLUSSEN, A. C. 2015. Heme oxygenase-1 is critically involved in placentation, spiral artery remodeling, and blood pressure regulation during murine pregnancy. *Frontiers in pharmacology,* 5**,** 291-291.

ZHANG, J. H., DUNK, C., CROY, A. B. & LYE, S. J. 2016. To serve and to protect: the role of decidual innate immune cells on human pregnancy. *Cell and Tissue Research,* 363**,** 249-265.

ZHANG, Q., HAO, J. & LI, G. 2019. Deletion of Prl7d1 causes placental defects at mid-pregnancy in mice. *Molecular Reproduction and Development,* 86**,** 696-713.

ZHANG, Q. & YAN, J. 2015. Update of Wnt signaling in implantation and decidualization. *Reproductive medicine and biology,* 15**,** 95-105.

ZHANG, S., REGNAULT, T., BARKER, P., BOTTING, K., MCMILLEN, I., MCMILLAN, C., ROBERTS, C. & MORRISON, J. 2015. Placental Adaptations in Growth Restriction. *Nutrients,* 7**,** 360.

ZHANG, X., QI, C. & LIN, J. 2010. Enhanced expressions of matrix metalloproteinase (MMP)-2 and-9 and vascular endothelial growth factors (VEGF) and increased microvascular density in the endometrial hyperplasia of women with anovulatory dysfunctional uterine bleeding. *Fertility and Sterility,* 93**,** 2362-2367.

ZHANG, Y.-H., HE, M., WANG, Y. & LIAO, A.-H. 2017. Modulators of the Balance between M1 and M2 Macrophages during Pregnancy. *Frontiers in Immunology,* 8**,** 120.

ZHAO, M., YUAN, L., YUAN, M. M., HUANG, L. L., SU, C., CHEN, Y. H., YANG, Y. Y., HU, Y. & XU, D. X. 2018. Maternal lipopolysaccharide exposure results in glucose metabolism disorders and sex hormone imbalance in male offspring. *Mol Cell Endocrinol,* 474**,** 272-283.

ZHU, C., ANDERSON, A. C., SCHUBART, A., XIONG, H., IMITOLA, J., KHOURY, S. J., ZHENG, X. X., STROM, T. B. & KUCHROO, V. K. 2005. The Tim-3 ligand galectin-9 negatively regulates T helper type 1 immunity. *Nat Immunol,* 6**,** 1245-1252.

ZŁOTKOWSKA, A. & ANDRONOWSKA, A. 2019. Chemokines as the modulators of endometrial epithelial cells remodelling. *Scientific Reports,* 9**,** 12968.